

**Faculty of Science and Engineering
School of Civil and Mechanical Engineering**

**Comparing CPT Results and Numerical Method Investigations to Assess
the Behaviour of Pile and Sand and Mixed Soil Using ABAQUS**

Reza Yadak

This thesis is presented for the Degree of

Doctor of Philosophy

of

Curtin University

January 2020

Declaration

To the best of my knowledge and belief, this thesis contains no materials previously published by any other person except where due acknowledgement has been made.

This thesis contains no material which has been accepted for the award of any other degree or diploma in any university.

Signature:

Date: 13/12/2019

Abstract

Geotechnical engineers often recommend the piles as foundations to support the high-rise buildings and other structures subjected to forces. Henceforth, pile lateral and axial carrying capacity is necessary to be estimated. It is well known that settlement and bearing capacity are two leading factors that govern the design procedure of pile foundations so that the serviceability necessities are attained.

This thesis demonstrates the expansion of numerical models which are purposed to be utilised to predict the load-settlement and the ultimate pile capacity of pile foundations embedded in sand and mixed soils. The finite element method and ABAQUS software are used to develop the models. To begin with, the finite element method (FEM) is used to model the bearing capacity and load-settlement behaviour of the bored piles, concrete driven piles and steel driven piles. Validating the load-settlement diagrams has been achieved by using this method.

The data used for developing the FEM models in ABAQUS are collected from the literature and comprise a total of 50 bored pile load tests and 58 driven pile load tests (28 concrete pile load tests and 30 steel pile load tests) as well as CPT profile data. The bored piles have different sizes and round shapes, with diameters ranging from 320 to 1800 mm and lengths from 6 to 27 m. The driven piles also have different sizes and shapes (i.e. circular, square and hexagonal), with diameters ranging from 250 to 660 mm and lengths from 8 to 36 m. All the information of case records in the data source is reviewed to ensure the reliability of used data.

The variables that are believed to have a major consequence on the bearing capacity of pile foundations are considered. They comprise pile diameter, embedded length, weighted average cone point resistance within tip influence region and weighted average cone point resistance and weighted average sleeve friction along the shaft. The sleeve friction values are not available in the bored piles data, so the weighted average sleeve friction along the shaft is excluded from bored piles models. The models output is the pile capacity (interpreted failure load) and settlement.

Additional input variables are included for modelling the load-settlement conduct of piles. They include pile materials (modulus of elasticity, Poisson's ratio), soil parameters (cohesion, modulus of elasticity, dilation angle, friction angle, groundwater level, installation technique).

Results were presented in terms of the settlement and ultimate bearing capacity. Firstly, three different piles in different soil profiles were chosen, and numerical analysis for each of them were expanded. Moreover, the sensitivity of each model to Young's modulus were carried out. Results of FEM in ABAQUS are presented with diagrams and visual presentations. Furthermore, validation of all 108 experimental and numerical models are shown in displacement-force diagrams. The validation method which consists of comparing CPT results and ABAQUS outcome shows they are the same in most cases, and the trend of diagrams are almost in the same orientation.

Above mentioned methods result the main purpose of this dissertation which is to validate a predictive FEM method based on relative difference between estimated and measured pile capacity. This was achieved by developing the ABAQUS package results and and finite element method in practical designing engineering process. The relationship of the results with other published reserchs is mentioned. It was found that considering soil-pile interaction can result in more optimistic design of deep foundations (piles).

The output of this study is very useful for designers and also for researchers who are going to apply this methodology on other problems in Geotechnical Engineering, like group piles foundationes. Moreover, the result of this study can be considered applicable worldwide because its input data is collected from different regions.

Acknowledgements

I would like to express my deepest gratitude to my advisors Professor Hamid Nikraz and Dr Amin Chegenizadeh.

I would like to extend my sincere gratitude and profound respect to my first supervisor, Professor Hamid Nikraz, for his patience, advice, support and encouragement during my study. I am greatly indebted to him for his timely advice, hearty concern for my research and the intensive, regular meetings to guide me throughout my time as his student.

I would also like to express my gratitude to Dr Amin Chegenizadeh, my second supervisor, for his invaluable suggestions, motivation, stimulating discussions and perpetual direction throughout my study time. His guidance and support have been invaluable on both personal and academic levels.

I would like to convey my gratitude to Dr Ranjan Sarukalige for being the chairperson of my thesis committee. I sincerely thank the Department of Civil Engineering at Curtin University for providing a pleasant research environment. I acknowledge the support of Dr Ahdyeh Mosadegh for her valuable advice and supports.

Last but not least, I deeply appreciate the emotional support of my beloved parents and all of my family members who kindly supported me during my thesis.

Reza Yadak

Curtin University

December 2019

Table of Contents

Declaration	II
Abstract	1
Acknowledgements	3
Table of Contents.....	4
List of Figures	7
List of Tables.....	13
Nomenclature	14
1 INTRODUCTION	18
1.1 BACKGROUND	18
1.2 PROBLEM STATEMENT	20
1.3 OBJECTIVES OF THESIS	21
1.4 STRUCTURE OF THESIS.....	22
2 LITERATURE REVIEW	24
2.1 INTRODUCTION AND CHAPTER OVERVIEW	24
2.2 SOIL-PILE-STRUCTURE INTERACTION ANALYSES.....	26
2.2.1 Method of Design Base on SPSI Analysis.....	26
2.2.2 Numerical Tools.....	28
2.3 <i>p-y</i> CURVES	31
2.3.1 Existing <i>p-y</i> Curves	32
2.3.2 Effects of pile dimension on <i>p-y</i> curves.....	40
2.3.3 <i>p-y</i> Curves with back evaluation	41
2.4 ARTIFICIAL INTELLIGENCE METHOD.....	48
2.4.1 Overview of ANNs	48
2.4.2 Extention of ANN instances	49

2.5 FINITE ELEMENT METHOD APPLIED TO SPSI PROBLEMS	54
2.5.1 Boundary Conditions	54
2.5.2 Pile-soil interface	56
2.5.3 Loading	57
2.5.4 Behaviour of soil	57
2.5.5 Applications	57
2.6 SUMMARY OF THE CHAPTER.....	64
3 Development of Experimental and Numerical Methods	65
3.1 INTRODUCTION AND CHAPTER OVERVIEW	65
3.2 CONE PENETRATION TEST (CPT).....	67
3.2.1 General Definitions	67
3.2.2 A Brief Background History of CPT	68
3.2.3 Methods of estimating pile bearing capacity based on CPT information.....	69
3.2.4 Settlement Prediction	80
3.3 FINITE ELEMENT METHOD	83
3.3.1 Build a Finite Element Model relied on CPT Outcomes	83
3.3.2 The Numerical Approach.....	87
3.4 DATA COLLECTION	95
3.4.1 Description of Piles	95
3.4.2 Choice of input variables	104
3.5 SUMMARY OF THE CHAPTER.....	115
4 Investigation of Pile Behaviour and Parametric Studies	117
4.1 INTRODUCTION AND CHAPTER OVERVIEW	117
4.2 RESULTS AND DISCUSSION FOR SELECTED PILES.....	119
4.2.1 Case 1 Profile	119
4.2.2 Case 2 Profile	120

4.2.3 Case 3 Profile	121
4.2.4 Description of Material properties in ABAQUS.....	122
4.2.5 Result Contours for Three Base Models	122
4.2.6 Parametric Study	131
4.2.7 Convergence Study	139
4.4 SUMMARY OF THE CHAPTER.....	142
5 Investigation of Soil Behaviour Based on CPT Data and Numerical Modeling 143	
5.1 INTRODUCTION AND CHAPTER OVERVIEW	143
5.2 VALIDATING ALL CASES	144
5.2.1 Regression Analysis	144
5.2.2 Evaluating the Model Performance.....	145
5.3 SUMMARY OF THE CHAPTER.....	182
6 CONCLUSIONS AND RECOMMENDATIONS	183
6.1 CONCLUSIONS.....	183
6.2 RECOMMENDATIONS	185
7 REFERENCES.....	186
8 APPENDICES.....	199
Appendix A - Bored Piles Case Records Summary	200
Appendix B - Concrete Driven Piles Case Records Summary	253
Appendix C - Steel Driven Piles Case Records Summary.....	283
Appendix D - Permissions from Copyright Owners.....	315

List of Figures

Figure 2- 1 Explanation for concept of p - y with a) foundation without loading b) foundation after loading (from[36])	32
Figure 2- 2 Formation of the p - y curvature of soil with soft clay criteria with a) load in static shape b) load in cyclic shape (from [31])	33
Figure 2- 3 Specification formation of the p - y curvature in soil with stiff clay criteria under water level with a) static load b) cyclical load c) quantity of permanent A (from [37]).....	35
Figure 2- 4 Specification formation of the p - y curvature in soil with stiff clay characteristic over water level for a) static load b) cyclical load (from [38], [37])	36
Figure 2- 5 Specification formation for p - y curvatures in sandy soils (from [30])	37
Figure 2- 6 Amount of factor A applied to expand p - y curvatures in sandy soil a) Factor A b) Factor B (from [30])	38
Figure 2- 7 Characteristic formation of p - y curves in sandy soil (from [30])..	40
Figure 2- 8 schematic demonstration of ANN patterns (from [53])	50
Figure 2- 9 Similar 3d pattern of soil-pile respond (from[36])	59
Figure 2- 10 outline of pile and structure (from[36])	60
Figure 3- 1 Supposed fracture models below piles (Source:[163]).....	70
Figure 3- 2 Dutch procedure for computing bearing of the end from the CPT results (Source: [165])	71
Figure 3- 3 LCPC procedure for measuring tantamount cone resistance in pile head (Source:[36, 167])	73
Figure 3- 4 a) Master surface pierce in the slave surface when it is not developed b) Additional master nodes per capita restraint are convoluted and coupled next to the slave surface (Source: [209]).....	86
Figure 3- 5 Shear persistence against standard stress (Source [210]).....	87
Figure 3- 6 Mohr-Coulomb fracture criteria (Source[36])	92
Figure 3- 7 Schematic sketch of the numerical model (Source[36])	94
Figure 3- 8 Comparing averaging techniques for cone point resistance inside head-impact region (Source: [36]).....	108

Figure 3- 9 Synopsis graph for driven steel pile sample data 15, (a) soil profile and pile geometry, (b) profile of cone head resistance, (c) profile of sleeve friction, (d) load–settlement plot (Source [36])	109
Figure 3- 10 Synopsis graph for driven steel pile sample data 1, (a) soil profile and pile geometry, (b) profile of cone head resistance, (c) profile of sleeve friction, (d) load–settlement plot (Source [36])	110
Figure 3- 11 Synopsis graph for the bored pile sample data 45, (a) soil profile and pile geometry, (b) profile of cone head resistance, (c) profile of sleeve friction, (d) load–settlement plot (Source [36])	111
Figure 4- 1 Summary sheet for case record A21, (a) pile geometry and soil profile, (b) cone tip resistance profile, (c) load deflection plot.....	119
Figure 4- 2 Summary sheet for case record B17, (a) pile geometry and soil profile, (b) cone tip resistance profile, (c) sleeve friction profile,	120
Figure 4- 3 Summary sheet for case record B17, (a) pile geometry and soil profile, (b) cone tip resistance profile, (c) sleeve friction profile,	121
Figure 4- 4 Case 1, elastic strain (maximum principal) – loading step – on soil	124
Figure 4- 5 Case 1, plastic strain (maximum principal) – loading step – on soil	124
Figure 4- 6 Case 1, total stress – loading step – on soil	125
Figure 4- 7 Case 1, vertical stress – loading step – on soil.....	125
Figure 4- 8 Case 1, total displacement magnitude – loading step – on soil.....	126
Figure 4- 9 Case 2, elastic strain (maximum principal) – loading step – on soil	126
Figure 4- 10 Case 2, plastic strain (maximum principal) – loading step – on soil.....	127
Figure 4- 11 Case 2, total stress – loading step – on soil	127
Figure 4- 12 Case 2, vertical stress – loading step – on soil.....	128
Figure 4- 13 Case 2, total displacement magnitude – loading step – on soil	128
Figure 4- 14 Case 3, elastic strain (maximum principal) – loading step – on soil.....	129
Figure 4- 15 Case 3, plastic strain (maximum principal) – loading step – on soil.....	129
Figure 4- 16 Case 3, total stress – loading step – on soil	130

Figure 4- 17 Case 3, vertical stress – loading step – on soil	130
Figure 4- 18 Case 3, total displacement magnitude – loading step – on soil	131
.....	
Figure 4- 19 Parametric study for case 1.....	132
Figure 4- 20 Load transfer mechanism study for case 1	133
Figure 4- 21 Parametric study for case 2.....	134
Figure 4- 22 Load transfer mechanism study for case 2.....	135
Figure 4- 23 Parametric study for case 3.....	136
Figure 4- 24 Load transfer mechanism for case 3	137
Figure 4- 25 Displacement-force diagram for different values of elements (mesh convergence study).....	141
Figure 5- 1 Model A-1.....	146
Figure 5- 2 Model A-2.....	146
Figure 5- 3 Model A-3.....	146
Figure 5- 4 Model A-4.....	147
Figure 5- 5 Model A-5.....	147
Figure 5- 6 Model A-6.....	147
Figure 5- 7 Model A-7.....	148
Figure 5- 8 Model A-8.....	148
Figure 5- 9 Model A-9.....	148
Figure 5- 10 Model A-10.....	149
Figure 5- 11 Model A-11.....	149
Figure 5- 12 Model A-12.....	149
Figure 5- 13 Model A-13.....	150
Figure 5- 14 Model A-14.....	150
Figure 5- 15 Model A-15.....	150
Figure 5- 16 Model A-16.....	151
Figure 5- 17 Model A-17.....	151
Figure 5- 18 Model A-18.....	151
Figure 5- 19 Model A-19.....	152
Figure 5- 20 Model A-20.....	152
Figure 5- 21 Model A-21.....	152
Figure 5- 22 Model A-22.....	153
Figure 5- 23 Model A-23.....	153
Figure 5- 24 Model A-24.....	153

Figure 5- 25 Model A-25.....	154
Figure 5- 26 Model A-26.....	154
Figure 5- 27 Model A-27.....	154
Figure 5- 28 Model A-28.....	155
Figure 5- 29 Model A-29.....	155
Figure 5- 30 Model A-30.....	155
Figure 5- 31 Model A-31.....	156
Figure 5- 32 Model A-32.....	156
Figure 5- 33 Model A-33.....	156
Figure 5- 34 Model A-34.....	157
Figure 5- 35 Model A-35.....	157
Figure 5- 36 Model A-36.....	157
Figure 5- 37 Model A-37.....	158
Figure 5- 38 Model A-38.....	158
Figure 5- 39 Model A-39.....	158
Figure 5- 40 Model A-40.....	159
Figure 5- 41 Model A-41.....	159
Figure 5- 42 Model A-42.....	159
Figure 5- 43 Model A-43.....	160
Figure 5- 44 Model A-44.....	160
Figure 5- 45 Model A-45.....	160
Figure 5- 46 Model A-46.....	161
Figure 5- 47 Model A-47.....	161
Figure 5- 48 Model A-48.....	161
Figure 5- 49 Model A-49.....	162
Figure 5- 50 Model A-50.....	162
Figure 5- 51 Model B-1.....	162
Figure 5- 52 Model B-2.....	163
Figure 5- 53 Model B-3.....	163
Figure 5- 54 Model B-4.....	163
Figure 5- 55 Model B-5.....	164
Figure 5- 56 Model B-6.....	164
Figure 5- 57 Model B-7.....	164
Figure 5- 58 Model B-8.....	165
Figure 5- 59 Model B-9.....	165
Figure 5- 60 Model B-10.....	165
Figure 5- 61 Model B-11.....	166

Figure 5- 62 Model B-12.....	166
Figure 5- 63 Model B-13.....	166
Figure 5- 64 Model B-14.....	167
Figure 5- 65 Model B-15.....	167
Figure 5- 66 Model B-16.....	167
Figure 5- 67 Model B-17.....	168
Figure 5- 68 Model B-18.....	168
Figure 5- 69 Model B-19.....	168
Figure 5- 70 Model B-20.....	169
Figure 5- 71 Model B-21.....	169
Figure 5- 72 Model B-22.....	169
Figure 5- 73 Model B-23.....	170
Figure 5- 74 Model B-24.....	170
Figure 5- 75 Model B-25.....	170
Figure 5- 76 Model B-26.....	171
Figure 5- 77 Model B-27.....	171
Figure 5- 78 Model B-28.....	171
Figure 5- 79 Model C-1	172
Figure 5- 80 Model C-2	172
Figure 5- 81 Model C-3	172
Figure 5- 82 Model C-4	173
Figure 5- 83 Model C-5	173
Figure 5- 84 Model C-6	173
Figure 5- 85 Model C-7	174
Figure 5- 86 Model C-8	174
Figure 5- 87 Model C-9	174
Figure 5- 88 Model C-10	175
Figure 5- 89 Model C-11	175
Figure 5- 90 Model C-12	175
Figure 5- 91 Model C-13	176
Figure 5- 92 Model C-14	176
Figure 5- 93 Model C-15	176
Figure 5- 94 Model C-16	177
Figure 5- 95 Model C-17	177
Figure 5- 96 Model C-18	177
Figure 5- 97 Model C-19	178
Figure 5- 98 Model C-20	178

Figure 5- 99 Model C-21	178
Figure 5- 100 Model C-22	179
Figure 5- 101 Model C-23	179
Figure 5- 102 Model C-24	179
Figure 5- 103 Model C-25	180
Figure 5- 104 Model C-26	180
Figure 5- 105 Model C-27	180
Figure 5- 106 Model C-28	181
Figure 5- 107 Model C-29	181
Figure 5- 108 Model C-30	181

List of Tables

Table 2- 1 Abstract of the method of expanding soil of soft clay p - y curvatures [31]	42
Table 2- 2 Abstract of the method of expanding soil of stiff clay by water-free p - y curvatures (from[39]).....	43
Table 2- 3 Abstract of the method of expanding soil of stiff clay water-free p - y curvatures (from[39] and [40]).....	44
Table 2- 4 Abstract of the method of expanding sandy soil p - y curvatures (from[30]).....	45
Table 2- 5 Abstract of the method of expanding soft clay soil p - y curvatures (from [51]).....	46
Table 2- 6 Abstract of method of expanding sand Cemented soil p - y Curvatures (from [44])	47
Table 2- 7 Statistics of ANN output and input for pile in mixed soils and sand soils (from [55])	53
Table 3- 1 w amounts for using in equation 3-1 (Source: [167]).....	72
Table 3- 2 The Empirical factors for LCPC procedure (Source: [168])	74
Table 3- 3 Axle correlation factor C_s (Source: [5]).....	80
Table 3- 4 Instantaneous of information applied for mounting FEM for bored piles (Source: [38]).....	97
Table 3- 5 Instantaneous of information applied for mounting FEM for concrete driven piles (Source: [38]).....	99
Table 3- 6 Instantaneous of information applied for mounting FEM for steel driven piles (Source: [38])	101
Table 3- 7 Young's modulus (MPa) values concerning different soil types and degrees of consolidation (Source [3])	112
Table 3- 8 Typical amounts of friction angle of soil for different soils agreeing to USCS (Source [223])	112

Nomenclature

A	Pile cross sectional area
A	Average cone point resistance within tip influence zone
a, b, c, d, e, f, g, h	Compound parameters
A_b	Area of shaft base
ANN	Artificial Neural Network
B	Shaft coefficient
BEM	Boundary Element Method
C	Cohesion
C	Dimensionless coefficient
c_0, c_1, c_2	Constants
Co.	Concrete piles
CPT	Cone Penetration Test
C_s	Shaft correlation coefficient
C_t	Tip correlation coefficient
D	Pile diameter
D_r	Relative density
E	Pile elastic modulus
E_B	Deformation secant modulus
E_0	Soil modulus under the tip
E_c	Young modulus for pile under compression
E_i	Soil modulus around element i
E_p	Pile material modulus
FEM	Finite element method
f_s	Side friction
\bar{f}_s	Average sleeve friction along shaft
G	Shear modulus of soil
GEP	Gene expression programming
GP	Genetic programming
H	Head size

J	Damping constant
K	Dimensionless coefficient, coefficient of lateral earth pressure
K_c	End bearing coefficient
K_0	Coefficient of earth pressure
K_s	Friction coefficient
K_s	Horizontal stress coefficient
L	Embedded length
L_0	Friction free zone
L_f	Friction load transfer length
M_s	Flexibility factor
N	Number of layers
N	Number of values
N_c	Capacity factor
N_k	Cone factor
N_q	Capacity factor
OCR	Over consolidation ratio
P	Applied load
P_m	Measured load
P_{pr}	Predicted load
PR	Penetration ratio
P_s	Applied load to pile carried by friction
P_t	Load applied at pile tip
Q	Mobilized end bearing capacity
Q	Total applied load
Q_c	Measured cone tip resistance
q_c (mechanical)	Readings of tip resistance of mechanical cone
q_c (electric)	Suggested electrical cone tip resistance reading corresponding the mechanical cone readings
q_c (tip)	Averages of cone point resistance over tip influence zone
q_{c1}, q_{c2}	Averages of cone point resistance
q_{c1}, q_{c2}, q_{cn}	Measured cone tip resistance
q_{c-eq}	Equivalent average cone resistance

q_{c-geo}	Geometric average of cone tip resistance values
q_{c-weld}	Weighted average of cone tip resistance values
q_e	Effective cone resistance
q_{Eg}	Geometric cone tip resistance over tip influence zone
Q_m	Measured pile capacity
Q_p	Total end bearing capacity
Q_p	Predicted pile capacity
q_t	Total measured cone resistance
Q_u	Ultimate pile capacity
R	Instantaneous soil resistance
R	Point coefficient
R	Coefficient of correlation
r_c	Pile radius
R_s	Static soil resistance
R_s	Total shaft resistance
R_s	Applied load to pile carried by friction
R_s	Ultimate shaft friction
$r_s (max)$	Maximum unit shaft resistance
r_s, r_{si}	Unit shaft resistance
R_{su}	Ultimate shaft friction
r_t	Unit end bearing
R_t	Total tip resistance
R_t	Load applied at pile base
S	Weighted sum
SA	Surface area
SD	Standard deviation
$St.$	Steel piles
S_u	Undrained shear strength
$S_u (shaft)$	Undrained shear resistance
u_2	Pore water pressure
V	Instantaneous velocity
VE	Variation element
w	Weight vector
X	Value of variable

x_{max}	Maximum value of variable
x_{min}	Minimum value of variable
x_n	Scaled value of variable
y_k	Predicted output
Z	Local pile deflection
ϕ	Internal friction angle
$\Delta\epsilon_i$	Settlement increment
A	Adhesion factor
β	Skin friction factor, shaft coefficient
ϵ_i	Measured settlement over pile diameter
λ	Shape coefficient
μ	Mean
μ_{ln}	Logarithmic mean
SD	Standard deviation
σ_0	Stress at soil pile tip interface
σ_i	Normal stress at the top of element i
σ_{i-1}	Normal stress at the bottom of element i
σ_{ln}	Logarithmic standard deviation
δ	Soil shaft friction angle
τ	Damping constant
γ	Soil unit weight
α	Adhesion factor

1 INTRODUCTION

1.1 BACKGROUND

Settlement and the bearing capability are noticed to be the prime features that control the scheme of piles (deep foundations). As a result, they have been the issue of concern for numerous engineering researchers all the way through the times past of the geomechanical engineering major. Therefore, various empirical and theoretical procedures have been suggested to govern the settlement and bearing capacity of deep foundations. The utmost trustworthy technique for defining the loading-settlement conduct and the pile capability is from outcomes of pile in-situ loading experiments. On the other hand, such experiments are costly, time-inefficient and need the accessibility of skilled human resources to administer them ([1]). Consequently, the capacity of piles and loading-settlement conduct are very regularly predicted and utilised for designing.

Generally, the capacity of piles is predicted relied on static analysis utilising in-situ experiments or soil properties and dynamic analysis relied on pile-driving dynamics, even though the settlement is measured relied on the numerical analysis or loading-transmission theory of elasticity ([2]). The complication of pile conduct underneath vertical loadings and the nonexistence of a specific explanation of soil-pile interaction, conversely, have produced faults in the prediction approaches and restricted their attainment in accomplishing a correct approximation of settlement and capacity of the pile. The static procedures that use the bearing capacity theory to determine the pile tip and shaft resistance include failings resulting from significant improbability concluded the factors that affect the bearing capacity. For instance, the proportion of vertical to effective horizontal stresses, K_s , is continuously varying through the period of setting up and as a result, numerous selections for K_s assumed

in the research have been proposed by diverse authors. Even though K_s values will to prepare sensible responses for more or less designers, they have the temper of giving unpredictable outcomes for others ([3]).

The dynamic approaches which are used to driven piles suffer from a number of obstacles. Initially, the dynamic analysis includes significant uncertainties due to erroneous approximations of energy dissipations ([1]). Also, the procedures tend to balance driving resistance and the loading bearing capacity which obviously, is almost not logical and would doubt ([4]). They also are governed by input presumptions which may noticeably bias the outcomes ([5]); the parameters, for instance, the effectiveness of energy transmission and the soil-pile quake, are presumed, and hence can not reflect the extraordinary mutability of the field circumstances. Furthermore, the theoretical analyses of the balanced pile formula relate the energy transmission mechanism to the Newtonian analyses of ram pile effect. This formulation is invalid theoretically for demonstrating the elastic wave proliferation mechanism, which in reality happens ([6]).

In recent times, the CPT-based techniques, mainly, those that use a direct relationship of CPT records with pile capacity, have developed favourably and widely utilised. This is due to the conductivity of soils in the CPT experiments, like cohesionless soils, from which uninterrupted models are incentive to attain. Furthermore, the CPT records may be correlated with properties of soil or straightly factored and utilised to predict bearing capacity of the pile without the necessity to supply intermediate factors like horizontal stress coefficient, K_s , and bearing capacity factor, N_q , ([5]). On the other hand, relative studies of the existing CPT based techniques performed by many researchers (i.e. [7], [8], [9] and [10]) have given away that the capacity predictions may be precise diverse for the same instance depending on the technique used. It is also set up that these approaches may not afford accurate and consistent pile capacity prediction.

The techniques that have been suggested to predict loading-settlement conduct of pile involve numerous restrictions. The load-transfer approaches pay no consideration to the continuousness of the mass of soil; consequently, they are not appropriate for analysing loading-settlement features of a group of piles. They also incline to extrapolate experiment records from one field to another, which is not constantly effective ([2]). The procedures that use the elasticity theory deliver estimated resolutions to the pile settlement which is installed in non-homogeneous

soils and can contain a substantial quantity of errors, if unexpected substantial variations in the module of soil occur alongside the pile length. The techniques also recommend an imprecise process to account for the soil-pile slip, henceforth can not get exact outcomes. Subsequently, the consistency and accurateness of suggested approaches for predicting the capacity of pile and loading-settlement are not definite, and the engineer may depend on his/her understanding to create a selection amongst these procedures utilising an extraordinary factor of safety for accounting for the improbability. Bearing in mind the insufficiencies in the beyond techniques, a better substitute for designing the pile and calculating the respective axial and lateral capacity and the loading-settlement conduct of piles is inevitable, and that can be the most recent technique, Finite Element Method (FEM).

In recent times, with the prompt growth of computational machinery, numerical analysis methods including finite element method (FEM) are extensively utilised to recognise the bearing capacity conduct of piles, particularly for piles underneath complex load situations ([11] and [12]). The superiority of the numerical analysis method relies on the interaction amongst pile and soil and its capability to state compound soil layers. In this study, some features on the numerical analysis of vertical load piles in homogeneous sand and mixed soils using software package ABAQUS is examined in details. Firstly the constitutive sample for neighbouring soil and the contact conduct of pile-soil boundary will be discussed; then founded on the recognised numerical sample, the approaches for recognising loaded stress state were examined; lastly, the presumed shaft persistence in terms of vertical forces and self-weight was compared with the CPT experiments outcomes.

1.2 PROBLEM STATEMENT

An experimental and numerical investigation to study the pile and soil behaviour under different loading conditions is needed due to several aspects. The contribution of the current research and its significances are resumed as below:

1. The study highpoints some of the deficiencies that are present in the commonly utilised approaches for predicting capacity and loading-settlement correlation of piles (deep foundations) and attempts to acquire the perfect model. This aim will advance the trustworthiness of the designing and the safety of the construction.

2. The study is parsimoniously essential, as utilising exact model involves a low factor of safety. Accordingly, the wasted capability will be minimised, directing to time and cost lessening.
3. Piles have numerous applications and any disaster in the foundation load transforming system will have several negative impacts in any economy and society.
4. This study is essential to recognise the factors affecting pile behaviour by implementing the numerical parametric study and validating it with experimental results.
5. The numerical model can be established to simulate the related aspects of the problem in order to obtain a better understanding of the model behaviour with respective visualisations.

1.3 OBJECTIVES OF THESIS

In the past few years, many types of research have been accomplished to investigate the conduct of piles subjected to diverse circumstances. On the other hand, a few works related to comparison the pile-soil behaviour in CPT results and finite element method outcomes, using ABAQUS package, are available. Thus, the leading goal of this study is to compare the experimental performance of a pile subjected to different loadings and soil profiles and numerical model of the particular case. Beforehand that, several numerical parametric works on different piles and soils are carried out by using finite element package, ABAQUS. In the next phase, a brief measurement to validate the numerical results versus experimental investigations will be performed. Therefore, 108 different CPT results have been involved in this research to evaluate the finite element analyses. This equate is the original and unique contributions of this research. Besides, degrees of error for numerical methods have been demonstrated. In the end, the conclusion and suggestions for future studies have been released. All and all, the main aim of this study is to determine the feasibility of using finite element technique for modelling the axial loading of piles and settlement capacity of soils and piles embedded in sand and mixed soils. The primary objectives of the offered research can be summarised as below:

- I. Developing a model for accurate prediction of the pile load-settlement curve using finite element method.
- II. Validation of the developed FEM model using cone penetration test results, which are reported in the available literature.
- III. Conducting a parametric study to assess the sensitivity of the developed FEM model.
- IV. Back-calculation of load-settlement curve for a large number of existing case studies in different soil profiles with different pile types using the developed FEM model.
- V. Comparing the developed FEM model with other modelling approaches to evaluate the effectiveness of the proposed model.

1.4 STRUCTURE OF THESIS

To launch the research objectives, this thesis is distributed into five chapters, and the contents of Chapters 1 to 5 are concisely outlined below:

Chapter one presents the studied problem and describes the scope and objectives of the research. A brief explanation of what will be enclosed in each chapter is incorporated.

Chapter two defines the basic concepts of finite element method. Firstly, two principal techniques including p - y curves method and artificial neural networks (ANNs), are described concisely. The main components of each procedure are clarified. Besides, the necessary steps for the development of the aforementioned models are discussed, and some of the present shortcomings in two methods are itemised. The review branches out into both numerical and experimental approaches to provide a scientific basis for further investigations. FEM numerical models published in the literature are the source of the material parameters to be implemented in the FE model, and the results of these experiments are employed for the purpose of verification.

Chapter three describes the methodology and specifications of experimental CPT setup and numerical modelling of piles under several loadings and soil types.

Chapters three to five focus on the investigation of comparing the outcomes of field CPT and numerical method in ABAQUS. In addition, the properties of the described models' materials and specifications have been presented. Moreover, data collection for the respective simulation has been defined.

Chapter four presents the results and discussion of the numerical analysis of pile samples. Firstly, three different piles in different soil profiles will be chosen, and numerical analysis for each of them will be expanded. Moreover, the sensitivity of each model to Young's modulus will be carried out. Results of FEM in ABAQUS will be presented with diagrams and visual presentations. Furthermore, validation of all 108 experimental and numerical models will be shown in displacement-force diagrams.

Chapter five summarises the main achievements of this work and presents the conclusions and some recommendations for further research and development.

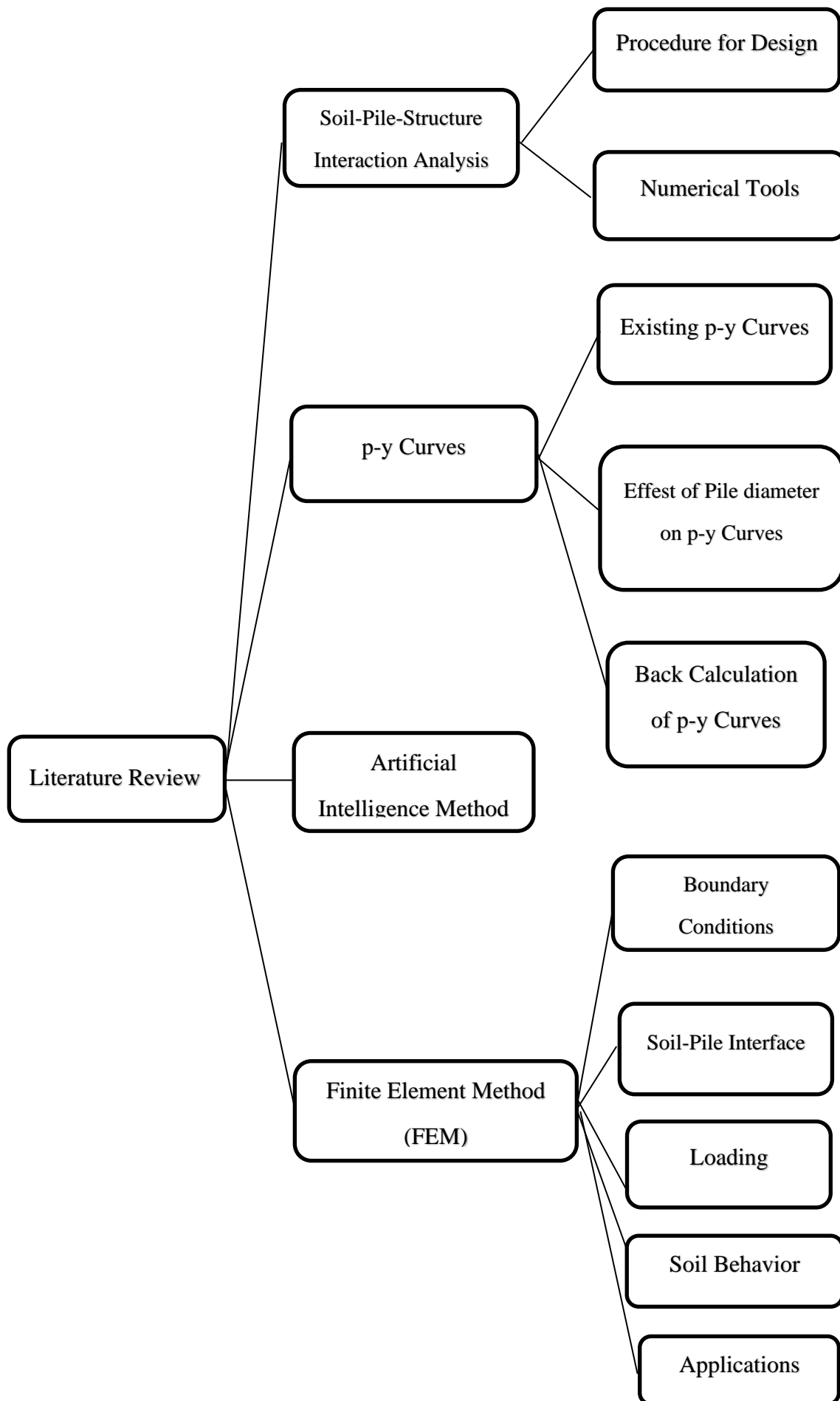
2 LITERATURE REVIEW

2.1 INTRODUCTION AND CHAPTER OVERVIEW

The primary purpose and function of structural foundations are to transfer the loads and forces applied to the super and upper structure to the adequate and capable layers of soils. In the case of lateral horizontal and cyclic loads in nature or by human-made machines, such as seismic earthquake loads or wind farms or traffic, and if the upper soil layers are weak to transmit the loads to lower layers, such as tall buildings on sand soils or subjected to critical conditions such as liquefaction, some special considerations must be taken in the design and analysis of elements of foundations. The reactance and reflexes of a structure under lateral, horizontal, harmonic or seismic loads are dependent on the sort and form of external loading, specification of the structure and importance of it, surrounding soil mechanic characteristics and interactions between superstructure, foundation and the soil. This problem called the soil–pile-structure interaction (SPSI), is the focus of this research.

Moreover, the settlement and bearing capacity of a foundation are considered significant factors that determine the plan of a foundation. Therefore, they are of interest to many researchers during the Geomechanics Science lifetime, and many theoretical empirical procedures have been performed to assume the settlement and bearing capability of one foundation [13].

In this chapter, a brief literature review is first conducted for SPSI problems, and then a study of static p-y curves is presented to estimate the pile capacity. Afterwards, we introduce an artificial intelligence (ANN) method and finite element method (FEM) and compare the results [14].



2.2 SOIL-PILE-STRUCTURE INTERACTION

ANALYSES

The results of SPSI could not achieve a common compromise and cooperation between civil engineering scientists on the entire efficiency of a structure, mainly in soft soils. Some researchers (e.g.[15]) proposed that SPSI efficiency can enhance structural requirements, while others believe that relinquishing SPSI would be a conservative approximation. The SPSI and input earth movement are the primary sources of a structure's response. A geotechnical engineer with cooperation with an earthquake engineer meets many challenges in designing foundations to overcome seismic forces because of complication issues and other loading cases. To maintain these problems, the engineering team needs to be proficient in soil geotech-mechanics, SPSI, foundation engineering and literacy science in structural dynamics. Currently, because of accessibility to FEM packages and nonlinear soil models, designing teams have concentrated on the nonlinear movement of soils and approximating the cyclic deficiency of foundations to yield correct and accurate SPSI forces [16].

Construction codes have traditionally calculated for SPSI just in an exceptionally clarified way (e.g.[17]). However, in the Eurocode series [18], some recommended techniques for designing foundations in harmonic and lateral loading have been included. In this literature review, the SPSI design method has been used to solve problems with numerical tools..

2.2.1 Method of Design Base on SPSI Analysis

The main problem of SPSI's features. There are two ways to accomplish SPSI analyses: one of them is considering appropriate interface behaviours and modelling the soil and structure together, and alternatively utilising primary of superposition. The second approximation has two stages which address two separate mechanisms, inertial interactions and kinematic interactions. Both ideas are based on the supposition that

the whole system remains linear. For the linear pile, soil and structure, the superposition remains valid ([19], [20]).

However, because of pile curvature as a result of horizontal loading transferred from the upper structure, superposition is valid for nonlinear systems with approximations that disappear quickly with depth. In a real situation, pile curvatures are less than 10 times the pile diameters under the ground level.

- **Interaction with Kinematic Interface**

If we ignore superstructure, the movement of the foundation is different from free ground movement. The term “free ground” refers to the movement of ground land, which is sufficiently separated from foundations so foundations do not have any effect on free ground. The reason for this difference is the kinematic interaction mechanism. These differences are observed because of wave inclination, stiff foundations or foundation supersedence. The method of describing kinematic effects includes using frequency interdependent transmission subordinates. The transmission subordinate is determined based on the ratio of foundation movement to free ground movement in the deficiency of one substructure. The transmission of the wave thru foundations increases an element’s foundation stress. These forces generate kinematic stress.

- **Interaction with Inertial Interface**

Movement at the foundation because of kinematic interface interactions makes the whole structure susceptible to stumbling. This action mentions which complete structure would generate internal power or reverse some kind of moments on the base level. Foundation or its circumambient land would gain extra kinetic control and displacement because of the aforementioned action. The main reason for these changes is its inertial interaction. The settlement related to the interaction between pile and earth and the inflexion of the foundation is described with a periodicity pile and impedance function (implement full impedance). Implement impedance is emulated with factors of dashpot and spring which affect the subgrade of the structure and its pile position.

The two aforementioned procedures occur during a concise time delay.

2.2.2 Numerical Tools

In the past, there were various methods used to solve SPSI problems [21]. Some of these models have been expanded and include boundary element procedures, numerical methods such as FEM, boundary element procedures, semi-analytical and semi-empirical and analytical resolutions. The first person who was successful to utilise a Winkler foundation beam method in the analysis of dynamic was [22]. The boundary element procedure was expanded ([23], [24, 25], [25], [26], [27], [28] and [29]). Boundary element method cannot combine the conduct of nonlinear soil or pile-soil jointing. However, several phenomenon wave fields such as bending body waves can be competent solutions. In the last part of this literature review, using the FEM model to solve the SPSI model has been reviewed.

2.2.3 Mohr-Coloumb Theory

Mohr–Coulomb theory is a mathematical model describing the response of brittle materials such as concrete, or rubble piles, to shear stress as well as normal stress. Most of the classical engineering materials somehow follow this rule in at least a portion of their shear failure envelope. Generally the theory applies to materials for which the compressive strength far exceeds the tensile strength.

In geotechnical engineering it is used to define shear strength of soils and rocks at different effective stresses. In structural engineering it is used to determine failure load as well as the angle of fracture of a displacement fracture in concrete and similar materials. Coulomb's friction hypothesis is used to determine the combination of shear and normal stress that will cause a fracture of the material. Mohr's circle is used to determine which principal stresses will produce this combination of shear and normal stress, and the angle of the plane in which this will occur. According to the principle of normality the stress introduced at failure will be perpendicular to the line describing the fracture condition.

It can be shown that a material failing according to Coulomb's friction hypothesis will show the displacement introduced at failure forming an angle to the

line of fracture equal to the angle of friction. This makes the strength of the material determinable by comparing the external mechanical work introduced by the displacement and the external load with the internal mechanical work introduced by the strain and stress at the line of failure. By conservation of energy the sum of these must be zero and this will make it possible to calculate the failure load of the construction. A common improvement of this model is to combine Coulomb's friction hypothesis with Rankine's principal stress hypothesis to describe a separation fracture.

The Mohr–Coulomb[5] failure criterion represents the linear envelope that is obtained from a plot of the shear strength of a material versus the applied normal stress. This relation is expressed as:

$$\tau = \sigma \tan(\phi) + c \quad 2.1$$

Where τ is the shear strength, σ is the normal stress, c is the intercept of the failure envelope with the τ axis, and $\tan(\phi)$ is the slope of the failure envelope. The quantity c is often called the cohesion and the angle ϕ is called the angle of internal friction. Compression is assumed to be positive in the following discussion. If compression is assumed to be negative then σ should be replaced with $-\sigma$.

If $\phi = 0$, the Mohr–Coulomb criterion reduces to the Tresca criterion. On the other hand, if $\phi = 90^\circ$ the Mohr–Coulomb model is equivalent to the Rankine model. Higher values of ϕ are not allowed. From Mohr's circle we have:

$$\sigma = \sigma_m - \tau_m \sin \phi ; \tau = \tau_m \cos \phi \quad 2.2$$

Where

$$\tau_m = \frac{\sigma_1 - \sigma_3}{2} ; \sigma_m = \frac{\sigma_1 + \sigma_3}{2} \quad 2.3$$

And σ_1 is the maximum principal stress and σ_3 is the minimum principal stress.

Therefore, the Mohr-Coulomb criterion may also be expressed as:

$$\tau_m = \sigma_m \sin \phi + c \cos \phi \quad 2.4$$

This form of Mohr-Coulomb criterion is applicable to failure on a plane that is parallel to the σ_2 direction.

2.2.4 Drucker-Prager yield criterion

The Drucker–Prager yield criterion is a pressure-dependent model for determining whether a material has failed or undergone plastic yielding. The criterion was introduced to deal with the plastic deformation of soils. It and its many variants have

been applied to rock, concrete, polymers, foams, and other pressure-dependent materials.

The Drucker–Prager yield criterion has the form:

$$\sqrt{J_2} = A + B I_1 \quad 2.5$$

Where I_1 is the first invariant of the Cauchy stress and J_2 is the second invariant of the deviatoric part of the Cauchy stress. The constants $A; B$ are determined from experiments. In terms of the equivalent stress (or von Mises stress) and the hydrostatic (or mean) stress, the Drucker–Prager criterion can be expressed as:

$$\sigma_e = a + b \sigma_m \quad 2.6$$

Where σ_e is the equivalent stress, σ_m is the hydrostatic stress, and $a; b$ are material constants. The Drucker–Prager yield criterion expressed in Haigh–Westergaard coordinates is:

$$\frac{1}{\sqrt{2}} \rho - \sqrt{3} B \xi = A \quad 2.7$$

The Drucker-Prager yield surface is a smooth version of Mohr-Coulomb yield surface.

The Drucker–Prager model can be written in terms of the principal stresses as:

$$\sqrt{\frac{1}{6} [(\sigma_1 - \sigma_2)^2 + (\sigma_2 - \sigma_3)^2 + ((\sigma_3 - \sigma_1)^2)]} = A + B(\sigma_1 + \sigma_2 + \sigma_3) \quad 2.8$$

If σ_t is the yield stress in uniaxial tension, the Drucker-Prager criterion implies:

$$\frac{1}{\sqrt{3}} \sigma_t = A + B \sigma_t \quad 2.9$$

If σ_c is the yield stress in uniaxial compression, the Drucker-Prager criterion implies:

$$\frac{1}{\sqrt{3}} \sigma_c = A - B \sigma_c \quad 2.10$$

Solving these two equations gives:

$$A = \frac{2}{\sqrt{3}} \left(\frac{\sigma_c \sigma_t}{\sigma_c + \sigma_t} \right); B = \frac{1}{\sqrt{3}} \left(\frac{\sigma_t - \sigma_c}{\sigma_c + \sigma_t} \right) \quad 2.11$$

Different uniaxial yield stresses in tension and in compression are predicted by the Drucker–Prager model. The uniaxial asymmetry ratio for the Drucker–Prager model is:

$$\beta = \frac{\sigma_c}{\sigma_t} = \frac{1 - \sqrt{3} B}{1 + \sqrt{3} B} \quad 2.12$$

Since the Drucker–Prager yield surface is a smooth version of the Mohr–Coulomb yield surface, it is often expressed in terms of the cohesion (c) and the angle of internal friction (ϕ) that are used to describe the Mohr–Coulomb yield surface. If

we assume that the Drucker–Prager yield surface circumscribes the Mohr–Coulomb yield surface then the expressions for A and B are:

$$A = \frac{6 c \cos \phi}{\sqrt{3}(3-\sin \phi)} ; B = \frac{2 \sin \phi}{\sqrt{3}(3-\sin \phi)} \quad 2.13$$

If Drucker-Prager yield surface middle circumscribes the Mohr-Coulomb yield surface then:

$$A = \frac{6 c \cos \phi}{\sqrt{3}(3+\sin \phi)} ; B = \frac{2 \sin \phi}{\sqrt{3}(3+\sin \phi)} \quad 2.14$$

If the Drucker–Prager yield surface inscribes the Mohr–Coulomb yield surface then:

$$A = \frac{3 c \cos \phi}{(9+3 \sin \phi)} ; B = \frac{\sin \phi}{(9+3 \sin \phi)} \quad 2.15$$

2.3 p - y CURVES

Engineers designing structures mostly prefer to use the beam Winkler foundation (BDWF) method instead of FEM or elastic progression solutions. Traditionally, p - y semi-empirical curves are used in BDWF such as those expanded ([30] and [31]). These curves showed the treatment of nonlinear soil with a chain of nonlinear sprigs, p represents the pressure of soil per unit longitude of pile and y represents the deflection. Some other researchers have expanded the p - y procedure to conflict with forces which are dynamic [32] and [33].

Almost all recent p - y curvatures which are standard has been expanded based on the idea of the tiny span of the diameter of pile related to full-scale horizontal load tests. However, Juirnarongrit discovered the effect of the diameter of the pile on compact weak cemented sand on p - y curves on movement levels under the ultimate resistance of the soil [34]. This kind of p - y curvatures has been used by some basic commercial software programmes such as FILPIER ([17]), LPILE ([35]) and COM624P ([36]). Applying these program packages can calculate the moment and deflection along with the pile because of the proposed load. This literature review reviews the calculated p - y curvatures for the lateral forces in the deep foundations and procedures in order to detect the p - y curvatures using the numeric method. Available p - y curves or sand and clay soils are presented, and then the consequence of diameter

on p - y curves is presented following an analysis of p - y curves which are an outcome from the numerical analysis.

2.3.1 Existing p - y Curves

Figure 2.3 shows the p - y curves, which they are obtained using graphical tools. It is assumed that the pile is perfectly straight prior to loading (i.e. we do not have any bending within pile driving). Before loading, the force of soil which is applied to the deep foundation is similar to the pile's radius (presented in Figure 2-1), determining that the lateral stress applied to the deep foundation is almost equal to zero. While increasing the pressure of the soil around the deep foundation, the load per unit of the deep foundation's length was obtained. This procedure may be extended for many curvatures which create a chain of pressures per length of the pile in terms of length, generating the p - y curvature. By using the same method, we can generate a series of p - y curvatures based on the pile [37].

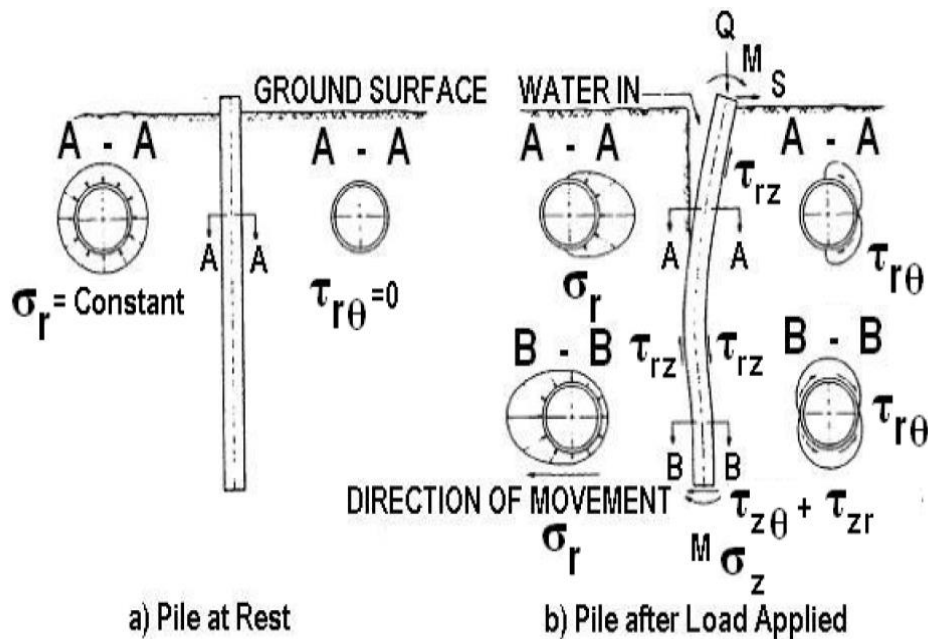


Figure 2- 1 Explanation for concept of p - y with a) foudation without loading b) foundation after loading (from[38])

2.3.1.1 p - y curvatures in soft clay soil type

A hip-and-tight straight force test was performed on a steel pipe pile with a diameter of 0.3 m inside soft clay at Lake Austin, Texas, USA ([31]). The specified shape of the clay p - y soft soil for the static loads was demonstrated by applying a parabolic equation in Figure 2.6 (a)

$$\frac{p}{p_u} = 0.5 \left(\frac{y}{y_{50}} \right)^{\frac{1}{3}} \quad 2-16$$

Which p_u is the maximum resistance of soil and demonstrates the shear stability of the soil and is a depth function, and y_{50} is the displacement of the soil at half the maximum soil stability.

Figure 2-5(b) shows the specification formation of soil with soft clay criteria p - y curvatures for the harmonic load. The noticeable differences among these two loadings show that tremendous tension decreased in cyclic loading. Table 2.1 shows the developing p - y curves methodology for harmonic and static loading.

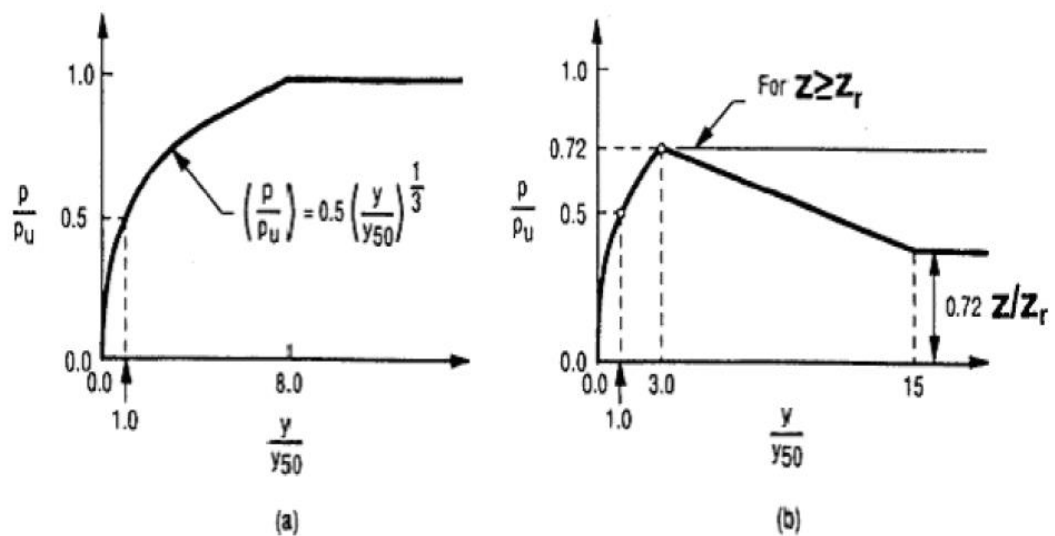
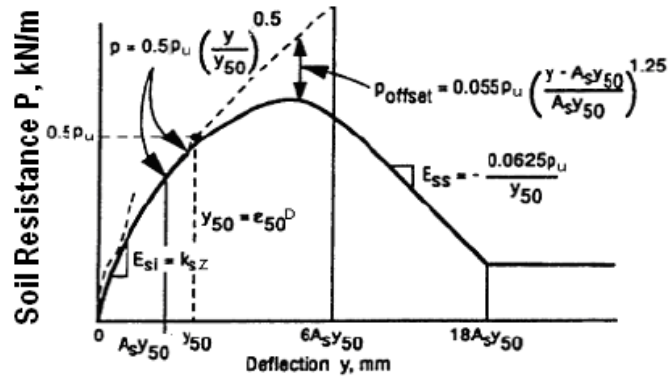


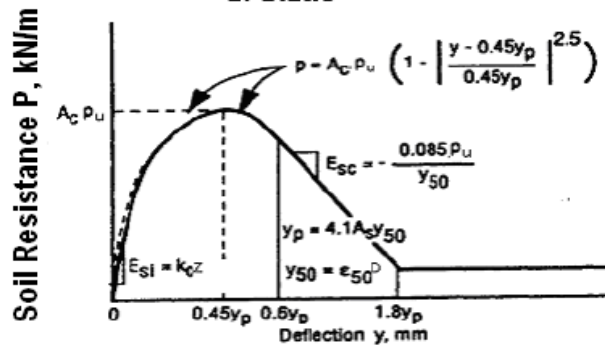
Figure 2- 2 Formation of the p - y curvature of soil with soft clay criteria with a) load in static shape b) load in cyclic shape (from [31])

2.3.1.2 *P*-*y* curvature for stiff clay soil under water table

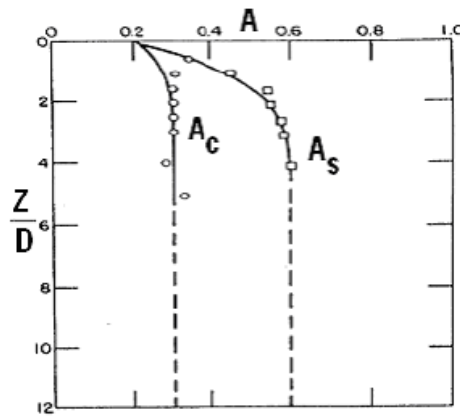
In Manor, Texas, USA, two pipe piles with each having a diameter of 0.6 m were embedded in stiff clay soil below the water level and examined ([37]). The characteristic form of *p*-*y* curves for the aforementioned static and harmonic loading is shown in Figure 2.6. The stabilities of both cases are lower than the maximum resistance at more significant tensions. The parameters utilised to qualify the specification form of soil with stiff clay criteria *p*-*y* curvature are the same as the previous case. Table 2-2 shows the methodology of expanding *p*-*y* curves for harmonic loading.



a) Static



b) Cyclic



c) Value of Constant A

Figure 2- 3 Specification formation of the p - y curvature in soil with stiff clay criteria under water level with a) static load b) cyclical load c) quantity of permanent A (from [39])

2.3.1.3 p - y curvetures for soils with stiff clay criteria over the water level

There were a series of tests for a horizontal load on a pile with a diameter of 0.76 m bored in stiff clay over the water level in Houston, Texas, USA ([40]). For describing the characteristic form of p - y curves, fourth polynomials were applied that are slightly similar but more rigid than the p - y curvature of soil with soft clay characteristics

(Matlock, 1970). If we apply cyclic loading, because the number of cycles of load application increases, the resistance of the soil decreases. Table 2-3 shows the method of developing p - y curves for this soil [41]. Figure 2-7 demonstrates the specification form of the p - y curvature in soil with stiff clay specification over the water level.

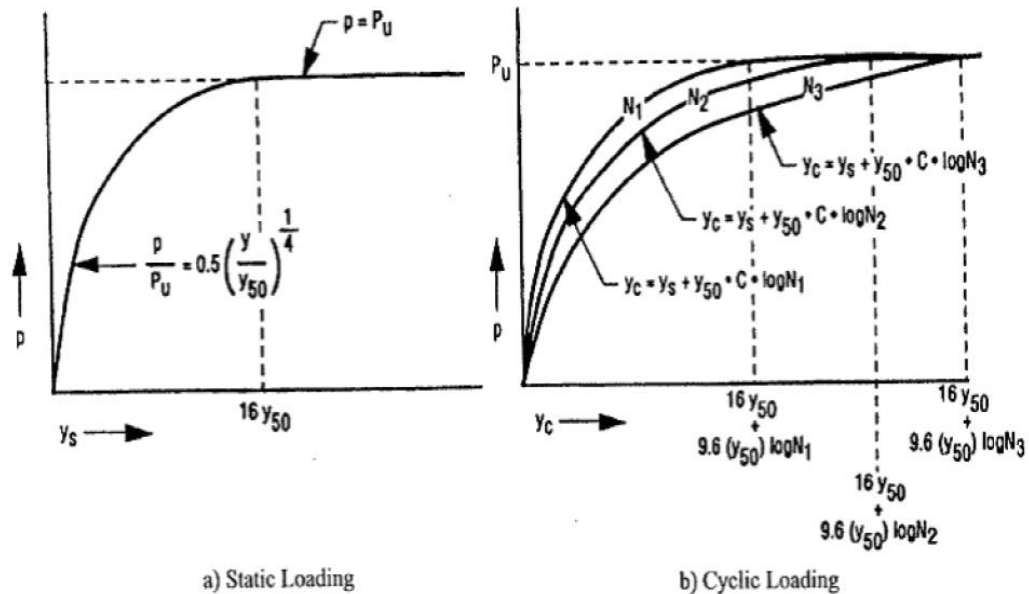


Figure 2- 4 Specification formation of the p - y curvature in soil with stiff clay characteristic over water level for a) static load b) cyclical load (from [40], [39])

2.3.1.4 p - y curvature for sandy soil

Two piles with each having a diameter of 0.6 m were embedded inside fine, de submerged, dense sand were tested by Reese et. al [30]. The result of the aforementioned experiment was used by Reese et. al to develop a system for acquiring p - y curves of sand [30].

The characteristic form of p - y curvature comprises three direct lanes and one parabolic curvature (Figure 2-9) [42]. This procedure uses the primary modulus of response from the subgrade and the final resistance of earth to expand the p - y curves. Competent worthiness of prime modulus of the reaction of subgrade for various relative sand density suggested by [30].

To obtain the ultimate resistance of a soil type on the ground level, wedge-type fracture theory ([30]) was utilised, and to obtain the largest opposing force from the soil with any spacing under the soil level, and flow fracture format was exerted. If we consider the aforementioned method, then the final strength of the soil was less than the outcomes acquired from experimental methods. Accordingly, [30] improved the stability of soil with proposing empirical modifications named A and B, shown in Figure 2-10, to cause the aforementioned lower value. Table 2-4 shows summaries of the procedure to expand the sand p - y curves.

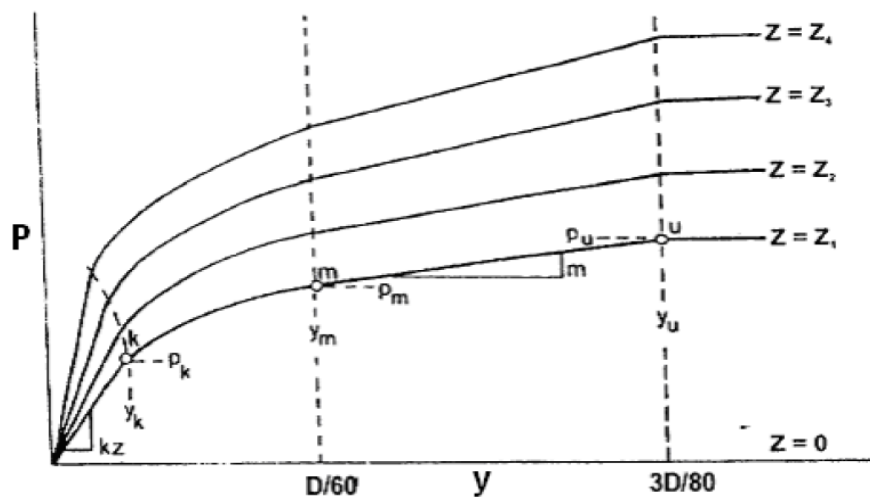
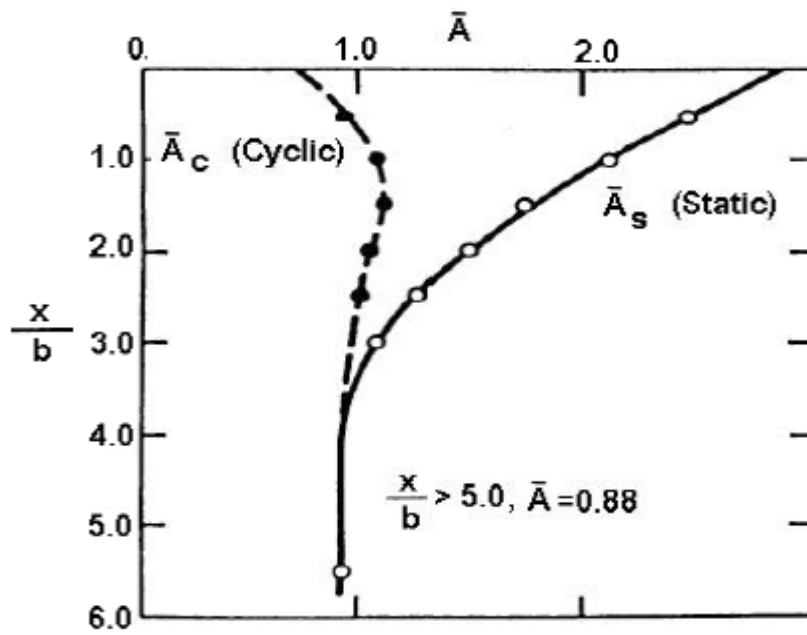
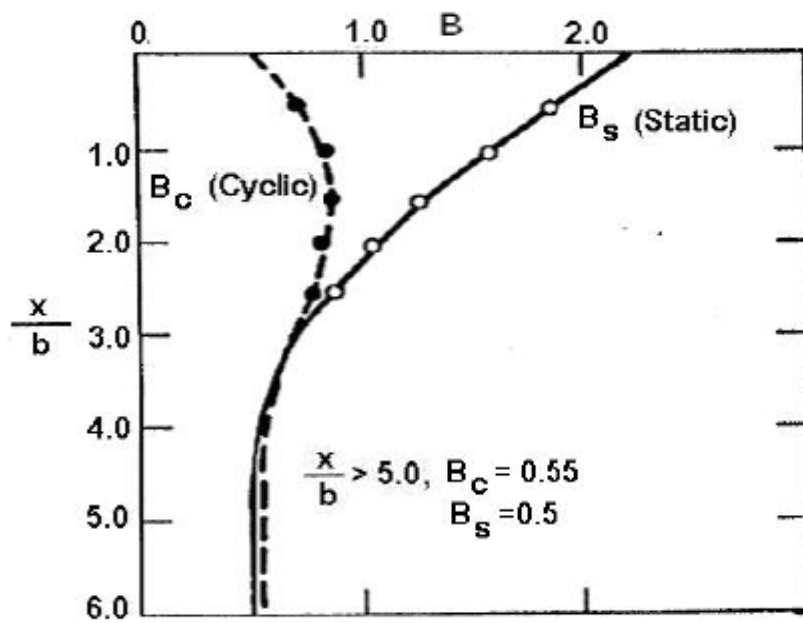


Figure 2- 5 Specification formation for p - y curvatures in sandy soils (from [30])



a) Coefficient A



b) Coefficient A

Figure 2- 6 Amount of factor A applied to expand p - y curvatures in sandy soil a) Factor A b) Factor B (from [30])

2.3.1.5 Sandy p - y Curvatures and API

One procedure presented with Reese, L.C., W.R. Cox, and F.D. Koop is entirely tiresome in usual utilisation [30]. A simplified technique by O'Neill suggested the American Petroleum Institute (API) accept method [43]. In that method, the specific p - y curvatures are explained by applying one hyperbolic tangent coefficient. The equalization applied for determining the final resistance of the soil had been separated into three tiny sections and streamlined with the presentation of three factors C_1 , C_2 and C_3 as factors of the friction angle. These coefficients are easily obtained from examining Figure 2.11(a). Similarly, the first modules of the undergrad reaction can be obtained from examining Figure 2.11(b). The experimental coefficient A for static loading trials was presented by a simplified linear equation. Table 2.1 summarises the method to expand p - y curvatures for the mentioned type of soil.

2.3.1.6 p - y curves for soils with c - Φ

By applying the usual simplified Mohr-Coulomb of a linear fracture envelope of the shear pressure vs. conventional pressure plane, soils can be ordered as cohesionless or cohesive. Based on the aforementioned assortment, theories were expanded to analyse geomechanical problems such as the interaction between soil and pile, which is our research subject. This concept can persuade to engage in substantial conservative designing for silt or cemented soil because the resistance the soil from the cohesion component is neglected.

Ismael, N.F. performed a full-scale vertical loading pile test subjected to static load in Kuwait [44]. Experiments were conducted using a reinforced bored pile filled with concrete with a diameter of 0.3 m, and the lengths of the piles were between 3 m and 5 m. The bending moment was evaluated for two piles by performing electrical resistance tension gauges. By applying a drained triaxial test, the friction angle and cohesion were determined as 35° and 20 KPa, respectively. The results show that assessed p - y curves for sand p - y curves expanded by Reese, L.C. were considerably underestimated with the experimental outcomes because of the presence of the cohesion ingredients [30]. A totally different method was then established to address

the pastiness parts. Figure 2.13 demonstrates the theoretical p - y parabolic curves for c - Φ soils type. Table 2.6 shows the technique used to expand p - y curves for soil with c - Φ type.

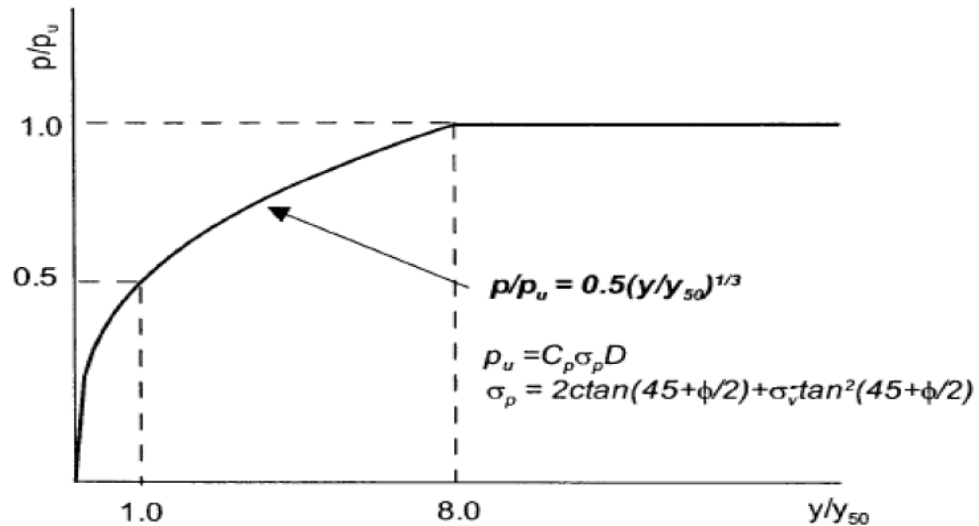


Figure 2- 7 Characteristic formation of p - y curves in sandy soil (from [30])

2.3.2 Effects of pile dimension on p - y curves

The literature review established in the previous section shows that for each soil type, there is a unique characteristic p - y curvature shape [45]. In contrast, almost all presented p - y curvatures were extended by relying on large-scale deep foundation exams on one restricted type of pile dimensions because of high-cost consumption for full-scale tests. Therefore, the validity of reaction when a large diameter (or micro-piles with small diameters) is used can still be discussed. The literature review in this section concentrated on the effects of the deep foundation's diameter on the p - y curvature in horizontally forced piles.

Reese, L.C. and Desai, C. used the information from tests on a 0.65-m pile in Manor, Texas, to backward compute the curves ([39] and [46]). These curvatures were operated to study the behaviour of a pile with a diameter of 0.15 m. The measured moment of bending was similar to the predicted one. However, the calculated deflection was less than the evaluated type. The conclusion of this regard was not demonstrated [47].

Dunnivant, T.W. and O'Neill, M.W. performed horizontally loaded deep foundation examination on piles with diameters of 1.83 m, 1.0 m, 0.22 m and 0.27 m

which were embedded in over-consolidated clay ([48] and [49]). They detected that the deviation at one half the final pressure of soil (y_{50}) was not linearly related to the pile diameter. Thus, y_{50} decreases whenever the deep foundation's radius rises. Therefore, the deep foundation third dimension (diameter) result was not completely interconnected in clay soil type p - y curvatures.

Stevens, J. and J. Audibert gathered publicised instance records at vertically loaded deep foundations inside clay soils [50]. Both of them exerted the available p - y curvatures suggested by API and Matlock, H. to respond to the deep foundation [51] and [31]. They determined that the ratio calculated to gauge deviation was larger than one and increased the deep foundation diameter. As a result, the calculated ultimate moments caused by bending are greater than the determined amount, and as much as 30 per cent in the first scenario. To push and argument among both of them, they proposed that y_{50} must be adequate to the square root of a radius multiplied by two of the piles. In addition, this case demonstrates that available p - y curvature for soil with soft clay characteristics does not correspond to the consequences of the pile radius [52].

2.3.3 p - y Curves with back evaluation

Serdaroglu, M.S. Finite element analyses (FEA) is applied to numeric testing to compute p - y curvatures [53]. P - y curvatures may be back evaluated by utilising from finite element analysis or full-scale experiments by using two procedures. The first procedure uses the moment caused by bending forward ahead of the deep foundation. In this approximate scenario, an analytical phrase is coordinated to the separate moment values ahead of the pile. The equation is differentiated twice to obtain the opposition of soil p . The other procedure includes the integration of the shear pressure and normal pressure placed on a deep foundation with soil instantly encompassing it [54]. These two procedures may be applied to statically p - y curvatures. However, the first procedure is formidable by dynamic p - y curvatures because of the difficulty in fitting the analytical expression for every time increment.

Table 2- 1 Abstract of the method of expanding soil of soft clay p - y curvatures [31]

Static Loading

1. Compute ultimate soil resistance, P_u (using the smaller values)	$P_u = \left[3 + \frac{\gamma'}{C_u} z + \frac{J}{D} z \right] C_u D$ $P_u = 9 C_u D$
2. Compute at one-half the ultimate soil resistance, y_{50}	$y_{50} = 2.5 \varepsilon_{50} D$
3. Develop p - y curves using the following expression	$\frac{P}{P_{ult}} = 0.5 \left(\frac{y}{y_{50}} \right)^{1/3}$

Cyclic Loading

1. Develop p - y curves	Construct p - y curves in the same manner as for static loading for values of P less than $0.72P_u$
2. Determine transition depth Z_r	$Z_r = \frac{6 C_u D}{(\gamma' D + J C_u)}$
3. If the depth is greater than or equal Z_r	$P = 0.72 P_u$ for $y > 3 y_{50}$
4. If the depth is less than Z_r	$P = 0.72 P_{ult}$ at $y = 3 y_{50}$ and $P = 0.72 P_{ult} \left(\frac{z}{Z_r} \right)$ at $y = 15 y_{50}$

- Where: C_u = Undrained shear strength
 D = Pile diameter
 J = Constant (0.5 for soft clay and 0.25 for medium clay)
 P_u = Ultimate soil resistance
 Y_{50} = Deflection at one-half the ultimate soil resistance
 Z = Depth
 Z_r = Transition depth
 γ' = Effective soil unit weight
 ε_{50} = Strain at one-half ultimate soil resistance
 0.020 for soft clay, 0.010 for medium clay, and 0.005 for stiff clay

Table 2- 2 Abstract of the method of expanding soil of stiff clay by water-free p - y curvatures (from[39])

Static Loading

1. Compute ultimate soil resistance, P_u (using the smaller values)	$P_{ut} = 2C_a D + \gamma' D Z + 2.83 C_a Z$ (wedge failure) $P_{ud} = 11 C_u D$ (flow failure)
2. Establish initial straight line portion	$P = (k_s Z) y$ for static, $P = (k_c Z) y$ for cyclic
3. Develop p - y curves using the following expression	$P = 0.5 P_u \left(\frac{y}{y_{50}} \right)^{0.5}$, $y_{50} = \epsilon_{50} D$
4. Develop the second parabolic portion of the p - y curves (from $A_s y_{50}$ to $6 A_s y_{50}$)	$P = 0.5 P_u \left(\frac{y}{y_{50}} \right)^{0.5} - 0.055 P_u \left(\frac{y - A_s y_{50}}{A_s y_{50}} \right)^{1.25}$
5. Establish straight line portion (from $6 A_s y_{50}$ to $18 A_s y_{50}$)	$P = 0.5 P_u (6 A_s)^{0.5} - 0.411 P_u - \frac{0.0625}{y_{50}} P_u (y - 6 A_s y_{50})$
6. Establish final straight line portion (beyond $18 A_s y_{50}$)	$P = 0.5 P_u (6 A_s)^{0.5} - 0.411 P_u - 0.75 P_u A_s$

Cyclic Loading

1. Follow step 1 to 3 of static case	Follow step 1 to 3 of static case
2. Establish parabolic portion (up to $6 y_p$)	$P = A_c P_u \left[1 - \left(\frac{y - 0.45 y_p}{0.45 y_p} \right)^{2.5} \right]$, $y_p = 4.1 A_c y_{50}$
3. Establish straight line portion (from $6 y_p$ to $1.8 y_p$)	$P = 0.936 A_c P_u - \frac{0.085}{y_{50}} P_u (y - 0.6 y_p)$
4. Establish final straight line portion (beyond $1.8 y_p$)	$P = 0.936 A_c P_u - \frac{0.102}{y_{50}} P_u y_p$

Where: A_s, A_c = Constants (from Figure 2.8c)
 C_a = Average undrained shear strength over depth Z
 C_u = Undrained shear strength
 D = Pile diameter
 k_s, k_c = Initial subgrade reaction constant for static and cyclic loading
 Y_{50} = Deflection at one-half the ultimate soil resistance
 Z = Depth
 ϵ_{50} = Strain at one-half ultimate soil resistance (0.004-0.007)
 γ' = Effective soil unit weight

Table 2- 3 Abstract of the method of expanding soil of stiff clay water-free p - y curvatures (from[39] and [40])

Static Loading

1. Compute ultimate soil resistance, P_u (using the smaller values)	$P_u = \left[3 + \frac{\gamma' z}{C_u} + \frac{J}{D} z \right] C_u D$ $P_u = 9C_u D$
2. Compute deflection at one-half the ultimate soil resistance, y_{50}	$y_{50} = 2.5\varepsilon_{50}D$
3. Develop p - y curves using the following expression	$\frac{P}{P_u} = 0.5 \left(\frac{y}{y_{50}} \right)^{1/4} \text{ for } y \leq 16y_{50}$ $P = P_u \quad \text{for } y > 16y_{50}$

Cyclic Loading

1. Develop p - y curves for static loading	Follow step 1 to 3
2. Determine parameter describing effect of repeated loading, C	$C = 9.6 \left(\frac{P}{P_u} \right)^4$
3. Determine y for cyclic loading, y_c	$y_c = y_s + y_{50}C \log N$

- Where: C_u = Undrained shear strength
 D = Pile diameter
 J = Constant =0.5
 N = Number of cycles
 P_{ult} = Ultimate soil resistance
 y_{50} = Deflection at Oone-half the ultimate soil resistance
 y_c = Deflection under N-cycles of load
 y_s = Deflection under short-term static
 Z = Depth
 ε_{50} = Strain at one-half ultimate soil resistance 0.020 for soft clay, 0.010 for medium clay, and 0.005 for stiff clay
 γ' = Effective soil unit weight

Table 2- 4 Abstract of the method of expanding sandy soil p - y curvatures (from[30])

1.Preliminary computation	$\alpha = \frac{\phi}{2}, \beta = 45 + \frac{\phi}{2}, \alpha = \frac{\phi}{2}, K_a = \tan^2 \left(45 - \frac{\phi}{2} \right)$
2. Theoretical ultimate soil resistance due to wedge failure, P_{st}	$P_{st} = \gamma'Z \left[\frac{K_0 Z \tan \phi \sin \beta}{\tan(\beta-\phi) \cos \alpha} + \frac{\tan \beta}{\tan(\beta-\phi)} (D + Z \tan \beta \tan \alpha) + K_a Z \tan \beta (\tan \phi \sin \beta - \tan \alpha) - K_a D \right]$
3. Theoretical ultimate soil resistance due to flow failure, P_{sd}	$P_{sd} = K_a D \gamma' Z (\tan^8 \beta - 1) + K_0 D \gamma' Z \tan \phi \tan^4 \beta$
4. Govern theoretical ultimate soil resistance, P_s	P_{sd} = the smaller of the values given from step 2 and 3
5. Ultimate soil resistance, P_u	$P_u = \bar{A}_s P_s$ for static loading or $P_u = \bar{A}_c P_s$ for cyclic loading
6. Soil pressure at $D/60$	$P_m = B_s P_s$ for static loading or $P_m = B_c P_s$ for cyclic loading
7. Establish initial straight line portion	$P = (kZ)y$
8. Establish parabolic section of p - y curves	$p = \bar{C} y^{1/n}, m = \frac{P_u - P_m}{y_u - y_m}, n = \frac{P_m}{m y_m}, \bar{C} = \frac{P_m}{y_m^{1/n}},$ $y_k = \left(\frac{\bar{C}}{kZ} \right)^{n/n-1}$

Where: \bar{A}_s, \bar{A}_c	=	Adjustment coefficient for static and cyclic p - y curves from Figure 2.11a
B_s, B_c	=	Non dimensional coefficient for static and cyclic p - y curves from Figure 2.11b
D	=	Pile diameter
k	=	Initial subgrade reaction constant (MN/m ³)
		Loose sand (submerge/ above water) 5.4/6.8
		Medium dense sand 16.3/24.4
		Dense sand 34/61
P_{sd}	=	Theoretical ultimate soil resistance due to flow failure
P_{st}	=	Theoretical ultimate soil resistance due to wedge failure
P_s	=	Govern ultimate soil resistance
P_u	=	Ultimate soil resistance
Z	=	Depth
ϕ	=	Friction angle
γ'	=	Effective soil unit weight for soil under water

Table 2- 5 Abstract of the method of expanding soft clay soil p - y curvatures (from [51])

1. Theoretical ultimate soil resistance due to wedge failure, P_{st}	$P_{st} = (C_1Z + C_2D)\gamma'Z$
2. Theoretical ultimate soil resistance due to flow failure, P_{sd}	$P_{sd} = C_3D\gamma'Z$
3. Govern theoretical ultimate soil resistance, P_s	P_s = the smaller of the values given from step 2 and 3
4. Determine adjustment coefficient for static and cyclic loading	$\bar{A}_s = \left(3.0 - 0.8\frac{Z}{D}\right) \geq 0.9$ for static loading $\bar{A}_c = 0.9$ for cyclic loading
5. Develop characteristic shape of p - y curves	$P = \bar{A}P_s \tan h\left(\frac{kZ}{\bar{A}P_u}y\right)$

Where: \bar{A}_s, \bar{A}_c = Adjustment coefficient for static and cyclic p - y curves
 C_1, C_2, C_3 = Coefficients from Figure 2.12a
 D = Pile diameter
 k = Initial subgrade reaction constant (MN/m^3) from Figure 2.12b
 P_{sd} = Theoretical ultimate soil resistance due to flow failure
 P_{st} = Theoretical ultimate soil resistance due to wedge failure
 P_s = Govern ultimate soil resistance
 P_u = Ultimate soil resistance
 Z = Depth
 ϕ = Friction angle
 γ' = Effective soil unit weight for soil under water

Table 2- 6 Abstract of method of expanding sand Cemented soil p - y Curvatures
(from [44])

1. Ultimate soil resistance, P_u	$P_u = C_p \sigma_p D$
2. Correction factor, C_p	$C_p = 1.5$ for $\phi \leq 15^\circ$ $C_p = \frac{\phi}{10}$ for $\phi > 15^\circ$
3. Passive earth pressure, σ_p	$\sigma_p = 2c \tan\left(45 + \frac{\phi}{2}\right) + \sigma_v \tan^2\left(45 + \frac{\phi}{2}\right)$
4. Characteristic shape of p - y curves	$\frac{P}{P_u} = 0.5 \left(\frac{y}{y_{50}}\right)^{1/3}$
5. Pile deflection at which $P = 0.5P_u$, y_{50}	$y_{50} = 2.5 \varepsilon_c D$

- Where: c = Soil cohesion
 C_p = Correction factor for small width of pile
 D = Pile diameter
 P_u = Ultimate soil resistance
 y_{50} = Pile deflection at $P = 0.5P_u$
 ϕ = Soil friction angle
 σ_p = Passive earth pressure
 σ_v = Effective vertical stress
 ε_c = Strain at $(\sigma_1 - \sigma_3) = 0.5 (\sigma_1 - \sigma_3)_u$
 $(\sigma_1 - \sigma_3)_u$ = Ultimate principal stress difference in triaxial test
 σ_1 = Major principal stress
 σ_3 = Minor principal stress

2.4 ARTIFICIAL INTELLIGENCE METHOD

Design procedure of a deep foundation (pile) is governed by serviceability and strength requirements. The settlement under load relations of the behaviour of the pile should be precisely identified to comply with the aforementioned requirements. Accordingly, the need for testing the in situ pile loading is required. However, because of time and cost consuming issues, the in situ loading tests are not always available [55]. In contrast, by using numerical and analytical procedures, the deep foundation load settlement relationships can be identified. In this respect, the pile foundation load settlement behaviours in various soil types are still complicated and not precisely understood. As a result, almost all existing procedures failed to generate stable success for predicting the response of deep foundations' settlement under specific loading. In this consideration, artificial neural networks (ANNs) may be utilised to prepare a more correct solution. The capability of ANNs to take the nonlinear and complicated correlation of behaviour of piles without requiring a former estimated formula is the advantage of this method over a prior traditional procedure [55]. Currently, a set of ANNs has been utilised to successfully address more geotech-mechanical civil engineering questions (e.g. [56]; [57]; [58])

In the following section of the literature review, (1) the ANN modelling method was used to simulate the relation of loading-settlement bored piles that were cohesive, (2) mixed and cohesionless soil results were used to compare experimental results with the efficiency of the expanded ANN model and (3) the correctness of ANN models using statistical analysis will be presented [55].

2.4.1 Overview of ANNs

An ANN is a question-resolving method which attempts to simulate the task of the nervous system and brain of an individual human. In this chapter, multilayer

perceptions (MLPs) enlightened with the backpropagation algorithm are studied [59]. More details about this type of neural networks could be discussed in some published papers (e.g. [60]). An MLP can be created with three layers: output layer, intermediate uncovered layer and input layer. Several processing basis elements, such as neurons or nodes, establish each layer. The neurons of each segment are partially or entirely connected to the processing basis elements of another layer through connectivity factors. Networks are instructed to achieve one objective and with one category of inputting models and liaising objective models [55]. The input models are boosted to networks for generating predictable outputting models. Outputting models are compared with objective models, and squared mistakes are assessed [61]. The main mistake is back reproduced through networks, and gradient fall principles are applied to improve the communication weight and minimise calculated square errors. The previous procedures are maintained until the finishing criteria are satisfied [55] [62].

As the deep foundation (pile) loading-settlement curves experience interdependence among the current and former cases of loading settlements stages, sequential (recurrent) nodes network are utilised. The following node networks were first suggested in [63] and contain two categories for standard state unit, plan unit and input unit. Functions of ongoing condition unit recall previous activities, and within instructing, the model of inputting information is presented to plan the unit whenever the standard condition unit is set to 0. During the first instructing period, outputting is generated or imitated back to ongoing case unit for the next instructing period. This procedure is maintained until the instructing stage ends. The efficiency of instructed networks is afterwards examined by utilising a self-determining validation category [55].

2.4.2 Extention of ANN instances

In this case, an ANN pattern is extended by using the existing software and *Neuroshell* (*version 2* and *version 4*) package [64]. Two ANN patterns are expanded out for this task. The first pattern uses deep foundations which are bored (piles) set up inside sandy soils and mixture soils. The second pattern uses sake deep foundations placed inside the cohesive type of soils. All deep foundations are exposed to gradual continued axial pressure forces [55]. The information utilised for ANN pattern development is

gathered from the experimental outcomes of 66 loading settlements exams and the cone-penetration-test (CPT) outcomes. The database contains 58 instances reported with Alsamman, 6 cases reported by Eslami, A. and 2 instances announced with Milovic, D. and S. Stevanovic ([65], [66] and [67]). The number of instances for a deep foundation in mixed soils or sandy soils are 50, while the number of deep foundations inside cohesive soil is 60. Piles have round shapes and various sizes have radius changes from 32 cm to 180 cm and lengths from 6 m to 27 m. The piles discussed in this research has numerous limit of radiuses, but they have been ordered in two classes: short radius deep foundations (for radius < 30 cm) and big radius deep foundations (for radius > 30 cm). These gradings agree with the work by Ng, C.W., N.E. Simons, and B.K. Menzies and rely on the reality that great scale foundations can be treated differently than short foundations [6] and [55].

To create a relationship between deep foundation loading settlements, a significant coefficient based on loading settlements treatment need to be recognised or introduced for node (neural) network regarding changeable inputs. The coefficient includes the deep foundation geometry and confidants of soil. In the geometry of deep foundation, y is demonstrated by the pile diameter (D), and pile incorporation length (L). The features of soil are introduced by the weighted intermediate cone point persistence above pile fracture zone (q_{c-tip}) and weighted intermediate cone point persistence above shaft longitude ($q_{c-shaft}$). These changeable inputting factors demonstrate the layout unity of node (neural) networks, as shown in Figure 2-12 [55].

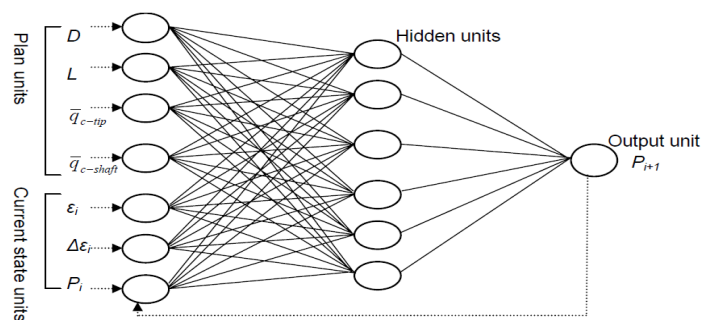


Figure 2- 8 schematic demonstration of ANN patterns (from [55])

The usual case of loading and settlements controls the next case of loading and settlements in imageries of the pile loading settlements curves. Accordingly, generic node networks for deep foundation loading settlements sketching consist of ongoing

cases, and those mentioned provide elements called former acting (e.g. neural of memory). The first step of the procedure presents an ongoing case of loading and/or settlements are placed into 0 and doctrine launches to foretell the subsequent awaited case of loading or/and settlements of an inputting loading and settlements increment. The anticipated loading and/or settlements are afterwards imitated backward to the ongoing case neural for a subsequent model of inputting information. Inputs of ANN patterns in existing case modules present an ongoing case of loading (P_i) and standard normalised settlement, ε_i ($\varepsilon_i = \frac{\text{settlement}}{\text{diameter}}$) which is increased normalised settlement, also known as $\Delta\varepsilon_i$, as demonstrated in Figure 2-12. The only result is a subsequent case of loading (P_{i+1}) [55].

In this literature review, to demonstrate this method, we mentioned the main points of this procedure. The normalised precipitation increments are selected as 0.01, 0.02, 0.03, 0.04, ..., 0.1, and 0.11. As presented by Penumadu, D. and R. Zhao [56], utilising vary strain increment amount eventuates in a well-done modelling ability without the need for a wide size of training information. Because of the need of information for the ANN, patterns on the settlements increment was not registered into the principal trials of the pile loading settlements trials, and the curvatures of operational trials were digitised for capturing the implicated information. One collection of 50 doctrines models was utilised to illustrate an individual loading-settlement curve [55].

In addition, for low-diameter deep foundations, the fracture zone, which q_{c-tip} medium was obtained following the procedure presented [66], above that when the pile end is placed in a homogenous kind soil, the fracture zone develops $4*D$ under and over the pile end; while when the pile end is placed in a firm kind soil layer over that incapable layer exists, the fracture zone develops from $4*D$ under and $8*D$ over the pile end. However, when the pile end is placed in a loose layer under a compact substrate, the fracture zone expands from $4*D$ under to $2*D$ over the pile end. In contrast, for vast radius deep foundations, the fracture region is obtained inside the range established to be $1*D$ under the deep foundation end. In addition, various deep foundation loading trials contain more geomechanical CPT than electrical CPT information; so afterwards, it was essential for transferring the geomechanical CPT records to equal electrical CPT contents. This trial was performed by utilising the formula suggested with [68], as shown below:

$$\left(\frac{q_c}{p_a}\right)_{Electric} = 0.408 \left(\frac{q_c}{p_a}\right)_{Mechanical}^{1.19} \quad 2-17$$

Where p_a is the atmospheric compression, while p_a and q_c would be in kPa.

The forthcoming stage in the expansion of ANN pattern is the information dispensation. In this study, information is accidentally distributed to two stable statistical complexes, as proposed with Masters, T. [69] and explained with Shahin, M.A., H.R. Maier, and M.B. Jaksa [70]. This involves an instructing collection for pattern verifying and one self-determining verification collection for verifying the pattern. Overall, 41 instances registered (80 per cent) of existing 50 instances of deep foundations set up in mixed soil or sand soil were utilised for instructing and 9 instances (20 per cent) were used for scaling and reliability. However, 13 instance recordings (81 per cent) of the available 16 instances of deep foundations placed in the soil with cohesive criteria were utilised for trial, and 3 instances (19 per cent) were used for scaling and reliability [38]. The census of information utilised for the prosecution or verifying and reliability cases for the pile inside mixed soil or sandy soil are shown in Table 2-7, including the maximum, standard deviation, mean, minimum or limit. Briefly, the statistical pieces of information utilised for deep foundation inside cohesive soil would not be presented. It must be mentioned that similar to every empirical sample, ANN accomplishes better explanation than extrapolation; afterwards, excessive amounts of information utilised comprised the trial collection [55] and [71].

The following stage in the improvement of the ANN pattern specifies the optimum sample's geometry. A mesh with a non-obvious substrate is utilised in this case, as it was suggested by [72] and [66] an uncovered substrate may prepare nearly any persistent subordinate where adequate connectivity gravities are utilised. The error-trial accede is utilised to specify optimal amounts of mesh parameters. After applying the aforementioned method, the number of non-obvious neural with assuming node network parameters would be determined. Alkroosh, I., M. Shahin, and H. Nikraz performed the numerical calculations for this method, so we refer the reader to that paper and satisfy this section by reviewing the procedure, errors and results [55].

The mean squared error (MSE) is among the real and auspicated amounts of loads of deep foundation invalidation, and the collection was utilised with ceasing criteria from the terminating trial. While the MSE of validity collection has attained the smallest amount without improving the efficiency of the training category, the trial has been stopped, and the output is tested.

Alkroosh, I., M. Shahin, and H. Nikraz demonstrated that the outcomes that illustrate ANN samples are qualified for the exact prediction of complicated nonlinear treatment of deep foundation loading settlements with a high measure of correctness [55]. The actuarial decomposition of factors of relationship demonstrates infinite quantity near unification in trial and examine collections utilised for ANN sample improvement.

Table 2- 7 Statistics of ANN output and input for pile in mixed soils and sand soils (from [55])

Model variables and data sets	Statistical parameters				
	Mean	Standard deviation	Minimum	Maximum	Range
Pile diameter, D (mm)					
Training set	591	327	320	1800	1480
Validation set	625	412	320	1500	1180
Pile embedment length, L (m)					
Training set	11	5	6	27	21
Validation set	9	4	6	17	11
Weighted average cone point resistance along pile tip failure zone, \bar{q}_{c-tip} (MPa)					
Training set	18	11	2	48	46
Validation set	17	9	6	31	25
Weighted average cone point resistance along shaft length, $\bar{q}_{c-shaft}$ (MPa)					
Training set	9	4	1	20	19
Validation set	9	6	3	19	16

2.5 FINITE ELEMENT METHOD APPLIED TO SPSI PROBLEMS

The FEM must be used to analyse boundary amount subjects for any continuing medium. There are innumerable subjects in solid mechanics where the FEM is the easiest analysis tool. For instance, in the scope of plasticity, performing nonlinear analysis by using analytical or semi-analytical equations is difficult, especially for entangled geometries such as a deep foundation in layered soil. Similarly, the nonlinear analysis may be dissolved by the FEM to a much more straightforward extent. Frequent loading questions may also be terminated by utilising the FEM. The aforementioned phenomena are generally encountered in geotechnical acquisitions.

There is comprehensive literature on the applications of FEM to geotechnical engineering. The literature review reported here concentrates on the usage of the FEM to dissolve SPSI questions under dynamic, vertical and horizontal loading. The standard treatment of the several elements of a FEM resolution (i.e. boundary conditions, loading utilisation, ...) in SPSI quandaries is first presented, and then a complete review of former function on the usage of FEM to dissolve individual SPSI cases is presented [73].

2.5.1 Boundary Conditions

The utilisation of finite element analysis differs from static analyses in assuming the soil's stratum is infinite in the lateral direction (and also between times in the upright direction). In FEA, the building beneath the soil level is commonly supposed to be restricted by the middle of infinite soils, while frames above and near the soil level lie over a semi-infinite damaged area. In static analysis, constant boundary conditions may be used at some spacing from the zone of interest. In contrast, infrequent subjects such boundary conditions would return exterior distributing waves back to the pattern. Besides, constant boundary conditions do not adequately shape the external radiation of strength at the boundaries of design. A more magnificent design may minimise this issue because of material damping, absorbing most of the force in the waves returned from confined boundaries [74]. As a result, the increase in pattern size indicates an

undesirable and perhaps excessive extension in the computational period. Besides, symmetrical and anti-symmetrical geometries inbound content issues may be utilised to decrease the FEA period. Instances of both states can be found in [75], where the authors took the benefit of symmetry by confining lateral movements perpendicular to the symmetric axis; and in [76], the writers took advantage of the symmetry and anti-symmetry as well.

There are three alternating procedures that exist in finite element software to properly make the infinite intermediate boundary conditions. These procedures are discussed in the following sections.

- **Kelvin elements**

Kelvin elements may be appended to abound to imitate an unlimited medium. A Kelvin element includes a spring and a dashpot affiliated in collateral [77]. The spring prepares stiffness essential to retain the static force in balance, while the cohesive dashpot imbrues the force that attains the bound. Spring and dashpot factors may be specified by utilising the solution expanded by [78]. This element is commonly utilised to imitate the bounds implicated in both dynamic and static analysis. In static analysis, the damping phrase disappears because of its interdependency on frequency. In contrast, in static analysis, a dashpot imbrues force as a subordinate of velocity, and because the velocity is zero, the dashpot energy is also zero. It was utilised by [75] and [76] the Kelvin element in their analyses for SPSI for the group and single deep foundations (piles).

- **Dashpot elements (cohesive elements)**

Cohesive elements were initially suggested been [79] for use in shallow foundations and utilised when the simulation only has a dynamic load (i.e. the frequency ingredient of the load is zero). The dashpots attract force until a maximum force. The dashpot factor per unit zone in the perpendicular and tangential orientations to the boundary may be computed from the addendum equations:

$$C_n = \rho_s V_P \quad \text{and} \quad C_t = \rho_s V_S \quad 2-18$$

Here, ρ_s is the soil's density, V_P is the wave's velocity, V_S is the shear wave's speed, C_n is the factor per unit zone perpendicular to bound and

C_t is the factor per unit zone tangent to bound. Cohesive dashpots are utilised mostly in site responses and SPSI issues (i.e. [80], [81], [82], among others).

- **Infinite elements**

Infinite elements are utilised in boundary quantity questions with unrestrained boundaries (infinite average) or questions with a lower zone of interest in comparison with the surrounding average [83]. Countless elements are commonly utilised in the continuity of finite elements. The treatment of infinite items is equivalent to the treatment of Kelvin elements, but far away nodes cannot move, while the infinite element acts linearly. Within static analysis, the effect of infinite elements stiffness at finite elements pattern boundaries relies on the pattern of [84]. Within dynamic analyses, infinite elements provide “quiet” boundaries on finite element model’s boundaries by relying on the patterns of [85] and [86]. The dynamic response of infinite elements relies on observation of smooth framework waves moving orthogonally to their boundaries. Nevertheless, the respond next to the boundary is small enough to assume average responses occur in a linear elastic style. A sample of the usage of the infinite element in dynamic issues is the wave dissemination analyses of [87] and [88].

2.5.2 Pile-soil interface

Pile-soil interfaces modelling chips in the behaviour of the pile–soil–structure regularity [89]. The pile-soil jointing is commonly modelled in two methods, either as a wholly bonded joint or as a frictional joint where pile-soil gapping or slipping can occur. In a realistic case, the joint should be modelled to combine gapping and slipping. Although computational modelling of hardness and time guidance requires researchers to remark complete bonding in some of the standard applications and the difficulty to be analysed is independent on gapping and slipping, this resolution can suffice. Usually, Coulomb’s rule of friction is utilised to model fapping and slipping in FEA. If the joint balance level is connected, the full transition of shear pressure is ensured. Plastic slipping can occur whenever the friction pressure exceeds the

maximum shear stress or friction stress because of the normal stress on the surface (μp). Differentiation occurs whenever there is tension among the pile and soil interface. Alongside the Coulomb friction pattern, there are other suggested interface patterns existing in the literature (e.g., [90], [91], [45, 92], [93], [94], [95], [96], [97], [98], [99], [100], [101], [102], [103], [104], [105] and [88]).

2.5.3 Loading

In a typical lateral, ramshackle and seismic analyses using finite element, the frequency and lateral load can be applied either at the basis, as displacement function or acceleration historical time, or as a pressure per unity volume ($f = -a_{base}\rho$, which ρ is density of soil and a_{base} is velocity and acceleration at the basis) divided through the mesh [106].

2.5.4 Behaviour of soil

Pile-soil interaction behaviour depends on the fundamental behaviour of soil pattern as well. Thus, selecting an appropriate fundamental pattern results in much better finite element analysis [107]. Fundamental patterns are widely utilised in numerical analyses of geomaterials, and they may be shaped to treat nonlinear elasticity, linear elasticity and elastoplasticity. Hardening laws may be used to shape elastoplastic behaviour. The Duncan–Chang pattern, which is extensively utilised to form soil dams, is a nonlinear elastic pattern [108]. A constitutive elastoplastic pattern may result in a better presentation for a typical corrugation and wave multiplication problem ([109], [110], [111] and [112]). Some of the fundamental patterns already exist in FE software, and new constitutive patterns may be combined in FEA packages with user-defined subroutines.

2.5.5 Applications

This research focuses only on FEM; therefore, in this section, a concise preview on published research of seismic and lateral SPSI problems using finite element method is summarised.

A similar 3D FEM was suggested for nonlinear and dynamic elastic analysis of soil–pile-structure interaction by [113]. The principle of a similar 3D pattern is shown in Figure 2.13 ([114], [115], [113]). This pattern was expanded under the following assumptions. First, shear waves in YZ and XY planes controlled dynamic motions, and the pressure waves in the vibratory direction, Y (see Figure 2.3). Second, deformations were omitted in the upright direction and normal to the vibratory direction. Dashpots were utilised to emulate the infinite soil intermediate. The pattern was accredited with centrifuge exams executed by Gohl, W.B. at the CalTech (California Institute of Technology) on one single pile and a 2 * 2 group of piles [116]. There were 8 nodes of brick shape elements utilised to represent the soil and 2 nodes of beam shape elements utilised to represent the pile [117]. Displacement adaptability between pile to soil is enforced. This model combined the soil laminated and gapping among the attached soil and pile. An equipollent linear procedure was used to create nonlinear hysteretic conduct of soil. Thus, a single efficient value was used for all-time history, instead of changing the shear modulus by strain [118] [119]. In a single pile pattern, the superstructure mass was rigid, and its movement was presented with a focused mass at its middle of gravity. A stiff beam shape element with a fine rigidity 1000 times that of a pile was utilised to link the superstructure and pile. Boundary conditions with a symmetric feature were utilised. In the model of group piles, a focused mass at the middle of gravity of the pile head presented the rigid pile hat, and less massed rigid bars were utilised to link piles. The pile and mass caps were linked by a stiffness less than the massed beam shape elements. The results of the FEA demonstrated that the pile's stiffness foundation reduced as the level of vibration increased. The analysis also presented the significance of the inertial 18 interactions. The suggested finite element analysis can detect the time-dependent damping and stiffness factors, and this detection is useful to combine into structural commercial analysis software for piles subjected to frequency vibration [120].

Cai, Y., P. Gould, and C. Desai suggested a 3-D nonlinear finite element subsystem method [121]. Figure 2.14 demonstrates the plan of the pile and structure foundation finite element model.

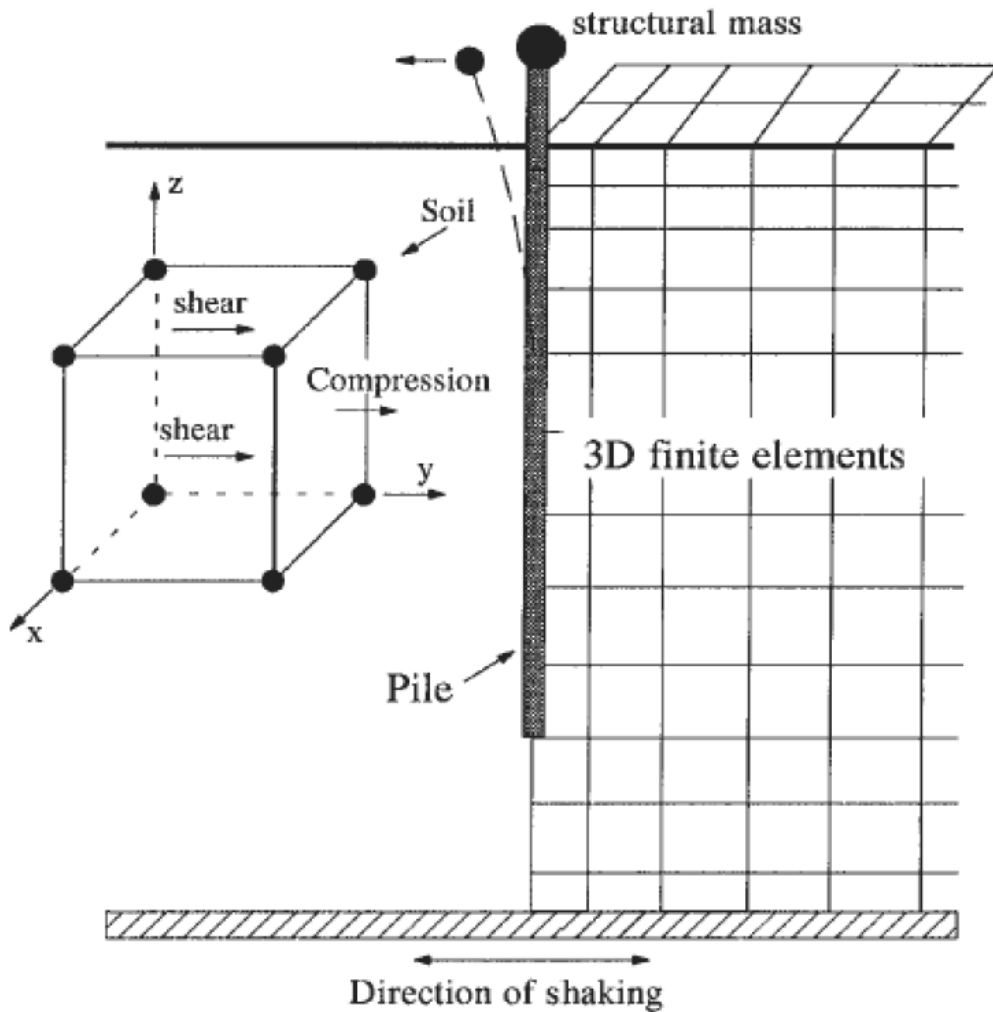


Figure 2- 9 Similar 3d pattern of soil-pile respond (from[38])

Progressive plasticity supported hierarchical single surface (HiSS) sample was utilised to create the soil. There were 8 nodes of hexahedral elements utilised to create the soil and pile, while 2 nodes of beam-column shape elements, which have 6 degrees of freedom in each node, were utilised to create the space frame of concrete super-structures [32] [122]. Moreover, 8 nodes thin layers of the isoparametric solid element with HiSS constitutive rule were utilised to combine the curvature face of slipping separation, bonding and rebounding off the soil-pile interface. Pertaining to the purification of the sample, the pile can behave as nonlinear or linear, and interracial and kinematic interactions may be simultaneously emulated by utilising this pattern. Infinite dynamic elements ([87]) were used to emulate the infinite medium. One recorded seism ground movement was utilised as a bedrock movement for this

literature review. They finalised that a based plasticity soil sample significantly changes the pile foundation response from bedrock movement [123] and [124].

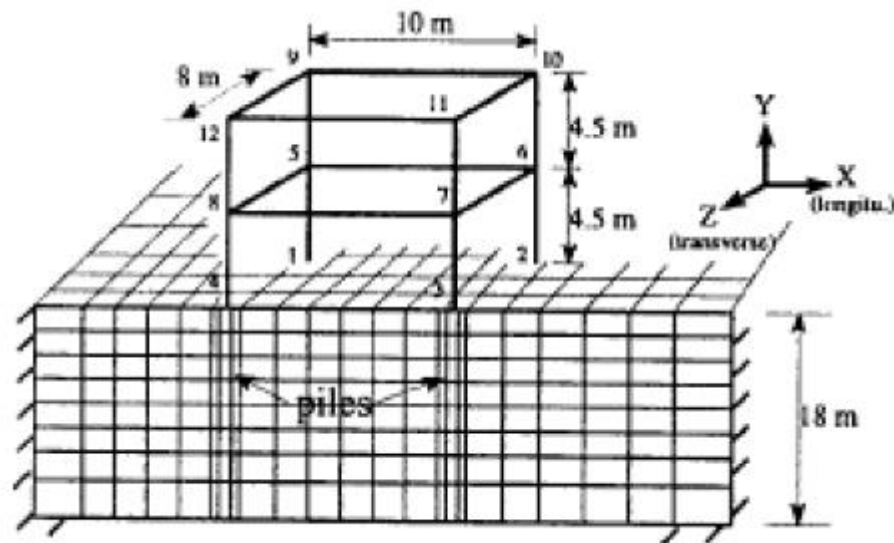


Figure 2- 10 outline of pile and structure (from[38])

Anandarajah, A. and J. Zhang expanded a simplified FE sample to analyse the dynamic nonlinear soil–pile interaction for one single pile [125]. This sample was investigated with data from one centrifuge test performed by Wilson ([126] and [127]). These analyses were performed utilising a fully coupled procedure ([83]), where pore water pressure and inflexion variations were emulated by shaping the dissipation and pore pressure build-up simultaneously. This soil sample can characterise the strain stress behaviour of sand with the liquefiable feature [128]. Beam shape elements were applied to shape the pile, and the soil was shaped with eight nodes elements. A specific radiation boundary was applied to emulate the infinite medium. A measured version of sequestration from the Kobe city event (Event J) was noticed as an input movement. The results from the finite element analysis and the centrifuge experiments agree well [129].

Kishishita, T., E. Saito, and F. Miura. performed nonlinear and linear analysis by applying 2-D FEA for friction type micro-piles [130]. The soil was created with two layers. In one linear analysis, three samples were expanded with changing shear surge velocity for upward layer whenever the shear surge velocity for the lower layer was stable in all instances. Moreover, four different types of pile (cast in situ piles,

precast piles, high capacity micro-piles for raked piles and high capacity micro-piles) were tested. The El Centro movement from the 1940 earthquake of the same name and the *K.P.83* movement from the Kobe 1995 earthquake were applied as input movements. The softest soils were through-out in the nonlinear analysis because they generally used piles in the softest soils. The soil was created with the adjusted Ramberg Osgood model [131]. Cast in situ piles, high capacity micro-piles and precast piles were created with tri-linear, improved Takeda, and bilinear samples, respectively. The results indicate that through their work, the horizontal respond of footing was approximately the same regardless of the type of pile because of the force from the soil was controlled. Piles had the greatest effects on both horizontal and vertical response of the footing in particular, while piles were raked for soft soils [132].

Bentley, K.J. and M.H.E. Naggar and Brown, D.A., et al. researched the effect of kinematic interaction on input motions at the pile level. In this research, they compounded soil–pile separation, soil plasticity, slippage and 3-D wave propagation [75] and [33]. The FEA was performed by applying ANSYS, a finite element software, ([133]). By noticing the symmetry feature, half of the real model was extended to decrease time-consuming computation. The Kelvin element was applied to emulate the infinite soil average, and the soil was created as an elastoplastic and linear material while applying the Drucker Prager failure criteria [134]. The elastic linear cylindrical pile was noticed for this research. Two various soil–pile interfaces were established: in one case, the frictional interface was applied between the soil and pile surface; while in the other case, the soil–pile interface was completely bonded. A Coulomb-frictional-sample was applied to combine the aforementioned behaviour. Socketed (fixed end) and piles were created in analyses. Two strong recorded motions were used in this research. Brown, D.A., et al. and Bentley, K.J. and M.H.E. Naggar derived in their researches that kinematic elastic interaction for one single pile slightly reinforces the free field transition function (i.e. the soil ratio of to bedrock movement) [33] and [75]. Overall, the kinematic interaction response is equal to the free field-effect used to respond to the assumptions created in their research [135].

Shahrour, I., M. Sadek, and R. Ousta performed a 3D FEA for micro-piles (minor diameter piles) [136]. The finite element analysis outcomes were compared with those of a streamlined sample based on the beam-on-Winkler pile approach. In this research, the behaviour of a single micro-pile and a micro-pile group amplifying a superstructure were discussed [137]. A unique degree of freedom structure

compound of a focused mass and one column was applied to create the superstructure. In group micro-pile analyses, three cases were introduced: a group compound of three micro-piles in a linear alignment ($1 * 3$), a square group containing nine elements ($3 * 3$), and one group of 15 micro-piles ($3 * 5$). In these analyses, square cross-sector micro-piles infixed in one homogenous layer of soil underlying by tough bedrock were discussed [138]. The behaviour of the structure-micropile-soil system was assumed to be elastic by Rayleigh material modification. Moreover, the conformance boundary conditions were imposed in this simulation: the base was fixed, and periodic conditions were constrained at horizontal boundaries for displacement field. In addition, harmonic acceleration ($a_g=0.2g$ and $f=0.67 \text{ Hz}$) was used at the basis of soil. The research demonstrated that the first effect is almost seen on the upward section of micro-piles. Inertial effects originally depend on aggregation and frequency of the superstructure. In group pile analyses, seismic and lateral loads are not distributed similarly in micro-piles. Furthermore, A group effect was noticed because of the inertial strength in this research [139].

Ousta, R. and I. Shahrour accomplished a 3D FEA to investigate the lateral and seismic behaviour of micro-piles applied for reinforcement in saturated sand soil [140] and [141]. The analysis was performed using (u-p) formulation (pore pressure for fluid phase and displacement for solid-phase) suggested by [77]. A model of soil based on bounding level concepts was applied, and isotropic and kinematic hardening was applied to obtain the elastoplastic behaviour. The micro-pile groups and a single micro-pile ($2 * 2$, $3 * 3$) were sampled in this analysis. Micro-piles were created with a linear elastic sample. The interface among pile and soil was assumed to correspond to complete bonding. The analysis was performed under the addendum boundary conditions: the basis of soil was impervious and fixed, the water level was presumed to be at the earth level, and the periodical conditions were used at horizontal boundaries for both displacement and pore pressure. A harmonic speed and acceleration ($f=2 \text{ Hz}$ and $a_g=0.1g$) were established as an input movement at the basis. The analysis for micro-piles underneath medium to loose sand demonstrated that vertical and seismic load induces growth in the pore pressure, and this growth is attributed to an increase in the micro-pile's bending moment. Although group consequences considerably decreased the bending moment, Sadek, M. and I. Shahrour researched the affection of pile tendency on motion behaviour of micro-pile groups using a 3D FEA [142]. The structure demonstrated by a centralised mass and columns

were created when the number of degrees of freedom was between 1 and 9 inclusive. The soil was created elastically with Rayleigh-damping and piles were shaped with 3-D elastic beam elements [36]. A pile head, which did not have any contact with the soil, was applied to link piles. 2 * 2 micro-pile groups with various inclinations (0°, 8°, 13°, 21°) with upright axis were noticed in this analysis. A frequency acceleration ($f=0.43$ Hz and $a_g=0.2$ g) was applied based on Young's modulus and input movement of the soil, $E_s(z)$ and was supposed to growth with depth, z , based on the following equations:

$$E_s(z) = E_{s0} x \left[\frac{p(z)}{p_a} \right]^{0.5} \quad 2-19$$

$$p(z) = \left[\frac{(1+2K_0)}{3} \right] \rho_s z \quad \text{if } z = z_0 \text{ and } p(z) = p(z_0) \quad 2-20$$

When, $p(z)$ is the average force due to the self-weight of soil at the profundity z , p_a is reference stress of 100.0 kPa, E_{s0} is Young's modulus of the soil when $p = p_0$, K_0 is the factor of horizontal earth force at rest, and z_0 is the width of the soil layer that is related to the surface when Young's modulus is fixed. The results show the micro-piles growth along their horizontal stiffness [143].

Maheshwari, B.K., et al. and Dobry, R. and G. Gazetas expanded a 3D FEM to test the effects of soil plasticity (included with work hardening) and separation at the pile-soil interface on the dynamic respond of pile groups and a single pile [144] and [145]. The pile was created with a linear elastic material, and the soil was shaped with an improved plasticity-based, HiSS model. Only a quarter of the sample was constructed by assuming symmetry and anti-symmetry. Kelvin elements (dashpot and spring) were applied in all three directions (X, Y and Z) to emulate the unlimited soil medium. Then, the sample was loaded (on the basis, which is presumed to demonstrate bedrock) with the north-south component of El Centro acceleration registered record from the El Centro 1940 Earthquake [121] and [53].

Moreover, the harmonic movement was applied to acquire the impedance and transition functions for the pile. The soil–pile separation was marked only in loading directions, while the soil and pile were presumed to be linked in the direction upright to the movement[143]. Friction among soil and pile were neglected. In every Gaussian

part, reasonable force in soil element (in the direction of applying load) and limiting press at that level were compared for every step and at every replication during a time step. The separation was presumed whenever common tensile stress was higher than the confining pressure[146].

Numerical analysis by Maheshwari, B.K., et al determined that the effect of separation was more considerable when using an elastic soil sample than the plastic sample [144]. Moreover, nonlinearity decreased the actual and conceptual parts of the impedance function for a pile system. Furthermore, the response of nonlinear soil in the pile-soil order has a significant effect on small excitation frequencies[143, 147].

2.6 SUMMARY OF THE CHAPTER

In this chapter, literature was reviewed for the research conducted on pile-soil interaction with different methods. In the first section, background and introduction about piles applications SPSI and its significant role in our modern society and tall and strategic constructions were explained. In the second section, the theory behind the design of piles with p - y curves and development through the past few decades were demonstrated. In the third section, a novel method based on artificial intelligence method was conducted. In the fourth section, different approaches based on computational methods and commercial software with an overview of the FEM were discussed. Then, factors affecting pile design under various load and soil types were briefly described. Moreover, some of the recent experimental and numerical studies dealing with pile-soil interaction analysis were reviewed in this chapter. However, based on the reviewed studies, research gaps still exist, and this proposed study compares the results of the CPT and FEA methods under different loads and with different soil and pile types.

3

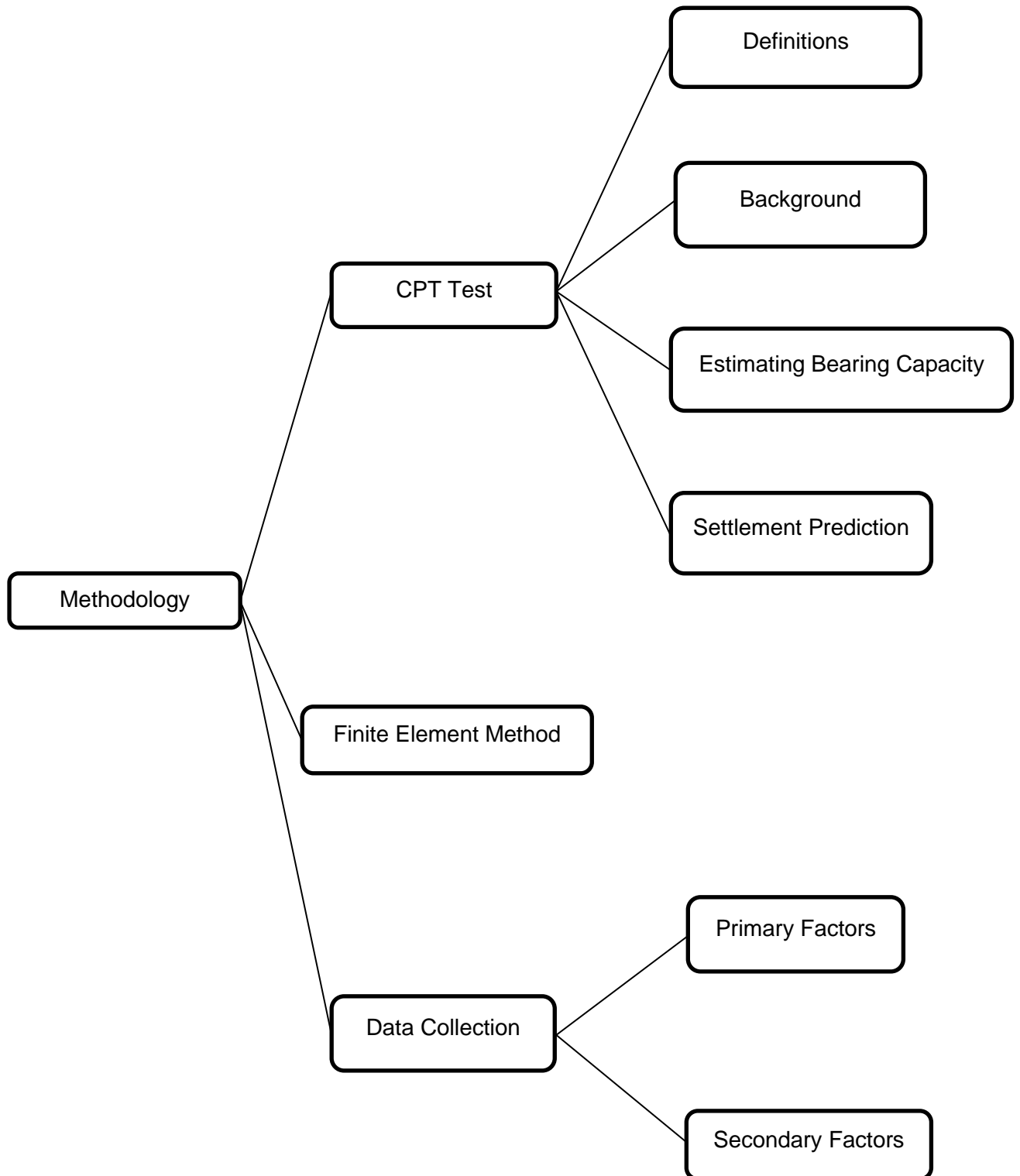
Development of Experimental and Numerical Methods

3.1 INTRODUCTION AND CHAPTER OVERVIEW

One of the utmost crucial characteristics that controls the designing of foundations and deep foundations (piles) is bearing capacity. Accordingly, it has been frequently been examined in the geotechnical engineering field. Accordingly, many experimental and theoretical techniques have been suggested to forecast the pile conduct and bearing capacity. However, exact assessments of certain interpretations of the pile load-transfer mechanisms and the pile's bearing capacity have not been completed because these calculations are complex. The objective is to conduct experimental tests and numerical simulations to assess the validation of the finite element method. Experimental tests have been performed by the cone penetration test (CPT) method in other resources and summaries of the results are presented in Appendices A, B and C.

This chapter introduces the experimental and numerical methodologies engaged for present research in three sections. Section 2 presents the CPT experiment and specifics of the experimental tests. Moreover, the specifications of the bearing capacity and displacement for exerting force are introduced. Then, Section 3 introduces the FEM (finite element method) analysis appropriate for pile simulations

and numerical approaches. The data accompanying this study are presented at the end of this chapter



3.2 CONE PENETRATION TEST (CPT)

Sampling the soils in combination with laboratory tests is the most trustworthy procedure to determine the properties of soils. However, because of limited schedules and budgets, few projects have suitable laboratory tests [148] [149]. Nonetheless, in many cases, subordinate soil consideration information such as CPT cone resistance or SPT strike count and sleeve erosion along with the type of soil and water level table can be obtained to adjudge the over-surface soil's characteristics [150] [151]. Therefore, whenever laboratory information does not exist, it is a common practice to evaluate soil exclusivities from the SPT/CPT outcomes. Many empirical relevancies have been built amongst SPT magnitude and CPT with other engineering exclusivities of soils. However, because of the variation of the soil exclusivities for similar kinds of soils from one place to another, it is difficult to predict the result of those dependencies without authentication from residential soil [152]. The residential soil may follow a previous relationship or follow a completely different relationship. For the posterior case, new relations for residential soil should be determined to fulfil the previously mentioned intention [153].

Currently, the CPT is becoming used globally as an in situ experiment for site inquiry and geotechnical designers, especially in deltaic regions, and it uses continuous confiscation that is separate from operator mutability [152, 154, 155].

3.2.1 General Definitions

In the CPT, a cone at the ending of a chain of shafts is compressed into the Earth at a fixed rate, and contiguous or interrupt measurements are made to measure the resistance of the cone to penetration. Measurement also consists of either the incorporated resistance to penetration of the cone and an external layer of a sleeve or the resistance of a scheme sleeve [156].

Ground investigations were performed originally by applying CPT and SPT experiments. Six couplings of SPT and CPT were added at different locations, and the maximum lateral interval was not more than 1 m [157].

SPT and CPT are commonly applied to prepare data comprising soil penetration resistance, pore water pressure and shear strength. The information acquired from SPT or CPT is applied to predict the pile capacity, and this application

comprises two steps: (1) The SPT or CPT information is correlated with contractual soil strength parameters, such as S_u or Φ , and a static procedure is performed to predict the valence, and (2) the outcomes of tests are correlated with the pile's bearing resistance [38].

The SPT studies have been performed to design piles for more than 50 years, and they have been applied frequently in South and North of America, Japan and the United Kingdom [158]. However, its main limitation is that it can be modified by numerous factors such as drilling, operating conditions, rate of blows and hammer efficiency. Then, high uncertainty and mutability depend on SPT information. In contrast, CPT is fast and simple, supplying direct recording resistance of the soil and permits significant information to be acquired in a short period. The information obtained from the CPT may be expounded analytically or empirically. Thus, CPT has been preferred testing for designing piles. Hence, this research briefly concentrates on the procedures that apply the CPT information for predicting the capacity of the pile.

3.2.2 A Brief Background History of CPT

The CPT is an in situ examination procedure that consists of pushing a specially instrumented penetrometer into the Earth at a fixed rate, commonly two cm per time unit (second) and continuously reading numerous evaluations [156]. There are two kinds of available cones: electrical and mechanical cones.

The mechanical cone was preliminarily invented by an engineer who worked in Holland at the Department of Public Work (DPW) in 1932 named P. Barenteson. Since then, various studies ([159-161]) have presented extensions on the primary designing of the cone for improving its correctness and increasing the number of evaluations.

The recent formation is Begemann's cone, and this method is demonstrated in Figure 3-1 and shows that the created internal shafts ambulate quickly inside of the external steel shafts. The cone point is conjoined to the internal shaft, the cone functions inside this path, and the cone is further increased in the external shaft into the cone resistance; then, the cone and external shafts are further combined to determine the total sum load. The difference between the total sum up force and cone resistance is the sleeve friction. Because of its low expense, robustness and simpleness,

the mechanical cone is utilised extensively. Nevertheless, the correctness of the information is shown in the operator experiments [156]. Moreover, the mechanical cone is sluggish and less efficient for soft soils [38].

In 1948, the electrical cones were expanded by the Delft Soil Mechanic Laboratory (DSML). Cone testing suggests performing consecutive evaluations for head resistance and drawing straight strip charts based on the sound record [162]. In addition, electrical cone testing with sleeve friction and head resistance readings was developed in 1960 ([163]). In this sort of cone penetrometer, there are no respective motions amongst the friction sleeve and cone. The cone penetrometer includes strain measure force cells installed on the friction sleeve and cone to determine the cone resistance and sleeve friction within the testing period [38].

The signals are transferred through cables transiting via the middle of the null push shafts to an in-field computer upon the face for automatised information attainment. This electronic cone can similarly include inclinometer electrics into gauge the deviance through the upright. An electronic cone that was expanded with Fugro in cooperation with the Dutch State Research Institute (TNO) is presented in Figure 3-2. The form and girths for this cone illustrate the basis on which the international reference test procedures are made ([156]).

3.2.3 Methods of estimating pile bearing capacity based on CPT information

There are two common procedures (direct approaches and indirect approaches) applied to correlate the valence of pile and CPT outcomes. The indirect procedures are currently unacceptable because of their particular applicability and their absence of resolution. The procedures that are used in sandy soils need criteria to be appropriate. The sandy soil should be cleansed, naturally consolidated and in-compressible. Therefore, indirect techniques have not been covered in this research, and we only concentrate on direct methods to obtain essential input data for ABAQUS. Most of these procedures are primarily derived for driven deep foundations and are then used

in bored deep foundations by reducing coefficients while considering the differences between the installation methods [38].

The direct procedures utilise direct correlation between side-friction resistances and pile tip with CPT outcomes. All the methods apply a mean cone resistance q_c near the height of the pile head to evaluate the unit top resistance, r_t . The middle area that is recognised as the impression area is a subordinate of the pile diameter. The increased impression area represents the fracture envelope and can revolve between 0.8 to 1.4 diameter of pile, D , below and above the foundation head, relatively. There are various models for fracture area proposed by scientists, as demonstrates in Figure 3-3. The unity axle resistance, r_s , is correlated with the cone spot resistance of the ahead axle of the pile or with residential flank cone's friction. Commonly, various direct procedures are suggested to estimate the valence of the pile from CPT information. The broadly applied methods related to this research are presented in the addendum sections [38].

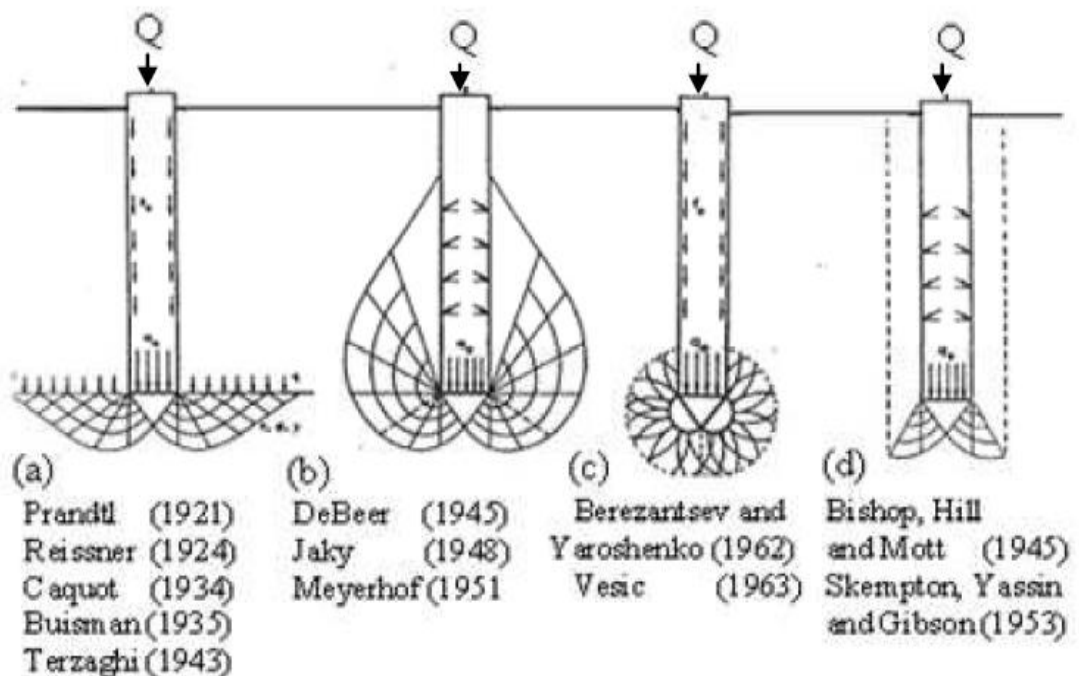


Figure 3- 1 Supposed fracture models below piles (Source:[164])

Schmertmann technique

The Schmertmann method relies on a job performed by Nottingham and Schmertmann which handled 108 force experiment outcomes on pattern piles to expand an equation for predicting the valence of a driven pile in sandy soils [165]. Schmertmann suggested that the following method be used to evaluate the unity top resistance:

1. q_c valence is cleared to pursue the smallest path, as presented in Figure 3-4.
2. q_{c1} has been characterised by calculating the mean of q_c valence ahead of line **abcd**.

Dot *b* is at a profundity x under suggested pile head and $0.7D \leq x \leq 4D$. The value of x that generated minim q_{c1} has been chosen.

3. q_{c2} is defined by computing the mean of q_c ahead the line **defgh**, which is demonstrated in Figure 3-4.

4. A reduction coefficient, w , has been produced to consider the gravel amount and over-consolidation ratio, which is listed in Table 3-1.

5. The bearing valence of the end is calculated using the following equation:

$$r_t = w \left(\frac{q_{c1} + q_{c2}}{2} \right) \quad 3-1$$

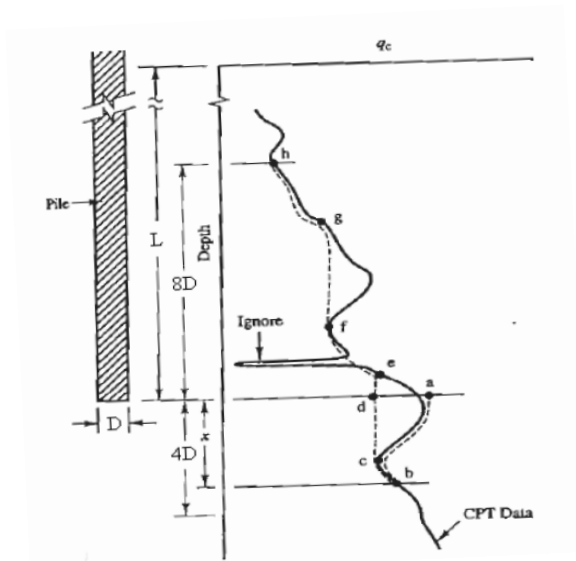


Figure 3- 2 Dutch procedure for computing bearing of the end from the CPT results
(Source: [166])

Table 3- 1 w amounts for using in equation 3-1 (Source: [167])

Condition of Soil	w
Sandy soil by OCR = 1	1.00
A lot gravelly coarse; sandy soil with OCR = 2 to 4	0.67
Fine gravel; sandy soil with OCR = 6 to 10	0.50

Note: OCR = Over-consolidation ratio

The resistance of unit shaft, r_s , is calculated by distributing the foundation into parts and assigning suitable residential side friction f_s to every single part. The f_s values of parts are considered, and the whole is multiplied by a factor to obtain r_s as:

$$r_s = K f_s \quad 3-2$$

Here, K is a dimensionless factor related to the foundation's form and material, type of cone and ratio of embedment size. K ranges from 0.8 to 2.0 in sandy soil and from 0.2 to 1.25 in clay soil.

If the friction of sleeve valence is not provided, r_s may be acquired from cone head resistance as follows:

$$r_s = C q_c \quad 3-3$$

Here, C is a dimensionless factor that depends on the type of pile and varies from 0.008 to 0.018. r_s should not more than 120 KPa.

Schmertmann suggested reducing the coefficient in Eq. 3-3 by 25% whenever it is applied to assume the bored piles capacity. The procedure executes an overhead range on the unity head resistance to not mount than 25 MPa in sandy soil and more than 9.5 MPa in very silty clay soil.

- 3- The tantamount mean cone head resistance, q_{eq} , is specified by averaging the remain cone head resistance (q_c) amounts upon the thick curvature.
- 4- The unit head resistance can then evaluated based on Eq. 3-4.

$$r_t = k_c q_{eq} \quad 3-4$$

Here, k_c is the bearing end factor, as demonstrated in Table 3-2.

The unit axle resistance r_s is obtained from the following:

$$r_s = \frac{q_c}{k_s} \quad 3-5$$

Here, k_s is the friction factor prepared in Table 3-2.

Utmost amounts of r_s , varying between 15 KPa to 120 KPa, have been nominated based on a type of pile and soil and installation method, as shown in Table 3-2.

Table 3- 2 The Empirical factors for LCPC procedure (Source: [168])

Nature of soil	q_c (MPa)	K_c	Driven Piles				Bored Piles			
			K_s		Upper limit of r_s (kPa)		K_s		Upper limit of r_s (kPa)	
			A	B	A	B	A	B	A	B
Soft clay and mud	<1	0.5	30	30	15	15	30	30	15	15
Moderately compact clay	1-5	0.45	40	80	35 (80)	35 (80)	40	80	35 (80)	35 (80)
Compact to stiff clay and compact silt	>5	0.55	60	120	35 (80)	35 (80)	60	120	35 (80)	35 (80)
Silt and loose sand	<5	0.5	60	120	35	35	60	150	35	35
Moderately compact sand gravel	5-12	0.5	100	200	80 (120)	80	100	200	80	35 (80)
Compact to very compact sand and gravel	>12	0.4	150	200	120 (150)	120	150	300	120 (150)	80 (120)

A: Driven precast piles, pre-stressed tubular and jacked concrete foundations

B: Jacked metal and driven metal and piles

P.S.: Bracket valences for r_s use to careful performance and minim the derangement of the soil.

Alsamman Method

Alsamman, O.M suggested two different patterns for predicting the valency of drilled deep piles: a pattern for foundations embedded inside of cohesive soils and the other pattern for deep foundations embedded in cohesionless soils [65]. This method was expanded by him by examining samples relying on the information, including 95 pile-load-tests and the CPT outcomes obtained from all over the world. Alsamman proposed an explanation of the factors applied with the LCPC procedure and proposed the following expressions for evaluating the valence of the pile.

For a foundation thrust inside a cohesive soil type, the unity head resistance, r_t , is predicted through:

$$r_t = 0.27 (\bar{q}_{c(tip)} - \sigma_{vo}) \quad 3-6$$

Here:

$\bar{q}_{c(tip)}$ = the mean of cone resistance above a region expanding to a pile diameter under the pile head

σ_{vo} = the total upright stress at the height of the axle basis

The unity axle resistance r_s is evaluated from (3-7), that is, concluded from the figures suggested by Alsamman. When the deep foundation is thrust into a layered type of soil, Equation (3-7) has been used for each of layers, and the sum unity axle resistance is the total of the unit axle resistance of the several layers.

$$r_s = \frac{1.75}{80} (\bar{q}_{c(shaft)} - \sigma_{vo}) \quad 3-7$$

Here:

$\bar{q}_{c(shaft)}$ = mean of the cone head resistance ahead of the pile's side

σ_{vo} = sum of upright stress at the medium depth of the layer of soil

The sum of pile head resistance, R_t , and resistance of sides, R_s , are obtained from:

$$R_t = (r_t \times A_b) + (\gamma \times L) A_b \quad 3-8$$

$$R_s = \sum_{i=1}^n (r_s \times SA)_i \quad 3-9$$

Here:

A_b = area of axle base

γ = unit weight of soil

L = length of pile

SA = plane area of the axle of each sublayer

n = numeral of layers.

For foundations (piles) in cohesionless soils, Alsamman similarly proposed a series of graphs to be utilised to evaluate the capacity of the pile. Equations (3-10 to 3-16) are concluded from the graphs. The unit head resistance is determined based on the following:

$$r_t = 0.15 (\bar{q}_{c(tip)}) \quad \bar{q}_{c(tip)} \leq 9.5 \text{ MPa} \quad 3-10$$

$$r_t = 1.44 + 0.075 (\bar{q}_{c(tip)} - 9.5) \quad \bar{q}_{c(tip)} > 9.5 \text{ MPa} \quad 3-11$$

r_t should not be more than 2.87 MPa.

The unity sides resistance is evaluated by means of the following equations:

$$r_s = 0.015 (\bar{q}_{c(shaft)}) \quad \bar{q}_{c(shaft)} \leq 4.75 \text{ MPa} \quad 3-12$$

$$r_s = 0.072 + 1.67 \times 10^{-3} (\bar{q}_{c(shaft)} - 4.79) \quad \bar{q}_{c(shaft)} > 4.75 \text{ MPa} \quad 3-13$$

r_s should not be more than 95 Kpa

In gravel and gravelly sand,

$$r_s = 0.02 (\bar{q}_{c(shaft)}) \quad \bar{q}_{c(shaft)} \leq 4.75 \text{ MPa} \quad 3-14$$

$$r_s = 0.095 + 2.5 \times 10^{-3} (\bar{q}_{c(shaft)} - 4.75) \quad \bar{q}_{c(shaft)} > 4.75 \text{ MPa} \quad 3-15$$

r_s should not be more than 130 KPa.

The sum of the pile's head resistance then can be calculated from the following:

$$R_t = r_t \times A_b \quad 3-16$$

The final total resistance of sides R_s is derived from Eq. 3-9.

DeRuiter and Beringen procedure

De Ruiter, J. and F. Beringen expanded a procedure based on the experimental results obtained from the off-shore structure in the North Sea [167]. The procedure uses the same pattern acquired by Schmertmann to estimate the unity head resistance of one pile in sandy soil.

In the clay soil type, the procedure relies on the total stress analyses and the definition of undrained shear strength, S_u , for evaluating the unity head resistance by the following equations:

$$S_u = \frac{\bar{q}_{c(tip)}}{N_k} \quad 3-17$$

$$r_t = N_C S_u \quad 3-18$$

Here:

N_k = the cone coefficient varying from 15 to 20 and depends on local experimental
 $\bar{q}_{c(tip)}$ = the mean cone dot resistance calculated similarly to the Schmertmann procedure.

$$N_C = 9$$

This procedure uses 15 MPa instead of a superior limitation of the unity head resistance.

The unity axle resistance has been acquired from Eq.3-19 and 3-20 utilising the correlation between the undrained shear resistance for each layer of soil along the pile axle, $S_{u(shaft)}$, and the adhesion coefficient, α , that is equal to 1 for normally consolidated clay soil types and 0.5 for over-consolidated clay soil types. A superior limitation of 120 KPa is imposed over the unity axle resistance.

$$S_{u(shaft)} = \frac{q_{c(shaft)}}{N_k} \quad 3-19$$

$$r_s = \alpha \times S_{u(shaft)} \quad 3-20$$

Eslami and Fellenius procedure

Eslami, A. and B.H. Fellenius suggested a procedure to predict pile valence based on piezocone outcomes [169]. Differing from the aforementioned procedure, the friction of sleeve and the cone head resistance were not purified. The impression of

peaks and troughs decreased thru the operation of the geometric average that was applied to measure the mean cone part resistance into the efficacy region. The procedure similarly calculates the pore water pressure and uses it to measure the effective stress by means of the long-term governing coefficient of the conduct of foundation.

Felleniuse and Eslami introduced the following phases to calculate unity head resistance:

- Outlining the measure of the impression area in the proximity of the foundation head. Once the deep foundation is fixed in a homogeneous soil type, the impression area increased to 4 times D under and over the pile head. The area extending 4 times D under to 8 times D over the pile head once deep foundation (pile) head is located in a firm soil layer beneath a faint soil layer or 4 times D under to 2 times D over the pile head when the foundation (pile) is fixed inside a strong soil or a faint soil.
- Reducing the pressure of pore water u_2 as of the calculated entire cone resistance, q_c , for specifying the effective cone resistance, q_E .
- The foundation (pile) unity head resistance has been acquired from:

$$r_t = C_t q_{Eg} \quad 3-21$$

Here:

C_t = head correlation factor assumed equal to 1

q_{Eg} = geometric mean of the cone pot resistance over the influence area

The unit axle resistance is acquired from the improved efficient cone point resistance as follows:

$$r_s = C_s q_E \quad 3-22$$

Here:

C_s = axle correlation factor shown in Table 3-3

q_E = cone point resistance after modification for pore pressure

Table 3- 3 Axle correlation factor C_s (Source: [5])

Type of soil	C_s %
Very soft clay and soft sensitive soil	8
Soft clay	5
Stiff clay and mixture of clay and silt	2.5
The mixture of silt and sand	1.0
Sand, gravely sand	0.4

3.2.4 Settlement Prediction

Commonly, a designing procedure treats the estimation of the settlement of pile as a second issue and focuses on using the proportional axial valence of the deep foundation to transport the structural loading ([1]). However, restricting movements to a passable state has been one of the most important reasons for applying piles and settlement, and differences between settlements is a major specification in designing deep foundation procedures ([170]). Nejad, F.P., et al. showed that pile designing should not just meet the strength criterion but also should satisfy serviceability commitments that fundamentally demand an accurate estimation of a deep foundation's settlement [171]. Therefore, determining the settlement-load relationship is an essential step for designing a valid criterion: the engineer would determine the permissible loadings that may be utilised and accomplish the serviceability necessities. The most trustable procedures for achieving the settlement-load relation is performing situ load-pile experiments. However, performing these experiments is not always possible. Therefore, pile loading settlement is evaluated and applied to the design procedure. Many methods are suggested to estimate the loading-settlement conduct of a single radially loaded deep foundation (pile), and they are commonly classified into three categories of closed-form resolution, load-transfer resolutions and numerical resolutions.

The closed-form resolutions have been primarily suggested to evaluate the behaviour of a single pile buried inside a homogenous elastic linear half space ([172])

and [173, 174]). These recommendations were expanded to evaluate the pile treat in the layered systems of the Gibson soil profile ([175-177]). Nevertheless, the main limitation of these approaches is that the closed-form answer simulations are not able to precisely create the conditions of a deep foundation entrenched in a subjectively nonhomogeneous soil outline that is originated to take the excessive impact in foundation movement ([178] and [179]). Numerical explanations (i.e. boundary element method (BEM), finite element method (FEM) and variation elements) may similarly be engaged to approximate the load–settlement conduct of solitary axially loaded deep foundations. Specifics of FEM are accessible in [180], [181] and [182], and the presentation of the technique in geotechnical engineering is presented in [183]. The BEM is examined in [25], and the presentation of the various elements in foundations are presented in [184] and [185].

The load-transfer technique in the investigation ([186]) is an additional method for demonstrating the load–settlement condition of the solitary deep foundation. Relying on this methodology, numerous speculative representations (e.g. [187-189], [190] and [191]) and empirical reproductions (e.g. [192], [193], [194], [186], [195], [177] and [196]) are suggested.

The load transfer is extensively utilised when estimating the load movement conduct of solitary piles exposed to the vertical loading because of its effortlessness and competence incorporating the nonlinear characteristics of soil ([197]). Consequently, this tactic has been comprehensive, and three approaches together with [191], [170] and [51] have been designated for the resolution of comparing outcomes of this revision. The approach presented in [191] is optimum because it examines a theoretic sample based on CPT statistics; the method presented in [170] is a well-known systematic attitude, and the [51] is a recognised technique that is based on the practice field. The explanation of the loading transfer idea is discussed in the next section.

3.2.4.1 The loading transfer technique

The loading transfer method has been mainly suggested by Seed, H.B. and L.C. Reese to compute the resident loading–displacement relationship of piles [198]. Subsequently, several scientists (e.g. [186], [190], [178], [179] and [197]) have

discussed the topic, and as a consequence, several load-transfer processes have been projected.

The load-transmission method contains forming the piles employing a chain of separate components. The corresponding component is linked to the subsequent component with a spring to represent the radial stiffness of the foundation and is laterally maintained with a nonlinear spring representing the resistance of the Earth infriiction of skin (T-Z spring). Similarly, this model uses a nonlinear spring on the deep foundation immoral to represent the tailing bearing (Q-Z springs). The nonlinear springs of soil represent the response of soil against the movement shown schematically in Figure 3-6. The load-transmission representations are mainly classified into two sets: theoretical and empirical models. The empirical models have been established by considering the loading and resident movement gained from the loading experiments of instrumented deep foundations (piles). The developed models characterise the purposes which may attain the finest probable appropriate by the measured information. Numerous kinds of these purposes are accessible in the collected works such as the exponential factors (i.e. [199], [200] and [201]), empirical functions (e.g. [195] and [51]), Osgood-Romberg functions (e.g. [202] and [203]), hyperbolic function (e.g. [204]) and polygonal functions (e.g. [205] and [206]).

Another methodology for creating the load–settlement relationship of the deep foundation is the theoretical model. In the mentioned method, the Earth has been presented in two coatings. The buckles on the superior coat (Z) have been produced with the axial pile loading (T), although the buckles on the subordinate coat (Z) have been produced with the baseload (Q). The buckles at the soil over the pile axle may have been idealised by concentric cylinders shearing ([190]), and they are for the most part upright, whereas the centrifugal bucklings have been insignificant. The bucklings underneath the base of the pile may have been assessed to utilise the elastic resolution for the stroke of the rigid figure performing on a half space. The explanations suggested by Mindlin, R.D. is utilised to determine the load-transmission function for the base of the pile [207], and this tactic is supplementarily detailed in [190].

3.3 FINITE ELEMENT METHOD

In this study, the numerical model is presented to examine the influence of diverse features affecting pile behaviour in the interior numerical context. This segment demonstrates the numerical pile's instance under axial load in the plane-strain condition. The explanation of methodology in this section is principally adopted from ABAQUS user's guide citations ([208]).

3.3.1 Build a Finite Element Model relied on CPT Outcomes

In simulating of the piles-soils interaction, several features need to be considered, for example, the mechanical conduct of the pile, conduct of the neighbouring earth, interaction between soils and piles, and geometry of the sample. In addition, appropriate element types for piles and soils and their interactions need to be selected. In the current investigation, the sample's geometry is formed and contains three portions together with pile and types of earth. Then, the mesh of finite element procedure is produced. In addition, properties of the material are allocated to the respective section in which pile has been presumed to be elastic, and the soil is demonstrated using an applicable elastoplastic constitutive pattern. Interactions, the boundary conditions and phases of exploration are presented in the following sections.

3.3.1.1 Modelling procedure

When determining a suitable type of the element for the pile-soil pattern, numerous element's limitations must be considered such as element intimate components (e.g. shell, continuum, rigid elements and beams), degrees of freedom (straight linked to the element domestic), quantity of nodes, preparation and integration. The family of FE is a broad conventional that is utilised for element arrangements. The elements of specimens frequently examined are beam, continuum, rigid, shell, and membrane elements.

Amongst diverse families of the element in ABAQUS, solid or continuum elements model the most extensive diversity of mechanisms. They basically model minor lumps of material in a constituent, and they may be linked to additional elements on to some extent of their faces and may be exposed to any load. Continuum elements may be utilised for linear-cooperation analyses and for multifaceted nonlinear analyses, which consist of touching base, plasticity, and enormous buckles. In the finite element method for common element, rotations, movement, loading and further grades of freedom are individual spontaneous at the element nodes, and they are incorporated amid nodes for another point in the element. This exclamation instruction is governed by the number of nodes on that element. First-order or linear interpolations in all directions are used for the elements with nodes merely at their curves, and are repeatedly entitled first-order elements or linear elements. Despite the elements with medium-size nodes, quadratic usage interpolation (second-order interpolation). Second-order elements are more responsible for advanced correctness than first-order elements. Subsequently, first-order elements are rigid and have an unimportant degree of convergence; thus, an exact fine mesh is needed. These results have been ignored in stress analysis computations because the results do not provide much value.

Consequently, second-order elements, where detention stresses attentiveness more efficiently, are improved selections for modelling geometric structures. The ABAQUS element reference library comprises linear and quadratic interpolation elements in one, two and three proportions in several figures. Quadrilaterals and triangles are accessible in two proportions, while tetrahedral and hexahedral (bricks) are in three sizes that are appropriate for substantial deflection assignments. In this project, soil and pile elements have been displayed as *C3D8R* (8-node bilinear plane strain quadrilateral), employing condensed integration.

The *C3D8R* element is a continuity displacement-stress element by means of first-order (linear) incorporation. The element has a hexahedron (brick form) shape by eight nodes. This shape is specified by decreased integration that has hourglass control and acquires significant computational period time. The element has three effective degrees of freedom: u_1 , u_2 , and u_3 , which coincide along three global Cartesian orientations X , Y , and Z ([209]).

3.3.1.2 Interaction

Between different interaction models accessible in ABAQUS software, the surface-to-surface interaction is preferred to create the boundary stuck between soil and pile. This boundary may define interactions in the middle of two deformable shells or stuck amongst a deformable shell and an inflexible shell. As the pile becomes stiffer, it is computer-generated as a master surface and its neighbouring soil is modelled as a slave surface. To solve technical convergence limitations, an asymmetrical solver matrix was applied to resolve the problems, as surface-to-surface discretisation has advanced propensity to produce asymmetrical stiffness relations; in particular, the minute slave and master surfaces are not equivalent. The interaction pair replacing the pile-soil boundary is revealed in Figure 3-8. To circumvent the penetration of the master surface nodes keen on the slave surface, the slave surface mesh was developed. The advantage of this model is to decrease the probability of principally limited to small-area penetration and to increase the accurateness of the interaction stress. The interaction material goods of the model were shaped by outlining in cooperation tangential and regular interactions. The tangential behaviour contains sliding flanked by two surfaces and conceivably frictional shear stresses. The standard behaviour is at right angles to the interaction surface. The pile-soil interaction was presumed to be adhesive friction, and no sliding occurs before the shear stress extents to its supreme significance. This is numerically attained by means of a large friction factor in the pile-soil boundary. The tangential friction factor between the soil and pile was assumed to be 0.5, and the average connection was measured as hard that permits departure after connection. To outline the interaction in ABAQUS software, the pile elements were selected as the master surface by a stiffer figure, and the soil was selected as a slave surface with extra refined meshes.

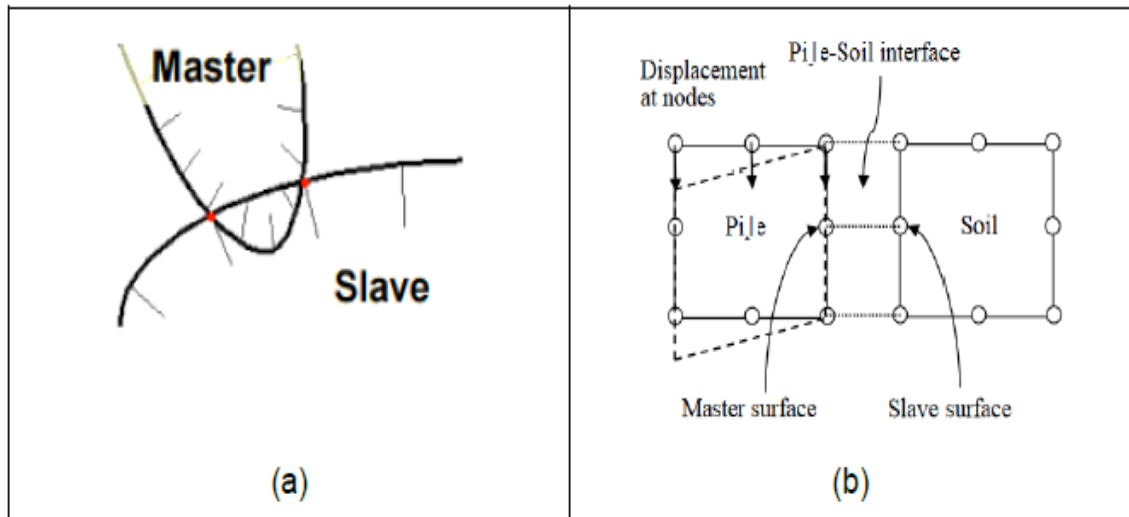


Figure 3- 4 a) Master surface pierce in the slave surface when it is not developed b) Additional master nodes per capita restraint are convoluted and coupled next to the slave surface (Source: [210])

The contact conducts at the soil–pile surface consist of the load-transfer mechanisms in both the tangent and rational orientations. The reasonable force is transferred only once soil and pile contact tightly; or else, there is no force transferred. This type of standard connection conduct could be determined as hard contact provided by ABAQUS software. The tangent conduct could vary from a rough connection with no comparative sliding amongst the pile, and the soil in friction-less sliding situations without friction develops along the axle of the pile. For the connection between the pile and soil, Coulomb frictional sample built-in ABAQUS can be selected to explain the interaction at the soil–pile interface by a recommended friction factor, μ , as demonstrated in Figure 3-9. These two ideal tangency situations can also be recognised and performed while suggesting a zero or higher frictional factor. The shear resistance is specified in Figure 3-9b, and it becomes constant after it reaches its limit (Figure 3-9a). The earlier is regularly utilised for undrained clay-pile interaction, and the latter is frequently utilised in sand-pile interaction. Once the tangent shear stress in the soil–pile interface surpasses the shear resistance, comparative slip between the soil and pile occurs.

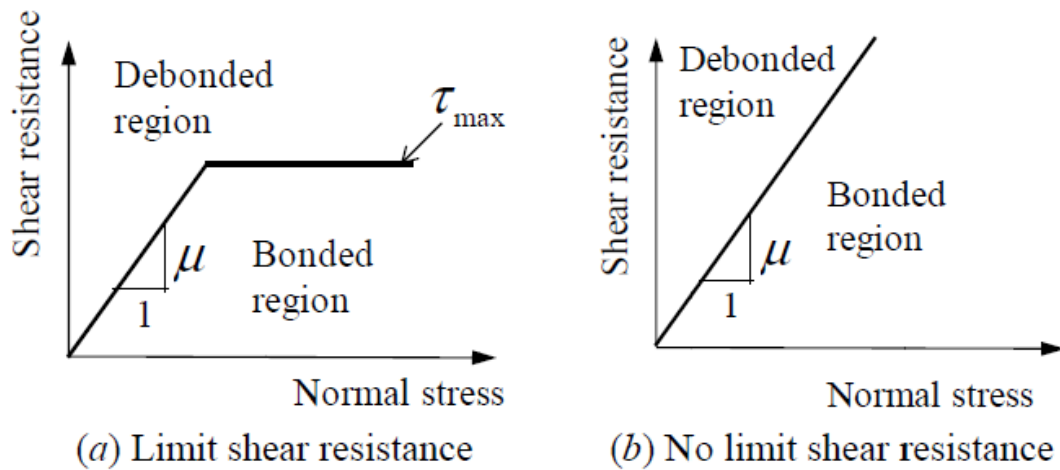


Figure 3- 5 Shear persistence against standard stress (Source [211])

3.3.2 The Numerical Approach

Pile's reaction

To estimate the reaction of a deep foundation (pile) to vertical load, the FEM software, ABAQUS, can be utilised in studies. In this programme, several constitutive samples are integrated to model the nonlinear behaviour of the soil and pile. Nevertheless, selecting a constitutive sample is generally unbiased by the material considerations that are accessible for the case studies under contemplation. For instance, when only repetitive parameters are presented, or there is a shortage of particular investigational information with reference to the parameters requested to simulate the mechanical conduct of the materials convoluted, the use of sophisticated samples may not be completely vindicated. While this is occasionally the case, the constitutive samples engaged in the current research are comparatively unpretentious and need limited material factors as inputted information. Moreover, these factors could be readily attained from conservative structural and geotechnical experiments [212].

In detail, a linear elastic entirely plastic sample with Mohr–Coulomb fracture principle and flow regulation of non-associated kind is presented for sampling the soil's conduct. The soil factors requested by this constitutive sample are Poisson's ratio, the shear modulus, shearing resistance angle, angle of dilatancy and effective cohesion. The pile is characterised by distinctive strain-stress relations for steel and

concrete and reinforcement. The constitutive pattern for concrete is established with the plasticity principle for compressive pressures and the failure mechanisms for tensile tensions. This pattern is appropriate for concrete constructions that are exposed to monotonic forcing. For compressive forces, concrete is estimated as a plastic-elastic material with isotropic hardening and related flow regulation, and the relationship of the surface of the yield is

$$q - \sqrt{3}a_0p_m - \sqrt{3}\tau_c = 0 \quad 3-23$$

Which p_m and q are well-defined in that order as

$$p_m = -\frac{1}{3} I_1 \quad 3-24$$

$$q = \sqrt{3J_2} \quad 3-25$$

Where I_1 is the 1st invariant of the pressure tensor and J_2 is the 2nd invariant of the deviatoric pressure tensor. In addition, the symbol convention utilised in the current research agrees with that generally implemented in solids mechanics; hence, tensile strains and stresses are considered to be positive. As a result, Equation 3-23 is not determined on the 3rd invariant of stresses, and this comparison must be utilised once the concrete is exposed to small confining stress (a lesser than 4 to 5 times of the most significant compressive stress which could be passed by the concrete in uniaxial compression). In Equation 3-23, a_0 is a constant that follows the following relationship.

$$a_0 = \sqrt{3} \frac{1 - r_{ba}^\sigma}{1 - 2r_{ba}^\sigma} \quad 3-26$$

Here, r_{ba}^σ is the proportion of the compression strength of concrete in biaxial situations to that beneath uniaxial situations (usually $r_{ba}^\sigma \cong 1.16$). Moreover, τ_c considers the dependence of the surface of yield on the plastic deflections because of the hardening action of the materials. The stresses τ_c are linked to the hardening parameters λ_c , and these parameters are determined by the following equation:

$$\lambda_c = \frac{\varepsilon_a^p}{\left(1 + \frac{c_0}{9}\right) \left(\frac{a_0}{\sqrt{3}} - 1\right)} \quad 3-27$$

Where

$$c_0 = 9 \frac{r_{ba}^\varepsilon (\sqrt{3} - a_0) + \left(a_0 - \frac{\sqrt{3}}{2}\right)}{r_{ba}^\varepsilon (a_0 - \sqrt{3}) + r_{ba}^\sigma (2\sqrt{3} - 4a_0)} \quad 3-28$$

ε_a^p is plastic strain dignified in a uniaxial trial, and r_{ba}^ε is the proportion of the plastic strain at fracture underneath biaxial circumstances to that underneath uniaxial circumstances (normally $r_{ba}^\varepsilon \cong 1.28$). The $\tau_c - \lambda_c$ correlation can be recognised using Equation 3-27 with Equation 3-23, and in uniaxial situations leads to the following equation:

$$\tau_c = \left(\frac{1}{\sqrt{3}} - \frac{a_0}{3}\right) \sigma_c \quad 3-29$$

Here, σ_c is the pressure related to ε_a^p in a uniaxial compress exam. In detail, λ_c is computed as a function of ε_a^p using Equation 3-27, and the related significance of τ_c is computed as a function of σ_c (which is experimentally associated with ε_a^p) using Equation 3-29. Afterwards, ultimate strength is increased, and the strain-softening condition is considered to model the decreased strength instigated by concrete crushing.

Under tensile stress, a dissimilar method is utilised to act out the improvement and occurrence of cracking. In detail, cracking occurs once the stress state extents a crack detection plasticity exterior. This surface similarly permits the bearings of the crack to be well-defined. It is presumed that the crack path is typical to this surface at a prearranged stress state. The plasticity exterior is of the Mohr–Coulomb category and is consequently defined with a correlation comparable to Equation 3-23. As soon as the incident and direction of crack are identified, the damaged elasticity theory is utilised to define the post-fracture conduct of the concrete through open cracks. Correctly, this is supposed that the material decreases in strength over and performs a softening mechanism that further decreases the strength, in the sense which open

cracks are epitomised with an absence of stiffness of the material, while any constant strain related to cracking is ignored. Consequently, the cracks could become closed by the stress converting to compressive stress. In addition, we assume that the cracks are smeared on the concrete sections that are modified with this procedure [212].

The first benefit of the defined constitutive method is that it merely necessitates, as inputting information, a strain-stress correlation of the concrete underneath uniaxial circumstances. The correlation assumed in the current method is presented in Figure 3-9, and this method comprises a piecewise linear function that is entirely well-defined with the following parameters: concrete's tensile strength f_{ct} , Young's modulus E_c (that composed of Poisson's ratio, ν_c , defines the elastic conduct of concrete) and compressive strength f_c . As shown in Figure 3-10, the conduct of concrete is elastic once compressive stress is smaller than $0.3 f_c$. For more significant levels of stress, plastic deflections occur because of the hardening conduct of the material. Fracture occurs at a strain of $1.81 f_c/E_c$, and afterwards, the material responds is strain-softening. In tensile stresses conditions, the conduct is linear elastic until the stress exceeds the tensile strength. Afterwards, the material is determined by strain-softening by the strength which slowly decreases by increasing the strain to account for almost the tension stiffening because of the concrete reinforcement interface. An extra in-depth explanation of the constitutive method for concrete could be introduced into the ABAQUS manuals [212].

The strain-stress correlation considered for the steel bars is presented in Figure 3-11. As shown, the steel behaviour is perfectly plastic-elastic, and it is compatible with compression and tension. The material factors required by this last fundamental method are the steel's yield strength f_y , Young's modulus E_s and Poisson's ratio ν_s . The reinforcement is supposed to be smeared in a pipe that is buried in concrete and is wholly joined to it.

Lastly, the shear strength criteria of the Mohr-Coulomb style are expressed in the pile-soil interaction. In cohesionless soils, these criteria are expressed by the following equation

$$F_{lim} = F_n \tan \delta$$

3-30

Here, F_{lim} is the restrictive shear stress, F_n is the standard force and δ is the friction angle at the pile-soil interface. Moreover, separation amongst soil and pile happens once tensile stress advances at the pile-soil interface. In other words, gap and slip could occur at the pile-soil boundary.

The FE mesh implemented in the analysis for discretising the pile and soil involves brick eight nodes solid linear decreased integration elements using the hourglass mechanism. The mesh modification is completed in the portions where high stages of strain are projected to happen. Reinforcement is discretised with four nodes with linear exterior elements with decreased integration. The lateral and the bottom sides of the field are situated sufficiently far from the foundation to elude any substantial boundary impact. In this fitting, the proposition by Karthigeyan, S., V. Ramakrishna, and K. Rajagopal of localising the lateral sides at an interval of $20D$ (which D is the diameter of the pile) from the foundation axle is determined to be effective [213]. The basis of the domain is completely fixed, and the horizontal borders are bounded through upright rollers.

The preliminary stress state in the interior of the soil domain (i.e. beforehand load) is computed with k_o -circumstances. After this phase, a vertical loading is exerted at the pile tip. The greatness of this force is continuously increased to the ultimate amount for which an answer is attained.

Constitutive Model of Soil

Recently, progressively more comprehensive constitutive models are being established to define the complicated conduct of geomaterials underneath diverse loading circumstances ([214] and [215]) that consecutively leads to complications in numerical identifying and implementing the model parameters by the purpose of the criterion material experiment. An Elasto-perfectly plastic sample with the Mohr–Coulomb

defeat criteria, regularly called the Mohr–Coulomb model, is extensively utilised in finite element analyses of geomechanical engineering because of its simpleness and sufficient accuracy ([216]). The fracture encompasses with their minor and major principle stresses (σ_1, σ_3), as shown in Figure 3-12, are determined by cohesion, c , and inner frictional angle, φ , by the following equation:

$$\frac{1}{2} (\sigma_1 - \sigma_3) + \frac{1}{2} (\sigma_1 + \sigma_3) \sin \varphi - c \cos \varphi = 0 \quad 3-31$$

When developed into three-dimensional stress, the defeat envelope shifts into a promiscuous hexagonal pyramid [211].

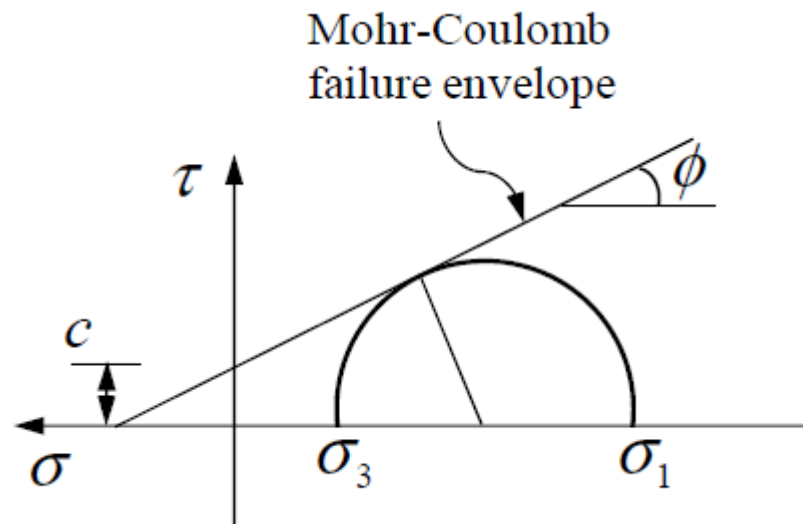


Figure 3- 6 Mohr-Coulomb fracture criteria (Source[38])

For the elastoplastic constitutive model, the possible functions are generally engaged as the same as defeat envelopes, with non-associated or associated flow law. Nevertheless, the probable flow, being completely different from the defeat envelope, has a hyperbolic profile in the climactic stress plane and has no angles in the deviatoric stress spaces was assumed in ABAQUS, referenced to [217]. The adequacy of this non-affiliated flow is in its exclusive description of the orientation of plastic flow and entire smoothness.

As mentioned, a 3-D numerical pattern was established to model the proposition of a piled foundation in each instance, and the pattern contained the soil continuity, connection zone, geometry of the pile elements and applied forces. The

modified Drucker–Prager constitutive rule was used in developing the models, and its cap plasticity procedure instance in the p - t plane is demonstrated.

The equations of its transition, share fracture and cap surfaces are

$$F_s = t - p \tan \beta - d = 0 \quad 3-32$$

$$F_c = \sqrt{(p - p_a)^2 + \left(\frac{R_t}{1 + \alpha - \frac{\alpha}{\cos \beta}}\right)^2} - R(d + p_a \tan \beta) = 0 \quad 3-33$$

$$F_t = \sqrt{(p - p_a)^2 + \left[1 - \left(1 - \left(1 - \frac{\alpha}{\cos \beta}\right)(d + p_a \tan \beta)\right)\right]^2} - \alpha(d + p_a \tan \beta) = 0 \quad 3-34$$

The correlation of cap factors d , β and k to Mohr-Coulomb's φ and c are as follows:

$$k = \frac{3 - \sin \varphi'}{3 + \sin \varphi'} \quad 3-35$$

$$\tan \beta = \frac{6 \sin \varphi'}{3 - \sin \varphi'} \quad 3-36$$

$$d = \left(1 - \frac{1}{3} \tan \beta\right) \frac{\cos \varphi'}{1 - \sin \varphi'} 2c' \quad 3-37$$

Figure 3-14 demonstrates a schematic sketch for numerical specimen expanded in this research. The specimen consisted of a raft (PQRS) and pile buried in the soil continuity (AA'BB'CC'DD'). Because of material isotropy and geometrical symmetry, $\frac{1}{4}$ of the block was analysed (AA'HH'FF'GG').

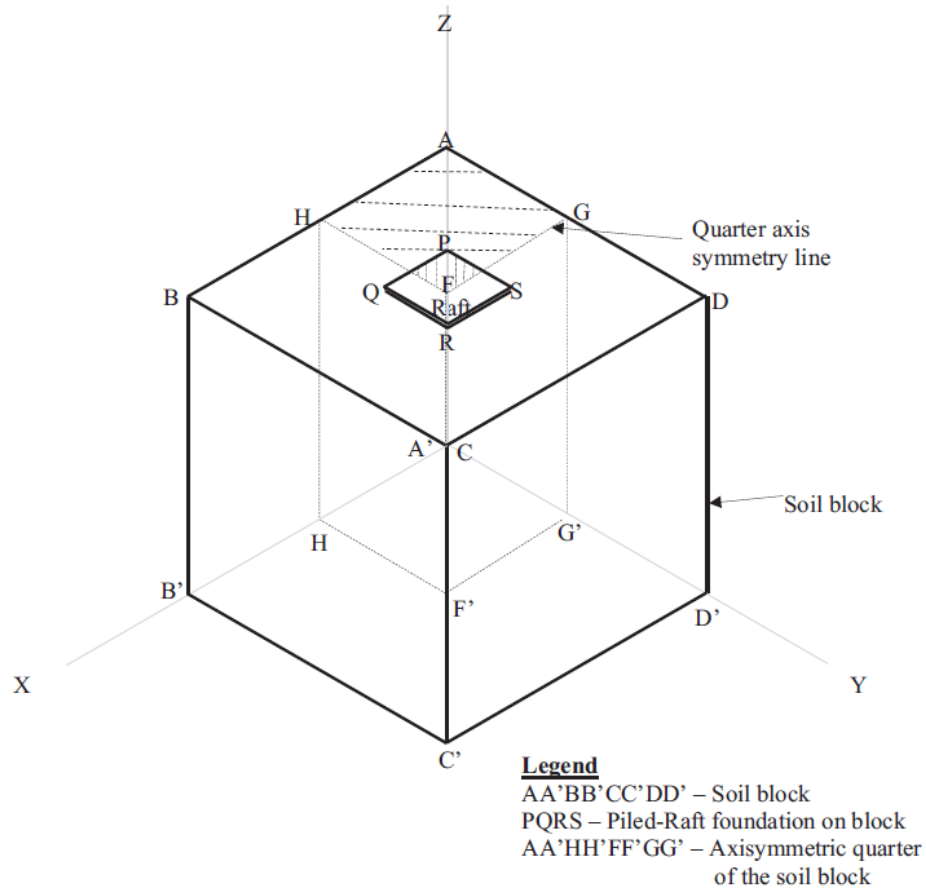


Figure 3- 7 Schematic sketch of the numerical model (Source[38])

Because of the symmetry in-plane, the boundary conditions alongside the mid-axis were established as XSIMM (symmetry about plane x is fixed) and YSIMM (symmetry about plane y is fixed). No translation was permissible in the underneath nodes, and no y or x translation was permissible in the angle nodes. Figure 3-15 shows a sample summary of these boundary conditions, composed with the upright movement contours. The figure shows that the fine elements are focused on the proximity of the piled raft tracked by a smooth transmission of elements from being fine to being coarse. Within this stage, the aspect ratio and the bias were retained within a proper limit to generate elements of decent modality and thus effectively run the software. To account for the contact amongst the foundation and the soil, the slave-master implication was utilised that the soil surface behaved like a slave surface and the raft acted like a master surface.

In the current research, the model treated the soil as a homogeneous isotropic single-stage medium. To decrease the computations period, several strain-stress analyses on elastoplastic and elastic soil sequences of different widths, depths and heights were tested. Based on the initial results, the horizontal dimension of the continuum was 20 times the pile diameter and the upright depth was two times the pile longitude so no significant strain and stress were detected at the boundaries. Moreover, the surface-to-node and surface-to-surface contiguity selections were tested, and surface-to-surface contiguity was determined because of its broad level of accuracy ([218]), and the penalty-type frictional limitation enforcement technique was utilised to formulate the contact surface's stiffness.

3.4 DATA COLLECTION

3.4.1 Description of Piles

The database for this study encompasses 58 driven piles and 50 bored piles (deep foundations) of two classes (concrete and steel piles). The bored deep foundations (piles) have diverse dimensions and circle forms, with a length from 6 to 27 m and a diameter from 320 mm to 1800 mm. The driven piles also do not have the same shapes and sizes (i.e. hexagonal, circular and square form) and have lengths ranging from 8 to 36 m and diameters ranging from 250 to 660 mm. Meanwhile, the piles measured in the existing research possess a wide-ranging variety of dimensions; they are categorised into large dimension piles ($D > 600$ mm) and small dimension piles ($D \leq 600$ mm). This arrangement follows [6] and relies on large diameter piles that demonstrate different behaviour from lesser-dimension piles. Comprehensive data of case experiments are shown in Appendixes A, B and C that contain the CPT side view and diagram soil profile underneath the pile and deep foundation (pile) geometry, establishing the technique and categories of foundation loading experiment. The CPT profile contains the cone spot resistance, q_c , for bored deep foundations and q_c and sleeve friction, f_s , for driven piles. The load–settlement figure is similarly provided.

The collected databank involves case histories composed from the references, mostly in situ experiments, and the CPT outcome records described by [65] and [5]. The cases were attained worldwide. The instantaneous information to each case recording utilised for advancing the models is revealed in Tables 3-4 to 3-7.

The bored piles in the record are exposed to upright compression loading experiments. The driven piles are similarly verified underneath vertical tension or compression forces. The loading experiments diverge in their method, apparatus, instrumentation, and loading presentation techniques. The loading experiment individually case recording has been demonstrated in the case recording excellent points in Appendixes A, B and C (Source [38]).

The cone penetration exams have been performed to a deepness of a minimum of eight times the pile radius underneath the pile head and at a remoteness sufficiently close to the loading experiment whereabouts to be illustrative; the interval amongst the CPT place and the force exam was at least higher than ten times the pile's radius. The results of cone spot resistance, q_c , against deepness are accessible in all loading experiments in the databank; nevertheless, the sleeve friction, f_s , only exists in the driven piles' case records.

Table 3- 4 Instantaneous of information applied for mounting FEM for bored piles (Source: [38])

Test No.	D (mm)	L (m)	\bar{q}_{c-tip} (MPa)	$\bar{q}_{c-shaft}$ (MPa)	Q_u (kN)	Soil profile	Site Location
1	1100	13.0	16.2	4.0	2624	Mud, peat, sand	Not available
2	421	5.8	22.9	11.8	912	Silt, peat, sand	Berlin, Germany
3	320	10.2	22.0	7.2	712	Silty clay, medium sand	Hamburg, Germany
4	457	15.2	1.6	8.1	1423	Sand, clay	Evanston, U.S.A
5	393	6.5	10.1	12.8	738	Sand	California, U.S.A
6	410	5.6	16.7	15.8	560	Sand	California, U.S.A
7	320	10.2	14.6	4.5	832	Silty clay, medium sand	Hamburg, Germany
8	320	7.7	8.3	2.6	445	Silty clay, medium sand	Hamburg, Germany
9	403	9.2	13.1	10.3	1352	Sand	California, U.S.A
10	814	24.2	6.5	9.6	5872	Sandy clay, sand	Houston, U.S.A
11	320	10.2	21.9	7.1	818	Silty clay, medium sand	Hamburg, Germany
12	671	13.0	25.6	17.2	4270	Gravelly sand, sandy gravel	Dusseldorf, Germany
13	1000	9.5	29.3	5.1	2358	Fine sand	Not available
14	1000	9.0	35.9	8.5	3692	Sand	Not available
15	840	24.4	47.6	9.2	9653	Silty clay, sand	Kuala Lumpur
16	600	7.2	10.9	7.6	1437	Clay, silty sand	Guimaraes, Portugal
17	1100	9.0	15.4	5.4	3247	Sand	Not available
18	500	10.2	8.9	2.2	1005	Sand, gravelly sand	Berlin, Germany
19	329	6.2	20.7	10.6	605	Sandy silt, medium sand	Berlin, Germany
20	408	5.8	17.6	8.2	765	Medium sand, fine sand	Berlin, Germany
21	521	8.2	12.9	9.6	1334	Gravelly sand	Berlin, Germany
22	1800	11.5	36.6	7.6	7651	Fine sand	Not available
23	405	8.4	33.4	11.5	1019	Silt & sand, gravelly sand	California, U.S.A

Table 3-4 (Continued)

Test No.	D (mm)	L (m)	\bar{q}_{c-tip} (MPa)	$\bar{q}_{c-shaft}$ (MPa)	Q_u (kN)	Soil profile	Site Location
24	405	10.4	8.9	11.3	1019	Sand	California, U.S.A
25	399	7.8	12.8	4.4	667	Sandy clay, medium sand	Berlin, Germany
26	671	10.2	13.7	20.1	4697	Gravelly sand, sandy gravel	Dusseldorf, Germany
27	430	8.7	31.7	14.5	516	Gravel, coarse sand	Berlin, Germany
28	320	7.7	7.9	2.6	356	Medium sand	Hamburg, Germany
29	399	10.0	24.6	12.7	756	Medium sand	Berlin, Germany
30	600	12.0	21.4	10.8	2687	Clayey sand, fine sand	Kallo, Belgium
31	600	12.0	21.3	11.1	2406	Clayey sand, fine sand	Kallo, Belgium
32	1100	27.0	7.0	9.4	8207	Sand & clay	Shandong, China
33	320	7.7	8.2	2.6	391	Silty clay, medium sand	Hamburg, Germany
34	400	9.4	2.4	1.4	480	Clay and silt, silty sand	Sao Paulo, Brazil
35	1085	25.1	32.0	9.0	7695	Sand & clay	Shandong, China
36	350	15.8	5.1	5.5	840	Sand	Seattle, U.S.A
37	500	10.2	14.7	3.2	1299	Sand, gravelly sand	Berlin, Germany
38	405	7.9	6.2	12.8	792	Silty sand, sandy silt	California, U.S.A
39	1100	6.0	21.0	7.8	2469	Fine sand & silt	Not available
40	631	18.3	30.0	11.7	1770	Clay, sand	Netherlands
41	521	8.2	12.8	9.5	1263	Gravelly sand	Berlin, Germany
42	405	7.0	17.8	14.3	1294	Sand	California, U.S.A
43	399	7.8	13.1	4.1	578	Sandy clay, medium sand	Berlin, Germany
44	1500	6.0	10.4	8.5	2669	Sand	Not available
45	400	7.8	10.6	3.6	543	Sandy clay, medium sand	Berlin, Germany
46	320	7.7	8.5	2.6	409	Silty clay, medium sand	Hamburg, Germany

Table 3-4 (Continued)

Test No.	D (mm)	L (m)	\bar{q}_{c-tip} (MPa)	$\bar{q}_{c-shaft}$ (MPa)	Q_u (kN)	Soil profile	Site Location
47	762	16.8	5.9	5.2	3425	Residual silty sand	Atlanta, U.S.A
48	430	8.7	26.8	11.7	627	Gravel, sand	Berlin, Germany
49	329	6.3	25.9	15.6	756	Medium sand	Berlin, Germany
50	1078	13.0	31.0	19.0	8825	Gravelly sand, sandy gravel	Dusseldorf, Germany

D , pile diameter; L , pile embedment length; \bar{q}_{c-tip} , middling cone point persistence surrounded by head-impact area; $\bar{q}_{c-shaft}$, middling cone point persistence along axle; Q_u , measured pile capacity.

Table 3- 5 Instantaneous of information applied for mounting FEM for concrete driven piles (Source: [38])

Test No.	D (mm)	L (m)	\bar{q}_{c-tip} (MPa)	\bar{f}_s (kPa)	$\bar{q}_{c-shaft}$ (MPa)	Q_u (kN)	Soil profile	Site Location
1	250	21.3	8.0	33	5.6	810	Sand, silty sand	Blount Island, U.S.A
2	400	11.3	10.8	105	5.0	870	Clay, sand	Washington, U.S.A
3	450	10.3	4.1	47	2.5	1250	Sand, clay	Wathall, U.S.A
4	350	8.6	5.7	25	4.6	600	Sand, clay	Perry, MS U.S.A
5	450	8	7.9	205	3.0	1140	Silty sand	West P Beach, U.S.A
6	285	15	7.7	56	5.0	1600	Silty sand, uniform sand	Baghdad, Iraq
7	450	14.9	5.3	38	6.3	1755	Sand	Blount Island, U.S.A
8	400	12.5	3.2	35	3.3	620	Sand	Hinds, MS U.S.A
9	350	15.85	6.0	50	5.6	1485	Silty sand	Blount Island, U.S.A
10	450	9.15	11.7	150	15.7	1845	Sand & clay	Jefferson County, U.S.A
11	610	18.2	10.5	43	9.6	3600	Sand, silty clay	Oklohama, U.S.A
12	400	11.2	7.0	88	8.4	1020	Sand	Hinds, MS U.S.A

Table 3-5 (Continued)

Test No.	D (mm)	L (m)	\bar{q}_{c-tip} (MPa)	\bar{f}_s (kPa)	$\bar{q}_{c-shaft}$ (MPa)	Q_m (kN)	Soil profile	Site Location
13	250	9.25	3.8	104	2.8	700	Clay, silty sand	Almere, Netherland
14	400	12.5	4.1	43	3.6	1170	Sand	Hinds, MS U.S.A
15	285	11	3.1	47	3.4	1000	Silty sand, uniform sand	Baghdad, Iraq
16	400	8.8	7.6	36	5.6	1140	Clay, sand	Smith, MS U.S.A
17	355	10.2	7.8	80	5.0	1300	Silt, sand, dens sand	Victoria, Australia
18	400	11.4	9.8	52	5.7	1140	Clay, sand	Madison, U.S.A
19	350	20.4	5.0	86	5.4	1260	Sand, silt	Florida, U.S.A
20	500	11	6.8	60	13.9	2070	Sand	Florida, U.S.A
21	350	16	7.5	60	7.3	1070	Clay, sand	Washington, U.S.A
22	350	16	7.6	154	7.5	1350	Sand	Florida, U.S.A
23	625	25.8	18.6	139	8.6	5455	Clay, sand	Los Angeles, U.S.A
24	450	15	10.3	46	6.0	1420	Sand	Harrison, MS U.S.A
25	400	13.4	8.8	48	4.4	1170	Clay, sand	Yazoo, MS U.S.A
26	450	11.3	1.1	195	2.5	830	Silty sand	West P Beach, U.S.A
27	350	9.5	4.5	124	6.6	900	Sand, clay	Louisiana, U.S.A
28	500	13.8	11.8	125	10.9	4250	Dense sand, lime stone	Victoria, Australia

D , pile diameter; L , pile embedment length; \bar{q}_{c-tip} , middling cone point persistence surrounded by head-impact area; $\bar{q}_{c-shaft}$, middling cone point persistence along axle; Q_m , measured pile capacity.

Table 3- 6 Instantaneous of information applied for mounting FEM for steel driven piles (Source: [38])

Test No.	D (mm)	L (m)	\bar{q}_{c-tip} (MPa)	\bar{f}_s (kPa)	$\bar{q}_{c-shaft}$ (MPa)	Q_m (kN)	Soil profile	Site Location
1	300	11.0	0.0	66	15.2	560	Sand	Lock & Dam 26, U.S.A
2	455	12.0	0.0	65	15.9	1170	Sand	''''
3	455	11.3	0.0	67	15.8	870	Sand	''''
4	273	22.5	23.9	46	8.1	1620	Sand, dense sand	Blount Island, U.S.A
5	660	18.2	10.2	46	9.5	3650	Sand, silty clay shale	Oklohama, U.S.A
6	609	34.3	13.3	48	9.5	4460	Sand, clay, sand	Taiwan
7	330	10.0	2.3	38	3.0	625	Clay, silty sand, clay	Milano, Italy
8	300	28.4	1.3	24	3.2	1240	Peat, sand, soft clay	Ruerto Rico, U.S.A
9	273	22.5	0.0	27	2.1	765	Sand, dense sand	Blount Island, U.S.A
10	455	16.2	0.0	67	9.8	1170	Sand	Lock & Dam 26, U.S.A
11	300	16.2	20.0	64	16.9	1310	Sand	''''
12	450	15.2	0.5	50	6.2	1020	Sand, clay	Evanston, U.S.A
13	455	16.8	0.0	66	17.5	1260	Sand	Lock & Dam 26, U.S.A
14	350	14.4	21.6	72	17.6	1300	Sand	''''
15	400	14.6	20.0	74	17.0	1800	Sand	''''
16	400	14.6	0.0	50	15.5	945	Sand	''''
17	273	9.2	6.5	18	5.4	490	fill, sand	S Farncisco, U.S.A
18	273	15.2	5.4	36	6.4	675	Sand, dense sand	Blount Island, U.S.A
19	455	16.2	15.5	89	9.7	3600	Sand	Lock & Dam 26, U.S.A
20	392	36.3	14.0	131	11.7	2130	Sand, silty clay, sand	Alabama, U.S.A

Table 3-6 (Continued)

Test No.	D_{eq} (mm)	L (m)	\bar{q}_{c-tip} (MPa)	\bar{f}_s (kPa)	$\bar{q}_{c-shaft}$ (MPa)	Q_m (kN)	Soil profile	Site Location
21	490	14.0	15.6	32	11.2	3500	Soft soil, dense sand	Kallo, Belgium
22	385	19.0	2.8	82	2.0	1370	Clay, sand	Washington DC, U.S.A
23	385	12.4	1.8	48	1.7	520	Clay, sand	'''
24	455	15.2	0.3	55	6.1	1010	Sand, clay	Evanston, U.S.A
25	321	8.5	5.0	70	1.5	590	Clay, sand	Lauderdale, U.S.A
26	350	31.1	5.6	19	1.4	1710	Clay, sand, clay	Louisiana, U.S.A
27	609	34.3	8.7	33	4.5	4330	Sand, clay, sand	Taiwan
28	455	11.3	0.0	65	15.5	817	Sand	Lock & Dam 26, U.S.A
29	350	11.1	0.0	60	15.5	630	Sand	'''
30	300	31.4	1.2	35	3.1	1690	Peat, sand, soft clay, sand	Ruerto Rico U.S.A

D , pile diameter; L , pile embedment length; \bar{q}_{c-tip} , middling cone point persistence surrounded by head-impact area; $\bar{q}_{c-shaft}$, middling cone point persistence along axle; Q_m , measured pile capacity

Numerous pile load experiments contain mechanical instead of electronic CPT records, and consequently, it was essential to convert the mechanical CPT evaluations into comparable electric CPT results. This is applied by using the following relationship suggested by [68]:

$$\left(\frac{q_c}{p_a}\right)_{Electric} = 0.47 \left(\frac{q_c}{p_a}\right)_{Mechanical}^{1.19} \quad 3-38$$

Here, p_a = atmospheric pressure in KPa and q_c = cone spot resistance in KPa.

For f_s values, the mechanical cones bounce more exceptional records than the electric cones in entire soils. [68] proposed a proportion of 2 for sandy soil and 2.5 to 3.5 for clay soil. In this research, a coefficient of 3 is assumed in clay and 2 in sand [38].

Soil profiles are principally categorised into two groups: sandy soils profiles containing loose to dens sands; mixed soils profiles containing coatings of cohesionless soils (gravel or sand) and coats of cohesive soil (clayey). While the soil profiles consist of a percentage of cohesive types of soil, the circumstances might be measured as the piles set in cohesionless soils for these explanations:

1. For most circumstances, the head of the pile is set in sandy soil. Thus, it is supposed that the sand delivers a maximum resistance on the pile head [5]. Consequently, the predictable behaviour of these piles is realised as piles inside cohesionless soils.
2. For a few circumstances, the head of the pile is located in clayey soil. In these situations, the head contribution in the overall capacity might be insignificant because the clay delivers most of its resistance on the pile axle. Henceforth, these piles may likewise be considered as piles inside cohesionless soils.

3.4.2 Choice of input variables

Appropriate approximation of deep foundation's bearing capacity necessitates the documents of the coefficients that affect the soil–pile interaction. These coefficients conclude material and geometry of the pile, properties of the soil, structural technique and experimenting process. As these coefficients possess various grades of impact on the capacity of the pile, they will be categorised into two classifications: primary and secondary factors. The primary factors have a substantial effect on the pile valence, while the secondary factors have a negligible effect.

3.4.2.1 The primary factors

Pile geometry

The geomechanical engineering resources show that the pile length and its diameter possess an essential effect on the bearing capacity of the pile. As a result, these factors have been chosen to present the geometry of the pile for the FEM's input.

Pile material

The friction amongst the neighbouring soil and the pile depends expressively on the external surface roughness of the pile that diverges with the material of the pile. Therefore, piles not constructed of the same materials (i.e. concrete or steel) possess diverse valence. While the database of current study contains two piles types (concrete and steel), the material of the pile should be considered. In contrast, in ABAQUS FEM, we only use the pile's Poisson's ratio and modulus of elasticity for each type of piles, which is 0.1 to 0.2 (take 0.2) and 25 GPa for concrete materials and 0.3 and 190 GPa to 215 GPa (take 200 GPa) for steel piles, respectively.

Average cone point resistance contained by the pile head-impact zone

Recent CPT-based approaches exert a correspondence coefficient to the middling cone tip resistance, q_c , and completed an assured zone recognised as the head-impact area to approximate the unity head resistance. Henceforth, the mean of q_c shows that the head-impact area has been involved as a changeable principal input. The penetration above that, the q_c is averaged and the averaging process is debated as follows:

The phrase of the impact zone states to the area spreads out for an interval downward and upward of the pile head, and in the zone, the defeat envelope can be located while the pile transports its ultimate head resistance. The levels and the system of the impact area around the head of forced pile rest on numerous coefficients such as the shearing resistance angle, volumetric strain, stiffness and the average operative stress of the pile head and the confined heterogeneity [219]. The interaction amongst the coefficients causes many problems and does not completely consistent. Therefore, researchers have proposed some forms of an influence zone, as presented in Figure 3-3.

There is no standard result amongst the investigators on the ranges of the impact area. Outcomes of the investigational and numerical researches on two concrete piles in intermediate dense sand performed have revealed that the head-impact zone developed starting 5D underneath to 5D overhead of the pile head [219]. A theoretic analysis indicates that in the homogeneous soil, the area can reach up to 1.5D underneath the pile head to 4 concluded 9D over the head [5]. Laterally, the area can spread to 5D. A study claimed that for piles in the clean sand, the impact zone over the pile head is in the middle of 1.5D up to 2.5D, and the area underneath the head of the pile varies between 3.5 and 5.5D [218]. There are, similarly, no general conclusion in the boundaries of the area amongst the present CPT-based techniques.

While considering the theoretical classifications and the existing results, in the current research and for minor-dimension piles, the levels of the impact zone may be assumed based on the description specified [5]. This assumption is made because for piles inside homogeneous soils, the description is specified by the technique with the explanation determined from the theoretical analyses, and for deep foundations in nonhomogeneous soils where no theoretical analyses are smeared, the description is established based on existing acts. Furthermore, the description which is set with the scheme counts for the heterogeneity of the soil that affects the levels of the head-impact area.

For large dimension piles, the model of the rapture area is expected to be similar to the impact area of the shallow foundation. In the mentioned circumstance, the characterisation stated is assumed [65].

Entirely CPT-created approaches show that defining a demonstrative significance for the cone point resistance, \bar{q}_{c-tip} , contained by the head-impact region is essential for computing the pile-unit head resistance. As soon as the unit head

resistance comes close to its final significance, the points lengthwise the rupture exterior, situated at the dissimilar lowest point, may have diverse friction angles or/and mobilised q_c significance to produce soil deviations and detaining stress. Therefore, cone resistance is essential for pile enterprise to consider for the differences of the soil features in most of the parts for unit head resistance [133]. The in-place of q_c is firm by being approximately the q_c amounts surrounded by the head rupture zone.

Three kinds of middling q_c values may be measured: arithmetic middling, geometric middling and weighted middling.

The arithmetic average is obtained from:

$$q_{c-arth} = \frac{q_{c1} + q_{c2} + \dots + q_{cn}}{n} \quad 3-39$$

Here, q_{c-arth} = arithmetic average of q_c amounts that varies from q_{c1} to q_{cn}

The geometric average is obtained from:

$$q_{c-geo} = \sqrt[n]{q_{c1} \cdot q_{c2} \cdot \dots \cdot q_{cn}} \quad 3-40$$

Here, q_{c-geo} = geometric average of amounts that vary from q_{c1} to q_{cn} .

The weighted average is obtained from:

$$q_{c-wetd} = \frac{\left(\frac{q_{c1} + q_{c2}}{2}\right) \Delta l_1 + \left(\frac{q_{c2} + q_{c3}}{2}\right) \Delta l_2 + \dots + \left(\frac{q_{cn-1} + q_{cn}}{2}\right) \Delta l_{n-1}}{\sum_{\Delta l=1}^{\Delta l=n-1} \Delta l} \quad 3-41$$

Here; q_{c-wetd} = weighted average of amounts that vary from q_{c1} to q_{cn}

Δl = length of the penetration section stuck between two consecutive q_c values

The arithmetic middling is convenient once mounts and furrows are disinterested from the information and likewise suitable for homogenous soil that amounts are uniform. The arithmetic middling is not considered in the current research

because most of the models in the databank include piles mounted in cohesionless soils. The CPT outcomes of this sort of soils typically comprise an enormous number of troughs and peaks that sort the arithmetic middling incorrectly an average value of q_c .

The geometric average is suitable once many severe troughs and peaks values are obtained, as may be originated for several sand deposits, and once governing significance is present amongst the together significances. Nevertheless, the geometric middling limitation is that if the composed values are small for a section of the deepness while being developed considerably higher for the other section, the geometric middling delivers unacceptable outcomes. In this circumstance, the weighted middling technique is improved, as it considers the average deepness values. The results in the following sample demonstrate that the geometric average and the weighted average of q_c amounts calculated inside the head-impact the region for a bored pile mounted in cohesionless soils (Case 13) a selection of the databank. The amounts of the pile head-impact region are presumed to develop for a region that is illustrated in Figure 3-16. The results show that the q_c amounts within the impact region stay small (ranging from 1 to 5 MPa) for a space of 6 metres of the region and then become much greater (ranging from 5 to 25 MPa) for a space of 8 metres of the region. The geometric middling of q_c amounts contained by the head-impact region is 5.6 MPa, although the weighted average is 10.3 MPa. Thus, the geometric middling is small and located close to the minor variety of q_c amounts, although there is a substantial total of high q_c values convoluted. The weighted middling, in contrast, is close to the average q_c values and accounts for the low-slung and the extraordinary variety q_c amounts. Therefore, for this issue, weighted average affords more proper demonstrations for the q_c than the geometric middling. Because numerous circumstances of this research in its databank are comparable to this case, the weighted middling technique is implemented.

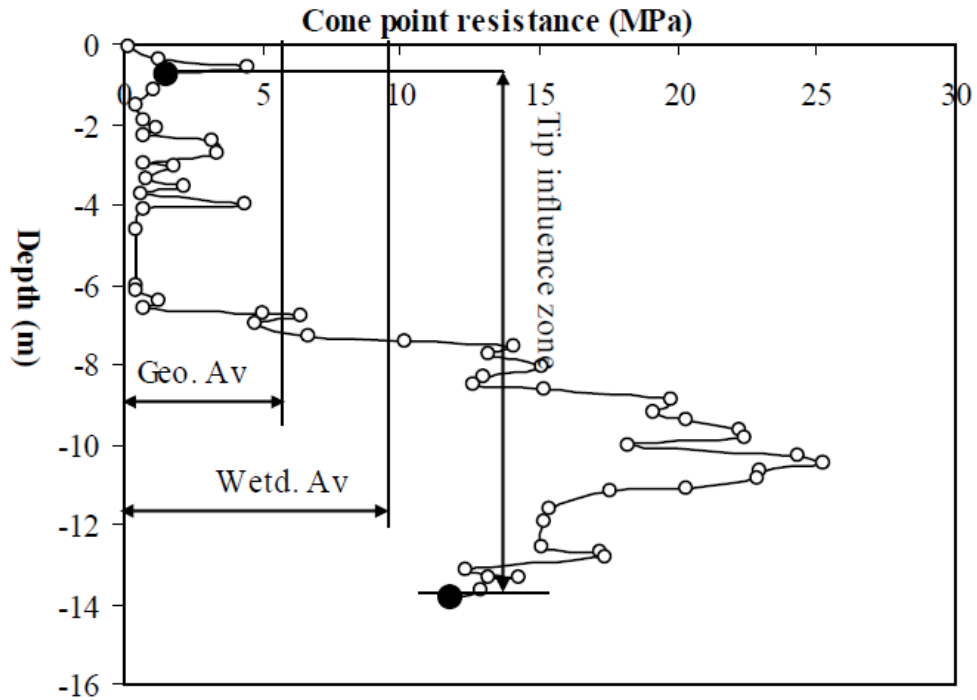


Figure 3- 8 Comparing averaging techniques for cone point resistance inside head-impact region (Source: [38])

Average cone spot resistance lengthwise the pile axle

Numerous CPT-based approaches (e.g. [65]; [9]; [167] and [220]) have suggested relationships to approximate the unit axle resistance from the middling point of cone resistance lengthwise axle of the pile. The procedures consider the q_c values to be more consistent for approximating pile shaft resistance. Consequently, this feature is applied by means of a changeable input.

Average sleeve friction lengthwise axle of the pile

Information of CPT-based techniques (i.e. [221] and [166]) have suggested representations to foresee unit axle resistance based on mediocre sleeve friction quantities f_s alongside pile axle. In contrast, other techniques (i.e. [65]; [168]) consider sleeve friction more adaptable than the cone dot resistance and thus do not focus on this resistance. In the current research, the friction of sleeve amounts was available in the database of the driven piles. Consequently, f_s affects the input variables, and its effect on the pile capability is confirmed in the sensibility analysis.

Calculated pile capacity

The pile capacity, Q_u , is another pattern output variable. For driven piles, the pile's capacity, Q_u , is shown in [5] as the immersion fracture, and for the clear failure samples and the 80% criterion of [222], the samples show that the fracture force is not obviously well-specified. For bored piles, the valence of pile, Q_u , agrees with [65] and indicates the vertical force at 5% of the pile diameter movement plus the elastic compression force of the pile (i.e. PL/EA where L is the length of embedded pile, P is the applied force, A is the pile cross-sectional area and E is the pile's elastic modulus). Figures 3-17 to 3-19 represent how the pile capacity is interpreted from load-assessment outcomes.

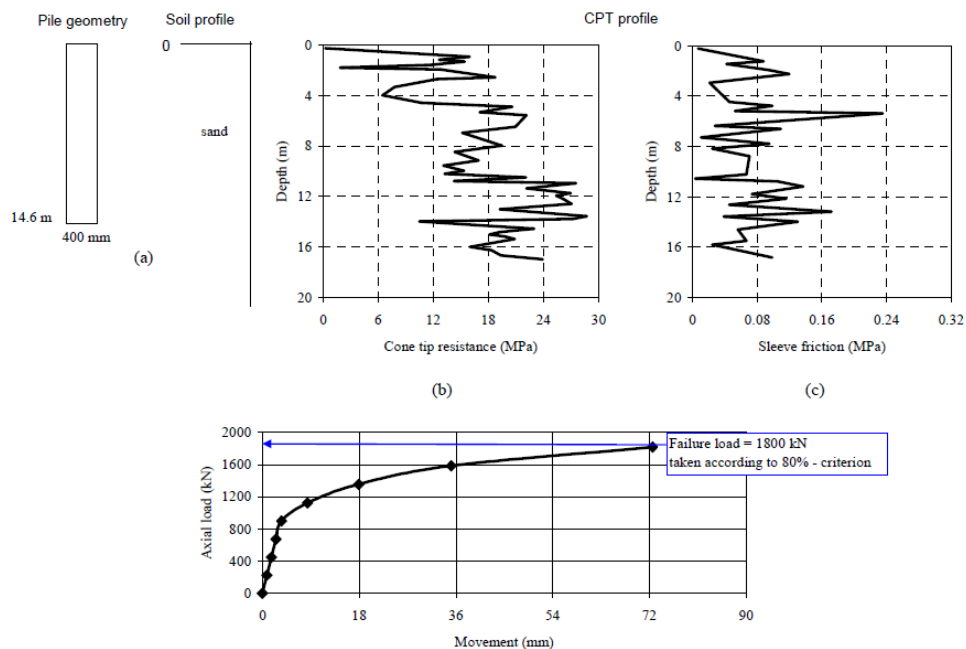


Figure 3- 9 Synopsis graph for driven steel pile sample data 15, (a) soil profile and pile geometry, (b) profile of cone head resistance, (c) profile of sleeve friction, (d) load–settlement plot (Source [38])

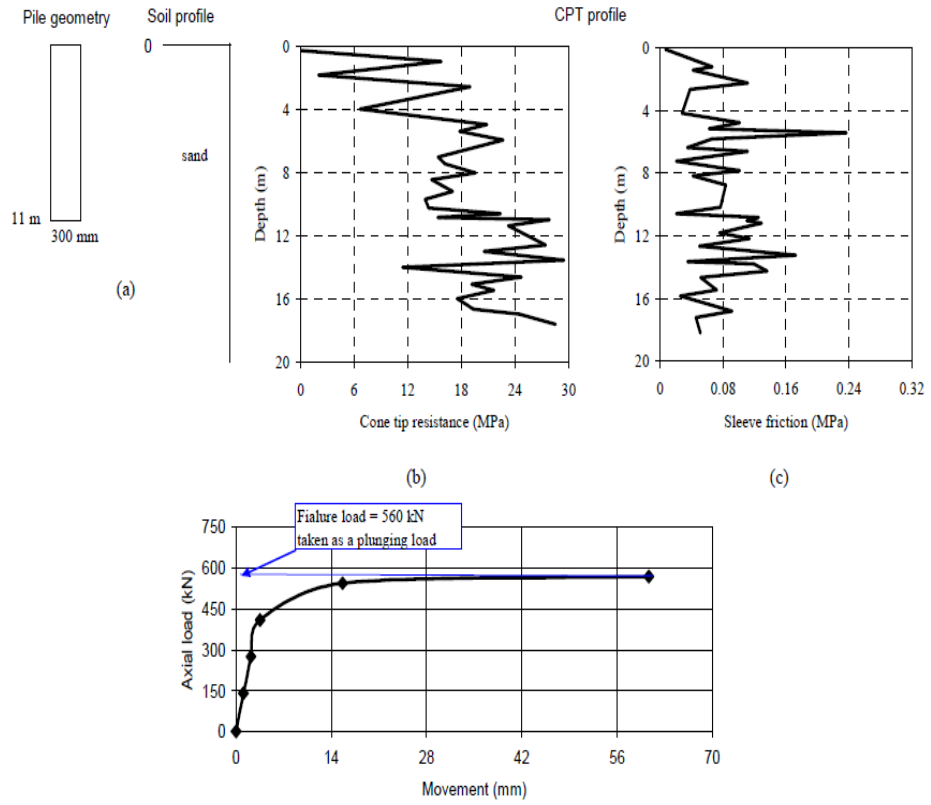


Figure 3- 10 Synopsis graph for driven steel pile sample data 1, (a) soil profile and pile geometry, (b) profile of cone head resistance, (c) profile of sleeve friction, (d) load–settlement plot (Source [38])

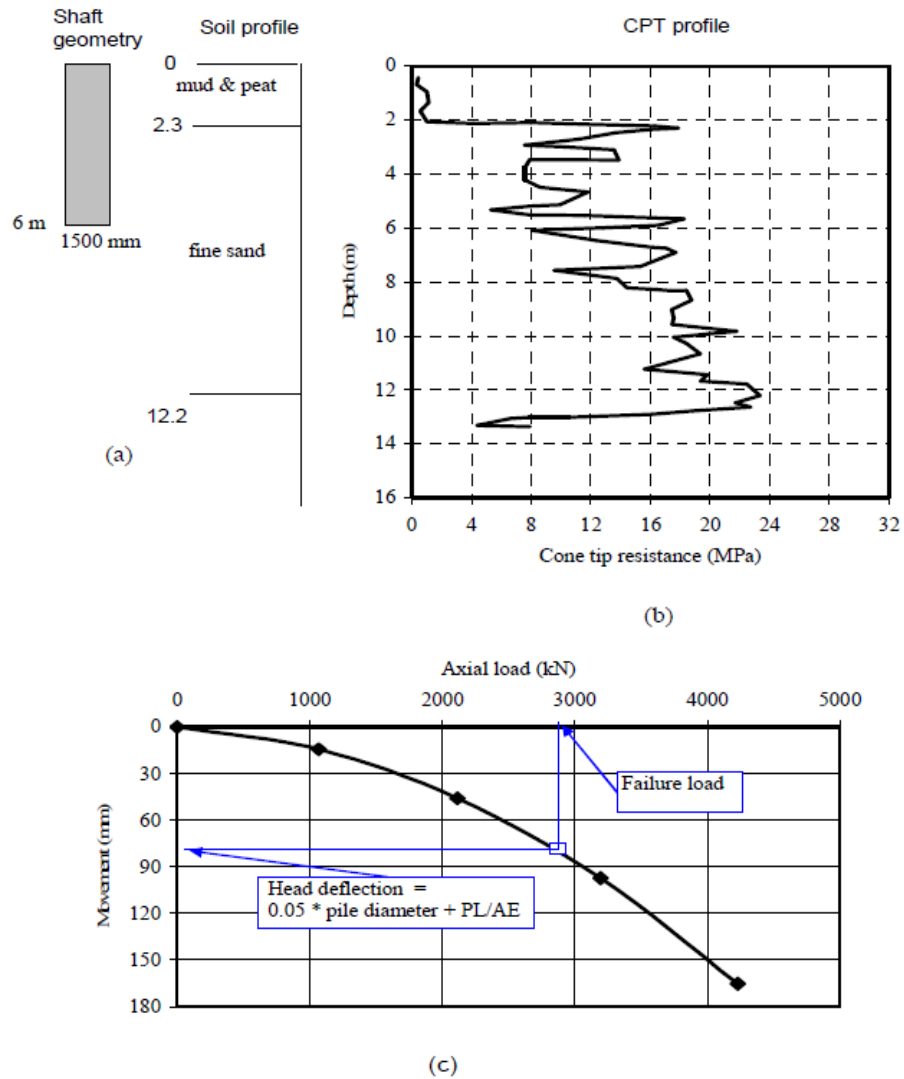


Figure 3- 11 Synopsis graph for the bored pile sample data 45, (a) soil profile and pile geometry, (b) profile of cone head resistance, (c) profile of sleeve friction, (d) load–settlement plot (Source [38])

Soil's modulus of elasticity

To obtain the modulus of elasticity for different types of soil, the following table is used based on the recommendations in [3].

Table 3- 7 Young's modulus (MPa) values concerning different soil types and degrees of consolidation (Source [3])

Soil Type	Modulus of Elasticity Range
Sand, normally consolidated	$(2 - 4)q_c$
Sand, over-consolidated	$(6 - 30)q_c$
Sand, Clayey (SC)	$(3 - 6)q_c$
Sand, silty (SM)	$(1 - 2)q_c$
Clay, soft	$(3 - 8)q_c$

Soil's friction angle

Friction angle of soil is the shear strength value soils. Its description is obtained from the failure criteria of Mohr–Coulomb, and it is used to define the soil's friction shear resistance composed by the standard adequate stress. In the shear normal stress-effective stress plane, the friction angle of the soil is the angle of inclination concerns the Mohr–Coulomb shear resistance line's lateral axis. Some typical amounts of friction angle of soil are given in Table 3-8 for different soil types of USCS at a normally consolidated situation or else if not identified. These amounts must be used just as a guideline for geomechanical subjects; nevertheless, a definite condition of each engineering issue regularly needs to be considered for an adequate selection of geomechanical factors.

Table 3- 8 Typical amounts of friction angle of soil for different soils agreeing to USCS (Source [223])

Description	USCS	Soil friction angle (°)		
		min	max	Specific value
Well graded gravel, sandy gravel, with little or no fines	GW	33	40	
Poorly graded gravel, sandy gravel, with little or no fines	GP	32	44	
Sandy gravels - Loose	(GW, GP)			35
Sandy gravels - Dense	(GW, GP)			50

Silty gravels, silty sandy gravels	GM	30	40	
Clayey gravels, clayey sandy gravels	GC	28	35	
Well graded sands, gravelly sands, with little or no fines	SW	33	43	
Well-graded clean sand, gravelly sands - Compacted	SW			38
Well-graded sand, angular grains - Loose	SW			33
Well-graded sand, angular grains - Dense	SW			45
Poorly graded sands, gravelly sands, with little or no fines	SP	30	39	
Poorly-graded clean sand - Compacted	SP			37
Uniform sand, round grains - Loose	SP			27
Uniform sand, round grains - Dense	SP			34
Sand	SW, SP	37	38	
Loose sand	SW, SP	29	30	
Medium sand	SW, SP	30	36	
Dense sand	SW, SP	36	41	
Silty sands	SM	32	35	
Silty clays, sand-silt mix - Compacted	SM			34
Silty sand - Loose	SM	27	33	
Silty sand - Dense	SM	30	34	
Clayey sands	SC	30	40	
Clayey sands, sandy-clay mix - compacted	SC			31
Loamy sand, sandy clay Loam	SM, SC	31	34	
Inorganic silts, silty or clayey fine sands, with slight plasticity	ML	27	41	
Inorganic silt - Loose	ML	27	30	

Inorganic silt - Dense	ML	30	35	
Inorganic clays, silty clays, sandy clays of low plasticity	CL	27	35	
Clays of low plasticity - compacted	CL			28
Organic silts and organic silty clays of low plasticity	OL	22	32	
Inorganic silts of high plasticity	MH	23	33	
Clayey silts - compacted	MH			25
Silts and clayey silts - compacted	ML			32
Inorganic clays of high plasticity	CH	17	31	
Clays of high plasticity - compacted	CH			19
Organic clays of high plasticity	OH	17	35	
Loam	ML, OL, MH, OH	28	32	
Silt Loam	ML, OL, MH, OH	25	32	
Clay Loam, Silty Clay Loam	ML, OL, CL, MH, OH, CH	18	32	
Silty clay	OL, CL, OH, CH	18	32	
Clay	CL, CH, OH, OL	18	28	
Peat and other highly organic soils	Pt	0	10	

Soil's dilation angle

Dilation angle was associated with some resources as the friction angle subtracted by 30 or $\frac{2}{3}$ of the friction angle. The dilation angle can vary from 5°–15° and can be checked by the range based on the type of soil. The dilation angle was considered for sand during the analysis and was close to the friction angle.

Furthermore, the dilation angle considered in the present research was correspondingly compared to [224], and dilation angles were found to be marginally less than [224]. The dilation angles derived according to the [224] method for loose, dense, medium dense and dense sands are 6°, 12° and 10°, respectively.

3.4.2.2 The secondary factors

These factors contain a smaller amount of grade of influence amongst the factors that impact the pile's bearing capability. They contain pile head (closed or open), pile shape, depth of the water table and the pile construction technique.

The greatest of the presently obtainable CPT-based approaches do not combine any factors for presenting the shape consequence of the pile. Research to predict the settlement of pile has illustrated that the shape of the pile has a negligible effect on pile efficiency; the research has also presented that the open-ended or closed head contains an alike and insignificant impact on the movement of the pile ([171]). As a result, these factors have not been involved in input variables. The water table's deepness did not exist in the bored piles' records; however, in several driven piles cases, the water table was delivered using the CPT index. The table shows that the water, therefore, affects all q_c values.

3.5 SUMMARY OF THE CHAPTER

In this section of the thesis, the methodology of this study was presented. In the first section, the experiential CPT method and its definitions and backgrounds, including methods of estimating pile's bearing capacity and settlement prediction, were

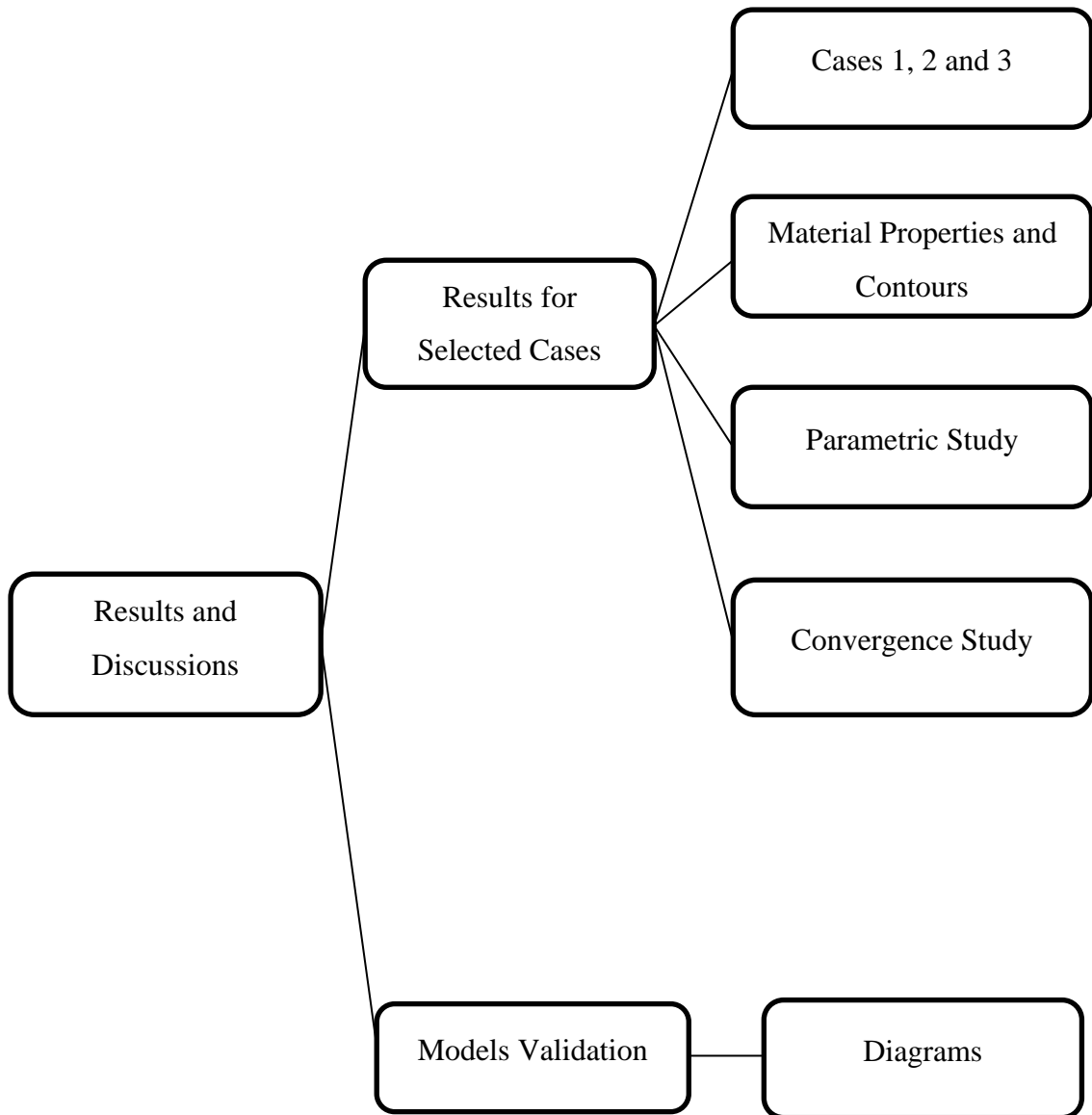
described. This section was followed by methods of data collection. Then, some of the input variables associated with this study were described. In the following chapter, the results of numerical method models, simulated by ABAQUS software based on pre-calculated experimental outcomes, are presented.

4

Investigation of Pile Behaviour and Parametric Studies

4.1 INTRODUCTION AND CHAPTER OVERVIEW

This chapter presents a comparison of the results from CPT tests due to various loading types and piles obtained from the literature ([38]) as well as findings from numerical simulations ABAQUS finite element software. The CPT tests and numerical simulations were carried out on different types of soil and pile. In the first section, the research approach will be discussed for three different types of proposed piles in the respective soil profile. It would be achieved by presenting visual and numerical results. Moreover, the sensitivity of modulus of elasticity parameter for each case will be discussed. Then, numerical test results will be presented, including 108 different piles in different soil profiles. Then, the validity of the obtained numerical results will be investigated. The overview of the chapter is illustrated below.



4.2 RESULTS AND DISCUSSION FOR SELECTED PILES

4.2.1 Case 1 Profile

In this section, the method of simulating three pile cases will be investigated. To achieve this, we need to input variables like modulus of elasticity for pile and soil, etc. that were discussed in chapter three (Methodology). In this part, three different cases with different properties and types will be investigated.

For bored piles, case number 21 from literature has been chosen. This model is a sample model from source [65], which is described in Table A-1. The pile is a square closed pile with 0.231 m^2 area, 521 mm diameter and 8200 mm length. Type of loading is CRP or constant rate of penetration. Type of cone in CPT experiment for this case is mechanical, which is convertible to electrical cone result and discussed in chapter 2 of this study. An overview of shaft geometry, soil profile, CPT profile and the respective load-deflection diagram has been presented in figure 4-1. As can be seen, there is a massive differential in soil properties when we passed 5.3m of shaft depth and soil changed to gravelly sand.

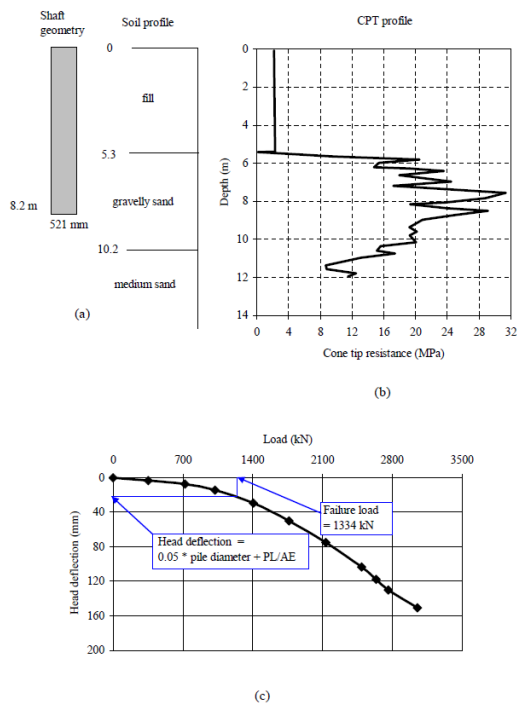


Figure 4- 1 Summary sheet for case record A21, (a) pile geometry and soil profile, (b) cone tip resistance profile, (c) load deflection plot

4.2.2 Case 2 Profile

For concrete driven piles, case number 17 from the source above has been selected. A brief description has been given in Table B-1 that shows this pile is a square closed sample with 0.292 m^2 area, 1020 mm length and 355 mm diameter and type of loading is QML or quick maintained load test. The type cone of in this case is electrical, which we do not need to convert from mechanical test results, as mentioned above. A brief review of CPT axle and soil geometry, cone tip resistance, sleeve friction profile and determined load-deflection diagram has been demonstrated in figure 4-2. It is evident that the mixed soil performance has complexity in this case and need more attention and time in simulating. The pile is embedded in 2 m silt soil as well as 4 m in the normal sand and the rest in dense sand soil. As it was mentioned before, we have the sleeve friction profile as well as other information in driven piles.

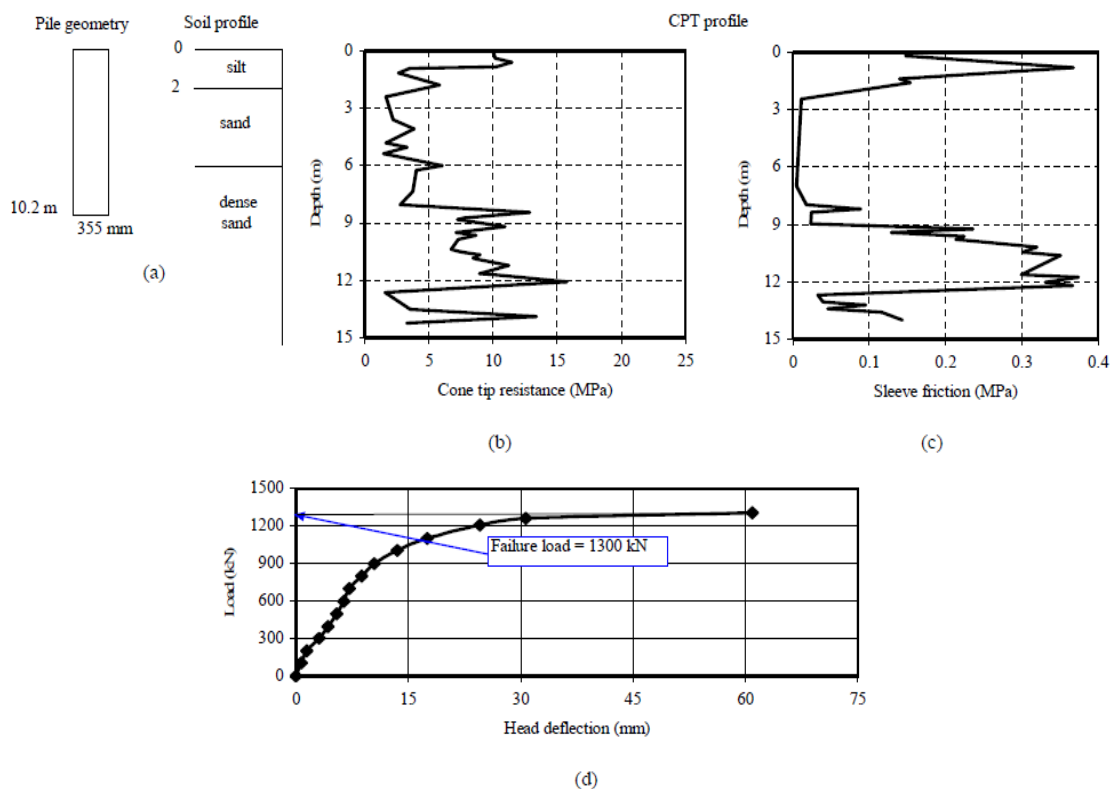


Figure 4- 2 Summary sheet for case record B17, (a) pile geometry and soil profile, (b) cone tip resistance profile, (c) sleeve friction profile, (d) load deflection plot

4.2.3 Case 3 Profile

For steel driven piles, case number 17 from the above source above has been selected. A brief description has been given in Table C-1 that shows this pile is a pipe closed sample with 0.059 m^2 area, 9200 mm length and 273 mm diameter and type of loading is SML or slow maintained load test. The type cone of in this case is electrical, which we do not need to convert from mechanical test results, as mentioned in case 1. A brief review of CPT axle and soil geometry, cone tip resistance, sleeve friction profile and determined load-deflection diagram has been demonstrated in figure 4-3. The pile is embedded in 2 m filled soil as well as 7.2 m in the hydraulic sand. As it was mentioned before, we have the sleeve friction profile as well as other information in driven piles.

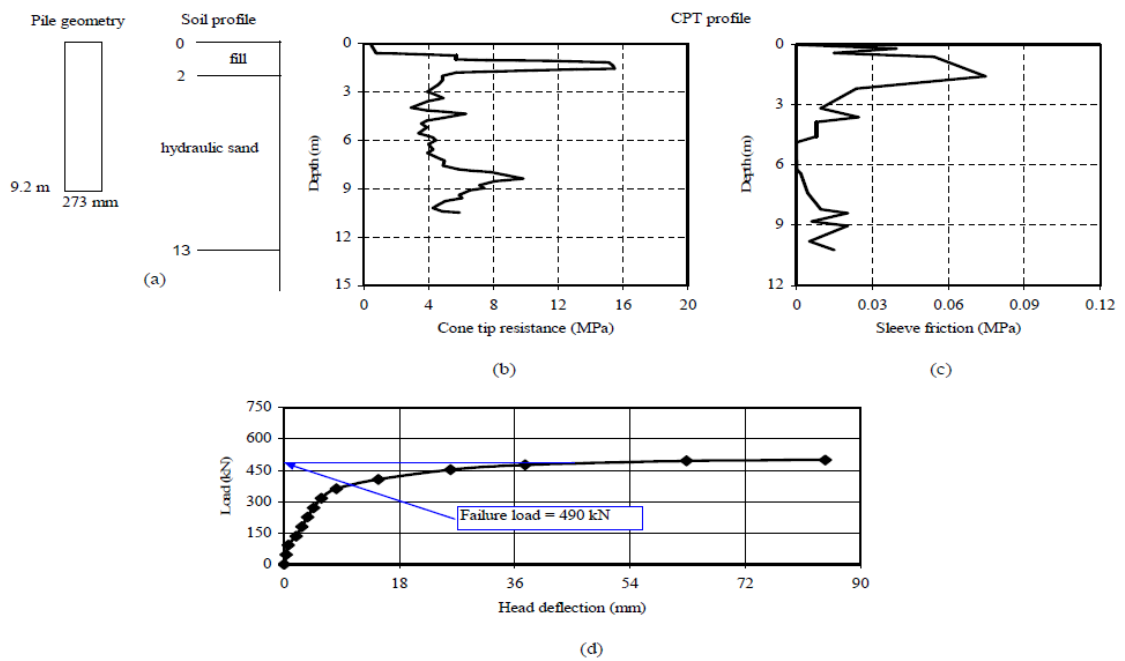


Figure 4- 3 Summary sheet for case record B17, (a) pile geometry and soil profile, (b) cone tip resistance profile, (c) sleeve friction profile, (d) load deflection plot

4.2.4 Description of Material properties in ABAQUS

In the model in ABAQUS.CAE subsequent explanations are used in describing material properties of existing project based on Drucker-Prager and Mohr-Coulomb simulations.

- The shear criterion parameter was set to linear and hyperbolic.
- The symmetrical solver was defined as *STEP, SYMM=YES for plastic flow rule as associated.
- For the elastic phase, young's modulus was set based on table 3-7.
- Based on the USA Army Stan Standard, the maximum friction angle between soil and concrete pile should be less than 27° and maximum tangential behaviour is 0.5.
- The Drucker-Prager plasticity selections were utilised to state β , ϵ and K , the flow potential eccentricity parameter was used as $\epsilon = 0.1$.
- The Drucker-Prager hardening preference was similarly defined as *Drucker-Prager Hardening 100000, 0 in which 100000 is yield stress and 0 is a plastic strain at failure.

4.2.5 Result Contours for Three Base Models

After running selected models in ABAQUS, several result contours can be obtained from outcome data in the software package, which some of the most important ones selected to illustrate results in visual presentation. Based on selected contours, definition of some terms will be determined.

A form of strain in which the distorted body returns to its original shape and size when the deforming force is removed is elastic strain. Strain is the response of a system to an applied stress. When a material is loaded with a force, it produces a stress, which then causes a material to deform. Engineering strain is defined as the amount of deformation in the direction of the applied force divided by the initial length of the material. Recall if a material experiences only elastic deformation, when the stress is removed the elastic strain will be recovered. If a material is loaded beyond its yield point it experiences both elastic and plastic strain. When the stress is removed, only the elastic strain is recovered; the plastic strain is permanent. This change in shape is called deformation. A temporary shape change that is self-reversing after the force is

removed, so that the object returns to its original shape, is called elastic deformation. When the stress is sufficient to permanently deform the metal, it is called plastic deformation.

The effective stress principle in soil engineering is one of the important theories put forward by Karl Terzaghi in the year 1936. It is the difference between total stress and pore water pressure. Effective stress is a force that keeps a collection of particles rigid. Usually this applies to sand, soil, or gravel. The principle of effective stresses applies only to normal stresses and not shear stresses. Total stress (σ) is equal to the sum of effective stress (σ') and pore water pressure (u) or, alternatively, effective stress is equal to total stress minus pore water pressure. The total stress is the sum of the weight of the soil up to the surface and the weight of water above this: Vertical total stress at depth z , $s_v = g \cdot z + g_w \cdot z$. More specifically, Karl von Terzaghi's Principle, also known as Terzaghi's theory of one-dimensional consolidation, states that all quantifiable changes in stress to a soil [compression, deformation, shear resistance] are a direct result of a change in effective stress.

Above-mentioned terms are presented in below contours to show principals in deformed soil under force on pile. It needs to be mentioned that units for visualisations are N and m.

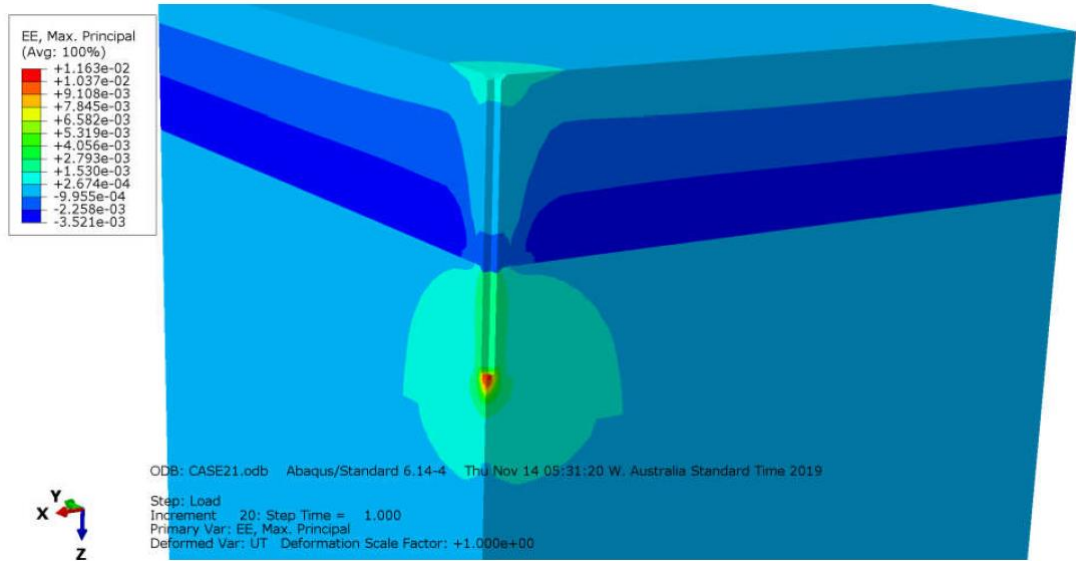


Figure 4- 4 Case 1, elastic strain (maximum principal) – loading step – on soil

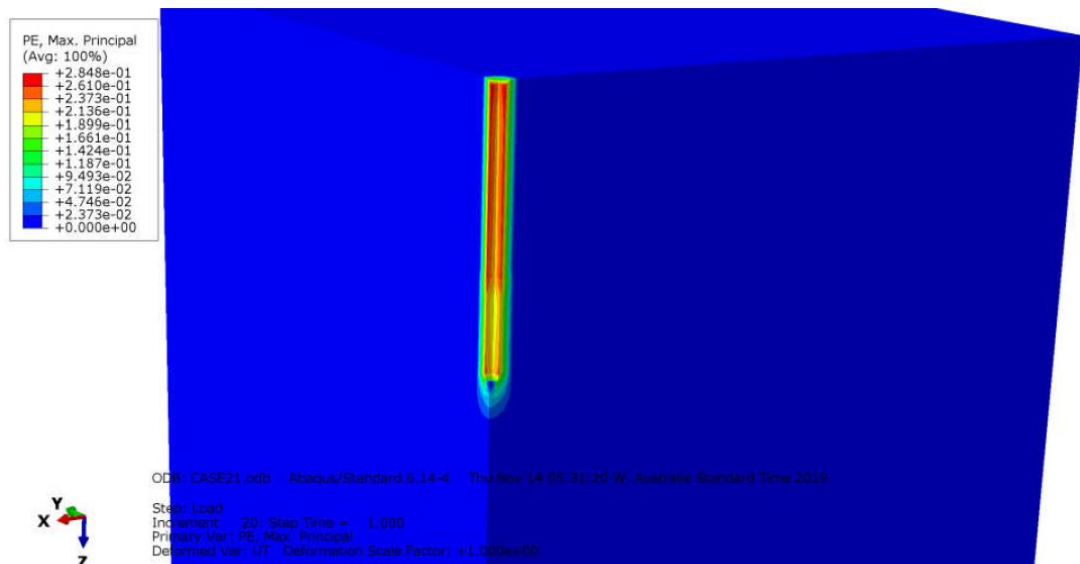


Figure 4- 5 Case 1, plastic strain (maximum principal) – loading step – on soil

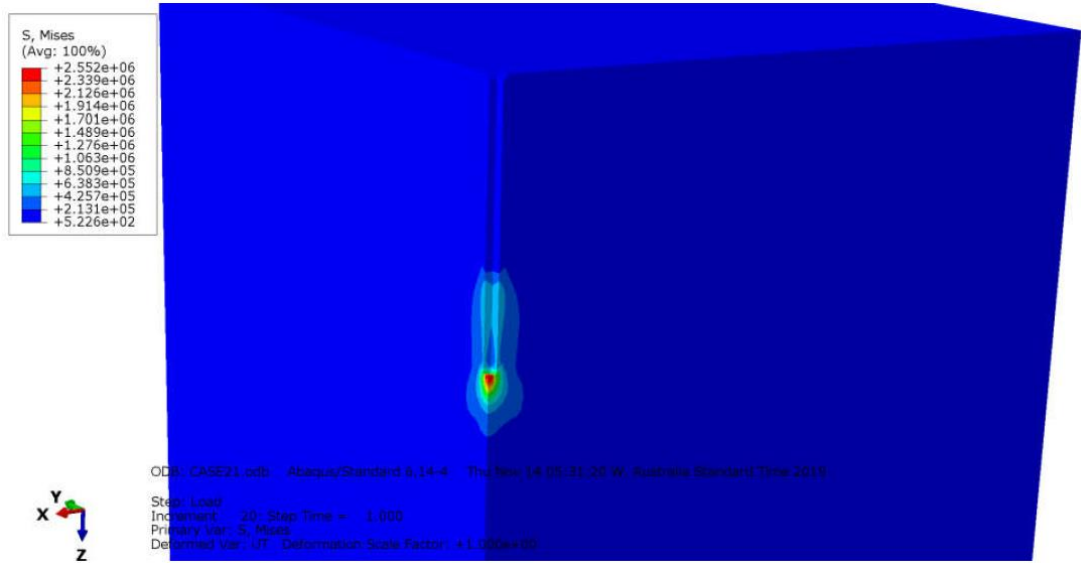


Figure 4- 6 Case 1, total stress – loading step – on soil

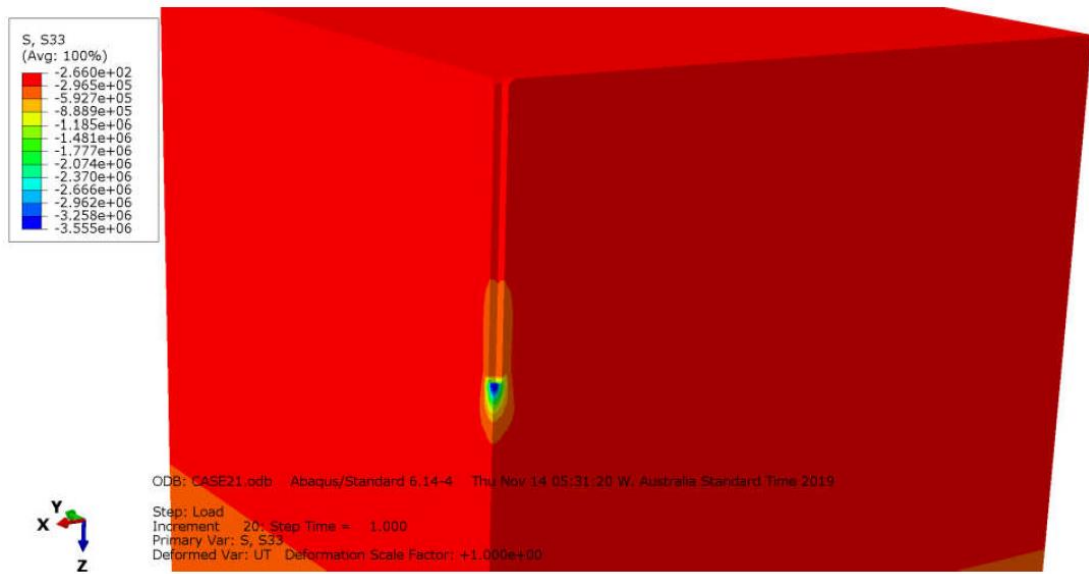


Figure 4- 7 Case 1, vertical stress – loading step – on soil

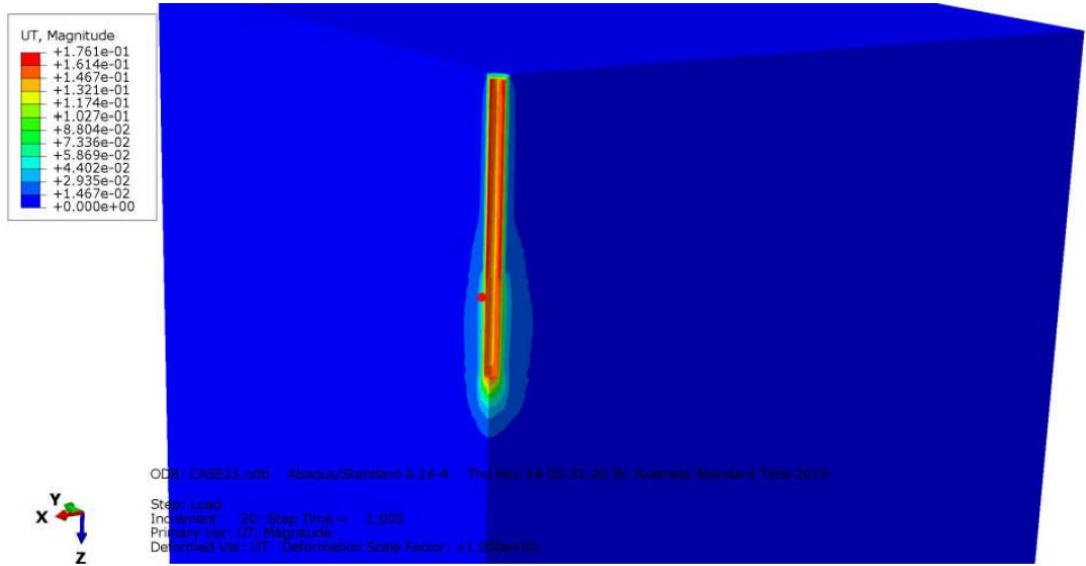


Figure 4- 8 Case 1, total displacement magnitude – loading step – on soil

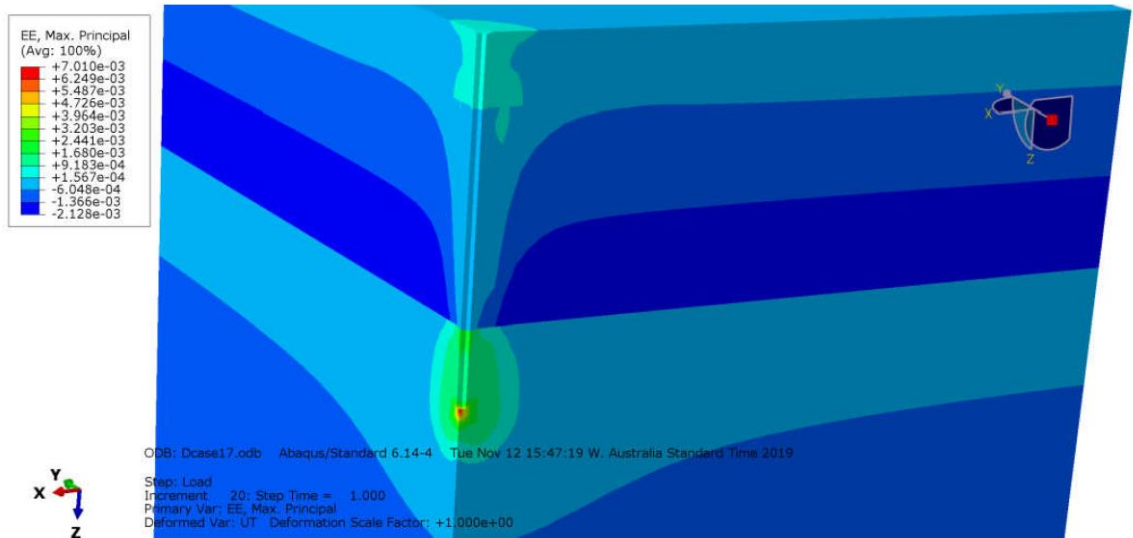


Figure 4- 9 Case 2, elastic strain (maximum principal) – loading step – on soil

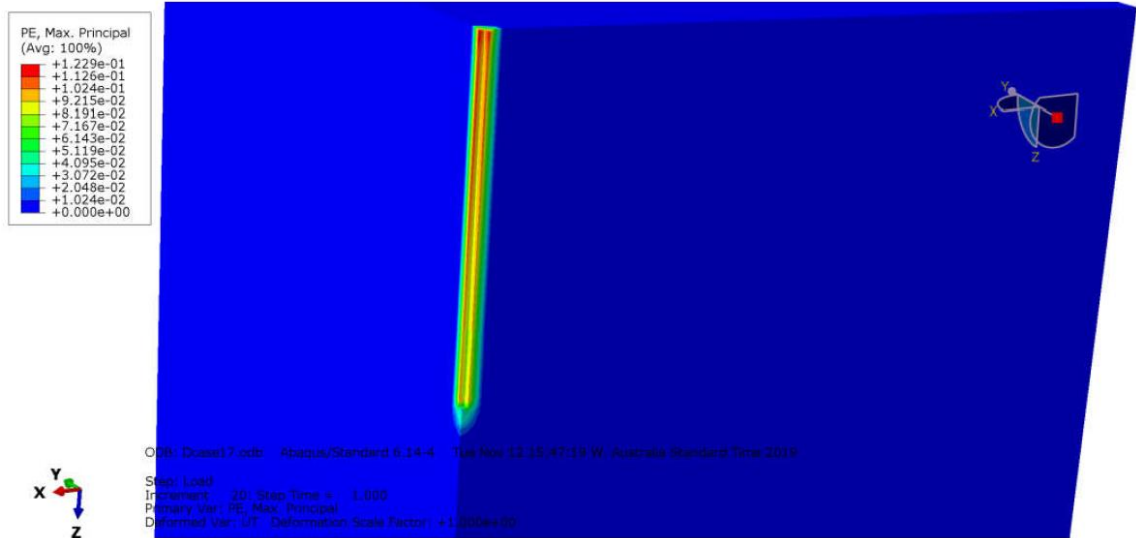


Figure 4- 10 Case 2, plastic strain (maximum principal) – loading step – on soil

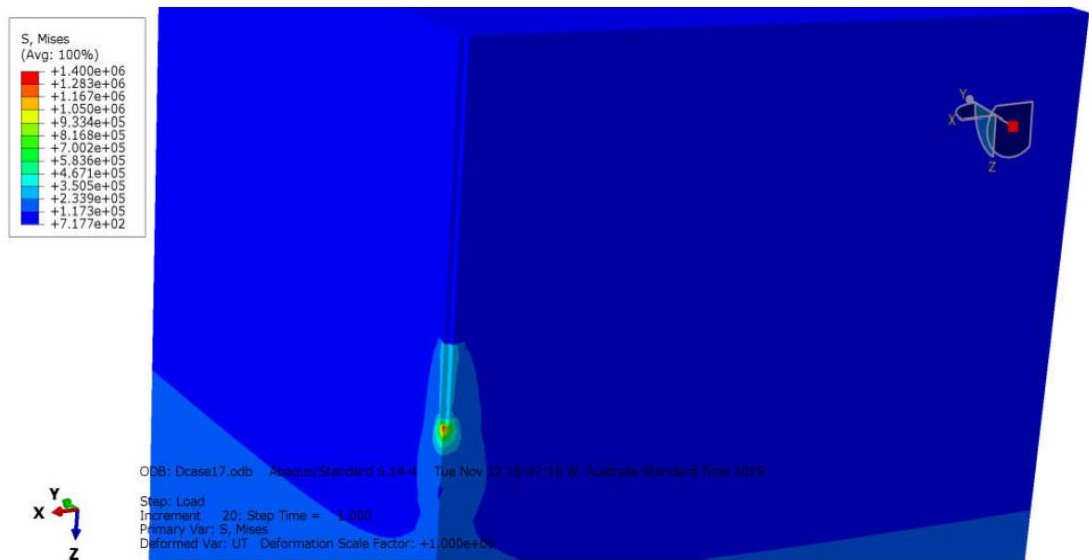


Figure 4- 11 Case 2, total stress – loading step – on soil

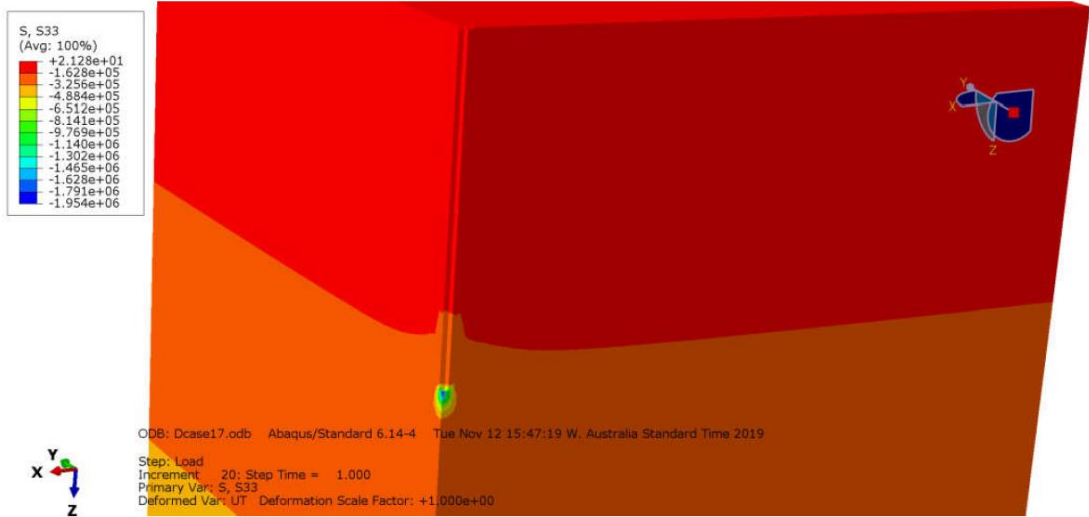


Figure 4- 12 Case 2, vertical stress – loading step – on soil

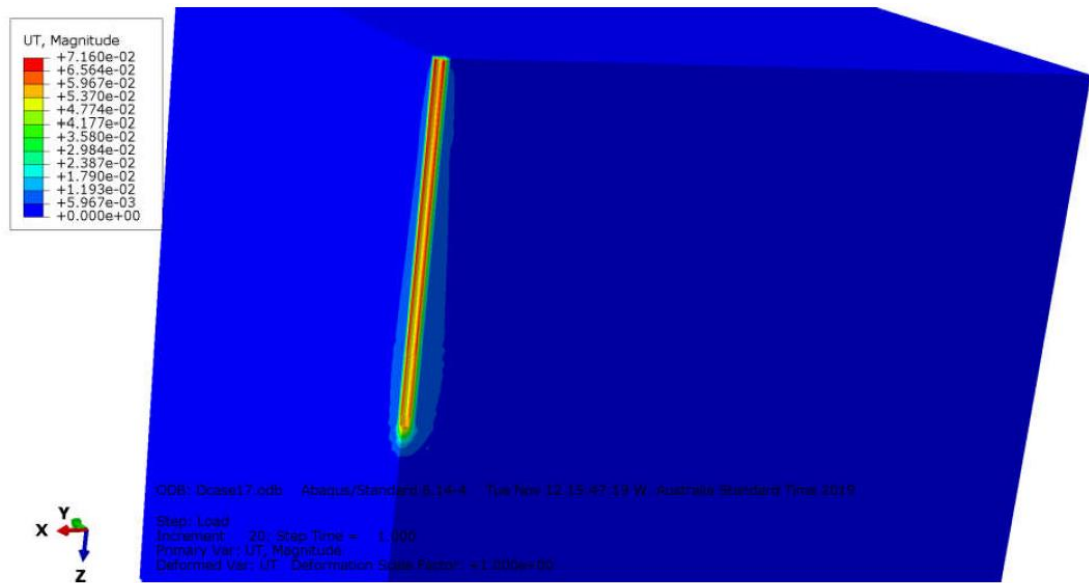


Figure 4- 13 Case 2, total displacement magnitude – loading step – on soil

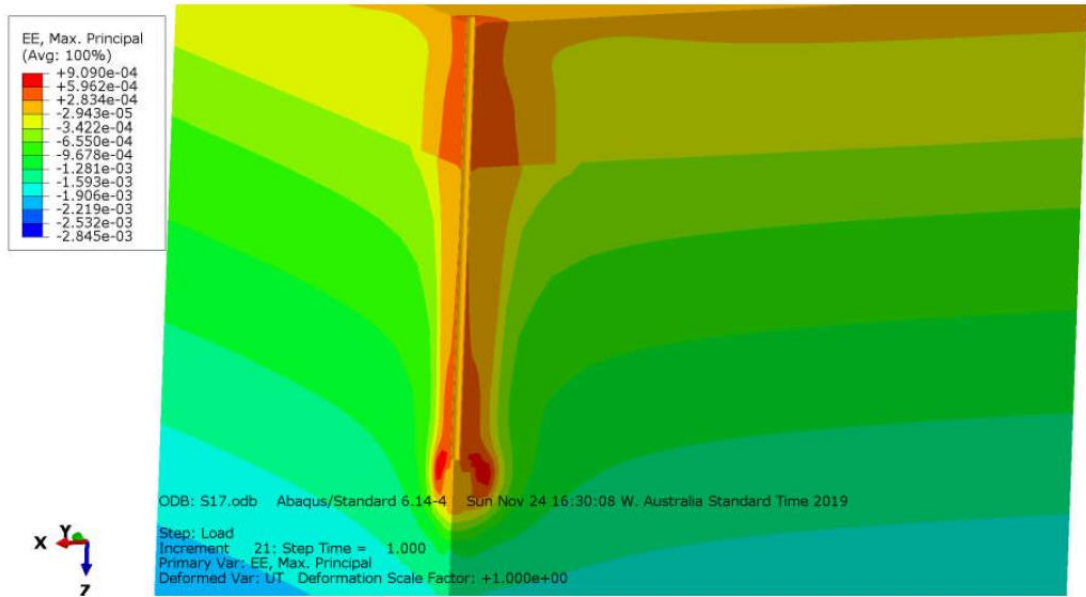


Figure 4- 14 Case 3, elastic strain (maximum principal) – loading step – on soil

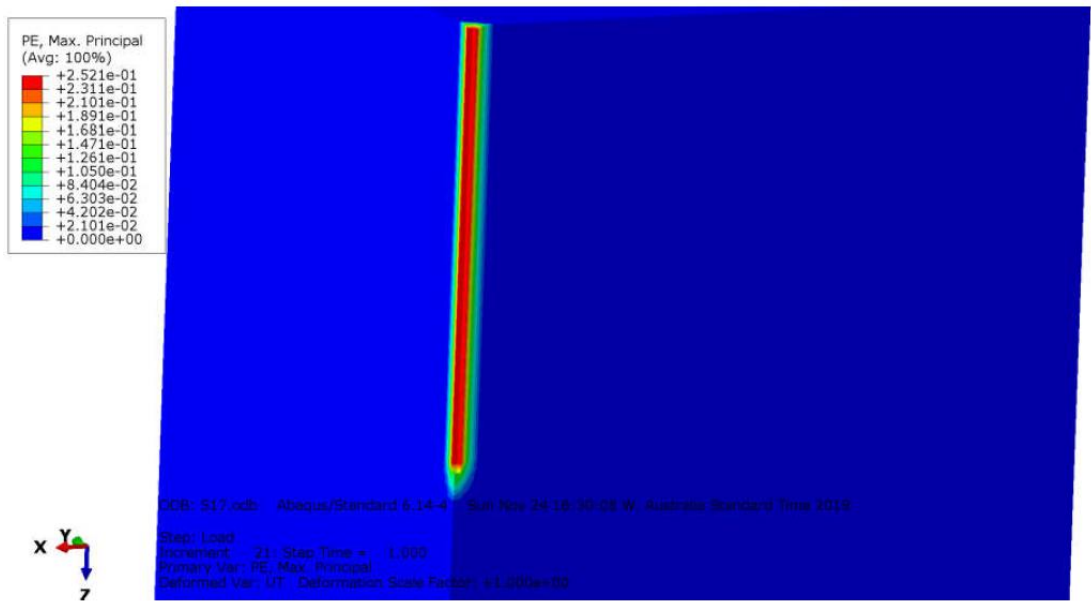


Figure 4- 15 Case 3, plastic strain (maximum principal) – loading step – on soil

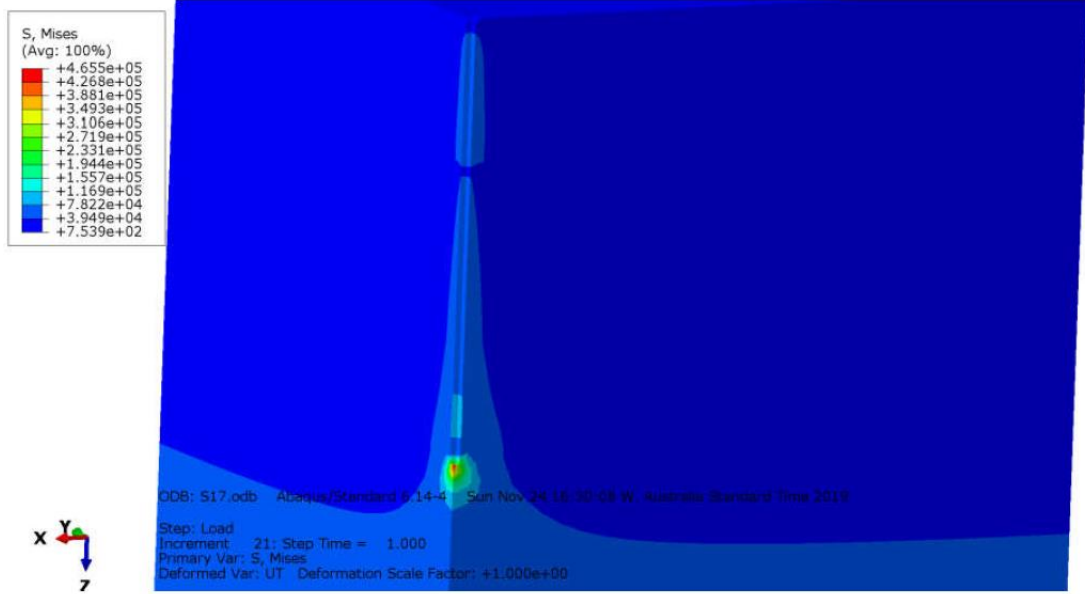


Figure 4- 16 Case 3, total stress – loading step – on soil

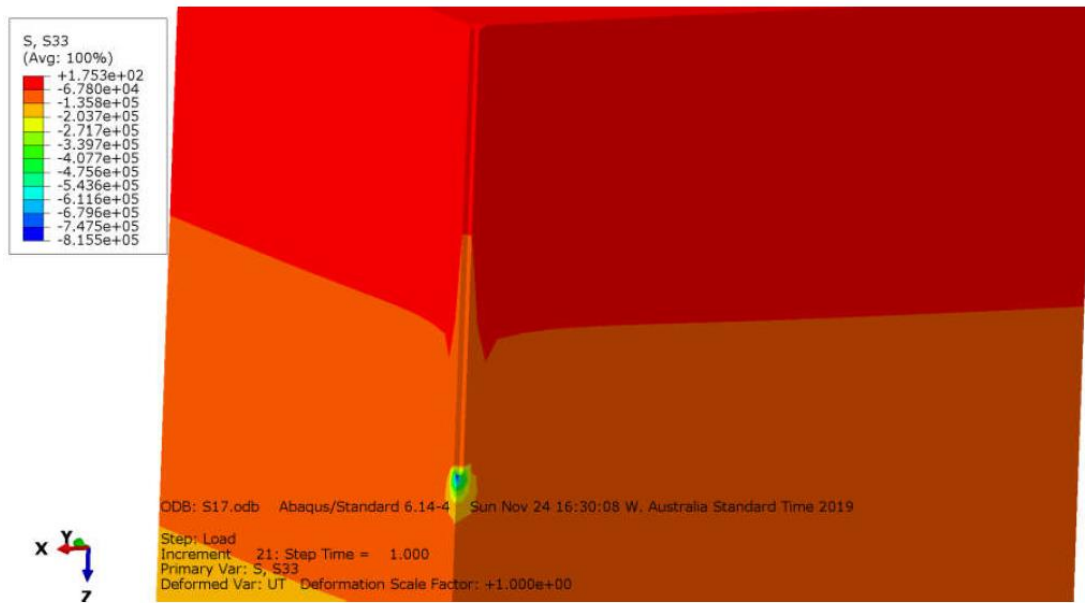


Figure 4- 17 Case 3, vertical stress – loading step – on soil

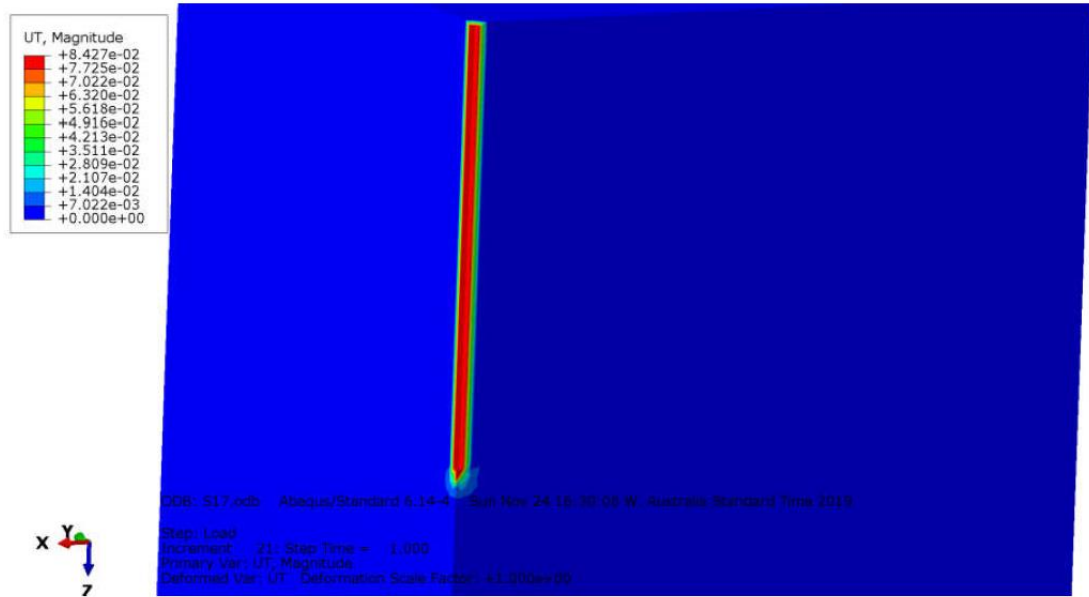


Figure 4- 18 Case 3, total displacement magnitude – loading step – on soil

4.2.6 Parametric Study

In this section of the study, the sensitivity of the proposed models to different values of young's modulus will be carried out. Table 3-7, shows different amounts for E respect to the soil type. Figures 4-19 to 4-21 show the effect of changing Young's modulus and friction angle to the shear stress between alongside the pile, which present the interaction of soil and foundation and load transfer mechanism.

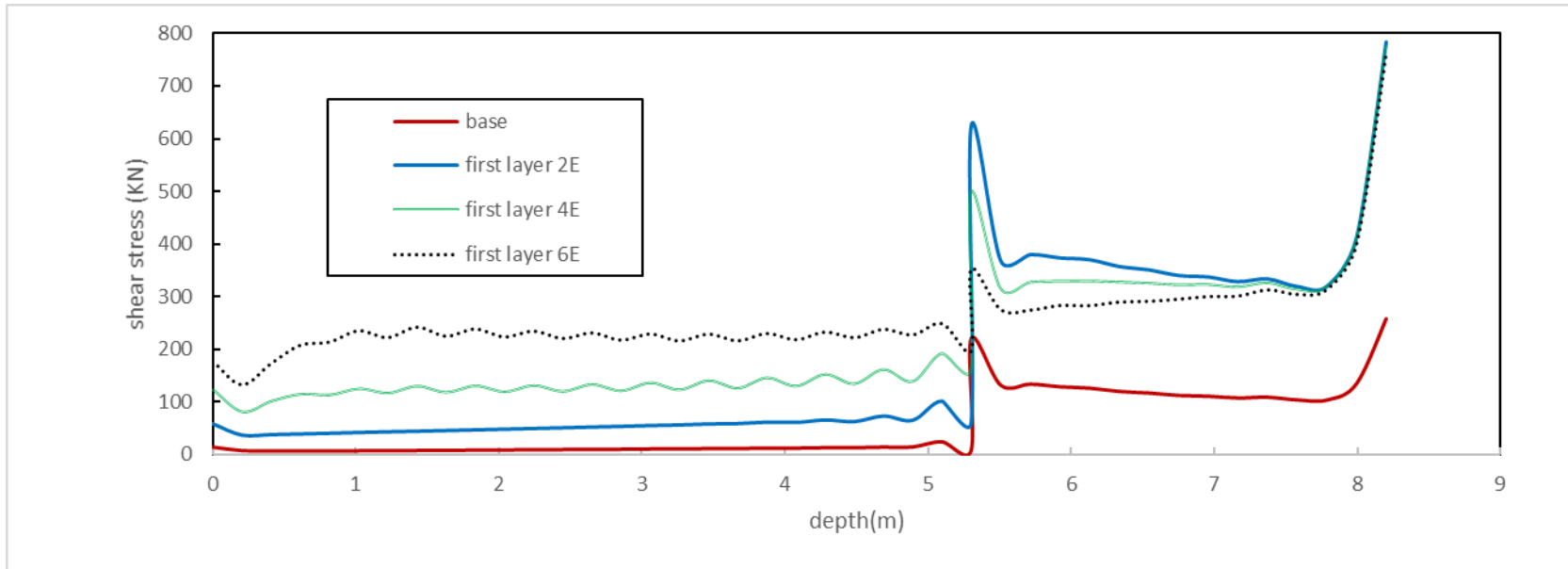


Figure 4- 19 Parametric study for case 1

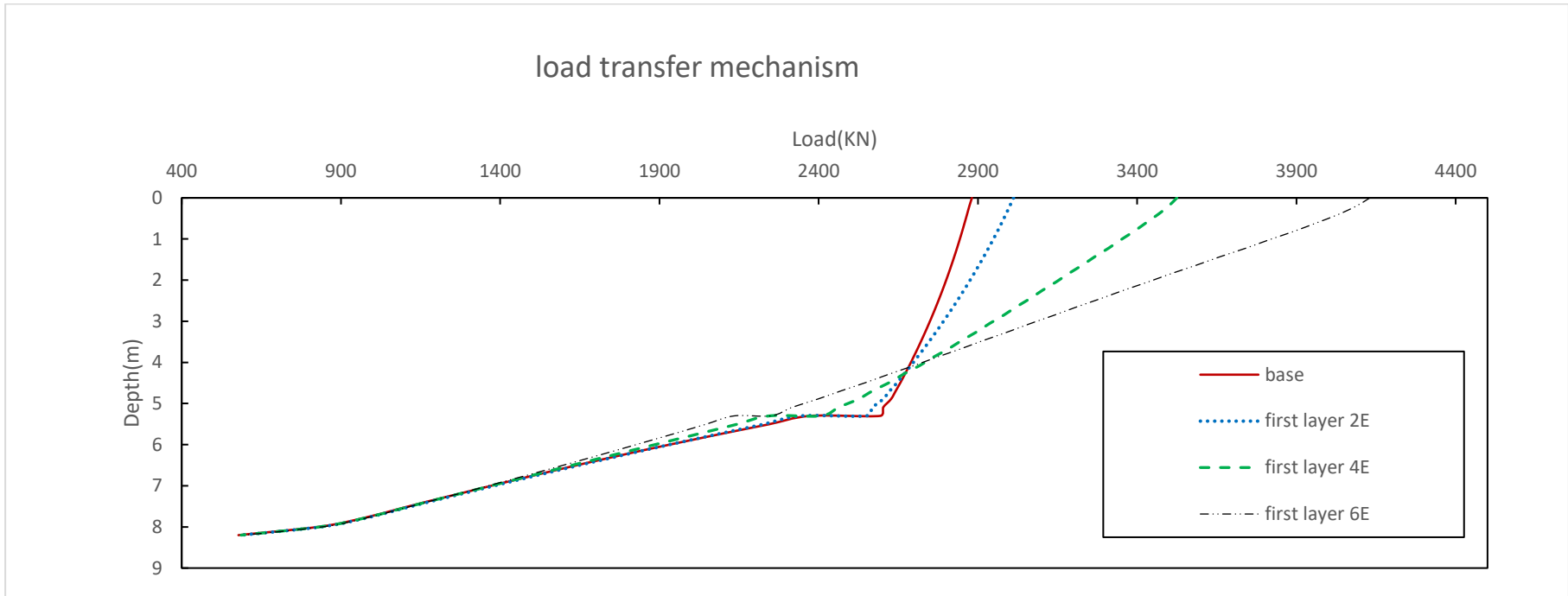


Figure 4- 20 Load transfer mechanism study for case 1

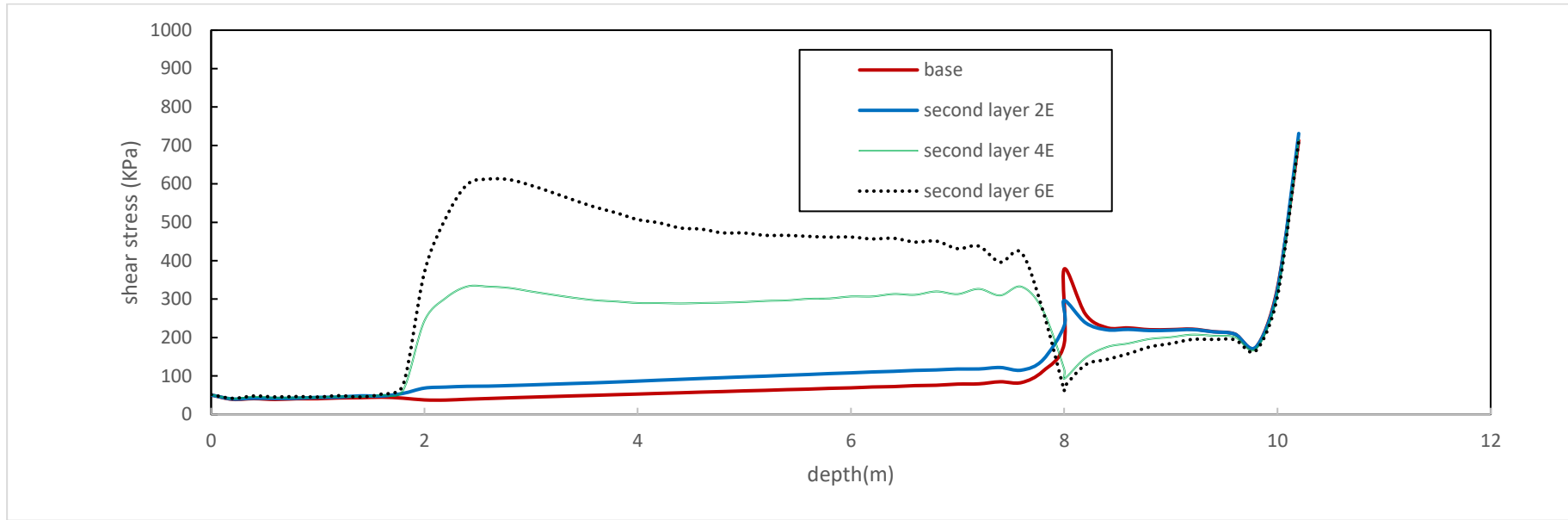


Figure 4- 21 Parametric study for case 2

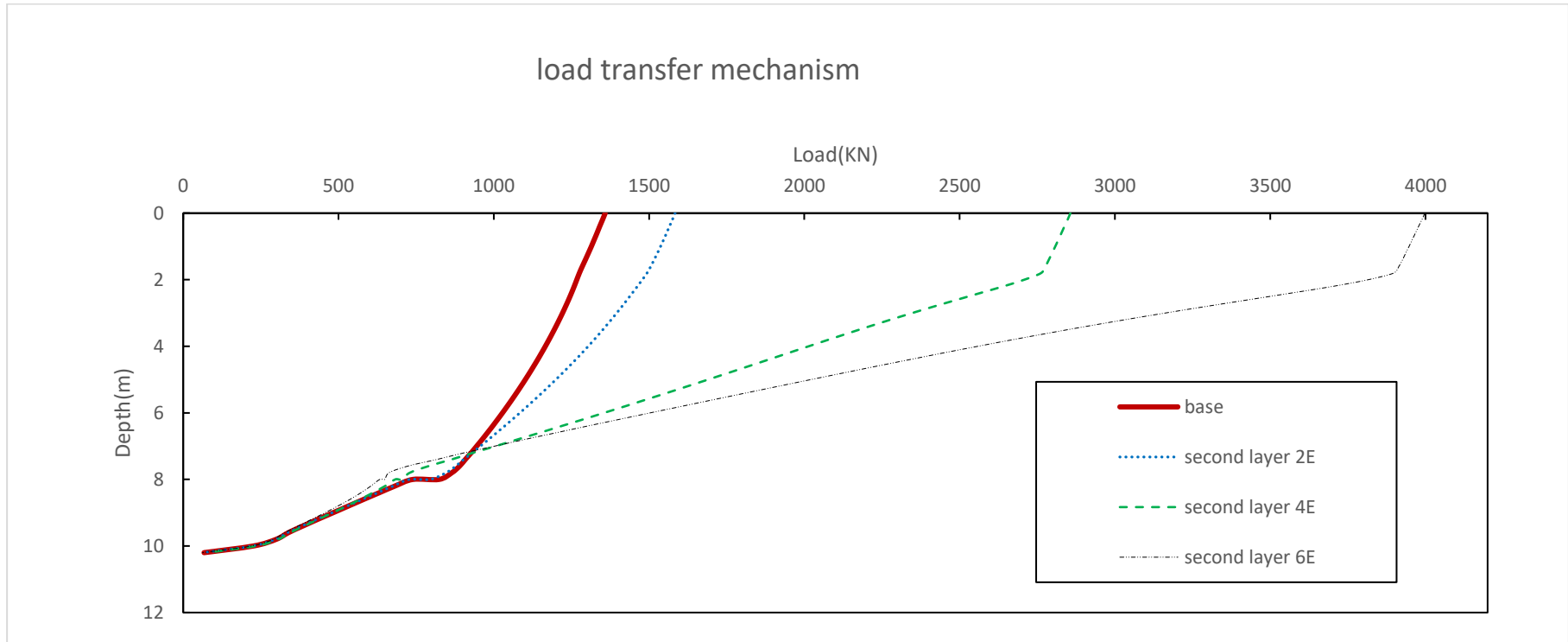


Figure 4- 22 Load transfer mechanism study for case 2

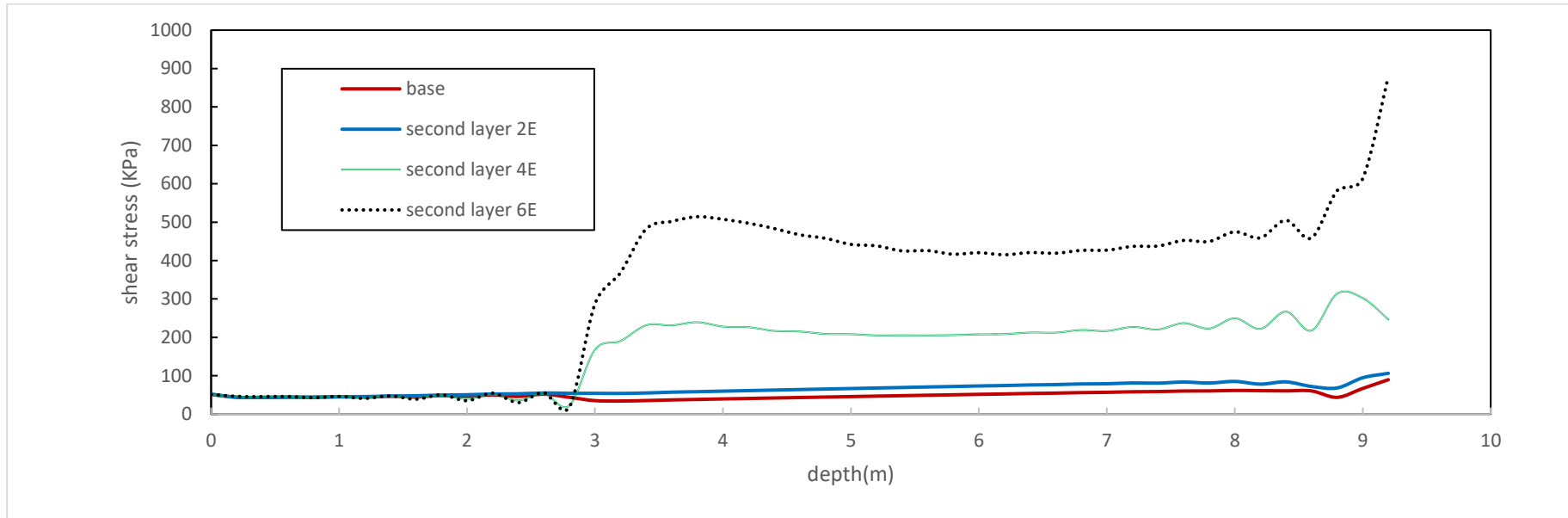


Figure 4- 23 Parametric study for case 3

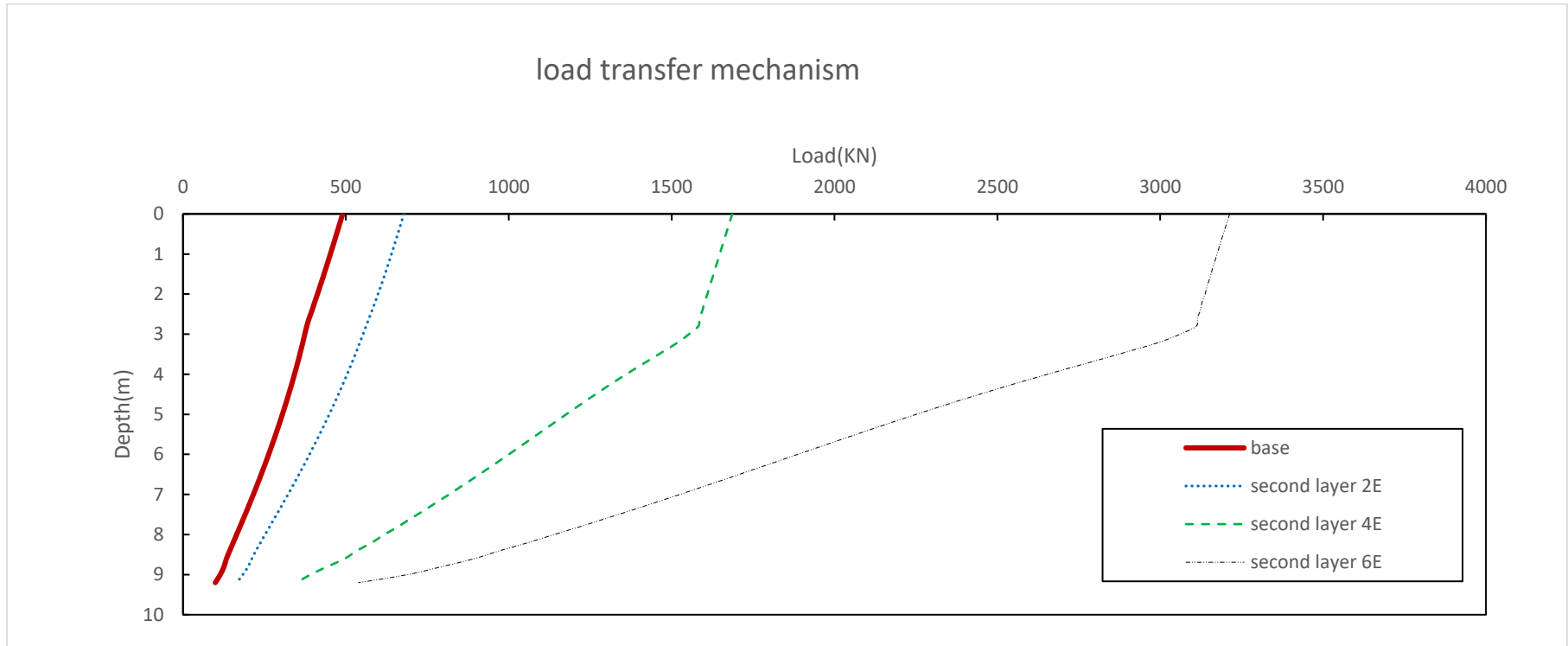


Figure 4- 24 Load transfer mechanism for case 3

For each case, four different amount of E (modulus of elasticity) has been carried out to study the effect of its changing on shear stress alongside pile and load transfer mechanism. The base model has $E_1=6$ MPa and $\phi_1= 13^\circ$ and then young's modulus doubles three times ($2*E$, $4*E$ and $6*E$) with values of $E_2=12$ MPa, $E_3=24$ MPa, $E_4=36$ MPa. When we change the young's modulus, the friction angle should be changed, respectively. In this case, we have $\phi_2=20^\circ$ $\phi_3=32^\circ$ $\phi_4=37^\circ$ in each respective models.

In case 1, the first layer has been chosen to apply changes in parameters. This layer has 5.3m thickness which type of material is filled soil. As can be seen in Figure 4-19, when we increase the value of E and ϕ , the shear stress along the pile and soil would be increased respectively. There is a jump in the diagram in depth of 5.3m as the type of soil has been changed to a stronger material (gravely sand). In a transition mechanism from fill soil to sand, models with larger values of E and ϕ have more significant changes in shear stress. Modifications in the first layer's parameters have minor effects on the interaction between soil and pile in other soil layers as well. There is still a growth in shear stress in layers two and three that the jumps are tending to be equal as the depth increases.

Figure 4-20 shows the load transfer mechanism based on the energy that each layer can carry out. By increasing the depth, the accumulative load that the soil can transfer to the next layers decreases. This decay ratio for stronger layer, like gravel sand soil, is less than the weak layer. By increasing the parameters E and ϕ in respective study layers, this value increases significantly.

In case 2, the second layer has been chosen to apply modifications in parameters and shown in figure 4-21. The thickness of this layer is 4m and it is embedded in depth of 2m with sand soil, beneath silt and above dense sand soil layers. CPT outcomes illustrated that we have a noticeable jump in cone tip resistance in depth of 8m from the ground level. As it was predictable, changing in second layer parameters does not have any effects on interaction between pile and soil in the first layer. However, these growths have significant consequences on shear stress in the respective layer (second layer). The ratio of abovementioned change increases by rising the multiplying E . Therefore, $6E$ has more increasing in shear stress than $4E$ and respectively same comparison between $2E$ and base model. As it was mentioned

before, the effect of significant change in CPT experimental cone tip resistance in depth of 8m has consequences in the diagram. Thus, we have a modification in the shear stress at that point for all four models. However, for base model and 2E model this change is increasing and for 4E and 6E is increasing in stresses. This shows that the performance of model in more dense soil is better than weaker soil.

Figure 4-22 shows the load transfer mechanism based on the energy that each layer can carry out. The results prove that the outlines in case 1 load transfer mechanism are repeated again. Therefore, By increasing the depth, the accumulative load that the soil can transfer to the next layers decreases. This decay ratio for stronger layer, like dense sand soil, is less than the weak layer, like silt. By increasing the parameters E and ϕ in respective study layers, this value increases significantly.

In case 2, the second layer has been chosen to apply adjustments in parameters. 7.2m of pile is embedded in this layer which contains hydraulic sand soil and placed under a fill soil layer. The CPT outcomes have distortions in depth between 8m and 9m from ground level and consequently, these distortions have slight effects in shear stress alongside the pile at that distance. Same as case 2, we do not see any consequences in interaction in first layer properties by changing second layers parameters. Effect of this modification has been shown in figure 4-23 which proves above conclusions for case 1 and 2. The influence of increasing the soil parameters is more evident in dense sands comparing to weaker soils.

Figure 4-24 demonstrate the load transition mechanism relying on carried out energy by each layer. Likewise case 2, this diagram proves first case outcomes. As a result, By growing the depth, the accumulative energy that the soil can handover to the next layers decreases. By increasing E and ϕ parameters in respective study layers, this value increases significantly. However, in this case, it can be seen that for the base model and 2E model we have almost straight lines.

4.2.7 Convergence Study

Numerical analysis is one of the central components of computational and finding an appropriate number of meshes in any project to reduce the time and cost of the project and to increase the accuracy of the analysis is very important. It takes scientific

contribution in many areas to successfully fit the software, network, etc. to perform computational tasks and numerical modelling. Computational science now constitutes what many call the third pillar of the scientific enterprise, a peer alongside theory and physical experimentation. The need to design structures using finite element packages is increasing rapidly, along with the demand for accurate and timely results. To achieve a reasonable number of meshes, mesh convergence study is carried out, and various models consisting of the different number of elements are created and subjected to the same amount loading. In this section, to achieve the reasonable number of meshes, mesh convergence study is carried out, and various models consisting of 6664, 9003, 14008, 24070 and 35694 element numbers are created and subjected to the same amount of surface pressure on top of the soil surface in case 1.

Figure 4- 25 shows the result of changing the number of elements in case 1. It is essential to find the right number of mesh in any finite element study because the not appropriate number of meshes could result in inaccurate results or could be time-consuming due to the bigger running time. It can be seen that the model with 24070 mesh elements is accurate enough for this study and 35694 elements mesh achieved the same results. More number of meshes needs more running time for each model and less number of meshes results in a more prominent element and less accurate results.

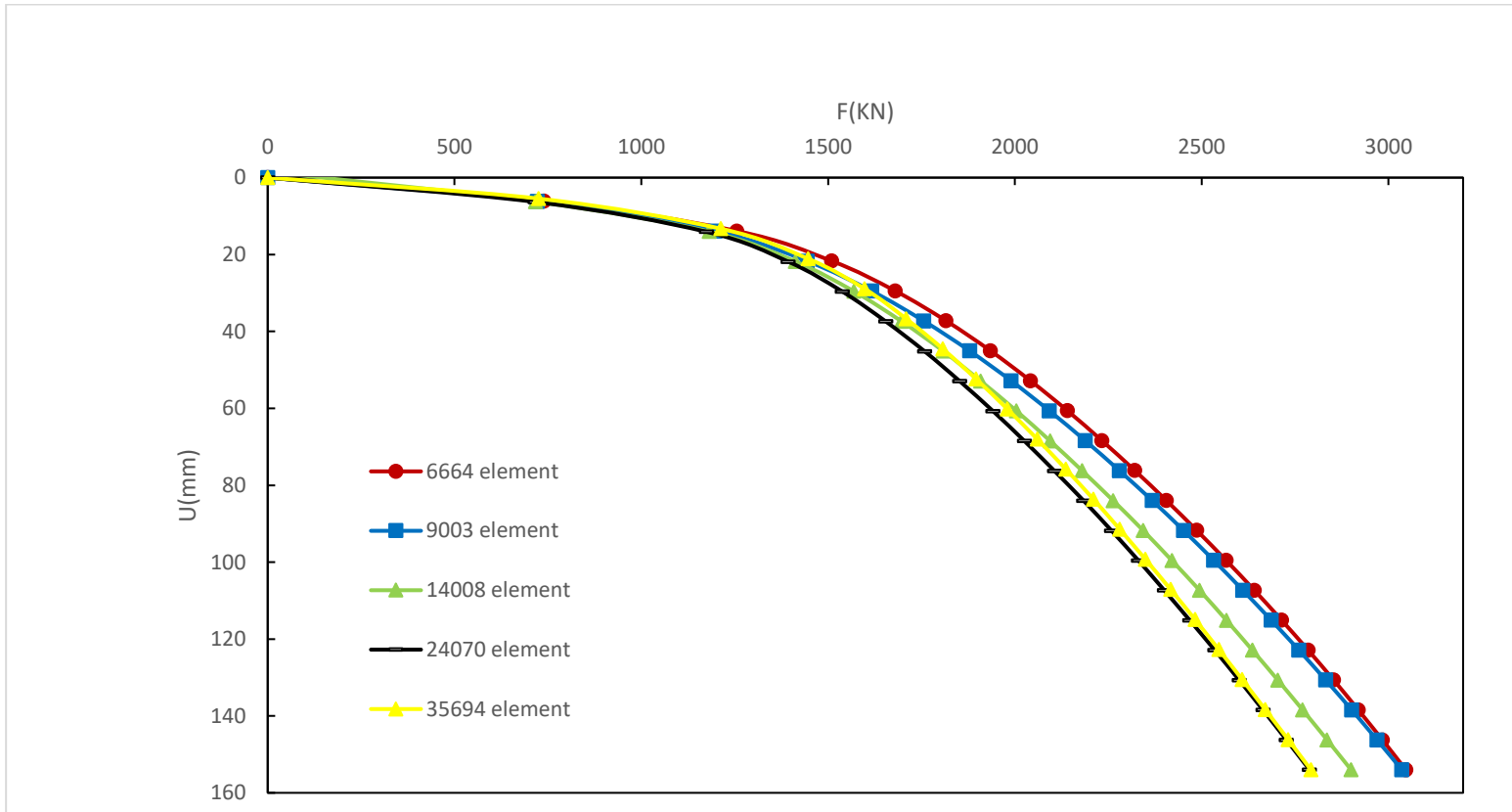


Figure 4- 25 Displacement-force diagram for different values of elements (mesh convergence study)

4.4 SUMMARY OF THE CHAPTER

In this chapter, results and discussion was reviewed for the research conducted on pile-soil behaviour for CPT experimental and ABAQUS numerical investigation. In the first section, respective results and discussion were explained for 3 selected profiles from the literature resources. In the second section, material properties for each model were demonstrated. In the third section, parametric study for different values of modulus of elasticity was conducted. In the fourth section, convergence study for various values of elements in different mesh sizes was discussed. In the chapter obtained displacement-force diagrams for each of 108 models were briefly described to validate ABAQUS results. All and all, based on the reviewed diagrams, this proposed study compares the results of the CPT and FEA methods under different loads and with different soil and pile types in a validated trend outcomes.

5 Investigation of Soil Behaviour

Based on CPT Data and Numerical Modeling

5.1 INTRODUCTION AND CHAPTER OVERVIEW

The effectiveness of the recently proposed models concerning the prediction of total stresses and displacement requires one to compare it with that of other modelling approaches or experimental outcomes. In order to validate the results from numerical analysis using ABAQUS, with the field outcomes, a comparison amongst the FEM and experimental methods is carried out to examine the accuracy of developed numerical models further. Firstly, the force-displacement diagrams for all 108 tests have been demonstrated to investigate the correctness of ABAQUS simulation. Moreover, the trend line for each experimental and numerical tests illustrated in the diagram with the respective equation and regression results.

5.2 VALIDATING ALL CASES

In order to validate obtained results from ABAQUS with CPT outcomes, both of data is prepared in the same diagram for each model. A polynomial trend line has been drawn for each series of data and respective regression value has been shown. As we have a total amount of 108 CPT experimental data, based on this information, the related model in ABAQUS has been created relied on chapter 3 methodology. Validation in discontinues values should be illustrated in diagrams to compare two methods. This is achieved by performing separate diagrams for each model. Related pile foundation and soil profile are accessible in appendices A, B and C. In each diagram the above equation and regression are referred to ABAQUS data and underneath equation and regression are connected to field outcomes.

5.2.1 Regression Analysis

In statistical modeling, regression analysis is a set of statistical processes for estimating the relationships between a dependent variable and one or more independent variables. The most common form of regression analysis is linear regression, in which one finds the line (or a more complex linear combination) that most closely fits the data according to a specific mathematical criterion. For example, the method of ordinary least squares computes the unique line (or hyperplane) that minimizes the sum of squared differences between the true data and that line (or hyperplane). For specific mathematical reasons, this allows the researcher to estimate the conditional expectation of the dependent variable when the independent variables take on a given set of values. Less common forms of regression use slightly different procedures to estimate alternative location parameters or estimate the conditional expectation across a broader collection of non-linear models.

In this research, for each sample, respected polynomial trend line for both ABAQUS and Field data obtained separately. Regression value and line formula were shown in each diagram.

5.2.2 Evaluating the Model Performance

The performance and the predictive ability of the finite element method and validation sets are shown graphically in Figures 5.1-5.50 for bored piles; in Figures 5.51-5.78 for concrete driven piles; and in Figures 5.79-5.108 for steel driven piles. The blue quadrangular points represents the experimental field data while the red triangle dots are for the finite element ABAQUS data.

A visual inspection the figures may conclude:

For bored piles, the ABAQUS model performs well and is capable in simulating the measured load-settlement behaviour of the piles. For most of the cases, there is an excellent correlation between FEM and measured load-settlement curve. Examining the predictive ability of the ABAQUS model in the validation set indicate that FEM is able to forecast the load-settlement behaviour accurately.

It can also be seen that in few computational cases records, the FE model may not perform as good as in the other cases. This cannot be considered as shortcoming, as in most of these cases (e.g. cases 10,28 and 32) the FEM under-predicts the load-settlement relationship and as a result this may assist with achieving safe design.

For driven piles, both of the FEM and field data are developed for concrete and steel piles perform well in validation sets. There is an excellent correlation can be seen between measured and simulated load-settlement relationship of modelled piles. The figures also show that the complex nonlinear relationship of pile load-settlement is well simulated by the ABAQUS models including the strain hardening behaviour.

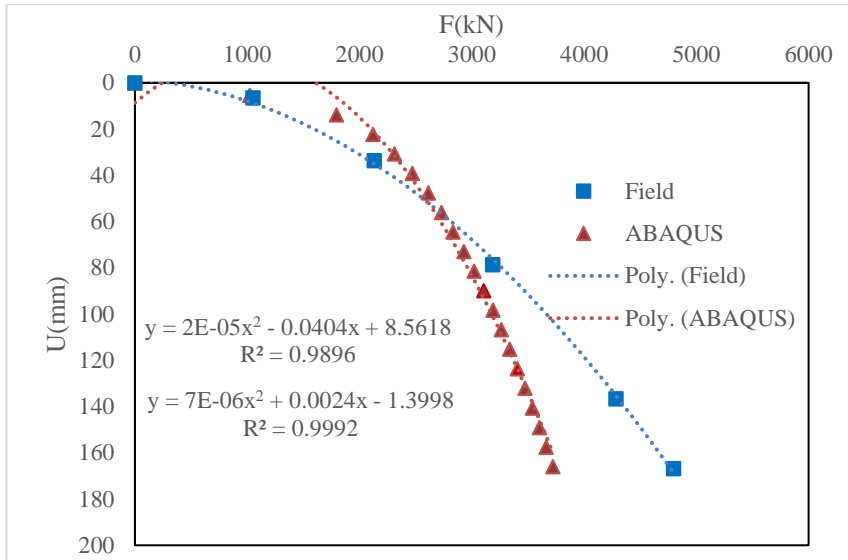


Figure 5- 1 Model A-1

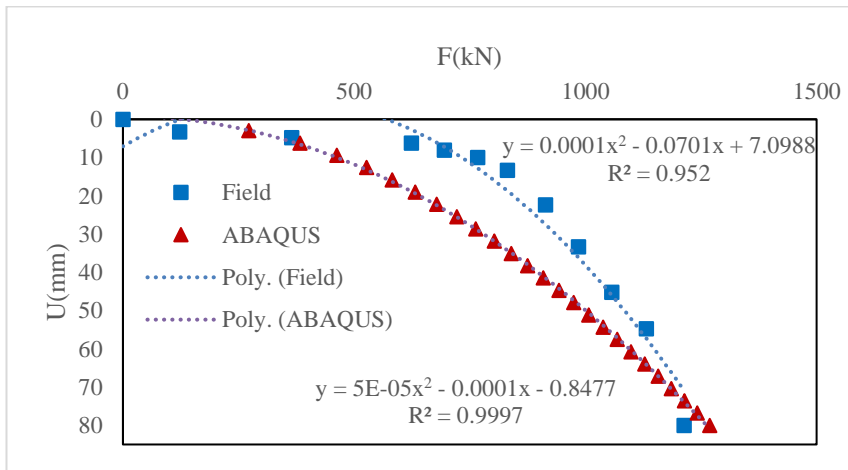


Figure 5- 2 Model A-2

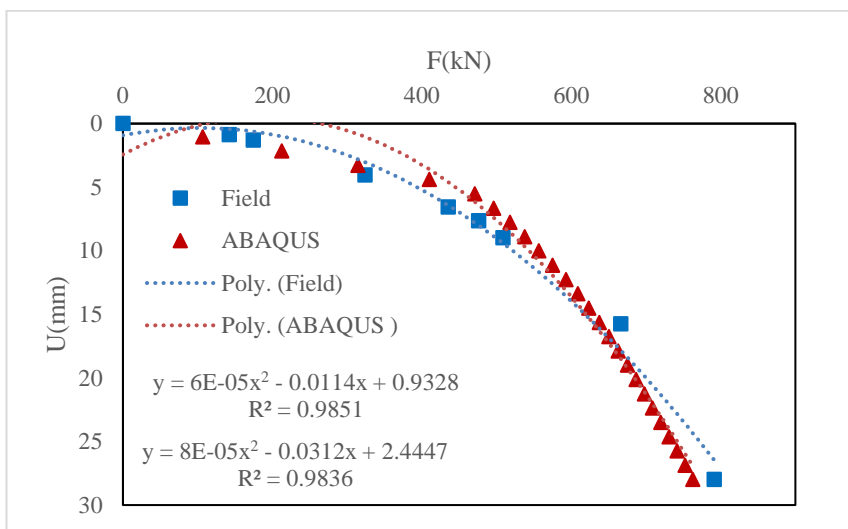


Figure 5- 3 Model A-3

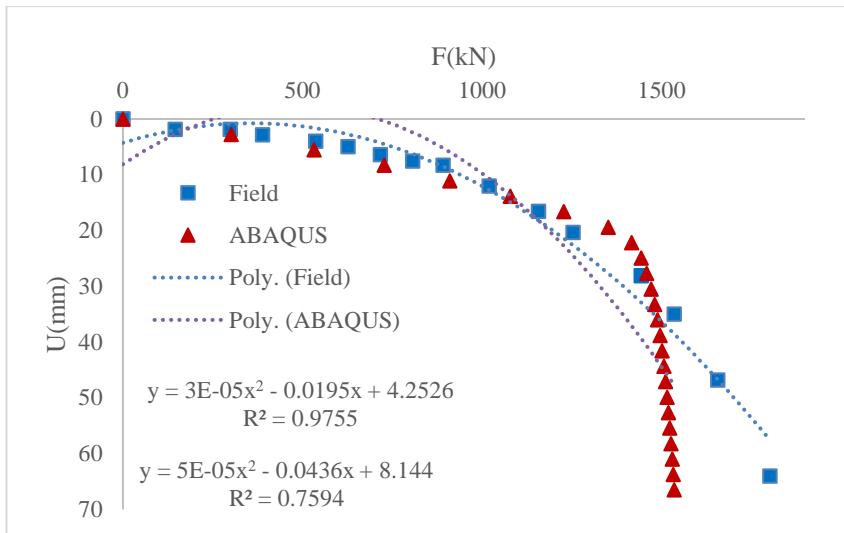


Figure 5- 4 Model A-4

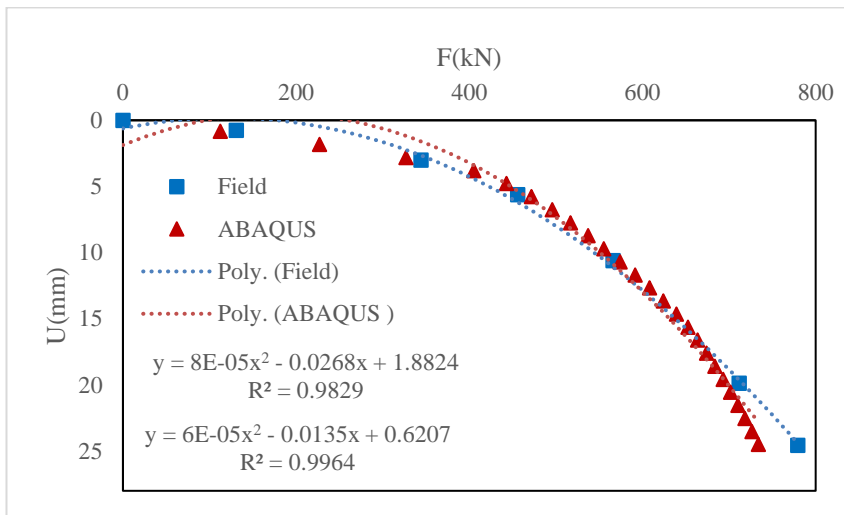


Figure 5- 5 Model A-5

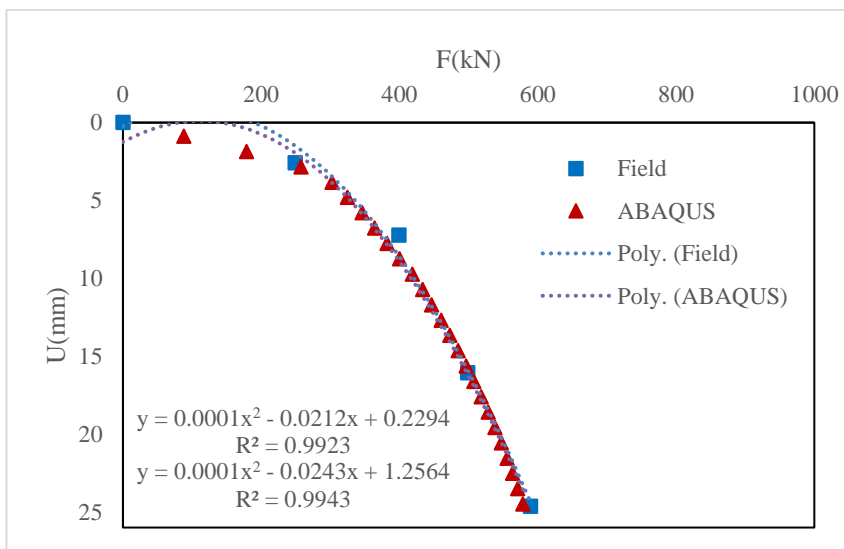


Figure 5- 6 Model A-6

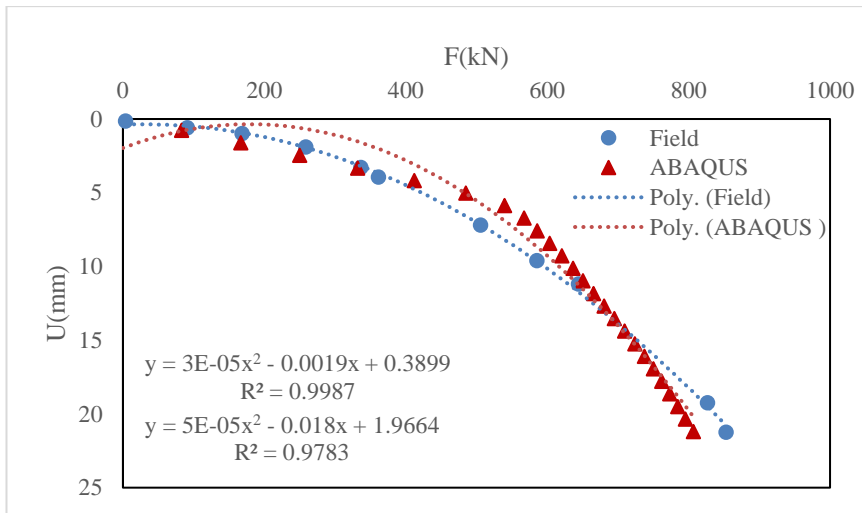


Figure 5- 7 Model A-7

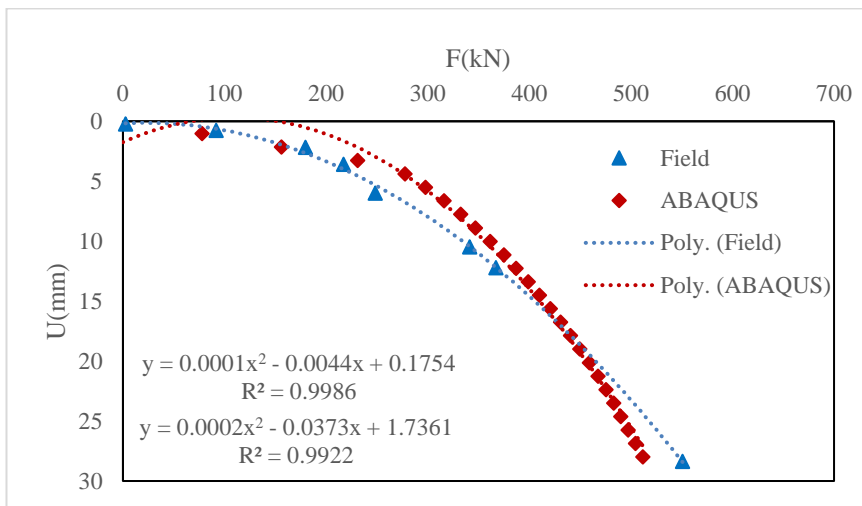


Figure 5- 8 Model A-8

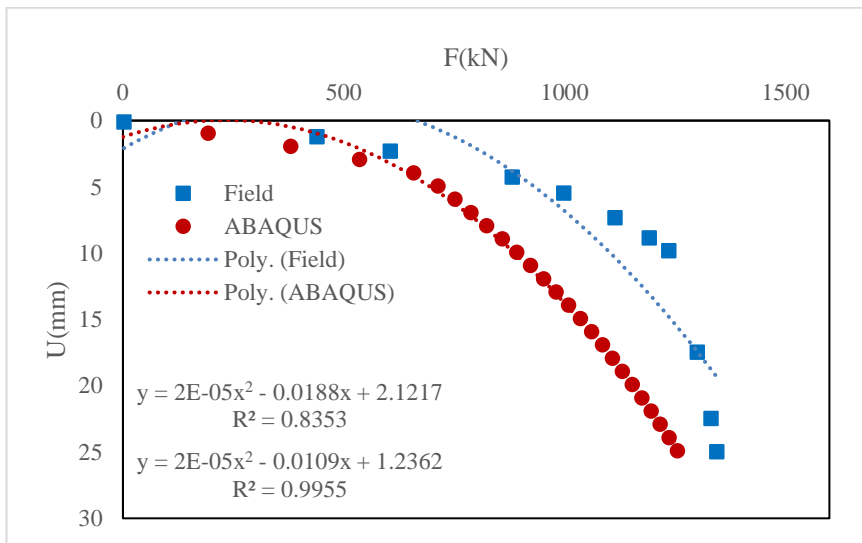


Figure 5- 9 Model A-9

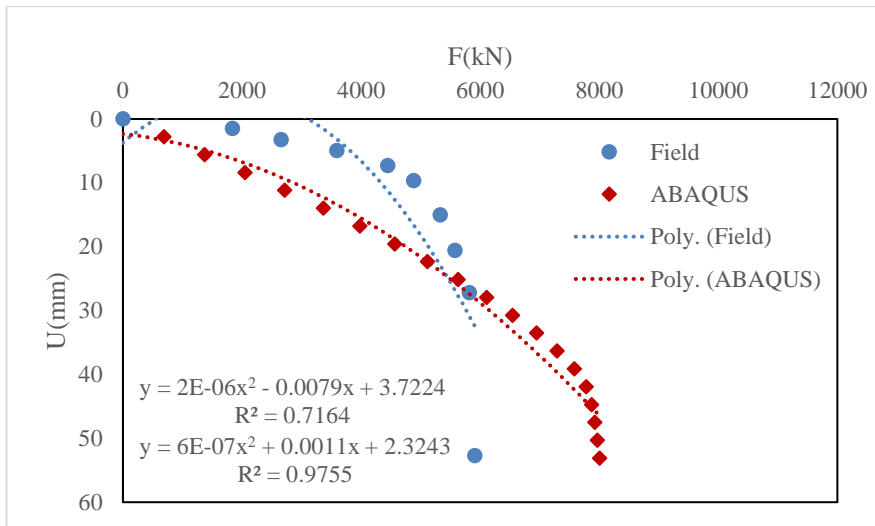


Figure 5- 10 Model A-10

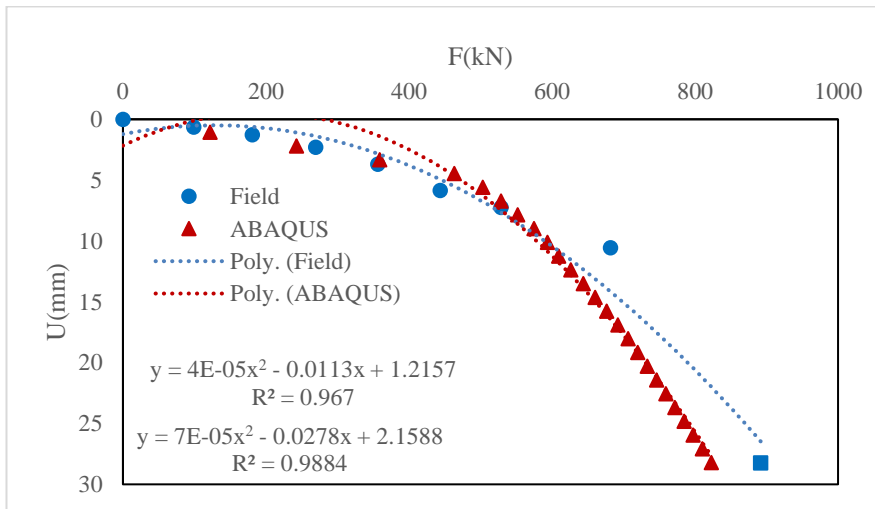


Figure 5- 11 Model A-11

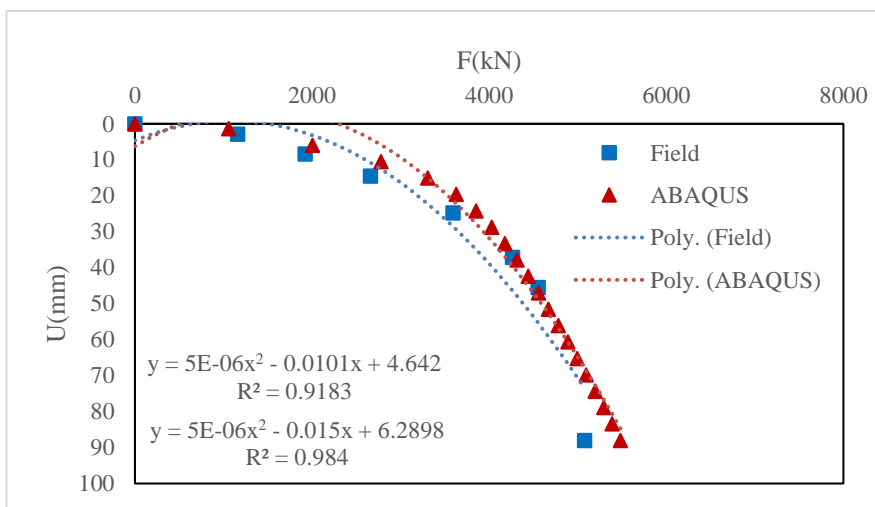


Figure 5- 12 Model A-12

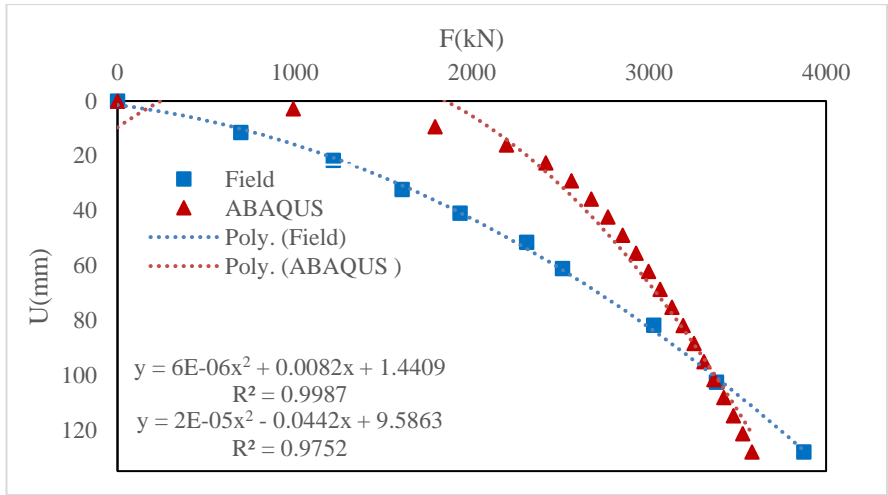


Figure 5- 13 Model A-13

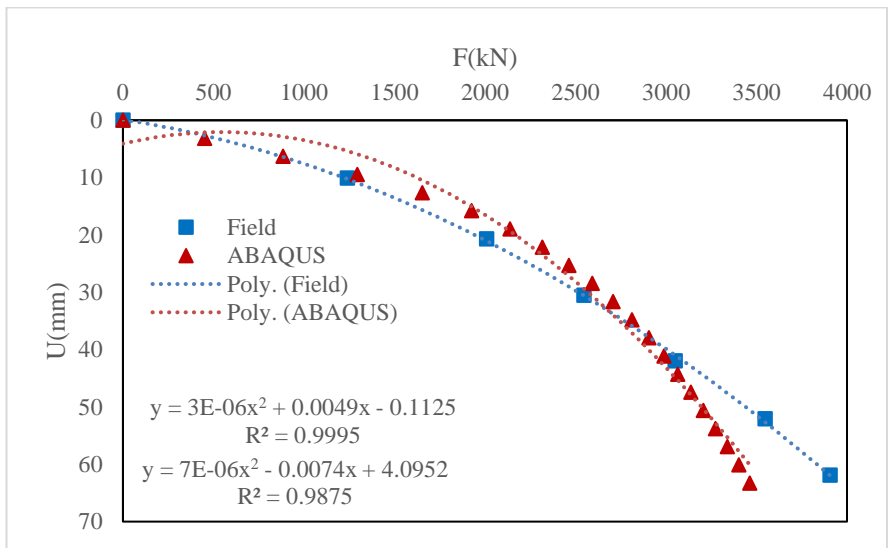


Figure 5- 14 Model A-14

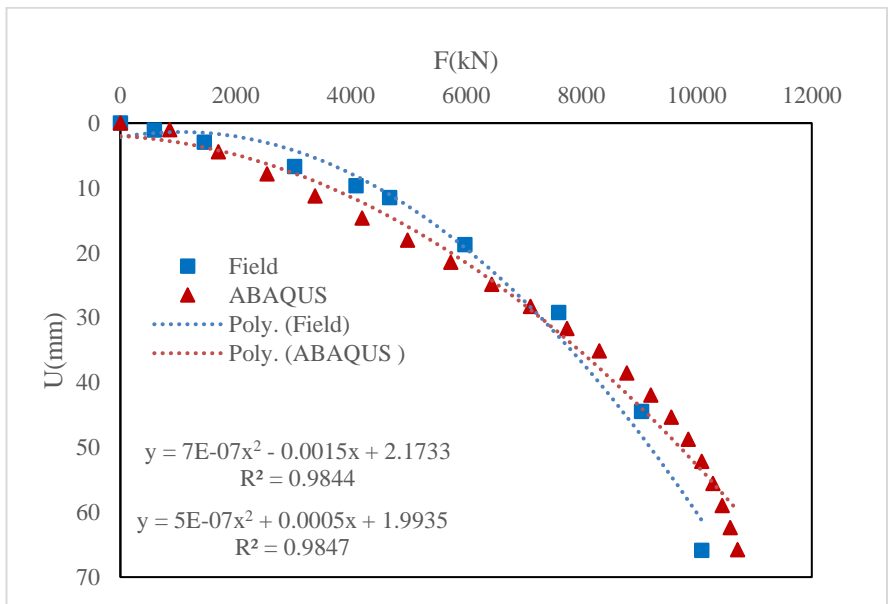


Figure 5- 15 Model A-15

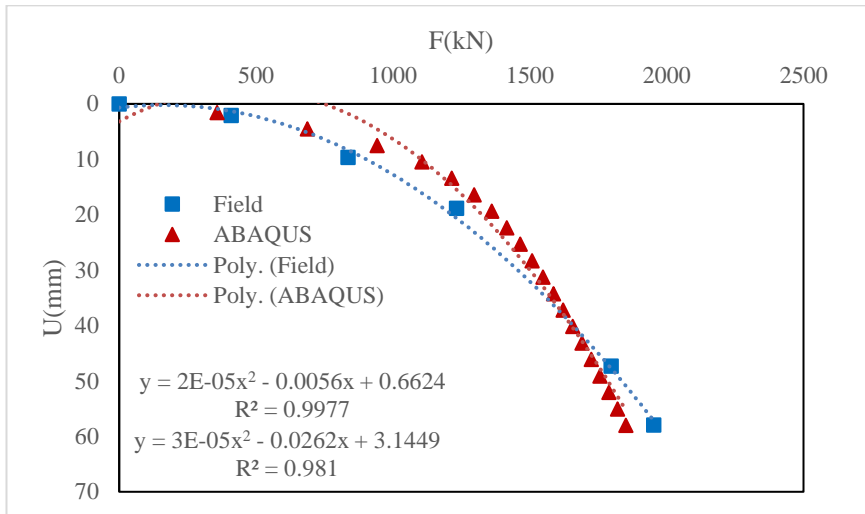


Figure 5- 16 Model A-16

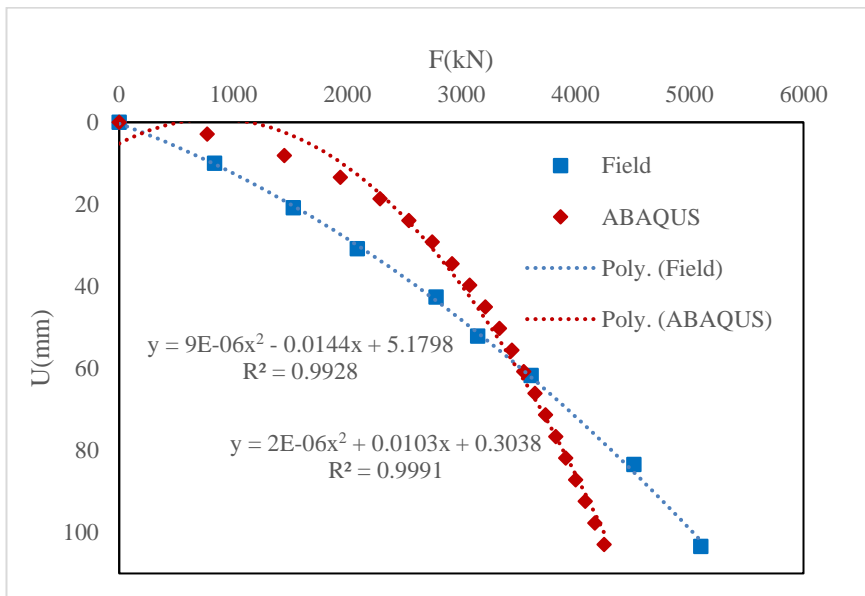


Figure 5- 17 Model A-17

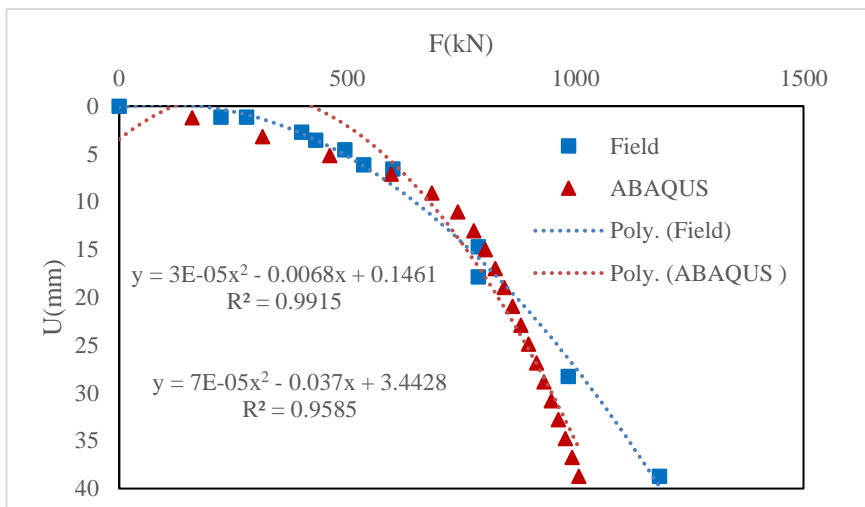


Figure 5- 18 Model A-18

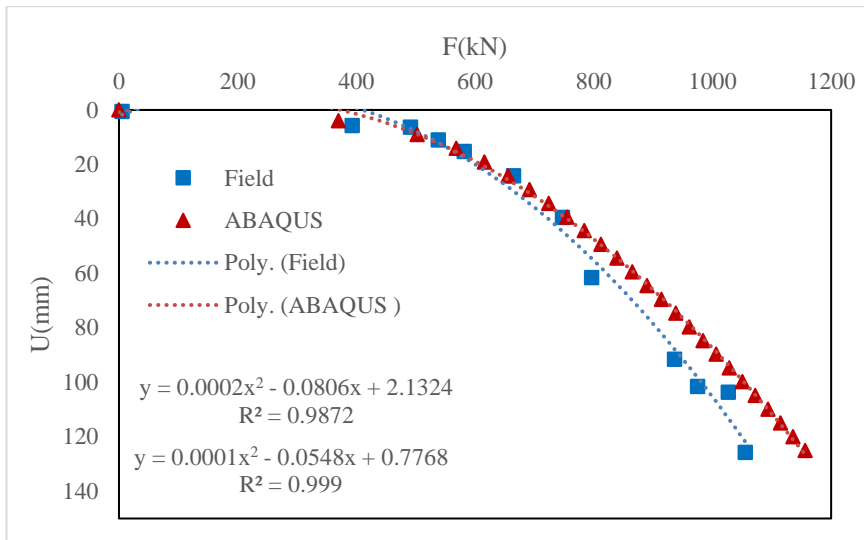


Figure 5- 19 Model A-19

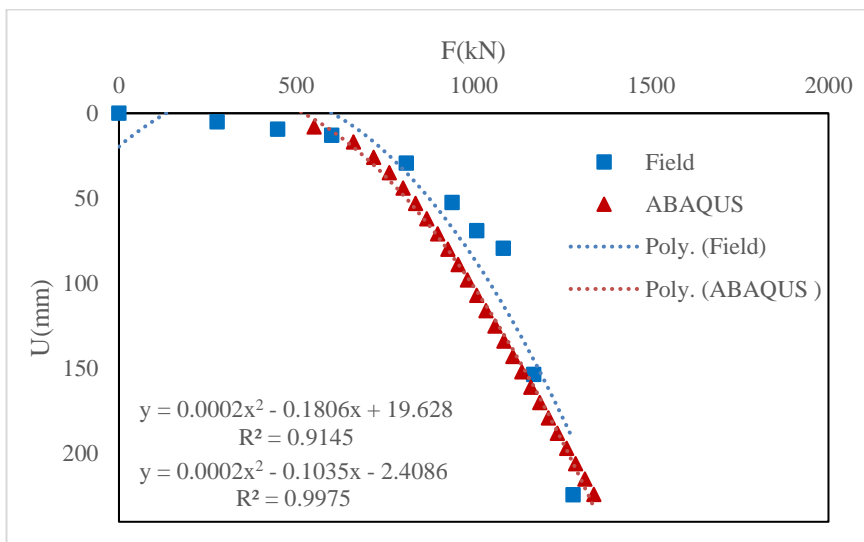


Figure 5- 20 Model A-20

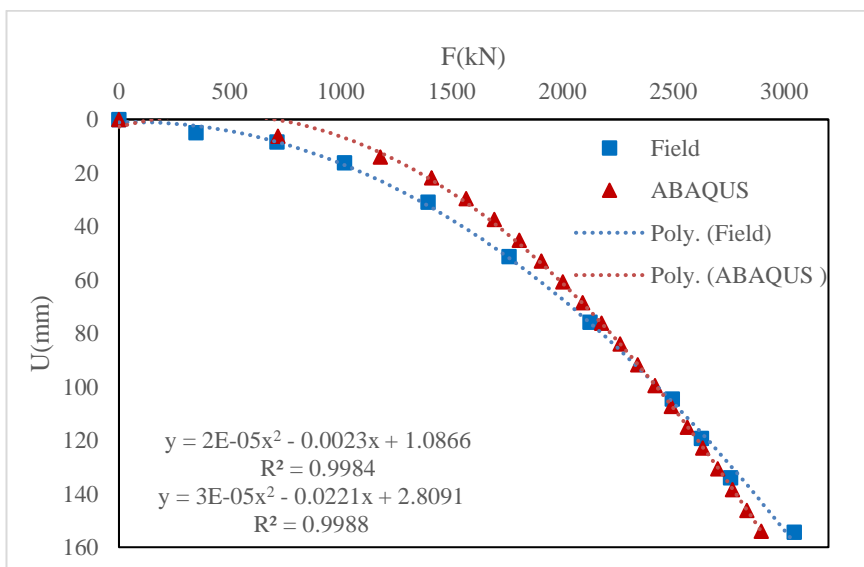


Figure 5- 21 Model A-21

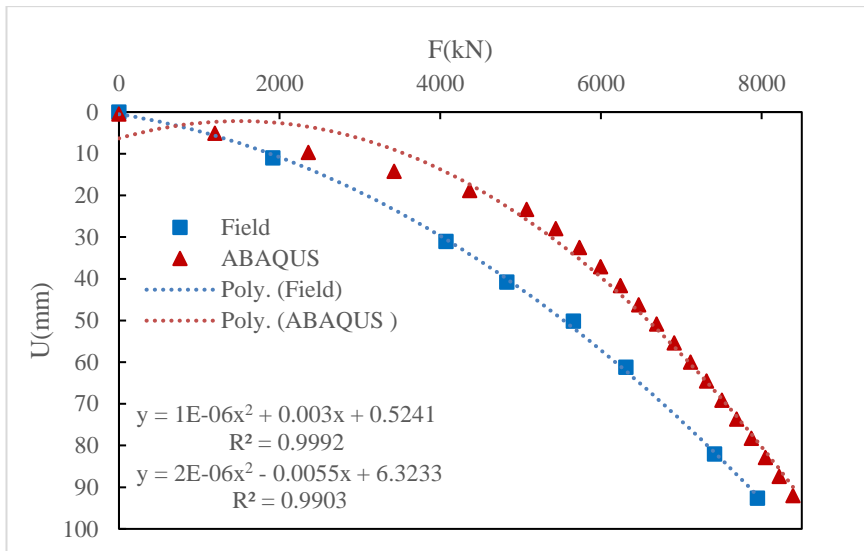


Figure 5- 22 Model A-22

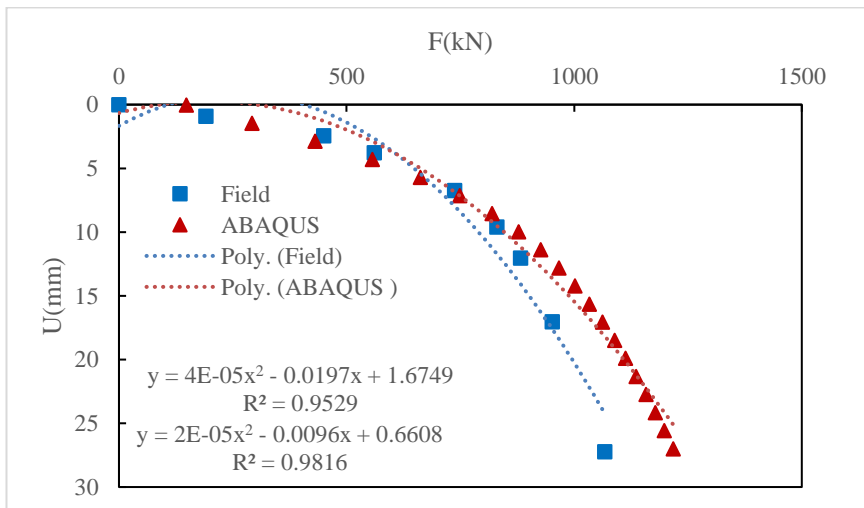


Figure 5- 23 Model A-23

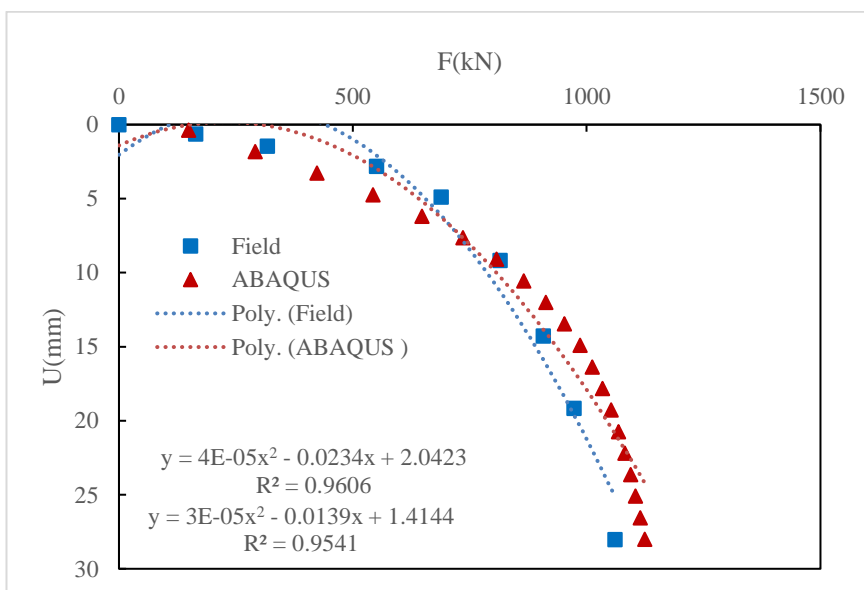


Figure 5- 24 Model A-24

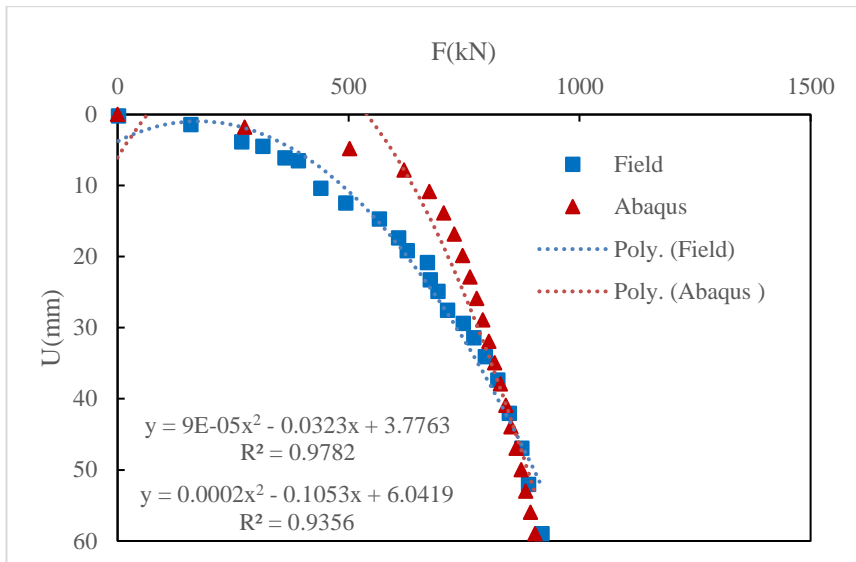


Figure 5- 25 Model A-25

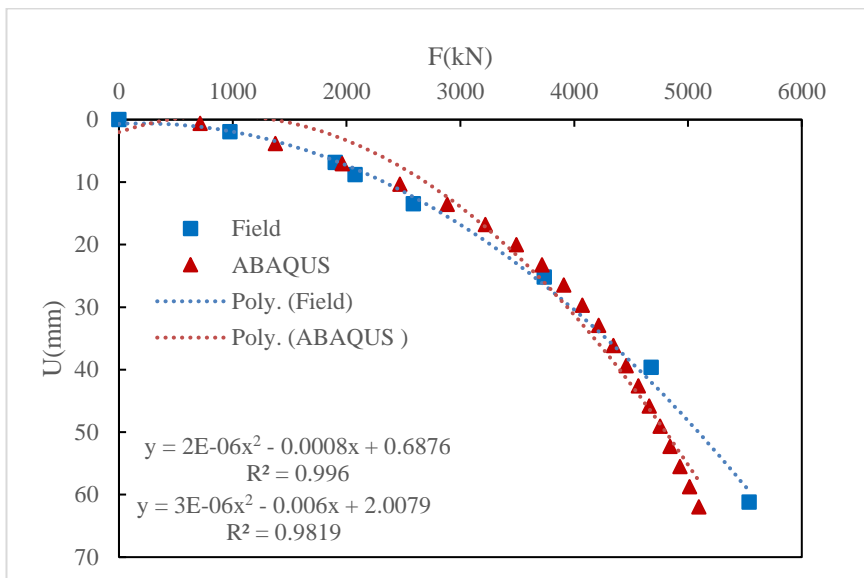


Figure 5- 26 Model A-26

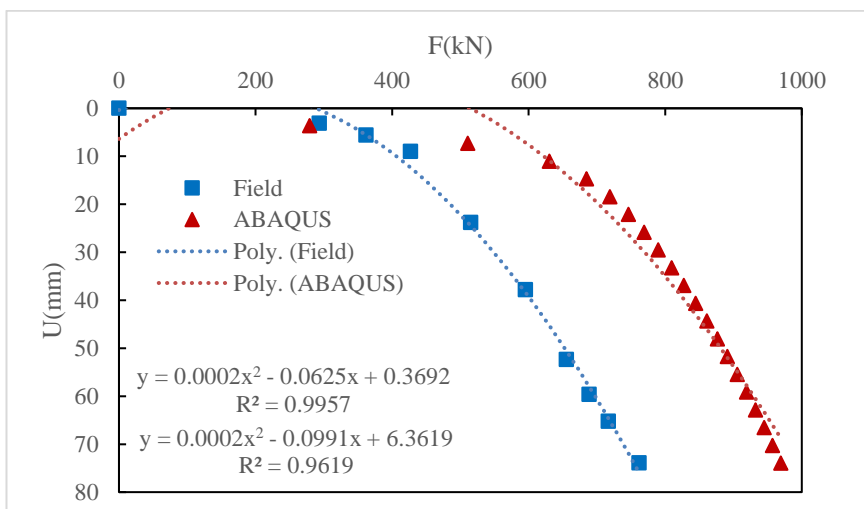


Figure 5- 27 Model A-27

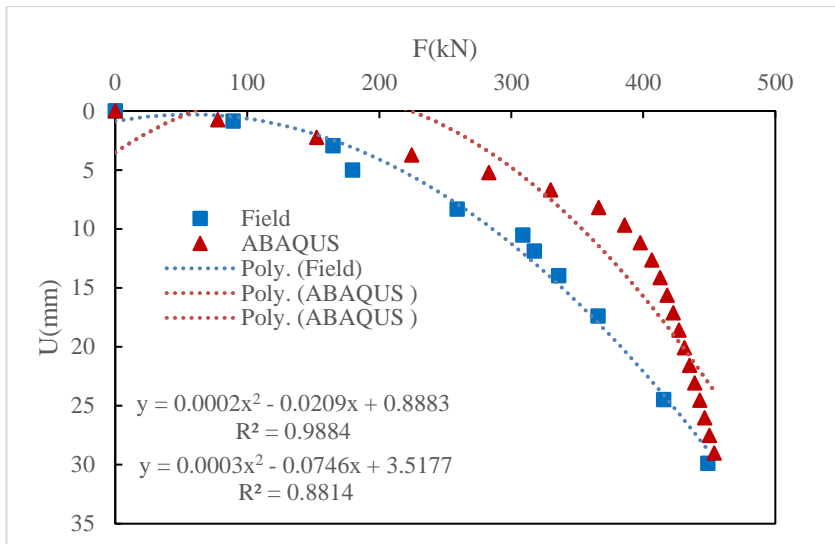


Figure 5- 28 Model A-28

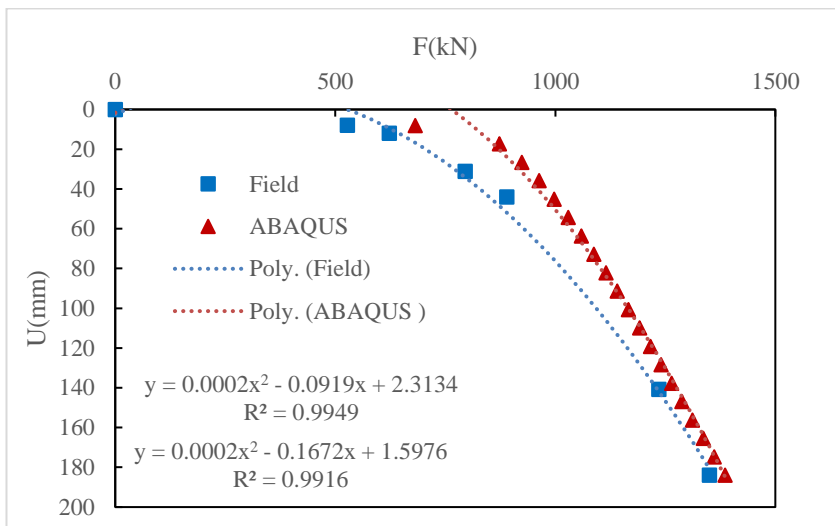


Figure 5- 29 Model A-29

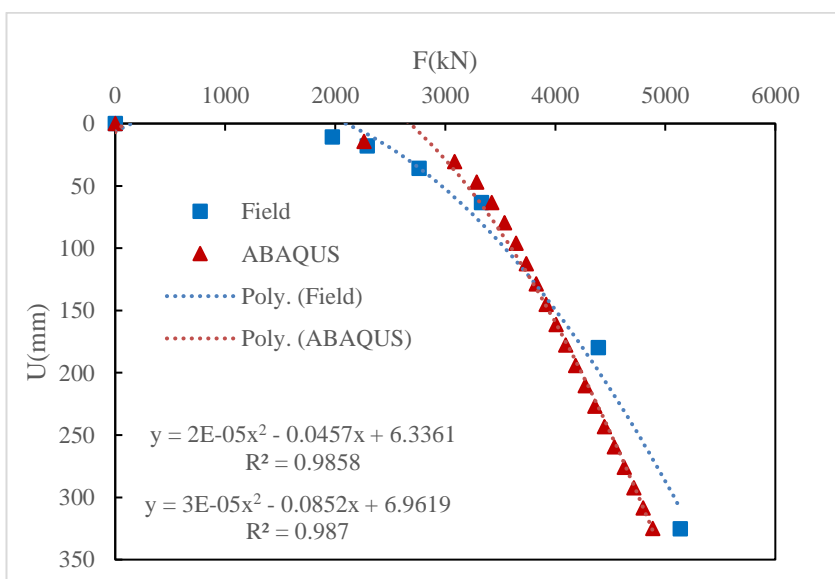


Figure 5- 30 Model A-30

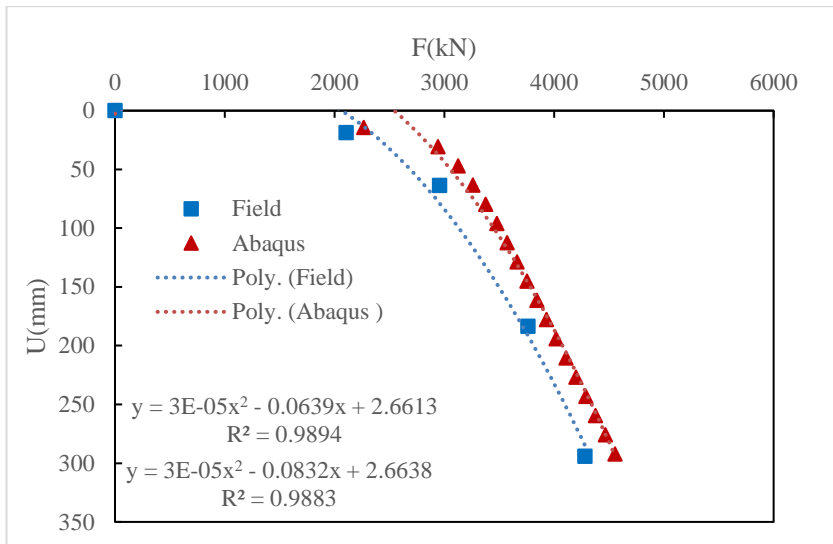


Figure 5- 31 Model A-31

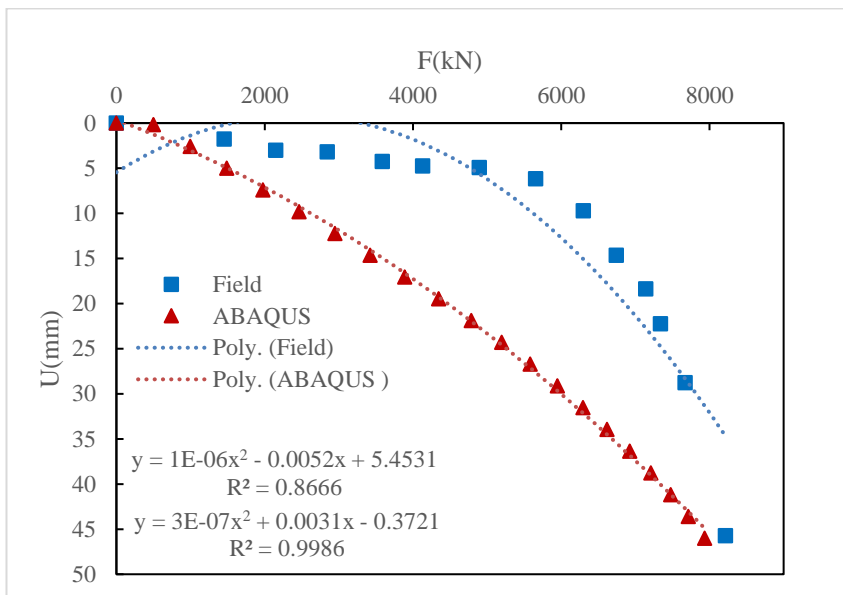


Figure 5- 32 Model A-32

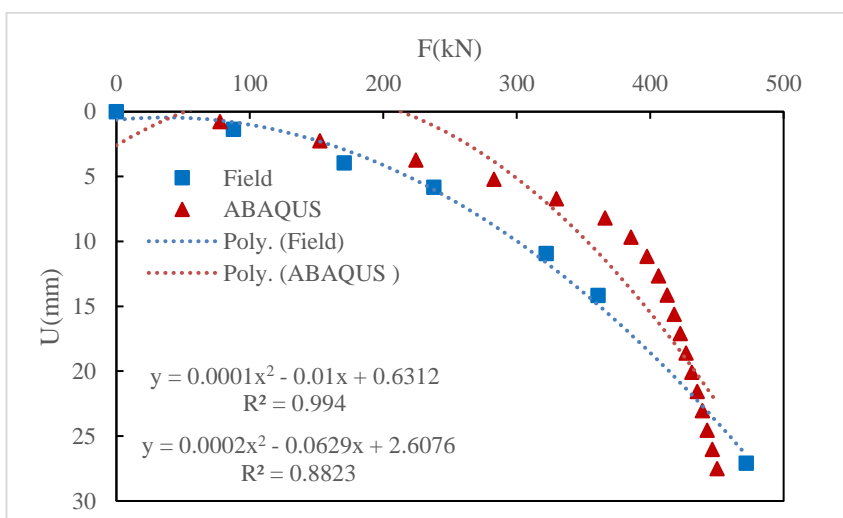


Figure 5- 33 Model A-33

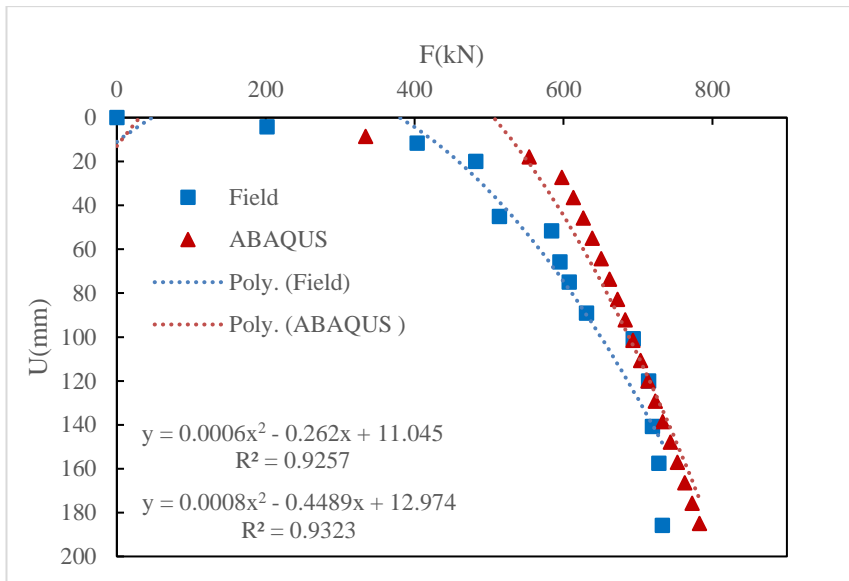


Figure 5- 34 Model A-34

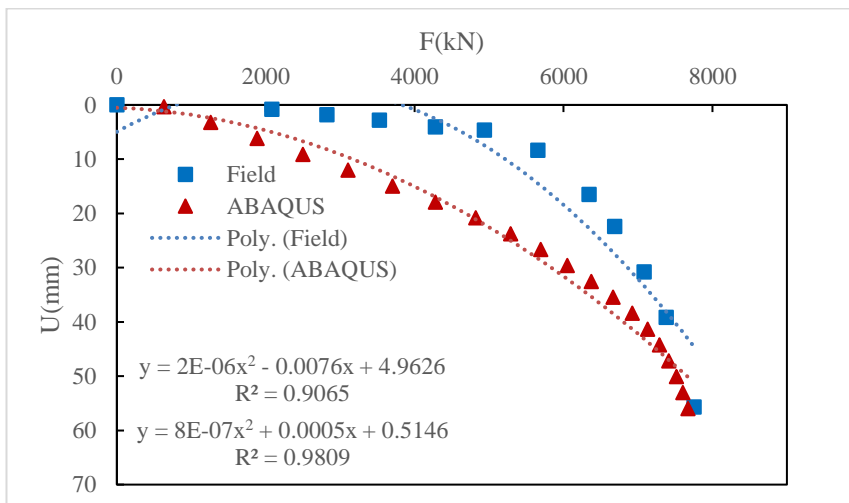


Figure 5- 35 Model A-35

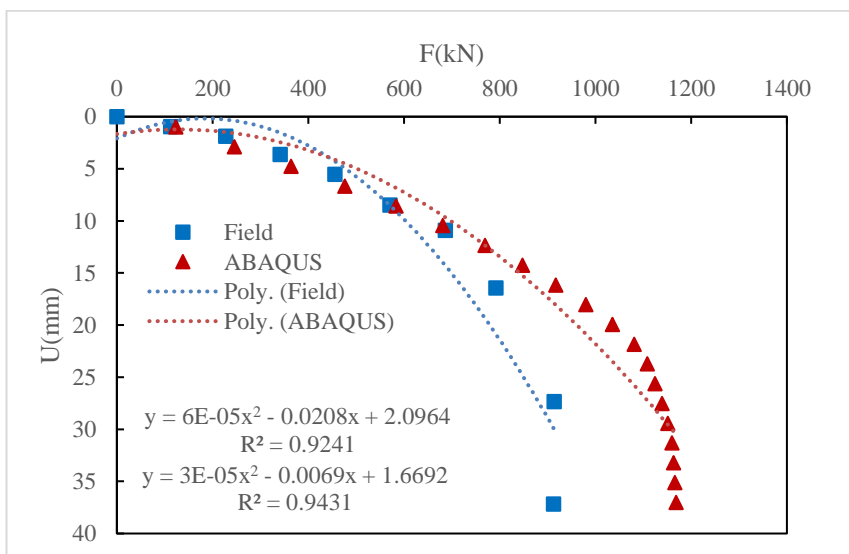


Figure 5- 36 Model A-36

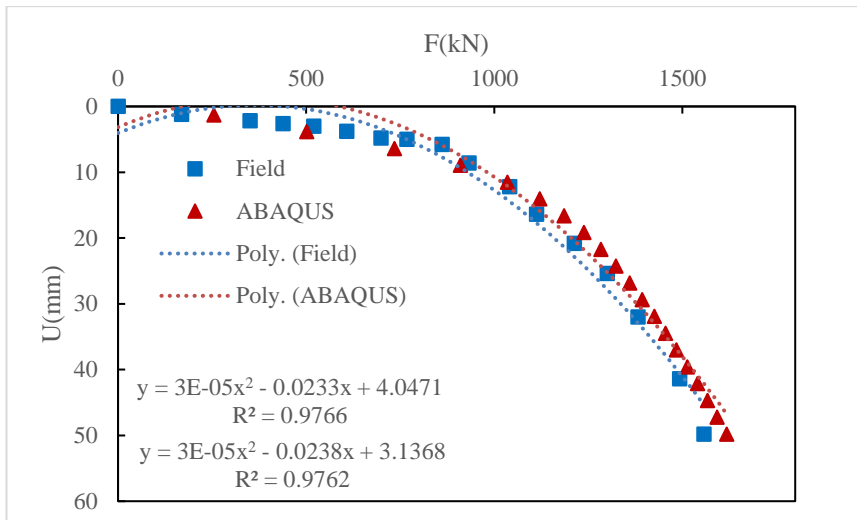


Figure 5- 37 Model A-37

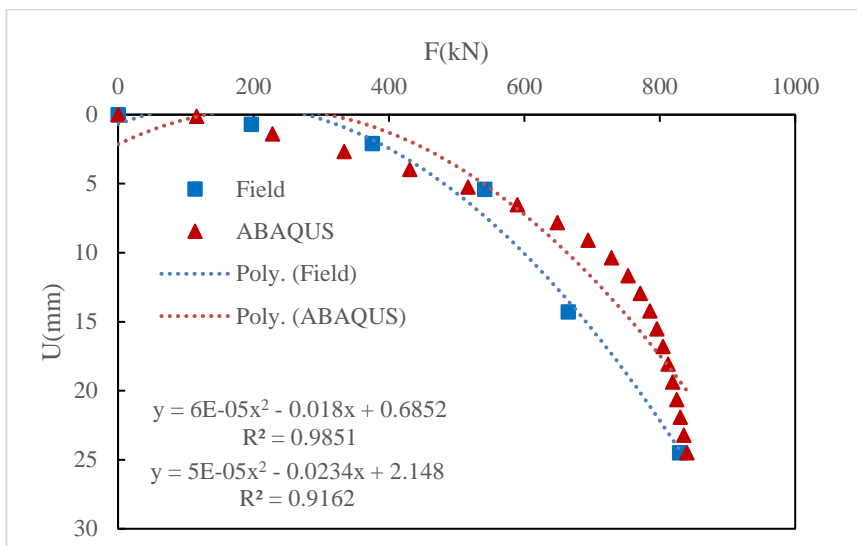


Figure 5- 38 Model A-38

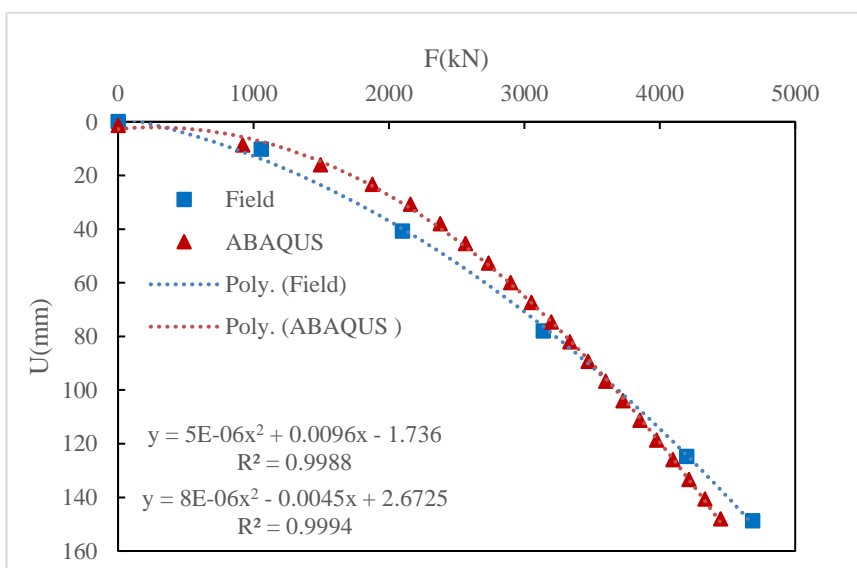


Figure 5- 39 Model A-39

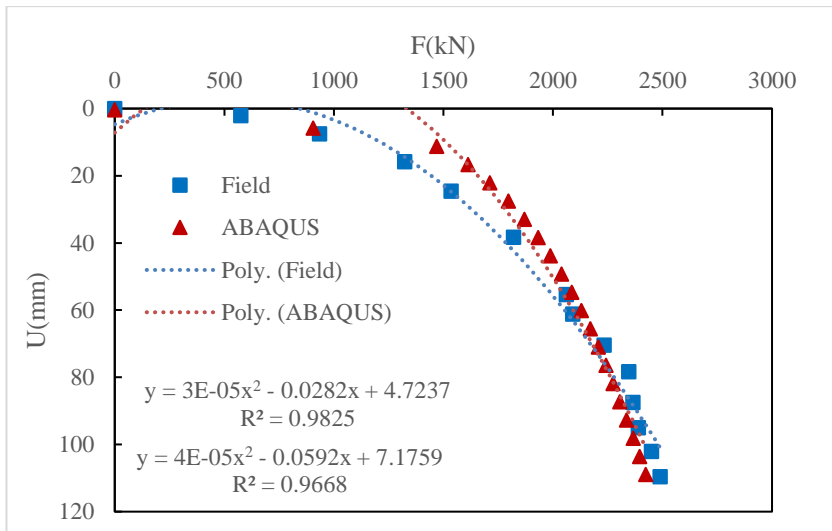


Figure 5- 40 Model A-40

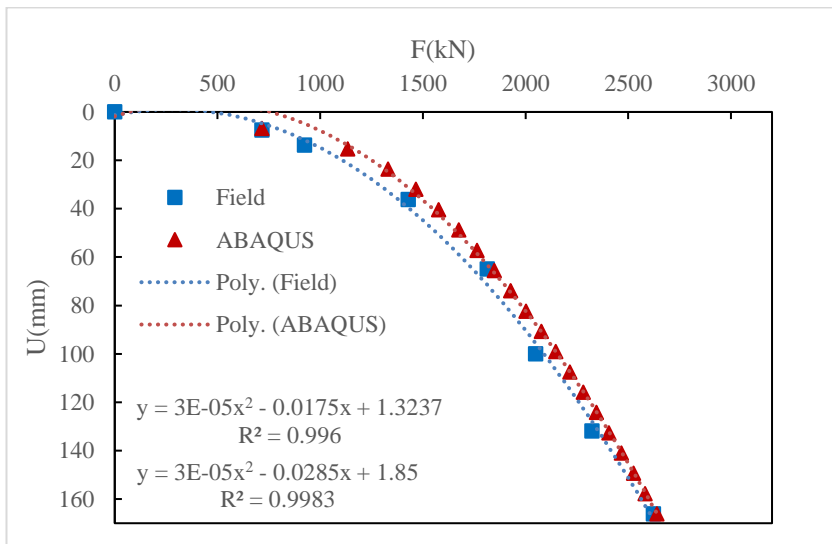


Figure 5- 41 Model A-41

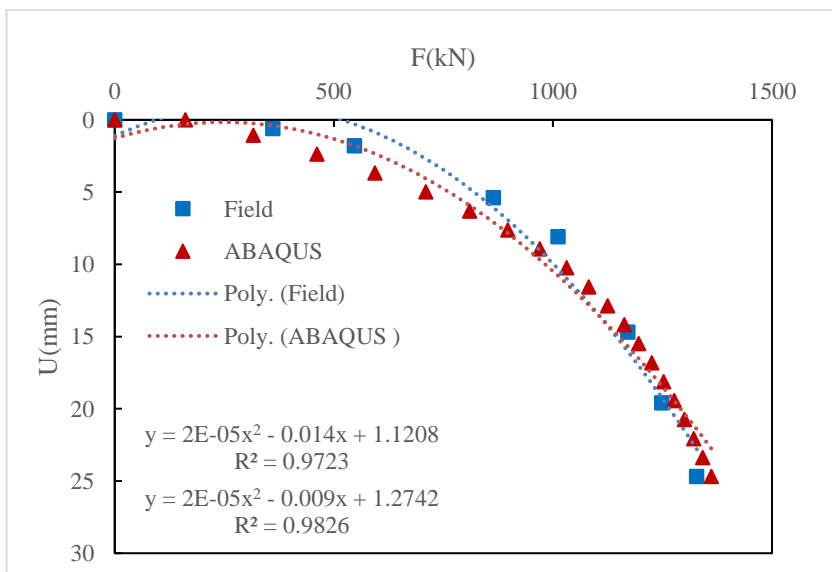


Figure 5- 42 Model A-42

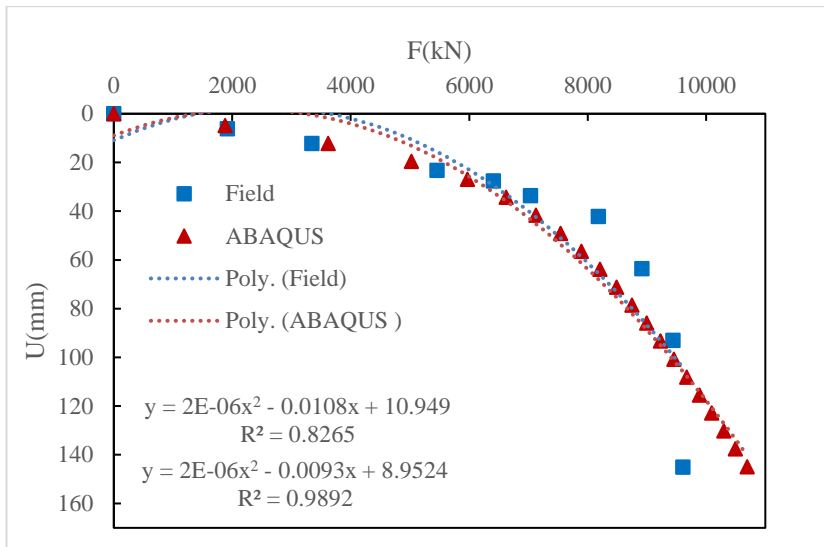


Figure 5- 43 Model A-43

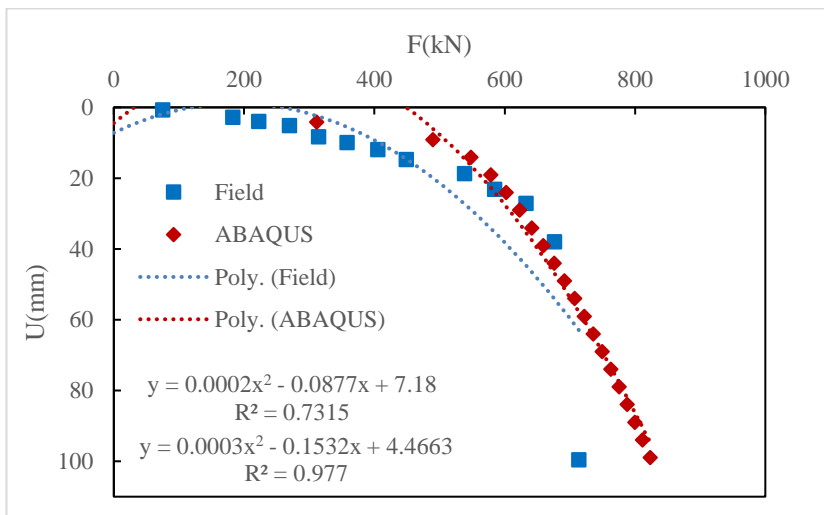


Figure 5- 44 Model A-44

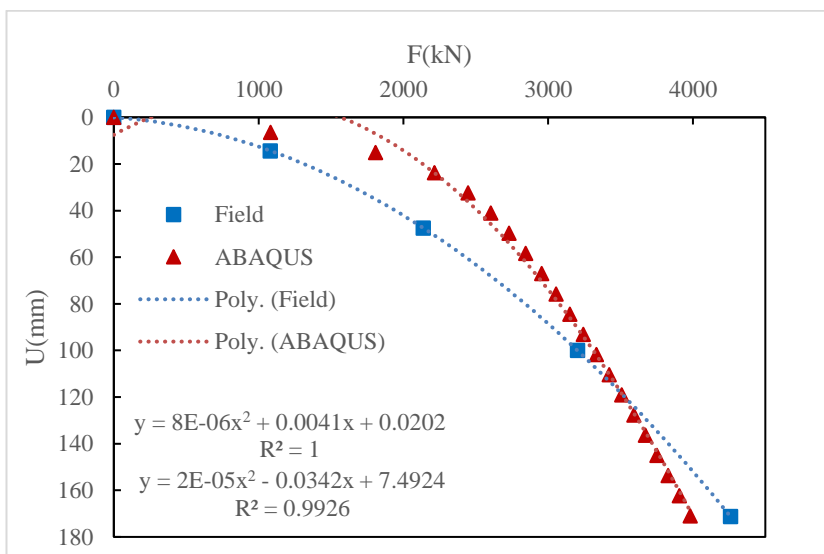


Figure 5- 45 Model A-45

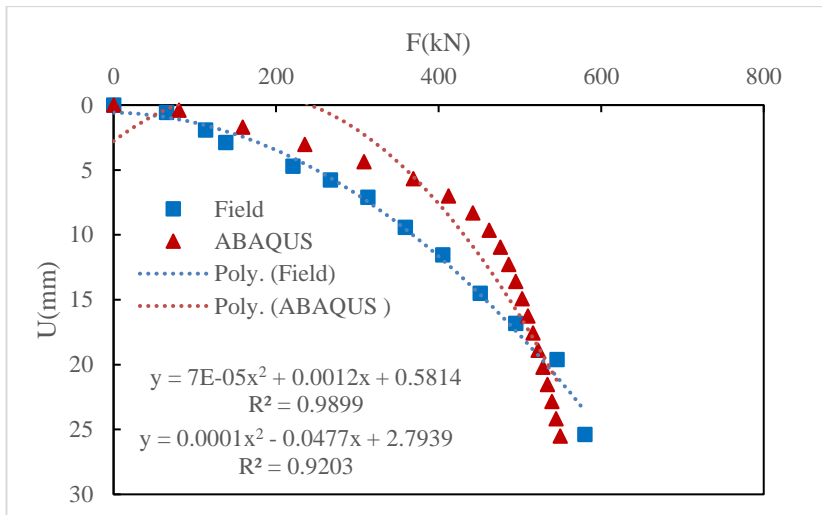


Figure 5- 46 Model A-46

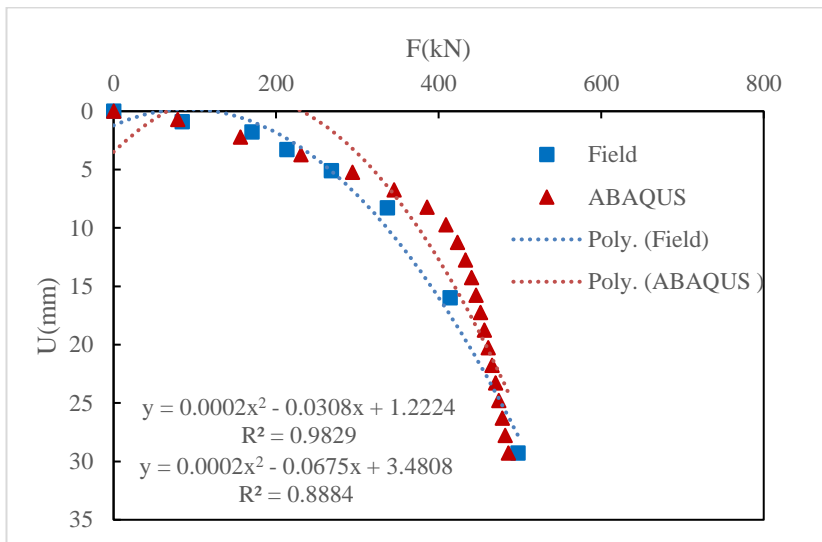


Figure 5- 47 Model A-47

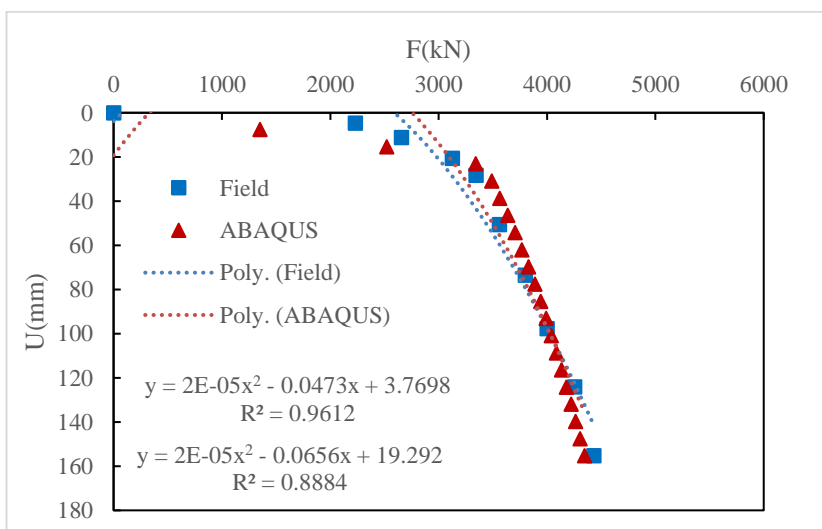


Figure 5- 48 Model A-48

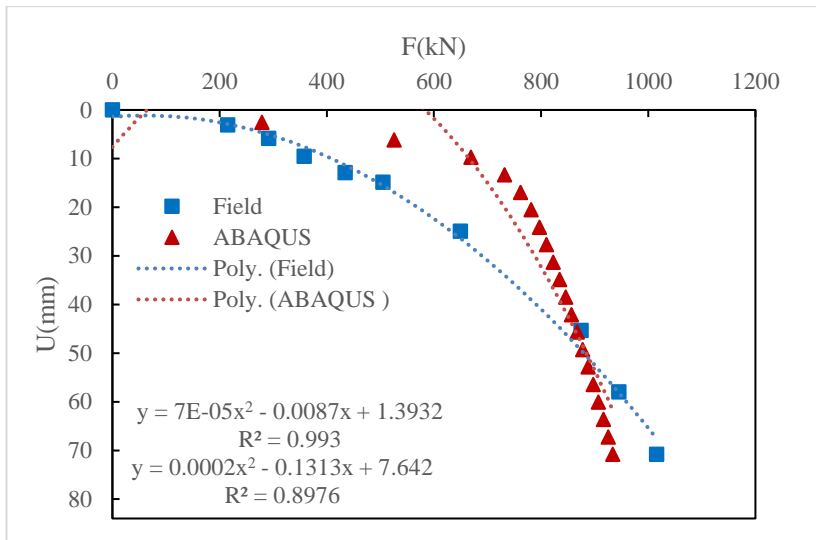


Figure 5- 49 Model A-49

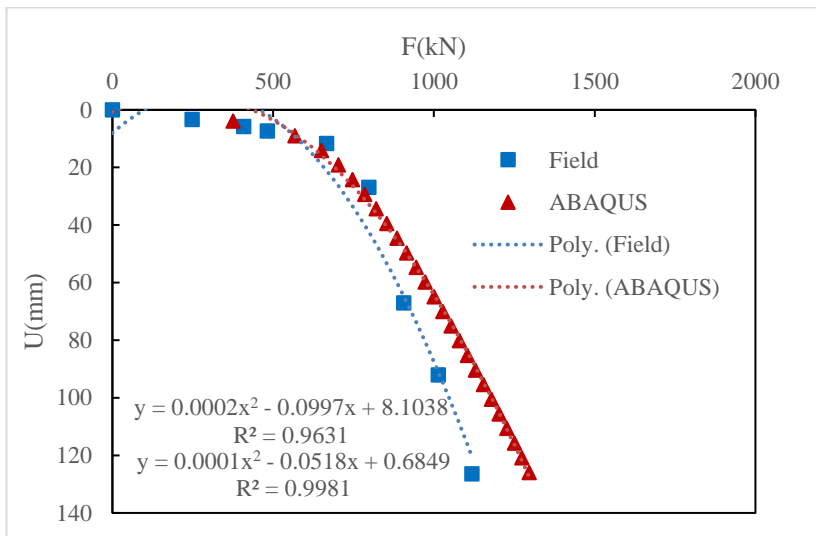


Figure 5- 50 Model A-50

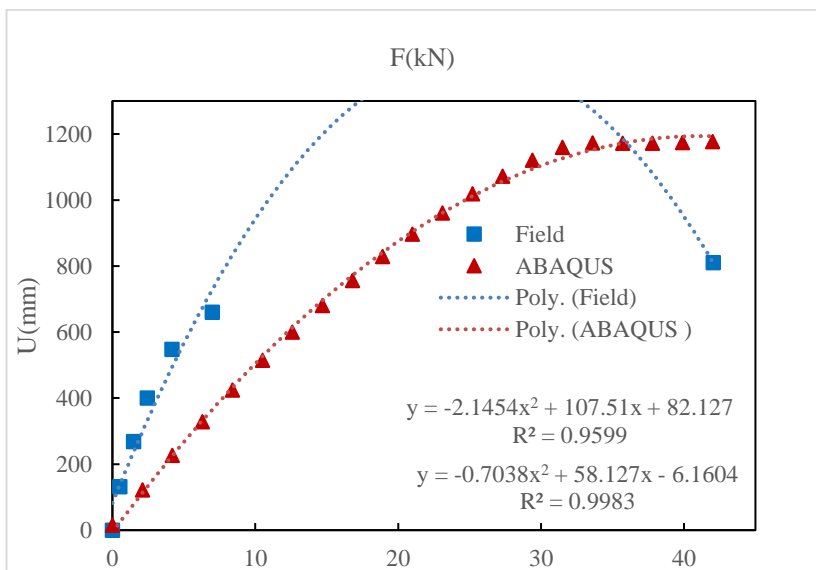


Figure 5- 51 Model B-1

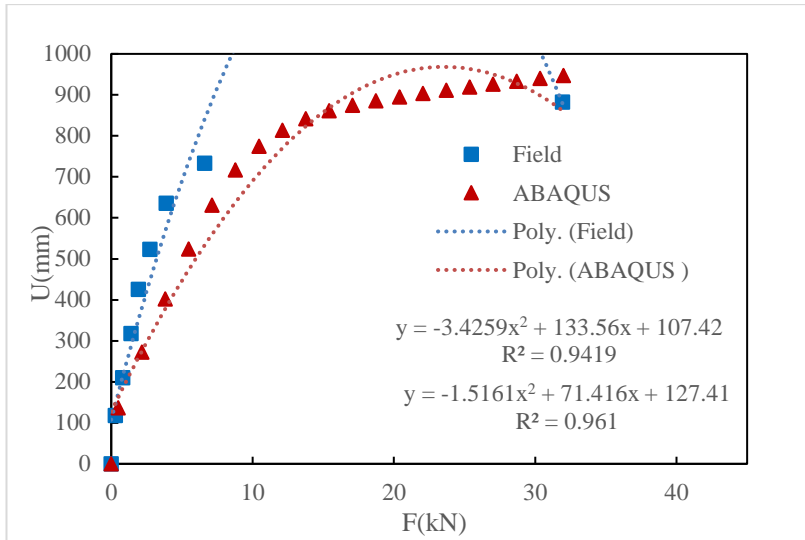


Figure 5- 52 Model B-2

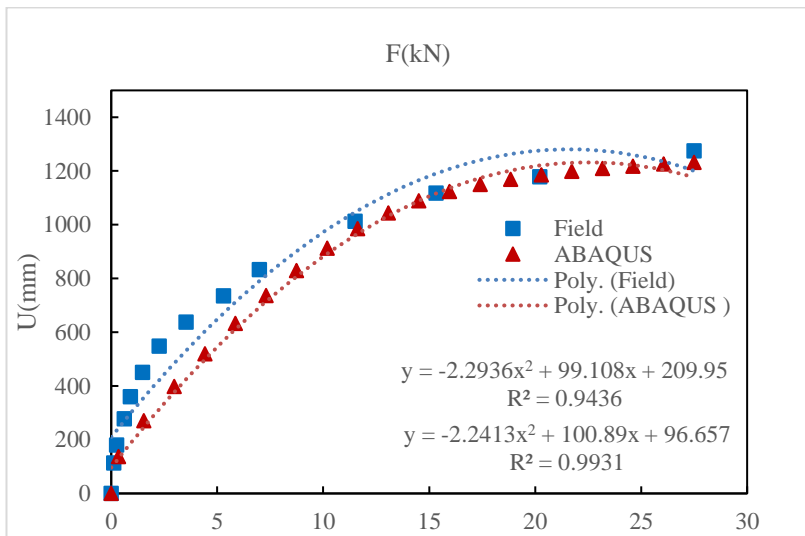


Figure 5- 53 Model B-3

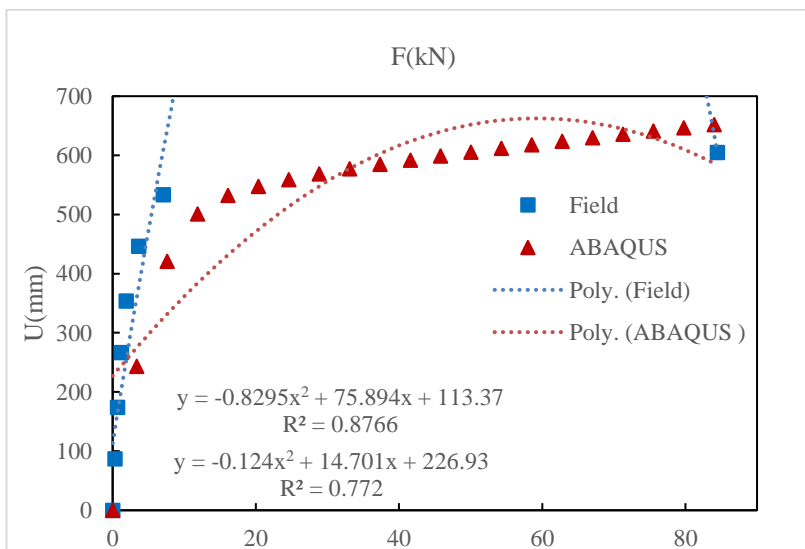


Figure 5- 54 Model B-4

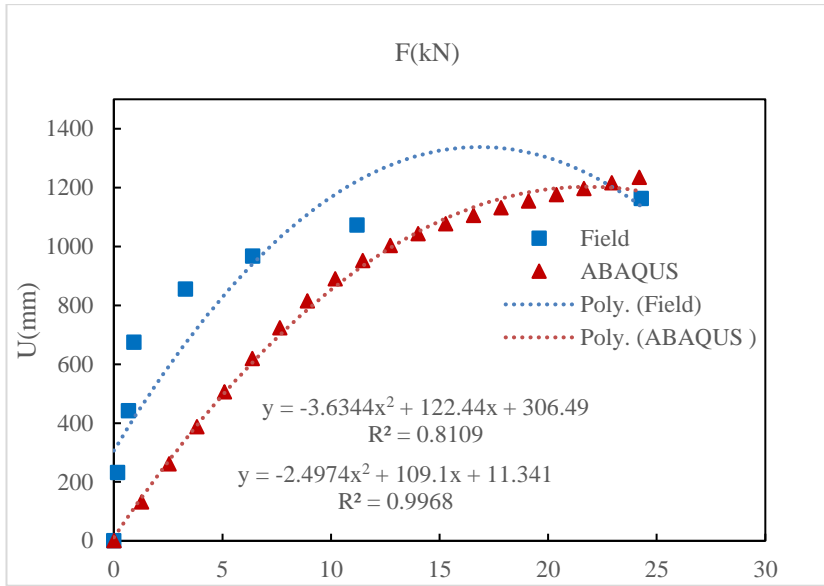


Figure 5- 55 Model B-5

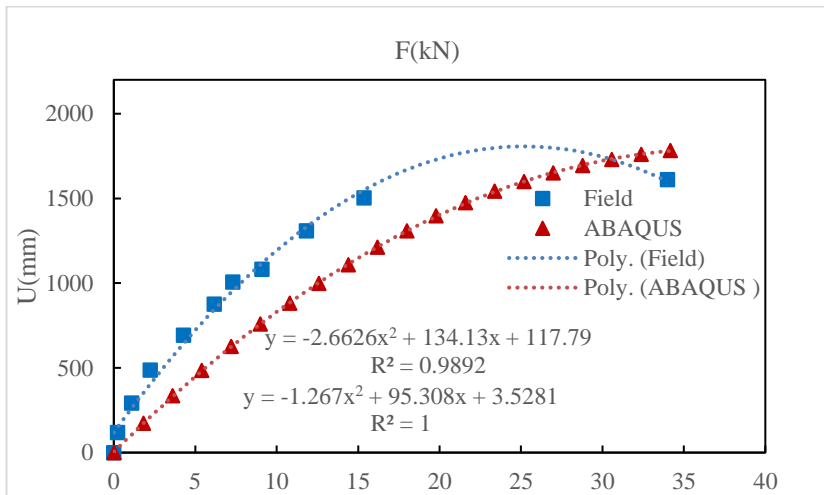


Figure 5- 56 Model B-6

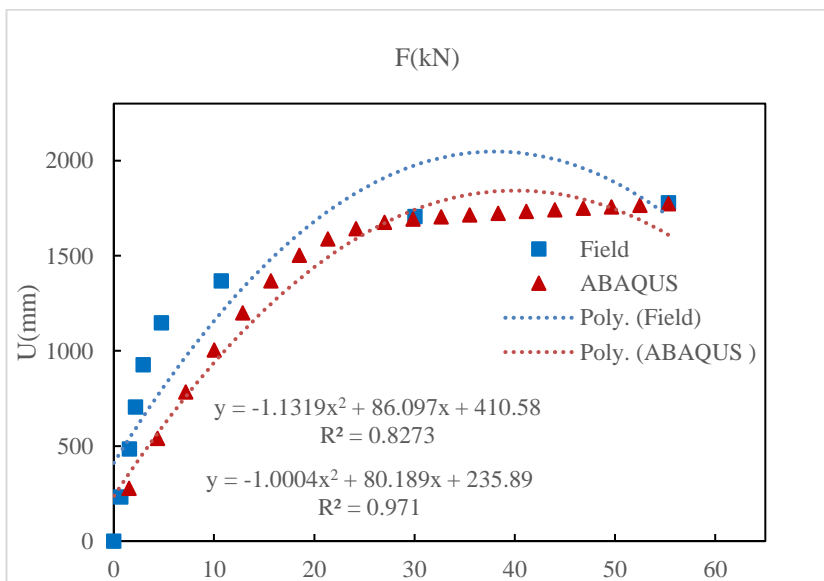


Figure 5- 57 Model B-7

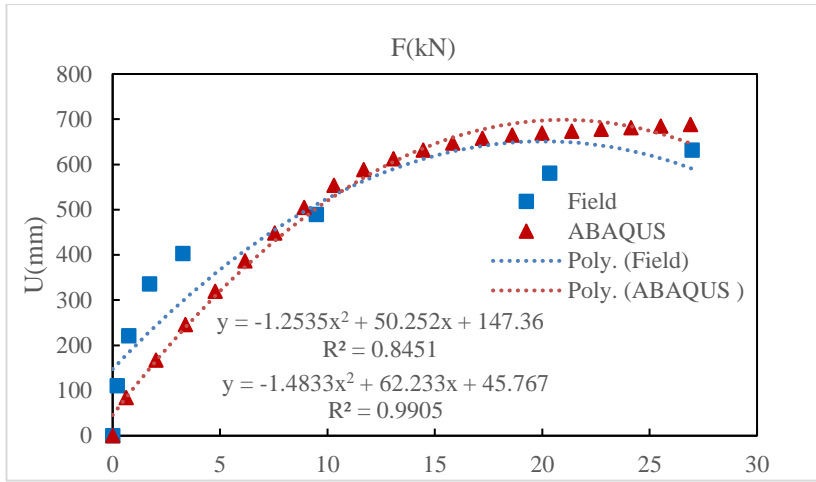


Figure 5- 58 Model B-8

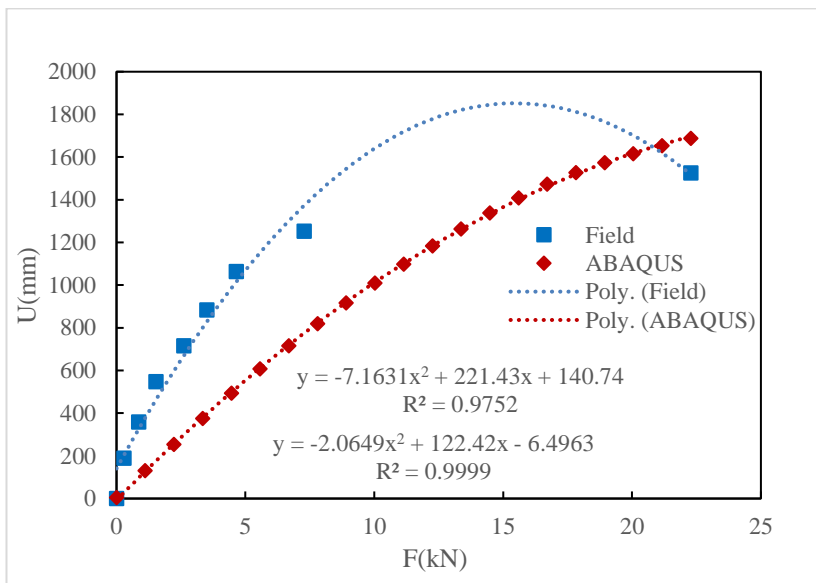


Figure 5- 59 Model B-9

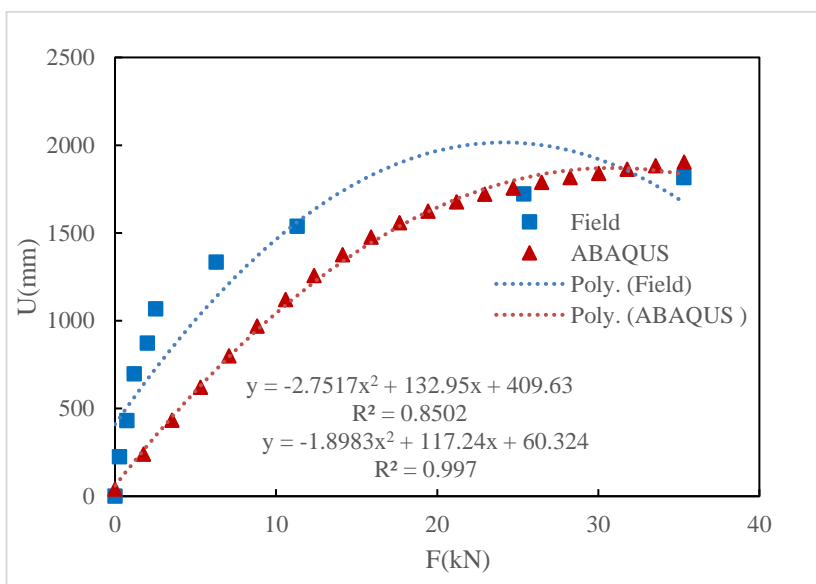


Figure 5- 60 Model B-10

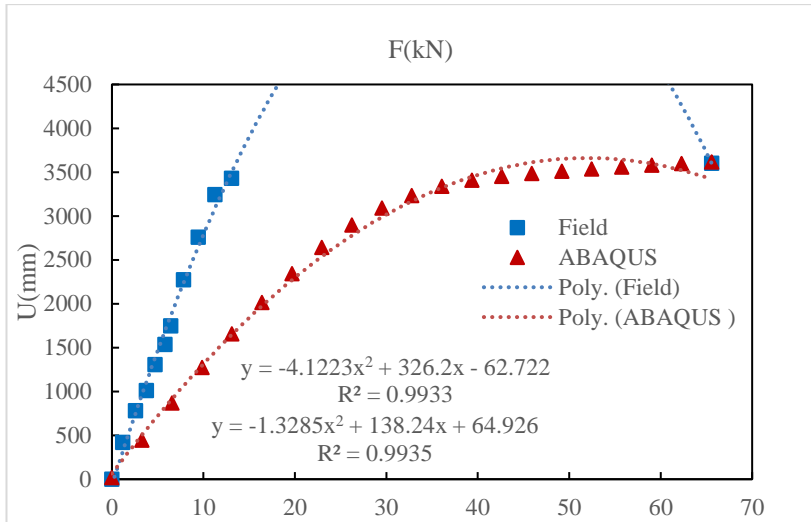


Figure 5- 61 Model B-11

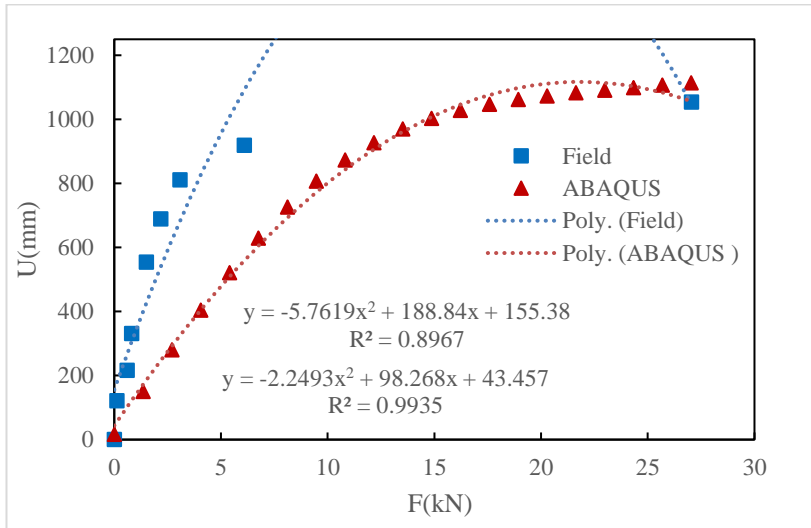


Figure 5- 62 Model B-12

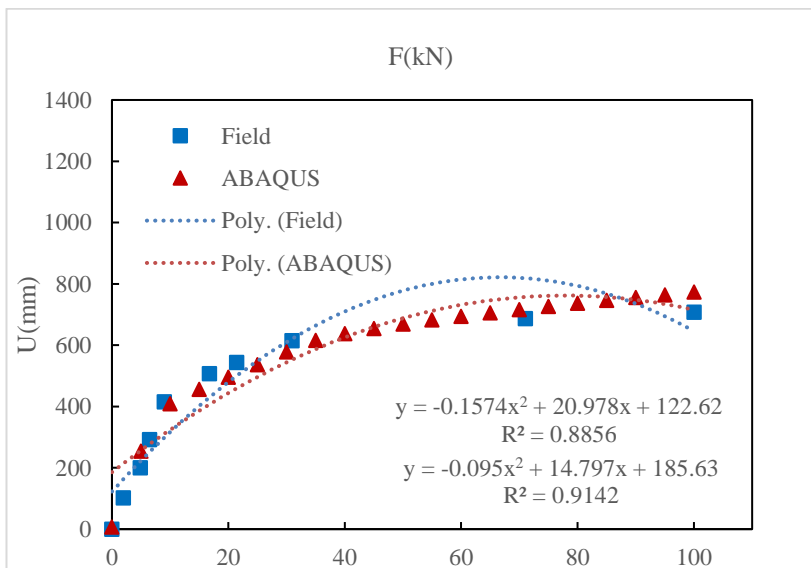


Figure 5- 63 Model B-13

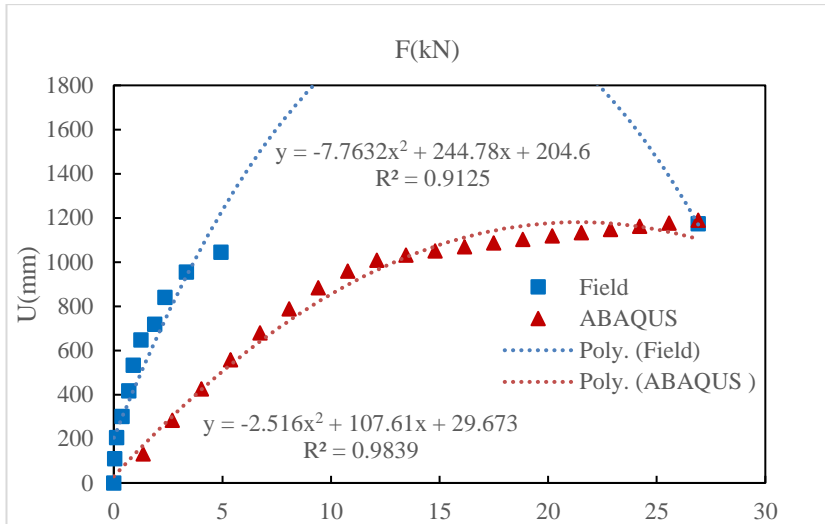


Figure 5- 64 Model B-14

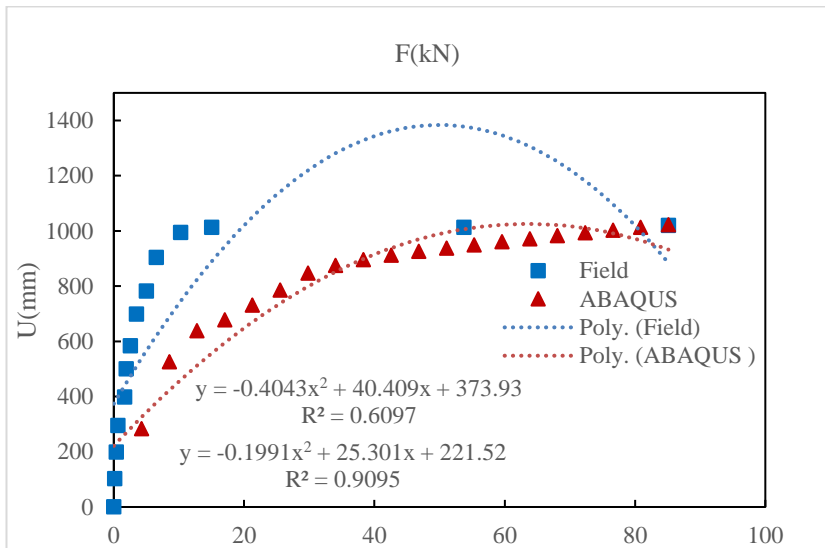


Figure 5- 65 Model B-15

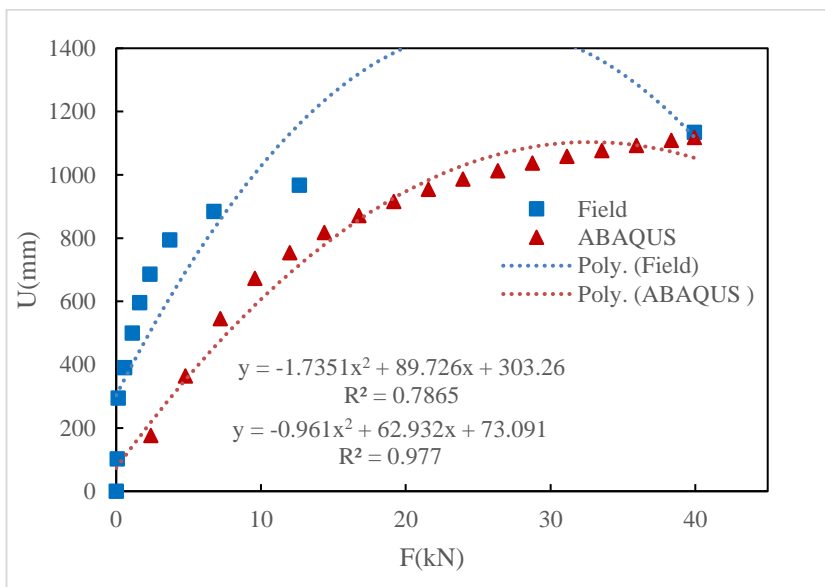


Figure 5- 66 Model B-16

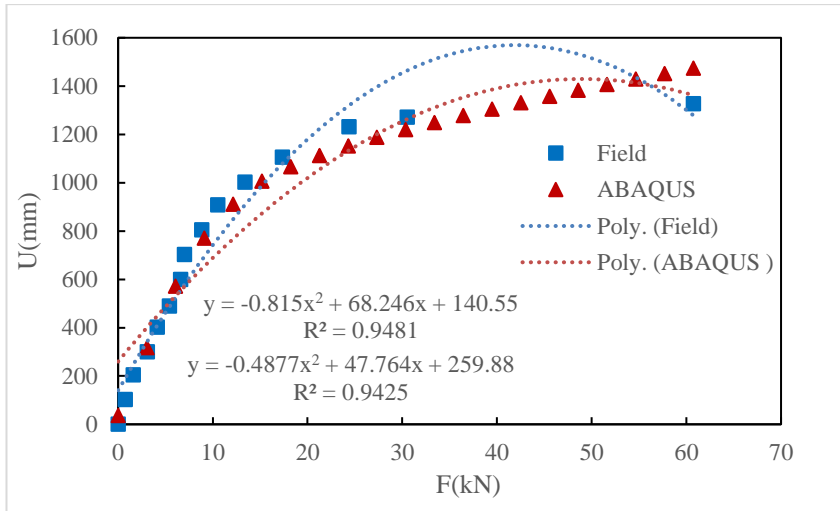


Figure 5- 67 Model B-17

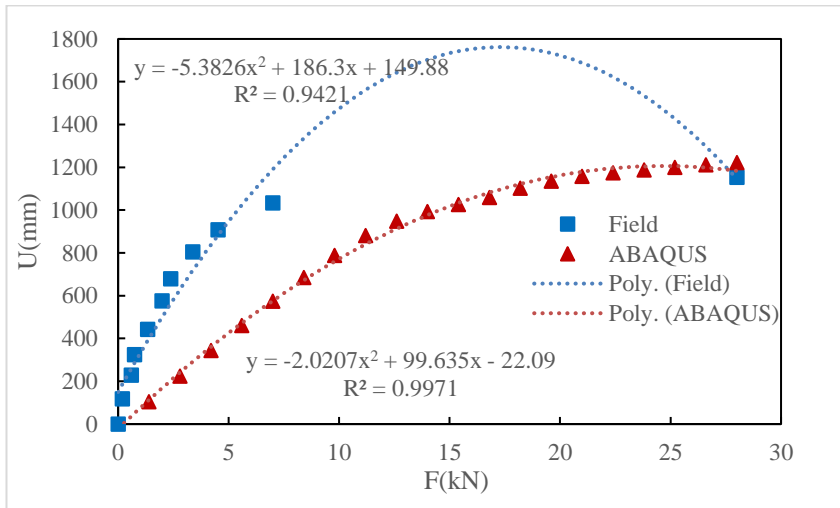


Figure 5- 68 Model B-18

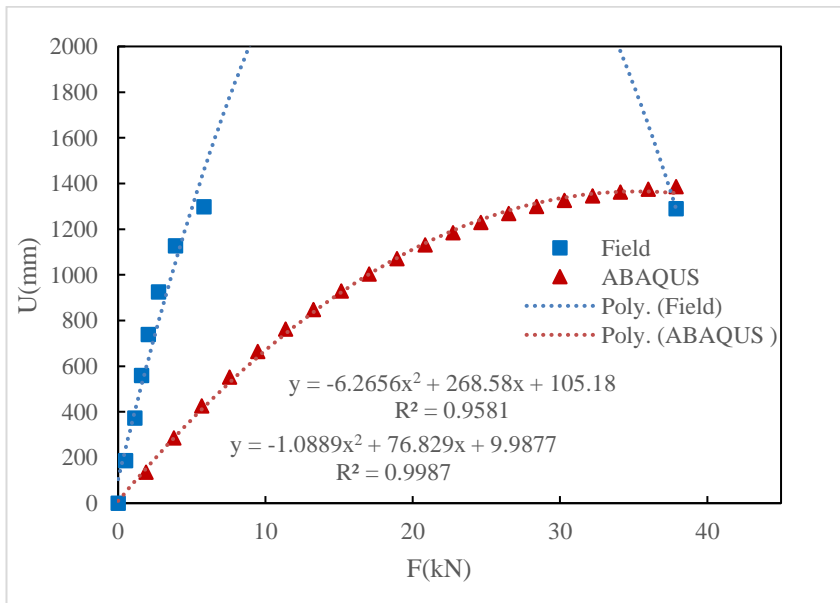


Figure 5- 69 Model B-19

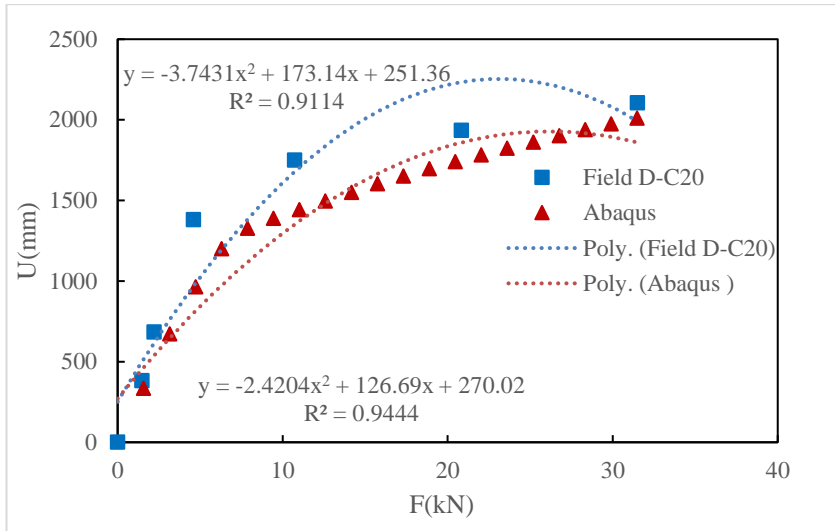


Figure 5- 70 Model B-20

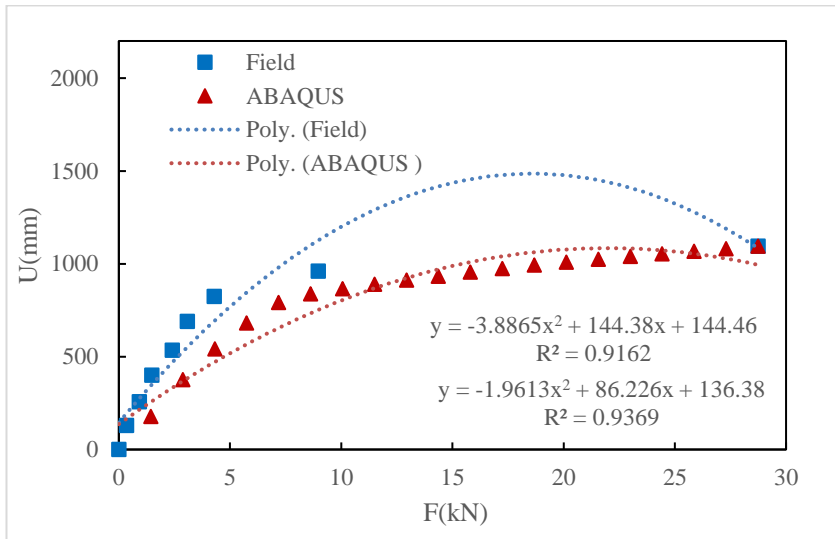


Figure 5- 71 Model B-21

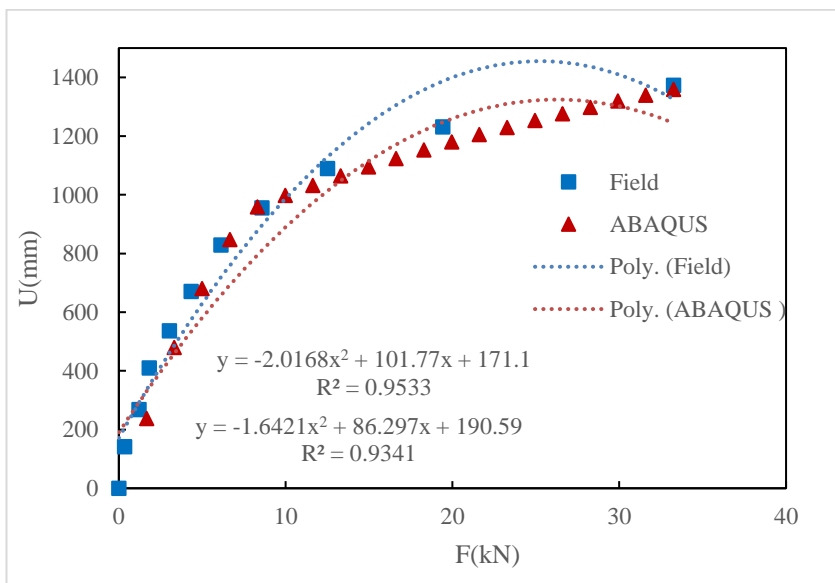


Figure 5- 72 Model B-22

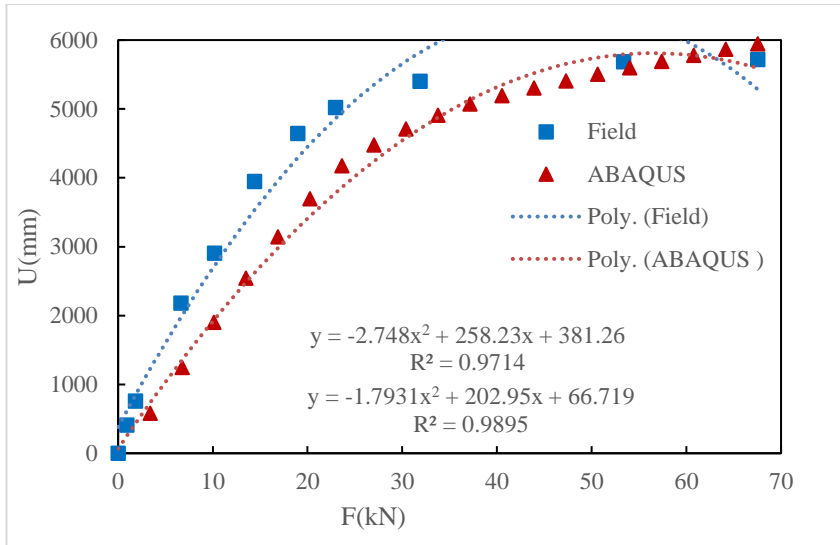


Figure 5- 73 Model B-23

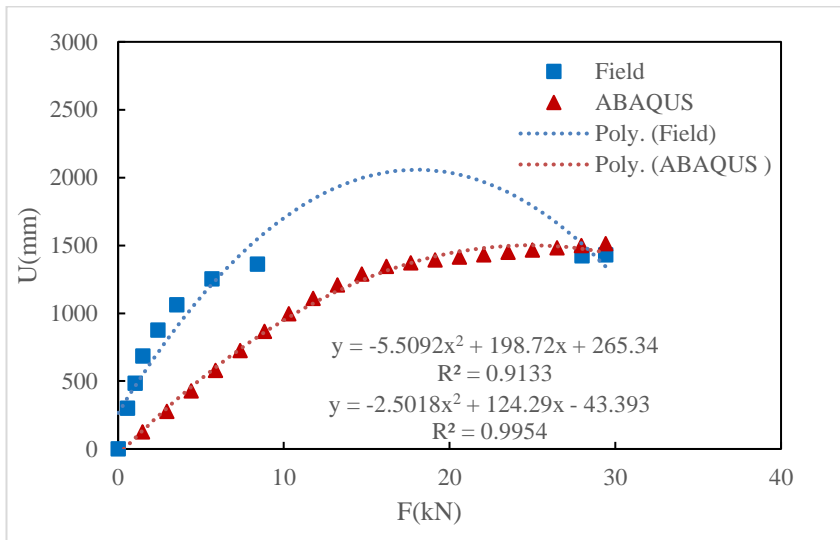


Figure 5- 74 Model B-24

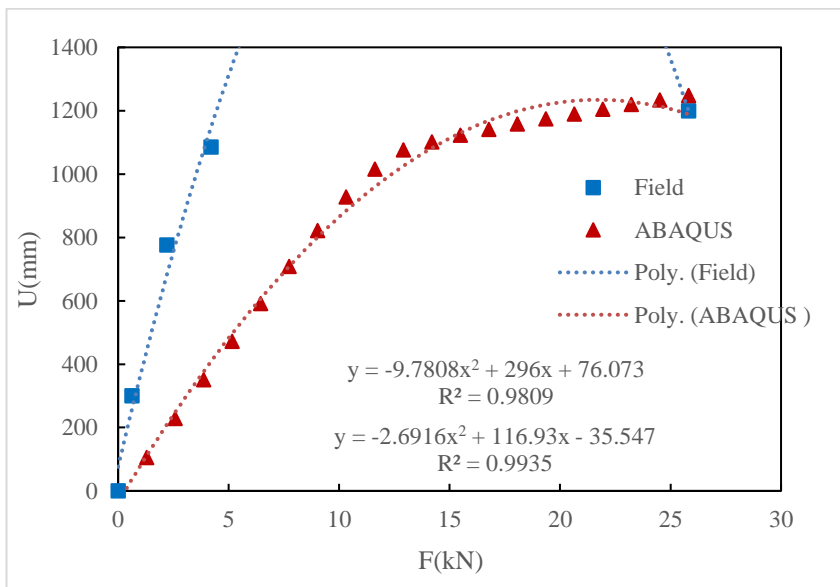


Figure 5- 75 Model B-25

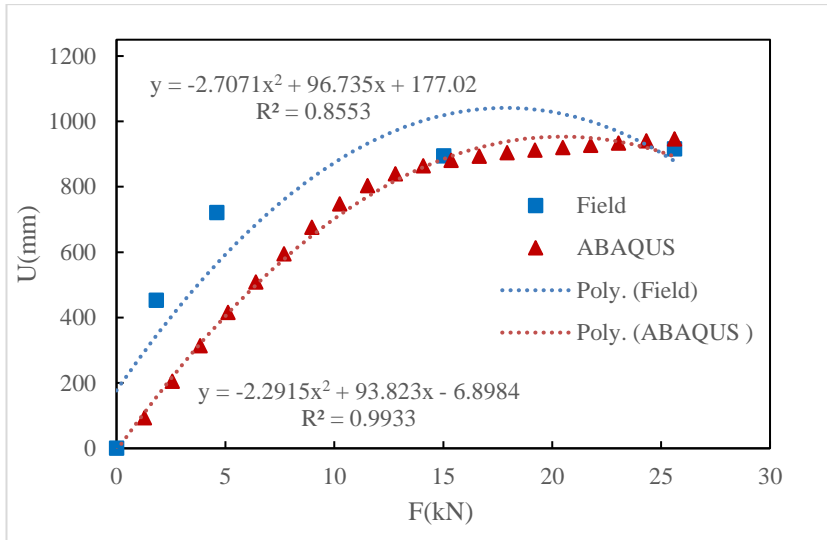


Figure 5- 76 Model B-26

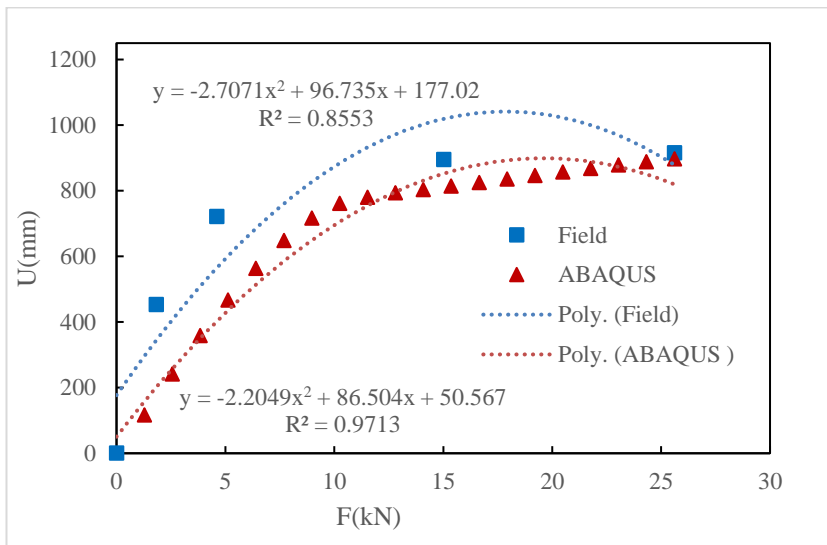


Figure 5- 77 Model B-27

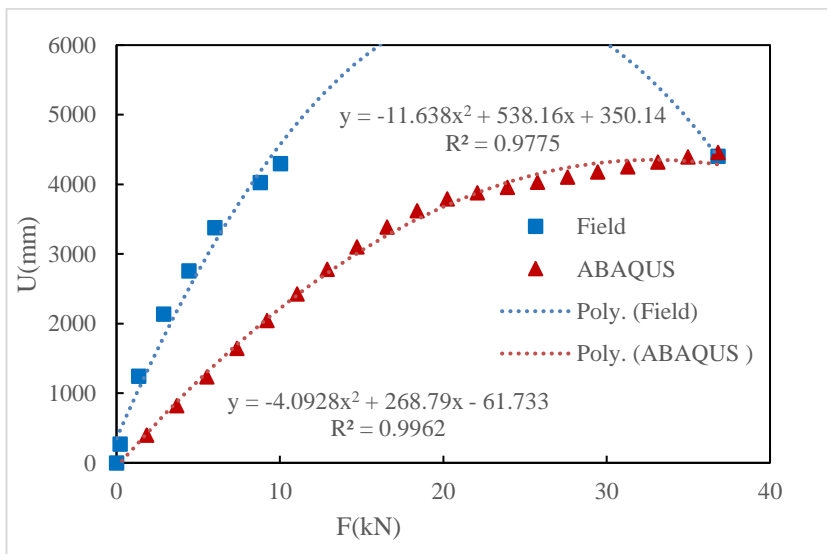


Figure 5- 78 Model B-28

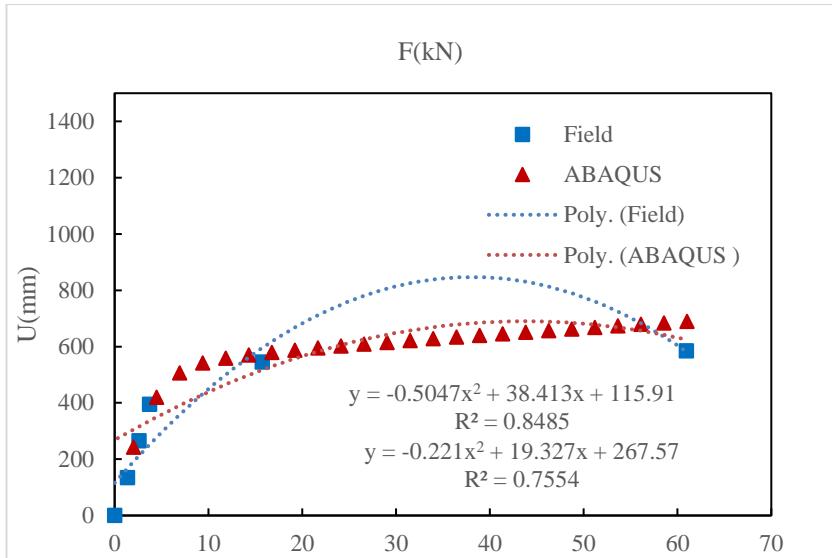


Figure 5- 79 Model C-1

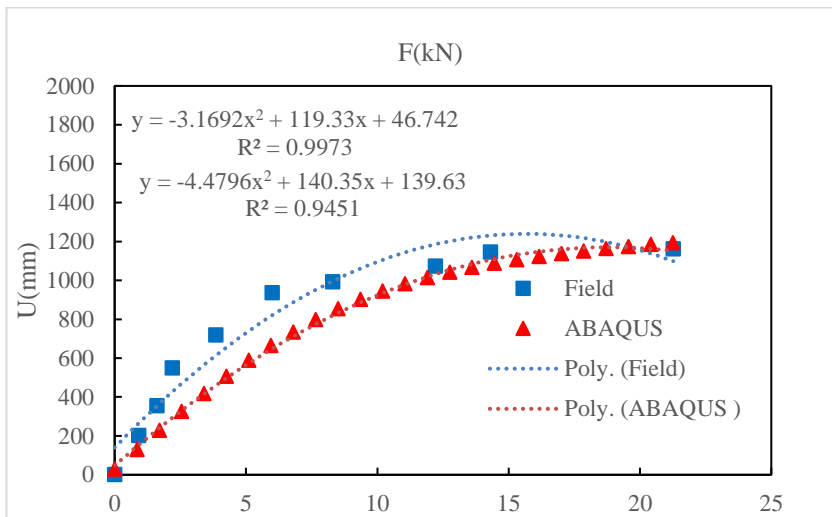


Figure 5- 80 Model C-2

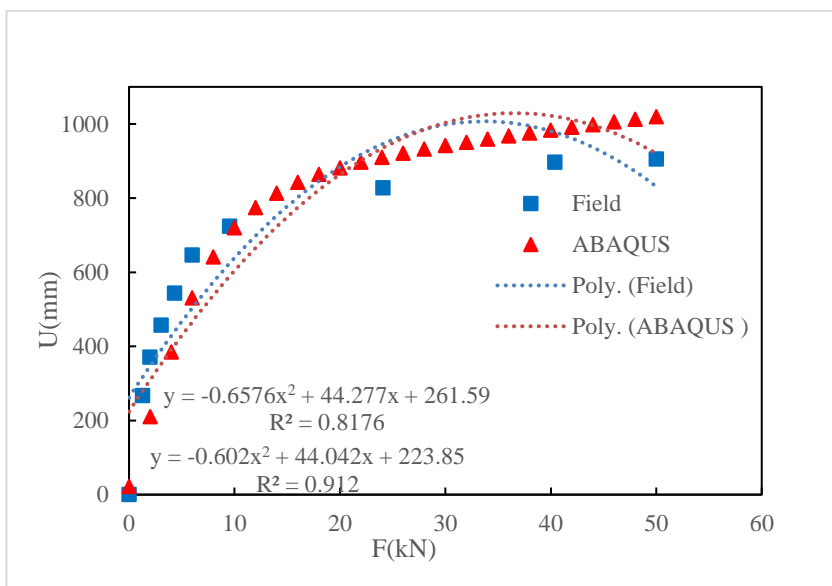


Figure 5- 81 Model C-3

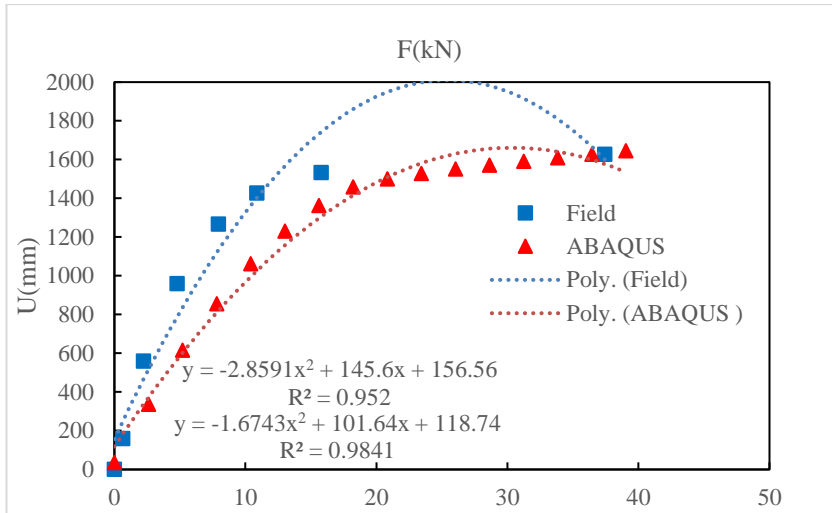


Figure 5- 82 Model C-4

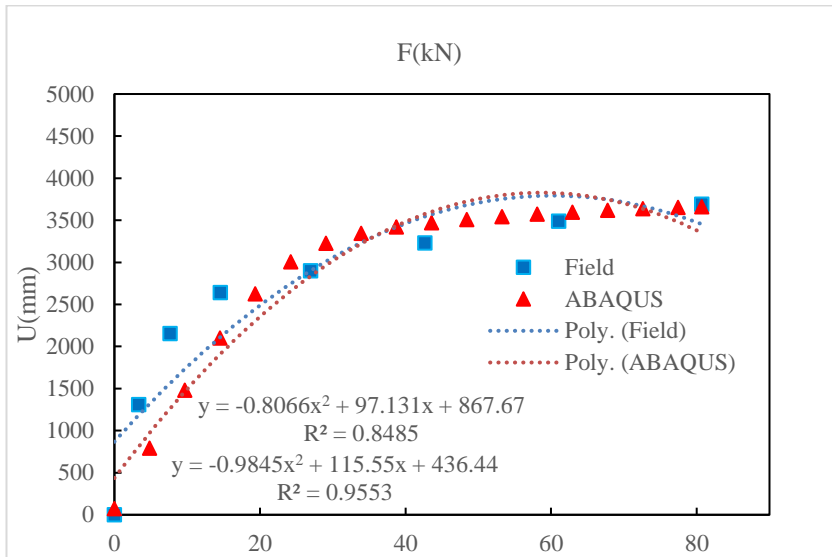


Figure 5- 83 Model C-5

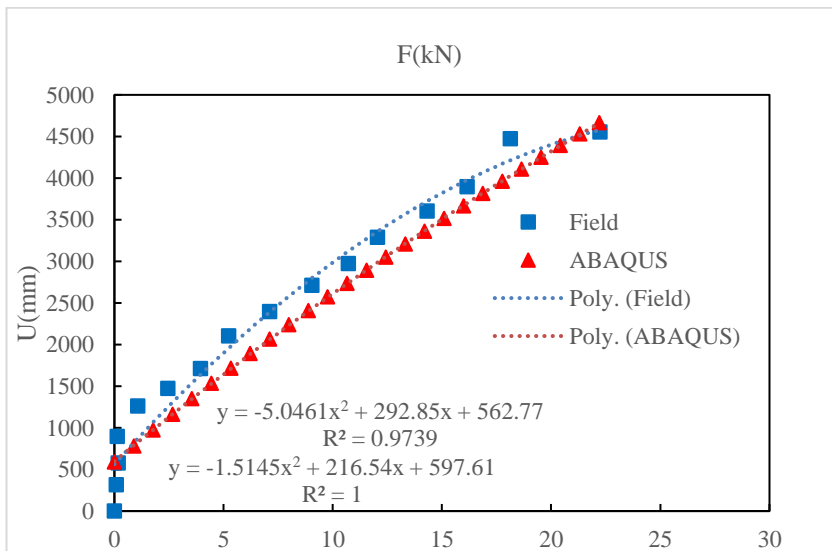


Figure 5- 84 Model C-6

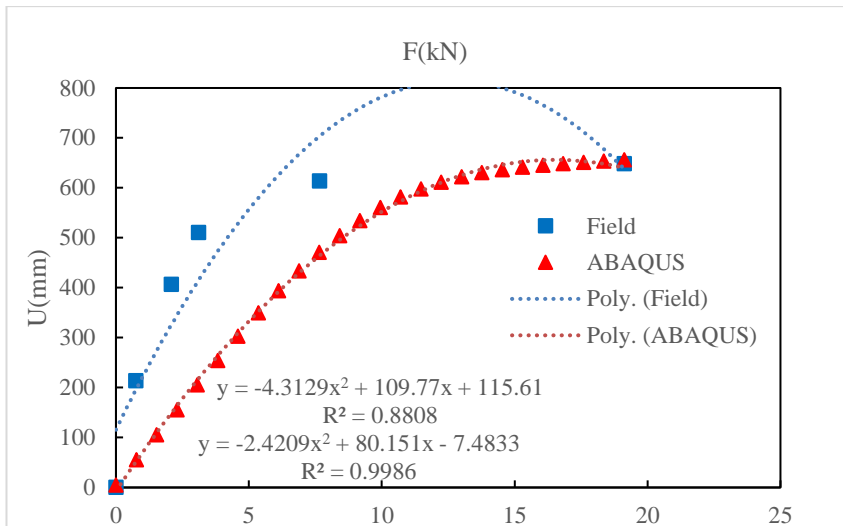


Figure 5- 85 Model C-7

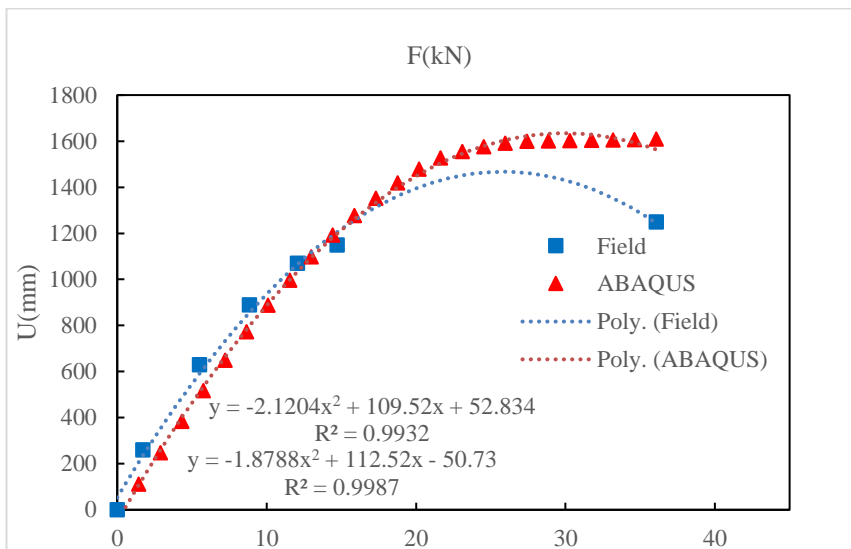


Figure 5- 86 Model C-8

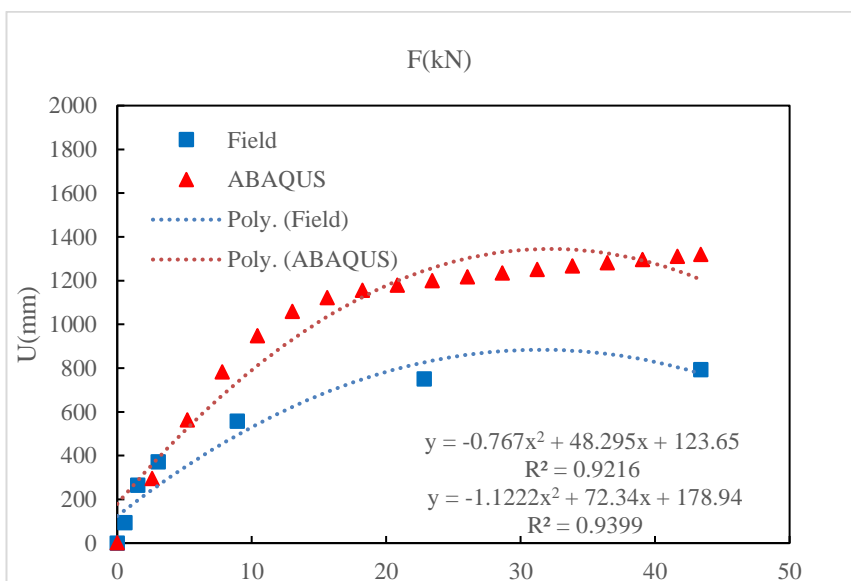


Figure 5- 87 Model C-9

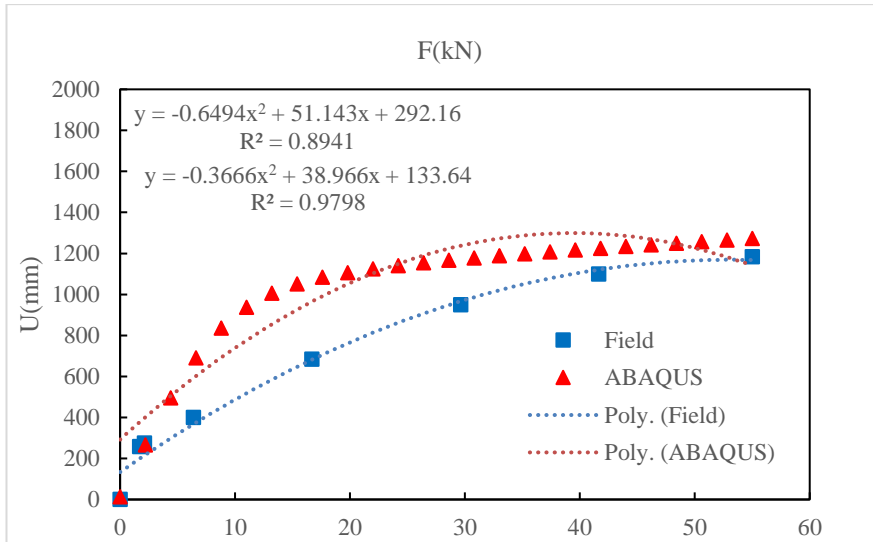


Figure 5- 88 Model C-10

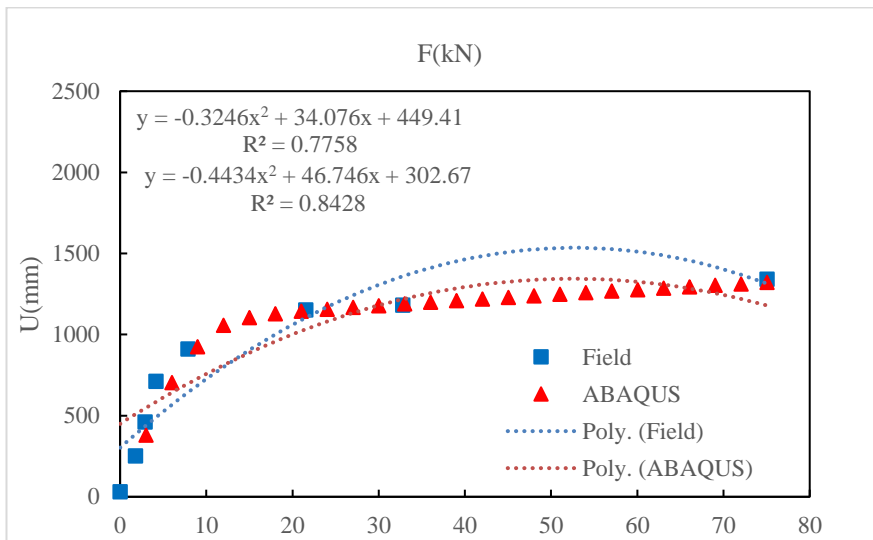


Figure 5- 89 Model C-11

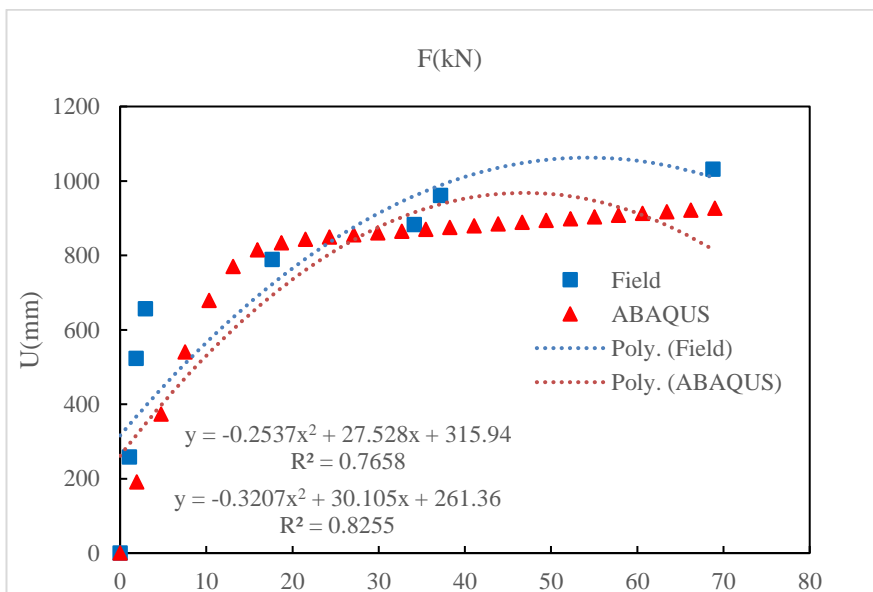


Figure 5- 90 Model C-12

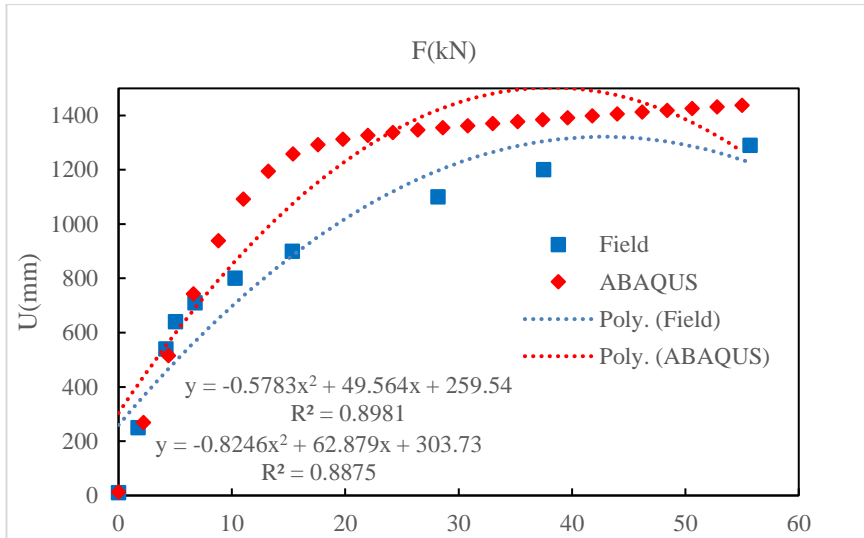


Figure 5- 91 Model C-13

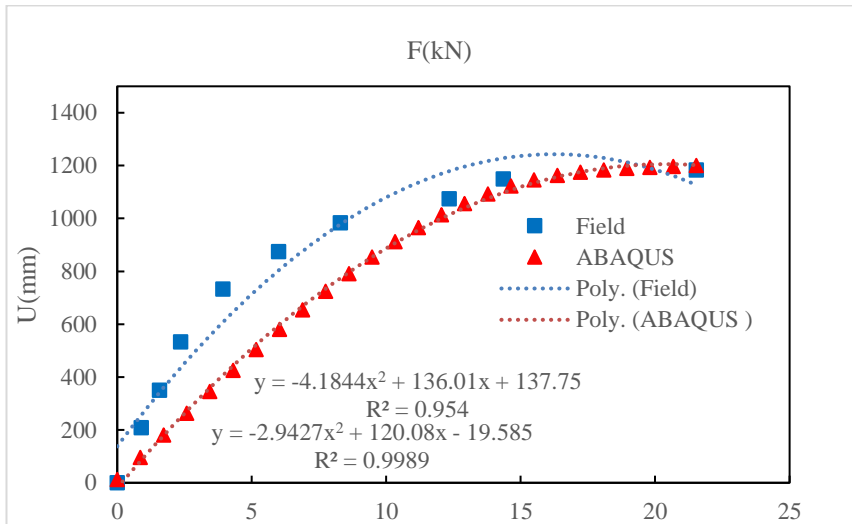


Figure 5- 92 Model C-14

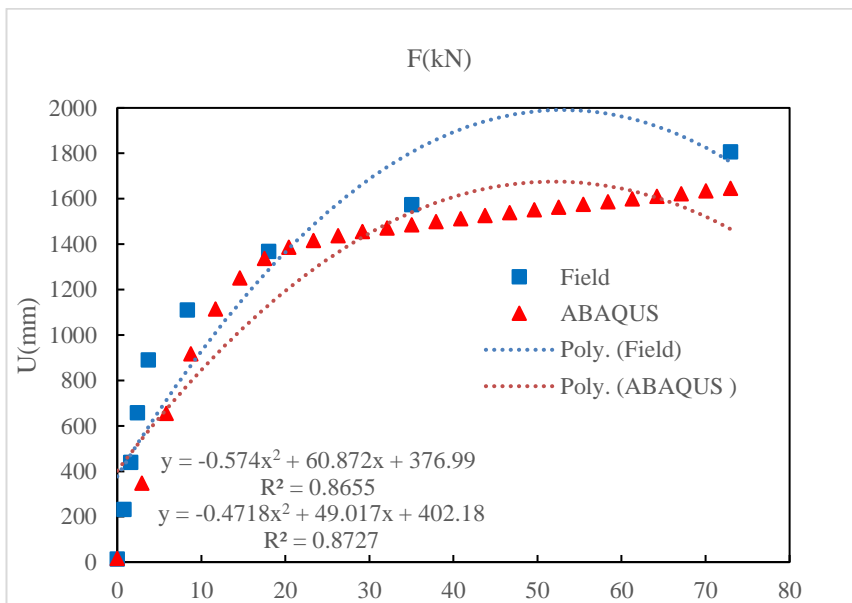


Figure 5- 93 Model C-15

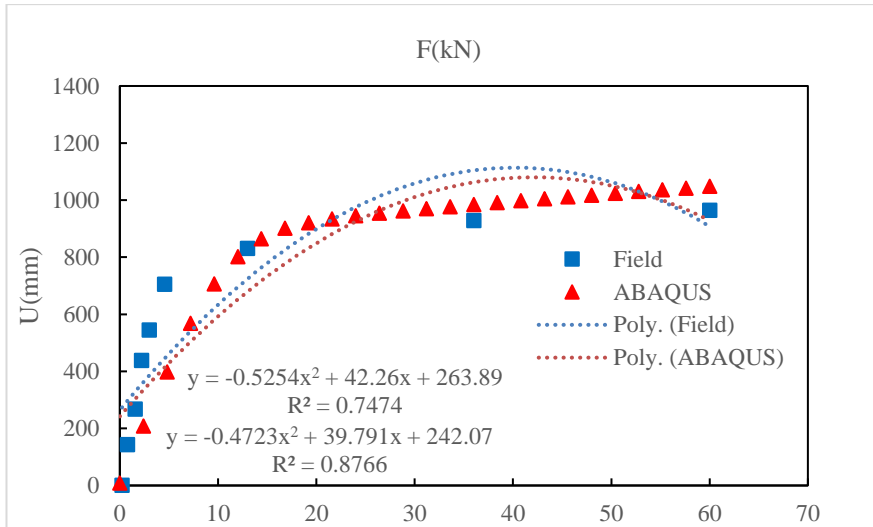


Figure 5- 94 Model C-16

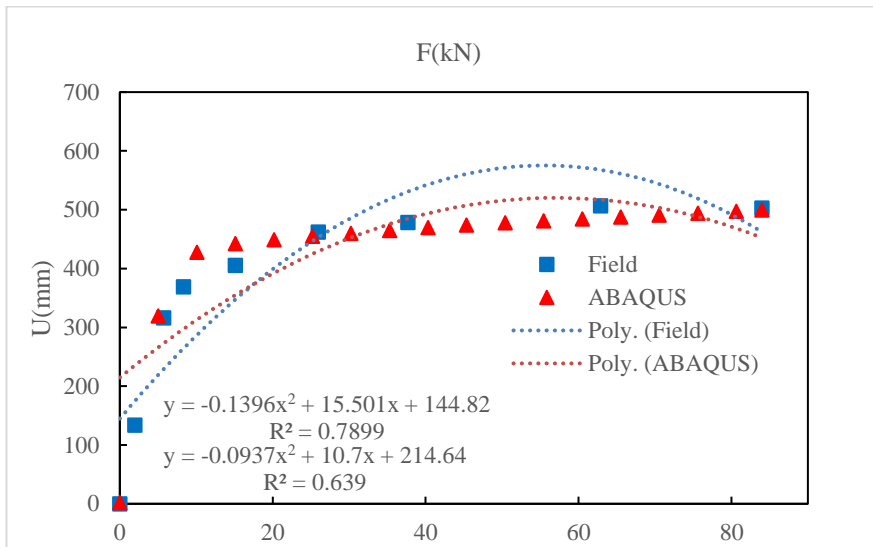


Figure 5- 95 Model C-17

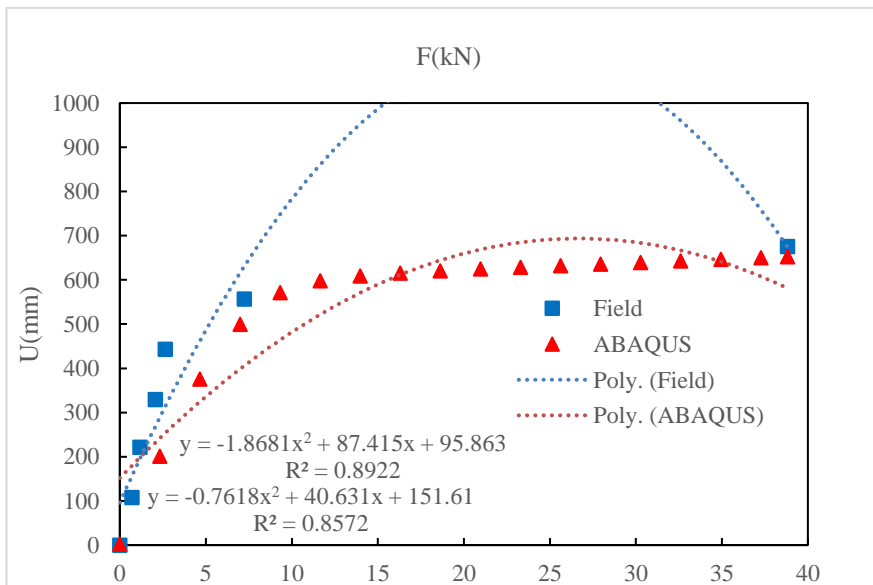


Figure 5- 96 Model C-18

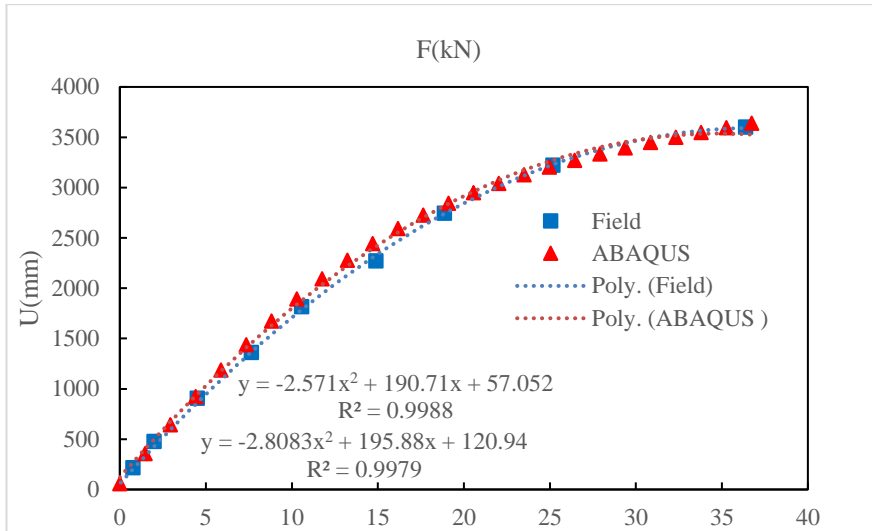


Figure 5- 97 Model C-19

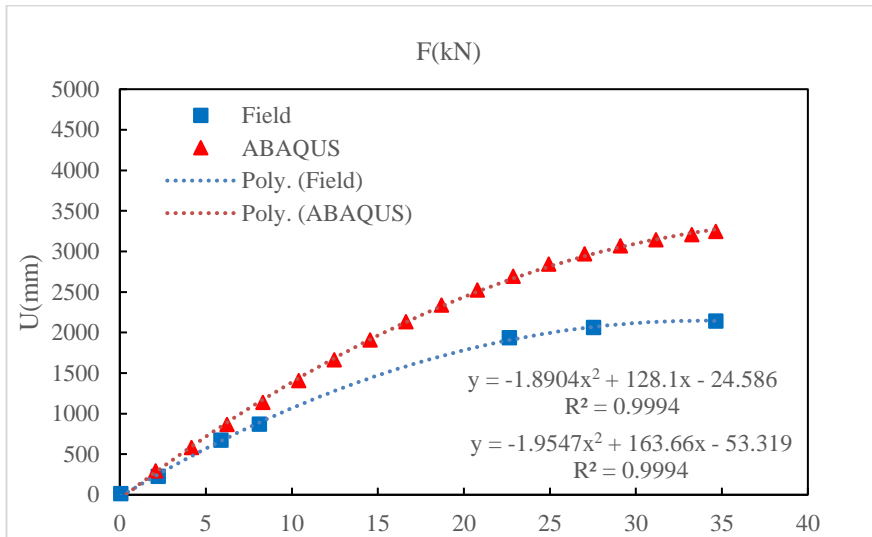


Figure 5- 98 Model C-20

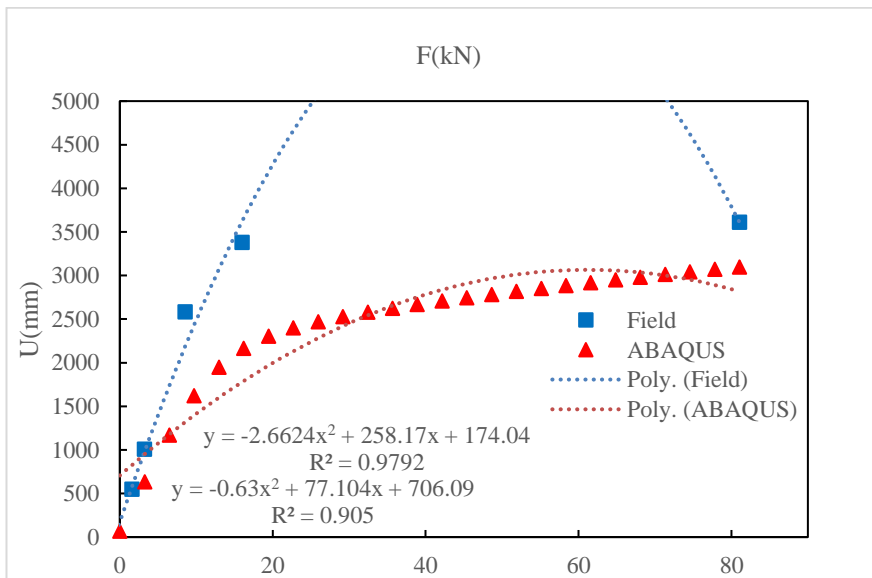


Figure 5- 99 Model C-21

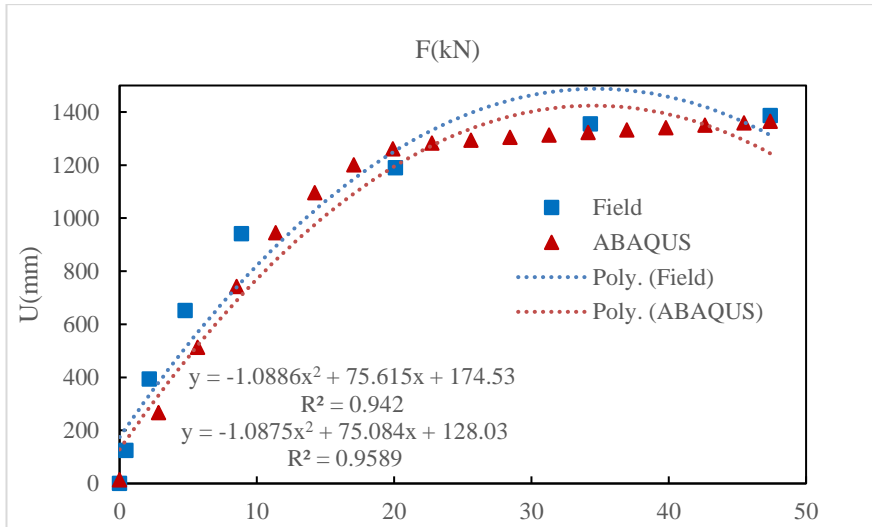


Figure 5- 100 Model C-22

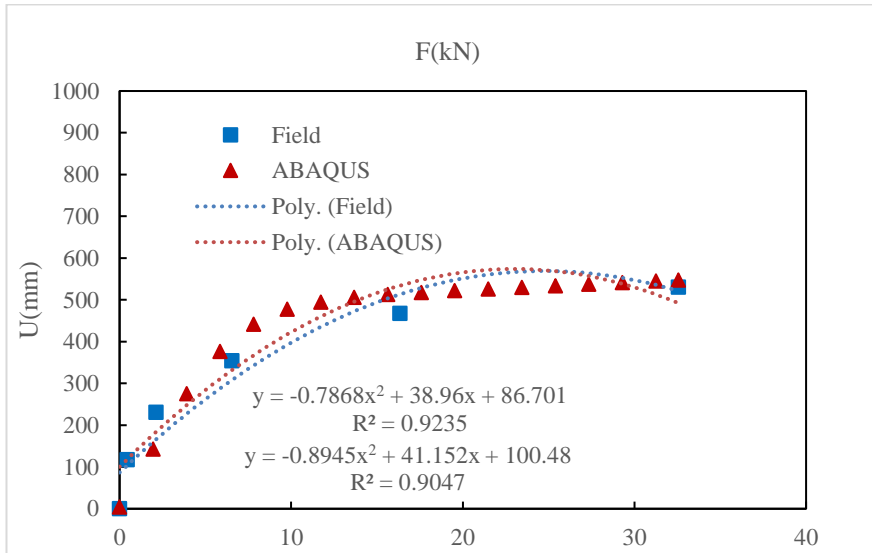


Figure 5- 101 Model C-23

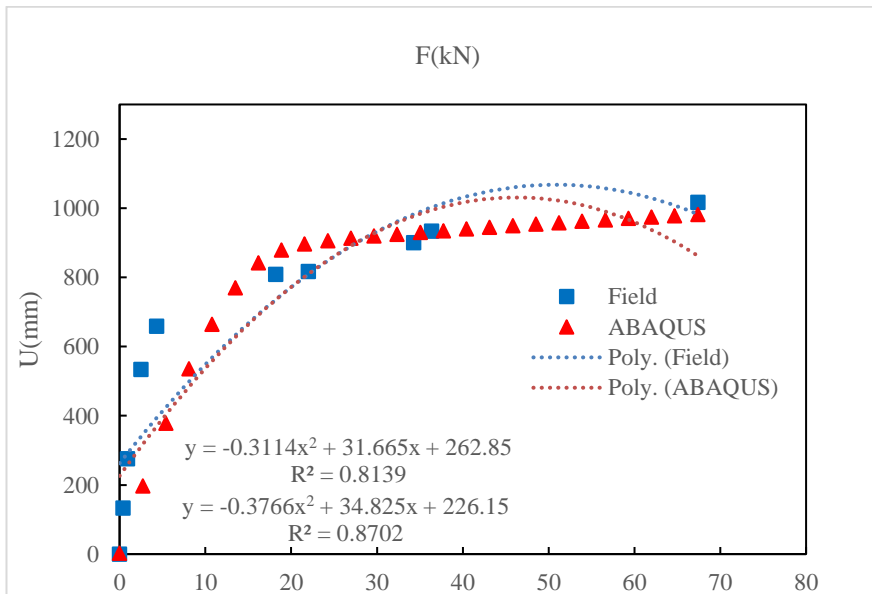


Figure 5- 102 Model C-24

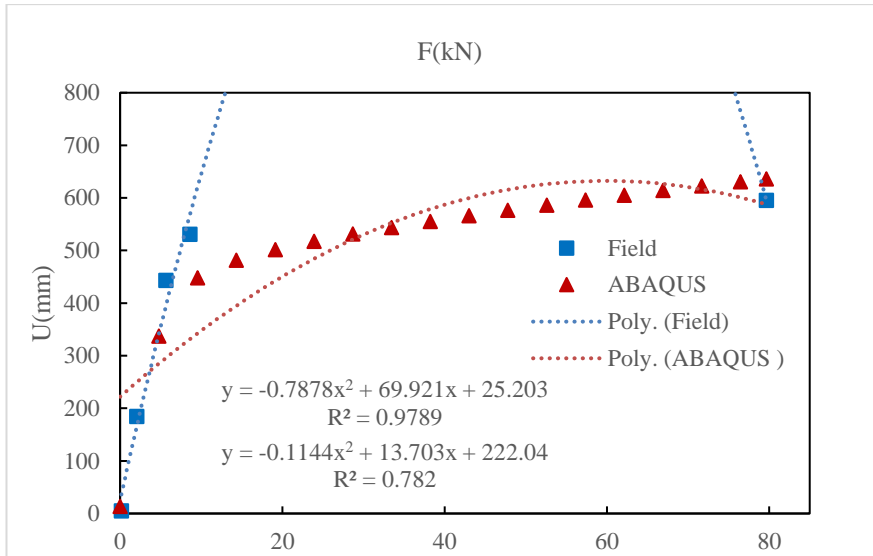


Figure 5- 103 Model C-25

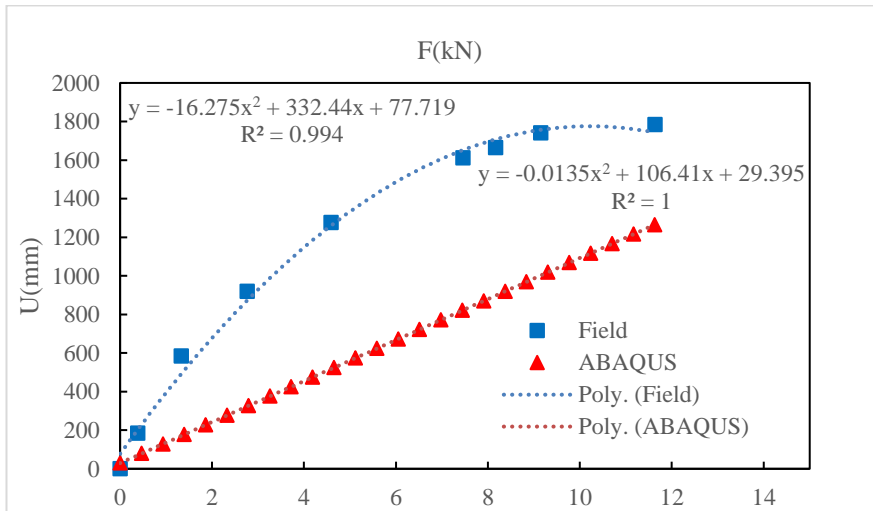


Figure 5- 104 Model C-26

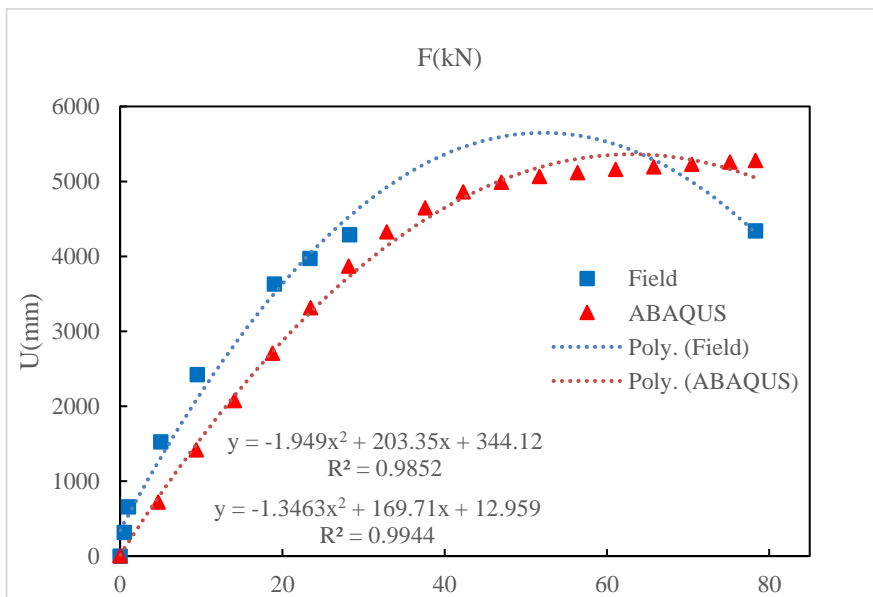


Figure 5- 105 Model C-27

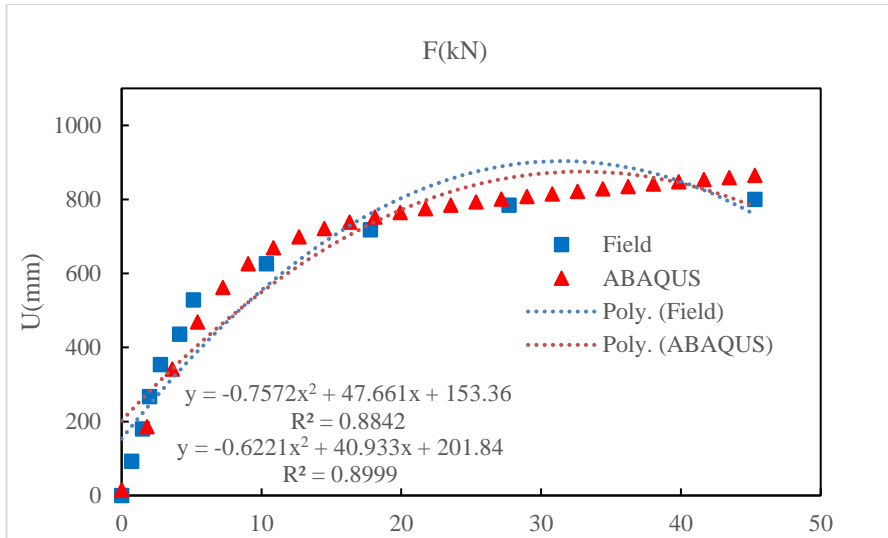


Figure 5- 106 Model C-28

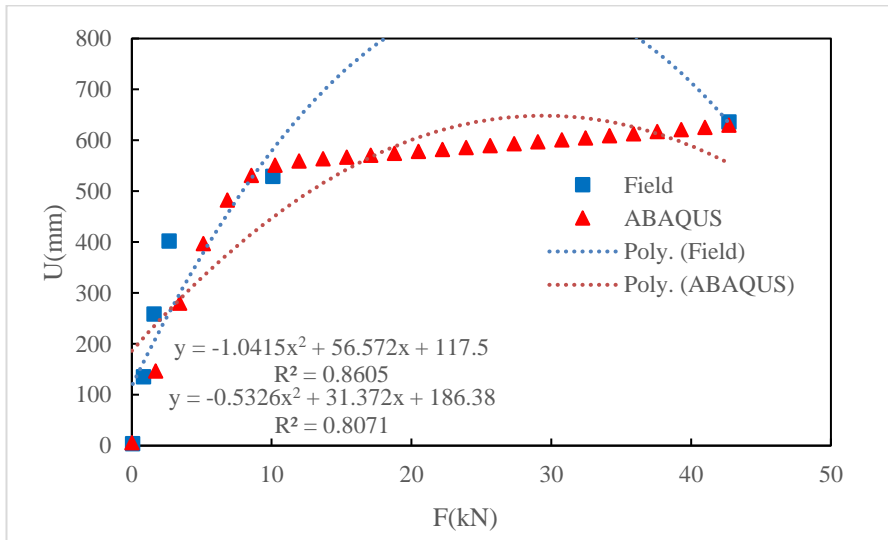


Figure 5- 107 Model C-29

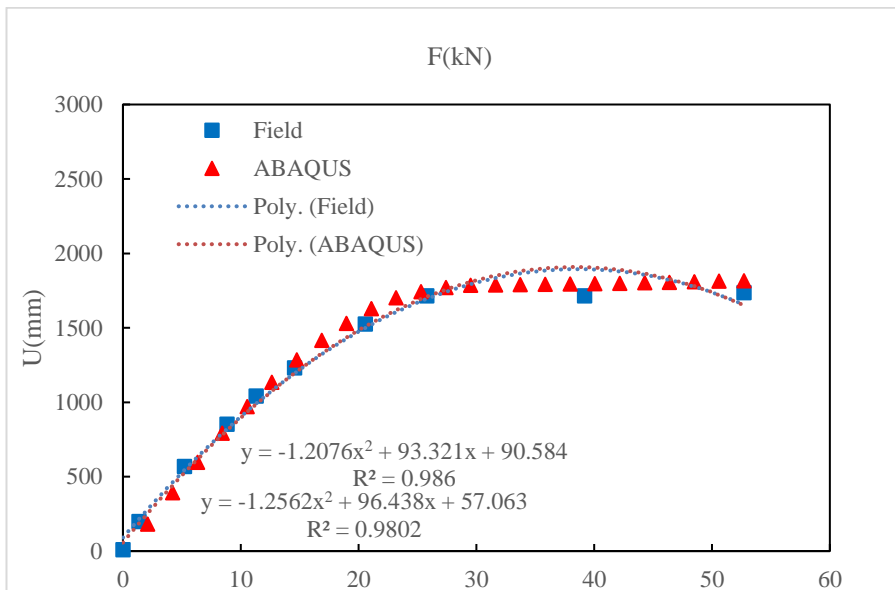


Figure 5- 108 Model C-30

5.3 SUMMARY OF THE CHAPTER

In this chapter, results and discussion was reviewed for the research conducted on pile-soil behaviour for CPT experimental and ABAQUS numerical investigation. In the first section, respective results and discussion were explained for 3 selected profiles from the literature resources. In the second section, material properties for each model were demonstrated. In the third section, parametric study for different values of modulus of elasticity was conducted. In the fourth section, convergence study for various values of elements in different mesh sizes was discussed. Then obtained displacement-force diagrams for each of 108 models were briefly described to validate ABAQUS results. All and all, based on the reviewed diagrams, this proposed study compares the results of the CPT and FEA methods under different loads and with different soil and pile types in a validated trend outcomes.

6 CONCLUSIONS AND RECOMMENDATIONS

6.1 CONCLUSIONS

The analysis, discussion and evidence created in the course of this research have endorsed the subsequent conclusions to be shown:

- The factors that have a major impact on the bearing capability of deep foundations (piles) consist of the length and diameter of embedded pile, the middling shaft point persistence within head impact region and weighted middling shaft point persistence alongside pile axle. The weighted middling sleeve friction has a negligible effect and may be well-thought-out as a secondary feature.
- The weighted middling technique for calculating the middling of shaft point persistence contained by head impact region or lengthwise pile axle delivers better averaging outcomes rather than the geometric and mathematic medians. The weighted middling proved advantageous mainly when many troughs and peaks are accessible in dignified values, and once great modifications occur in the values of shaft point persistence from one section of the deep foundation length to a different.
- The parameters of the ABAQUS model have dissimilar stages of impact on the qualification of the outcome. The modulus of elasticity and the friction angle are the utmost influential factors.
- When the value of E and ϕ increased, the shear stress along the pile and soil would be increased respectively. There would be a jump in the shear

stress-depth diagram as the type of soil has been changed to a stronger material. In a transition mechanism from a kind of soil to another, models with larger values of E and ϕ have more significant changes in shear stress.

- In the load transfer mechanism diagram, which is based on the energy that each layer can carry out, by increasing the depth, the accumulative load that the soil can transfer to the next layers decreases. This decay ratio for stronger layers, like gravel sand soil, is less than the weaker layers. By increasing the parameters E and ϕ in respective study layers, this value increases significantly.
- When CPT results show that there is a noticeable jump in the cone tip resistance profile, there would be a consequence in the shear stress-depth diagram. Therefore, we have a modification in the shear stress at that point for all parametric study models. This research shows that the performance of the model in more dense soil is better than weaker soil.
- When the CPT outcomes have distortions in any depth from ground level, consequently these distortions have slight effects in soil pile interaction alongside the pile at that distance.
- It is essential to find the right number of element in meshes in any finite element study because the not appropriate number of meshes could result in inaccurate results or could be time-consuming due to the longer running time. More number of meshes needs more running time for each model and less number of meshes results in a more prominent element and less accurate results.
- In order to validate the results from numerical analysis using ABAQUS, with the field outcomes, a comparison amongst the FEM and experimental methods should be carried out to examine the accuracy of developed numerical models further. Firstly, the force-displacement diagrams have to be demonstrated to investigate the correctness of ABAQUS simulation. Moreover, the trend line for each experimental and numerical tests should be illustrated in the diagram with the respective equation and regression results.

6.2 RECOMMENDATIONS

- The proposed FEM model can be used for accurate prediction of pile groups behaviour including axial capacity and load-settlement curve due to lateral loading.
- The FEM ABAQUS technique can also be used to predict the capacity of the deep foundations (piles) utilising the data of dynamic approaches.
- The competency of FEM ABAQUS to model the constitutive conduct of soils can considerably be developed if the method is prepared qualified of performing a feedback function in which the predicted result in the existing state is fed back to be an input for the next state.
- It is recommended that designers notice the expanded models as alternative for predicting the loading-settlement conduct and the axial capability of piles embedded in sand and mixed soil.
- The limitation of FEM ABAQUS package to model saturated and partially saturated soils can be of interest for engineers to find other finite element software.
- For validating FEM ABAQUS outcome with CPT results, other diagrams rather than force-displacement can be performed to obtain more reliable technique.
- A parametric study with other functions, like cohesion, dilation angle, groundwater level, lateral earth pressure coefficient, length of pile outside of soil and other installation methods can be performed to evaluate the FEM ABAQUS results.
- Convergence study can be extended to more comparing functions, like settlement, ultimate capacity and stresses.
- The results of this study, which are based on plane-strain analysis can be compared with results of three-dimensional (3D) finite element modelling to evaluate the accuracy of plane-strain model.
- The application of the proposed FEM model for raked piles can be investigated
- The application of the proposed FEM model for piles socketed into rock can be investigated.

7 REFERENCES

1. Randolph, M. *Design methods for pile group and piled rafts*. in *Proc. 13th Int. Conf. on SMFE*. 1994.
2. Poulos, H.G. and E.H. Davis, *Pile foundation analysis and design*. 1980.
3. Bowles, J.E., *Foundation Analysis and Design*. 4th ed. 1988.
4. Young, F., et al., *PILES AND FOUNDATIONS (CONTD)*. 1981.
5. Eslami, A., *Bearing capacity of piles from cone penetration test data*. 1997, University of Ottawa (Canada).
6. Ng, C.W., N.E. Simons, and B.K. Menzies, *A short course in soil-structure engineering of deep foundations, excavations and tunnels*. Vol. 5. 2004: Thomas Telford.
7. Briaud, J. *Evaluation of cone penetration test methods using 98 pile load tests*. in *Proceedings of the 1st International Symposium on Penetration Testing* Vol. 1988.
8. Robertson, P., et al., *Axial capacity of driven piles in deltaic soils using CPT*. *Penetration Testing 1988*, 1988. **2**: p. 919-928.
9. Abu-Farsakh, M.Y. and H.H. Titi, *Assessment of direct cone penetration test methods for predicting the ultimate capacity of friction driven piles*. *Journal of Geotechnical and Geoenvironmental Engineering*, 2004. **130**(9): p. 935-944.
10. Cai, G., et al., *Assessment of direct CPT and CPTU methods for predicting the ultimate bearing capacity of single piles*. *Engineering Geology*, 2009. **104**(3-4): p. 211-222.
11. Lee, C., M. Bolton, and A. Al-Tabbaa, *Numerical modelling of group effects on the distribution of dragloads in pile foundations*. *Geotechnique*, 2002. **52**(5): p. 325-335.
12. Rajagopal, K. and S. Karthigeyan, *Influence of combined vertical and lateral loading on the lateral response of piles*. *International Association for*

- Computer Methods and Advances in Geomechanics (IACMAG), 2008: p. 3272-3282.
13. Shahin, M.A., *Load–settlement modeling of axially loaded steel driven piles using CPT-based recurrent neural networks*. Soils and Foundations, 2014. **54**(3): p. 515-522.
 14. Shahin, M.A., *Use of evolutionary computing for modelling some complex problems in geotechnical engineering*. Geomechanics and Geoengineering, 2015. **10**(2): p. 109-125.
 15. Kavvads, M. and G. Gazetas, *Kinematic seismic response and bending of free-head piles in layered soil*. Geotechnique, 1993. **43**(2): p. 207-222.
 16. Mujah, D., et al., *The design method of slope stabilizing piles: a review*. International Journal of Current Engineering and Technology, 2013. **3**(2): p. 224-229.
 17. ICC(International_Code_Council), *International Building Code*, C.C. Hills, Editor. 2003, International Code Council
 18. Eurocode8 and P. 5, *Foundation, retaining structures and geotechnical aspects*. 1999.
 19. Whitman, R.V., *Analysis of Soil-Structure Interaction: State-of -the-Art Review*, I.O.S.a.V. Experimental and Structural Dynamics, Editor. 1972: Southampton.
 20. Kausel, E. and J. Roesset, *Soil structure interaction problems for nuclear containment structures*, in *Electric power and the civil engineer*. 1974, Proc. ASCE: Boulder, Colorado.
 21. Shahin, M.A., *Intelligent computing for modeling axial capacity of pile foundations*. Canadian Geotechnical Journal, 2010. **47**(2): p. 230-243.
 22. J., P., *Soil-Pile Foundation Interaction*. Earthquake Engineering, 1970: p. 349-381.
 23. Sen, R., T. Davies, and P. Banerjee, *Dynamic analysis of piles and pile groups embedded in homogeneous soils*. Earthquake engineering & structural dynamics, 1985. **13**(1): p. 53-65.
 24. Ahmad, S. and S. Mamoon, *Seismic Response of Floating Piles to Obliquely Incident Waves*, in *Proc. of 2nd International Conference on Recent Advances in Geotechnical Earthquake Engineering and Soil Dynamics*. 1991, University of Missouri-Rolla Publication: St. Louis, MO. p. 805-814.
 25. Butterfield, R. and P. Banerjee, *The elastic analysis of compressible piles and pile groups*. Geotechnique, 1971. **21**(1): p. 43-60.
 26. Poulos, H.G., *Analysis of the Settlement of Pile Groups*. Geotechnique, 1968. **18** (4): p. 449-471.
 27. Poulos, H.G., *Behavior of laterally loaded piles II. Pile groups*. Journal of Soil Mechanics & Foundations Div, 1971. **97**(SM5): p. 773-751.
 28. Kaynia, A.M. and E. Kausel, *Dynamic Behavior of Pile Groups*, in *2nd int. Conference, On Numerical Methods in Offshore Piling*. 1982: Texas University, Austin. p. 509-532.
 29. Kausel, E. and R. Peek, *Boundary integral method for Stratified Soils*. MIT Department of Civil Engineering, Order, 1982(746).
 30. Reese, L.C., W.R. Cox, and F.D. Koop, *Analysis of laterally loaded piles in sand*. Offshore Technology in Civil Engineering Hall of Fame Papers from the Early Years, 1974: p. 95-105.

31. Matlock, H., *Correlations for design of laterally loaded piles in soft clay*. Offshore technology in civil engineering's hall of fame papers from the early years, 1970: p. 577-594.
32. El Naggar, M. and M. Novak, *Nonlinear analysis for dynamic lateral pile response*. Soil Dynamics and Earthquake Engineering, 1996. **15**(4): p. 233-244.
33. Brown, D.A., et al., *Static and dynamic lateral loading of pile groups*. 2001: TRB Washington, DC, USA.
34. Juirnarongrit, T., *Effect of diameter on the behavior of laterally loaded piles in weakly cemented sand*. 2003.
35. Reese, L., et al., *Computer program LPILE plus version 4.0 technical manual*, Ensoft. Inc., Austin, Texas, 2000.
36. Wang, S.-T. and L.C. Reese, *COM624P-Laterally loaded pile analysis program for the microcomputer, version 2.0*. 1993, United States. Federal Highway Administration. Office of Technology Applications.
37. Reese, L.C., W.R. Cox, and F.D. Koop. *Field testing and analysis of laterally loaded piles on stiff clay*. in *Offshore Technology Conference*. 1975. Offshore Technology Conference.
38. Alkroosh, I.S.J., *Modelling pile capacity and load-settlement behaviour of piles embedded in sand & mixed soils using artificial intelligence*. 2011, Curtin University.
39. Reese, L.C. and R.C. Welch, *Lateral loading of deep foundations in stiff clay*. Journal of Geotechnical and Geoenvironmental Engineering, 1975. **101**(ASCE# 11456 Proceeding): p. 663-649.
40. Welch, R.C. and L.C. Reese, *Laterally loaded behavior of drilled shafts*. 1972: University of Texas, Austin. p. 3-5-65-89.
41. Nogami, T. and K. Konagai, *Time domain flexural response of dynamically loaded single piles*. Journal of Engineering Mechanics, 1988. **114**(9): p. 1512-1525.
42. Mujah, D., et al., *Numerical analysis of multirow arrangement of small diameter steel piles for landslide prevention*. International Journal of Current Engineering and Technology, 2013. **3**(1): p. 1-20.
43. O'Neill, M.W. and J.M. Murchison, *An evaluation of py relationships in sands*. 1983: University of Houston.
44. Ismael, N.F., *Behavior of laterally loaded bored piles in cemented sands*. Journal of Geotechnical Engineering, 1990. **116**(11): p. 1678-1699.
45. Bahrami, A. and H. Nikraz. *Initial Soil Springs Stiffness for laterally loaded Piles*. in *Proceedings of the 11th Australia-New Zealand Conference on Geomechanics (ANZ 2012)*. 2012. The Australian Geomechanical Society and New Zealand Geotechnical Society.
46. Desai, C. and B. Nagaraj, *Modeling for normal and shear behavior of interfaces*. Journal of engineering mechanics, 1987. **110**(7): p. 1198-1217.
47. El Naggar, M. and M. Novak, *Nonlinear lateral interaction in pile dynamics*. Soil Dynamics and Earthquake Engineering, 1995. **14**(2): p. 141-157.
48. Dunnivant, T.W. and M.W. O'Neill, *Performance, Analysis, and Interpretation of a Lateral Load Test of a 72-inch-diameter Bored Pile in Overconsolidated Clay*. 1985: University of Houston, Department of Civil Engineering.

49. O'Neill, M.W. and T.W. Dunnavant, *A study of the effects of scale, velocity, and cyclic degradability on laterally loaded single piles in overconsolidated clay*. 1984: University of Houston, Department of Civil Engineering.
50. Stevens, J. and J. Audibert. *Re-examination of py curve formulations*. in *Offshore technology conference*. 1979. Offshore Technology Conference.
51. (API), *Recommended Practice for Ultrasonic Examination of Offshore Structural Fabrication and Guidelines for Qualification of Ultrasonic Technicians*. 17th ed. 1987: American Petroleum Institute.
52. Prager, W., *A new methods of analyzing stresses and strains in work hardening plastic solids*. J. Appl. Mech.(ASME), 1956. **23**: p. 493-496.
53. Serdaroglu, M.S., *Nonlinear analysis of pile driving and ground vibrations in saturated cohesive soils using the finite element method*. 2010.
54. Bransby, M., *Selection of p-y curves for the design of single laterally loaded piles*. International Journal for numerical and analytical methods in geomechanics, 1999. **23**(15): p. 1909-1926.
55. Alkroosh, I., M. Shahin, and H. Nikraz. *Modeling load-settlement curves of behaviour bored piles using artificial neural networks*. in *Proceedings of the 14th Danube-European Conference on Geotechnical Engineering*. 2010. Slovak University of Technology.
56. Penumadu, D. and R. Zhao, *Triaxial compression behavior of sand and gravel using artificial neural networks (ANN)*. Computers and Geotechnics, 1999. **24**(3): p. 207-230.
57. Banimahd, M., S. Yasrobi, and P.K. Woodward, *Artificial neural network for stress-strain behavior of sandy soils: Knowledge based verification*. Computers and Geotechnics, 2005. **32**(5): p. 377-386.
58. Shahin, M.A. and B. Indraratna, *Modeling the mechanical behavior of railway ballast using artificial neural networks*. Canadian Geotechnical Journal, 2006. **43**(11): p. 1144-1152.
59. Rumelhart, D., G. Hinton, and R. Williams, *Learning internal representations by error propagation*, in *Parallel Distributed Processing*, DE Rumelhart, JL McClelland eds. 1986, MIT Press, Cambridge.
60. Fausett, L., *Fundamentals of neural networks: architectures, algorithms, and applications*. 1994: Prentice-Hall, Inc.
61. Nogami, T., et al., *Nonlinear soil-pile interaction model for dynamic lateral motion*. Journal of Geotechnical Engineering, 1992. **118**(1): p. 89-106.
62. Alkroosh, I. and H. Nikraz, *Evaluation of pile lateral capacity in clay applying evolutionary approach*. International Journal of GEOMATE, 2013. **4**(1): p. 462-465.
63. Jordan, M. *Attractor dynamics and parallelism in a connectionist sequential machine*. in *Proc. of the Eighth Annual Conference of the Cognitive Science Society (Erlbaum, Hillsdale, NJ)*, 1986. 1986.
64. Ward, *NeuroShell 2*. 2000, Ward System Groups, Inc. Mass.
65. Alsamman, O.M., *The use of CPT for calculating axial capacity of drilled shafts*. 1995, University of Illinois at Urbana-Champaign.
66. Eslami, A., *Bearing capacity of piles from cone penetration test data*. 1997: University of Ottawa (Canada).
67. Milovic, D. and S. Stevanovic. *Deformation modulus determined by pile load test*. in *Proceedings of 12th International Conference on Soil Mechanics and Foundation Engineering*. 1989.

68. Kulhawy, F.H. and P.W. Mayne, *Manual on estimating soil properties for foundation design*. 1990, Electric Power Research Inst., Palo Alto, CA (USA); Cornell Univ., Ithaca
69. Masters, T., *Practical neural network recipes in C++*. Academic Press, San Diego, CA. Practical neural network recipes in C++. Academic Press, San Diego, CA., 1993: p. -.
70. Shahin, M.A., H.R. Maier, and M.B. Jaksa, *Data division for developing neural networks applied to geotechnical engineering*. Journal of Computing in Civil Engineering, 2004. **18**(2): p. 105-114.
71. Odom, M.D. and R. Sharda. *A neural network model for bankruptcy prediction*. in *1990 IJCNN International Joint Conference on neural networks*. 1990. IEEE.
72. Hornik, K., M. Stinchcombe, and H. White, *Multilayer feedforward networks are universal approximators*. Neural networks, 1989. **2**(5): p. 359-366.
73. Mosadegh, A., *Experimental and Numerical Investigations to Assess the Performance of a Buried Pipe Subjected to Traffic Load/Non-Treated and Cement-Treated Trench*. 2018, Curtin University.
74. Nogami, T. and K. Konagai, *Time domain axial response of dynamically loaded single piles*. Journal of Engineering Mechanics, 1986. **112**(11): p. 1241-1252.
75. Bentley, K.J. and M.H.E. Naggar, *Numerical analysis of kinematic response of single piles*. Canadian Geotechnical Journal, 2000. **37**(6): p. 1368-1382.
76. Maheshwari, B.K., et al., *Three-dimensional finite element nonlinear dynamic analysis of pile groups for lateral transient and seismic excitations*. Canadian Geotechnical Journal, 2006. **51**(1): p. 120-135.
77. Zienkiewicz, O., C. Chang, and P. Bettess, *Drained, undrained, consolidating and dynamic behaviour assumptions in soils*. Geotechnique, 1980. **30**(4): p. 385-395.
78. Novak, M. and H. Mitwally, *Transmitting boundary for axisymmetrical dilation problems*. Journal of engineering mechanics, 1988. **114**(1): p. 181-187.
79. Lysmer, J. and R.L. Kuhlemeyer, *Finite element model for infinite media*. Journal of the Engineering Mechanics Division, 1971. **102**(4): p. 776-795.
80. Rodriguez-Marek, A. and J.D. Bray, *Seismic site response for near-fault forward directivity ground motions*. Journal of Geotechnical and Geoenvironmental Engineering, 2006. **132**(12): p. 1611-1620.
81. Borja, R.I., B.G. Duvernay, and C.-H. Lin, *Ground response in Lotung: total stress analyses and parametric studies*. Journal of Geotechnical and Geoenvironmental Engineering, 2002. **128**(1): p. 54-63.
82. Wu, G. and W.L. Finn, *Dynamic elastic analysis of pile foundations using finite element method in the frequency domain*. Canadian Geotechnical Journal, 1997. **33**(1): p. 45-58.
83. Zienkiewicz, O. and T. Shiomi, *Dynamic behaviour of saturated porous media; the generalized Biot formulation and its numerical solution*. International journal for numerical and analytical methods in geomechanics, 1984. **8**(1): p. 71-96.
84. Zienkiewicz, O., C. Emson, and P. Bettess, *A novel boundary infinite element*. International Journal for Numerical Methods in Engineering, 1983. **19**(3): p. 393-404.

85. Lysmer, J. and R.L. Kuhlemeyer, *Finite dynamic model for infinite average*. Journal of the Engineering Mechanics Division, 1969. **95**(4): p. 859-878.
86. Hibbitt, K., *Sorensen Inc. ABAQUS/standard user's manual, Version 6.5*. Hibbitt, Karlsson, & Sorensen, Inc, 2005.
87. Zhao, C. and S. Valliappan, *A dynamic infinite element for three-dimensional infinite-domain wave problems*. International journal for numerical methods in engineering, 1993. **36**(15): p. 2567-2580.
88. Bahrami, A. and H. Nikraz. *Characteristics of Radiated Waves in Viscoelastic Soil Layer due to Lateral Flexural Vibration of Single Pile*. in *Proceedings of the International Conference on Advances in Geotechnical Engineering*. 2011. Australian Geomechanics Society.
89. Kim, S. and J.P. Stewart, *Kinematic soil-structure interaction from strong motion recordings*. Journal of Geotechnical and Geoenvironmental Engineering, 2003. **129**(4): p. 323-335.
90. Desai, C., et al., *Thin-layer element for interfaces and joints*. International Journal for Numerical and Analytical Methods in Geomechanics, 1984. **8**(1): p. 19-43.
91. Fakharian, K. and E. Evgin, *An automated apparatus for three-dimensional monotonic and cyclic testing of interfaces*. Geotechnical Testing Journal, 1996. **19**(1): p. 22-31.
92. Desai, C. and B. Nagaraj, *Constitutive Modeling in Nonlinear Soil-Structure Interaction*. Mechanics of Material Interfaces, APS Selvadurai and GZ Voyiadjis, eds., Elsevier Science Publishers, Amsterdam, 1986.
93. Drumm, E.C., *TESTING, MODELLING, AND APPLICATIONS OF INTERFACE BEHAVIOR IN DYNAMIC SOIL-STRUCTURE INTERACTION*. 1983.
94. Drumm, E. and C. Desai, *Determination of parameters for a model for the cyclic behaviour of interfaces*. Earthquake engineering & structural dynamics, 1986. **14**(1): p. 1-18.
95. Ghaboussi, J., E.L. Wilson, and J. Isenberg, *Finite element for rock joints and interfaces*. Journal of Soil Mechanics & Foundations Div, 1973. **99**(Proc Paper 10095).
96. Goodman, R.E., R.L. Taylor, and T.L. Brekke, *A model for the mechanics of jointed rock*. Journal of Soil Mechanics & Foundations Div, 1968.
97. Herrmann, L.R., *Finite element analysis of contact problems*. Journal of the Engineering Mechanics Division, 1978. **104**(5): p. 1043-1057.
98. Desai, C. and B. Nagaraj, *Modeling for cyclic normal and shear behavior of interfaces*. Journal of engineering mechanics, 1988. **114**(7): p. 1198-1217.
99. Isenberg, J. and D. Vaughan. *Nonlinear effects in soil-structure interaction*. in *Proc. of the symposium on implementation of Comp. Procedures and Stress-Strain Laws in Geotechnical Engineering, held at Chicago, III*. 1981.
100. Katona, M.G., *A simple contact-friction interface element with applications to buried culverts*. International Journal for Numerical and Analytical Methods in Geomechanics, 1983. **7**(3): p. 371-384.
101. Kausel, E. and J. Roesset, *Soil structure interaction for structures*, in *Electric power and the civil engineer*. 1978.
102. Toki, K., T. Sato, and F. Miura. *Separation and sliding between soil and structure during strong ground motion*. in *Proceedings of the Japan Society of Civil Engineers*. 1980. Japan Society of Civil Engineers.

103. Vaughan, D. and J. Isenberg, *Non-linear rocking response of model containment structures*. Earthquake Engineering & Structural Dynamics, 1983. **11**(2): p. 275-296.
104. Wolf, J.P., *Soil-structure interaction*. Prentice Hall Inc., Englewood Cliffs, New Jersey ISBN 0 13, 1985. **221565**(9): p. 01.
105. Zaman, M.M.-u., C.S. Desai, and E.C. Drumm, *Interface model for dynamic soil-structure interaction*. Journal of Geotechnical Engineering, 1984. **110**(9): p. 1257-1273.
106. Juirnarongrit, T., *Effect of diameter on the behavior of seismic loaded piles in weakly sand*. 2005.
107. Alderlieste, E.A., *Experimental modelling of lateral loads on large diameter mono-pile foundations in sand*. 2011.
108. Duncan, J.M. and C.-Y. Chang, *Nonlinear analysis of stress and strain in soils*. Journal of Soil Mechanics & Foundations Div, 1970.
109. Prévost, J.H., *Mathematical modelling of monotonic and cyclic undrained clay behaviour*. International Journal for Numerical and Analytical Methods in Geomechanics, 1977. **1**(2): p. 195-216.
110. Bardet, J., *Prediction of deformations of Hostun and Reid Bedford sands with a simple bounding plasticity model*. Constitutive Equations for Granular Noncohesive Soils, A. Saada and G. Bianchini, Eds, 1989: p. 131-148.
111. Dafalias, Y.F., *Bounding surface plasticity. I: Mathematical foundation and hypoplasticity*. Journal of Engineering Mechanics, 1986. **112**(9): p. 966-987.
112. Finn, W. *Dynamic analysis in geotechnical engineering*. in *Earthquake Engineering and Soil Dynamics II—Recent Advances in Ground-Motion Evaluation*. 1988. ASCE.
113. Wu, G. and W.L. Finn, *Dynamic elastic analysis of pile foundations using finite element method in the frequency domain*. Canadian Geotechnical Journal, 1998. **37**(1): p. 115-129.
114. Wu, G., *Dynamic soil-structure interaction: Pile foundations and retaining structures*. 1994, University of British Columbia.
115. Wu, G. and W.L. Finn, *Dynamic nonlinear analysis of pile foundations using finite element method in the time domain*. Canadian Geotechnical Journal, 1997. **34**(1): p. 44-52.
116. Gohl, W.B., *Response of pile foundations to simulated earthquake loading: experimental and analytical results volume I*. 1991, University of British Columbia.
117. SKANSEBO, E. and Y. VENEV, *Lateral stability of pile groups Old timber piles in clay deposit*. 1989.
118. Makris, N. and G. Gazetas, *Dynamic pile-soil-pile interaction. Part II: Lateral and seismic response*. Earthquake engineering & structural dynamics, 1992. **21**(2): p. 145-162.
119. Borja, R.I. and A.P. Amies, *Multiaxial cyclic plasticity model for clays*. Journal of geotechnical engineering, 1994. **120**(6): p. 1051-1070.
120. Hudson, M., I. Idriss, and M. Beikae, *QUAD4M: a computer program to evaluate the seismic response of soil structures using finite element procedures and incorporating a compliant base*. 1994: Center for Geotechnical Modeling, Department of Civil and Environmental
121. Cai, Y., P. Gould, and C. Desai, *Nonlinear analysis of 3D seismic interaction of soil-pile-structure systems and application*. Engineering Structures, 2000. **22**(2): p. 191-199.

122. Borja, R.I., et al., *Nonlinear ground response at Lotung LSST site*. Journal of geotechnical and geoenvironmental engineering, 1999. **125**(3): p. 187-197.
123. Kwok, A.O., et al., *Use of exact solutions of wave propagation problems to guide implementation of nonlinear seismic ground response analysis procedures*. Journal of Geotechnical and Geoenvironmental Engineering, 2007. **133**(11): p. 1385-1398.
124. Borja, R.I., et al., *Modelling non-linear ground response of non-liquefiable soils*. Earthquake engineering & structural dynamics, 2000. **29**(1): p. 63-83.
125. Anandarajah, A. and J. Zhang, *Simplified finite element modeling of nonlinear dynamic pile-soil interaction*. Retrieved February, 2000. **10**: p. 2005.
126. Wilson, D., *Soil-pile superstructure interaction in liquefiable sand and soft clay*. 1998, Doctoral dissertation, University of California, Davis.
127. Boulanger, R.W., et al., *Soil-pile-superstructure interaction in liquefiable sand*. Transportation research record, 1997. **1569**(1): p. 55-64.
128. Fekadu, P., *Simulating the dynamic response of a soil-pile system using ABAQUS*. 2010.
129. Mosadegh, A. and H. Nikraz, *Buried pipe response subjected to traffic load experimental and numerical investigations*. International Journal of Geomate, 2017. **13**(39): p. 1-8.
130. Kishishita, T., E. Saito, and F. Miura. *Dynamic-response characteristics of structures with micropile foundation system*. in *12th World Conference on Earthquake Engineering, Auckland, New Zealand*. 2000.
131. Novak, M. and T. Nogami, *Soil-pile interaction in horizontal vibration*. Earthquake Engineering & Structural Dynamics, 1977. **5**(3): p. 263-281.
132. Hardin, B.O. and V.P. Drnevich, *Shear modulus and damping in soils: measurement and parameter effects*. Journal of Soil Mechanics & Foundations Div, 1972. **98**(sm6).
133. El-sawy, M.K., *Seismic Performance of Steel Helical Piles*. 1996.
134. Gazetas, G. and R. Dobry, *Horizontal response of piles in layered soils*. Journal of Geotechnical engineering, 1984. **110**(1): p. 20-40.
135. Ho, I.-H., *Optimization of pile reinforced slopes using finite element analyses*. 2009.
136. Shahrour, I., M. Sadek, and R. Ousta, *Seismic behavior of micropiles: used as foundation support elements: three-dimensional finite element analysis*. Transportation Research Record, 2001. **1772**(1): p. 84-90.
137. Gazetas, G., *Seismic response of end-bearing single piles*. International Journal of Soil Dynamics and Earthquake Engineering, 1984. **3**(2): p. 82-93.
138. Rodriguez-Marek, A., *Near-fault seismic site response*. Vol. 1. 2000: University of California, Berkeley.
139. Møller, I.F. and T. Christiansen, *Laterally loaded monopile in dry and saturated sand—Static and cyclic loading*. Master Project, June, 2011.
140. Ousta, R. and I. Shahrour, *Three-dimensional analysis of the seismic behaviour of micropiles used in the reinforcement of saturated soil*. International Journal for Numerical and Analytical Methods in Geomechanics, 2001. **25**(2): p. 183-196.
141. Ismail, M. and M. Shahin. *Finite element analyses of granular pile anchors as a foundation option for reactive soils*. in *Proceedings of the International Conference on Advances in Geotechnical Engineering*. 2011. Australian Geomechanics Society.

142. Sadek, M. and I. Shahrour. *Influence of piles inclination on the seismic behavior of groups of flexible piles*. in *82nd Annual Meeting of the Transportation Research Board*. 2003.
143. Balendra, S., *Numerical modeling of dynamic soil-pile-structure interaction*. 2005.
144. Maheshwari, B.K., et al., *Three-dimensional finite element nonlinear dynamic analysis of pile groups for lateral transient and seismic excitations*. Canadian Geotechnical Journal, 2004. **41**(1): p. 118-133.
145. Dobry, R. and G. Gazetas, *Simple method for dynamic stiffness and damping of floating pile groups*. Geotechnique, 1988. **38**(4): p. 557-574.
146. Kwon, S., et al. *3D dynamic numerical modeling for soil-pile-structure interaction in centrifuge tests*. in *Proc of the 18th International Conference on Soil Mechanics and Geotechnical Engineering, Paris*. 2013.
147. Dafalias, Y. and E. Popov, *A model of nonlinearly hardening materials for complex loading*. Acta mechanica, 1975. **21**(3): p. 173-192.
148. Kasim, A.G., M.-Y. Chu, and C.N. Jensen, *Field correlation of cone and standard penetration tests*. Journal of geotechnical engineering, 1986. **112**(3): p. 368-372.
149. Robertson, P., *Cone penetration test (CPT)-based soil behaviour type (SBT) classification system—an update*. Canadian Geotechnical Journal, 2016. **53**(12): p. 1910-1927.
150. McNulty, G. and M. Harney. *Comparison of CPT-and DMT-correlated effective friction angle in clayey and silty sands*. in *Proceedings of the 2nd International Conference on Cone Penetration Testing*. 2010.
151. Long, M., *Design parameters from in situ tests in soft ground—recent developments*, in *Geotechnical and Geophysical Site Characterization*. 2008, CRC Press. p. 97-124.
152. Urmi, Z.A. and M. Ansary, *Interpretation of geotechnical parameters from CPT and SPT for the reclaimed areas of Dhaka, Bangladesh*. Dep. **12**: p. 14.
153. Douglas, B. *Soil classification using electric cone penetrometer*. in *Symp. on Cone Penetration Testing and Experience, Geotech. Engrg. Div.* 1981. ASCE.
154. Urmi, Z.A. and M. Ansary, *Interpretation of geotechnical parameters from CPT and SPT for the reclaimed areas of Dhaka, Bangladesh*. Dep, 1998. **12**: p. 14.
155. Jefferies, M.G. and M.P. Davies, *Use of CPTU to estimate equivalent SPT N 60*. Geotechnical Testing Journal, 1993. **16**(4): p. 458-468.
156. Lunne, T., J.J. Powell, and P.K. Robertson, *Cone penetration testing in geotechnical practice*. 2002: CRC Press.
157. Hettiarachchi, H. and T. Brown, *Use of SPT blow counts to estimate shear strength properties of soils: energy balance approach*. Journal of Geotechnical and Geoenvironmental Engineering, 2009. **135**(6): p. 830-834.
158. Liu, H., B. Luke, and C. Calderón. *A scheme to generate starting models for interpretation of shallow surface wave data*. in *Symposium on the Application of Geophysics to Engineering and Environmental Problems 2002*. 2002. Society of Exploration Geophysicists.
159. Vermeiden, J. *Improved sounding apparatus as developed in Holland since 1936*. in *Proc. 2nd Int. Conf. on Soil Mech. and Found. Eng., Rotterdam*. 1948.
160. Begemann, H. *Improved method of determining resistance to adhesion by sounding through a loose sleeve placed behind the cone*. in *Proceedings of the*

- 3rd International Conference on Soil Mechanics and Foundation Engineering, ICSMFE, August. 1953.*
161. Faccioli, E. and D. Resendiz, *Soil dynamics: behavior including liquefaction*, in *Developments in geotechnical engineering*. 1976, Elsevier. p. 71-139.
 162. Vlasblom, A., *The electrical penetrometer: A historical account of its development*. 1985: Delft Soil Mechanics Laboratory.
 163. Robertson, P. *Sixty years of the CPT—How far have we come*. in *International Conference on In situ Measurement of Soil Properties and Case Histories, Bali*. 2001.
 164. Vesic, A.S., *A study of the bearing capacity of deep foundations*. 1967.
 165. Nottingham, L. and J. Schmertmann, *An investigation of pile capacity design procedures*. Final Report D629 to Florida Department of Transportation, Department of Civil Engineering, University of Florida, 1975.
 166. Schmertmann, J.H., *Guidelines for cone penetration test: performance and design*. 1978, United States. Federal Highway Administration.
 167. De Ruiter, J. and F. Beringen, *Pile foundations for large North Sea structures*. Marine Georesources & Geotechnology, 1979. **3**(3): p. 267-314.
 168. Bustamante, M. and L. Ganeselli. *Pile bearing capacity prediction by means of static penetrometer CPT*. in *Proceedings of the 2-nd European symposium on penetration testing*. 1982.
 169. Eslami, A. and B.H. Fellenius, *Pile capacity by direct CPT and CPTu methods applied to 102 case histories*. Canadian Geotechnical Journal, 1997. **34**(6): p. 886-904.
 170. Fleming, W., *A new method for single pile settlement prediction and analysis*. Geotechnique, 1992. **42**(3): p. 411-425.
 171. Nejad, F.P., et al., *Prediction of pile settlement using artificial neural networks based on standard penetration test data*. Computers and geotechnics, 2009. **36**(7): p. 1125-1133.
 172. Murff, J.D., *Response of axially loaded piles*. Journal of the Geotechnical Engineering Division, 1975. **101**(3): p. 356-360.
 173. Bhattacharya, S. and S. Madabhushi, *A critical review of methods for pile design in seismically liquefiable soils*. Bulletin of Earthquake Engineering, 2008. **6**(3): p. 407-446.
 174. Onoue, A., et al., *Slope failures at Yokowatashi and Nagaoka College of Technology due to the 2004 Niigata-ken Chuetsu earthquake and their analytical considerations*. Soils and Foundations, 2006. **46**(6): p. 751-764.
 175. Seo, H. and M. Prezzi, *Analytical solutions for a vertically loaded pile in multilayered soil*. Geomechanics and Geoengineering, 2007. **2**(1): p. 51-60.
 176. Guo, W.D. and H. Qin, *Thrust and bending moment of rigid piles subjected to moving soil*. Canadian Geotechnical Journal, 2010. **47**(2): p. 180-196.
 177. Lee, K. and Z. Xiao, *A simplified nonlinear approach for pile group settlement analysis in multilayered soils*. Canadian Geotechnical Journal, 2001. **38**(5): p. 1063-1080.
 178. Guo, W.D. and M.F. Randolph, *Vertically loaded piles in non-homogeneous media*. International Journal for Numerical and Analytical Methods in Geomechanics, 1997. **21**(8): p. 507-532.
 179. Pando, M.A., *A laboratory and field study of composite piles for bridge substructures*. 2003, Virginia Tech.

180. Zienkiewicz, O., *Origins, milestones and directions of the finite element method—a personal view*. Archives of computational methods in engineering, 1995. **2**(1): p. 1.
181. Hinton, E., T. Rock, and O. Zienkiewicz, *A note on mass lumping and related processes in the finite element method*. Earthquake Engineering & Structural Dynamics, 1976. **4**(3): p. 245-249.
182. Zienkiewicz, O.C., R.L. Taylor, and J.Z. Zhu, *The finite element method: its basis and fundamentals*. 2005: Elsevier.
183. Christian, J.T. and C.S. Desai, *Constitutive laws for geologic media*. Numerical methods in geotechnical engineering, McGraw Hill, New York, 1977. **65**: p. 115.
184. Lee, C. and J. Small, *Finite-layer analysis of axially loaded piles*. Journal of geotechnical engineering, 1991. **117**(11): p. 1706-1722.
185. Kulkarni, R. and D. Dewaikar, *Analysis of rock-socketed piles loaded in axial compression in Mumbai region based on load transfer characteristics*. International Journal of Geotechnical Engineering, 2019. **13**(3): p. 261-269.
186. Coyle, H.M. and L.C. Reese, *Load transfer for axially loaded piles in clay*. Journal of the Soil Mechanics and Foundations Division, 1966. **92**(2): p. 1-26.
187. Seo, H., M. Prezzi, and R. Salgado, *Settlement analysis of axially loaded piles*. 2008.
188. Castelli, F. and E. Motta, *An Analytical Expression for the Nonlinear Evaluation of the Soil-Pile Interaction*, in *Art of Foundation Engineering Practice*. 2010. p. 179-189.
189. Maharaj, D.K., *The Effect of Raft Size and Pile Length on Load-Settlement Behaviour of Axisymmetric Piled Raft Foundation*. Electronic Journal of Geotechnical Engineering, 2004.
190. Randolph, M.F. and C.P. Wroth, *Analysis of deformation of vertically loaded piles*. Journal of Geotechnical and Geoenvironmental Engineering, 1978. **104**(ASCE 14262).
191. Verbrugge, J., *Pile foundations design using CPT results*. Structural engineering practice, analysis, design, management, 1986. **3**(2): p. 93-112.
192. Gudmestad, O.T. and G. Moe, *Hydrodynamic coefficients for calculation of hydrodynamic loads on offshore truss structures*. Marine Structures, 1996. **9**(8): p. 745-758.
193. Mangiavacchi, A., et al. *API offshore structure standards: RP 2A and much more*. in *Offshore Technology Conference*. 2005. Offshore Technology Conference.
194. Clausen, C., P. Aas, and K. Karlsrud. *Bearing capacity of driven piles in sand, the NGI approach*. in *Proceedings of Proceedings of International Symposium. on Frontiers in Offshore Geotechnics, Perth*. 2005.
195. Van Impe, W.F. and L.C. Reese, *Single piles and pile groups under lateral loading*. 2010: CRC press.
196. Kim, N.-K., J.-S. Park, and S.-K. Kim, *Numerical simulation of ground anchors*. Computers and geotechnics, 2007. **34**(6): p. 498-507.
197. Zhu, H. and M.-F. Chang, *Load transfer curves along bored piles considering modulus degradation*. Journal of Geotechnical and Geoenvironmental Engineering, 2002. **128**(9): p. 764-774.
198. Seed, H.B. and L.C. Reese, *The action of soft clay along friction piles*. American Society of Civil Engineers Transactions, 1955.

199. Kezdi, A., *Pile foundation*. Foundation engineering handbook, 1975: p. 556-600.
200. Liu, Q.-f. and G.G. Meyerhof, *New method for non-linear analysis of rigid piles in clay*. Computers and Geotechnics, 1987. **3**(4): p. 185-212.
201. Vaziri, H. and J. Xie, *A method for analysis of axially loaded piles in nonlinear soils*. Computers and Geotechnics, 1990. **10**(2): p. 149-159.
202. Abendroth, R.E. and L.F. Greimann, *Pile behavior established from model tests*. Journal of geotechnical engineering, 1990. **116**(4): p. 571-587.
203. O'Neill, M.W. and R.D. Raines, *Load transfer for pipe piles in highly pressured dense sand*. Journal of Geotechnical Engineering, 1991. **117**(8): p. 1208-1226.
204. HIRAYAMA, H., *Load-settlement analysis for bored piles using hyperbolic transfer functions*. Soils and Foundations, 1990. **30**(1): p. 55-64.
205. Chen, X., *Settlement calculation on high-rise buildings*. 2011: Springer.
206. Kodikara, J. and I. Johnston, *Analysis of compressible axially loaded piles in rock*. International journal for numerical and analytical methods in geomechanics, 1994. **18**(6): p. 427-437.
207. Mindlin, R.D., *Force at a point in the interior of a semi-infinite solid*. physics, 1936. **7**(5): p. 195-202.
208. Systems, D., *ABAQUS/CAE User's Manual*. 2013, USA: Dassault Systems.
209. Hibbitt, H., *General purpose finite element analysis program, version 6.8*. Habbitt, Karlsson & Sorensen. Inc., Pawtucket, RI, 2008.
210. King, S. and T. Richards, *Solving contact problems with abaqus*. Dassault Systemes, Coventry, UK, 2013.
211. Zhan, Y., H. Wang, and F. Liu, *Modeling vertical bearing capacity of pile foundation by using ABAQUS*. Electronic Journal of Geotechnical Engineering, 2012. **17**: p. 1855-1865.
212. Conte, E., A. Troncone, and M. Vena, *Nonlinear three-dimensional analysis of reinforced concrete piles subjected to horizontal loading*. Computers and Geotechnics, 2013. **49**: p. 123-133.
213. Karthigeyan, S., V. Ramakrishna, and K. Rajagopal, *Numerical investigation of the effect of vertical load on the lateral response of piles*. Journal of Geotechnical and Geoenvironmental Engineering, 2007. **133**(5): p. 512-521.
214. Hashiguchi, K., *Subloading surface model in unconventional plasticity*. International Journal of Solids and Structures, 1989. **25**(8): p. 917-945.
215. Collins, I. and P. Kelly, *A thermomechanical analysis of a family of soil models*. Geotechnique, 2002. **52**(7): p. 507-518.
216. Chen, W. and A. Saleeb, *Constitutive equations for engineering materials, Vol. 1: Elasticity and modeling*. 1982, Wiley, New York.
217. Menetrey, P. and K. Willam, *Triaxial failure criterion for concrete and its generalization*. Structural Journal, 1995. **92**(3): p. 311-318.
218. Sinha, A. and A. Hanna, *3D numerical model for piled raft foundation*. International Journal of Geomechanics, 2016. **17**(2): p. 04016055.
219. Yang, J., *Influence zone for end bearing of piles in sand*. Journal of geotechnical and geoenvironmental engineering, 2006. **132**(9): p. 1229-1237.
220. Philipponnat, G., *Méthode pratique de calcul d'un pieu isolé, à l'aide du pénétromètre statique*. Revue Française de Geotechnique, 1980(10): p. 55-64.
221. Clisby, M., et al., *An evaluation of pile bearing capacities*. Volume I, Final Report, Mississippi State Highway Department, 1978.

222. Brinch Hansen, J., *Discussion of Hyperbolic Stress-Strain Response: Cohesive Soil*. by Robert L. Kondner. J. Soil Mech., Found. Div., ASCE, 1963. **89**(4): p. 241-242.
223. Geotechdata.info, *Soil friction angle*. 2013.
224. Bolton, M., *Strength and dilatancy of sands*. Geotechnique, 1986. **36**(1): p. 65-78.

Every reasonable effort has been made to acknowledge the owners of copyright material. I would be pleased to hear from any copyright owner who has been omitted or incorrectly acknowledged.

8 APPENDICES

Appendix A - Bored Piles Case Records Summary

Piles group	Case record number	Reference	Case number at the reference	Shape	Tip, closed or open	A_c (m ²)	A_{cir} (m ² /m)	D or D_{eq} (mm)	L (m)	Type of load test	Type of cone
Bored piles	1	Alsamman (1995)	LTN 89	round	closed	0.951	3.458	1100	13.0	na	M
	2	****	LTN 894	****	****	0.139	1.322	421	5.8	****	****
	3	****	LTN 865	****	****	0.080	1.006	320	10.2	****	****
	4	****	LTN 652	****	****	0.164	1.437	457	15.2	****	E
	5	****	LTN 928	****	****	0.121	1.236	393	6.5	CYC	****
	6	****	LTN 923	****	****	0.132	1.289	410	5.6	****	****
	7	****	LTN 870	****	****	0.080	1.006	320	10.2	SML	M
	8	****	LTN 869	****	****	0.080	1.006	320	7.7	****	****
	9	****	LTN 938	****	****	0.128	1.267	403	9.2	CYC	E
	10	****	LTN 742	****	****	0.520	2.558	814	24.2	QML	****
	11	****	LTN 866	****	****	0.080	1.006	320	10.2	SML	M
	12	****	LTN 911	****	****	0.353	2.107	671	13.0	****	****
	13	****	LTN 860	****	****	0.785	3.142	1000	9.5	na	****
	14	****	LTN 861	****	****	0.785	3.142	1000	9.0	****	****
	15	****	LTN 857	****	****	0.554	2.640	840	24.4	CYC	****
	16	****	LTN 302	****	****	0.283	1.887	600	7.2	IE	****
	17	****	LTN 859	****	****	0.951	3.457	1100	9.0	na	****

Table A-1 Bored piles case records summary (continued)

A_c = cross section area, A_{cir} = unit circumferential area; D = diameter; D_{eq} = equivalent diameter; L = embedment length; SML = slow maintained load test; na = not available; CYC = cyclic load test; QML = quick maintained load test; CRP = constant rate of penetration; IE = incremental equilibrium; M = Mechanical; E = Electrical

Piles group	Case record number	Reference	Case number at the reference	Shape	Tip, closed or open	A_c (m ²)	A_{cir} (m ² /m)	D or D_{eq} (mm)	L (m)	Type of load test	Type of cone
Bored piles	18	Alsamman (1995)	LTN 886	****	****	0.196	1.571	500	10.2	SML	****
	19	****	LTN 896	****	****	0.085	1.035	329	6.2	****	****
	20	****	LTN 895	****	****	0.131	1.284	408	5.8	****	****
	21	****	LTN 881	round	closed	0.213	1.638	521	8.2	CRP	M
	22	****	LTN 862	****	****	2.546	5.657	1800	11.5	na	****
	23	****	LTN 937	****	****	0.129	1.274	405	8.4	CYC	E
	24	****	LTN 936	****	****	0.129	1.274	405	10.4	****	E
	25	****	LTN 893	****	****	0.125	1.255	399	7.8	SML	M
	26	****	LTN 912	****	****	0.353	2.107	671	10.2	****	****
	27	****	LTN 887	****	****	0.145	1.351	430	8.7	CRP	****
	28	****	LTN 871	****	****	0.080	1.006	320	7.7	SML	****
	29	****	LTN 872	****	****	0.125	1.255	399	10.0	CRP	****
	30	****	LTN 406	****	****	0.283	1.887	600	12.0	SML	****
	31	****	LTN 407	****	****	0.283	1.887	600	12.0	****	****
	32	****	LTN 159	****	****	0.951	3.458	1100	27.0	****	****
	33	****	LTN 868	****	****	0.080	1.006	320	7.7	****	****
34	Eslami (1996)	USPB2	****	****	0.126	1.257	400	9.4	****	E	

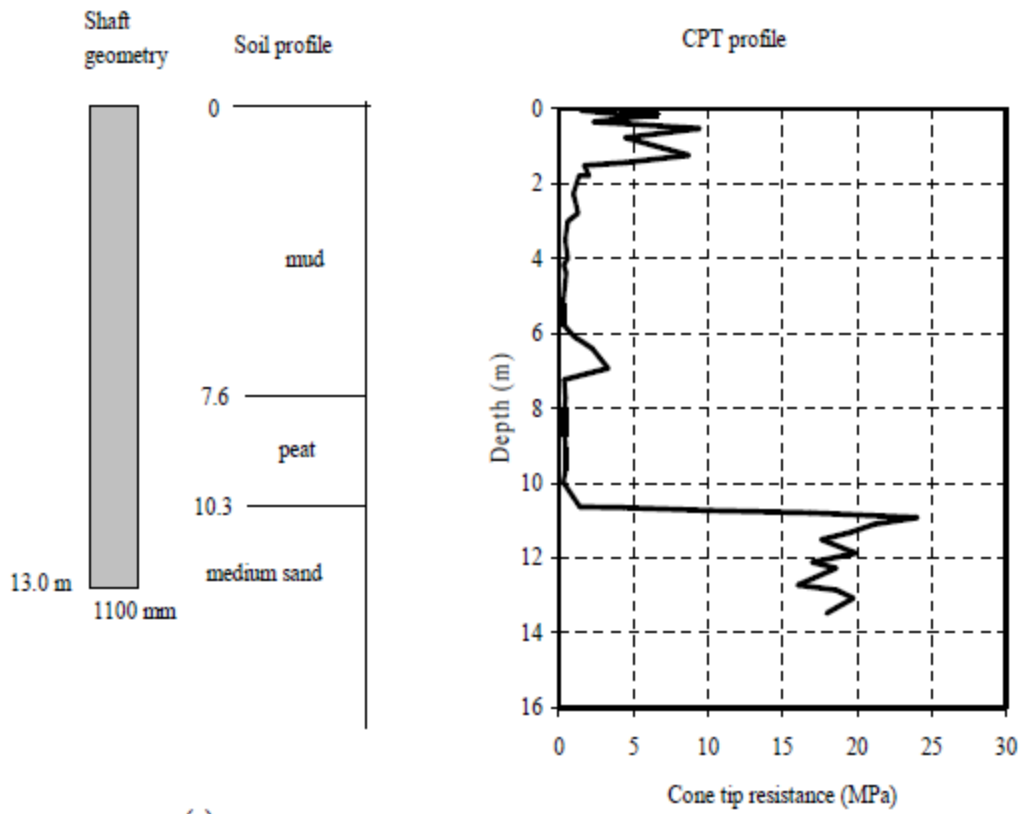
Table A-1 Bored piles case records summary (continued)

A_c = cross section area, A_{cir} = unit circumferential area; D = diameter; D_{eq} = equivalent diameter; L = embedment length; SML = slow maintained load test; na = not available; CYC = cyclic load test; QML = quick maintained load test; CRP = constant rate of penetration; IE = incremental equilibrium; M = Mechanical; E = Electrical

Piles group	Case record number	Reference	Case number at the reference	Shape	Tip, closed or open	A_c (m ²)	A_{cir} (m ² /m)	D or D_{eq} (mm)	L (m)	Type of load test	Type of cone
Bored piles	35	Alsamman (1995)	LTN 158	****	****	0.925	3.410	1085	25.1	****	M
	36	Eslami (1996)	SEATW	****	****	0.096	1.100	350	15.8	****	E
	37	Alsamman (1995)	LTN 885	****	****	0.196	1.571	500	10.2	SML	M
	38	****	LTN 925	****	****	0.129	1.274	405	7.9	CYC	E
	39	****	LTN 93	****	****	0.951	3.458	1100	6.0	CRP	M
	40	****	LTN 404	****	****	0.313	1.983	631	18.3	CYC	****
	41	****	LTN 880	round	closed	0.213	1.638	521	8.2	CRP	M
	42	****	LTN 935	****	****	0.129	1.274	405	7.0	****	****
	43	****	LTN 910	****	****	0.915	3.391	1079	13.0	****	****
	44	****	LTN 892	****	****	0.125	1.255	399	7.8	****	****
	45	****	LTN 95	****	****	1.768	4.714	1500	6.0	****	****
	46	****	LTN 891	****	****	0.126	1.257	400	7.8	****	****
	47	****	LTN 867	****	****	0.080	1.006	320	7.7	****	****
	48	****	LTN 941	****	****	0.456	2.395	762	16.8	****	****
	49	****	LTN 888	****	****	0.145	1.351	430	8.7	****	****
50	****	LTN 897	****	****	0.085	1.035	329	6.3	****	****	

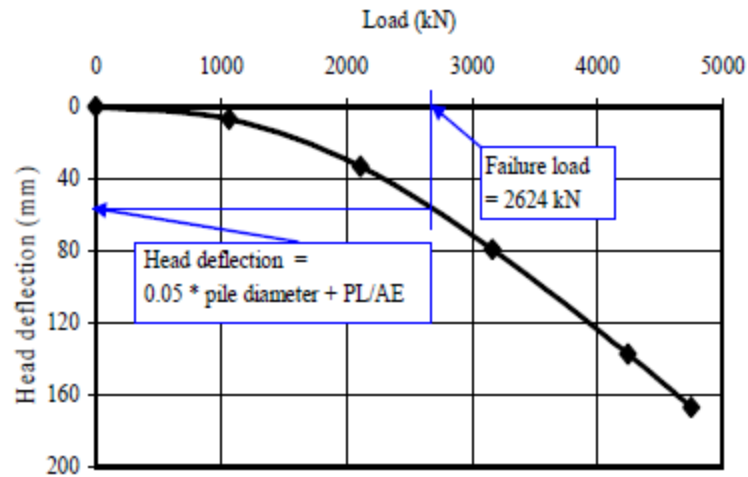
Table A-1 Bored piles case records summary (continued)

A_c = cross section area, A_{cir} = unit circumferential area; D = diameter; D_{eq} = equivalent diameter; L = embedment length; SML = slow maintained load test; na = not available; CYC = cyclic load test; QML = quick maintained load test; CRP = constant rate of penetration; IE = incremental equilibrium; M = Mechanical; E = Electrical



(a)

(b)



(c)

Figure A-1 Summary sheet for case record 1, (a) pile geometry and soil profile, (b) cone tip resistance profile, (c) load deflection plot

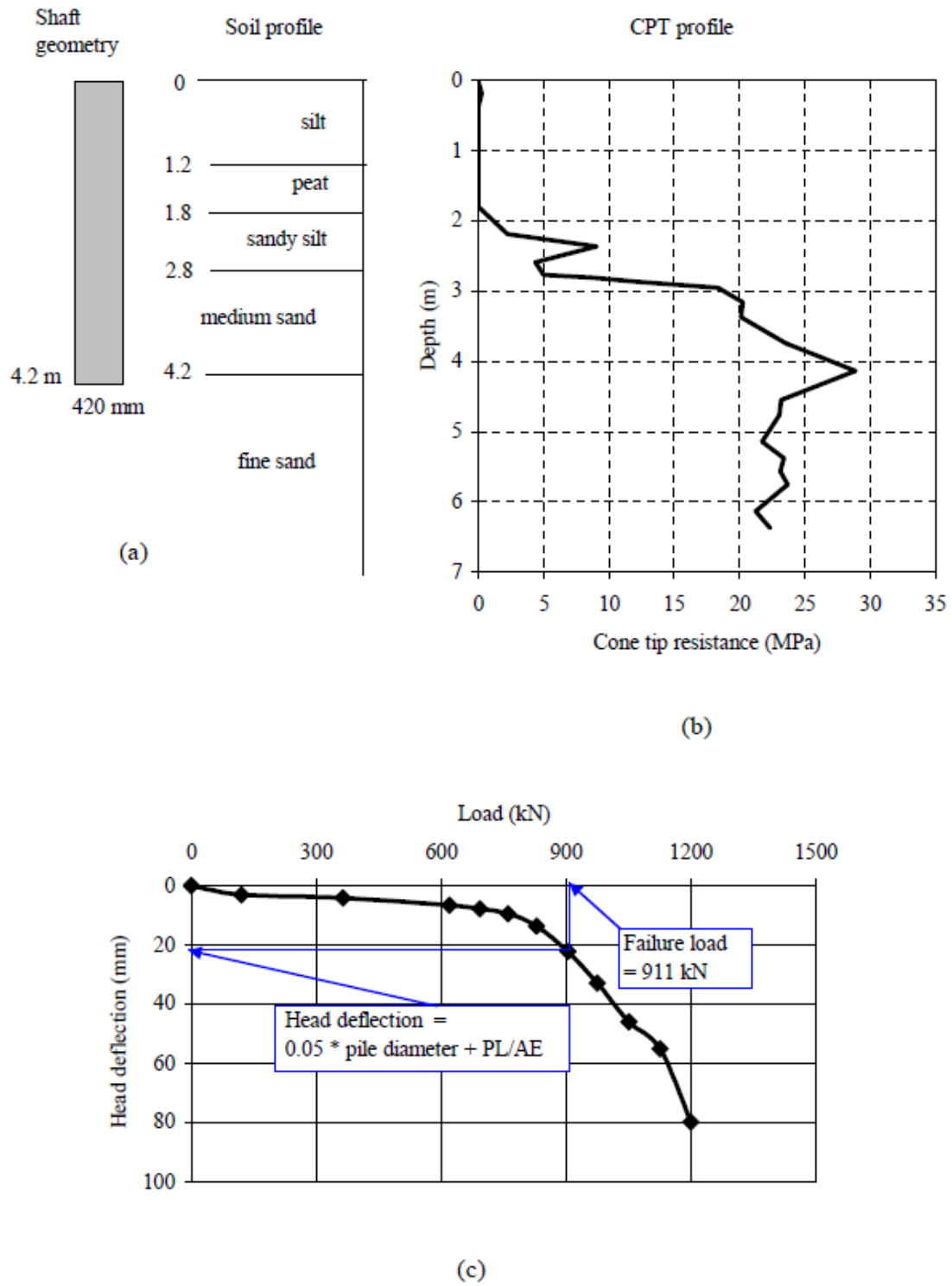
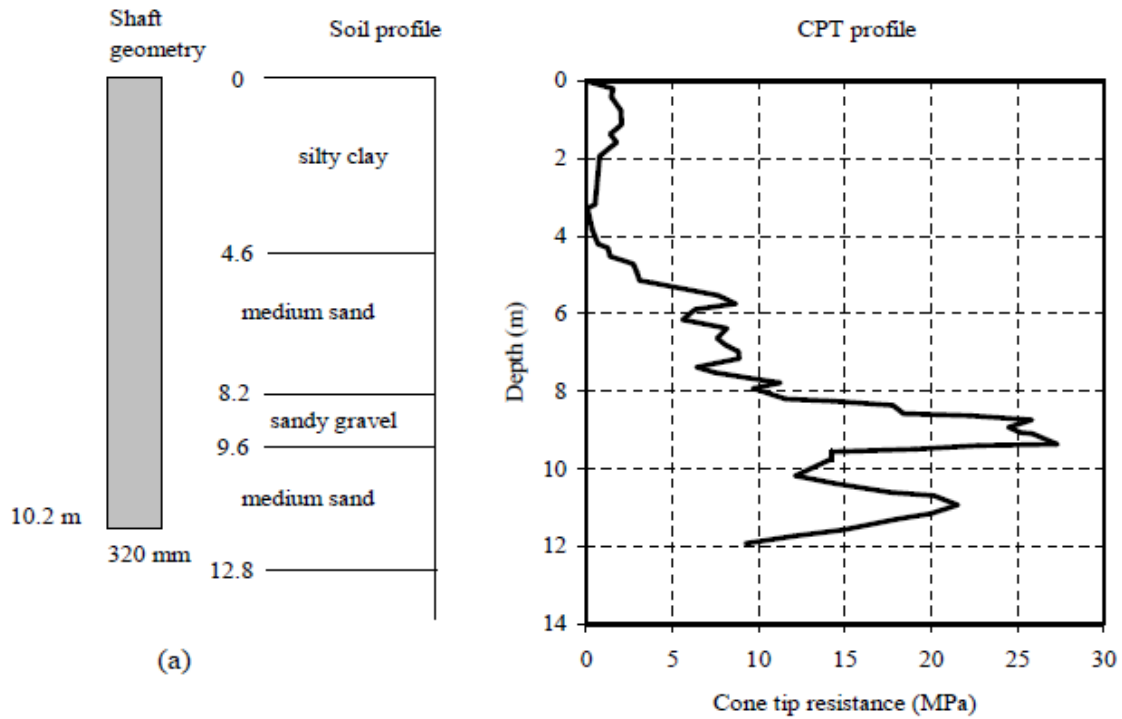
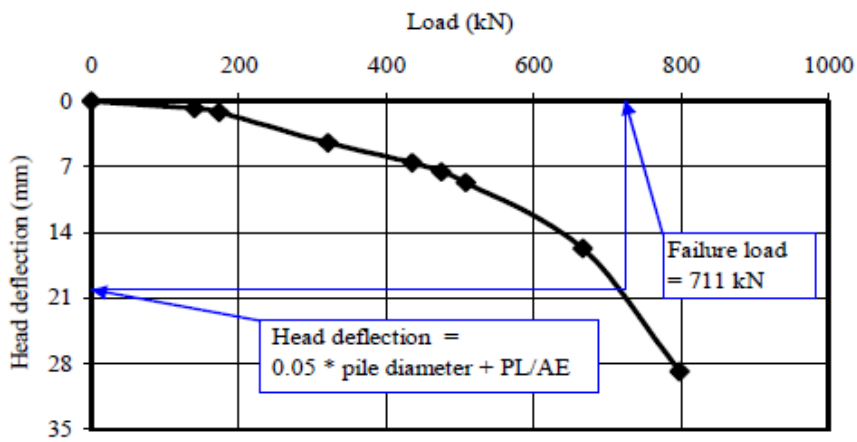


Figure A-2 Summary sheet for case record 2, (a) pile geometry and soil profile, (b) cone tip resistance profile, (c) load deflection plot



(b)



(c)

Figure A-3 Summary sheet for case record 3, (a) pile geometry and soil profile, (b) cone tip resistance profile, (c) load deflection plot

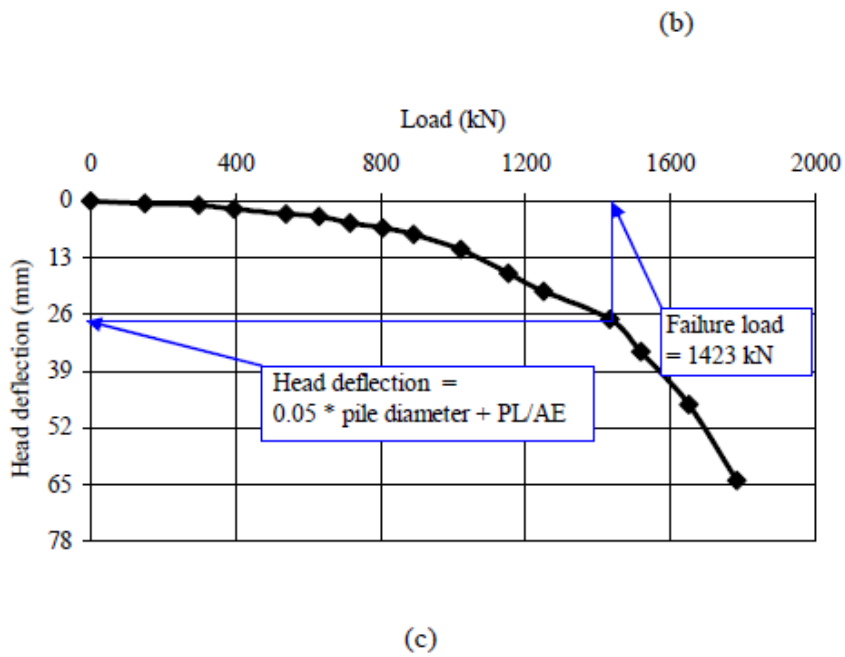
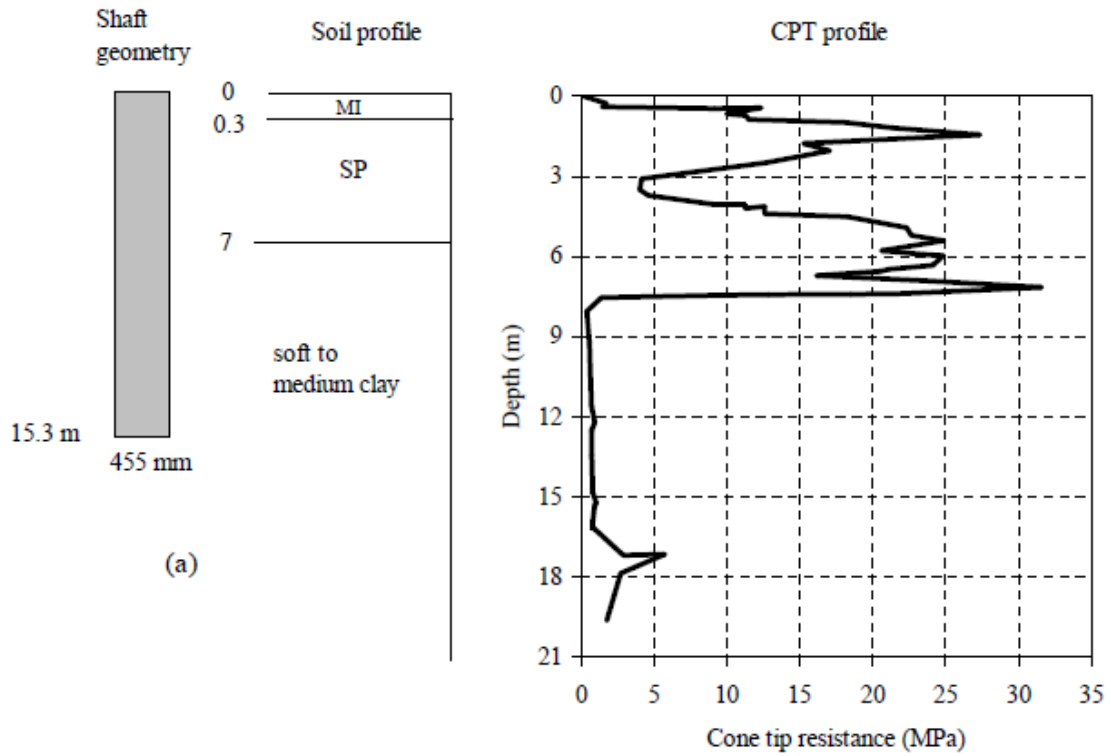


Figure A-4 Summary sheet for case record 4, (a) pile geometry and soil profile, (b) cone tip resistance profile, (c) load deflection plot

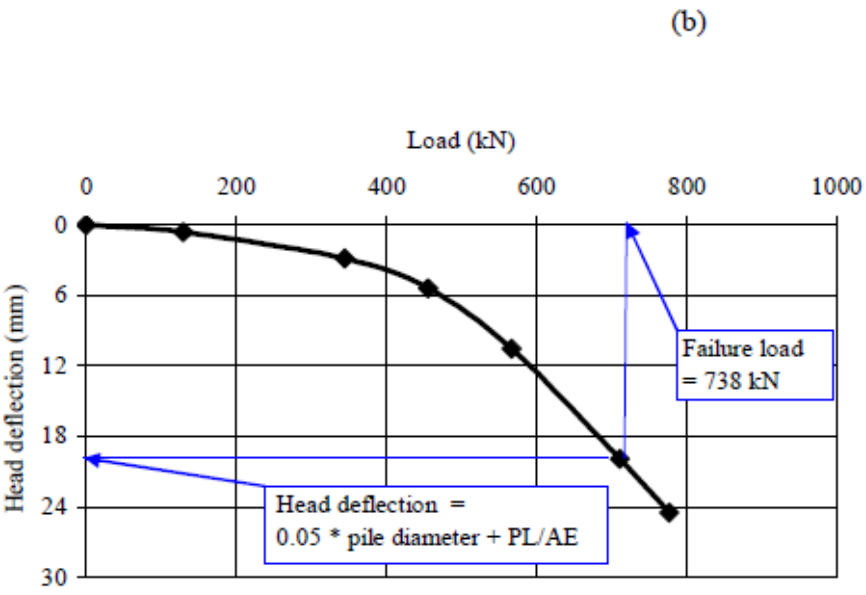
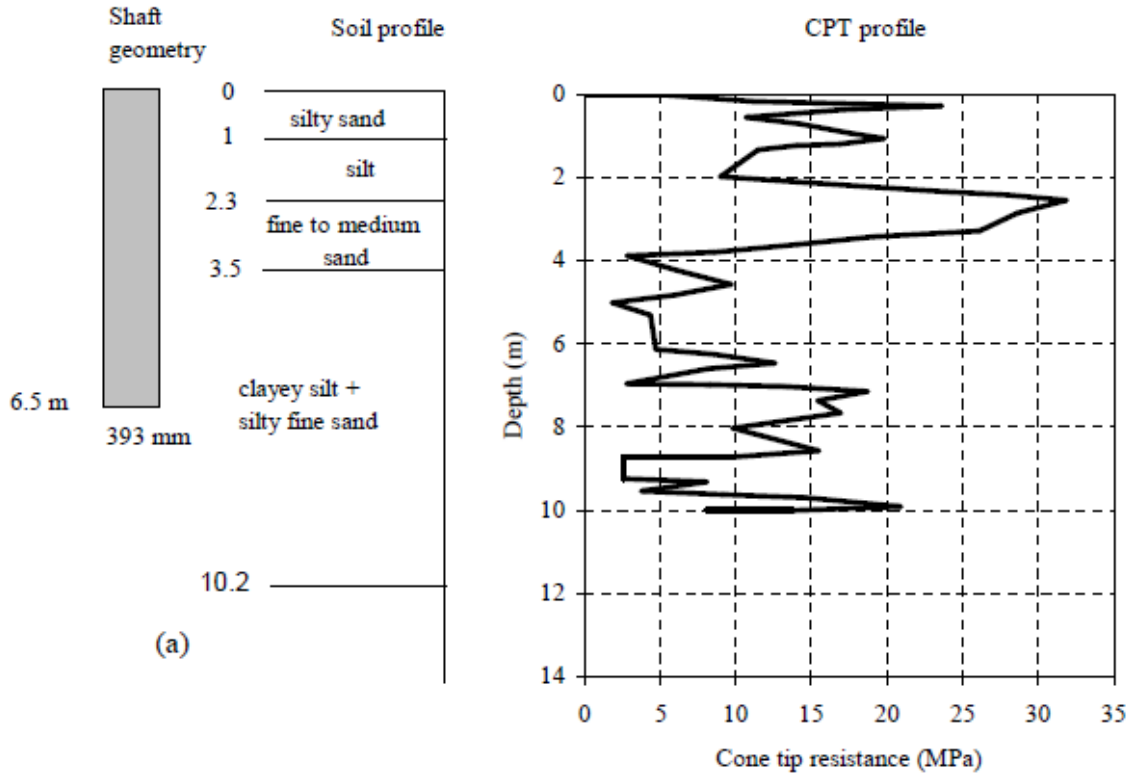


Figure A-5 Summary sheet for case record 5, (a) pile geometry and soil profile, (b) cone tip resistance profile, (c) load deflection plot

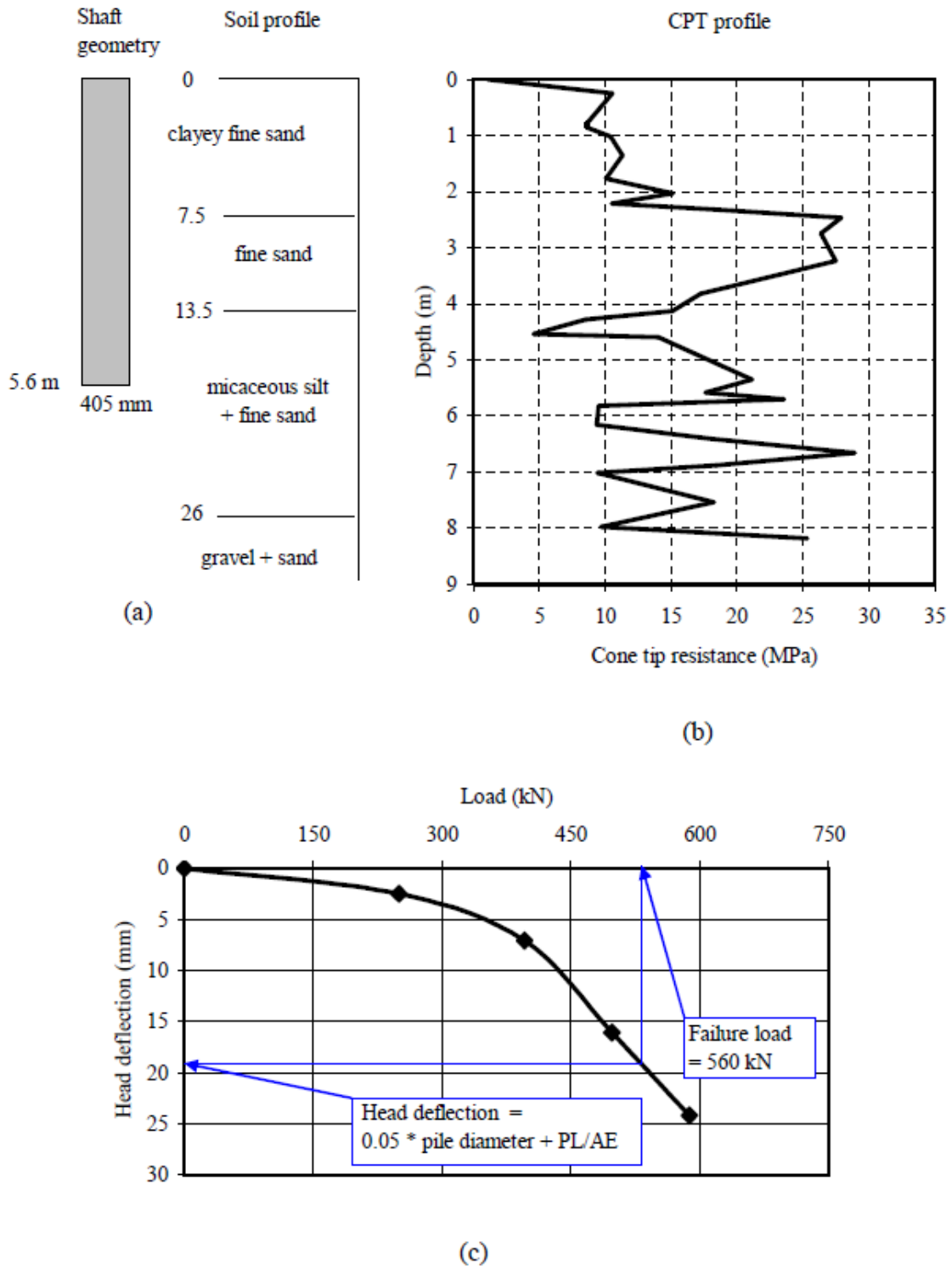


Figure A-6 Summary sheet for case record 6, (a) pile geometry and soil profile, (b) cone tip resistance profile, (c) load deflection plot

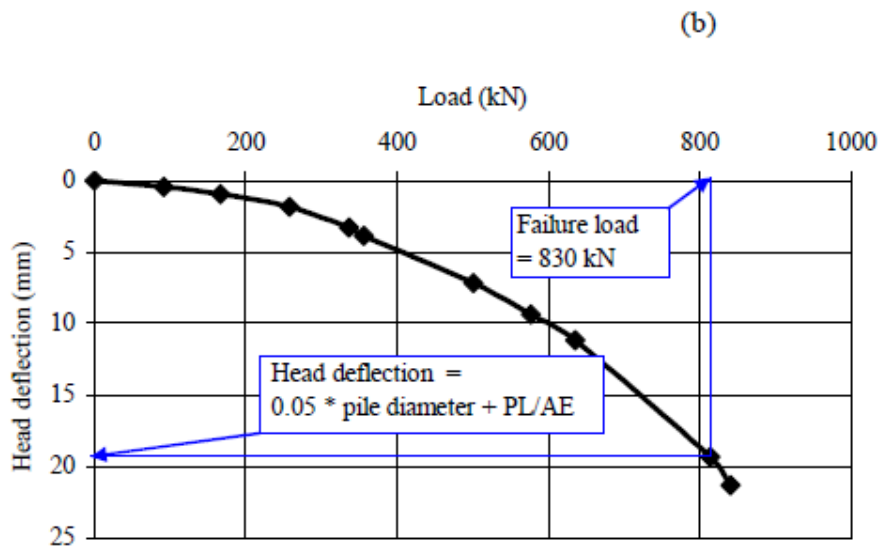
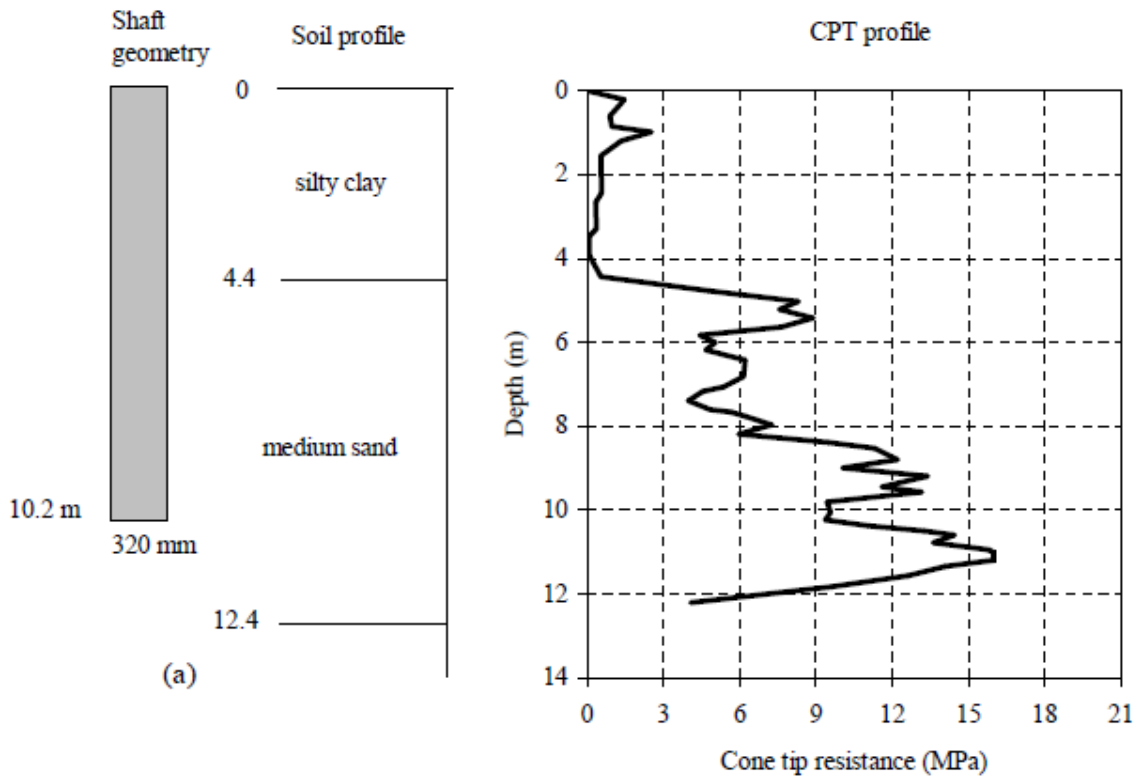


Figure A-7 Summary sheet for case record 7, (a) pile geometry and soil profile, (b) cone tip resistance profile, (c) load deflection plot

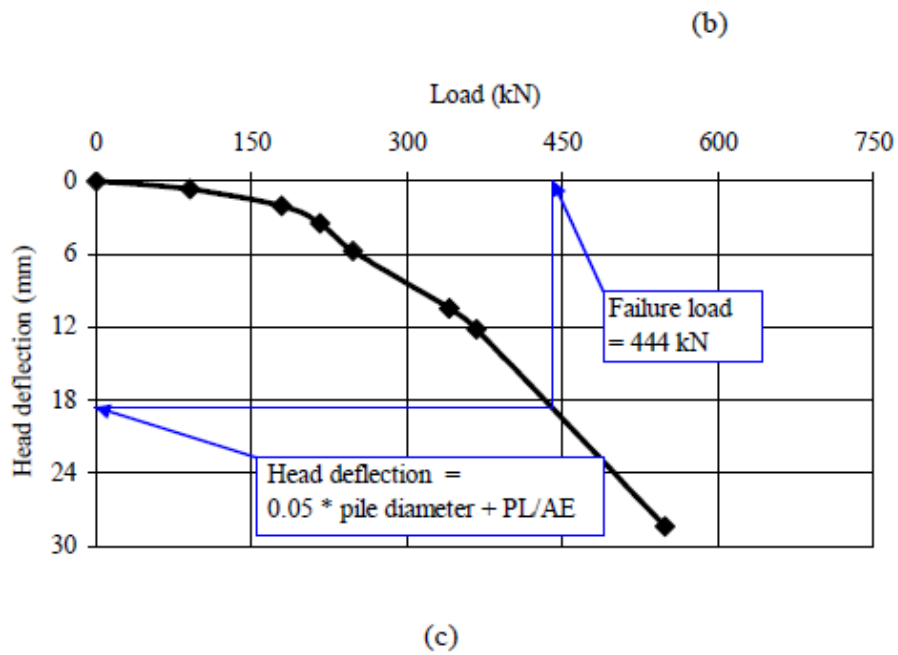
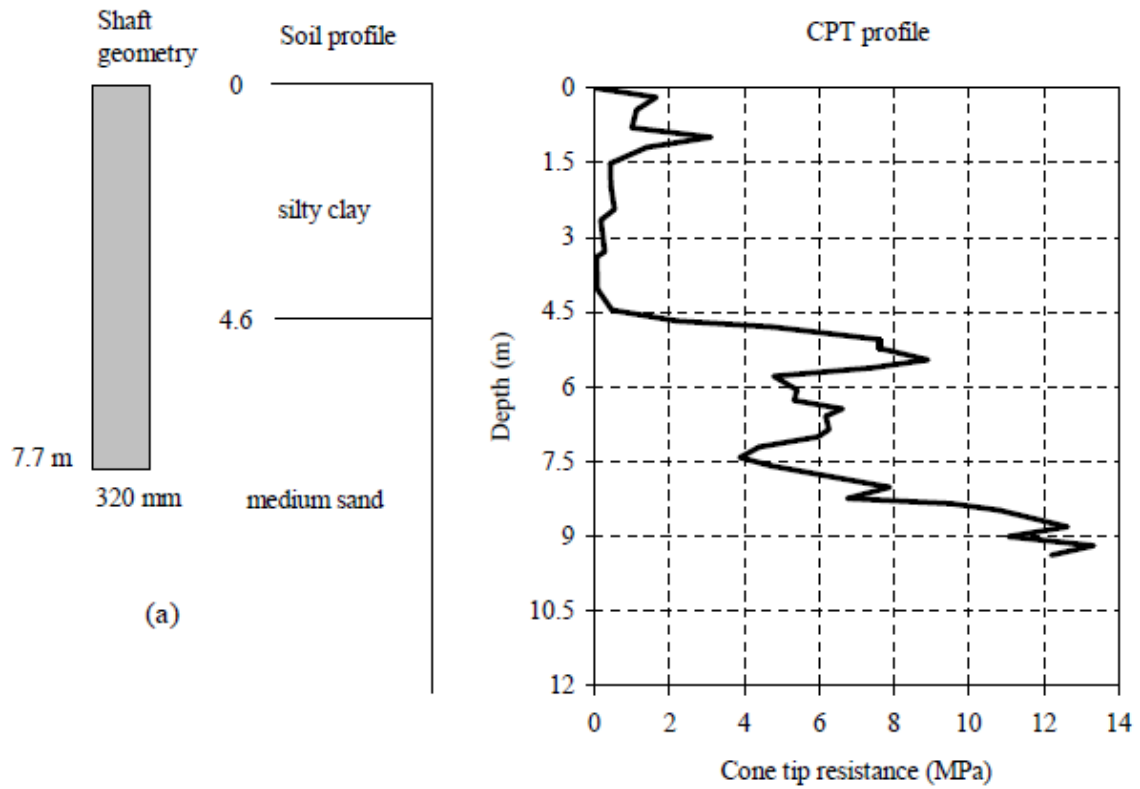


Figure A-8 Summary sheet for case record 8, (a) pile geometry and soil profile, (b) cone tip resistance profile, (c) load deflection plot

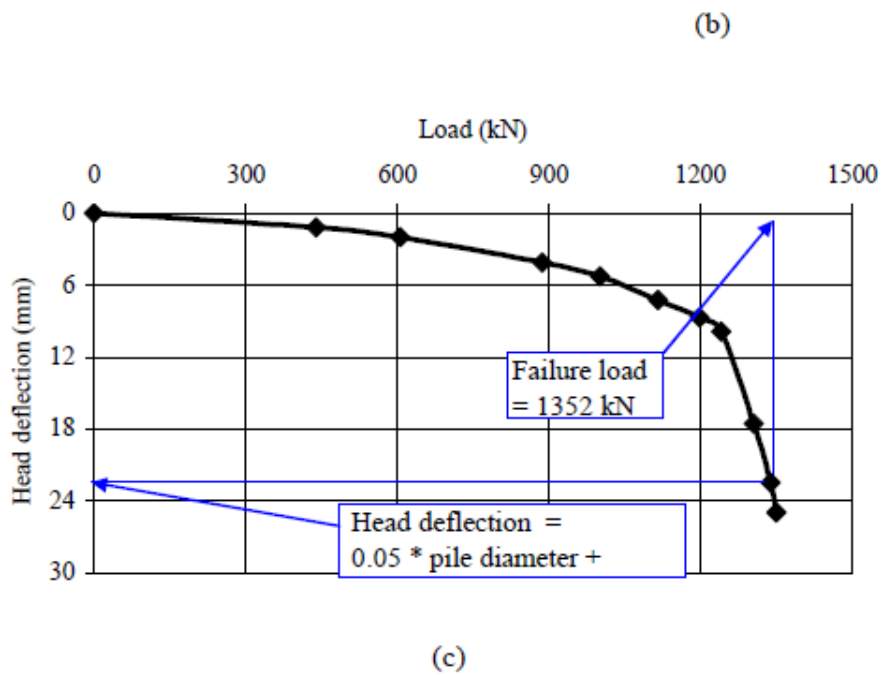
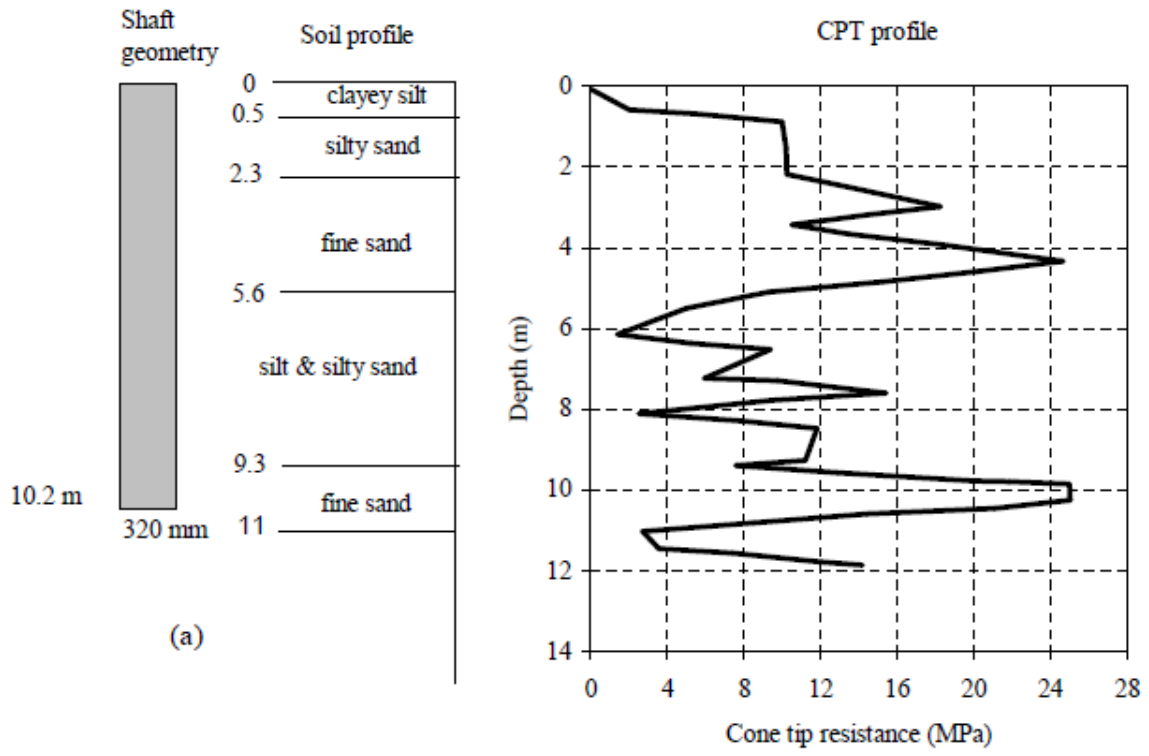


Figure A-9 Summary sheet for case record 9, (a) pile geometry and soil profile, (b) cone tip resistance profile, (c) load deflection plot

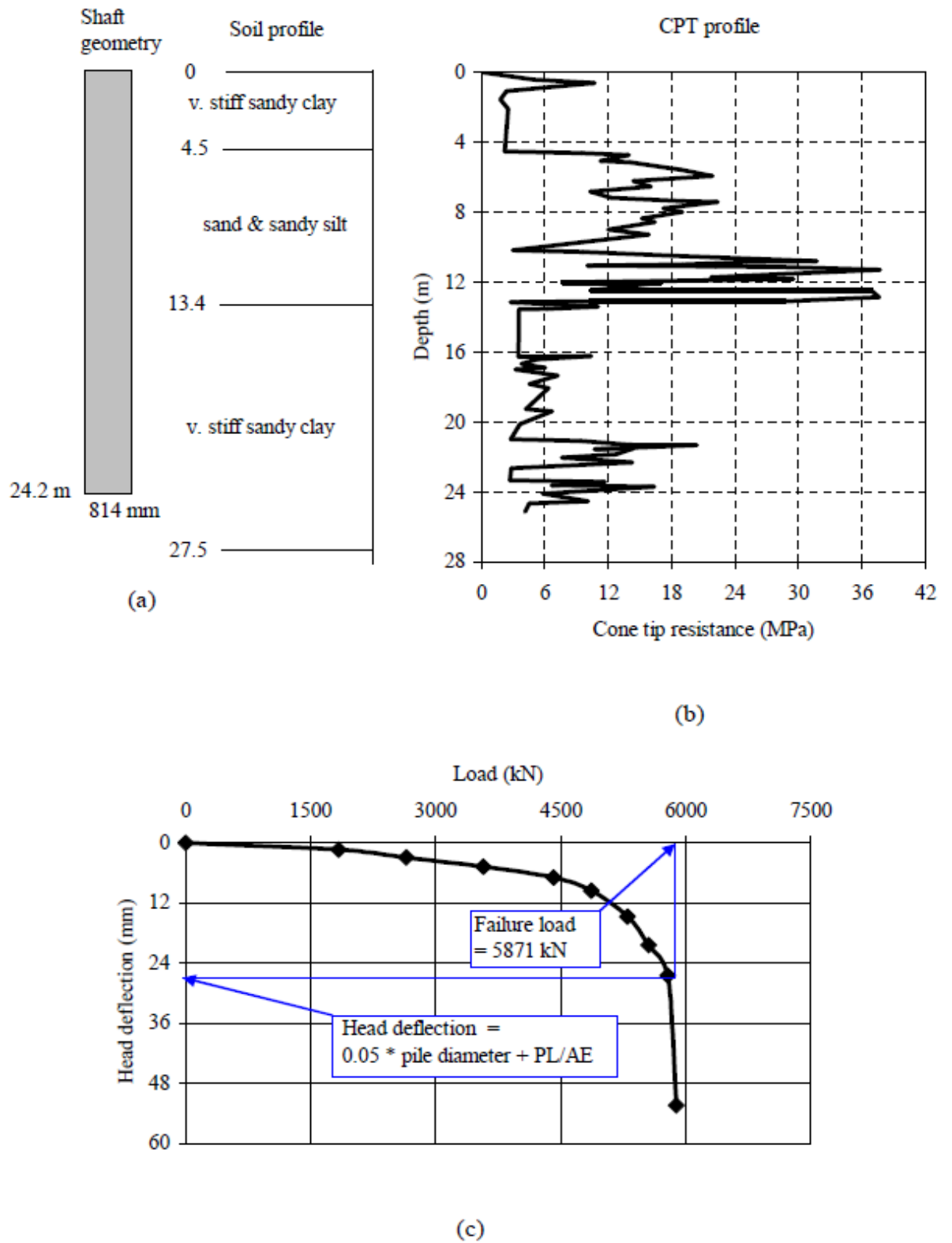


Figure A-10 Summary sheet for case record 10, (a) pile geometry and soil profile, (b) cone tip resistance profile, (c) load deflection plot

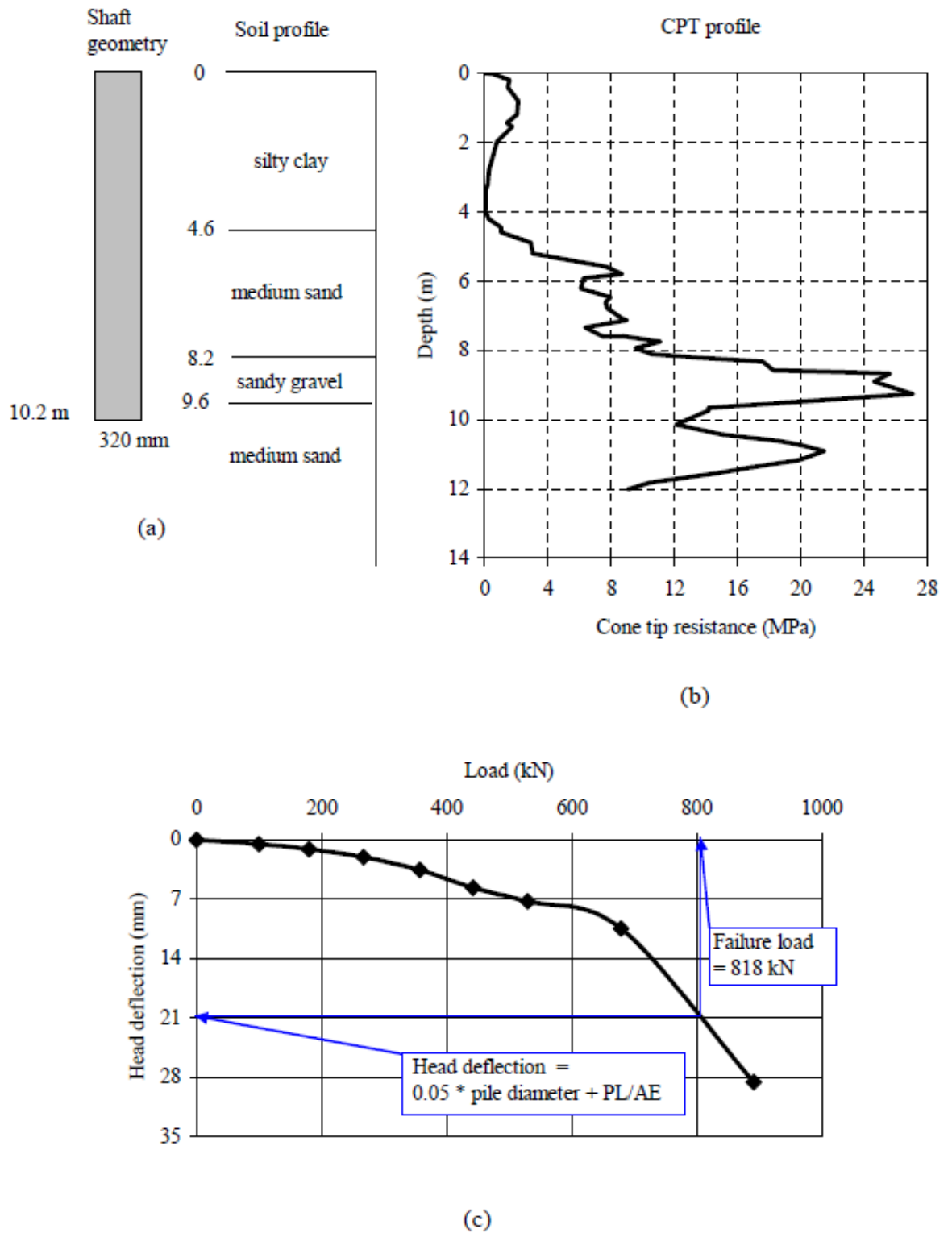


Figure A-11 Summary sheet for case record 11, (a) pile geometry and soil profile, (b) cone tip resistance profile, (c) load deflection plot

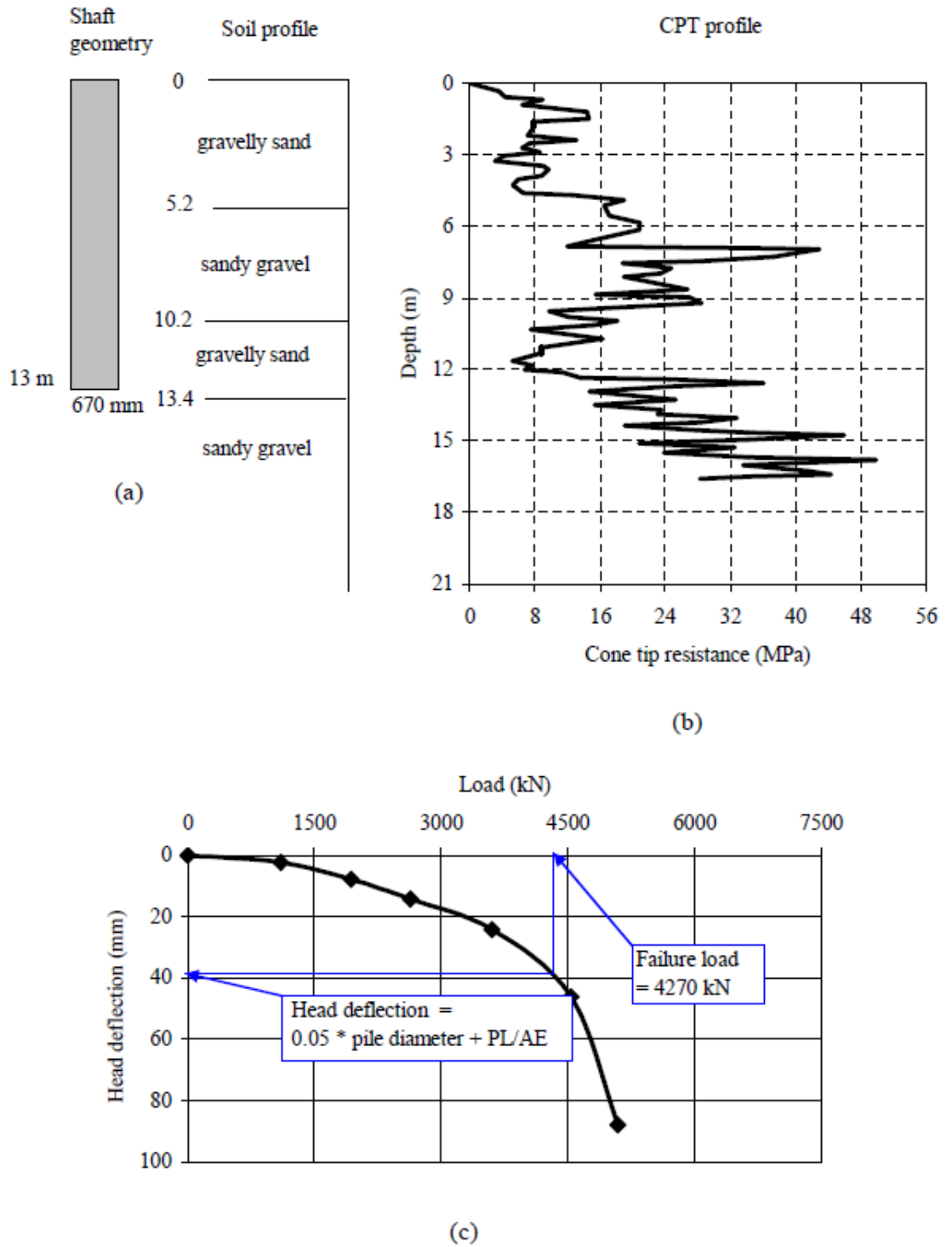


Figure A-12 Summary sheet for case record 12, (a) pile geometry and soil profile, (b) cone tip resistance profile, (c) load deflection plot

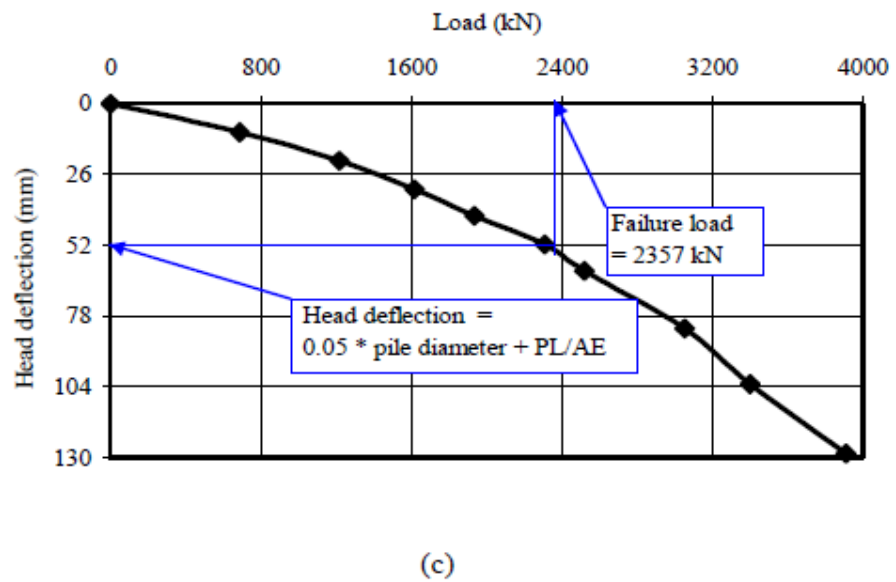
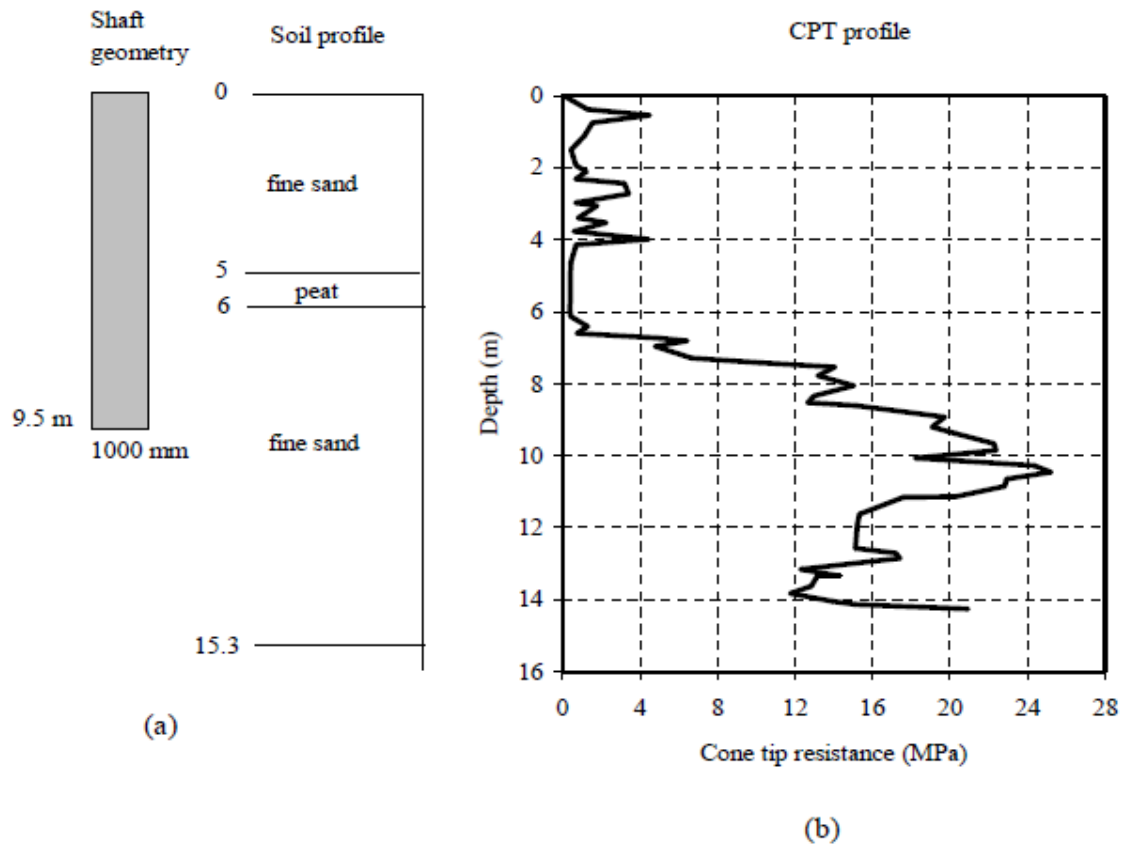
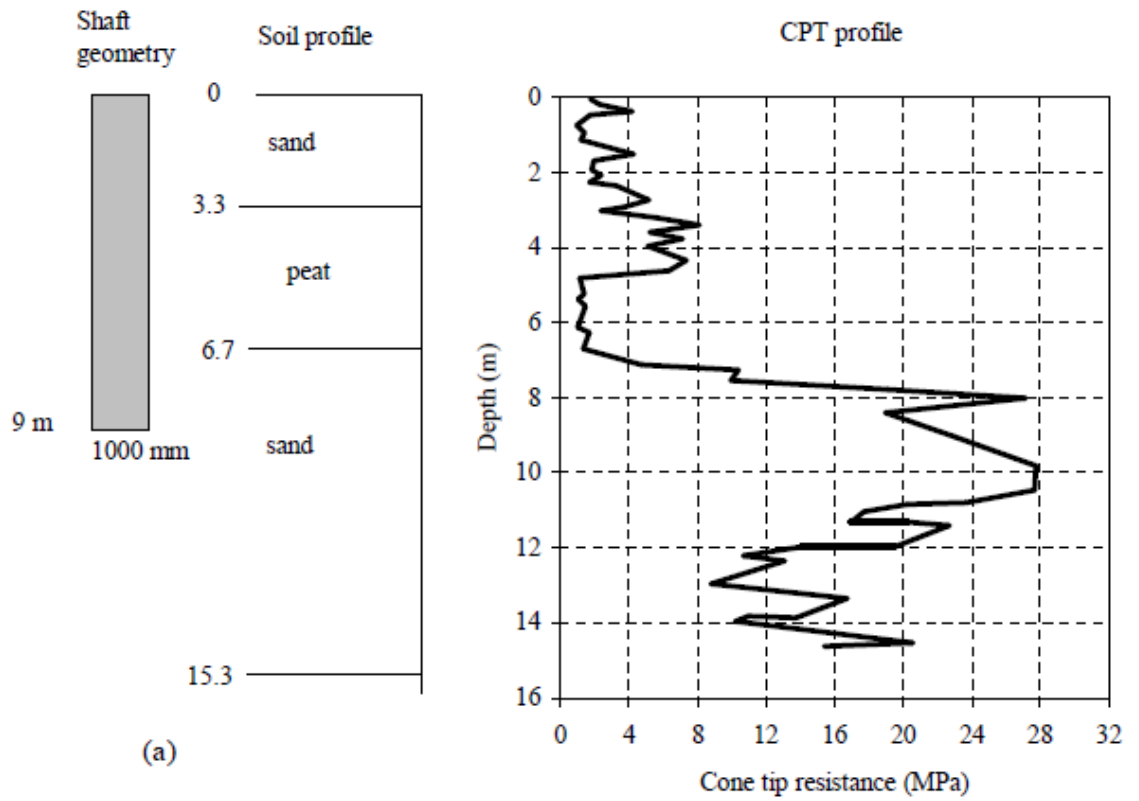
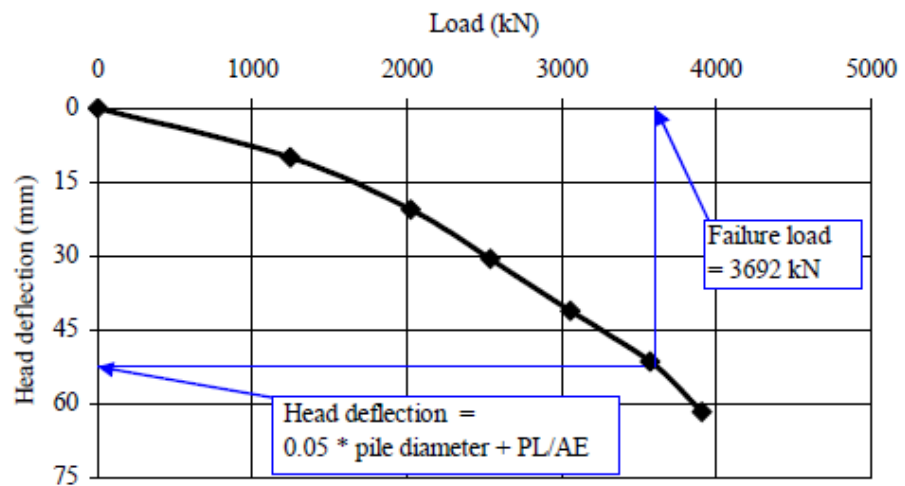


Figure A-13 Summary sheet for case record 13, (a) pile geometry and soil profile, (b) cone tip resistance profile, (c) load deflection plot



(a)

(b)



(c)

Figure A-14 Summary sheet for case record 14, (a) pile geometry and soil profile, (b) cone tip resistance profile, (c) load deflection plot

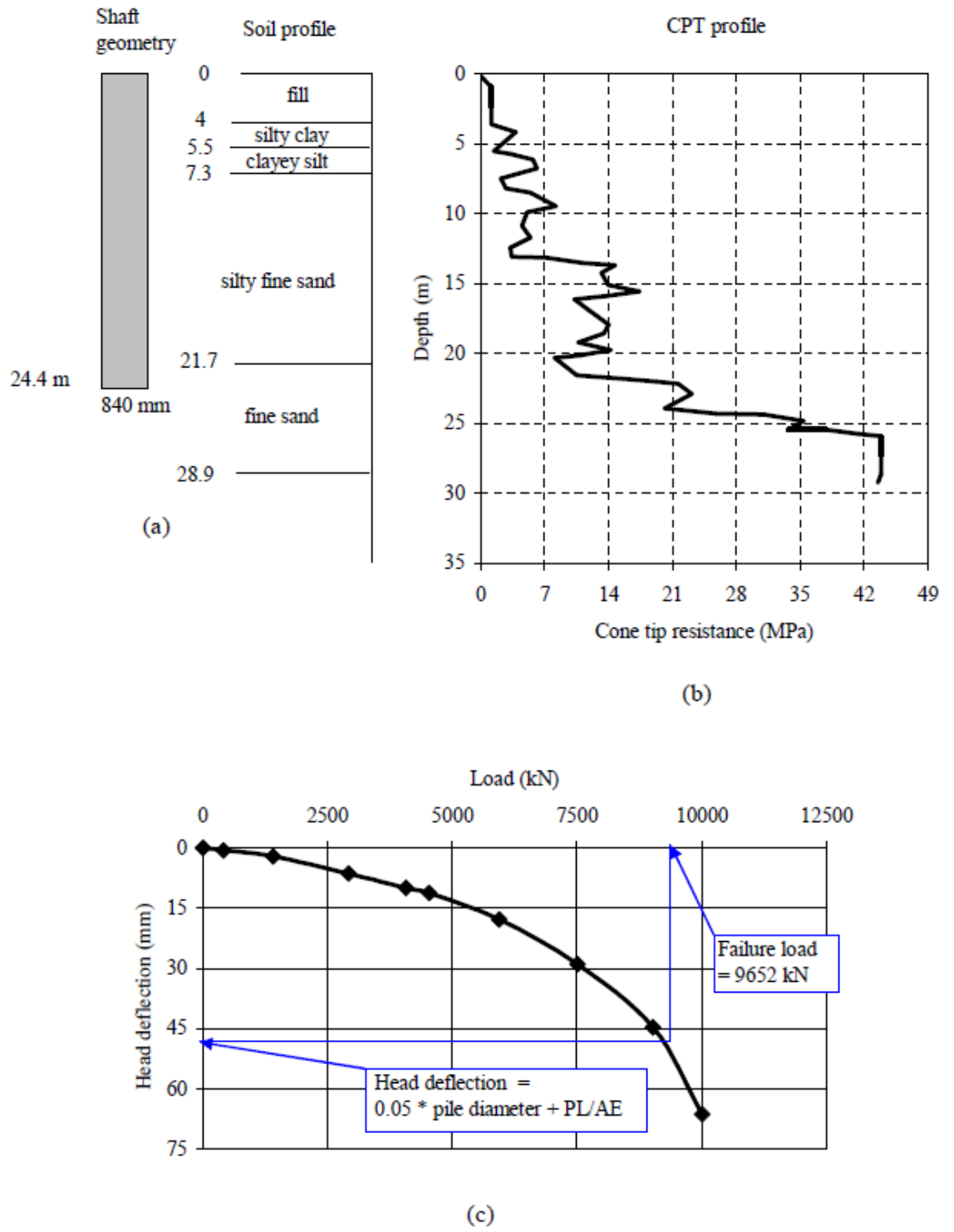
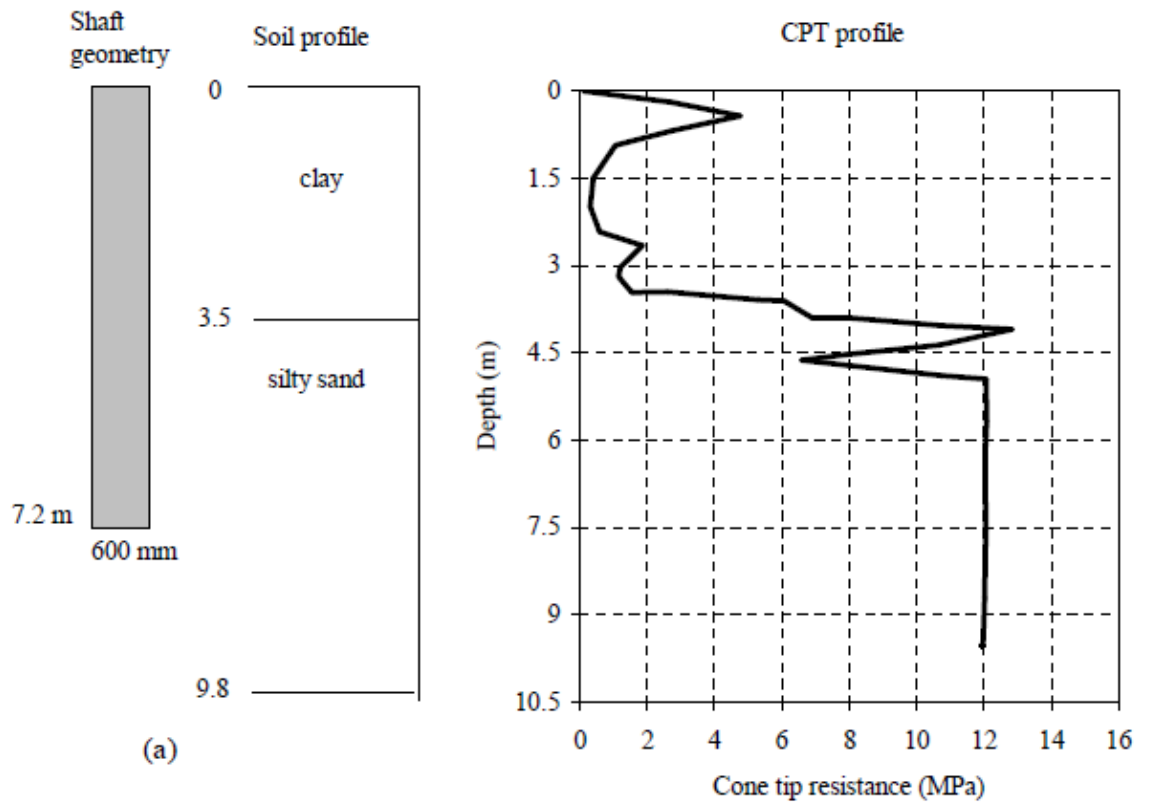
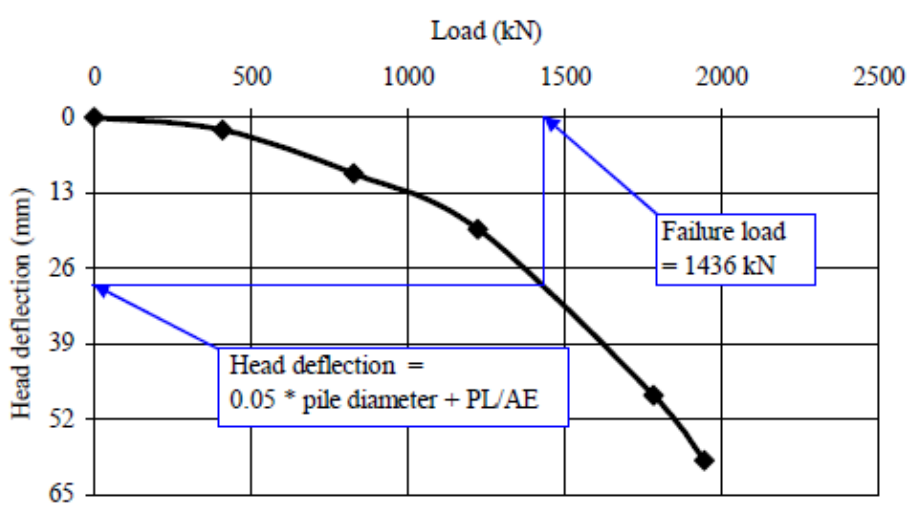


Figure A-15 Summary sheet for case record 15, (a) pile geometry and soil profile, (b) cone tip resistance profile, (c) load deflection plot



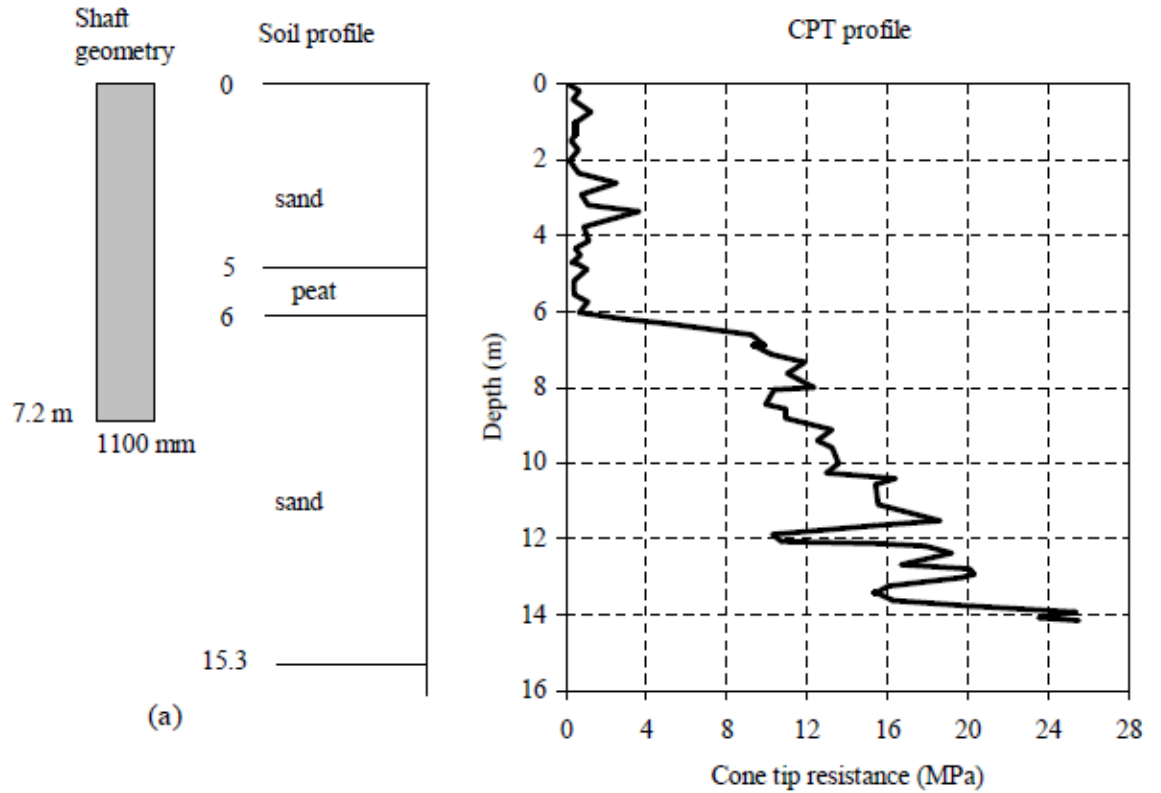
(a)

(b)



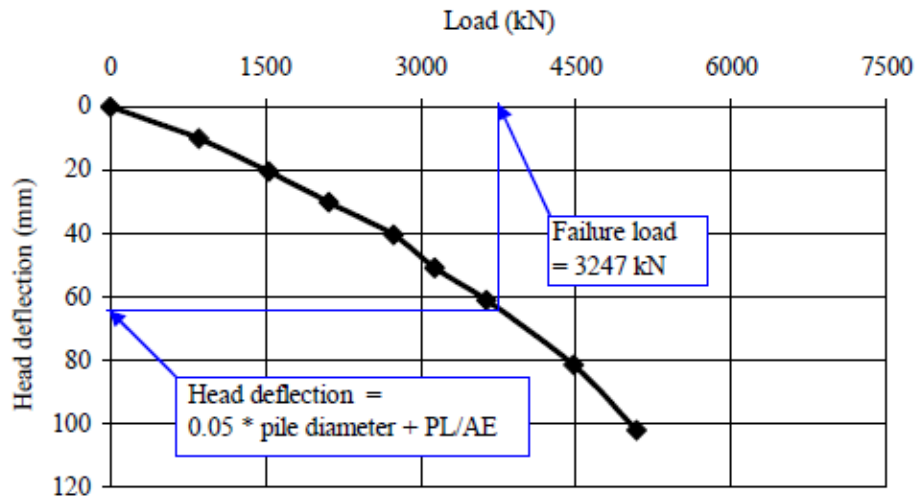
(c)

Figure A-16 Summary sheet for case record 16, (a) pile geometry and soil profile, (b) cone tip resistance profile, (c) load deflection plot



(a)

(b)



(c)

Figure A-17 Summary sheet for case record 17, (a) pile geometry and soil profile, (b) cone tip resistance profile, (c) load deflection plot

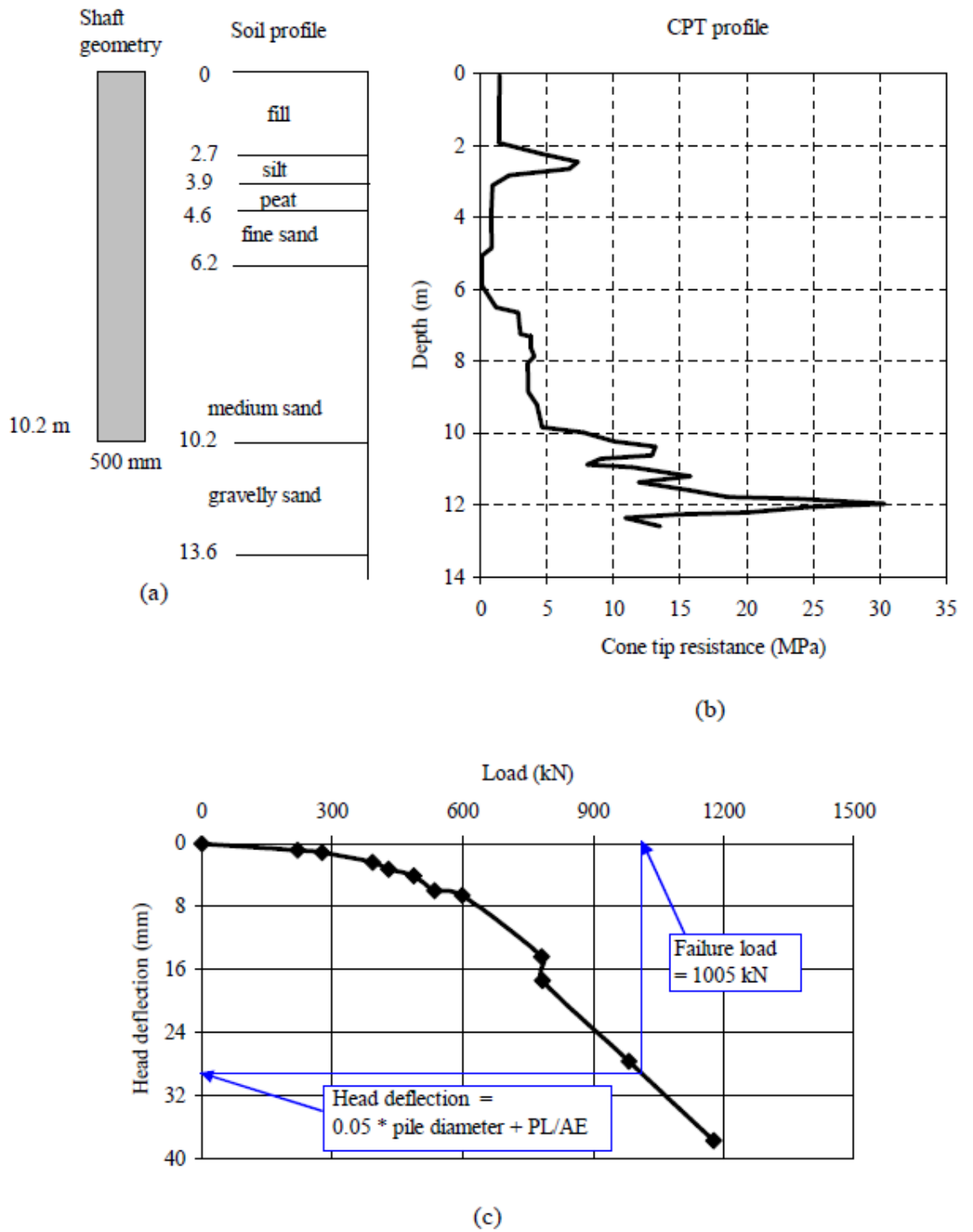


Figure A-18 Summary sheet for case record 18, (a) pile geometry and soil profile, (b) cone tip resistance profile, (c) load deflection plot

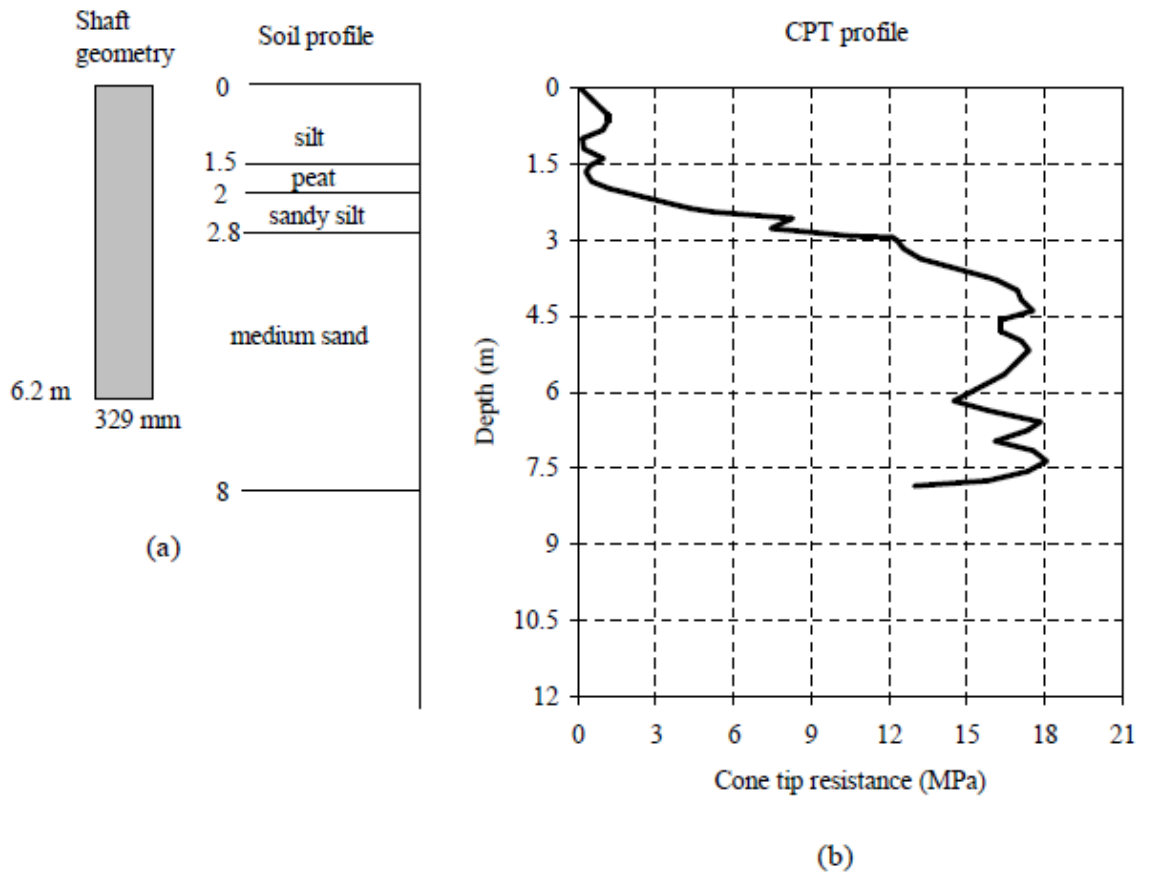


Figure A-19 Summary sheet for case record 19, (a) pile geometry and soil profile, (b) cone tip resistance profile, (c) load deflection plot

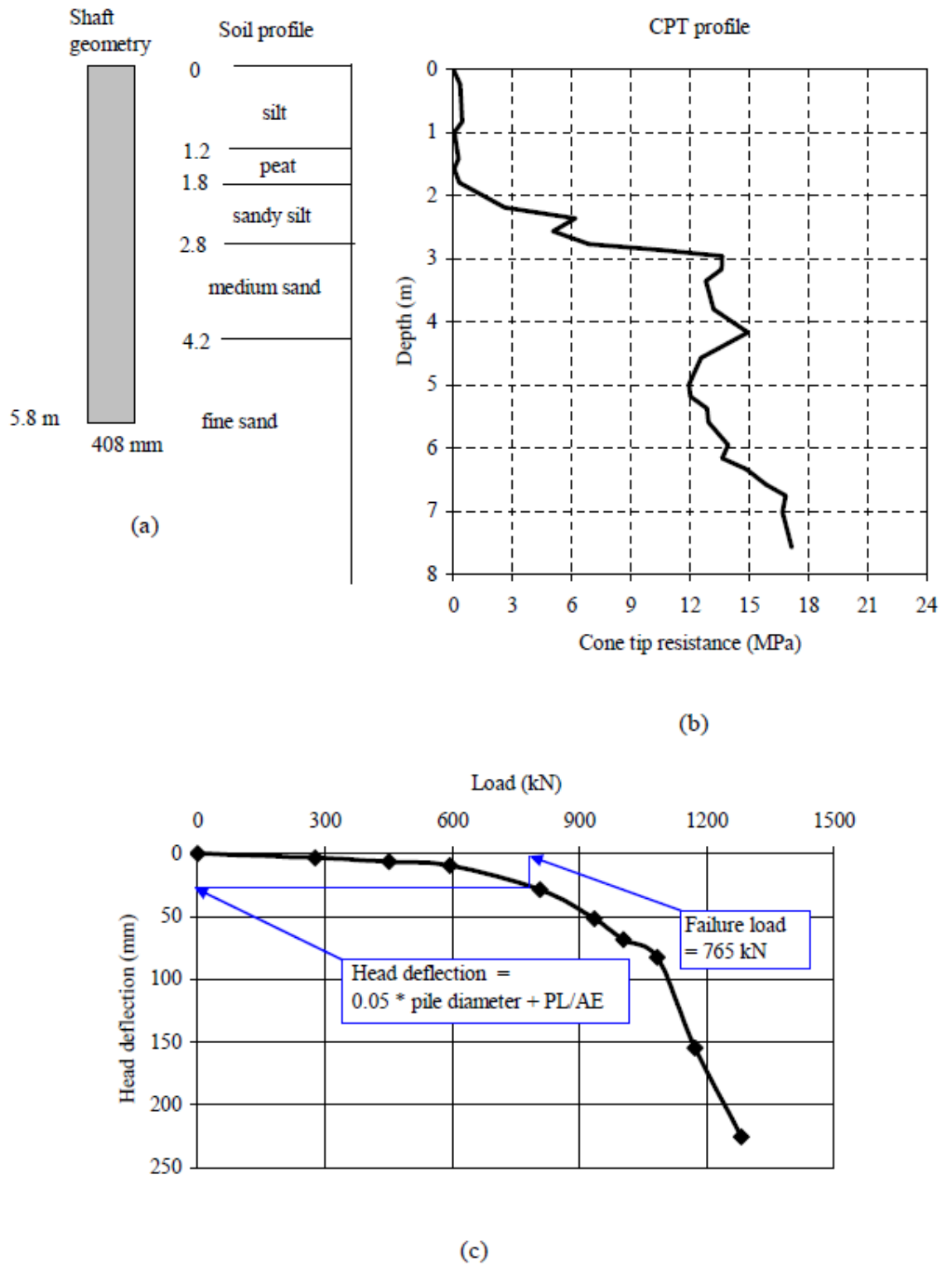
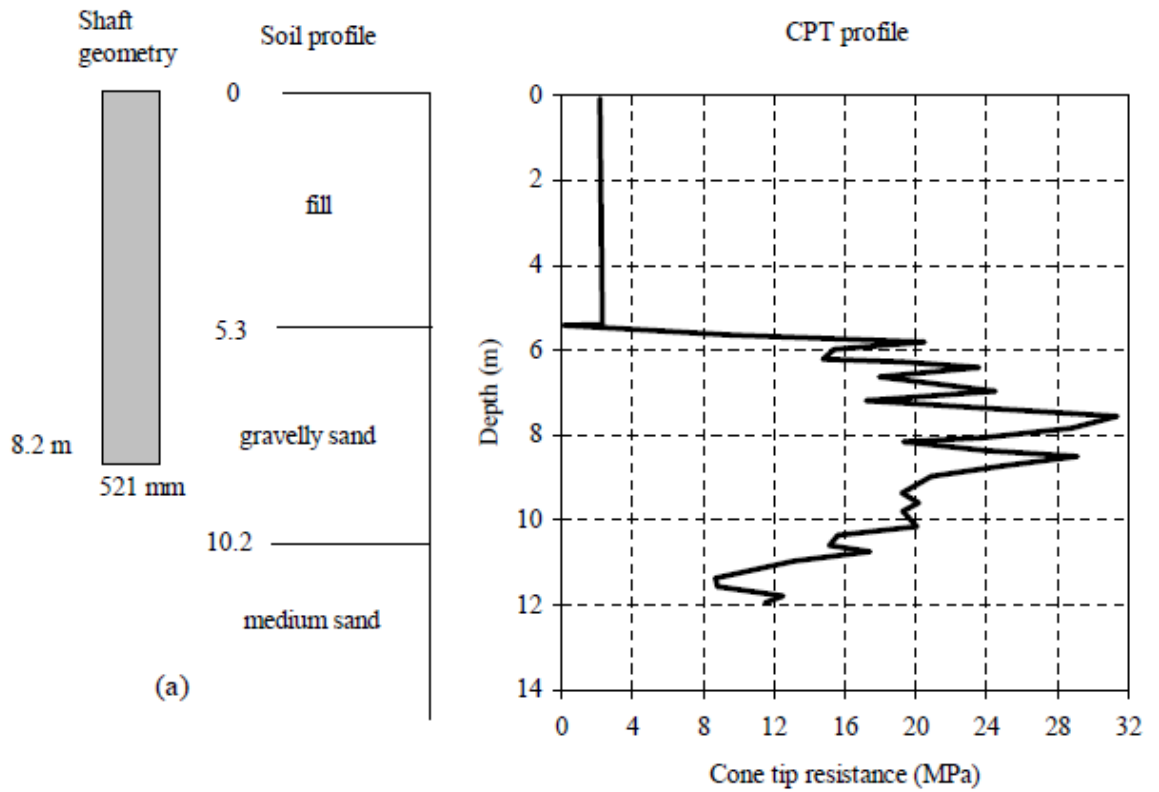
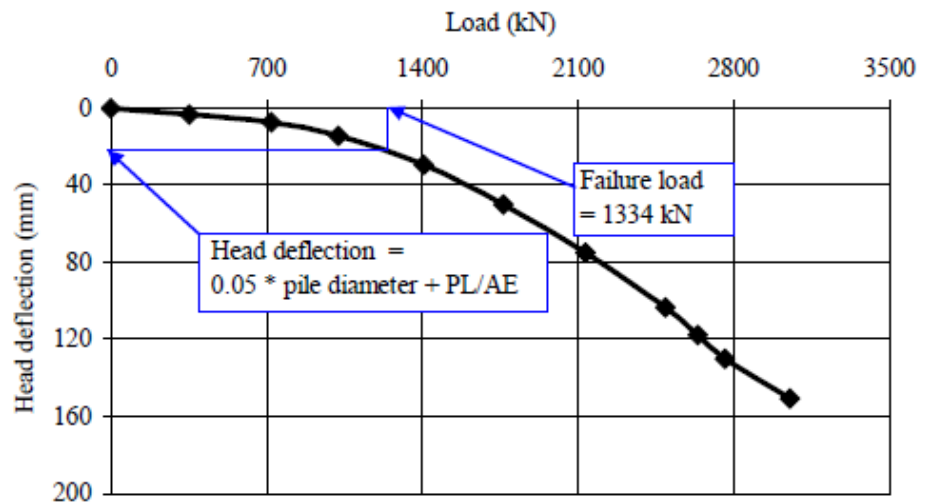


Figure A-20 Summary sheet for case record 20, (a) pile geometry and soil profile, (b) cone tip resistance profile, (c) load deflection plot



(b)



(c)

Figure A-21 Summary sheet for case record 21, (a) pile geometry and soil profile, (b) cone tip resistance profile, (c) load deflection plot

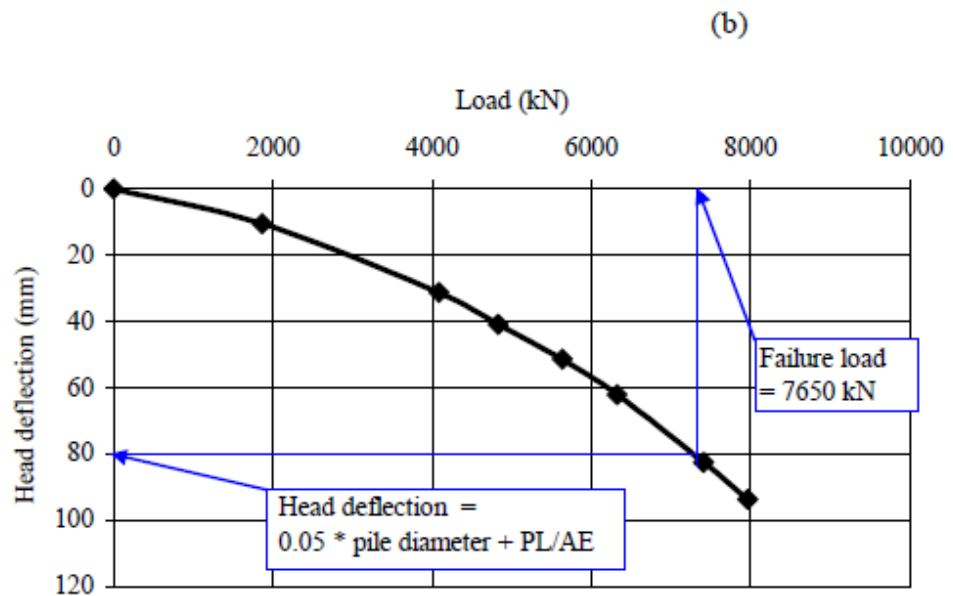
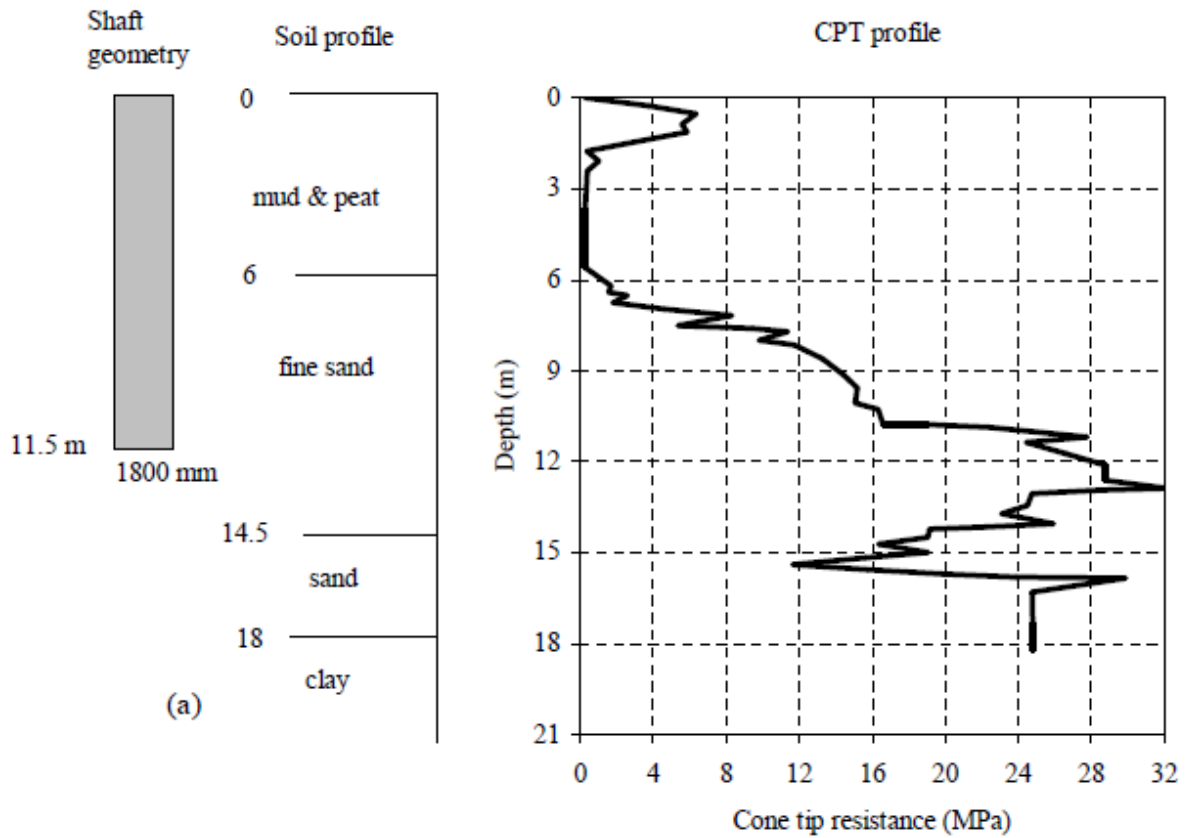


Figure A-22 Summary sheet for case record 22, (a) pile geometry and soil profile, (b) cone tip resistance profile, (c) load deflection plot

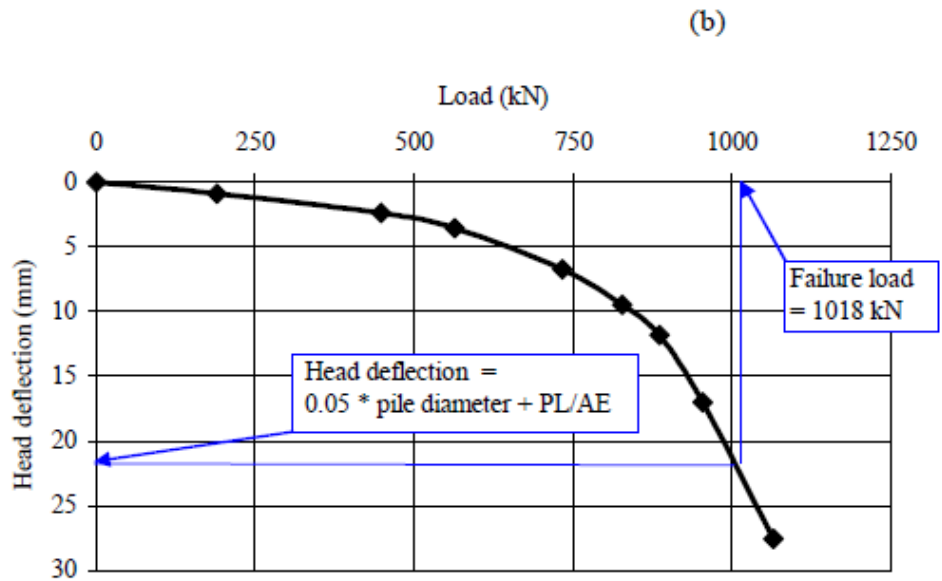
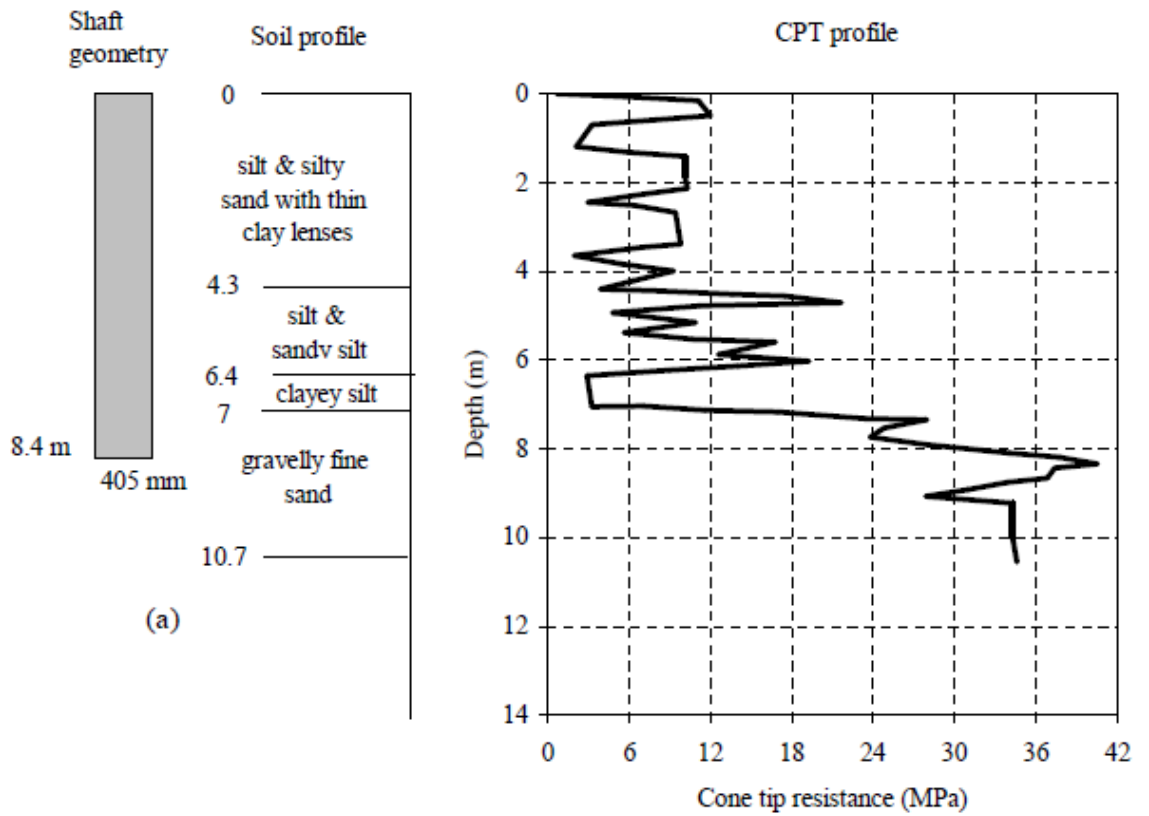


Figure A-23 Summary sheet for case record 23, (a) pile geometry and soil profile, (b) cone tip resistance profile, (c) load deflection plot

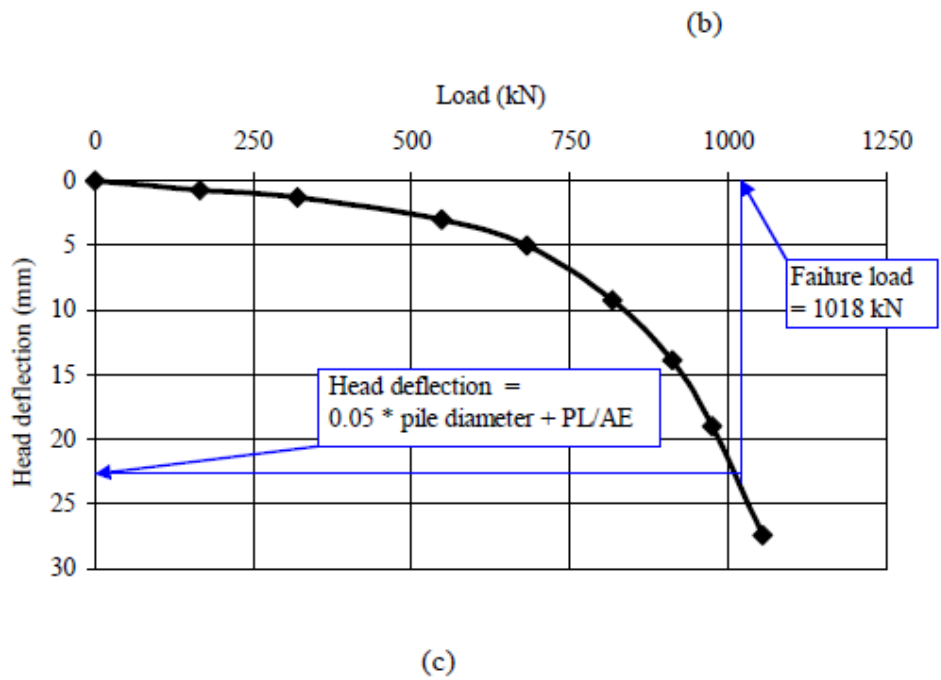
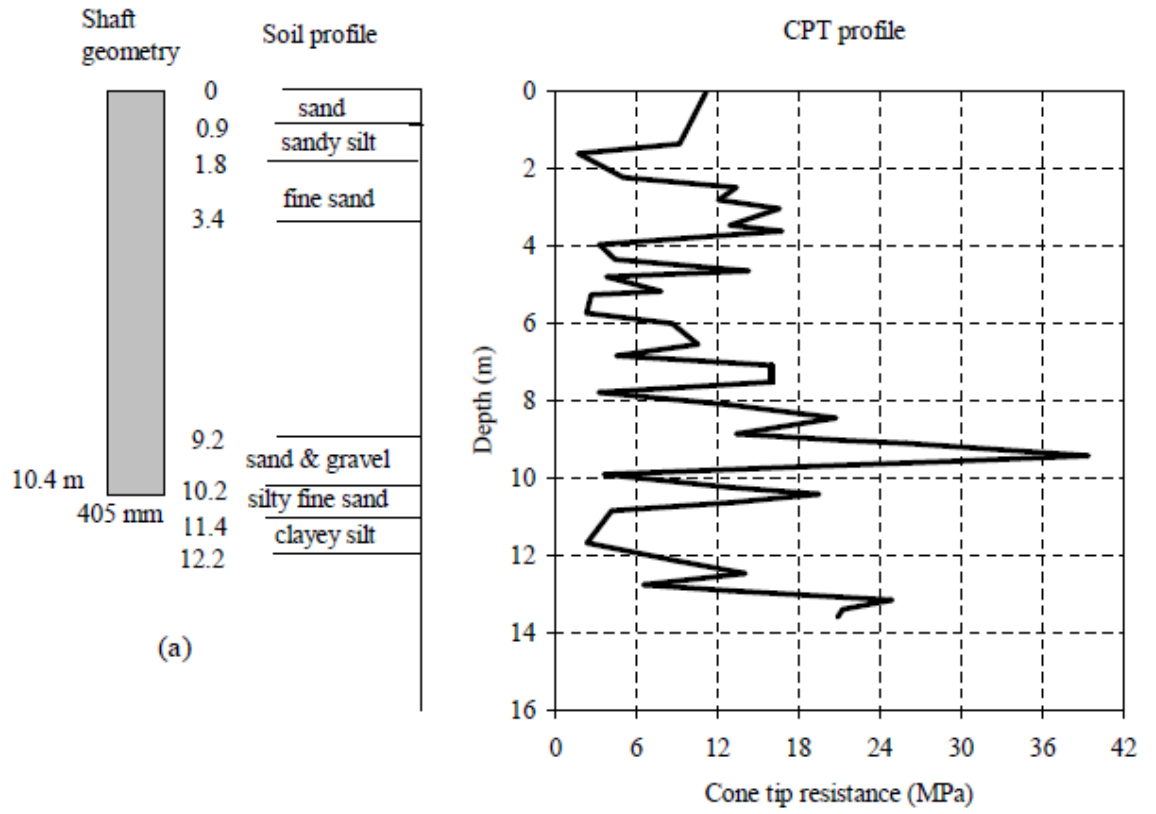


Figure A-24 Summary sheet for case record 24, (a) pile geometry and soil profile, (b) cone tip resistance profile, (c) load deflection plot

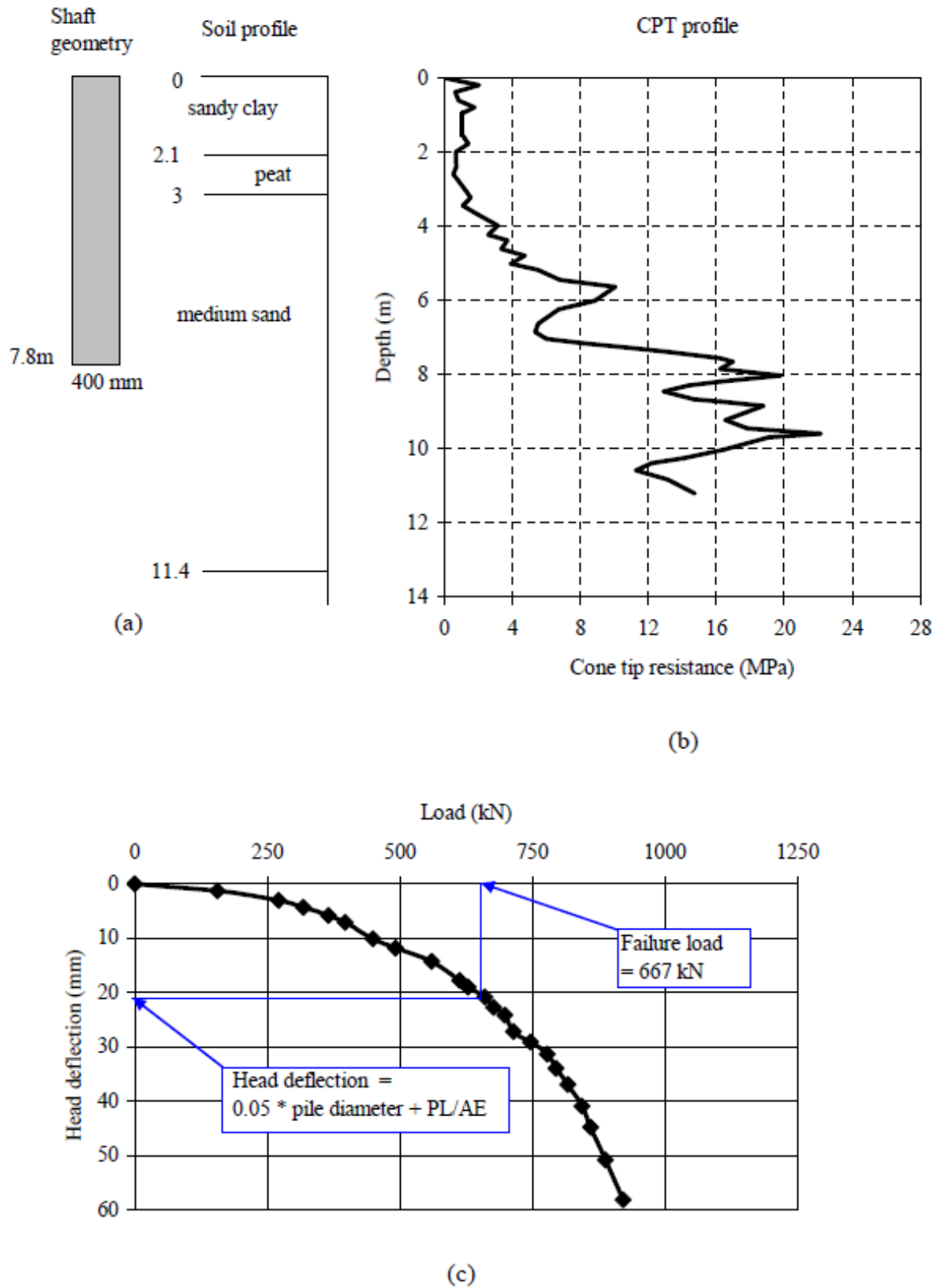


Figure A-25 Summary sheet for case record 25, (a) pile geometry and soil profile, (b) cone tip resistance profile, (c) load deflection plot

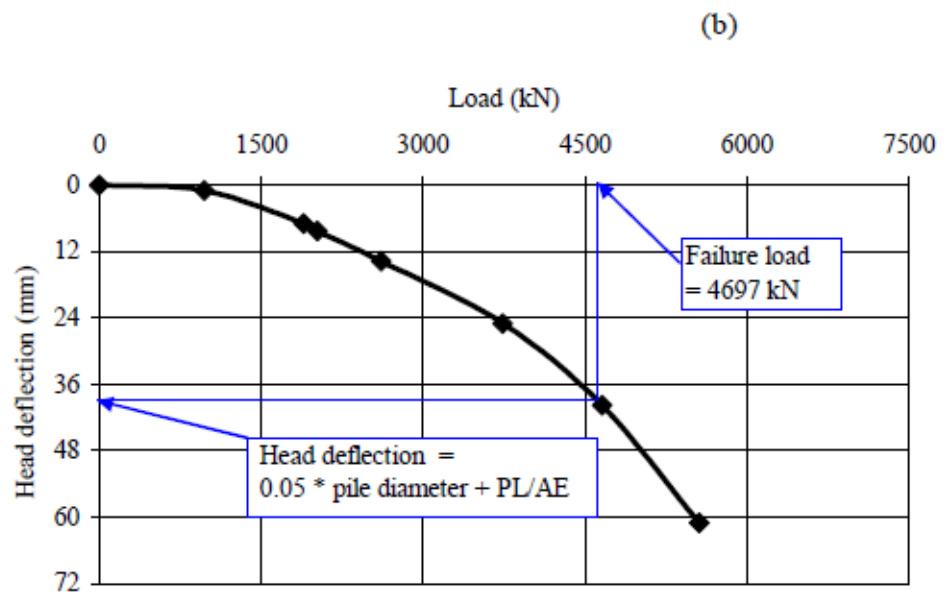
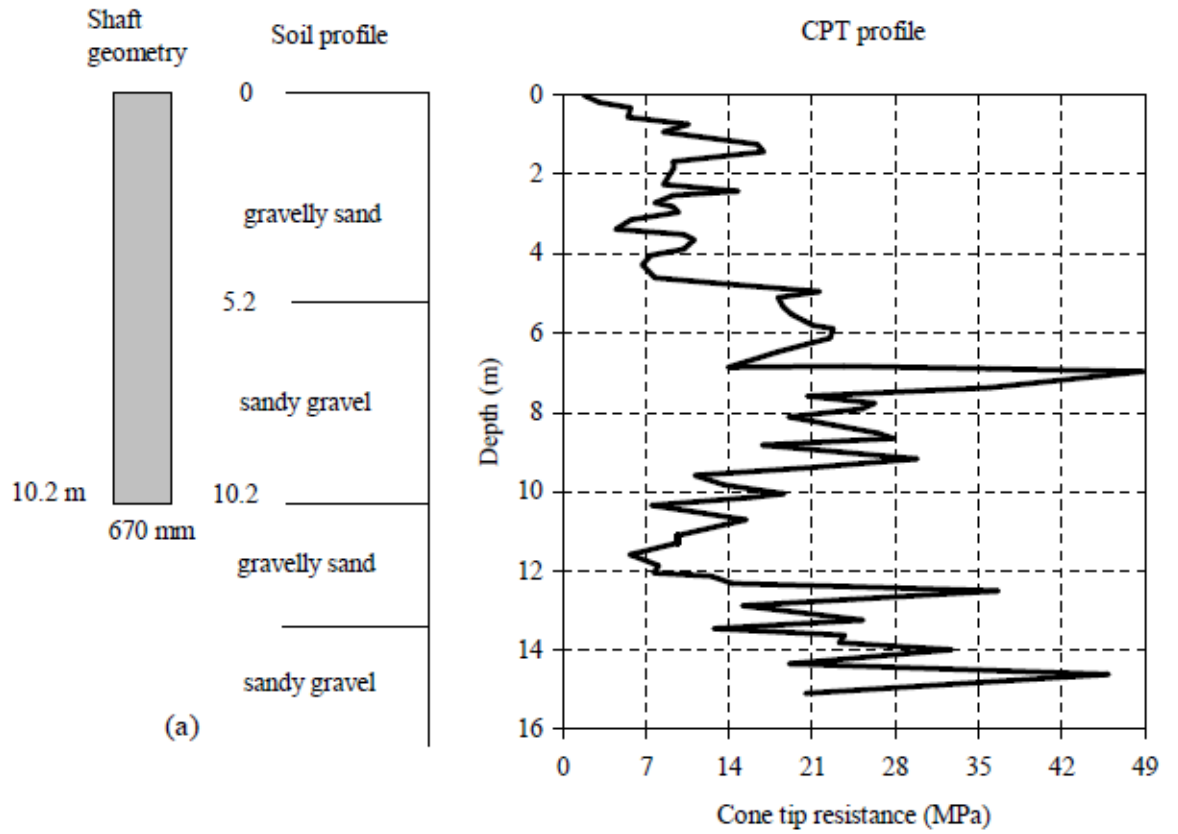


Figure A-26 Summary sheet for case record 26, (a) pile geometry and soil profile, (b) cone tip resistance profile, (c) load deflection plot

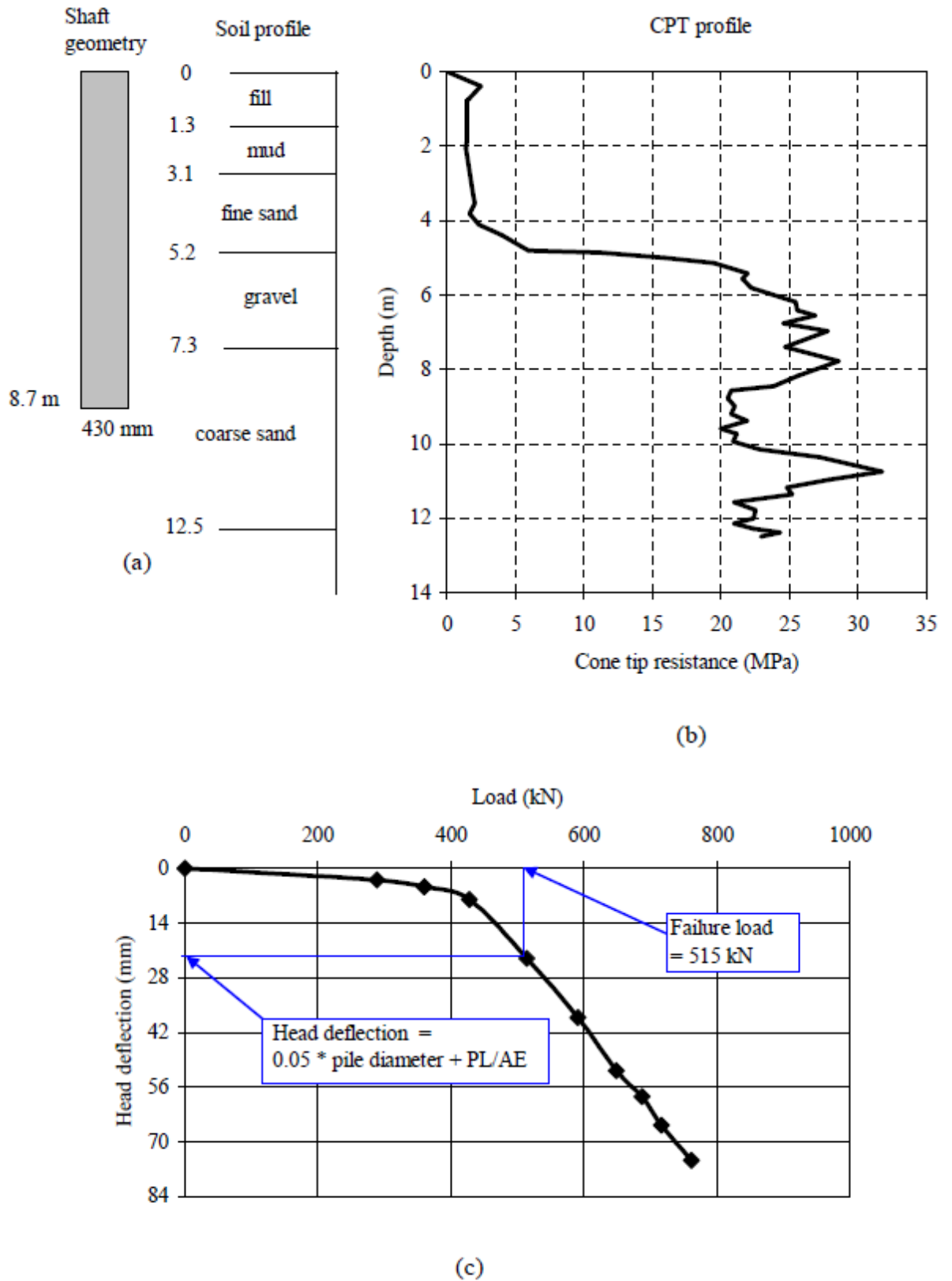
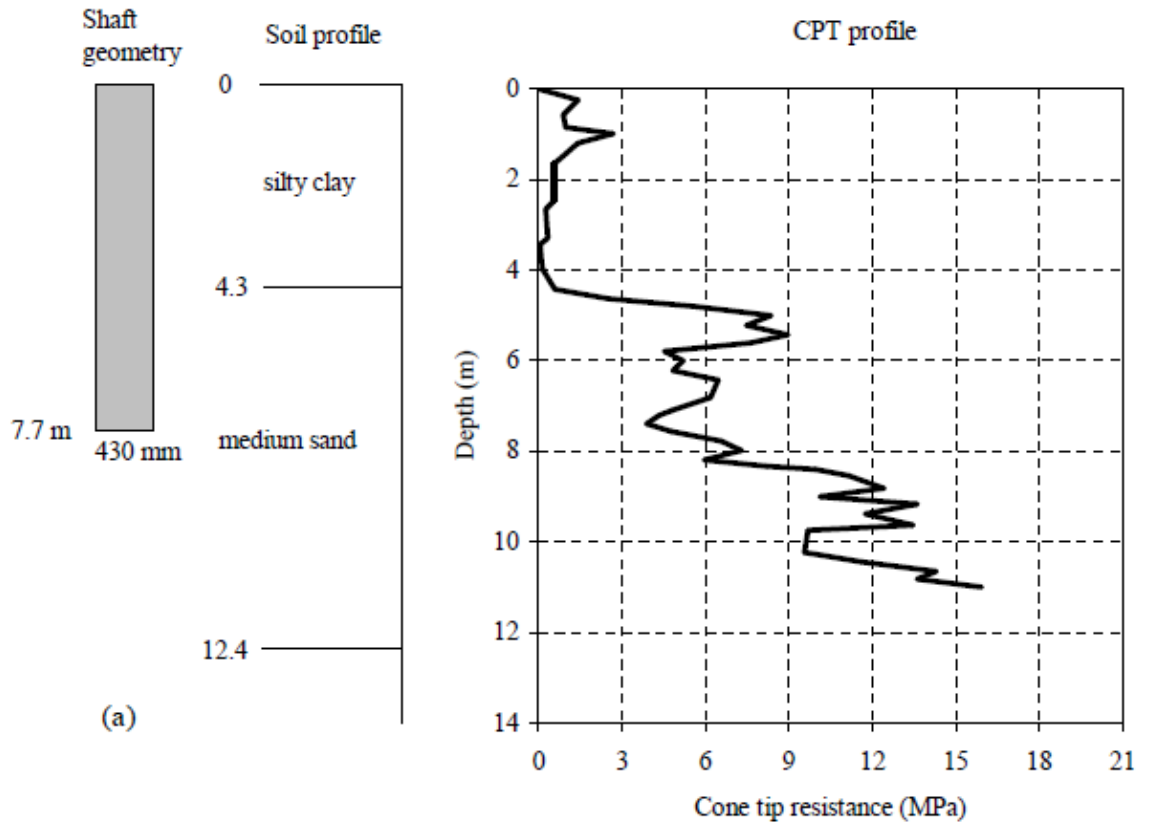
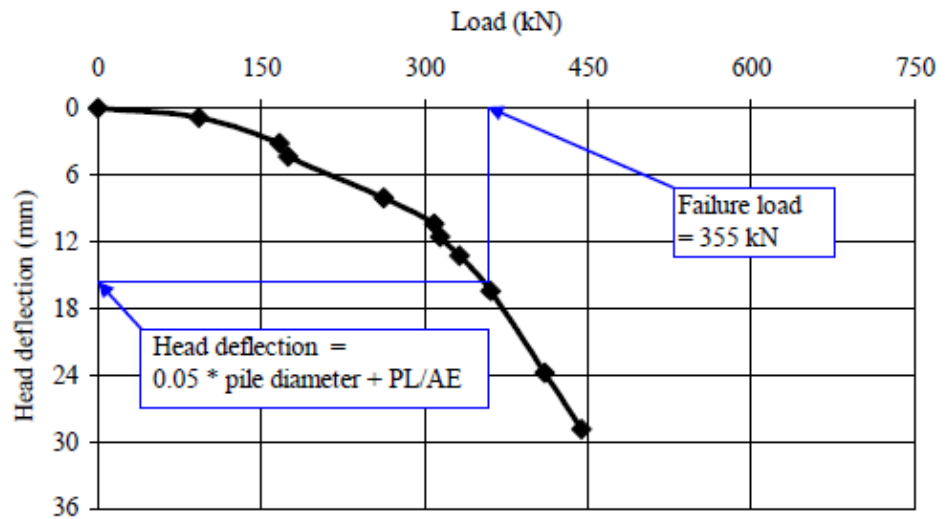


Figure A-27 Summary sheet for case record 27, (a) pile geometry and soil profile, (b) cone tip resistance profile, (c) load deflection plot



(a)

(b)



(c)

Figure A-28 Summary sheet for case record 28, (a) pile geometry and soil profile, (b) cone tip resistance profile, (c) load deflection plot

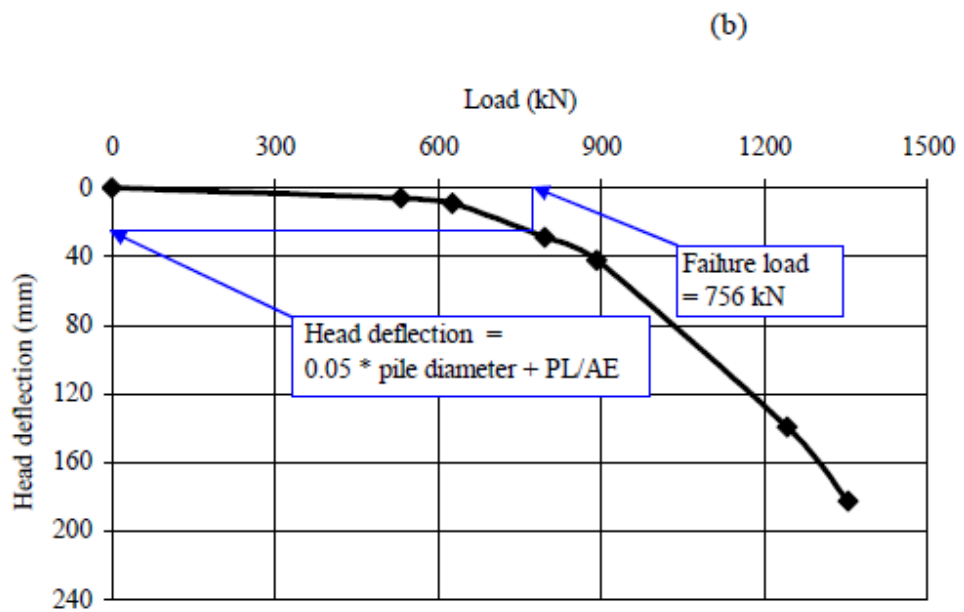
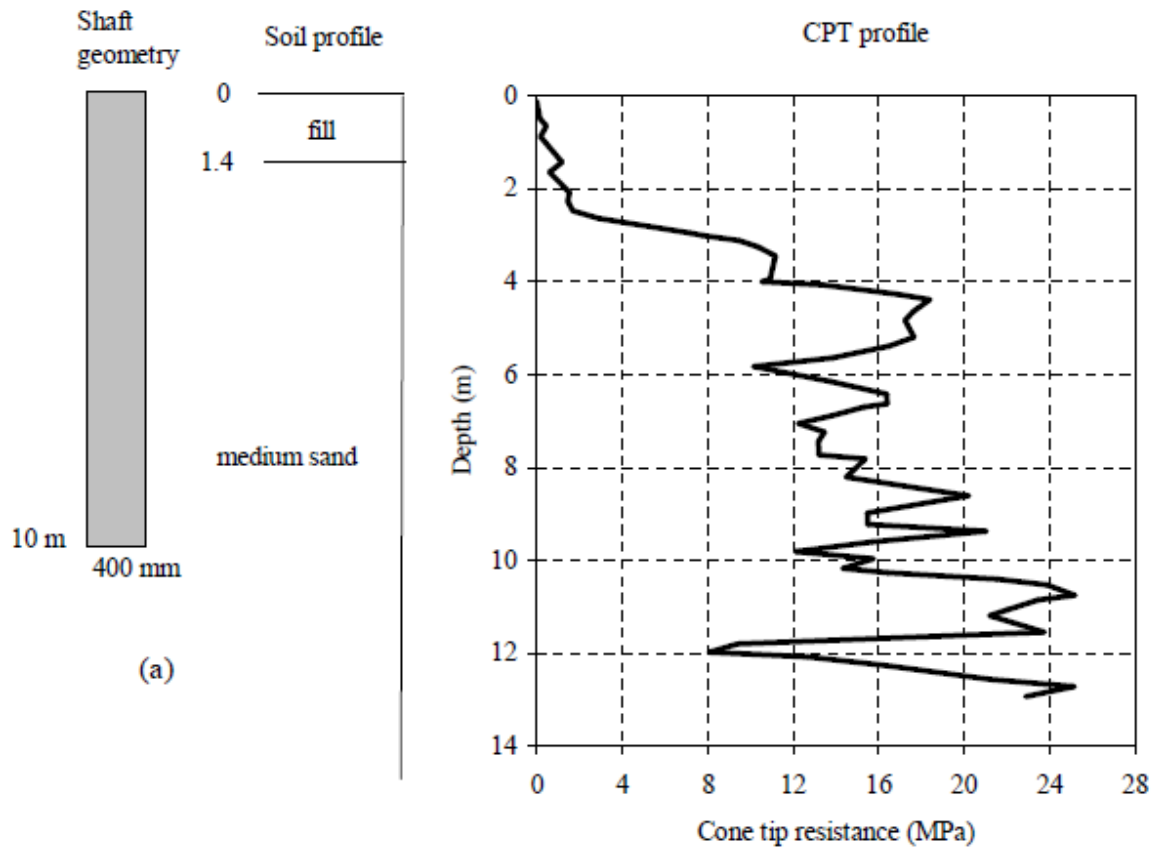
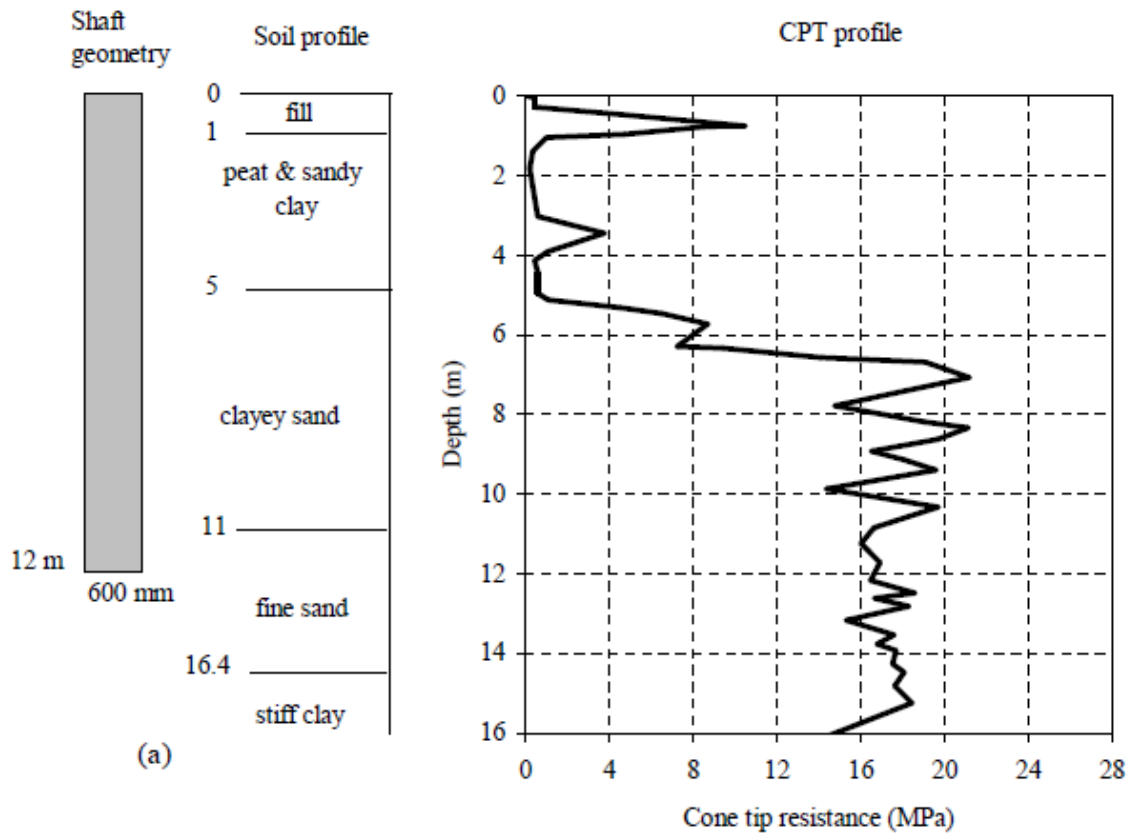
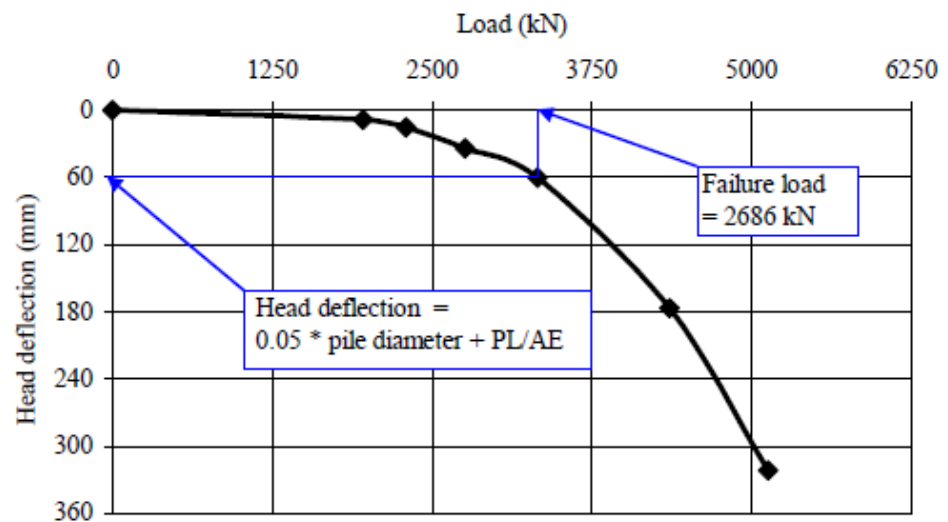


Figure A-29 Summary sheet for case record 29, (a) pile geometry and soil profile, (b) cone tip resistance profile, (c) load deflection plot



(a)

(b)



(c)

Figure A-30 Summary sheet for case record 30, (a) pile geometry and soil profile, (b) cone tip resistance profile, (c) load deflection plot

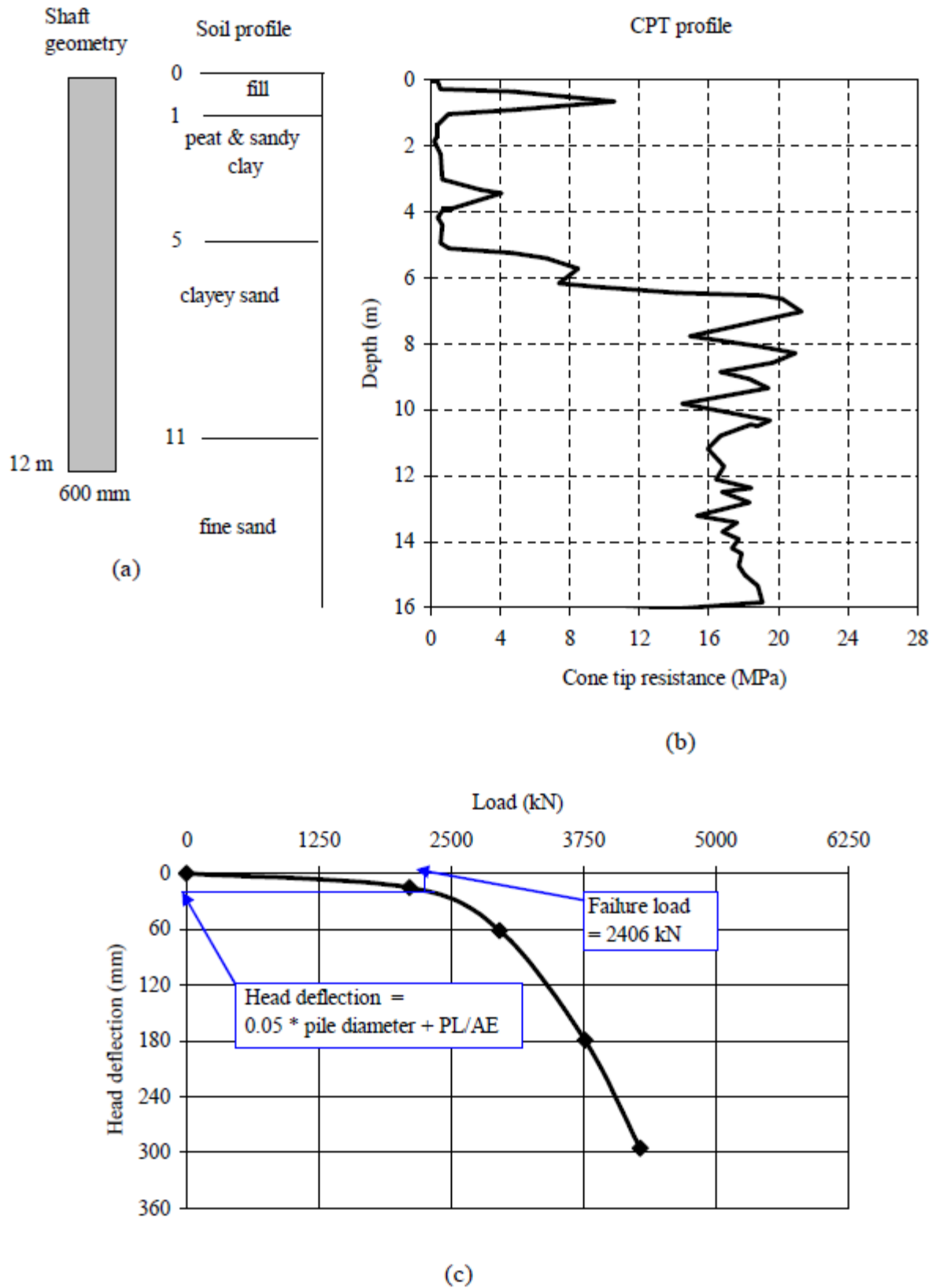


Figure A-31 Summary sheet for case record 31, (a) pile geometry and soil profile, (b) cone tip resistance profile, (c) load deflection plot

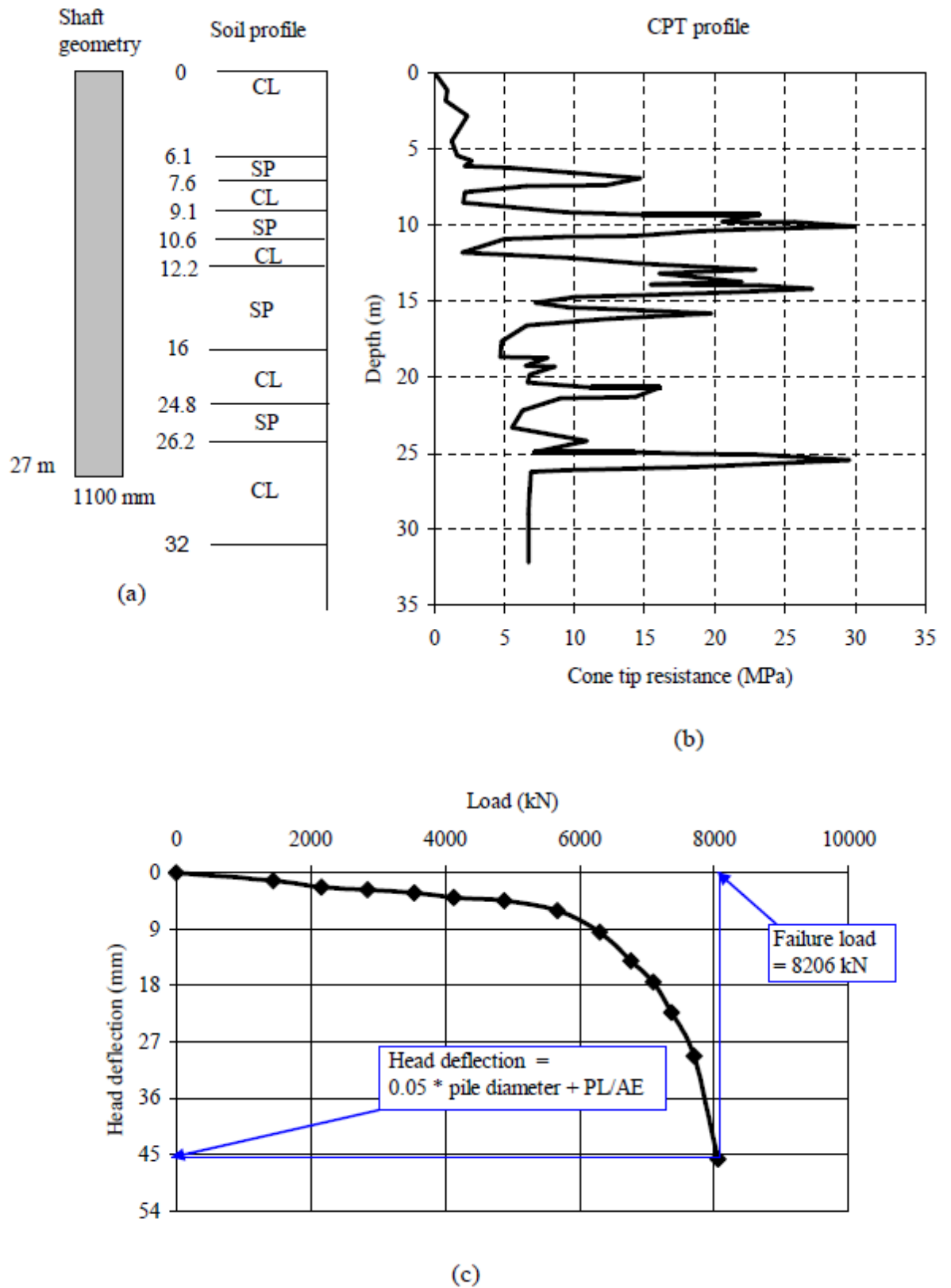


Figure A-32 Summary sheet for case record 32, (a) pile geometry and soil profile, (b) cone tip resistance profile, (c) load deflection plot

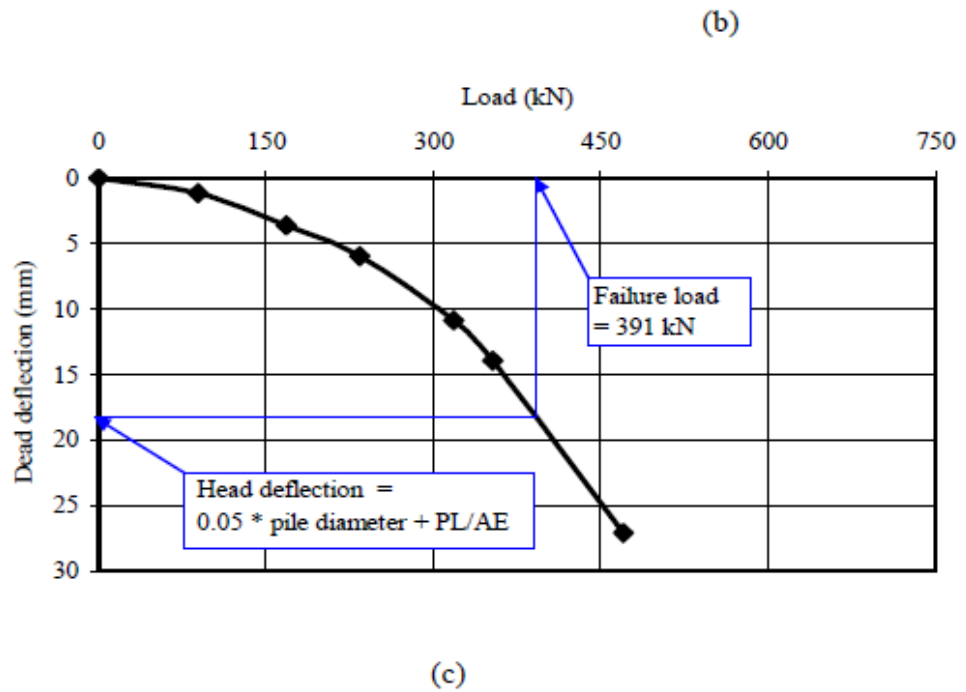
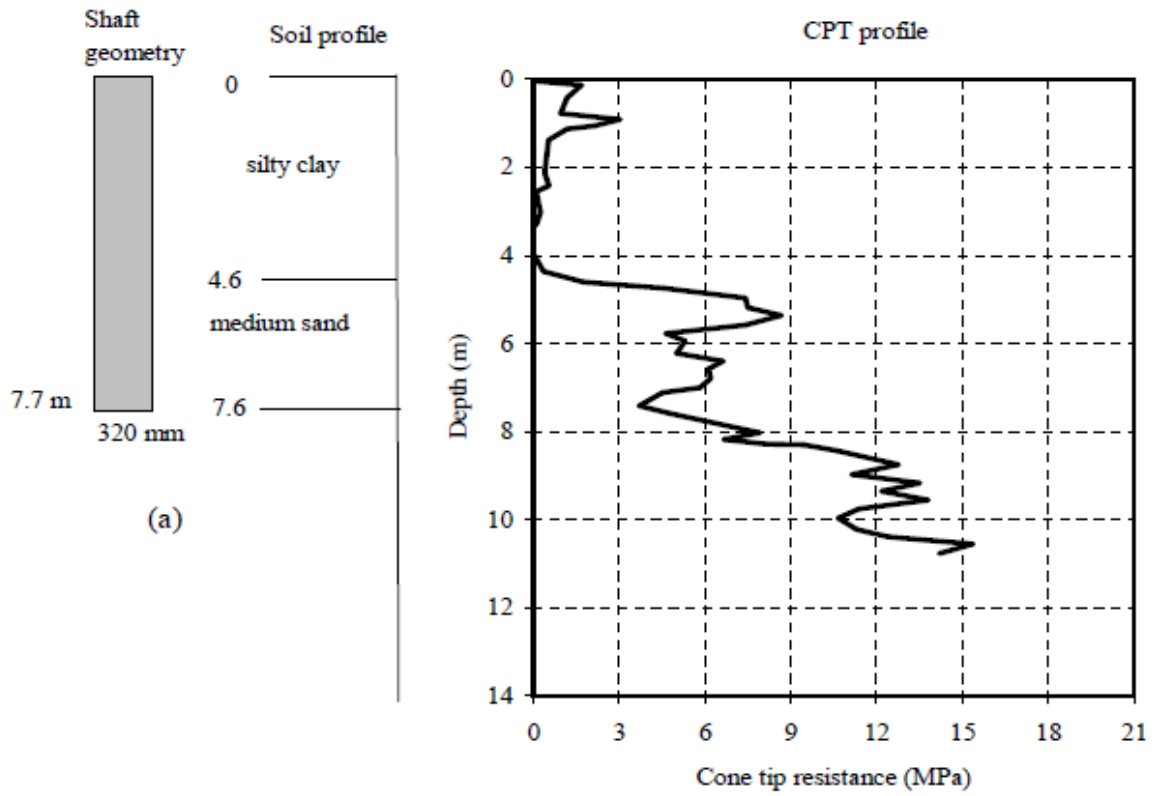


Figure A-33 Summary sheet for case record 33, (a) pile geometry and soil profile, (b) cone tip resistance profile, (c) load deflection plot

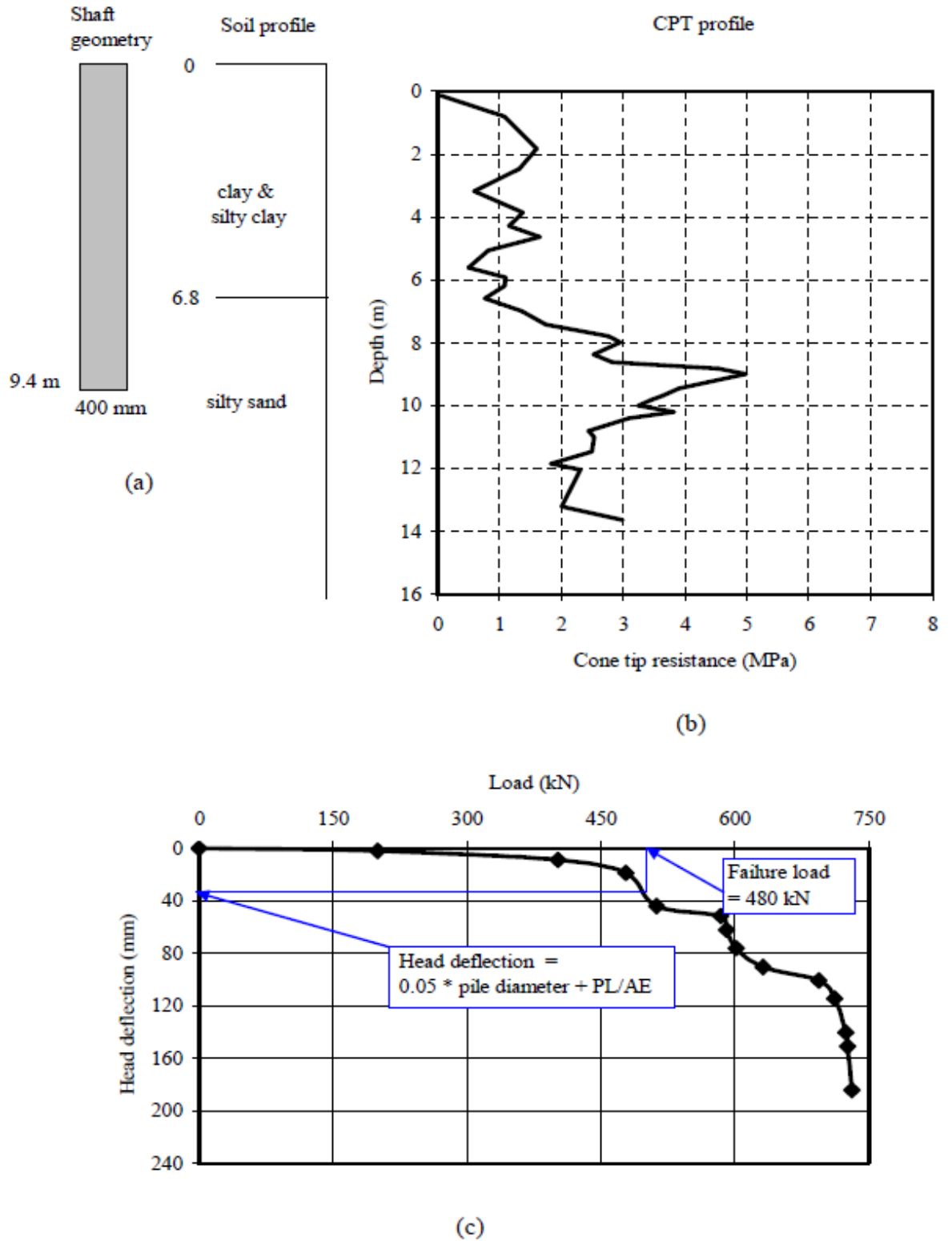


Figure A-34 Summary sheet for case record 34, (a) pile geometry and soil profile, (b) cone tip resistance profile, (c) load deflection plot

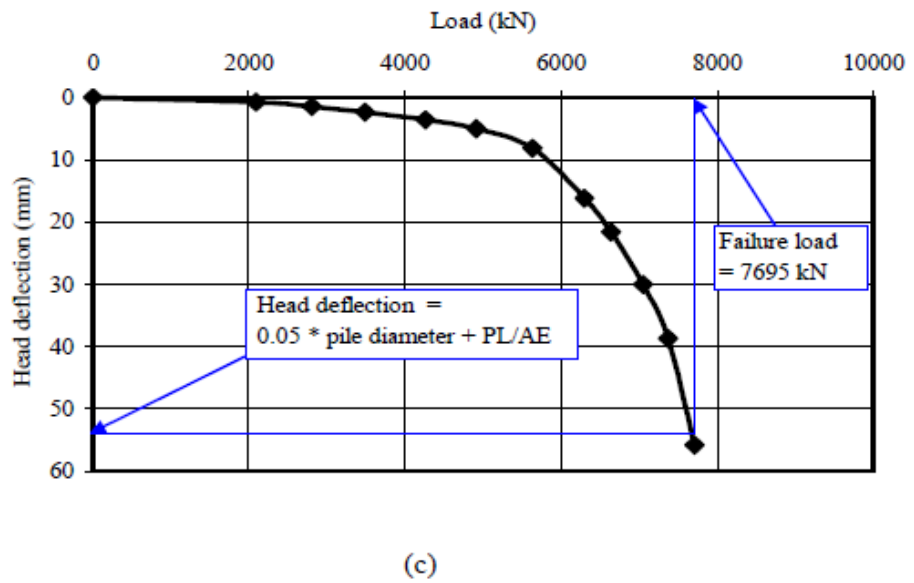
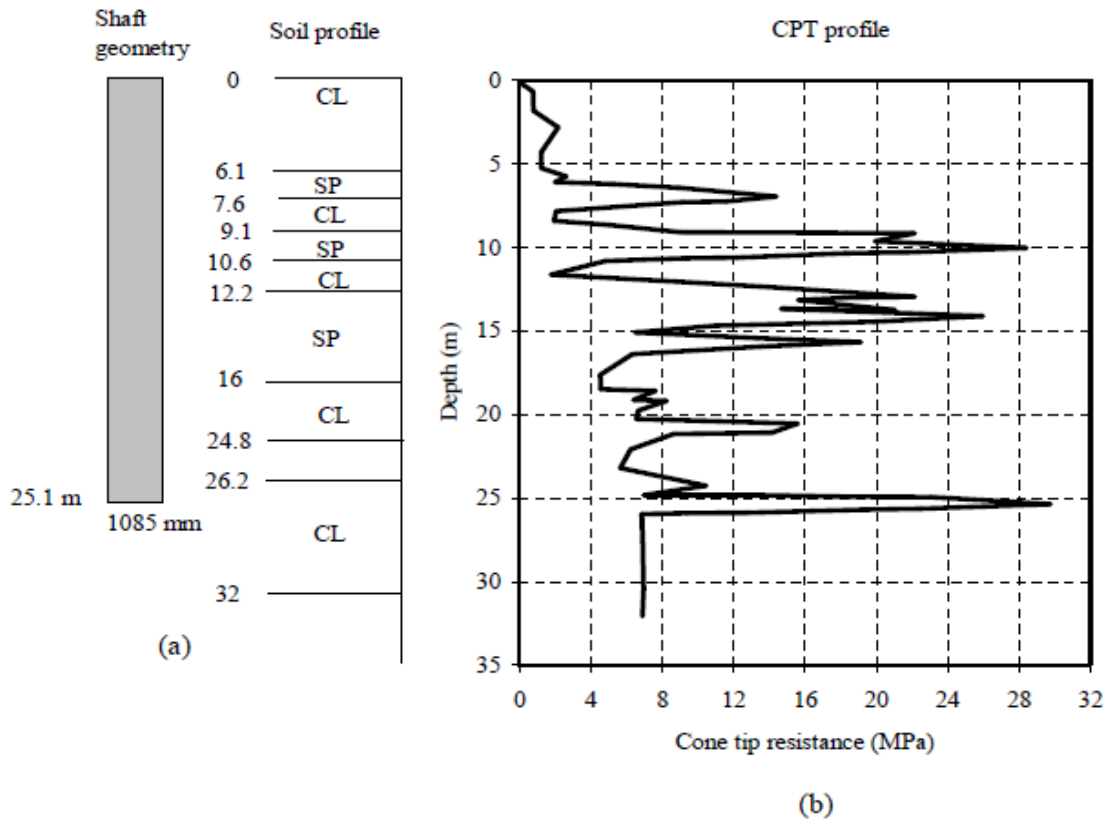


Figure A-35 Summary sheet for case record 35, (a) pile geometry and soil profile, (b) cone tip resistance profile, (c) load deflection plot

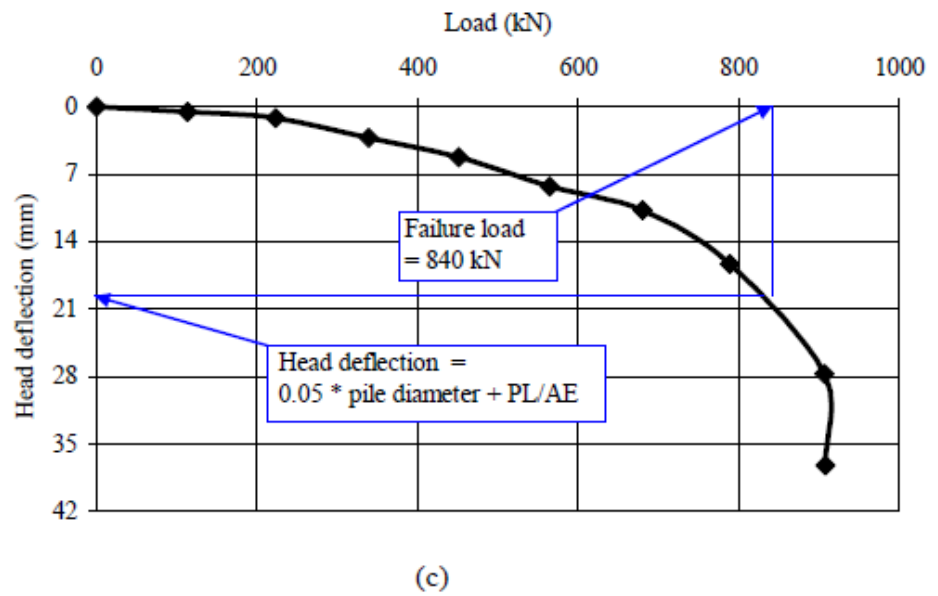
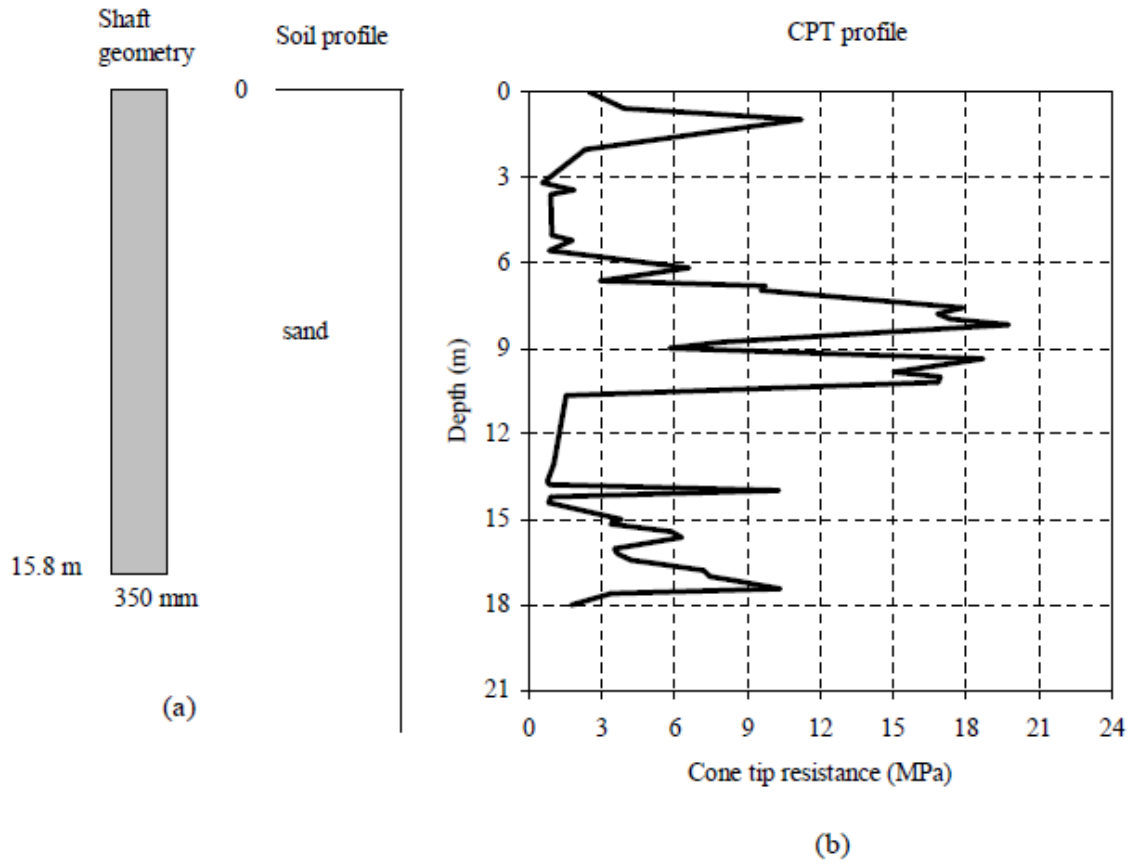


Figure A-36 Summary sheet for case record 36, (a) pile geometry and soil profile, (b) cone tip resistance profile, (c) load deflection plot

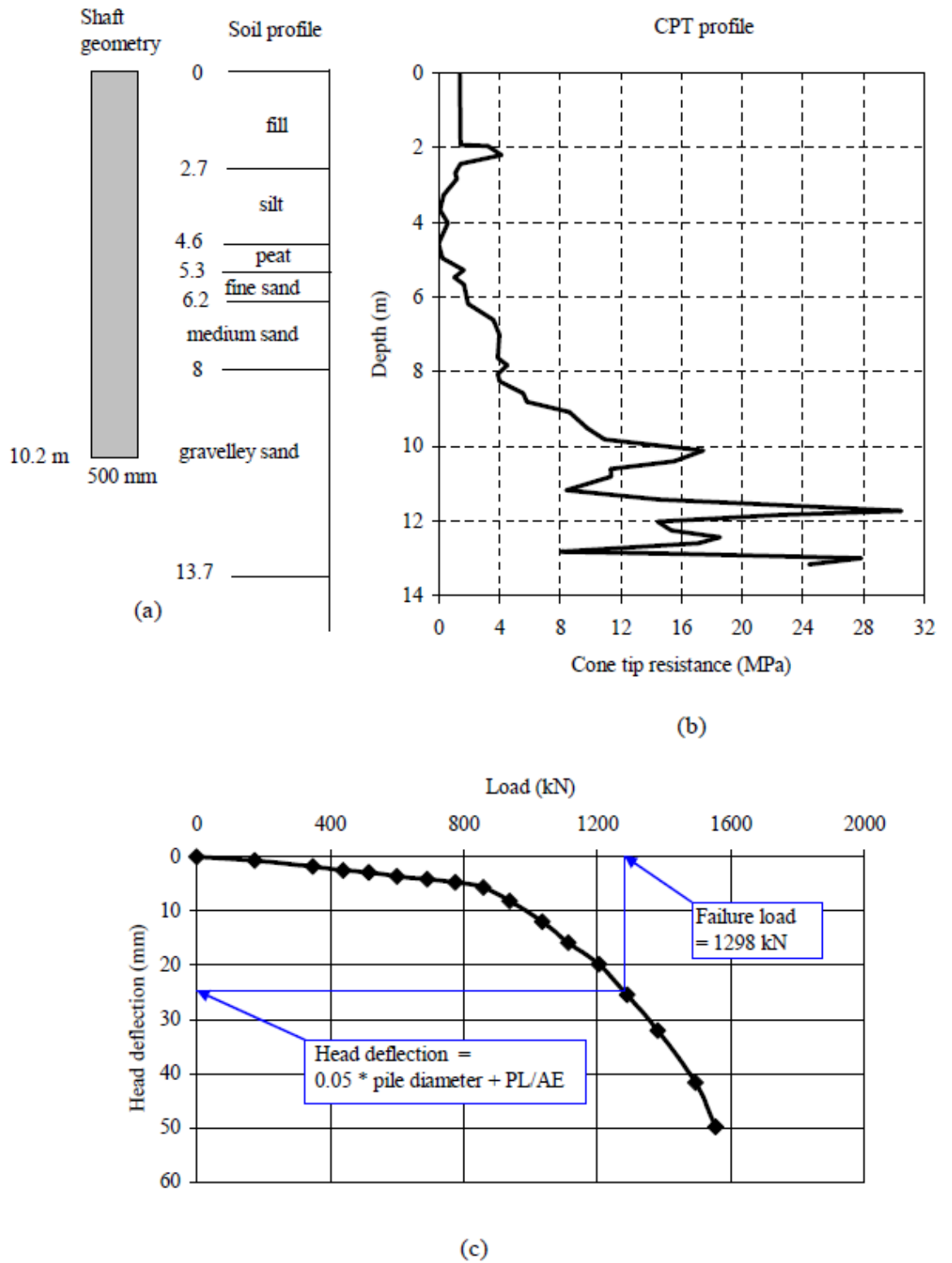


Figure A-37 Summary sheet for case record 37, (a) pile geometry and soil profile, (b) cone tip resistance profile, (c) load deflection plot

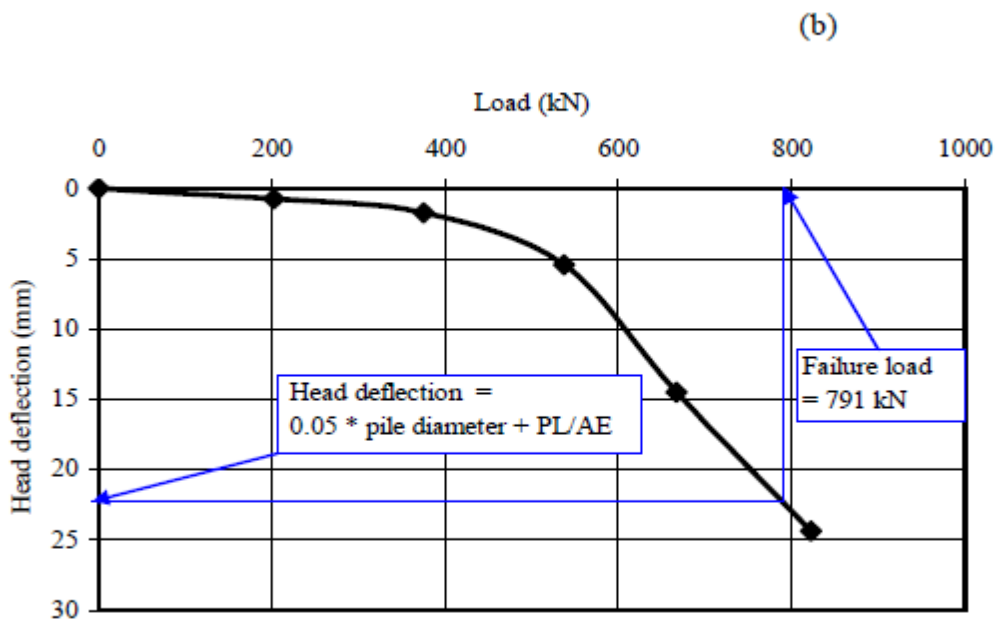
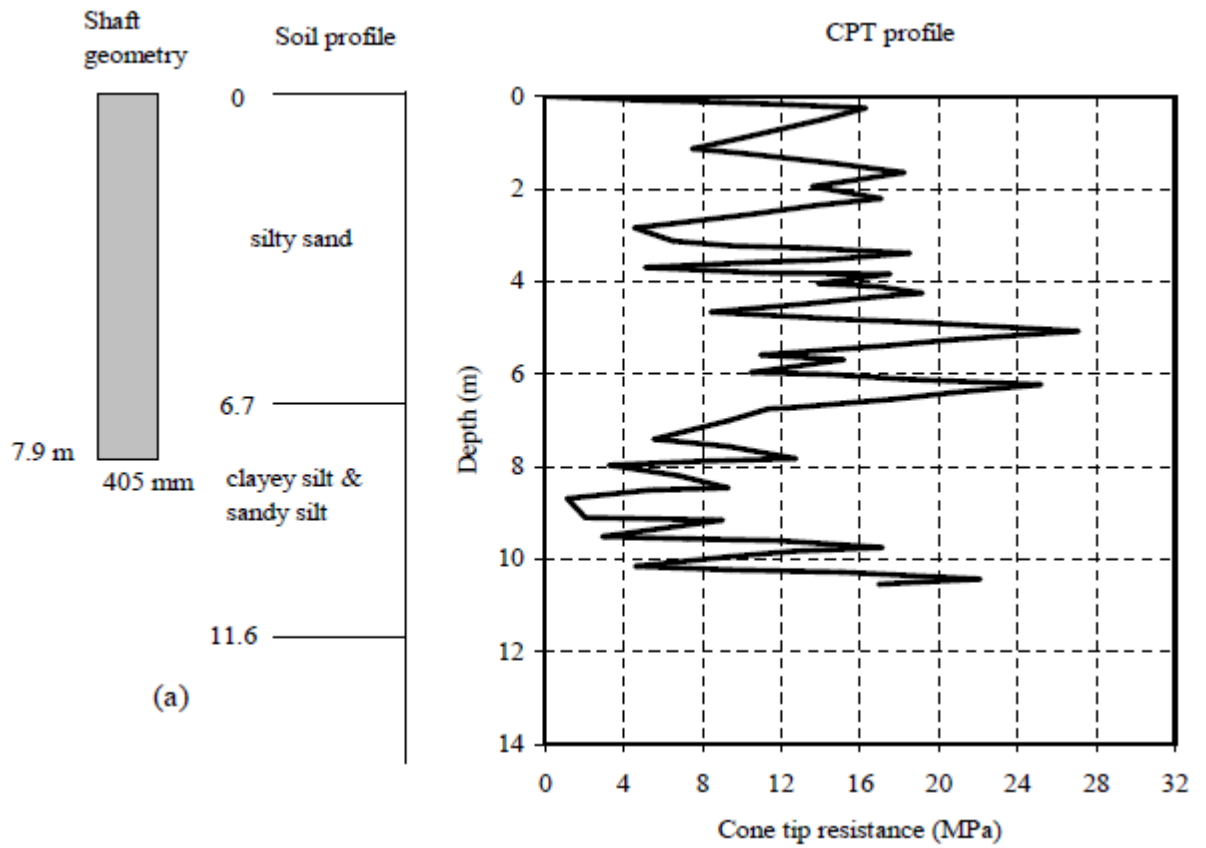


Figure A-38 Summary sheet for case record 38, (a) pile geometry and soil profile, (b) cone tip resistance profile, (c) load deflection plot

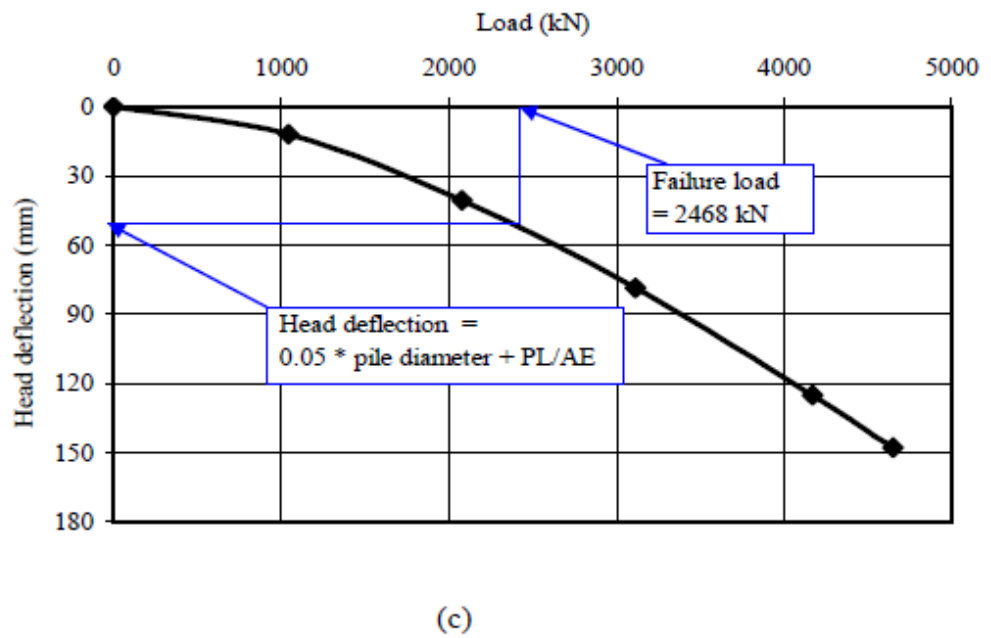
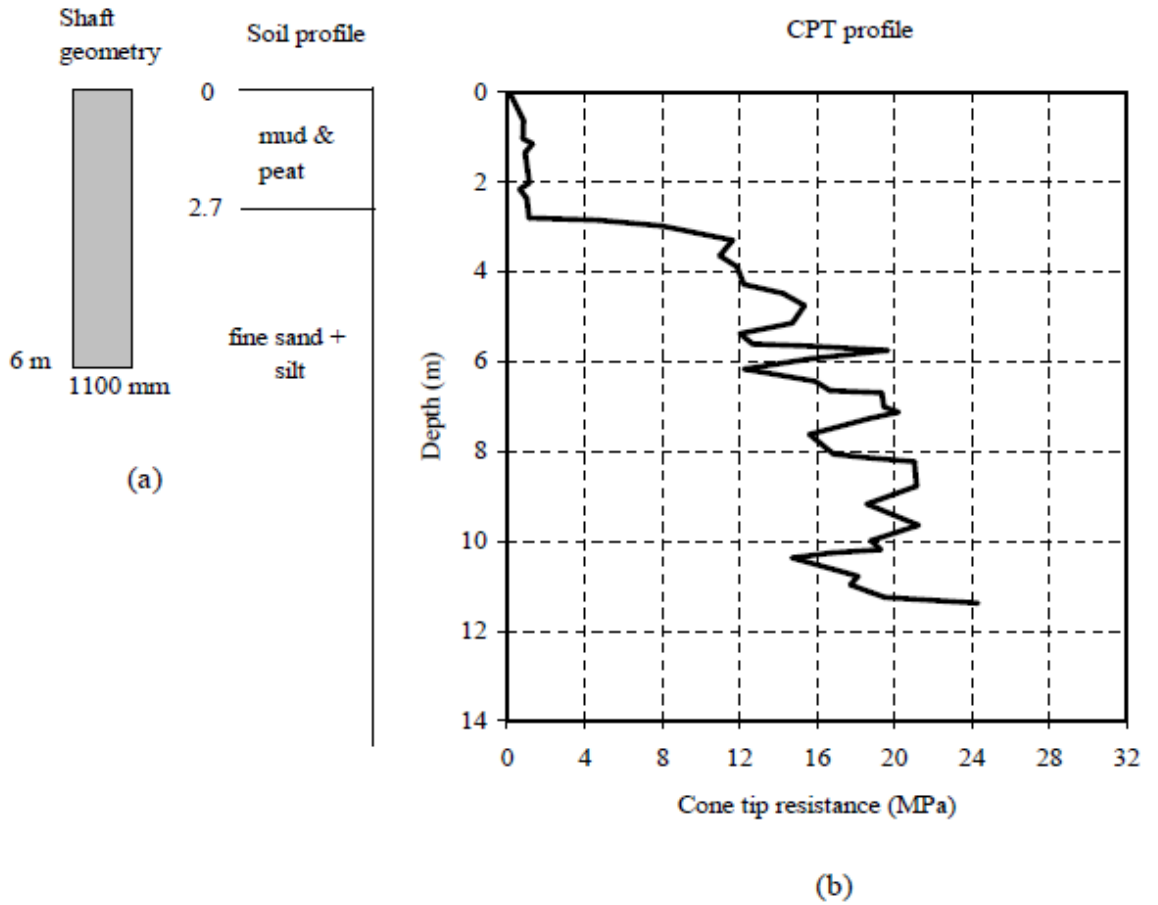


Figure A-39 Summary sheet for case record 39, (a) pile geometry and soil profile, (b) cone tip resistance profile, (c) load deflection plot

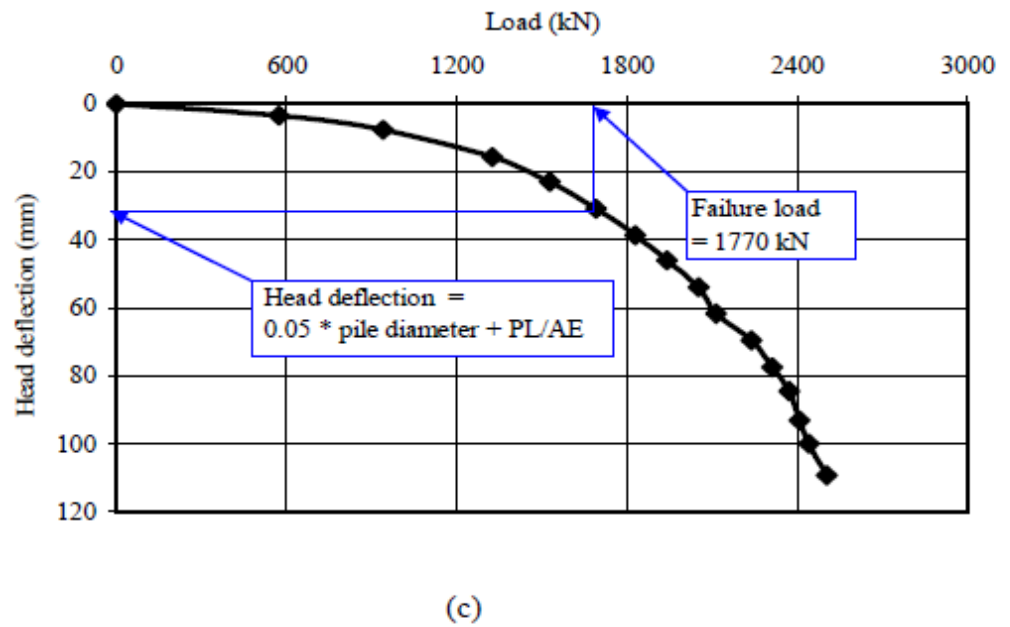
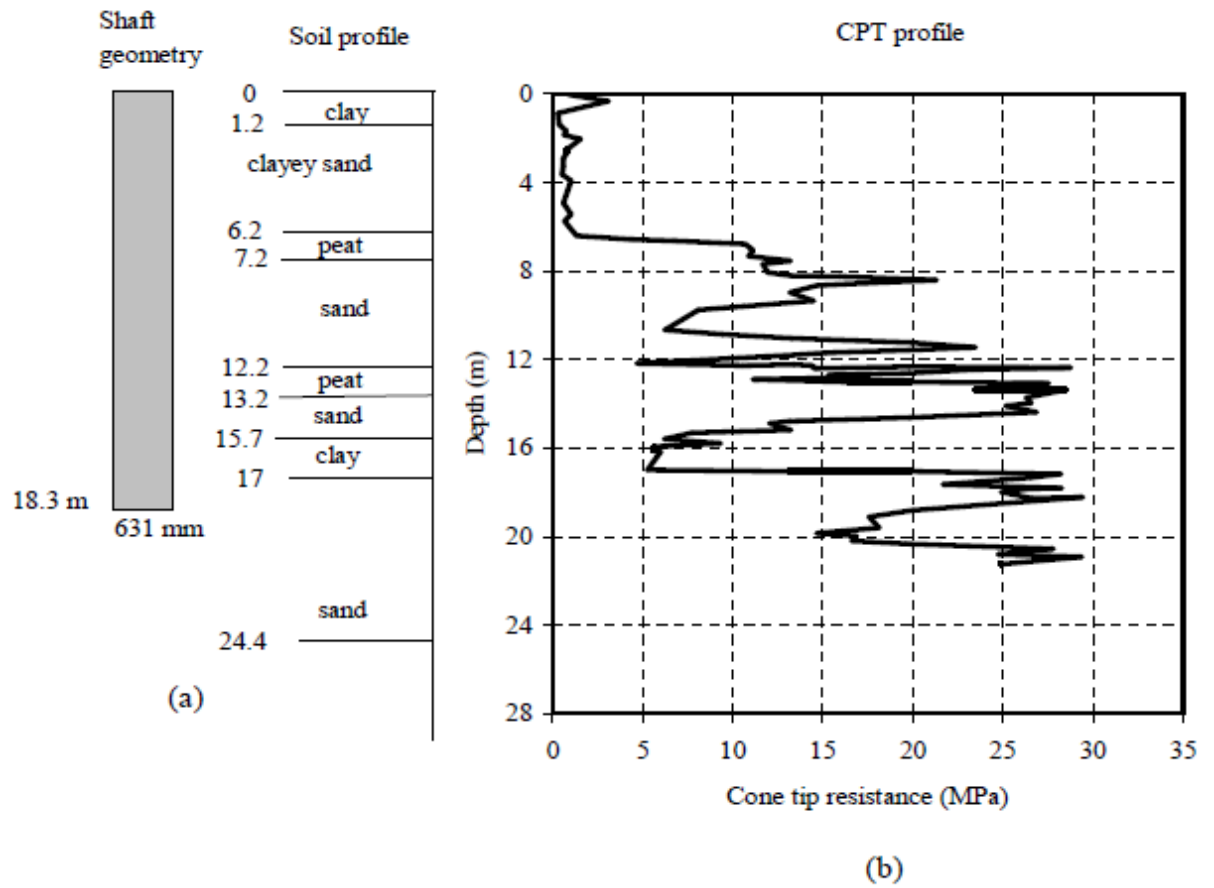


Figure A-40 Summary sheet for case record 40, (a) pile geometry and soil profile, (b) cone tip resistance profile, (c) load deflection plot

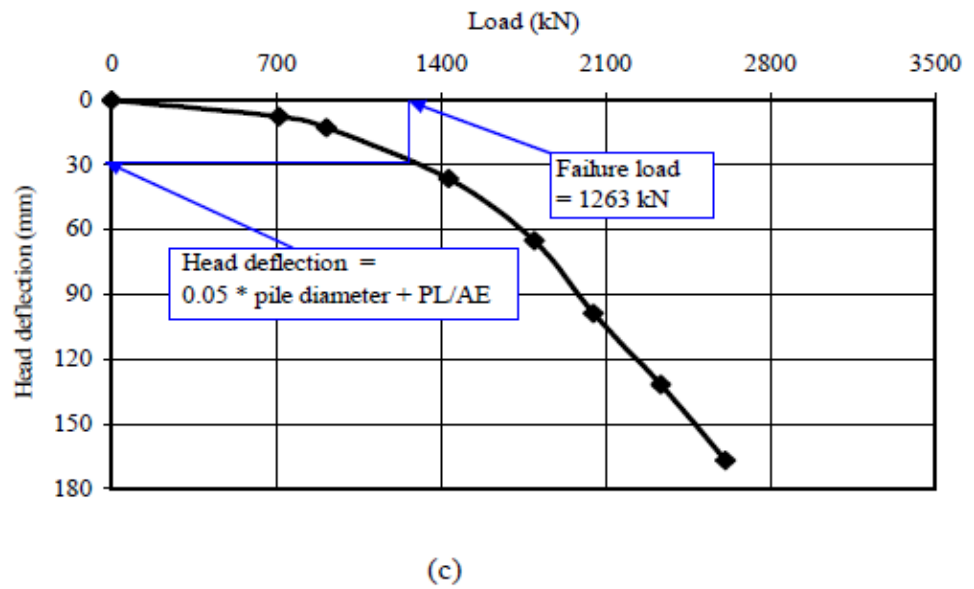
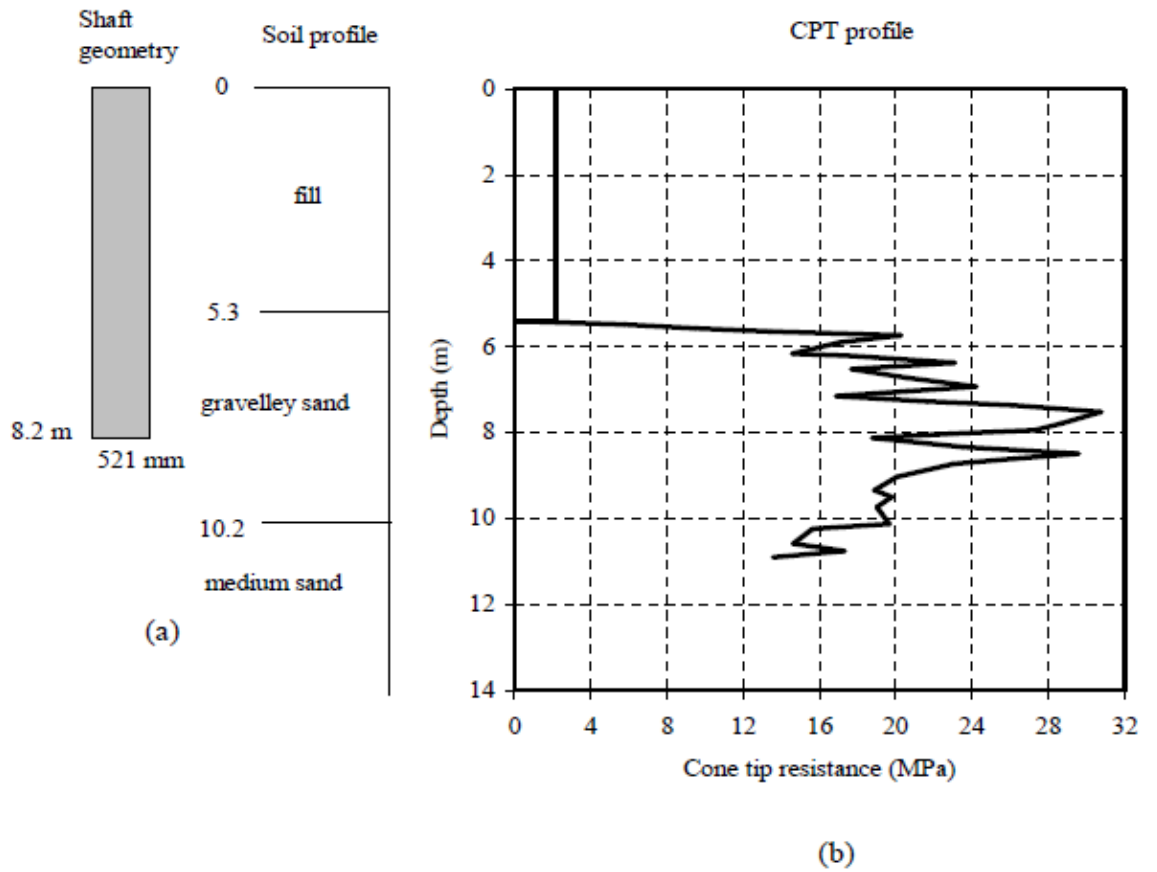


Figure A-41 Summary sheet for case record 41, (a) pile geometry and soil profile, (b) cone tip resistance profile, (c) load deflection plot

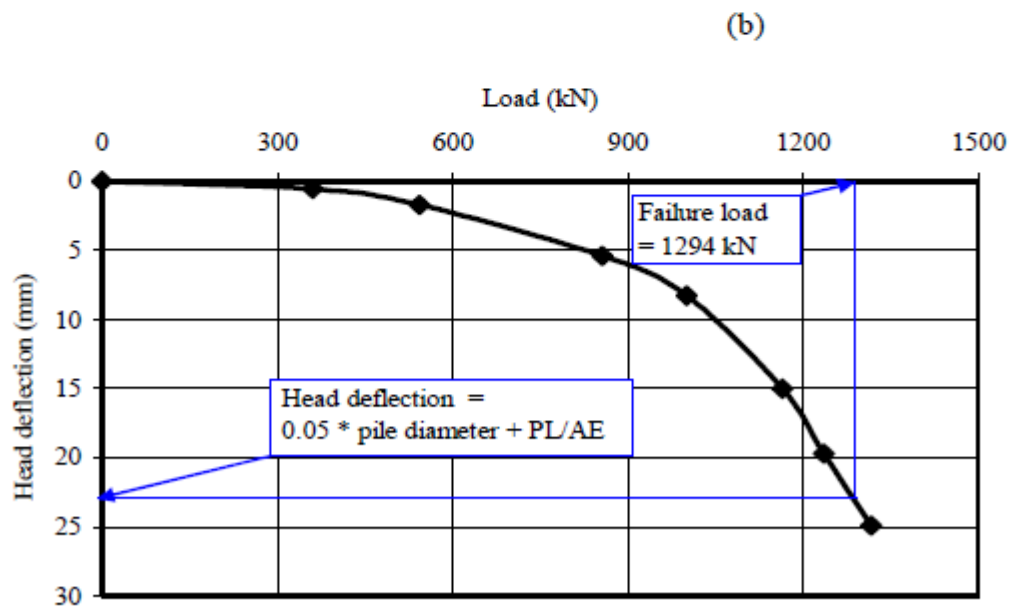
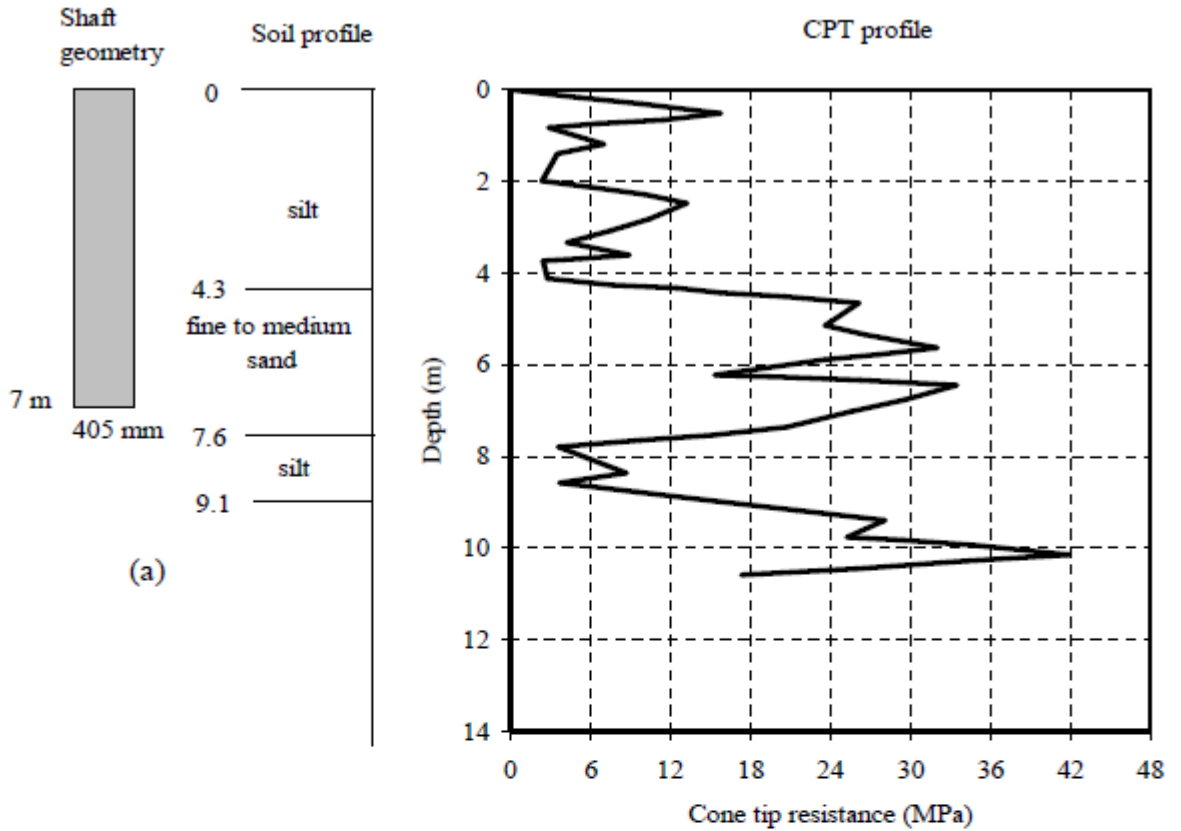


Figure A-42 Summary sheet for case record 42, (a) pile geometry and soil profile, (b) cone tip resistance profile, (c) load deflection plot

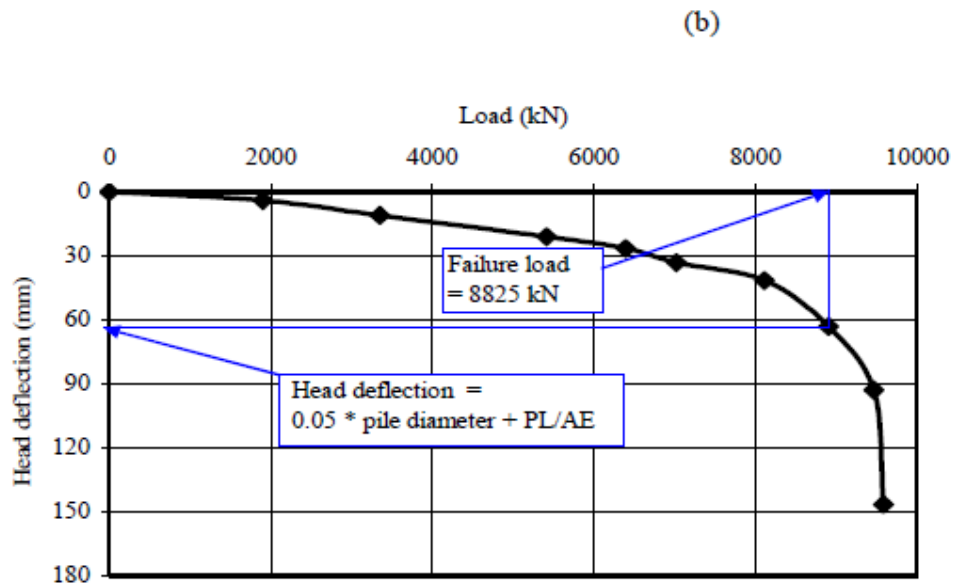
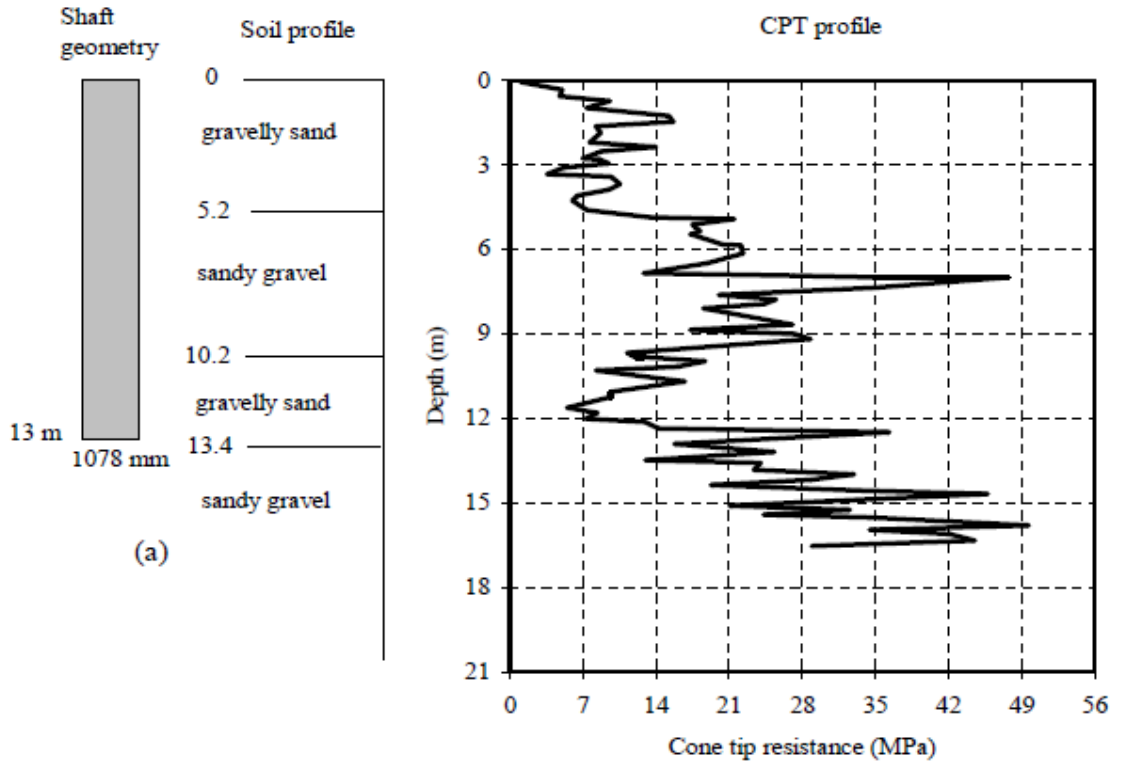


Figure A-43 Summary sheet for case record 43, (a) pile geometry and soil profile, (b) cone tip resistance profile, (c) load deflection plot

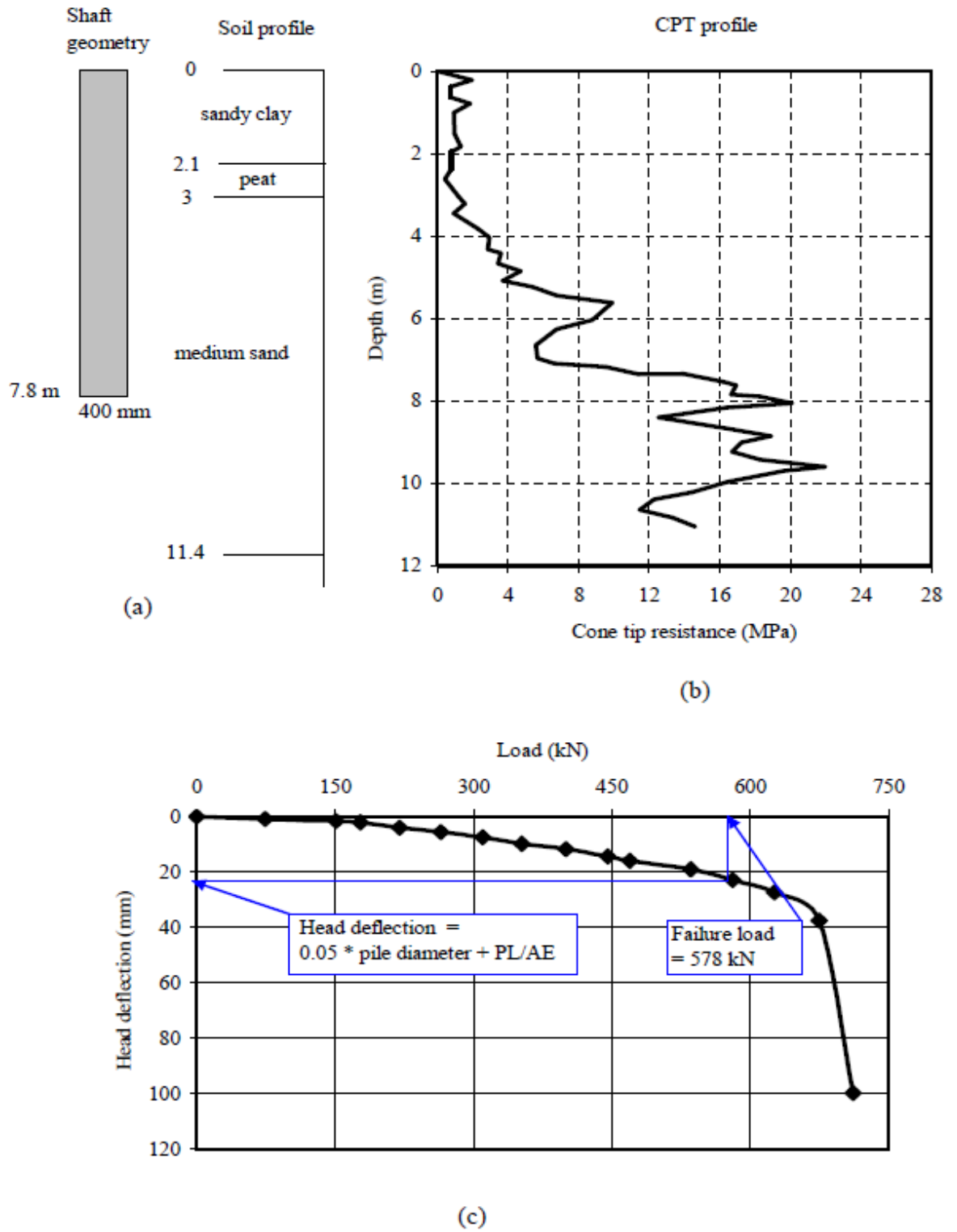


Figure A-44 Summary sheet for case record 44, (a) pile geometry and soil profile, (b) cone tip resistance profile, (c) load deflection plot

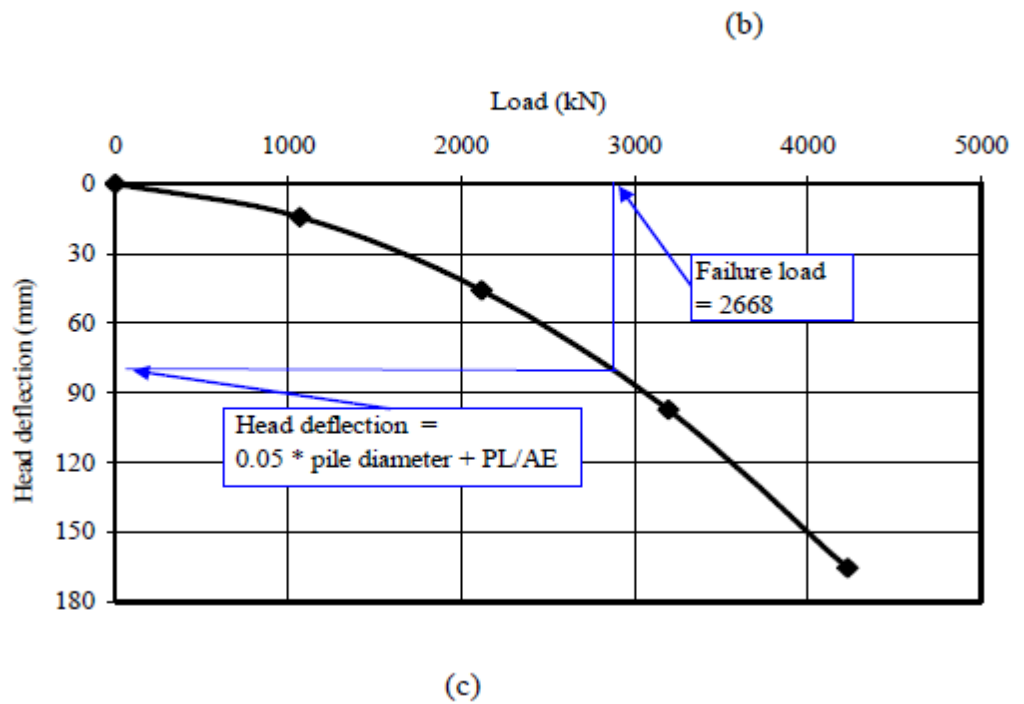
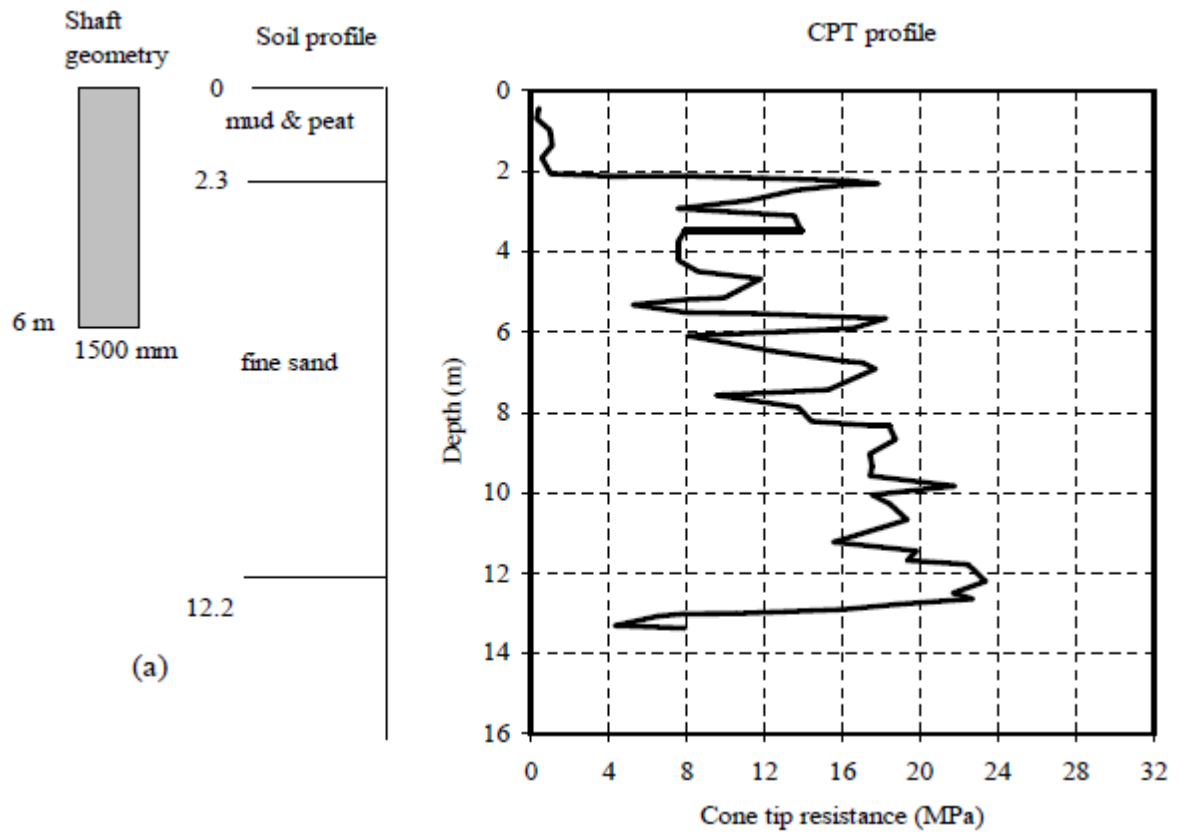


Figure A-45 Summary sheet for case record 45, (a) pile geometry and soil profile, (b) cone tip resistance profile, (c) load deflection plot

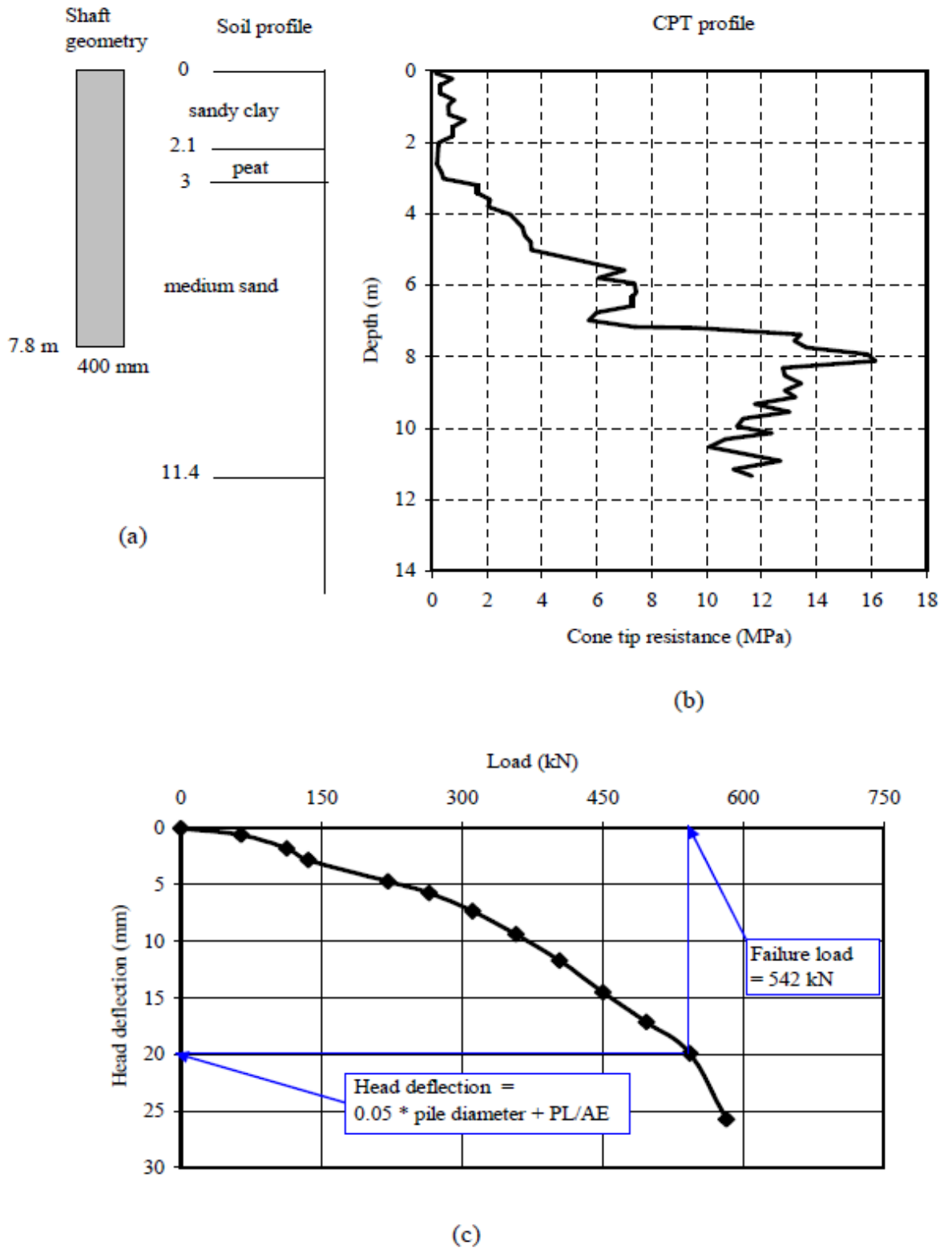


Figure A-46 Summary sheet for case record 46, (a) pile geometry and soil profile, (b) cone tip resistance profile, (c) load deflection plot

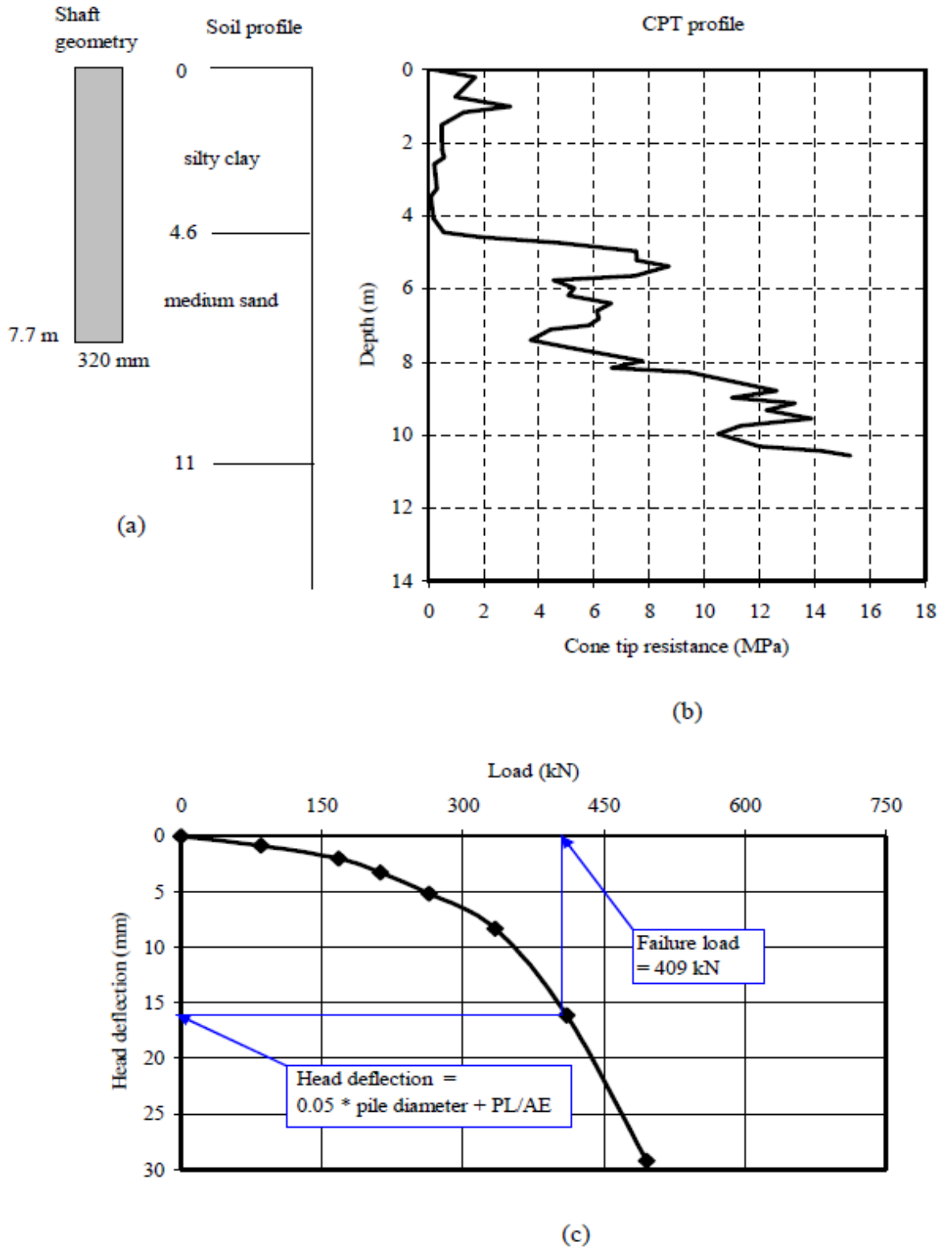


Figure A-47 Summary sheet for case record 47, (a) pile geometry and soil profile, (b) cone tip resistance profile, (c) load deflection plot

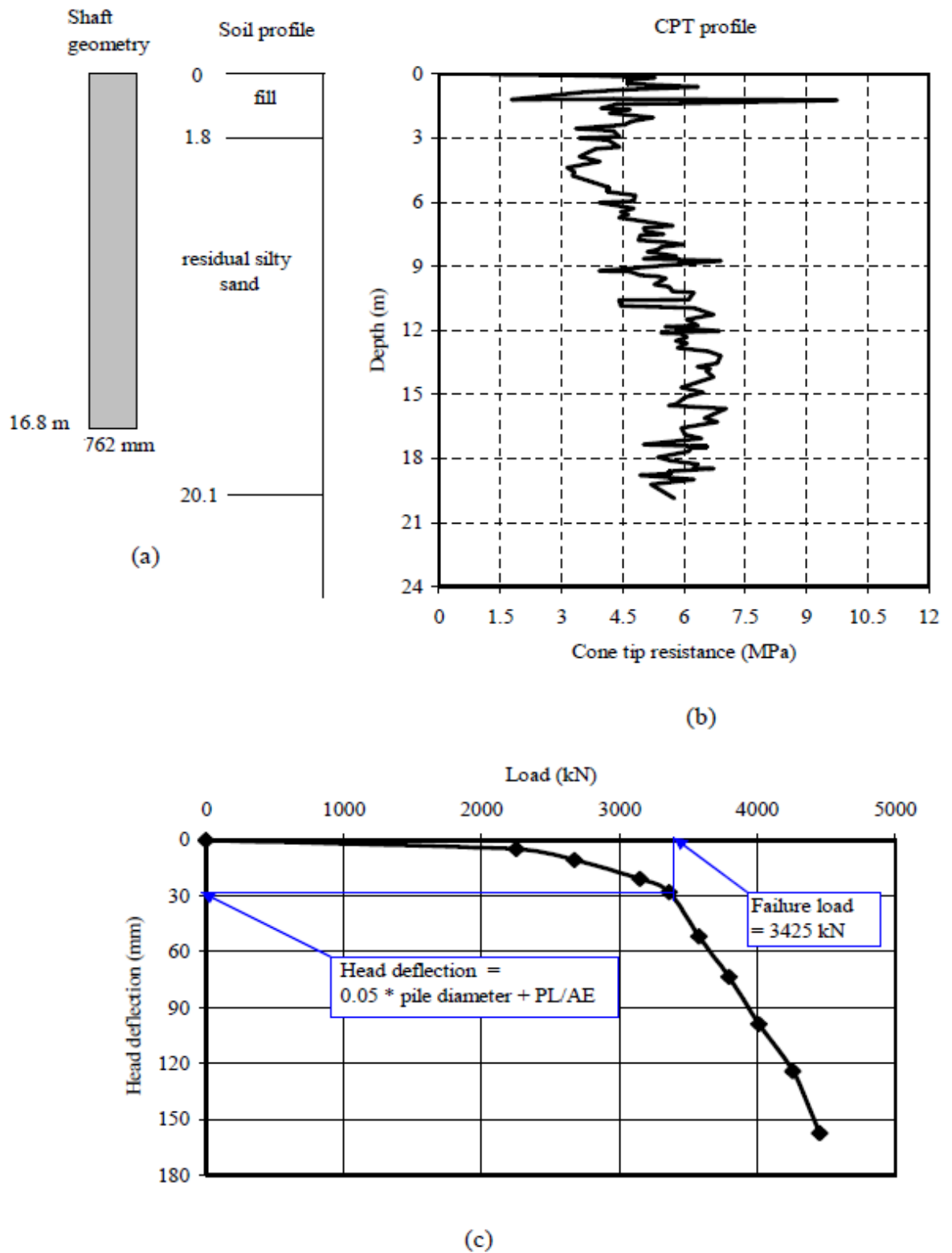


Figure A-48 Summary sheet for case record 48, (a) pile geometry and soil profile, (b) cone tip resistance profile, (c) load deflection plot

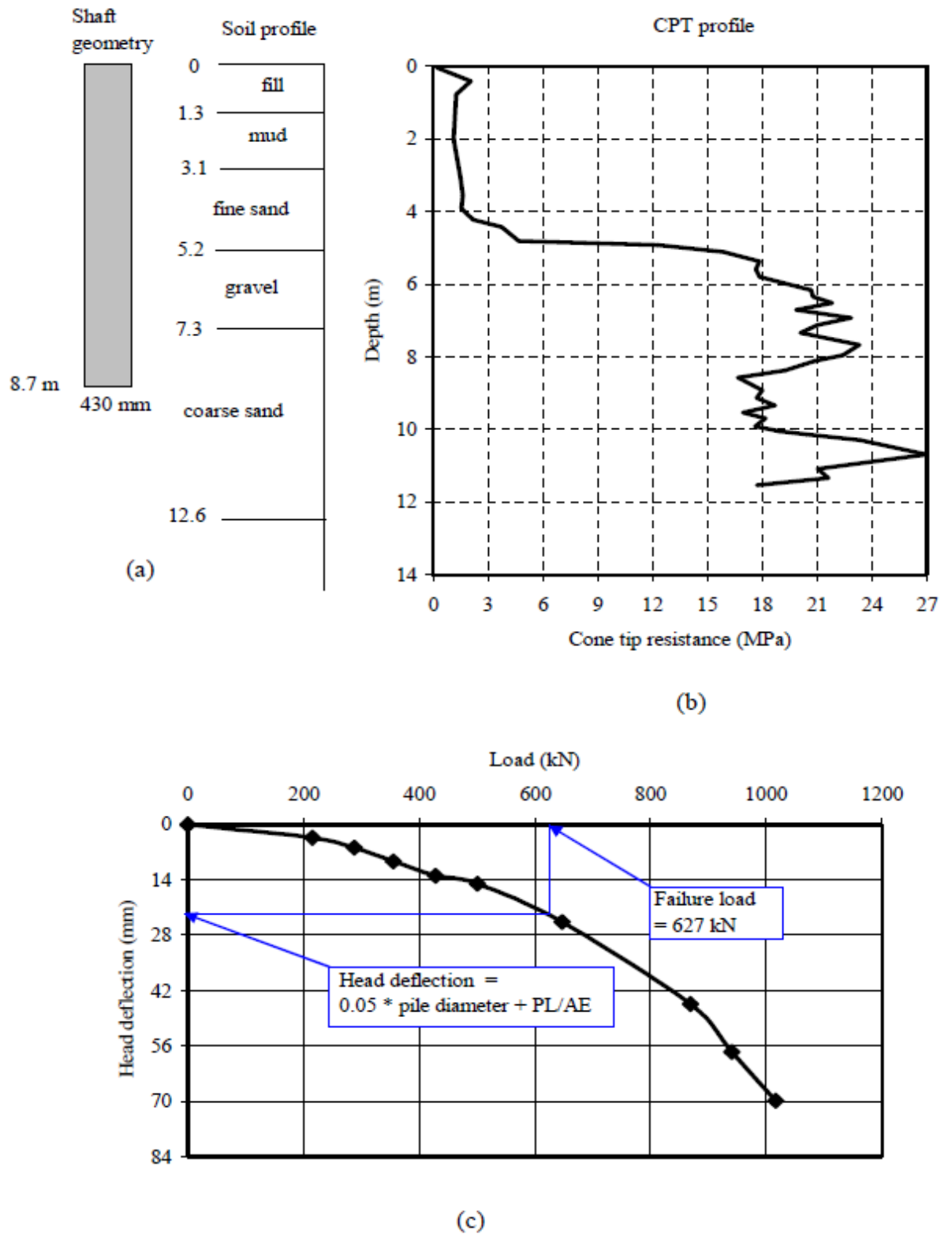


Figure A-49 Summary sheet for case record 49, (a) pile geometry and soil profile, (b) cone tip resistance profile, (c) load deflection plot

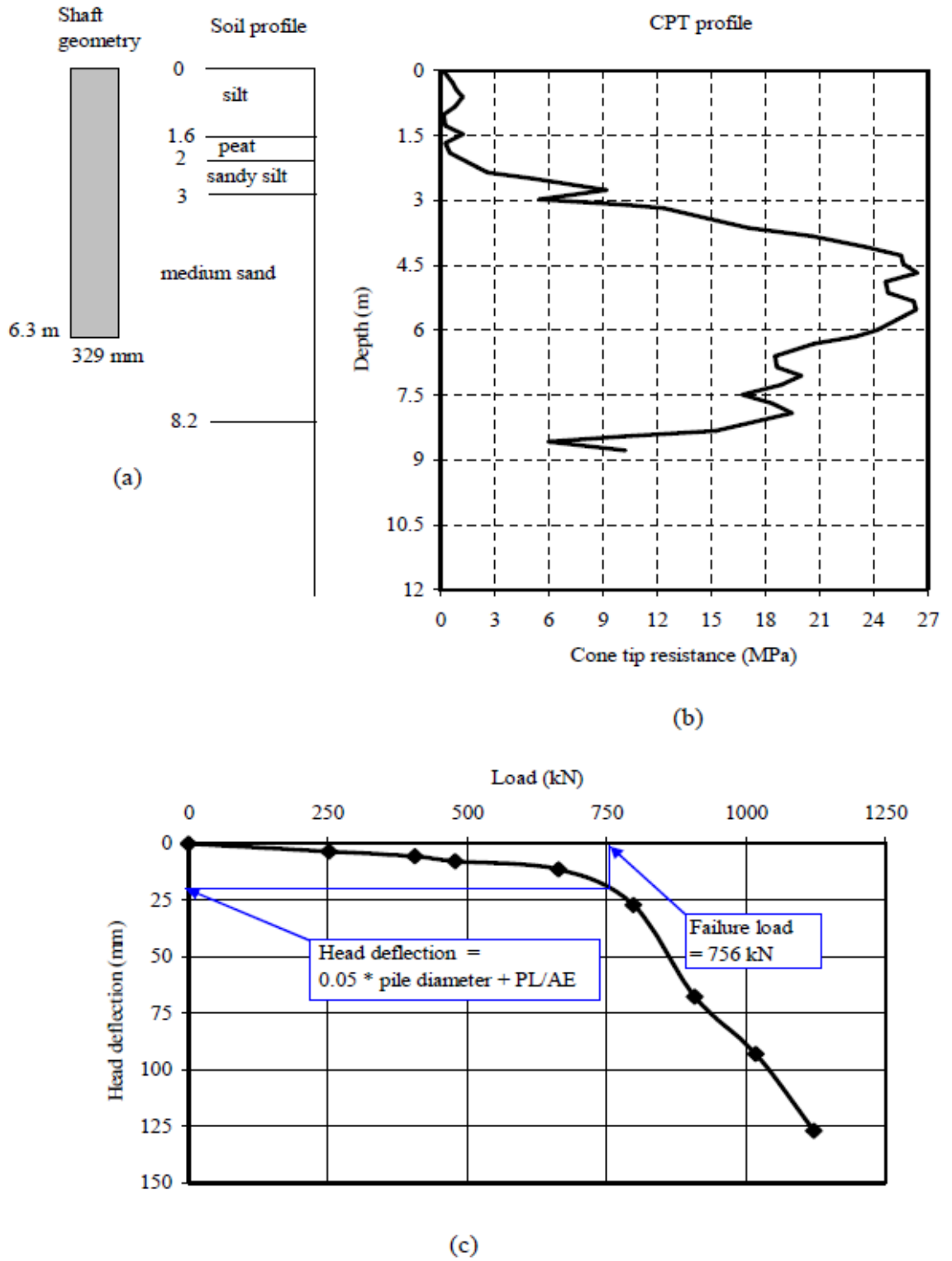


Figure A-50 Summary sheet for case record 50, (a) pile geometry and soil profile, (b) cone tip resistance profile, (c) load deflection plot

Appendix B - Concrete Driven Piles Case Records Summary

Piles group	Case record number	Reference	Case number at the reference	Shape	Tip, closed or open	A_c (m ²)	A_{cir} (m ² /m)	D or D_{eq} (mm)	L (m)	Type of load test	Type of cone	
Driven piles (concrete)	1	Eslami (1996)	N&SB1-215	****	****	0.049	0.785	250	21.3	****	****	
	2	****	A&M38	****	****	0.16	1.6	400	11.3	****	****	
	3	****	A&M22	****	****	0.203	1.8	450	10.3	****	****	
	4	****	A&M26	****	****	0.123	1.4	350	8.6	****	****	
	5	****	N&SWPB1	****	****	0.203	1.8	450	8.0	****	****	
	6	****	POLA1	****	****	0.081	1.14	285	15.0	****	****	
	7	****	N&SB1348	****	****	0.202	1.8	450	14.9	****	****	
	8	****	A&M48	****	****	0.16	1.6	400	12.5	****	****	
	9	****	N&SB1316	****	****	0.123	1.4	350	15.9	****	****	
	10	****	N&SJC1	****	****	0.203	1.8	450	9.2	****	****	
	11	****	OKLACO	****	round	closed	0.292	1.92	610	18.2	QML	E
	12	****	A&M47	****	square	****	0.16	1.6	400	11.2	SML	M
	13	****	NETH2	****	****	****	0.83	1.0	250	9.3	****	****
	14	****	A&M49	****	****	****	0.16	1.6	400	12.5	SML	****
	15	****	BGHD1	****	****	****	0.081	1.14	285	11.0	****	****
	16	****	A&M1	****	****	****	0.16	1.6	400	8.8	****	****
	17	****	A&N3	****	round	****	0.292	1.92	355	10.2	QML	E

Table B-1 Concrete driven piles case records summary

A_c = cross section area, A_{cir} = unit circumferential area; D = diameter; D_{eq} = equivalent diameter; L = embedment length; SML = slow maintained load test; na = not available; CYC = cyclic load test; QML = quick maintained load test; CRP = constant rate of penetration; IE = incremental equilibrium; M = Mechanical; E = Electrical

Piles group	Case record number	Reference	Case number at the reference	Shape	Tip, closed or open	A_c (m ²)	A_{cir} (m ² /m)	D or D_{eq} (mm)	L (m)	Type of load test	Type of cone
Driven piles (concrete)	18	Eslami (1996)	A&M46	square	****	0.16	1.6	400	11.4	SML	M
	19	****	UFL53	****	****	0.123	1.4	350	20.4	****	E
	20	****	UFL52	square	****	0.25	2	500	11.0	****	E
	21	****	A&M40	****	****	0.123	1.4	350	16.0	****	M
	22	****	UFL22	****	****	0.096	1.1	350	16.0	****	E
	23	****	POLA1	octagonal	****	0.308	2.02	625	25.8	QML	****
	24	****	A&M30	square	****	0.203	1.8	450	15.0	SML	M
	25	****	A&M24	****	****	0.16	1.6	400	13.4	****	****
	26	****	N&SWPB2	****	****	0.203	1.8	450	11.3	****	****
	27	****	LSUA1	****	****	0.096	1.1	350	9.5	****	E
	28	****	A&N2	****	****	0.203	1.8	500	13.8	****	****

Table B-1 Concrete driven piles case records summary (continued)

A_c = cross section area, A_{cir} = unit circumferential area; D = diameter; D_{eq} = equivalent diameter; L = embedment length; SML = slow maintained load test; na = not available; CYC = cyclic load test; QML = quick maintained load test; CRP = constant rate of penetration; IE = incremental equilibrium; M = Mechanical; E = Electrical

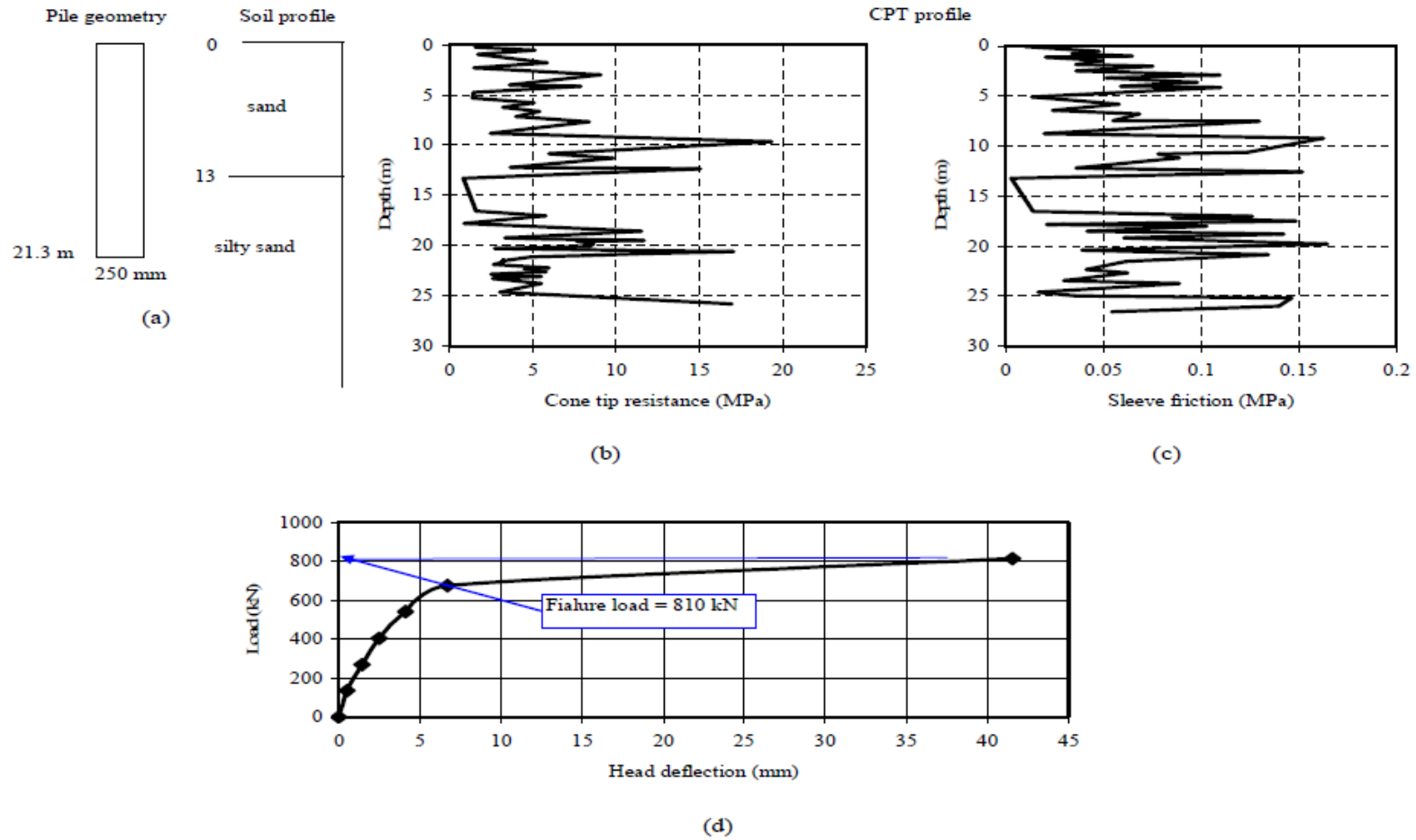


Figure B-1 Summary sheet for case record 1, (a) pile geometry and soil profile, (b) cone tip resistance profile, (c) sleeve friction profile, (d) load deflection plot

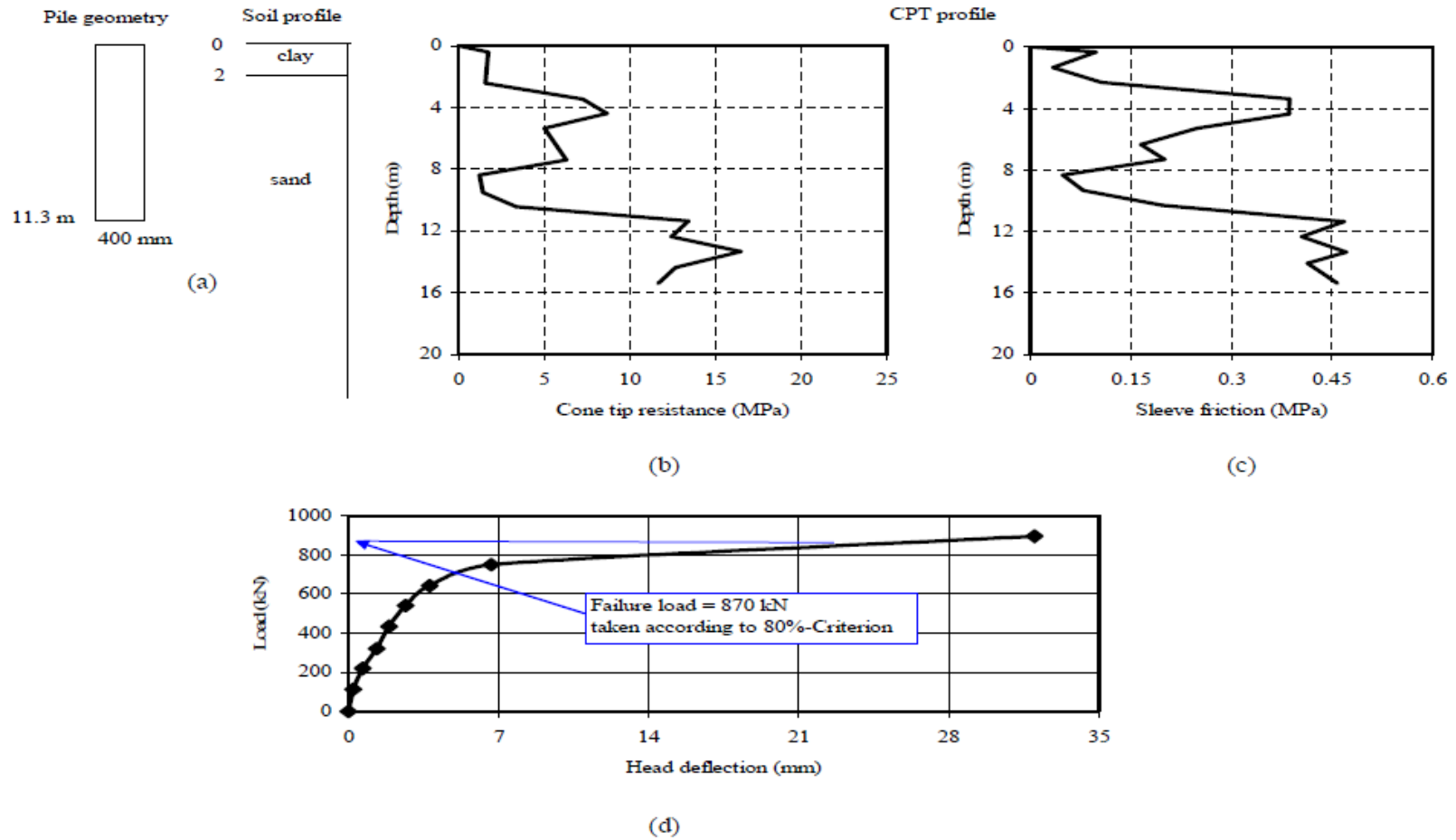


Figure B-2 Summary sheet for case record 2, (a) pile geometry and soil profile, (b) cone tip resistance profile, (c) sleeve friction profile, (d) load deflection plot

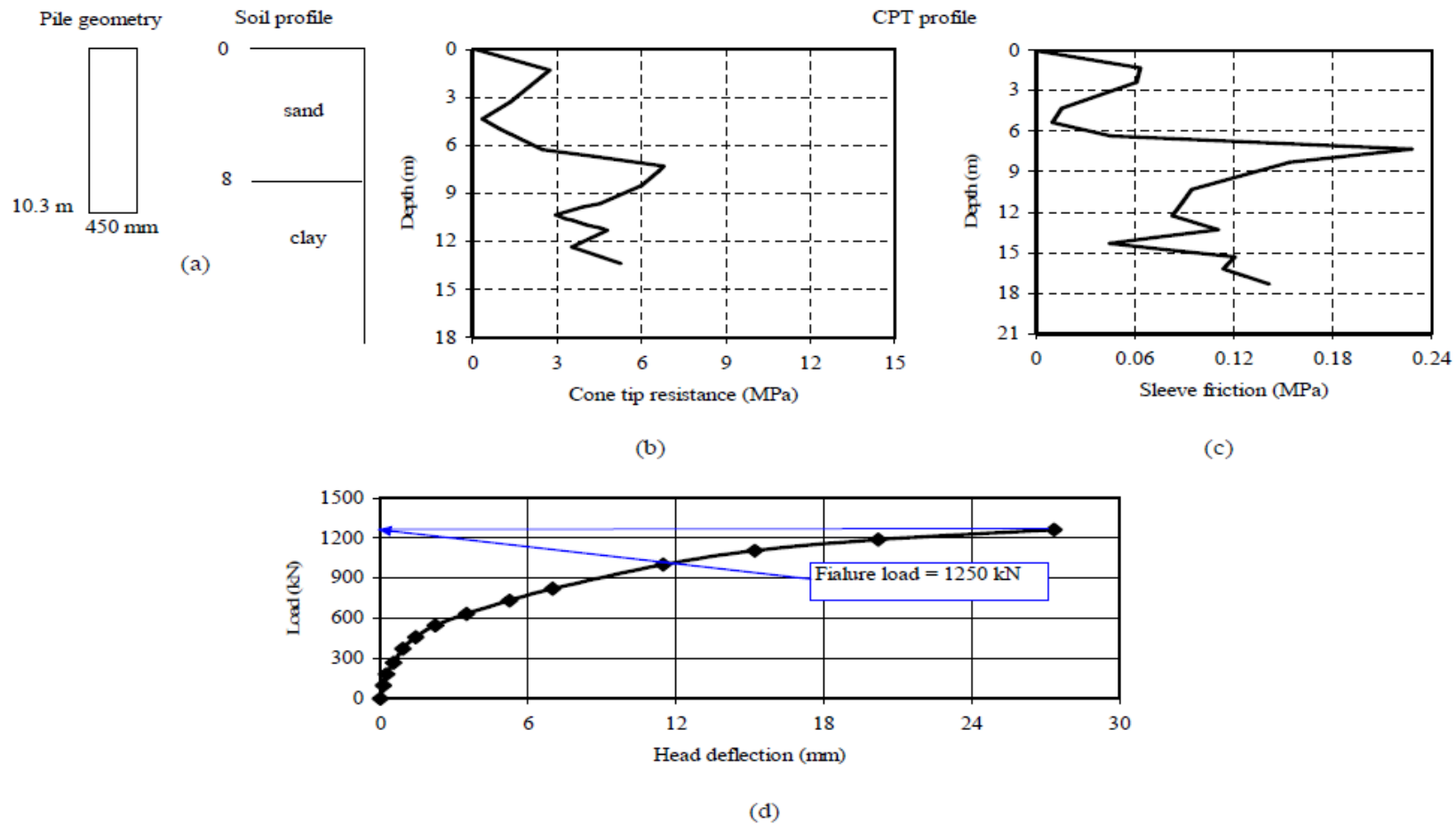


Figure B-3 Summary sheet for case record 3, (a) pile geometry and soil profile, (b) cone tip resistance profile, (c) sleeve friction profile, (d) load deflection plot

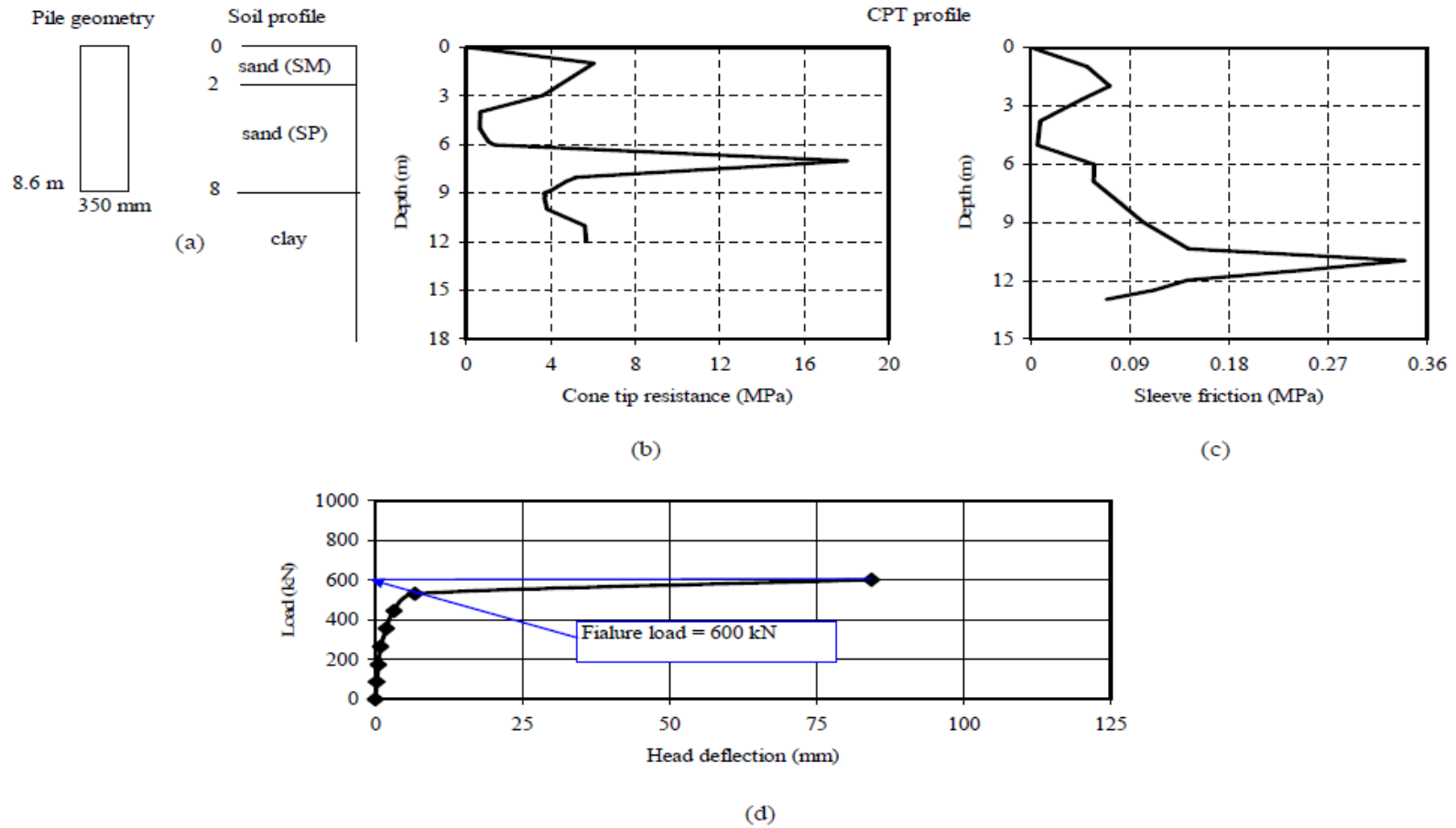


Figure B-4 Summary sheet for case record 4, (a) pile geometry and soil profile, (b) cone tip resistance profile, (c) sleeve friction profile, (d) load deflection plot

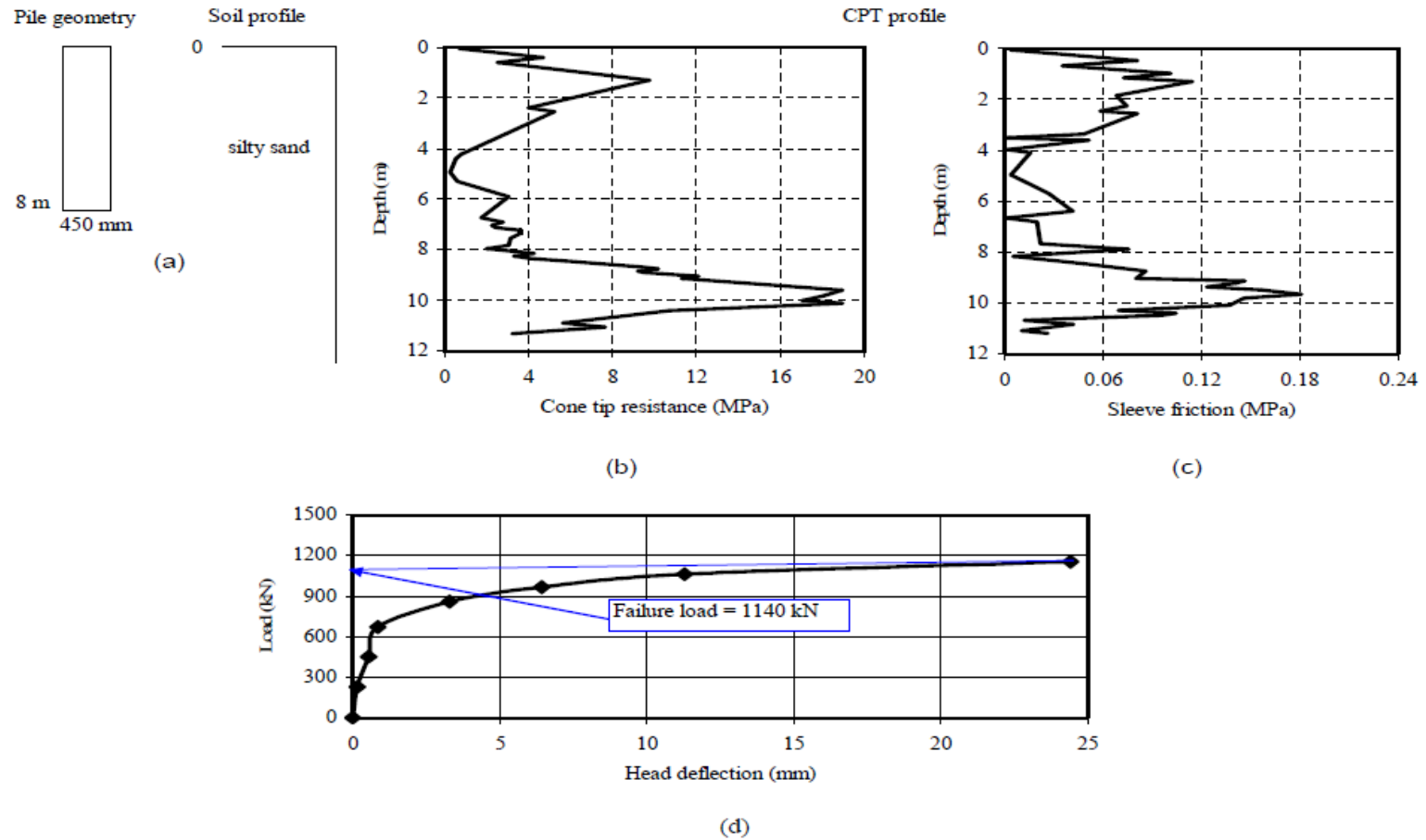


Figure B-5 Summary sheet for case record 5, (a) pile geometry and soil profile, (b) cone tip resistance profile, (c) sleeve friction profile, (d) load deflection plot

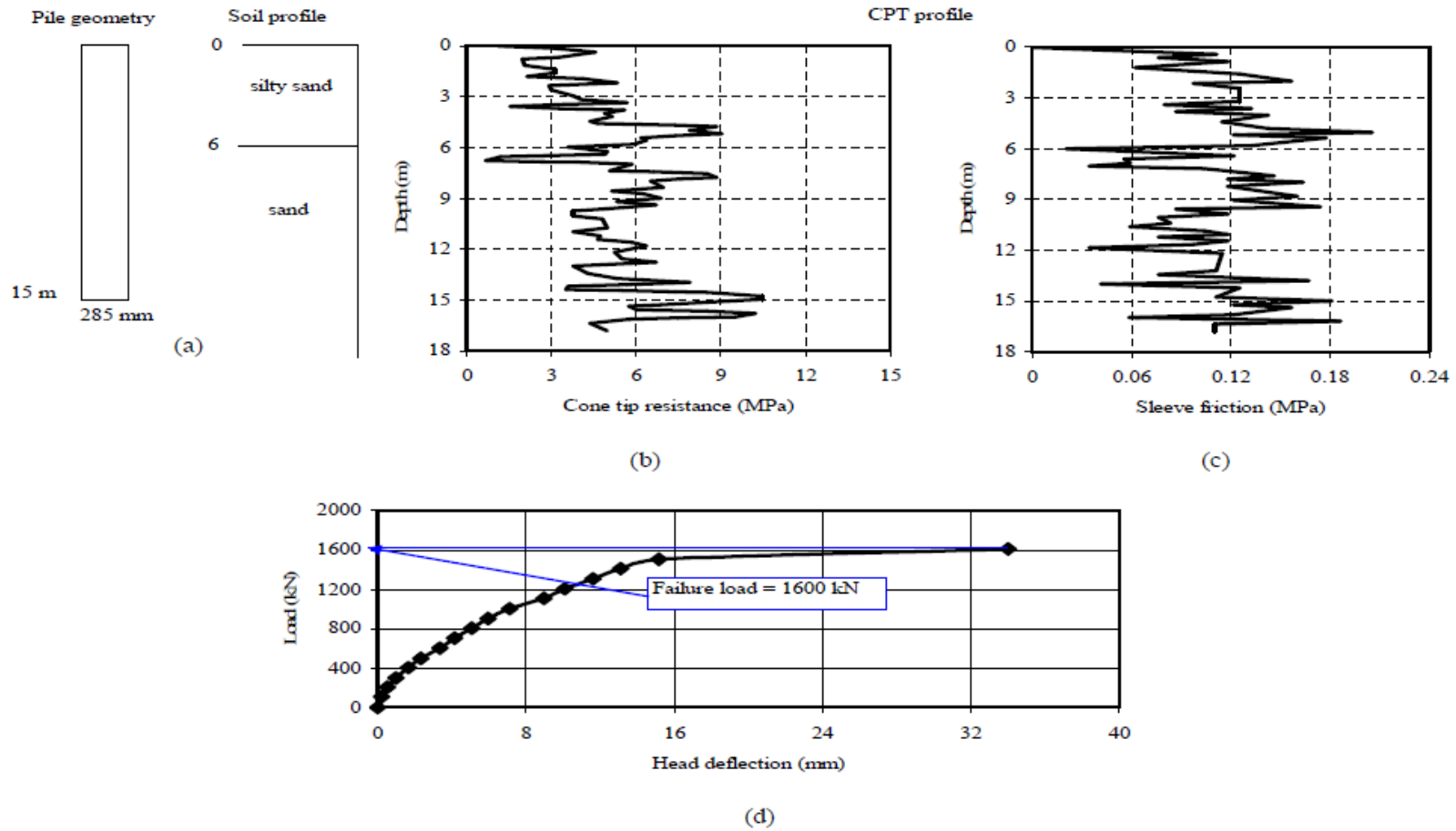


Figure B-6 Summary sheet for case record 6, (a) pile geometry and soil profile, (b) cone tip resistance profile, (c) sleeve friction profile, (d) load deflection plot

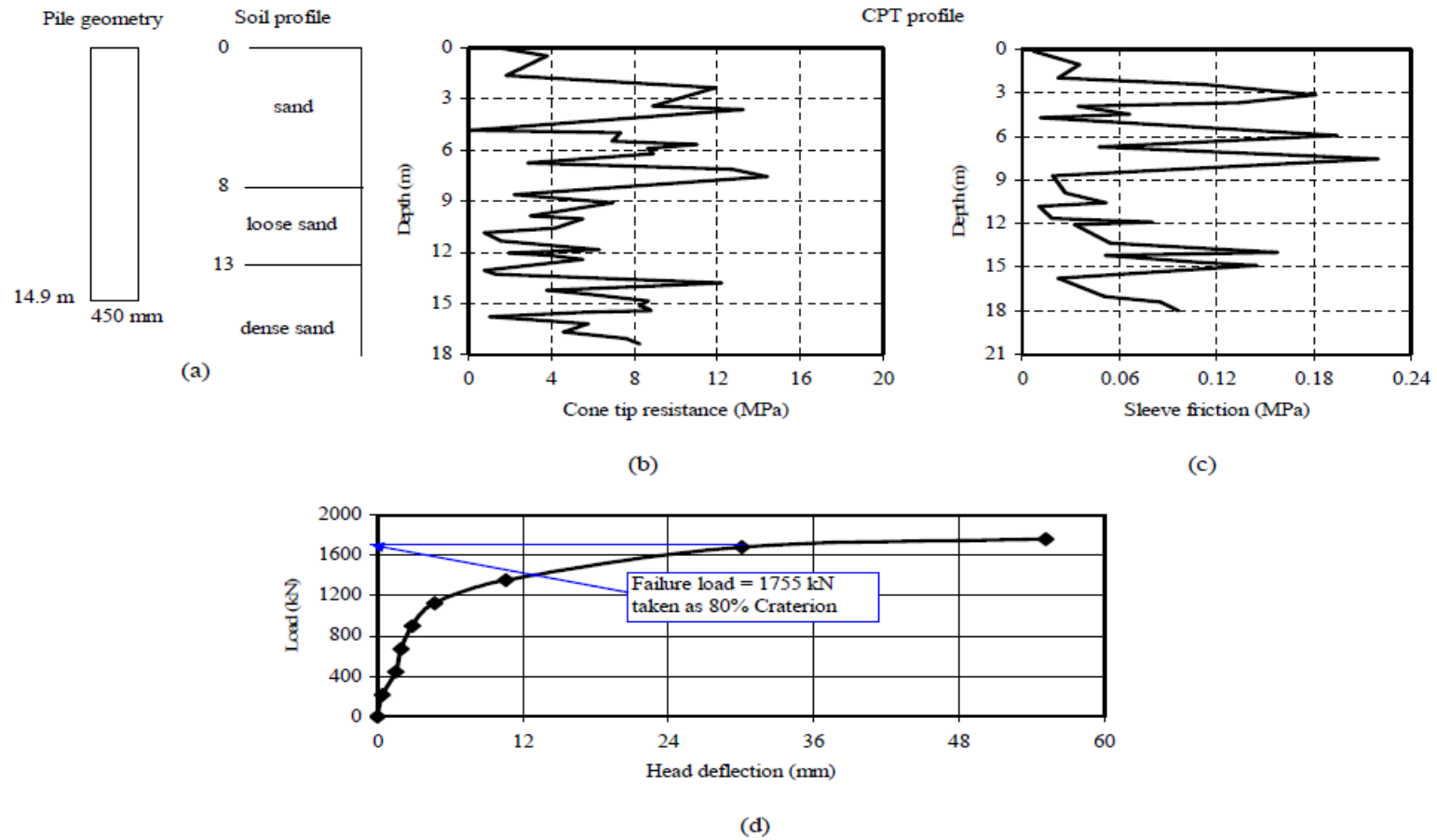


Figure B-7 Summary sheet for case record 7, (a) pile geometry and soil profile, (b) cone tip resistance profile, (c) sleeve friction profile, (d) load deflection plot

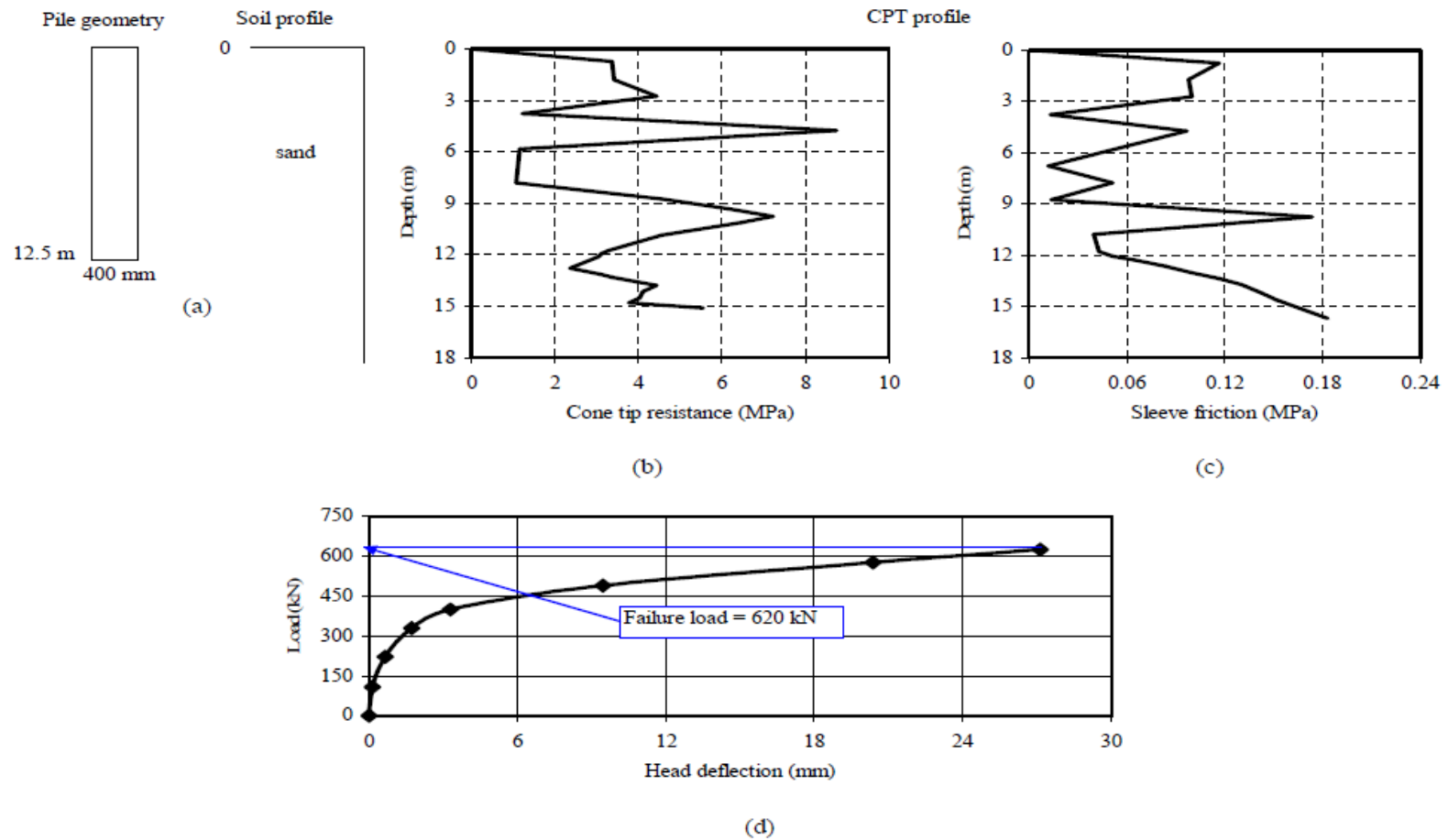


Figure B-8 Summary sheet for case record 8, (a) pile geometry and soil profile, (b) cone tip resistance profile, (c) sleeve friction profile, (d) load deflection plot

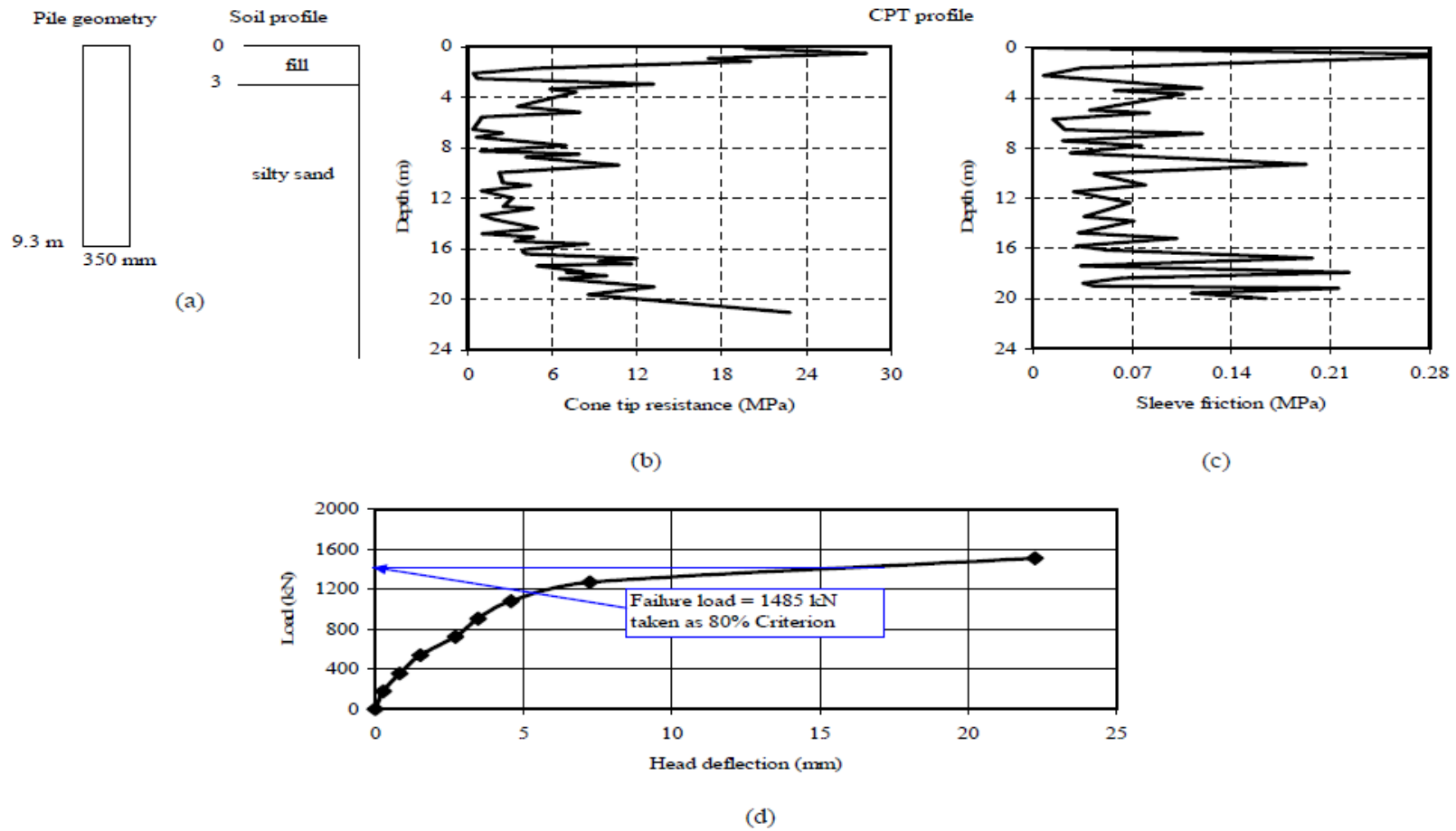


Figure B-9 Summary sheet for case record 9, (a) pile geometry and soil profile, (b) cone tip resistance profile, (c) sleeve friction profile, (d) load deflection plot

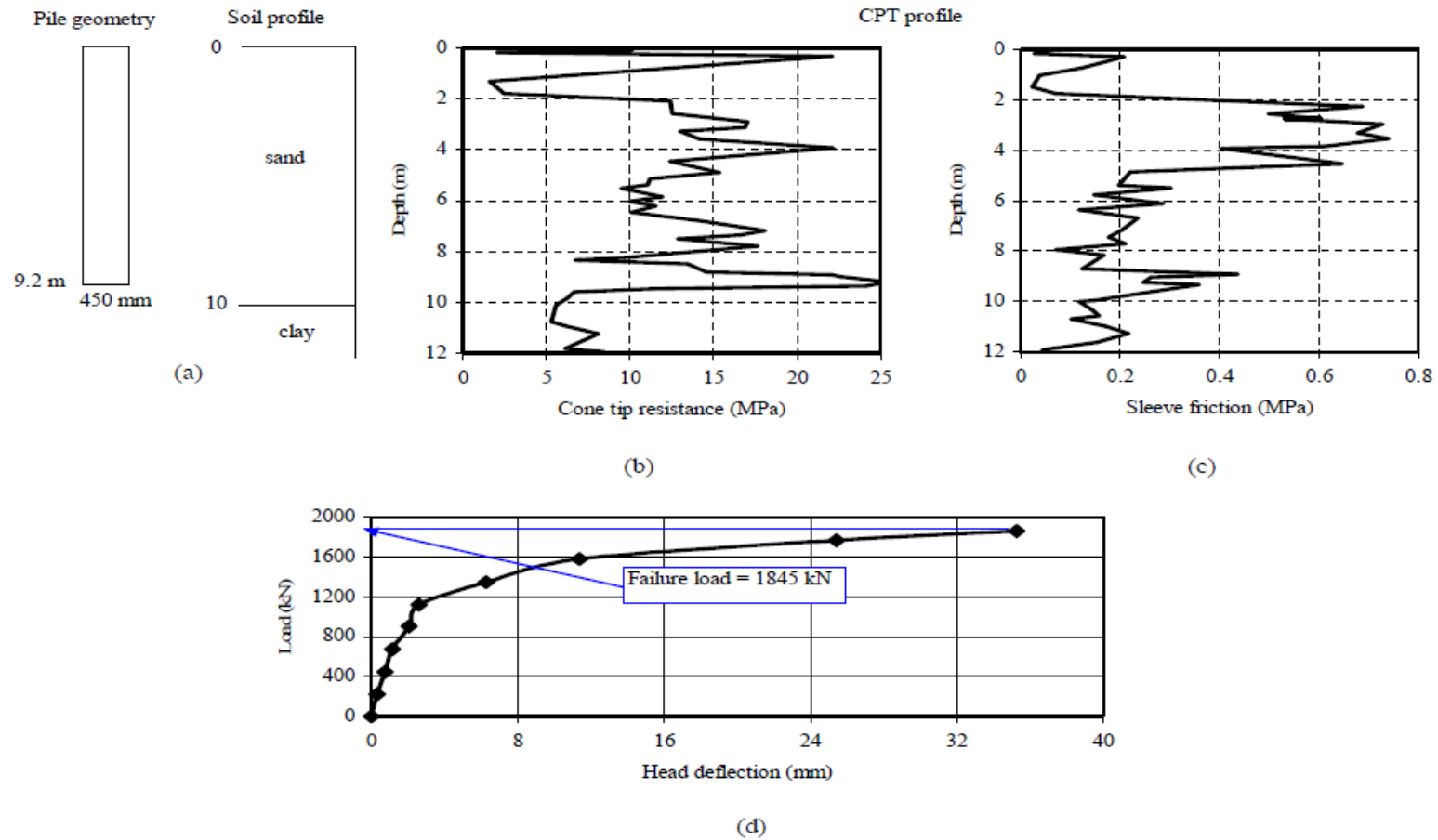


Figure B-10 Summary sheet for case record 10, (a) pile geometry and soil profile, (b) cone tip resistance profile, (c) sleeve friction profile, (d) load deflection plot

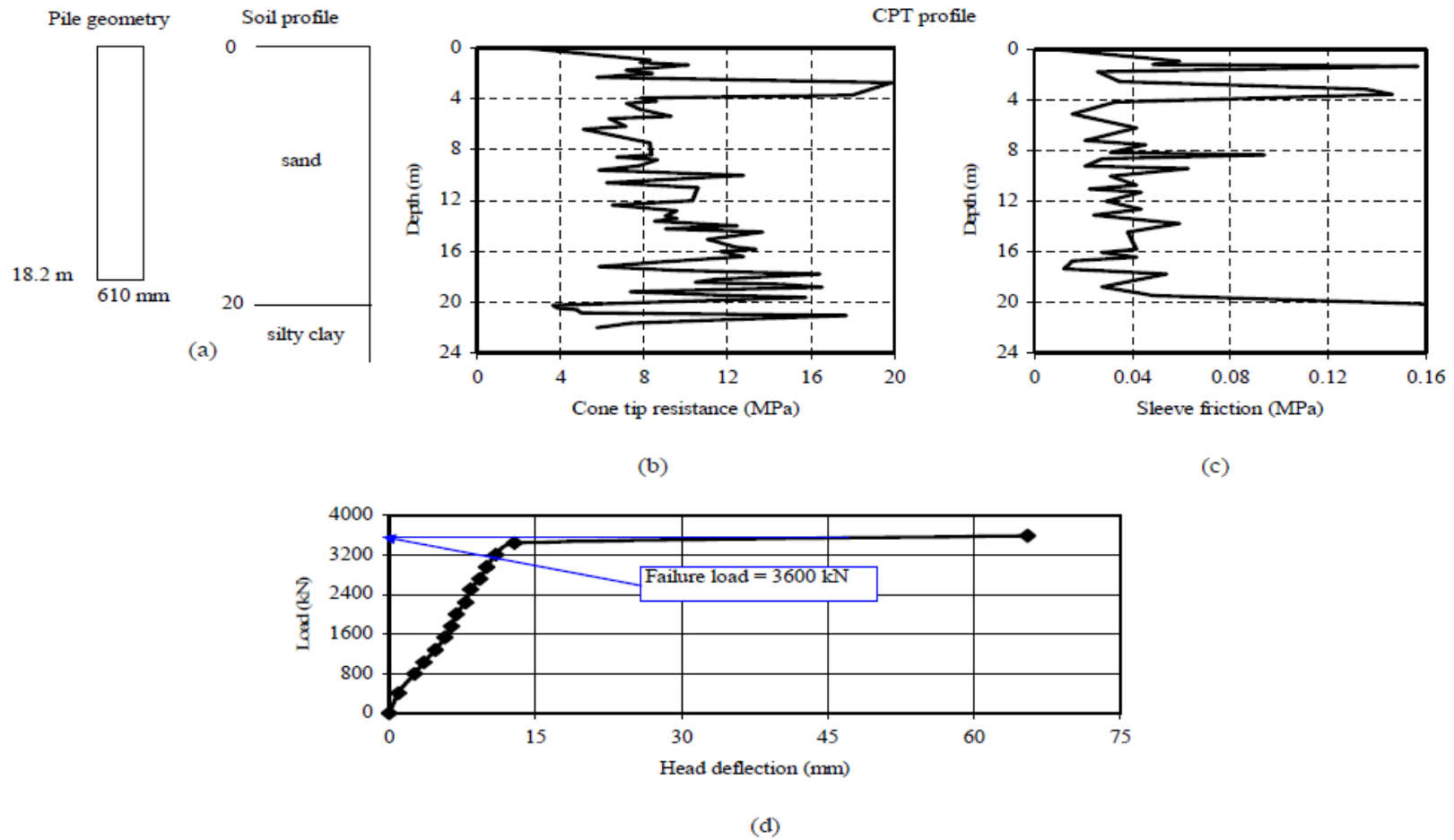


Figure B-11 Summary sheet for case record 11, (a) pile geometry and soil profile, (b) cone tip resistance profile, (c) sleeve friction profile, (d) load deflection plot

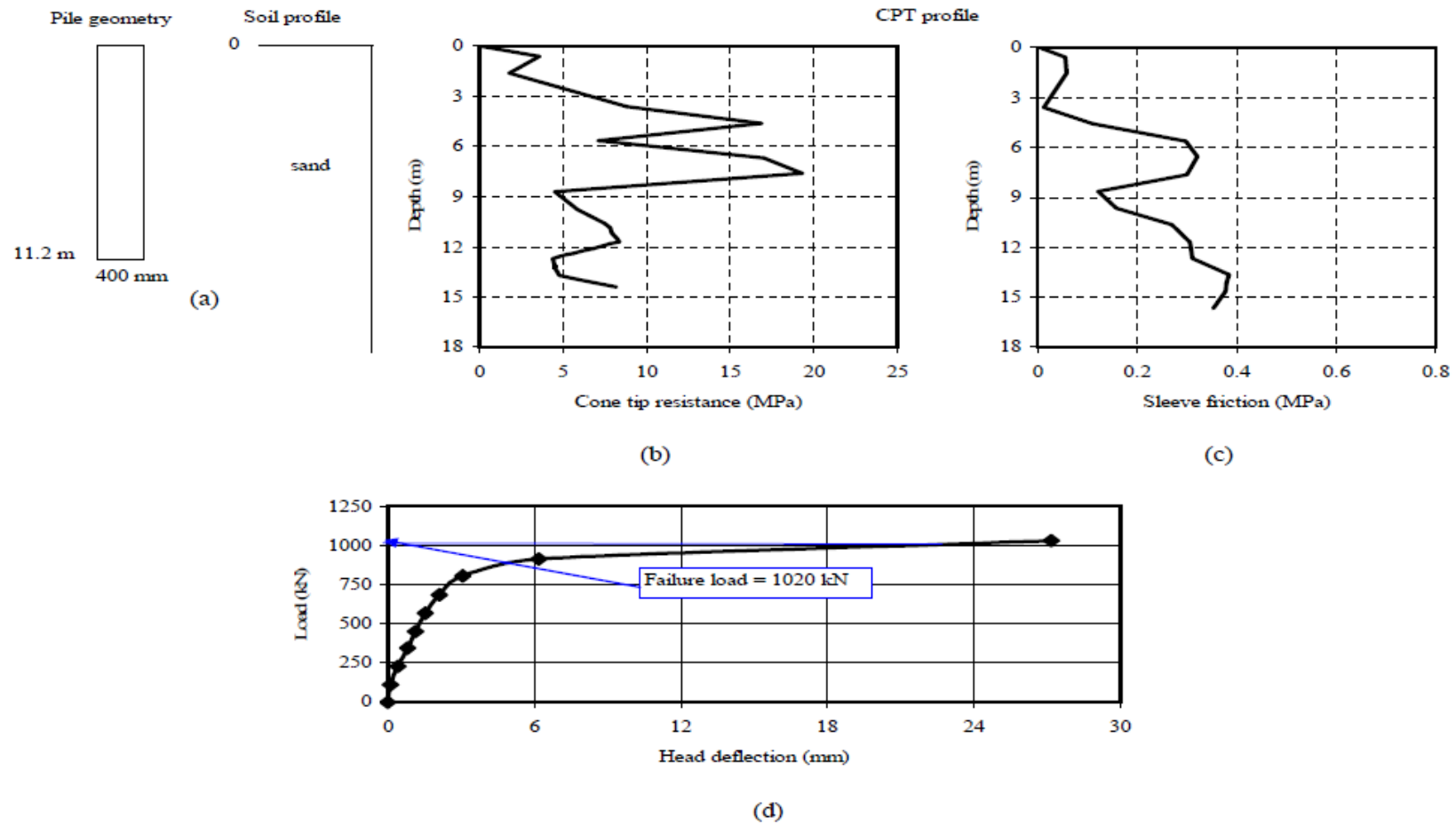


Figure B-12 Summary sheet for case record 12, (a) pile geometry and soil profile, (b) cone tip resistance profile, (c) sleeve friction profile, (d) load deflection plot

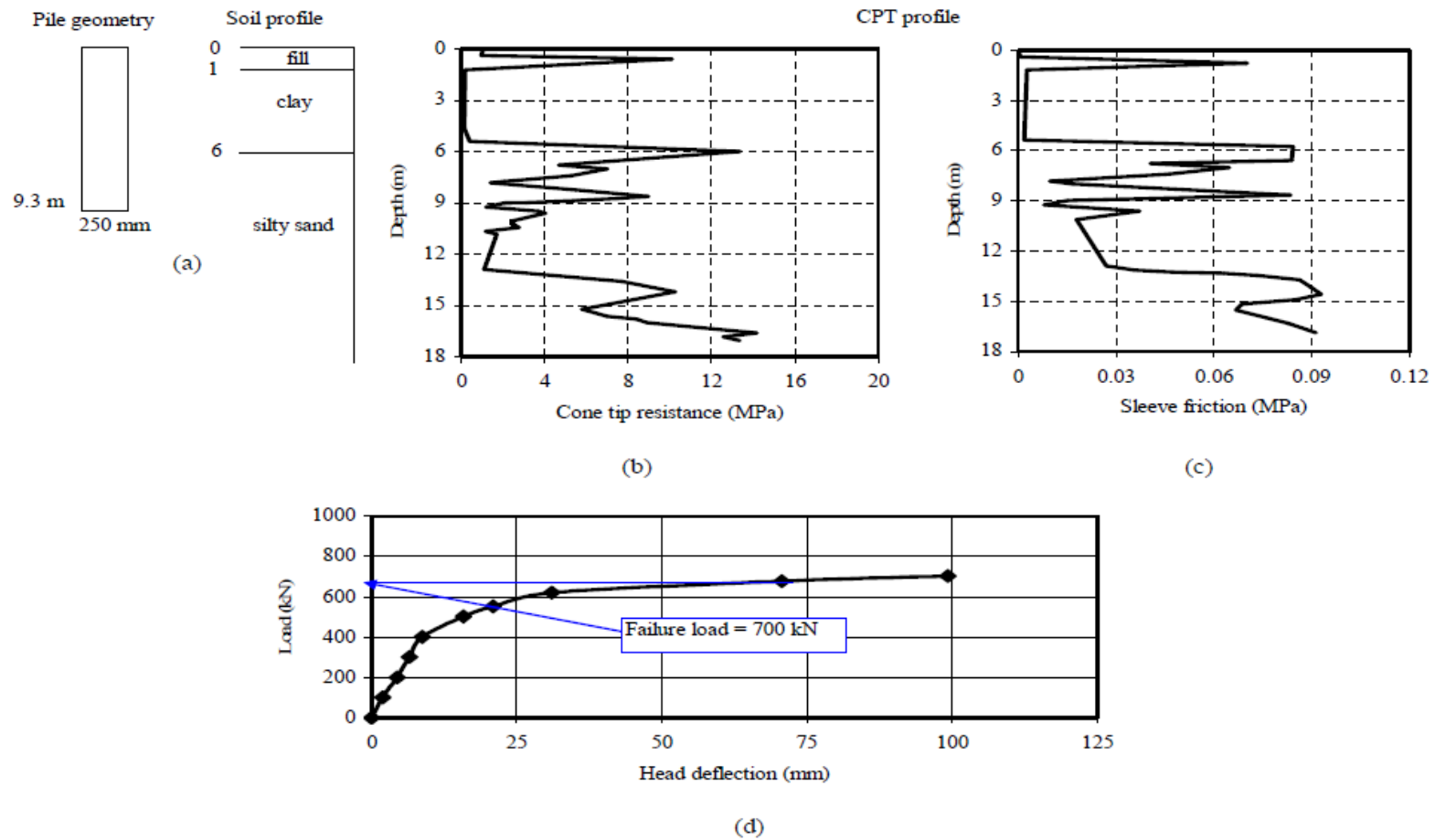


Figure B-13 Summary sheet for case record 13, (a) pile geometry and soil profile, (b) cone tip resistance profile, (c) sleeve friction profile, (d) load deflection plot

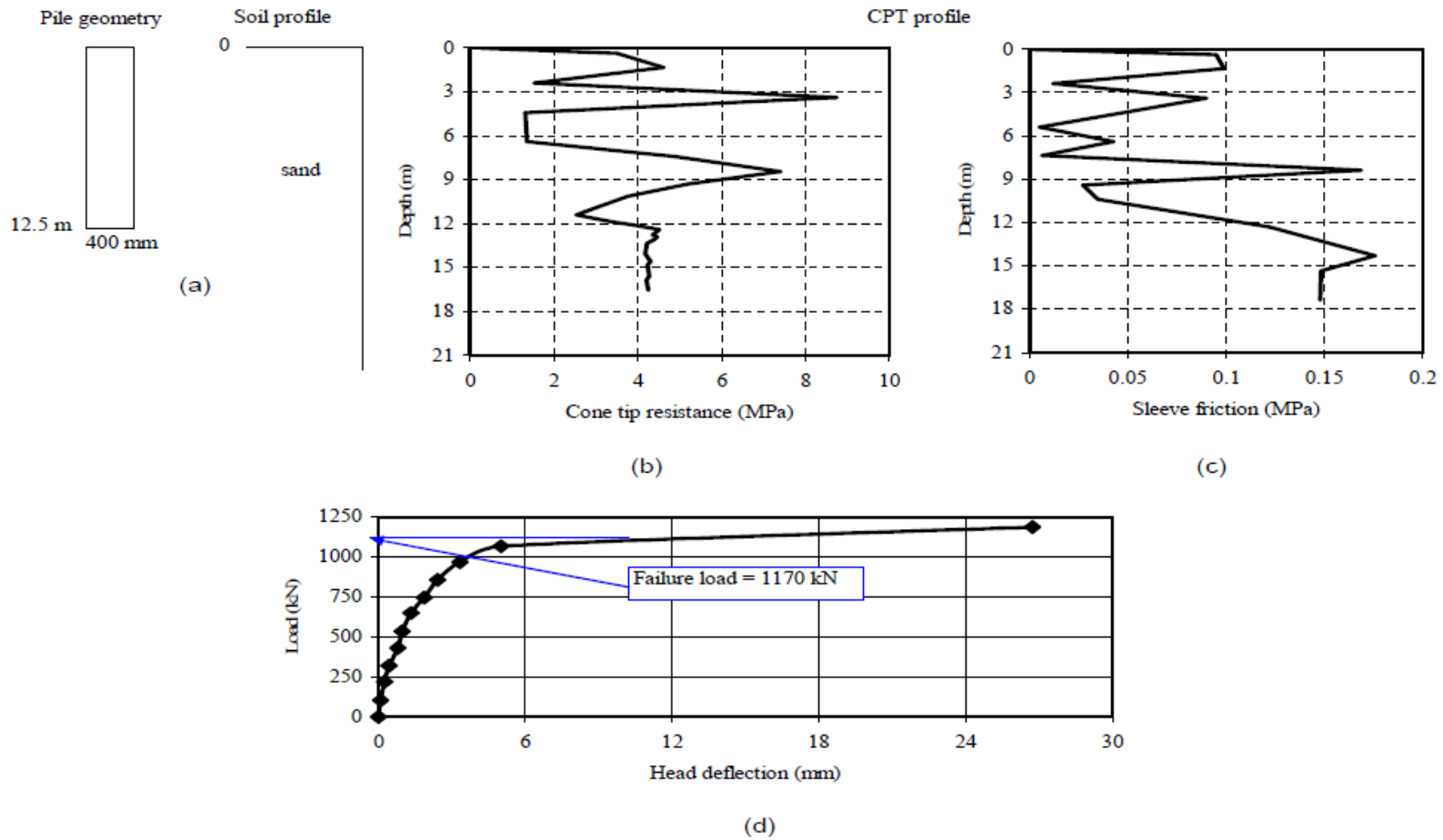


Figure B-14 Summary sheet for case record 14, (a) pile geometry and soil profile, (b) cone tip resistance profile, (c) sleeve friction profile, (d) load deflection plot

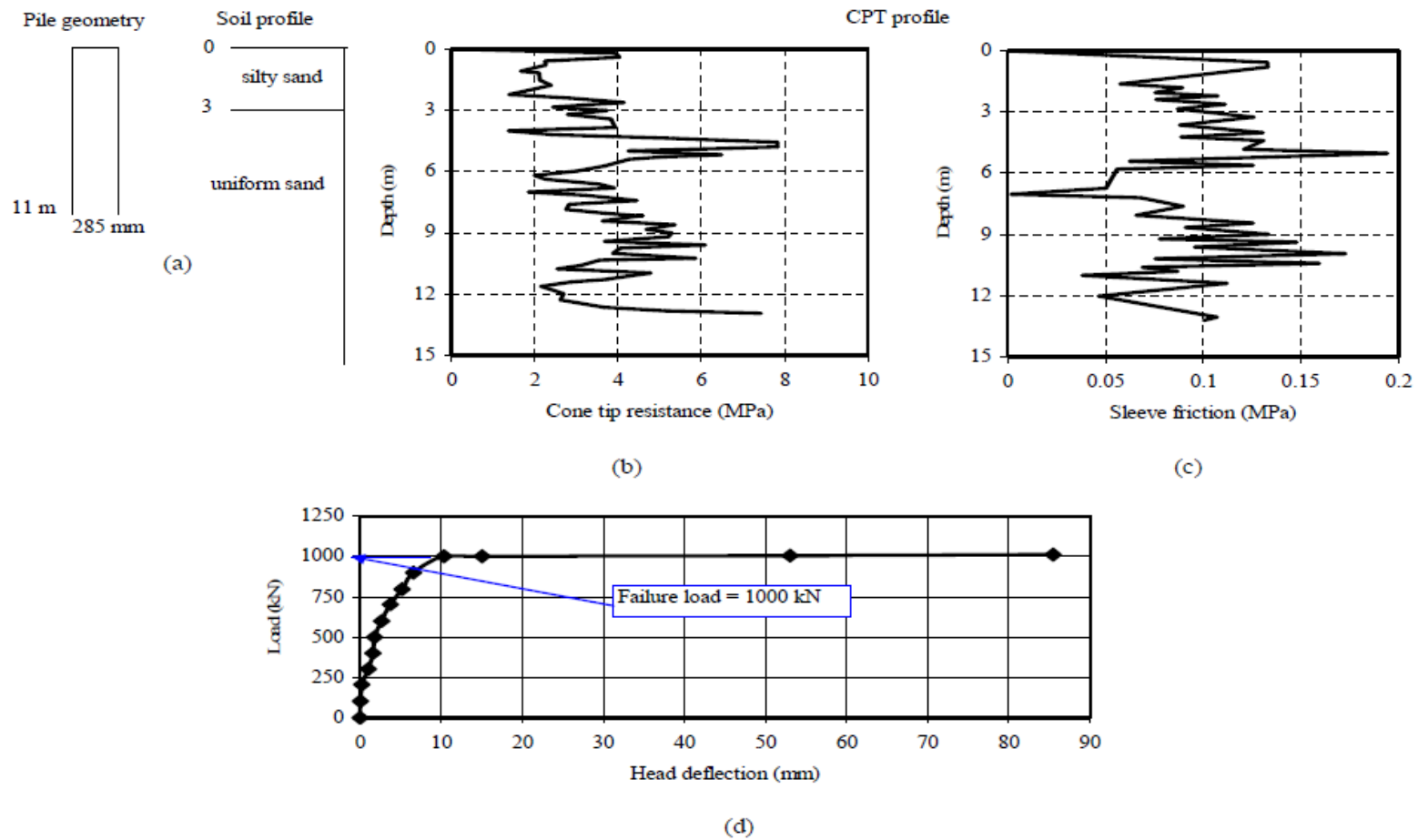


Figure B-15 Summary sheet for case record 15, (a) pile geometry and soil profile, (b) cone tip resistance profile, (c) sleeve friction profile, (d) load deflection plot

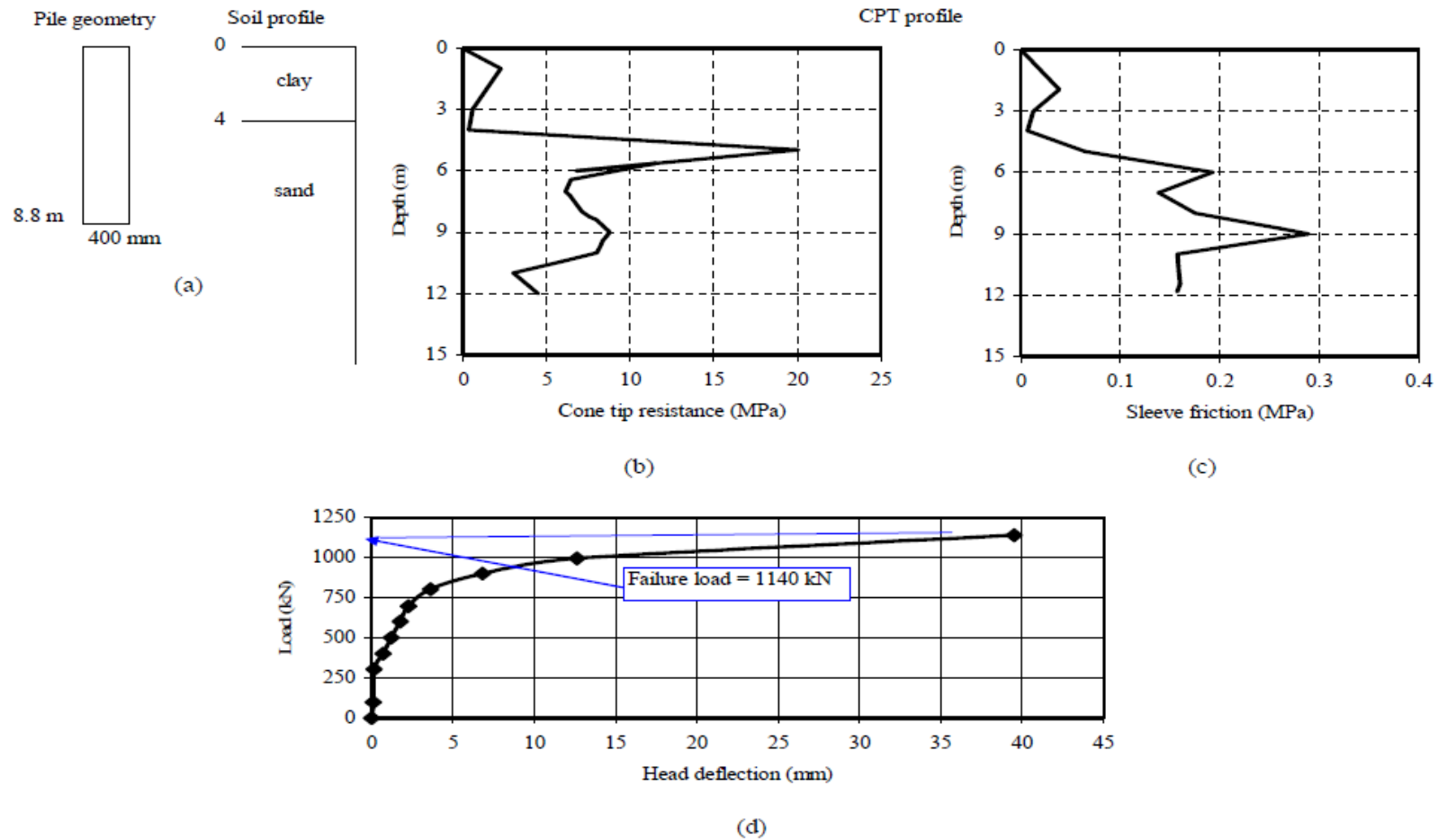


Figure B-16 Summary sheet for case record 16, (a) pile geometry and soil profile, (b) cone tip resistance profile, (c) sleeve friction profile, (d) load deflection plot

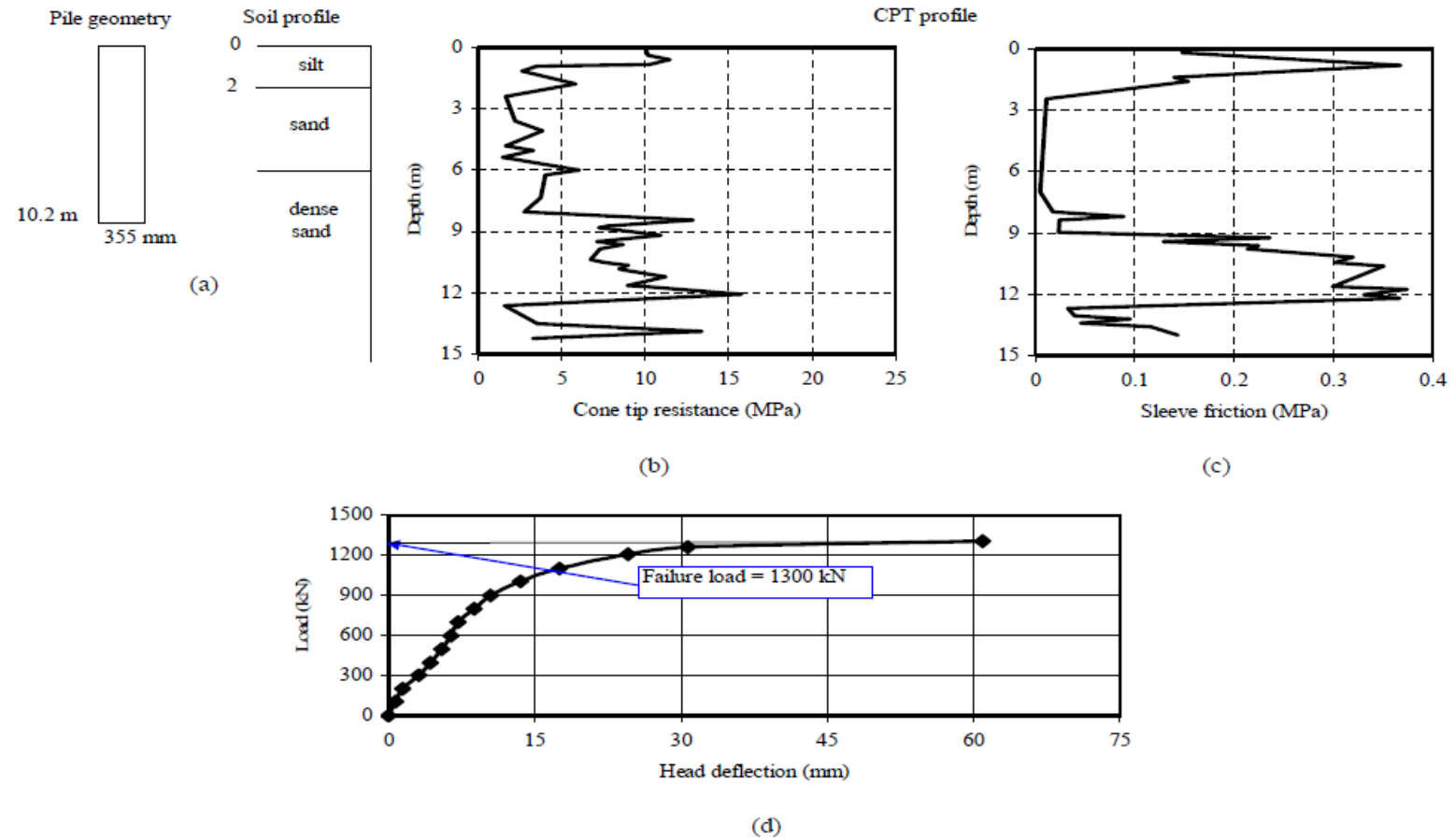


Figure B-17 Summary sheet for case record 17, (a) pile geometry and soil profile, (b) cone tip resistance profile, (c) sleeve friction profile, (d) load deflection plot

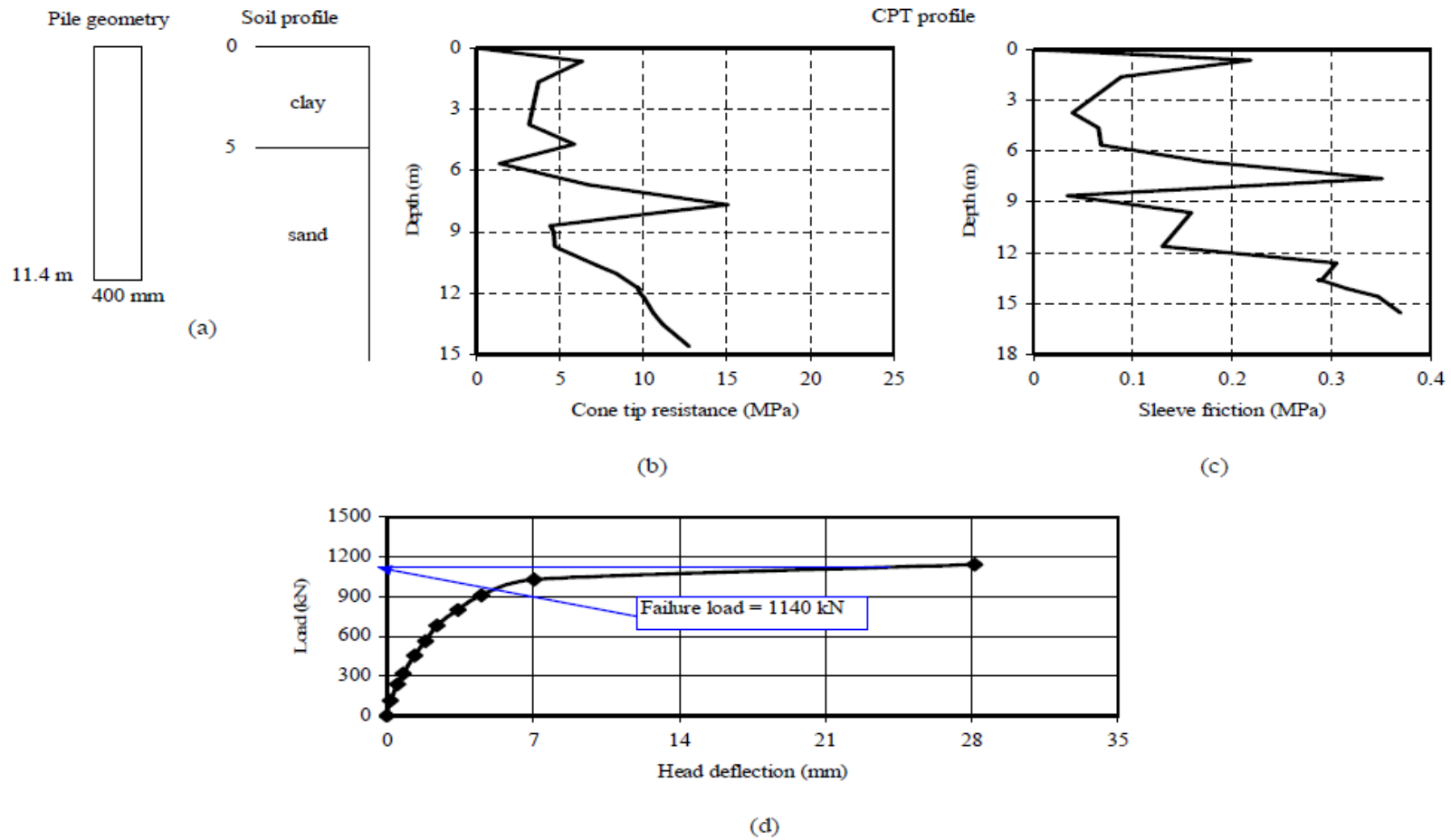


Figure B-18 Summary sheet for case record 18, (a) pile geometry and soil profile, (b) cone tip resistance profile, (c) sleeve friction profile, (d) load deflection plot

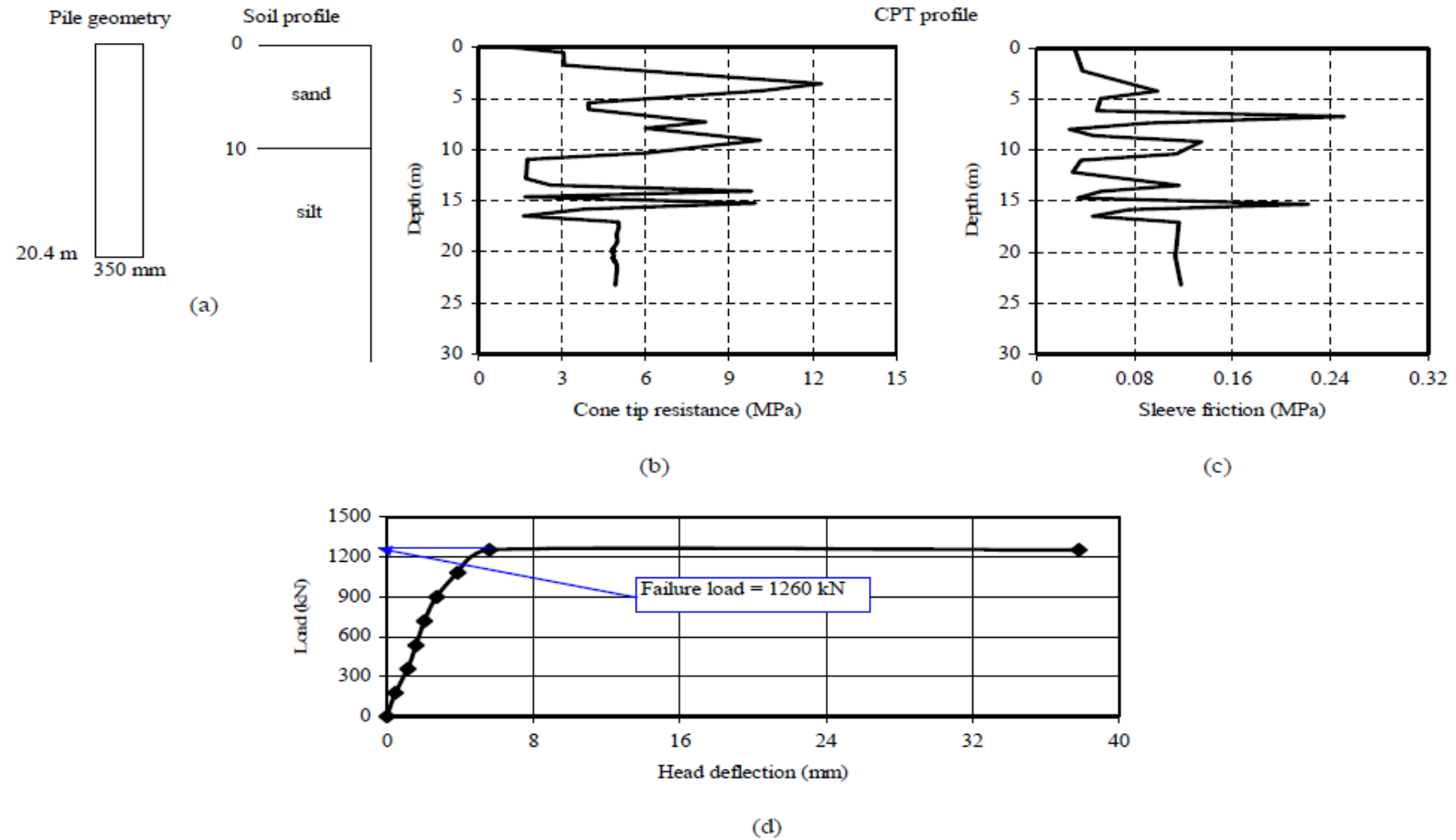


Figure B-19 Summary sheet for case record 19, (a) pile geometry and soil profile, (b) cone tip resistance profile, (c) sleeve friction profile, (d) load deflection plot

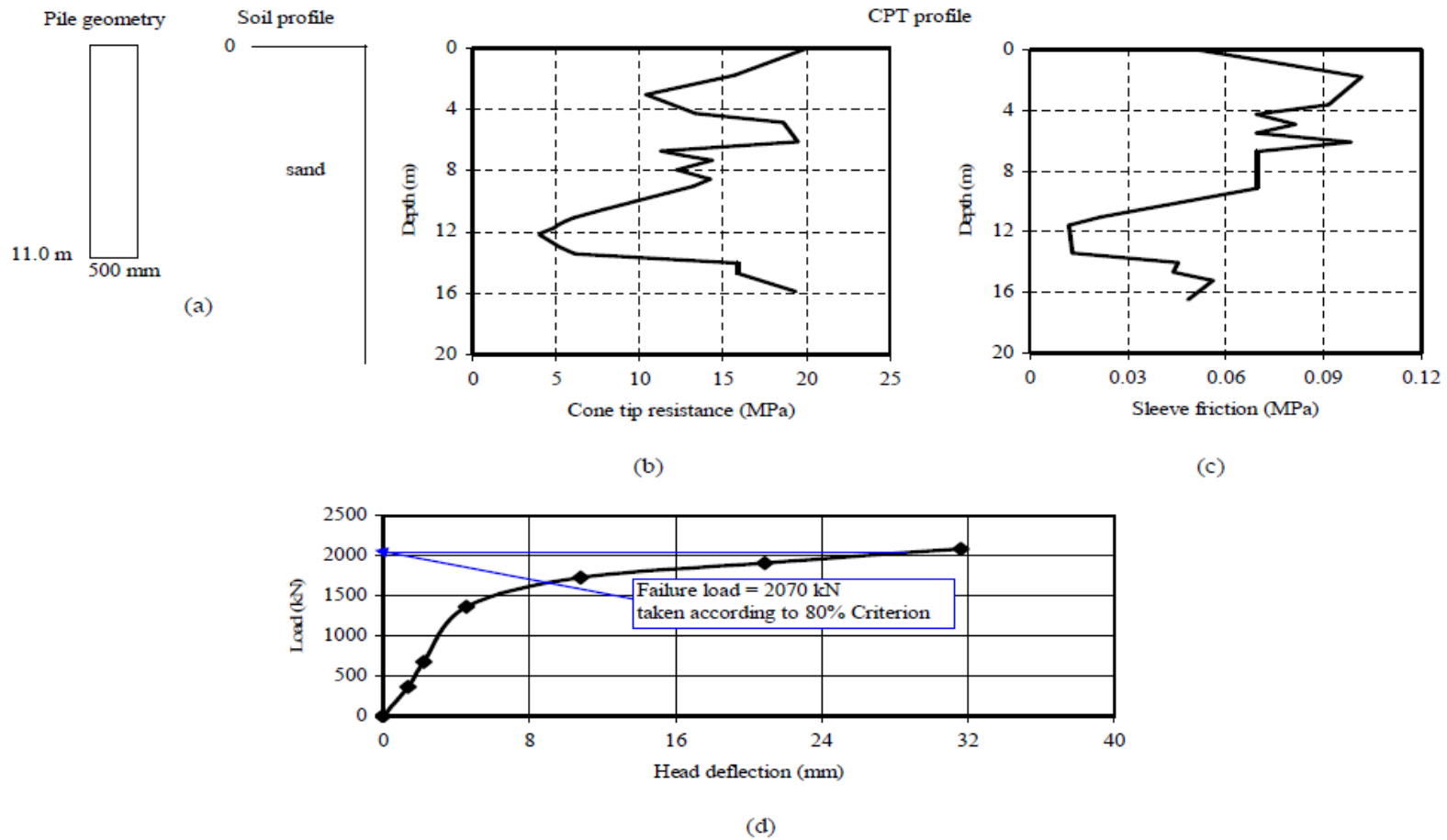


Figure B-20 Summary sheet for case record 20, (a) pile geometry and soil profile, (b) cone tip resistance profile, (c) sleeve friction profile, (d) load deflection plot

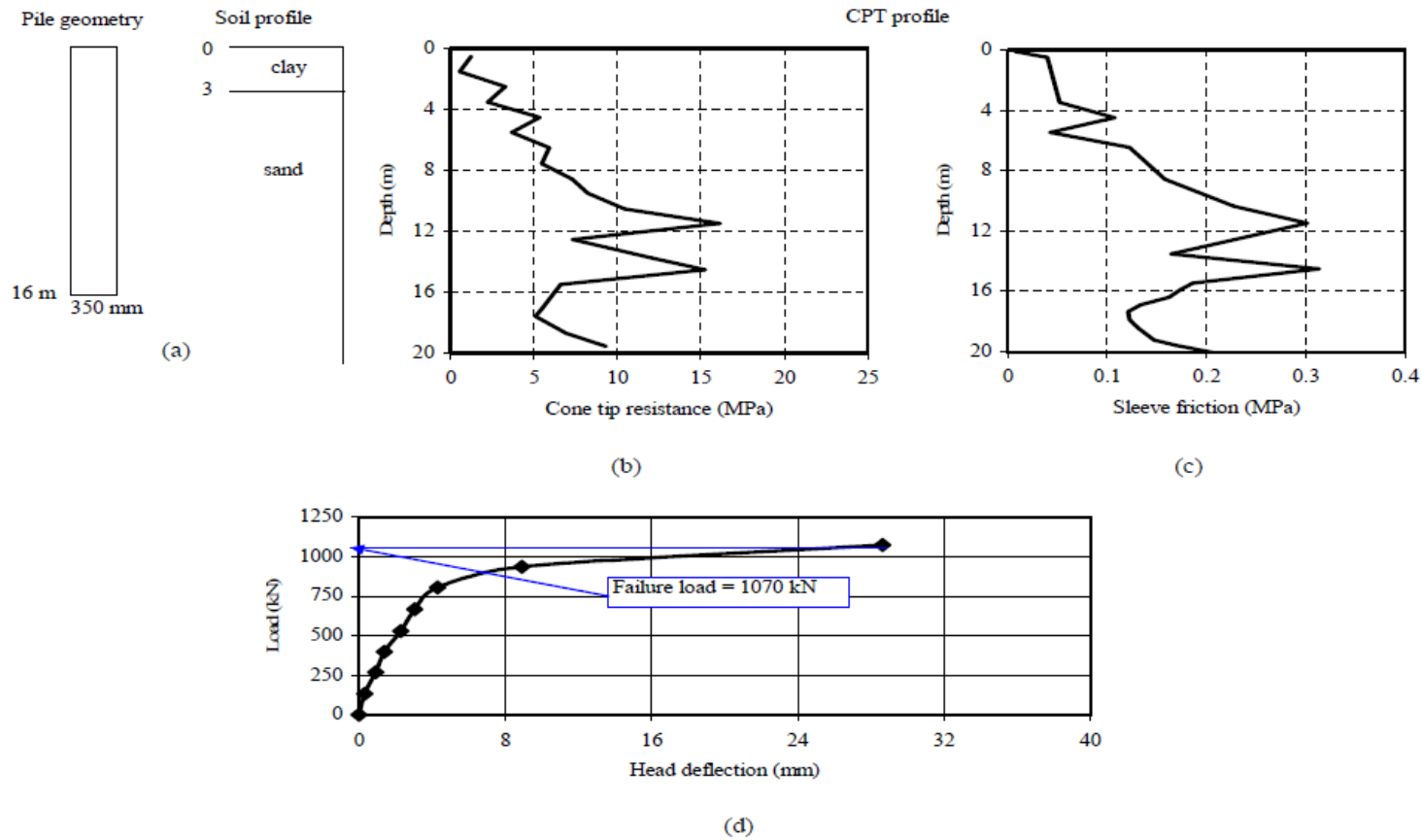


Figure B-21 Summary sheet for case record 21, (a) pile geometry and soil profile, (b) cone tip resistance profile, (c) sleeve friction profile, (d) load deflection plot

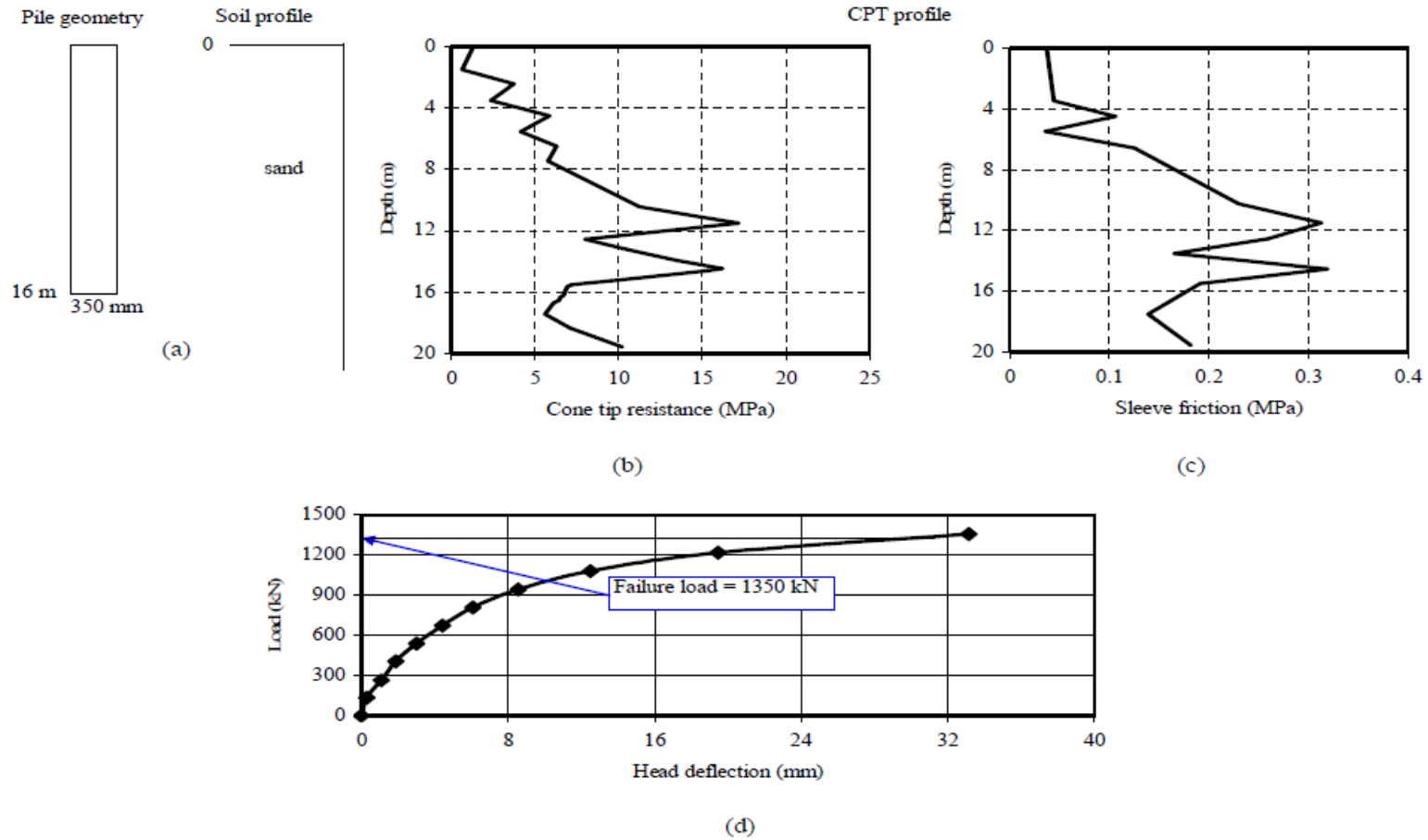


Figure B-22 Summary sheet for case record 22, (a) pile geometry and soil profile, (b) cone tip resistance profile, (c) sleeve friction profile, (d) load deflection plot

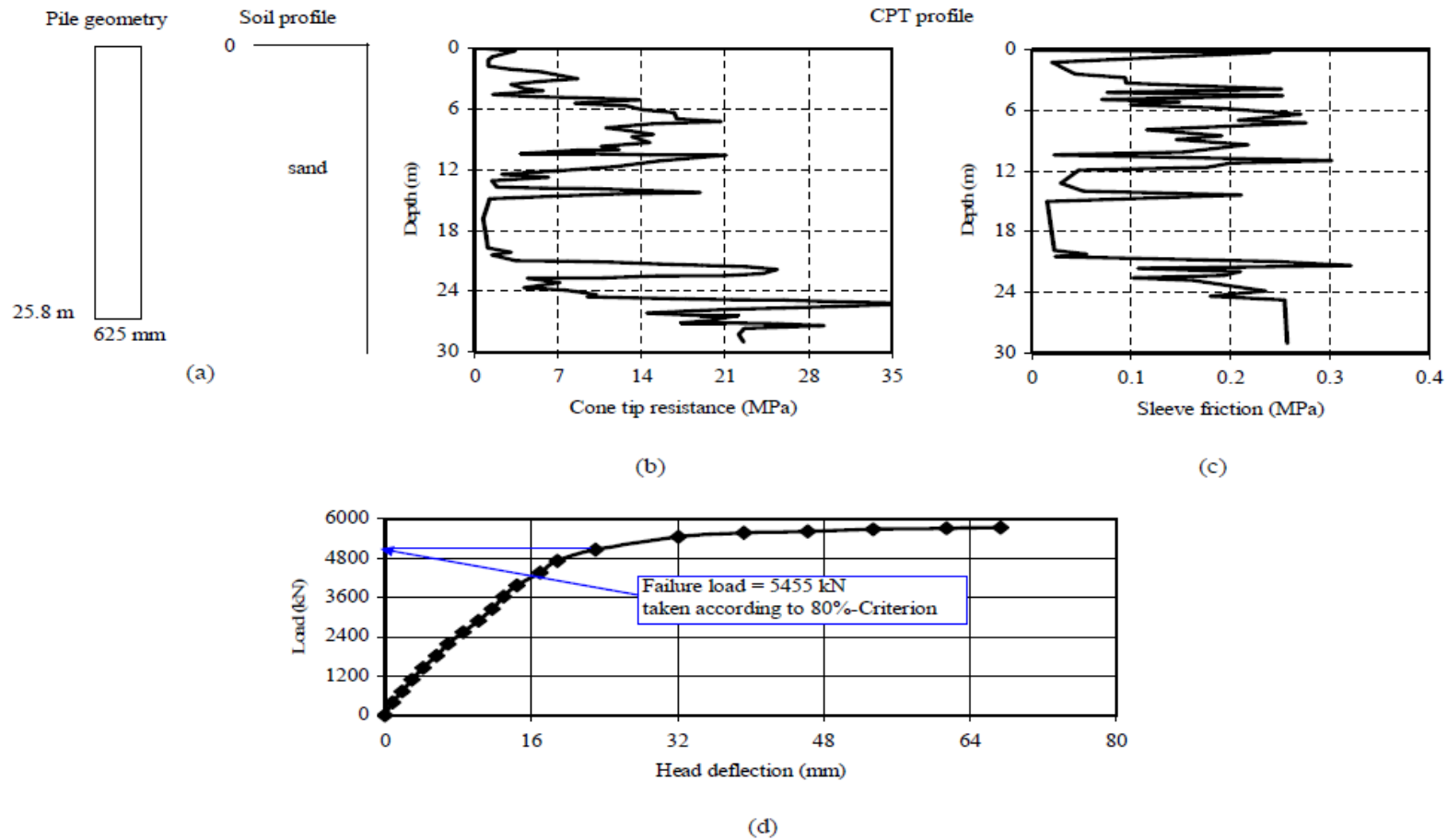


Figure B-23 Summary sheet for case record 23, (a) pile geometry and soil profile, (b) cone tip resistance profile, (c) sleeve friction profile, (d) load deflection plot

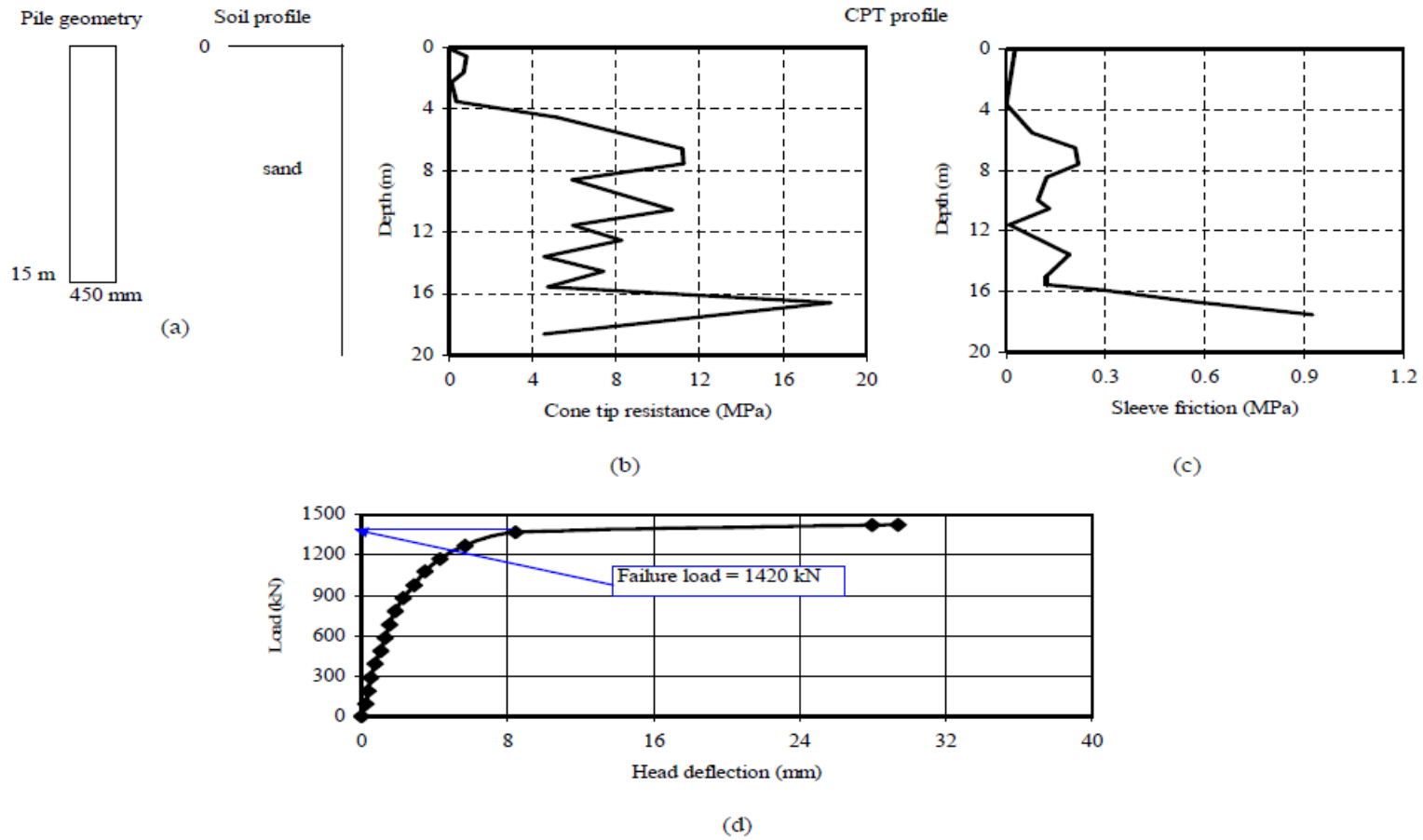


Figure B-24 Summary sheet for case record 24, (a) pile geometry and soil profile, (b) cone tip resistance profile, (c) sleeve friction profile, (d) load deflection plot

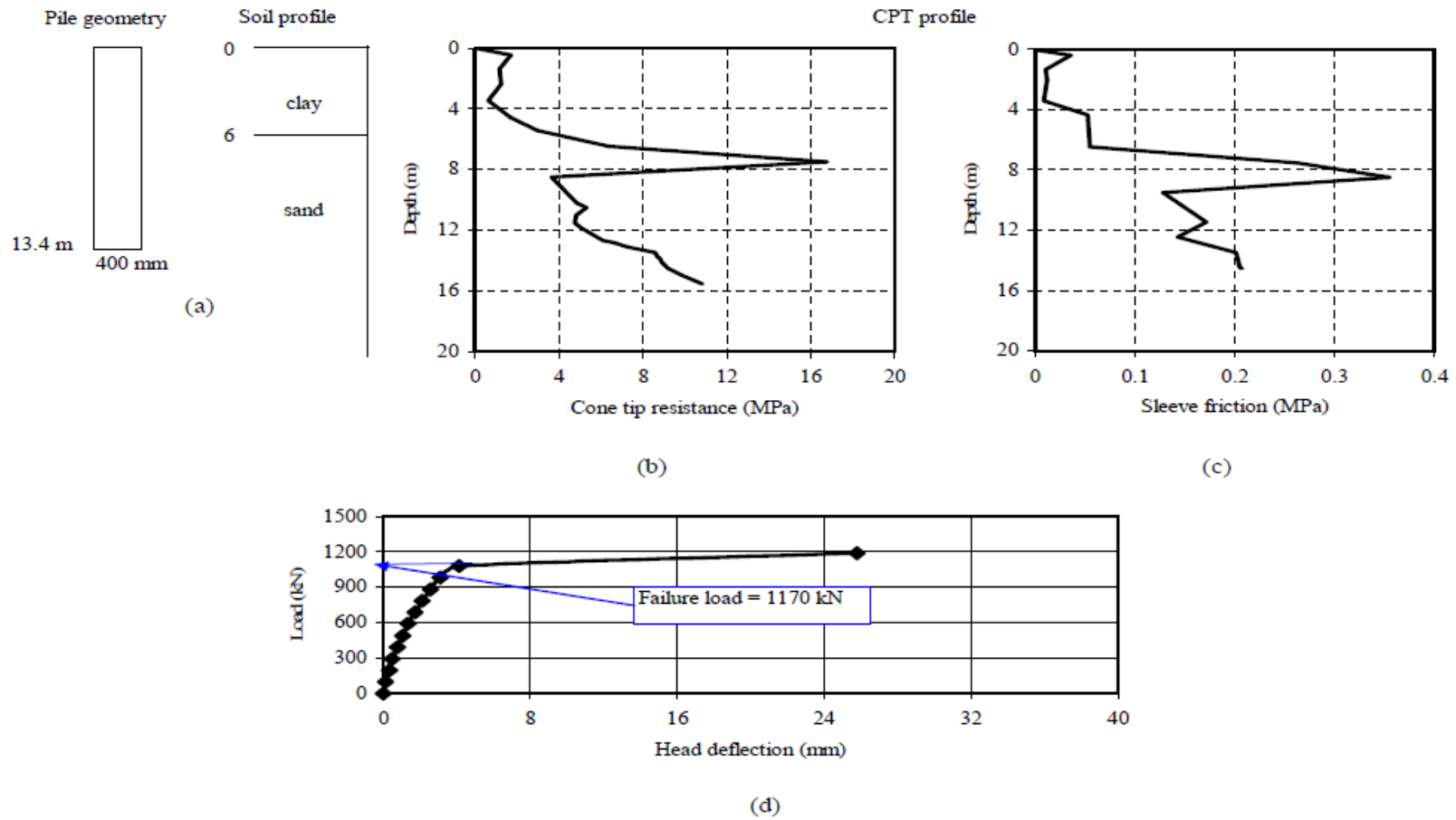


Figure B-25 Summary sheet for case record 25, (a) pile geometry and soil profile, (b) cone tip resistance profile, (c) sleeve friction profile, (d) load deflection plot

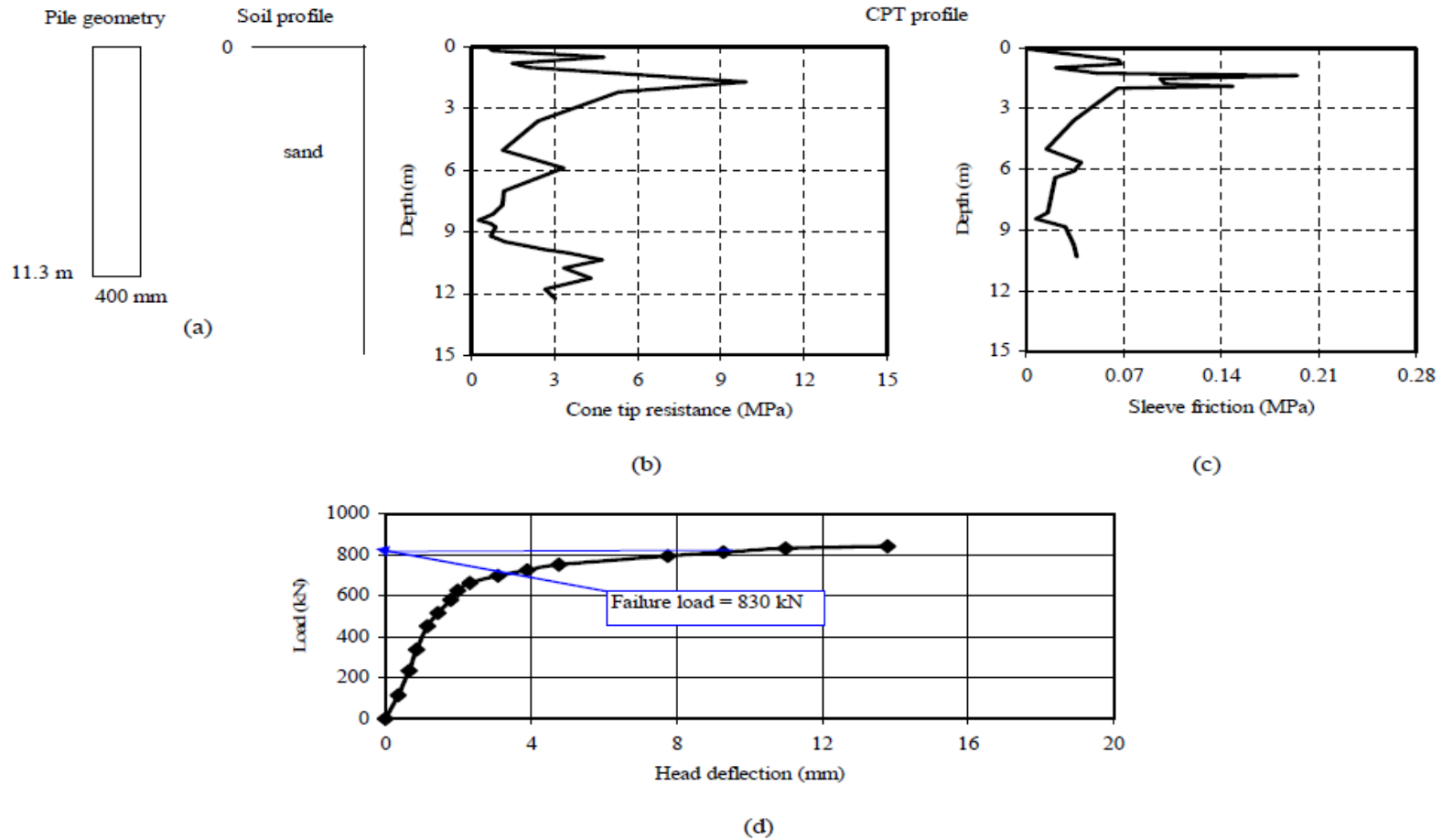


Figure B-26 Summary sheet for case record 26, (a) pile geometry and soil profile, (b) cone tip resistance profile, (c) sleeve friction profile, (d) load deflection plot

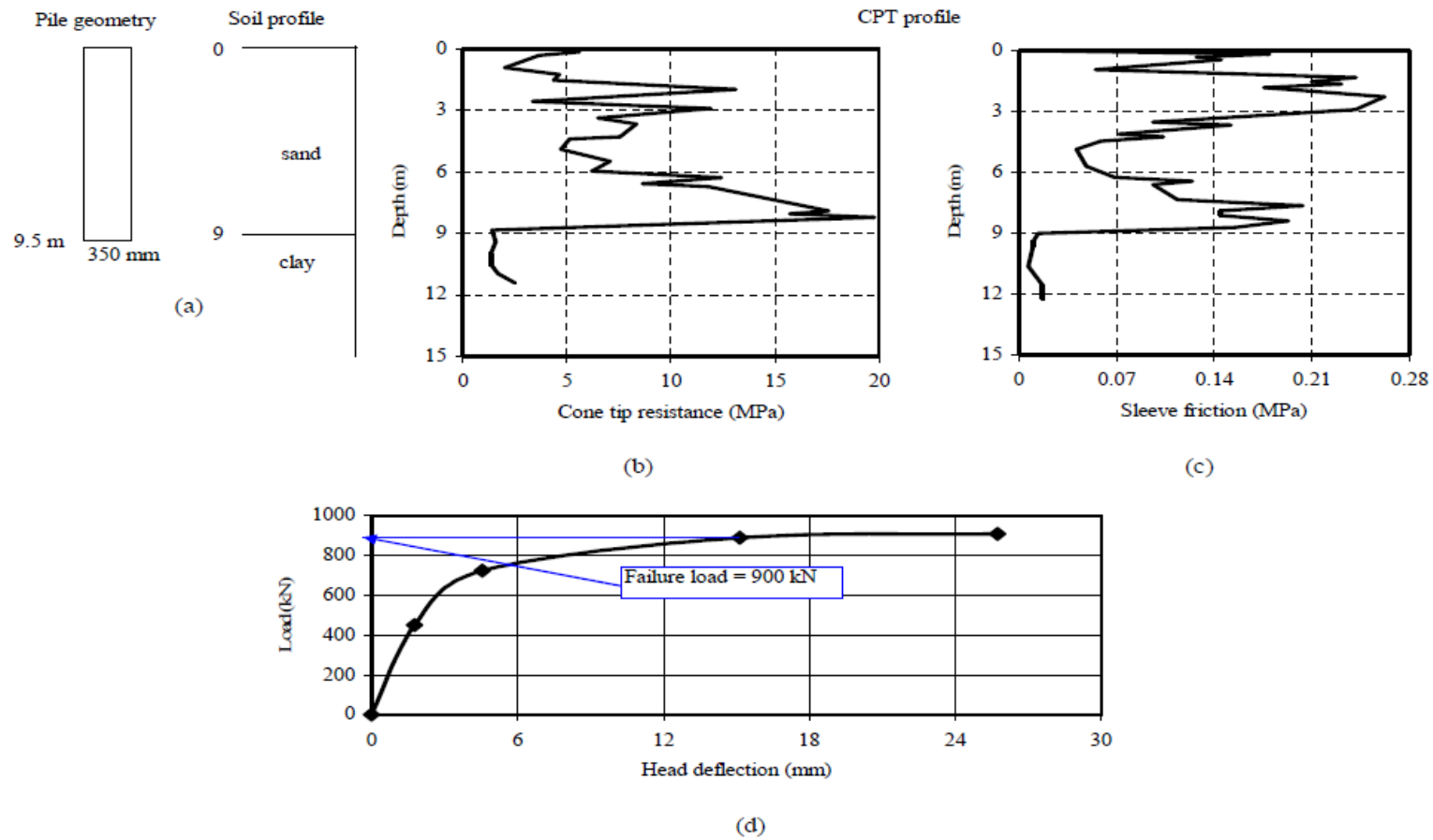


Figure B-27 Summary sheet for case record 27, (a) pile geometry and soil profile, (b) cone tip resistance profile, (c) sleeve friction profile, (d) load deflection plot

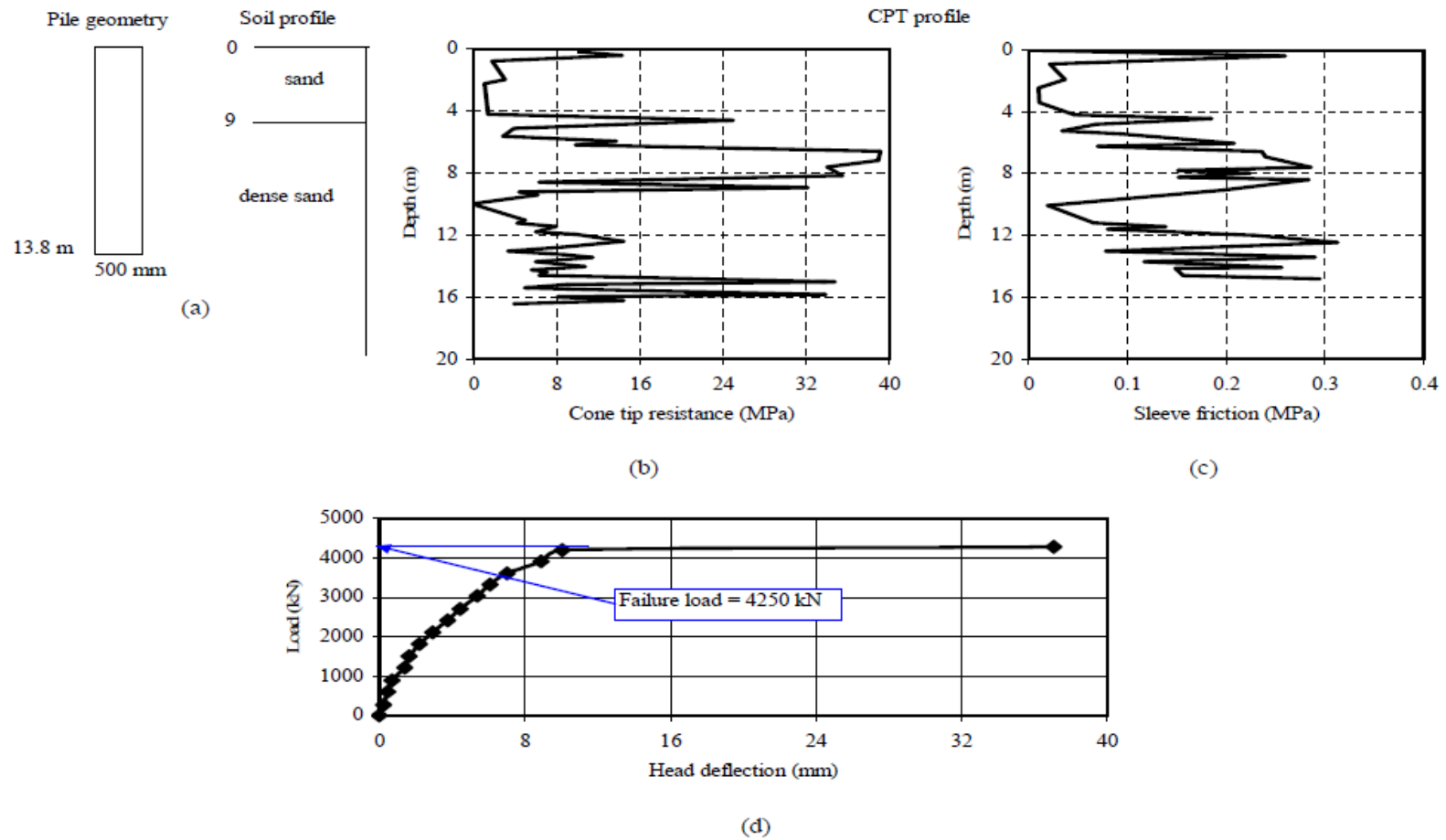


Figure B-28 Summary sheet for case record 28, (a) pile geometry and soil profile, (b) cone tip resistance profile, (c) sleeve friction profile, (d) load deflection plot

Appendix C - Steel Driven Piles Case Records Summary

Piles group	Case record number	Reference	Case number at the reference	Shape	Tip, closed or open	A_c (m ²)	A_{cir} (m ² /m)	D or D_{eq} (mm)	L (m)	Type of load test	Type of cone
Driven piles (steel)	1	Eslami (1996)	L&D32	pipe	closed	0.071	0.94	300	11.0	SML (T)	E
	2	****	L&D314	H-pile	open	0.014	1.43	455	12	****	****
	3	****	L&D316	****	****	0.014	1.43	455	11.3	****	****
	4	****	N&SBI43	pipe	closed	0.059	0.858	273	22.5	SML	M
	5	****	OKLAST	****	****	0.342	2.07	660	18.2	****	E
	6	****	TWNTP6	****	****	0.291	1.91	609	34.25	****	****
	7	****	MILANO	****	****	0.066	1.037	330	10.0	****	****
	8	****	PRICOS	****	****	0.071	0.942	300	28.4	****	****
	9	****	N&SBI44	****	****	0.059	0.858	273	22.5	SML (T)	M
	10	****	L&D12	H-pile	open	0.014	1.43	455	16.2	****	E
	11	****	L&D31	pipe	closed	0.071	0.94	300	16.2	SML	****
	12	****	NWUP	****	****	0.159	1.41	450	15.2	****	****
	13	****	L&D21	H-pile	open	0.014	1.43	455	16.8	QML (T)	****
	14	****	L&D34	pipe	closed	0.096	1.1	350	14.4	SML	****
	15	****	L&D37	****	****	0.126	1.26	400	14.6	****	****
	16	****	L&D38	****	****	0.126	1.26	400	14.6	SML (T)	****
	17	****	FHWASF	****	****	0.059	0.858	273	9.2	SML	****
	18	****	N&SBI42	****	****	0.059	0.858	273	15.2	****	M

Table C-1 Steel driven piles case records summary

A_c = cross section area, A_{cir} = unit circumferential area; D = diameter; D_{eq} = equivalent diameter; L = embedment length; SML = slow maintained load test; na = not available; CYC = cyclic load test; QML = quick maintained load test; CRP = constant rate of penetration; IE = incremental equilibrium; M = Mechanical; E = Electrical

Piles group	Case record number	Reference	Case number at the reference	Shape	Tip, closed or open	A_c (m ²)	A_{cir} (m ² /m)	D or D_{eq} (mm)	L (m)	Type of load test	Type of cone
Driven piles (steel)	19	Eslami (1996)	L&D16	H-pile	open	0.014	1.43	455	16.2	QML	E
	20	****	ALABA	****	****	0.014	1.23	392	36.3	SML	****
	21	****	KP1	****	****	0.046	1.54	490	14.0	SML (T)	****
	22	****	A&M39	****	****	0.01	1.21	385	19	SML	M
	23	****	A&M41	****	****	0.01	1.21	385	12.4	****	****
	24	****	NWUH	H-pile	open	0.128	1.43	455	15.2	SML	E
	25	****	A&M14	****	****	0.008	1.01	321	8.5	****	M
	26	****	LSUN215	pipe	closed	0.096	1.01	350	31.1	QML	E
	27	****	TWNT4	****	****	0.291	1.91	609	34.3	SML	****
	28	****	L&D315	H-pile	open	0.014	1.43	455	11.3	SML (T)	****
	29	****	L&D35	pipe	closed	0.096	1.1	350	11.1	****	****
	30	****	PRICOL	****	****	0.71	0.942	300	31.4	SML	****

Table C-1 Steel driven piles case records summary (Continued)

A_c = cross section area, A_{cir} = unit circumferential area; D = diameter; D_{eq} = equivalent diameter; L = embedment length; SML = slow maintained load test; na = not available; CYC = cyclic load test; QML = quick maintained load test; CRP = constant rate of penetration; IE = incremental equilibrium; M = Mechanical; E = Electrical

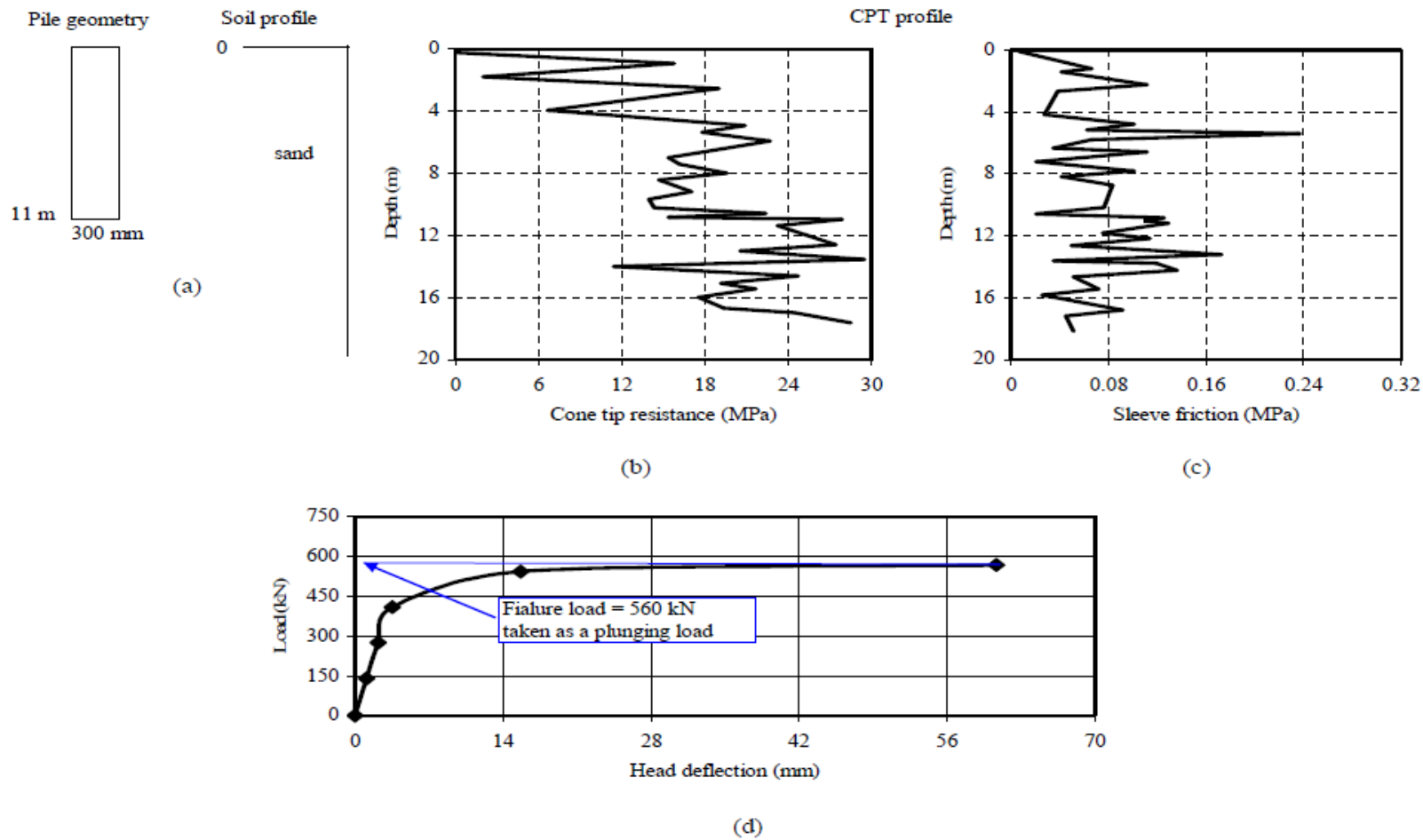


Figure C.1 Summary sheet for case record 1, (a) pile geometry and soil profile, (b) cone tip resistance profile, (c) sleeve friction profile, (d) load deflection plot

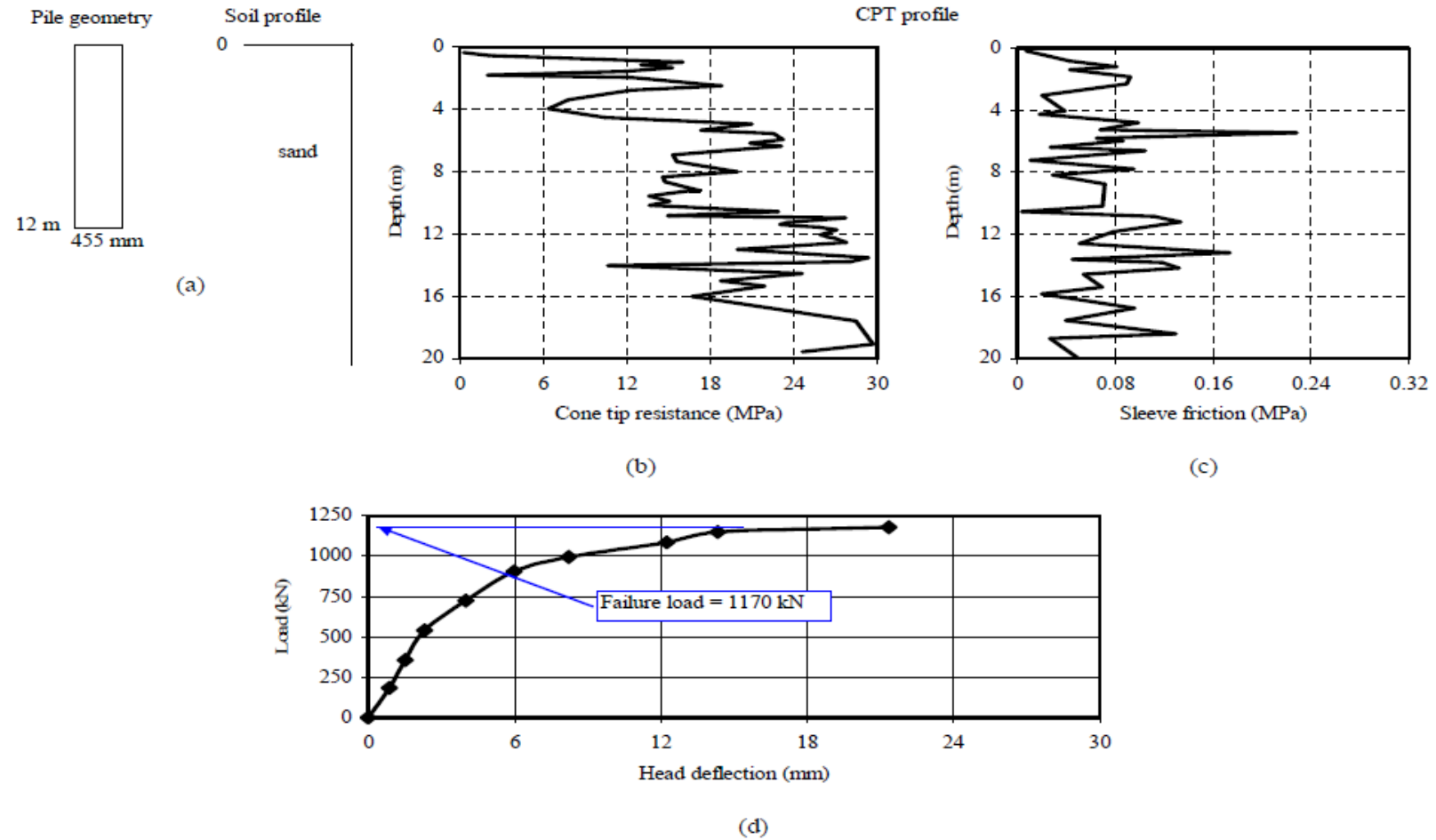


Figure C.2 Summary sheet for case record 2, (a) pile geometry and soil profile, (b) cone tip resistance profile, (c) sleeve friction profile, (d) load deflection plot

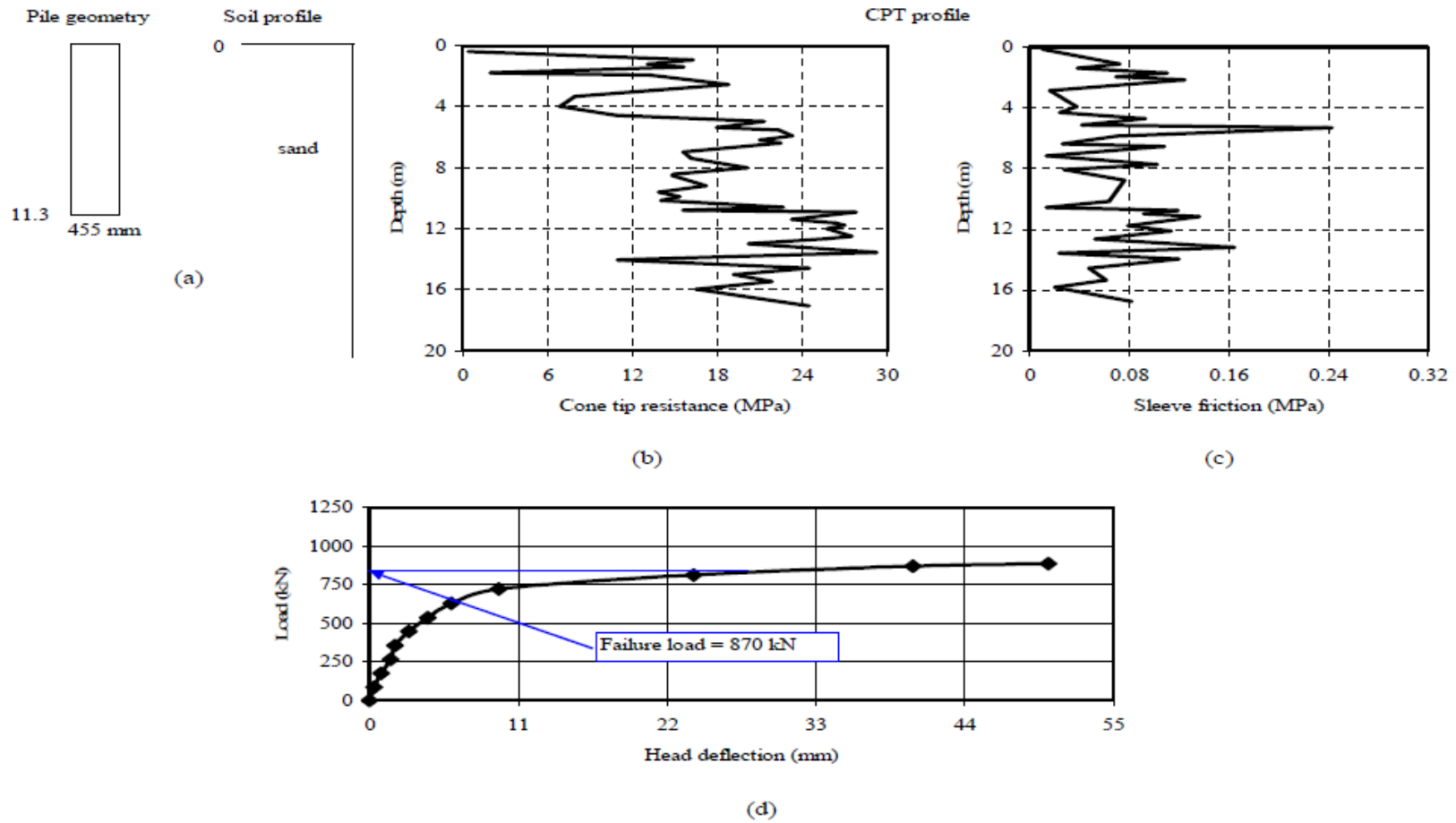


Figure C.3 Summary sheet for case record 3, (a) pile geometry and soil profile, (b) cone tip resistance profile, (c) sleeve friction profile, (d) load deflection plot

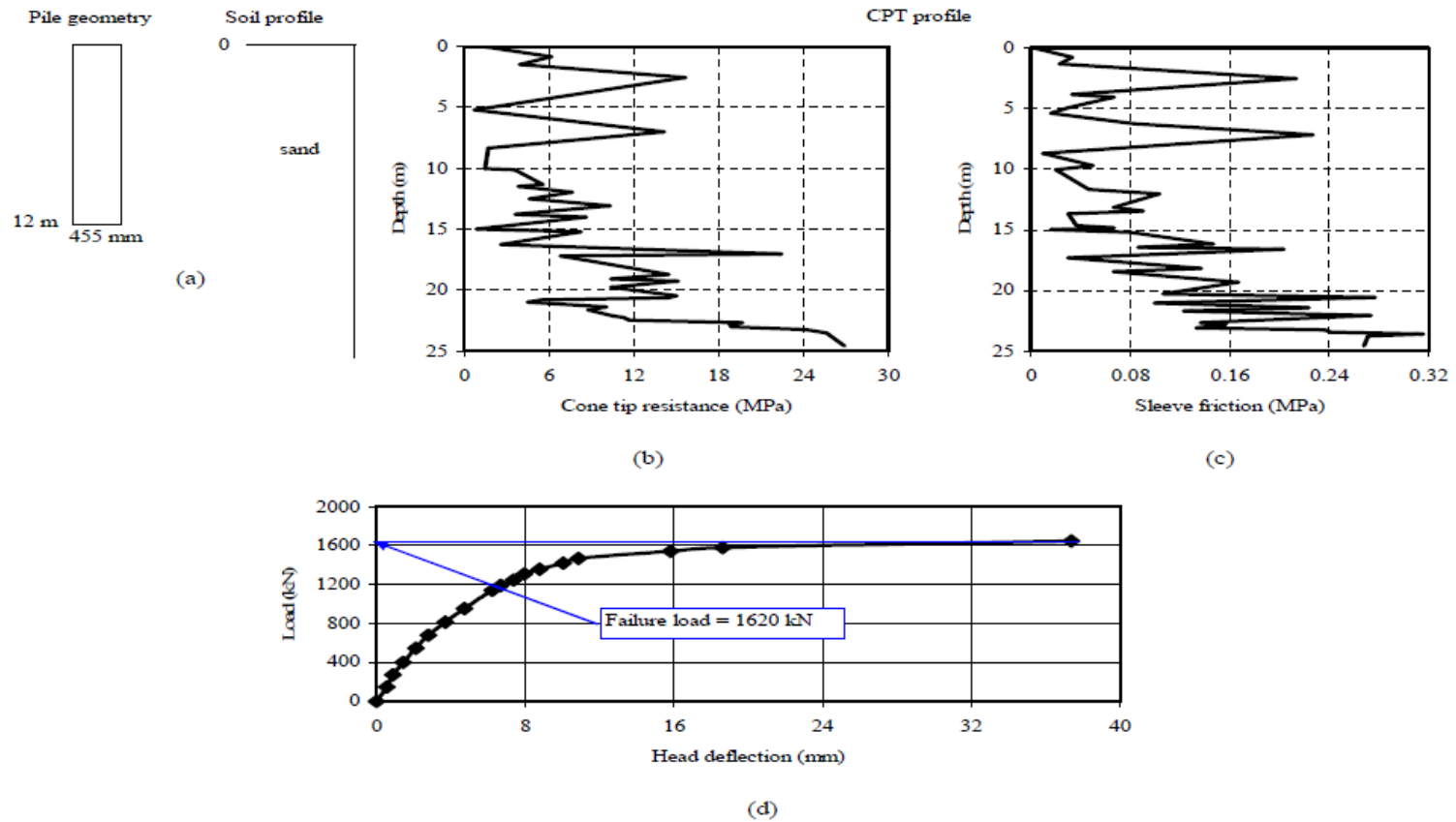


Figure C.4 Summary sheet for case record 4, (a) pile geometry and soil profile, (b) cone tip resistance profile, (c) sleeve friction profile, (d) load deflection plot

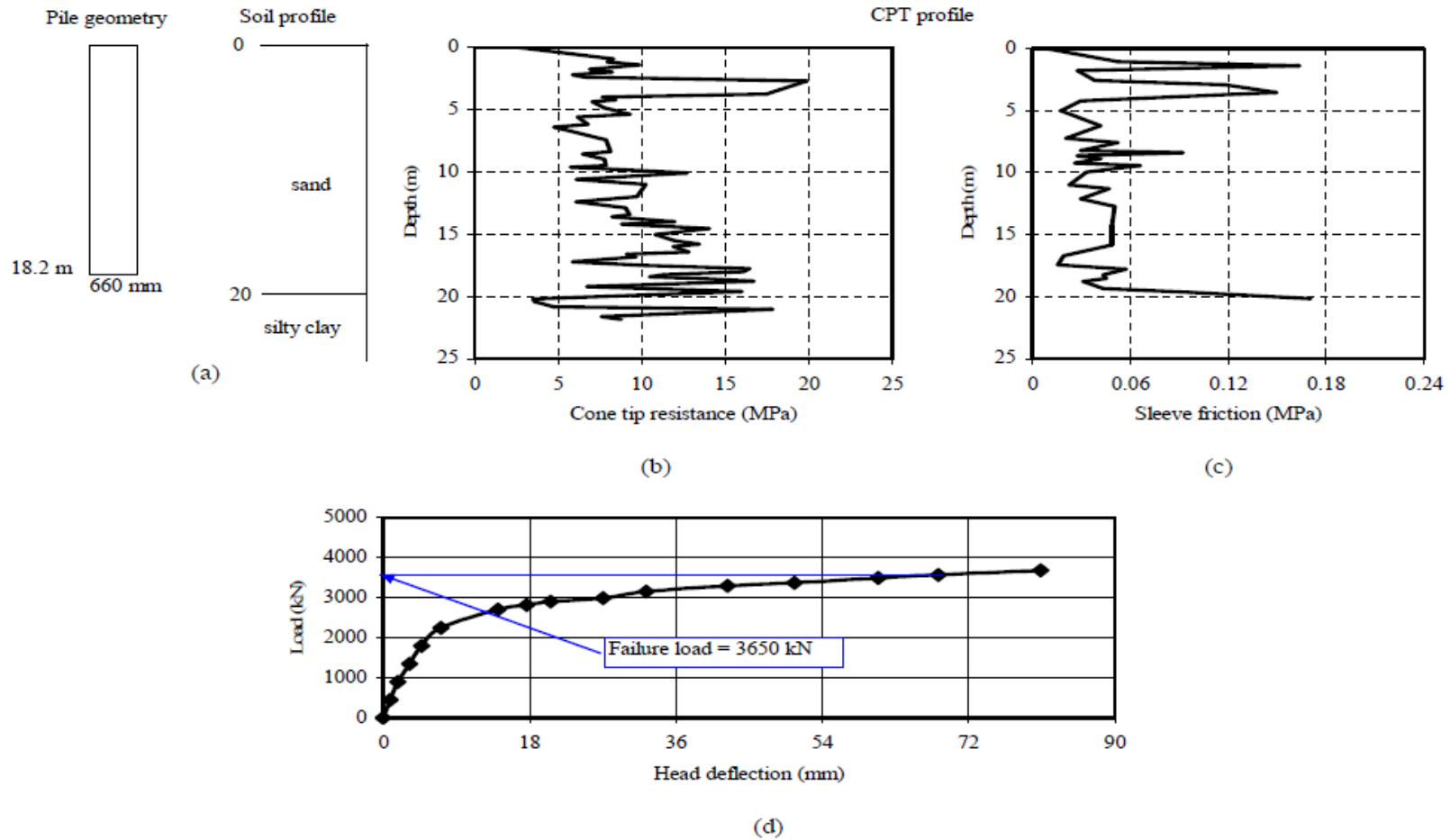


Figure C.5 Summary sheet for case record 5, (a) pile geometry and soil profile, (b) cone tip resistance profile, (c) sleeve friction profile, (d) load deflection plot

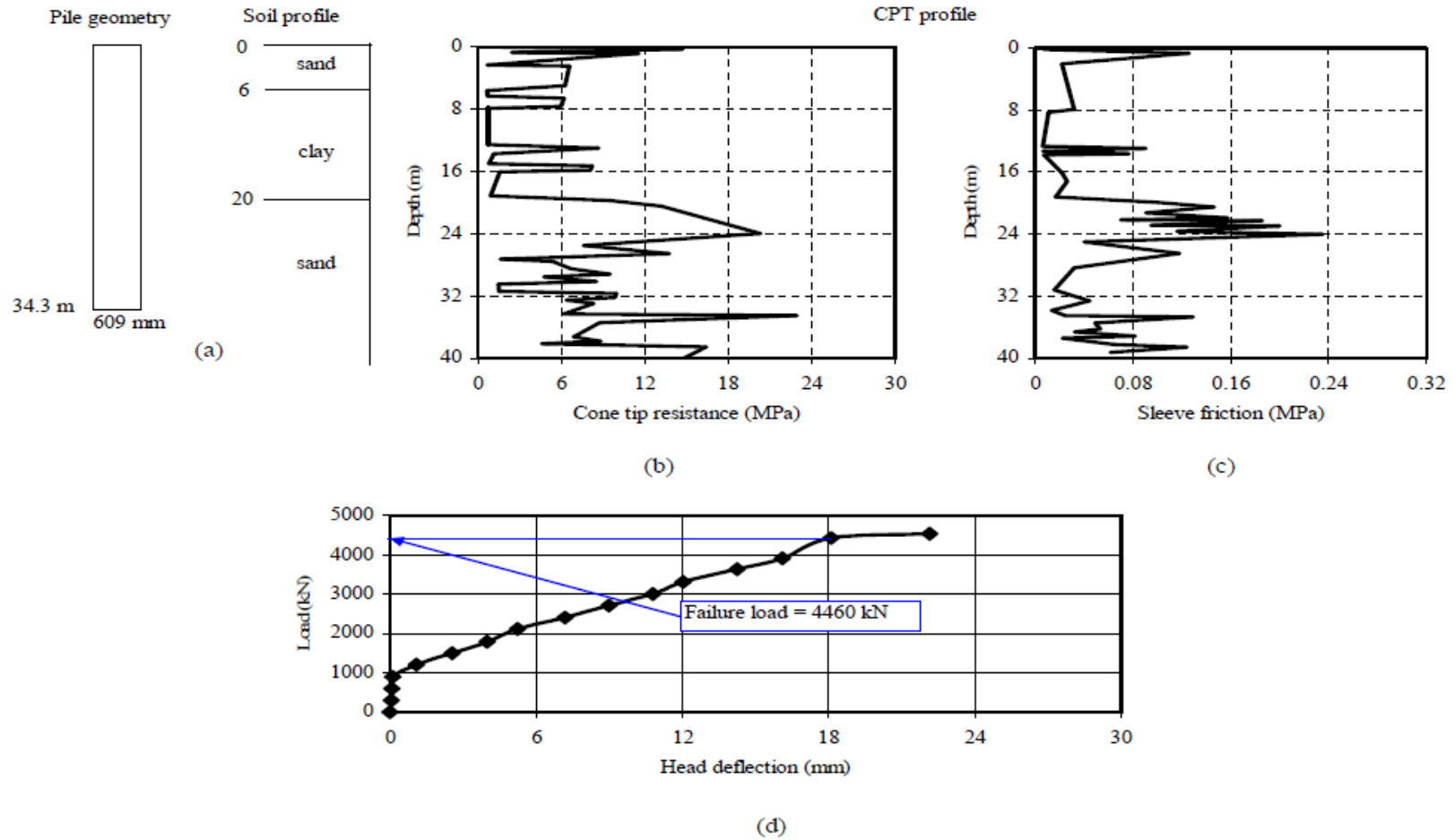


Figure C.6 Summary sheet for case record 6, (a) pile geometry and soil profile, (b) cone tip resistance profile, (c) sleeve friction profile, (d) load deflection plot

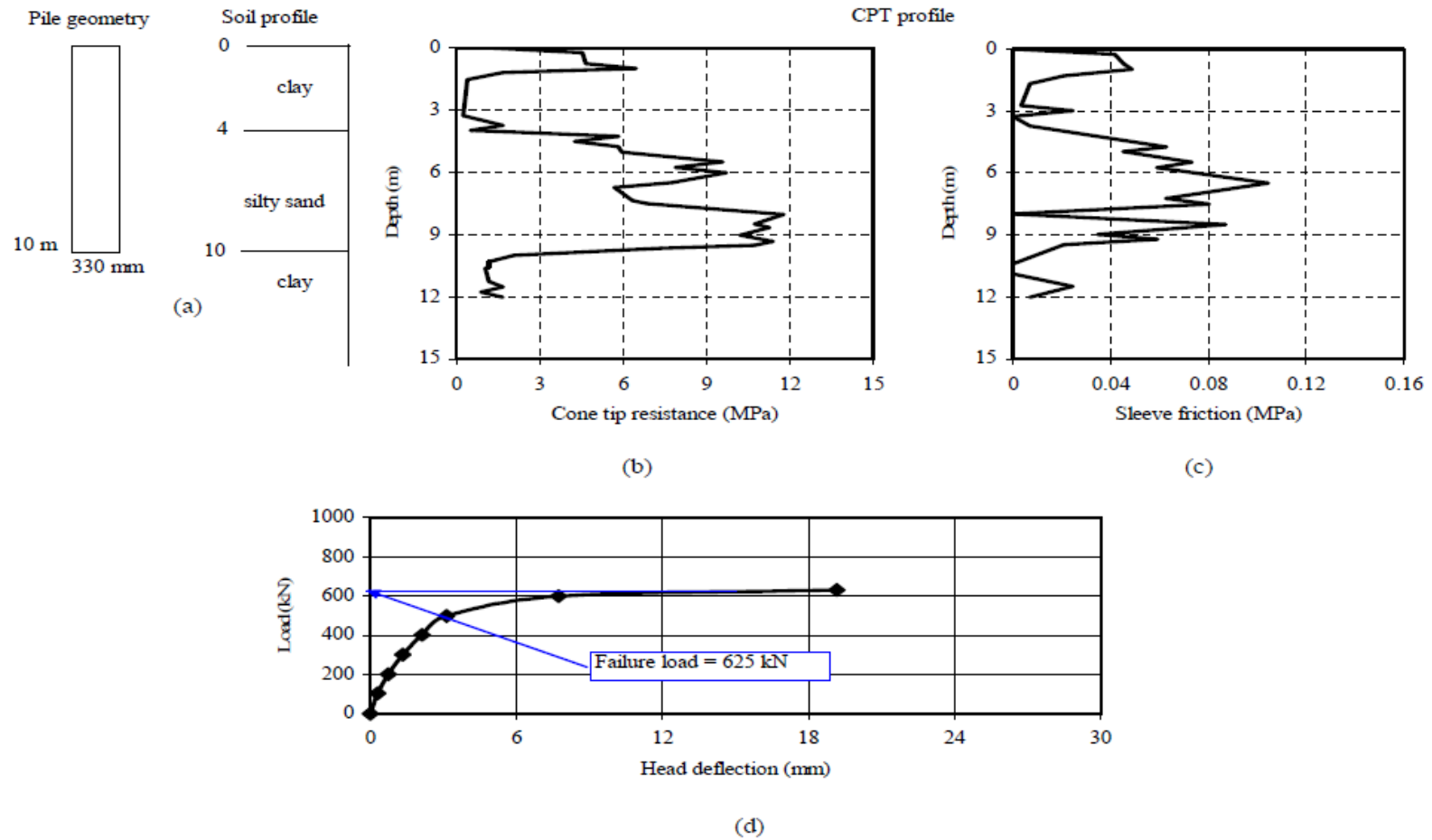


Figure C.7 Summary sheet for case record 7, (a) pile geometry and soil profile, (b) cone tip resistance profile, (c) sleeve friction profile, (d) load deflection plot

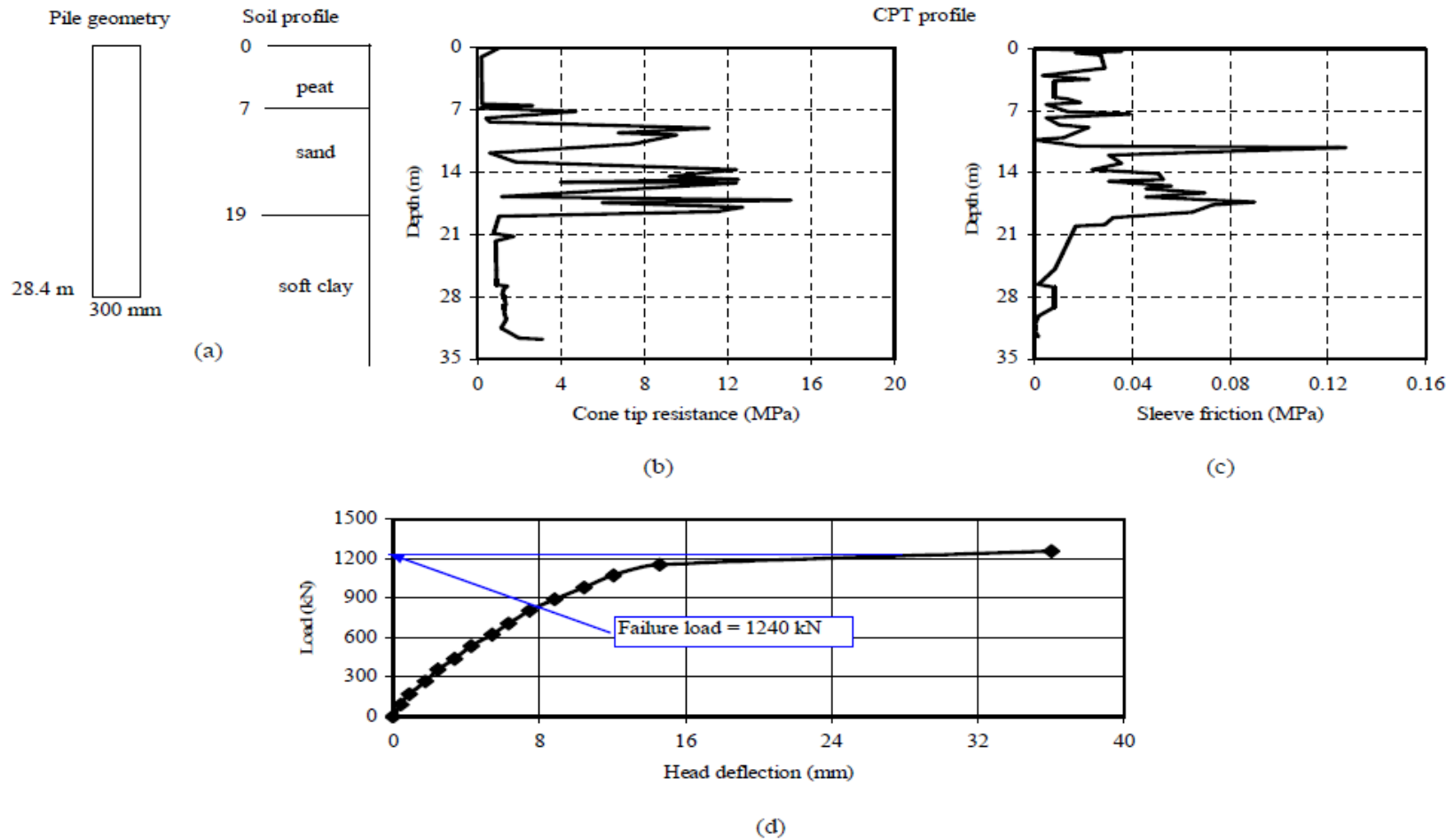


Figure C.8 Summary sheet for case record 8, (a) pile geometry and soil profile, (b) cone tip resistance profile, (c) sleeve friction profile, (d) load deflection plot

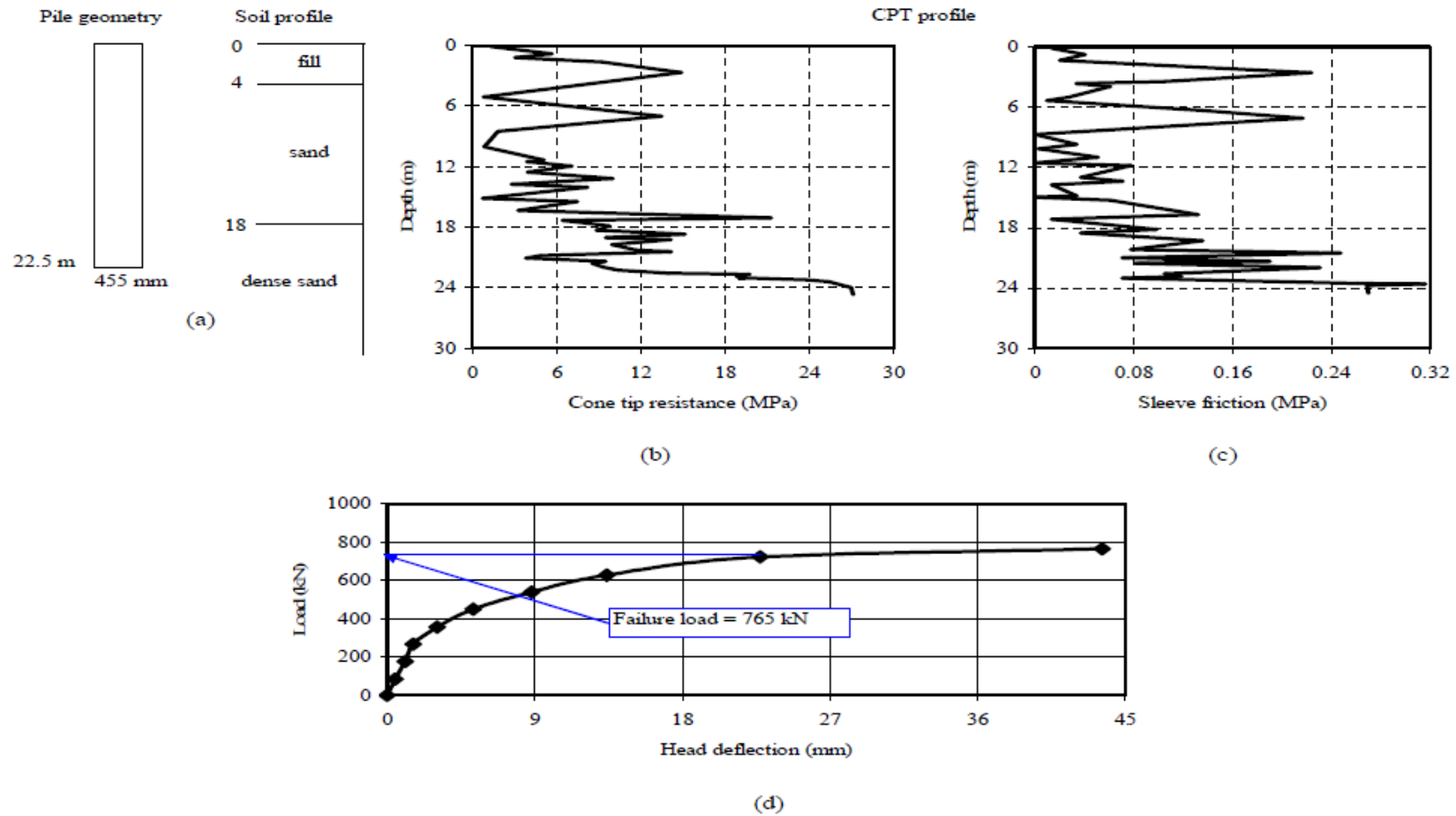


Figure C.9 Summary sheet for case record 9, (a) pile geometry and soil profile, (b) cone tip resistance profile, (c) sleeve friction profile, (d) load deflection plot

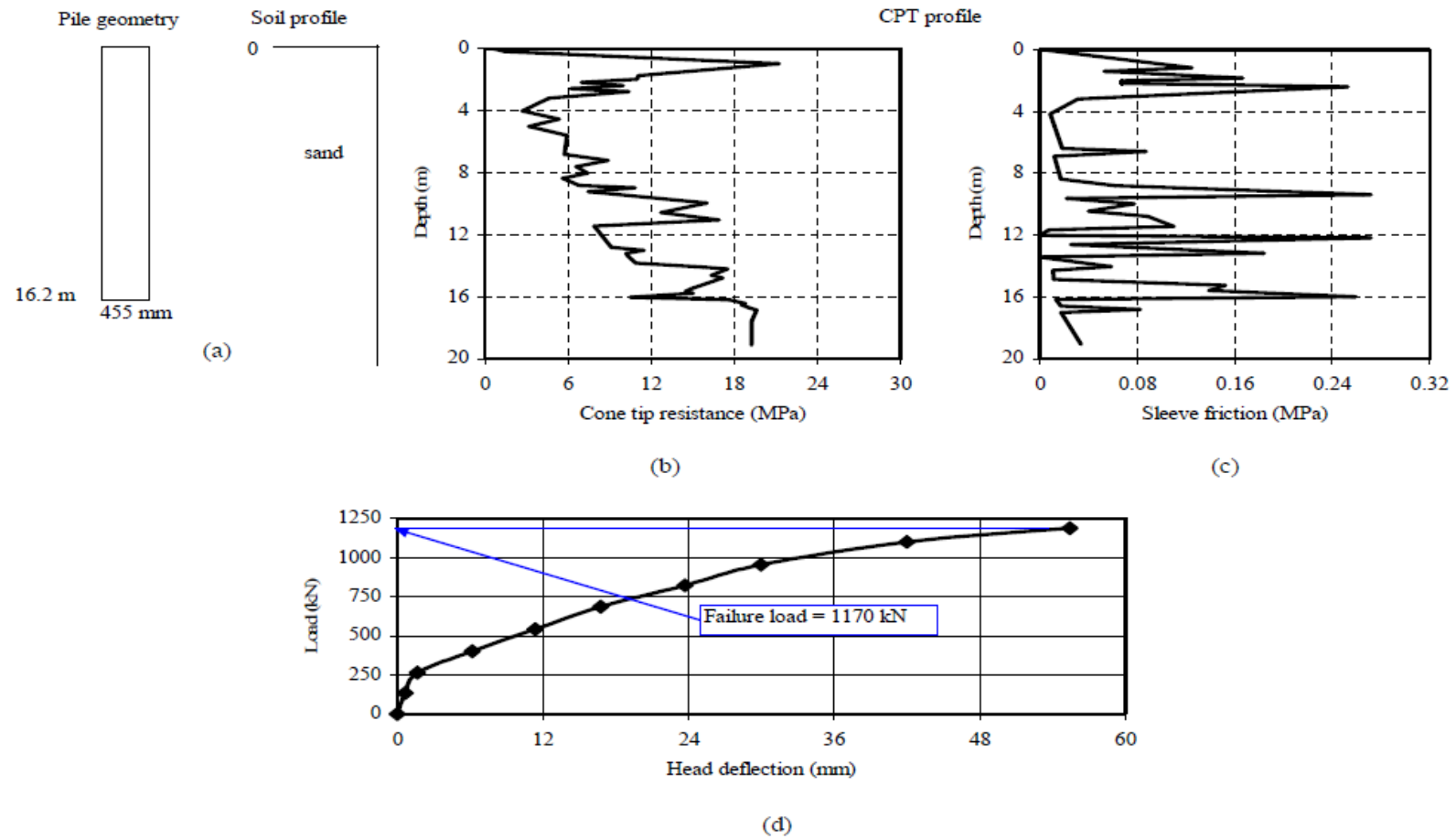


Figure C.10 Summary sheet for case record 10, (a) pile geometry and soil profile, (b) cone tip resistance profile, (c) sleeve friction profile, (d) load deflection plot

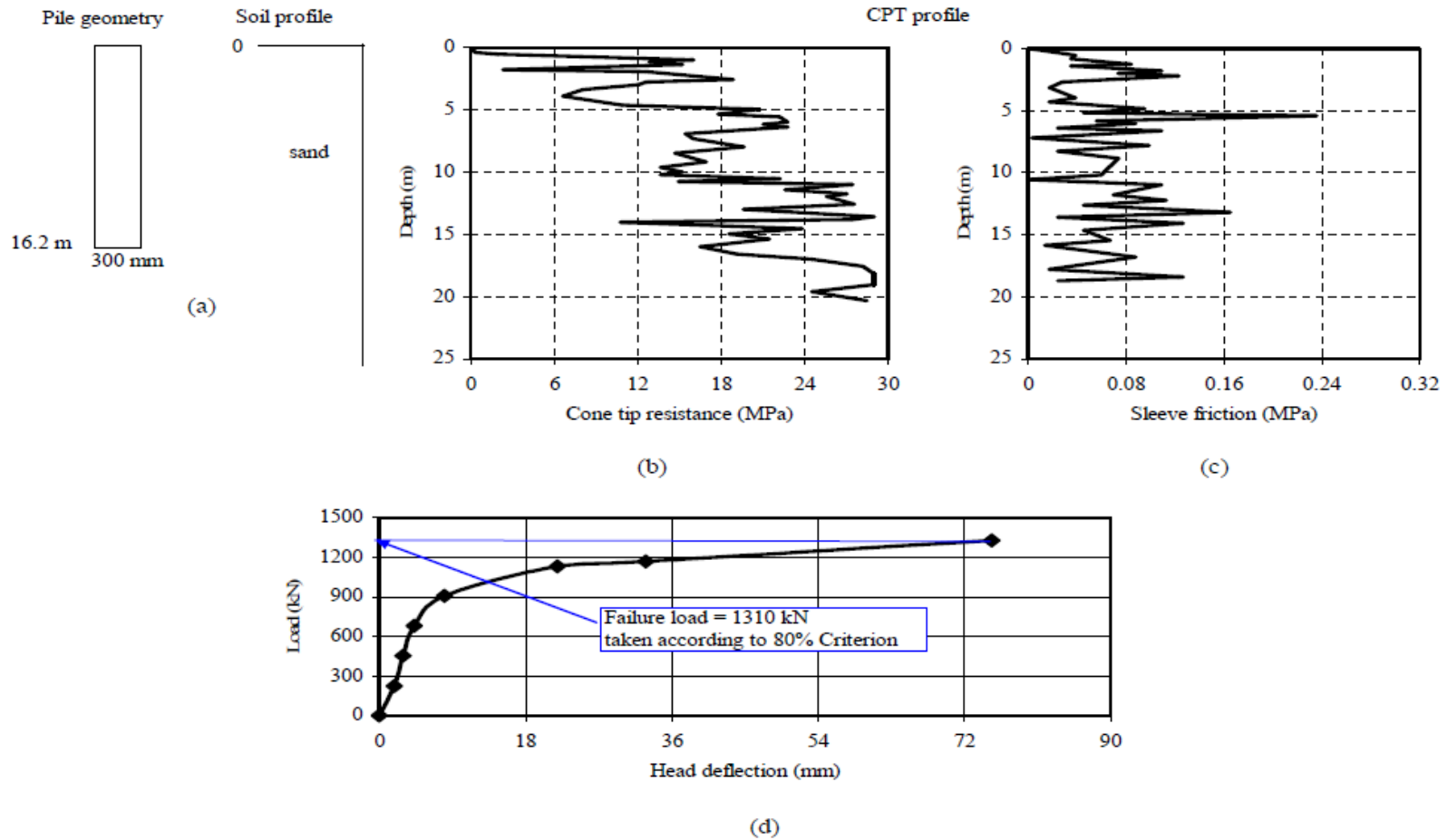


Figure C.11 Summary sheet for case record 11, (a) pile geometry and soil profile, (b) cone tip resistance profile, (c) sleeve friction profile, (d) load deflection plot

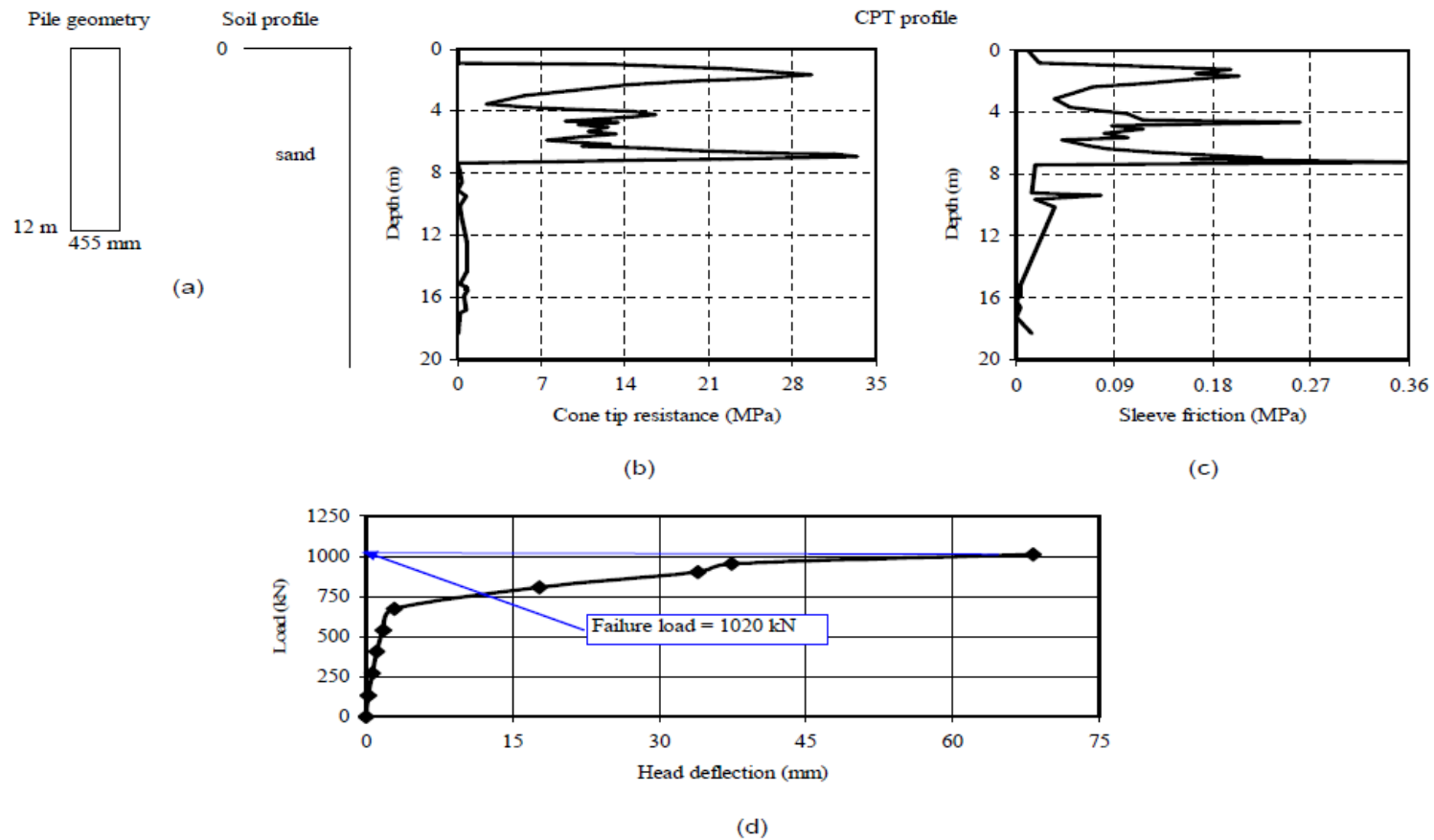


Figure C.12 Summary sheet for case record 12, (a) pile geometry and soil profile, (b) cone tip resistance profile, (c) sleeve friction profile, (d) load deflection plot

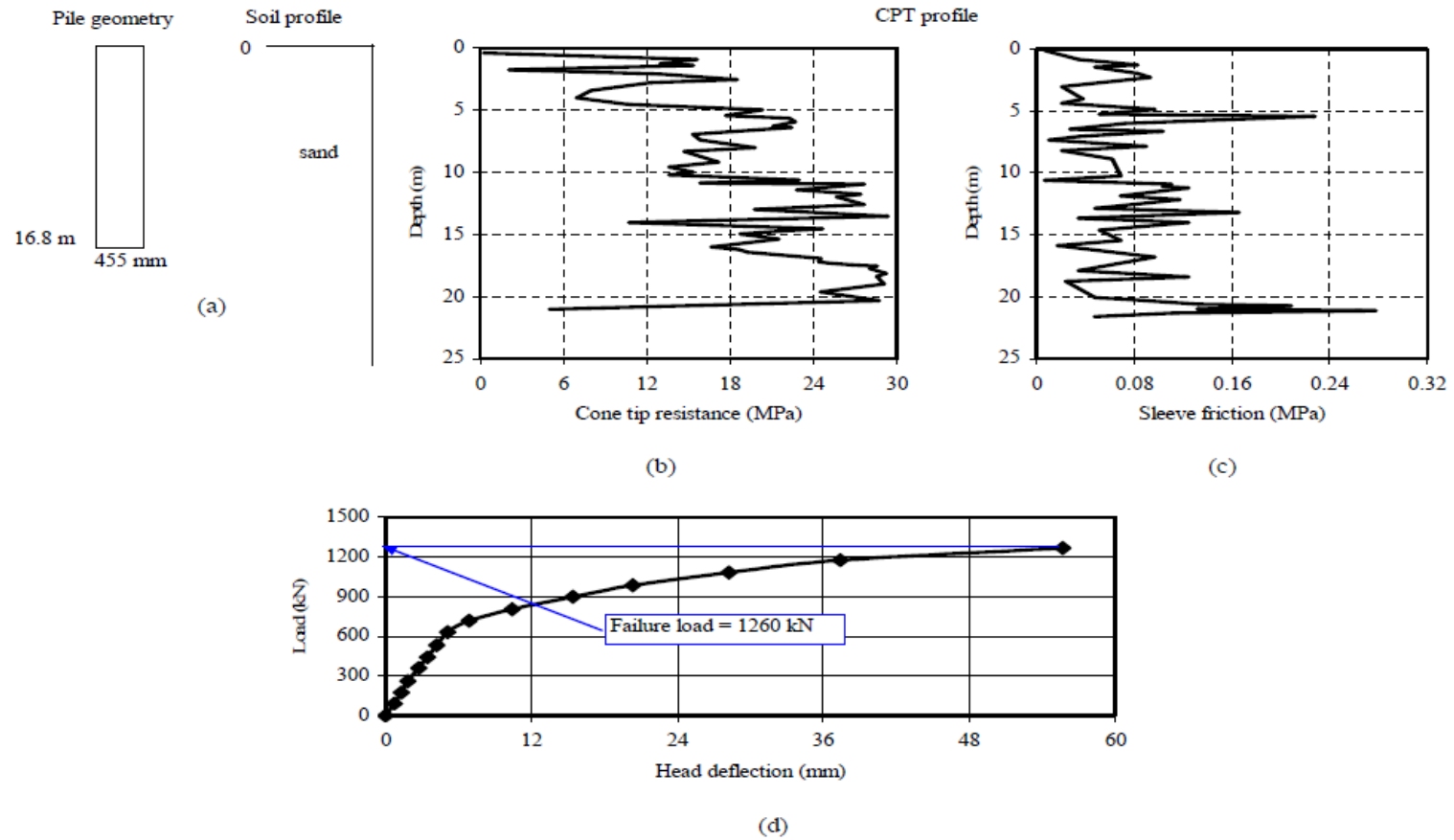


Figure C.13 Summary sheet for case record 13, (a) pile geometry and soil profile, (b) cone tip resistance profile, (c) sleeve friction profile, (d) load deflection plot

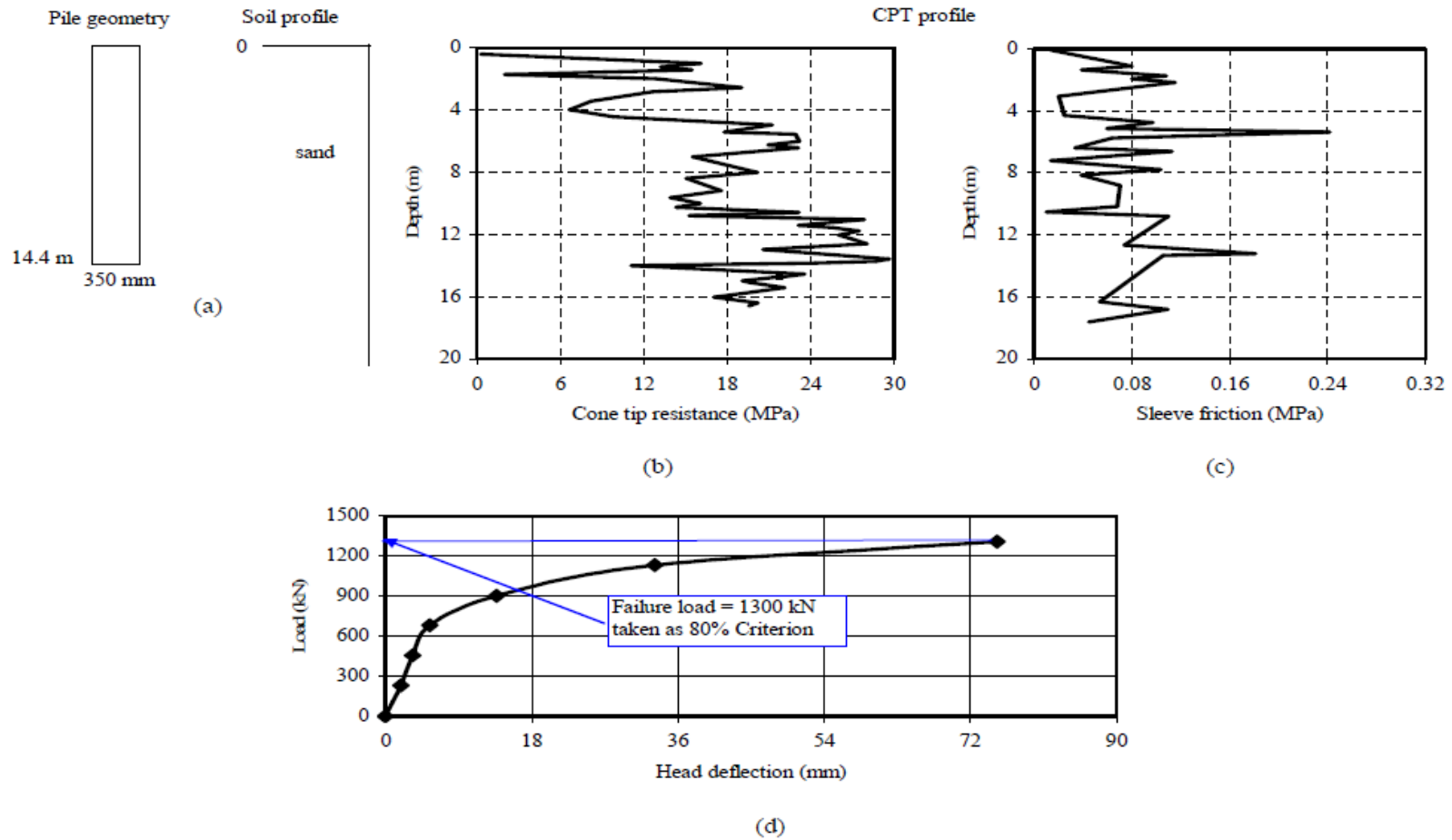


Figure C.14 Summary sheet for case record 14, (a) pile geometry and soil profile, (b) cone tip resistance profile, (c) sleeve friction profile, (d) load deflection plot

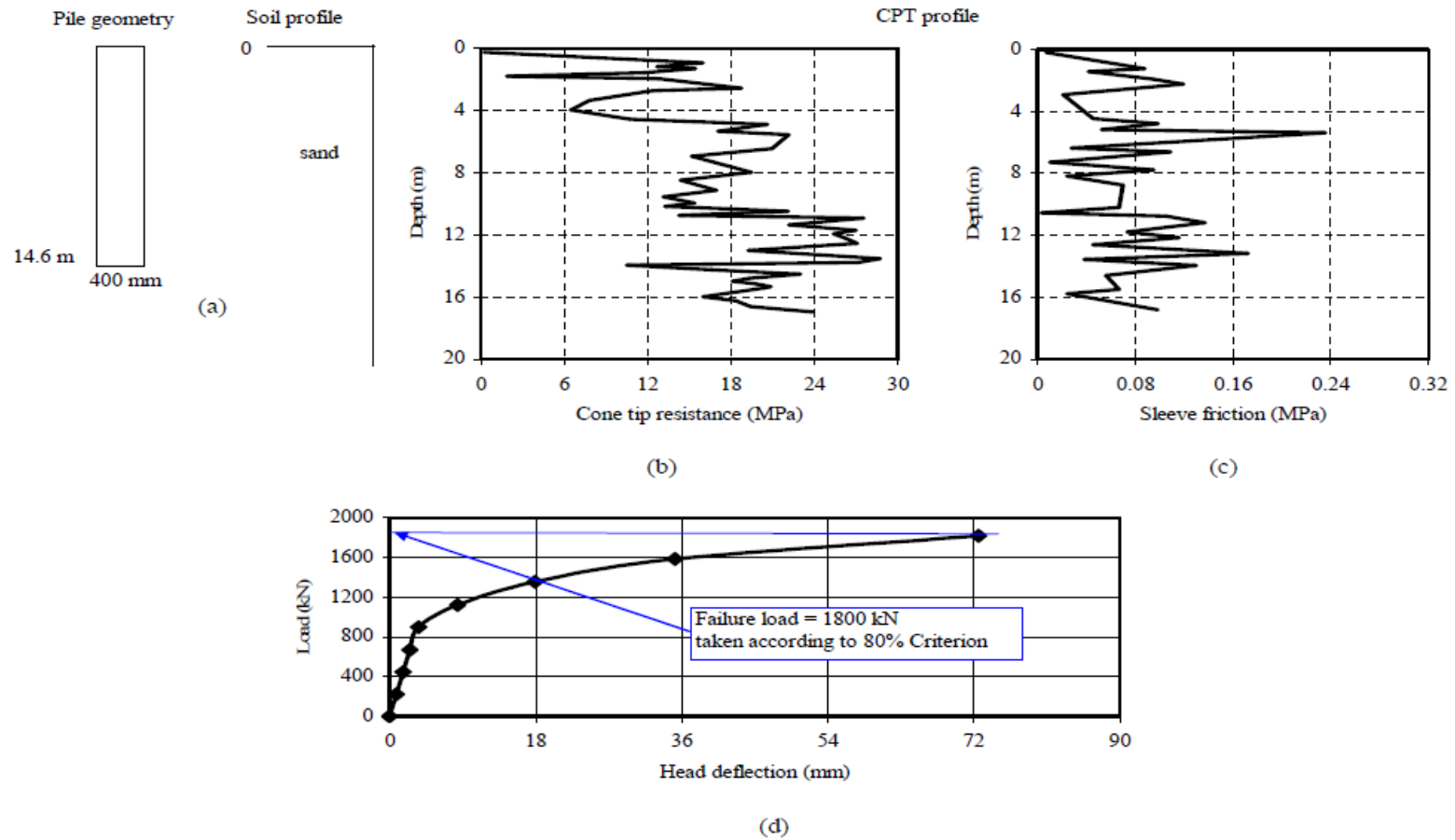


Figure C.15 Summary sheet for case record 15, (a) pile geometry and soil profile, (b) cone tip resistance profile, (c) sleeve friction profile, (d) load deflection plot

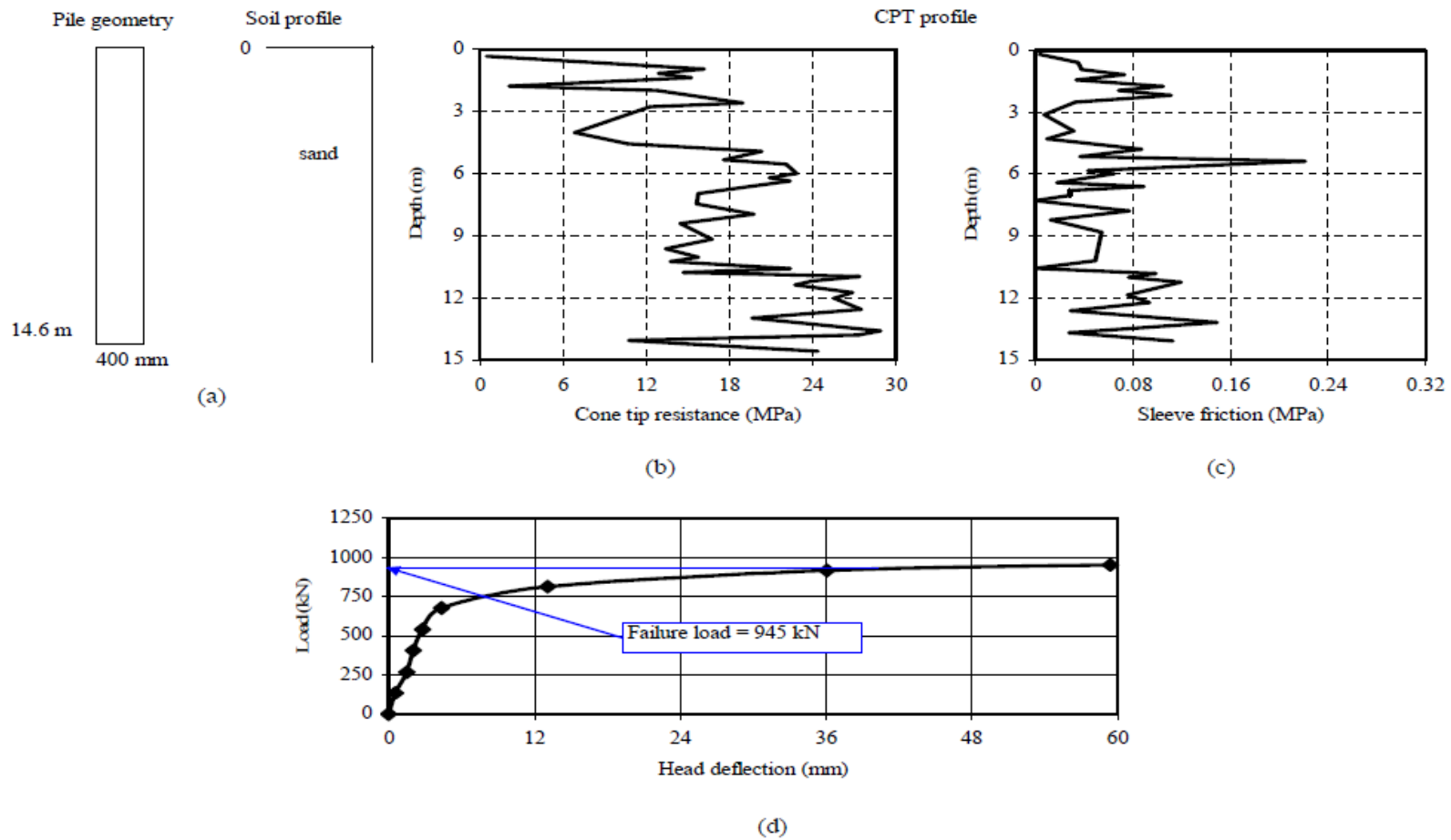


Figure C.16 Summary sheet for case record 16, (a) pile geometry and soil profile, (b) cone tip resistance profile, (c) sleeve friction profile, (d) load deflection plot

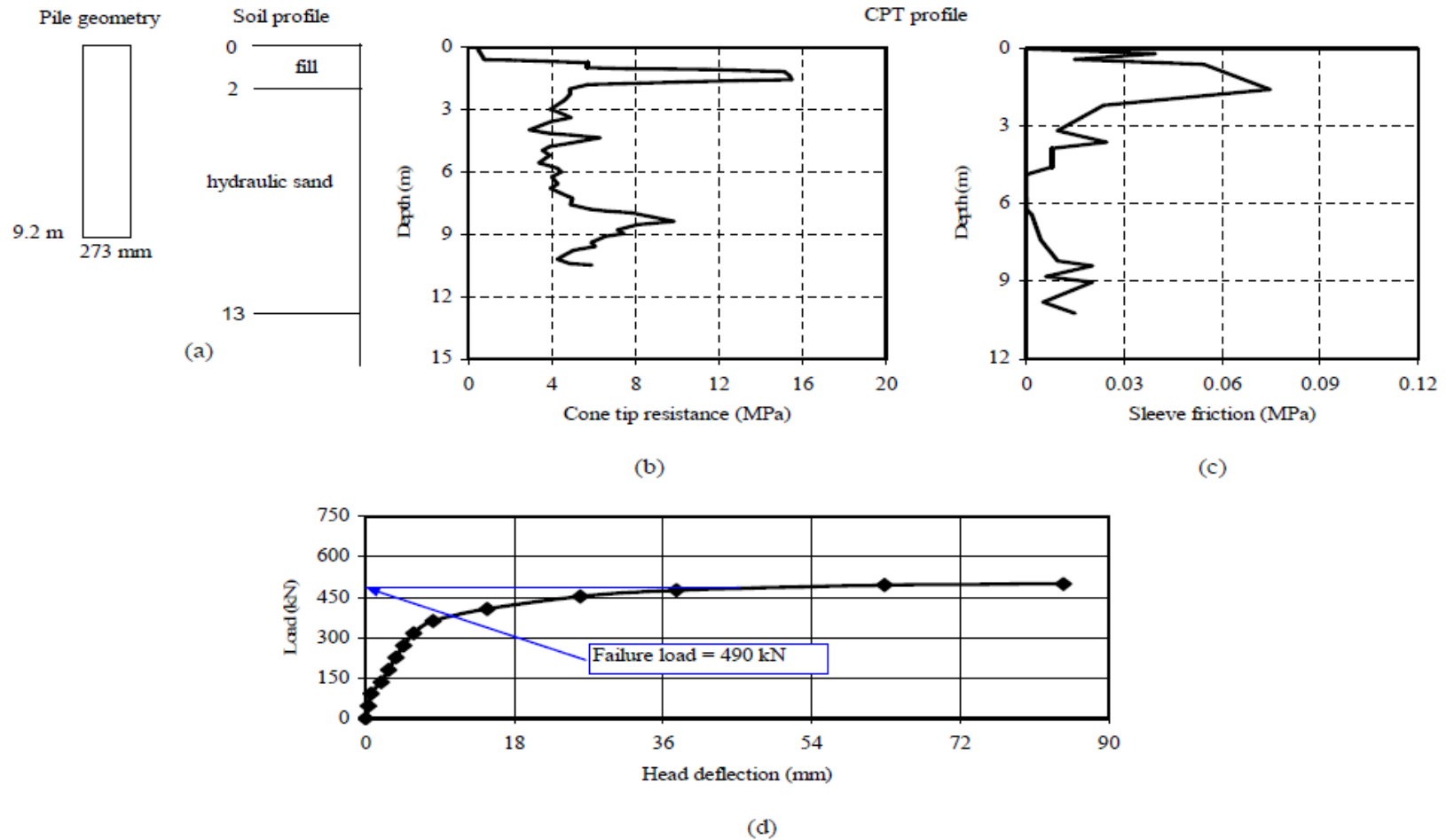


Figure C.17 Summary sheet for case record 17, (a) pile geometry and soil profile, (b) cone tip resistance profile, (c) sleeve friction profile, (d) load deflection plot

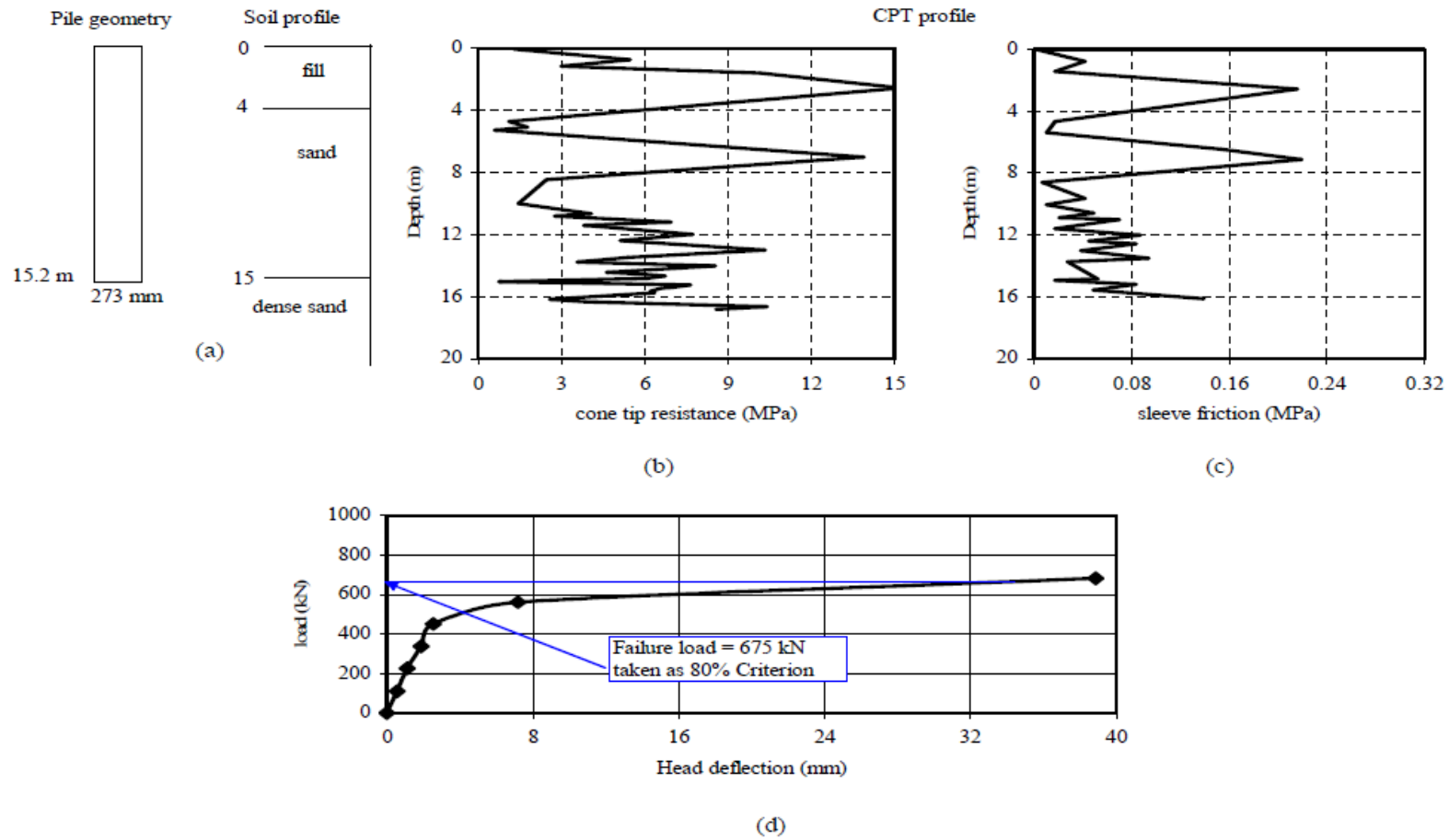


Figure C.18 Summary sheet for case record 18, (a) pile geometry and soil profile, (b) cone tip resistance profile, (c) sleeve friction profile, (d) load deflection plot

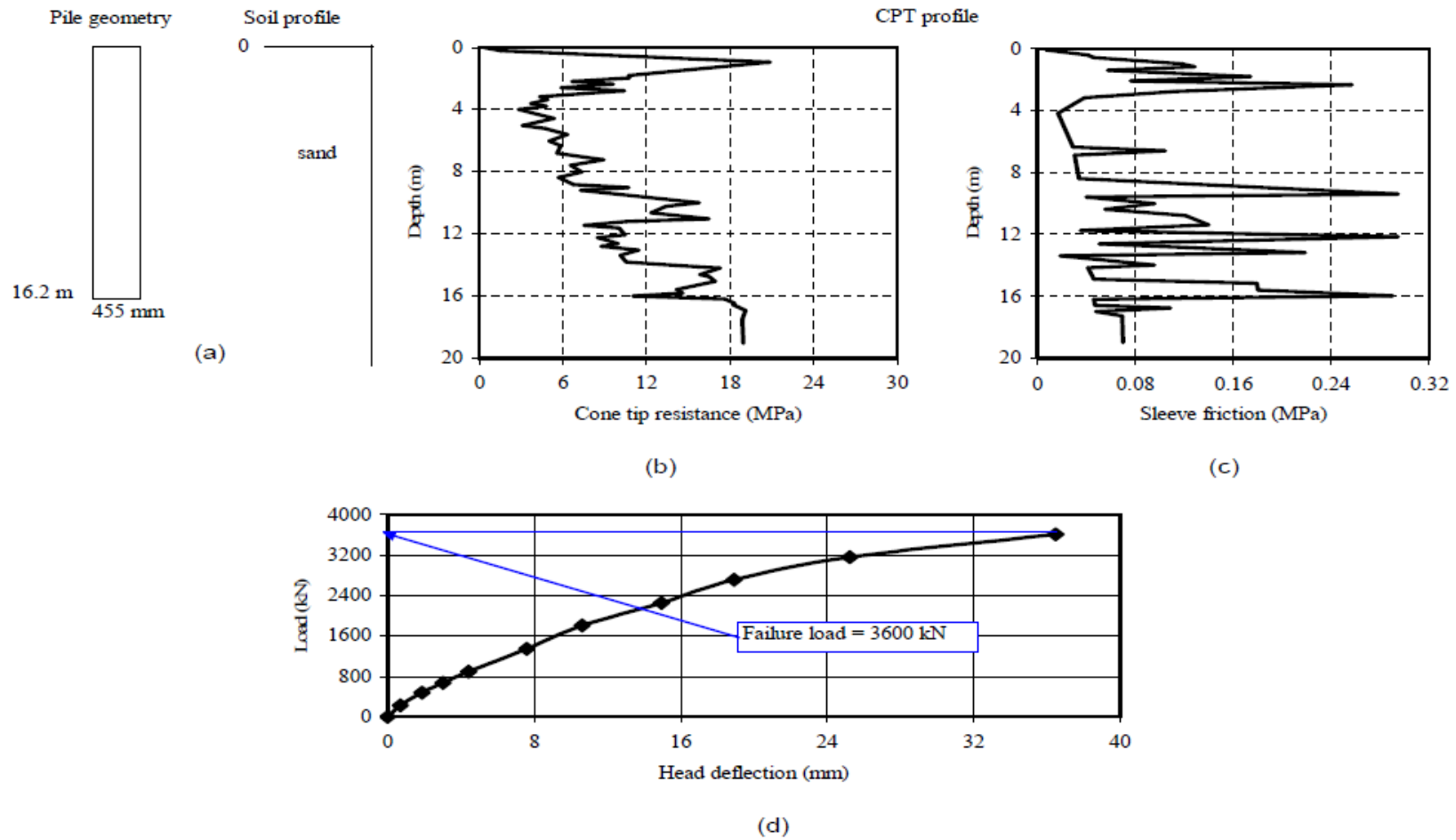


Figure C.19 Summary sheet for case record 19, (a) pile geometry and soil profile, (b) cone tip resistance profile, (c) sleeve friction profile, (d) load deflection plot

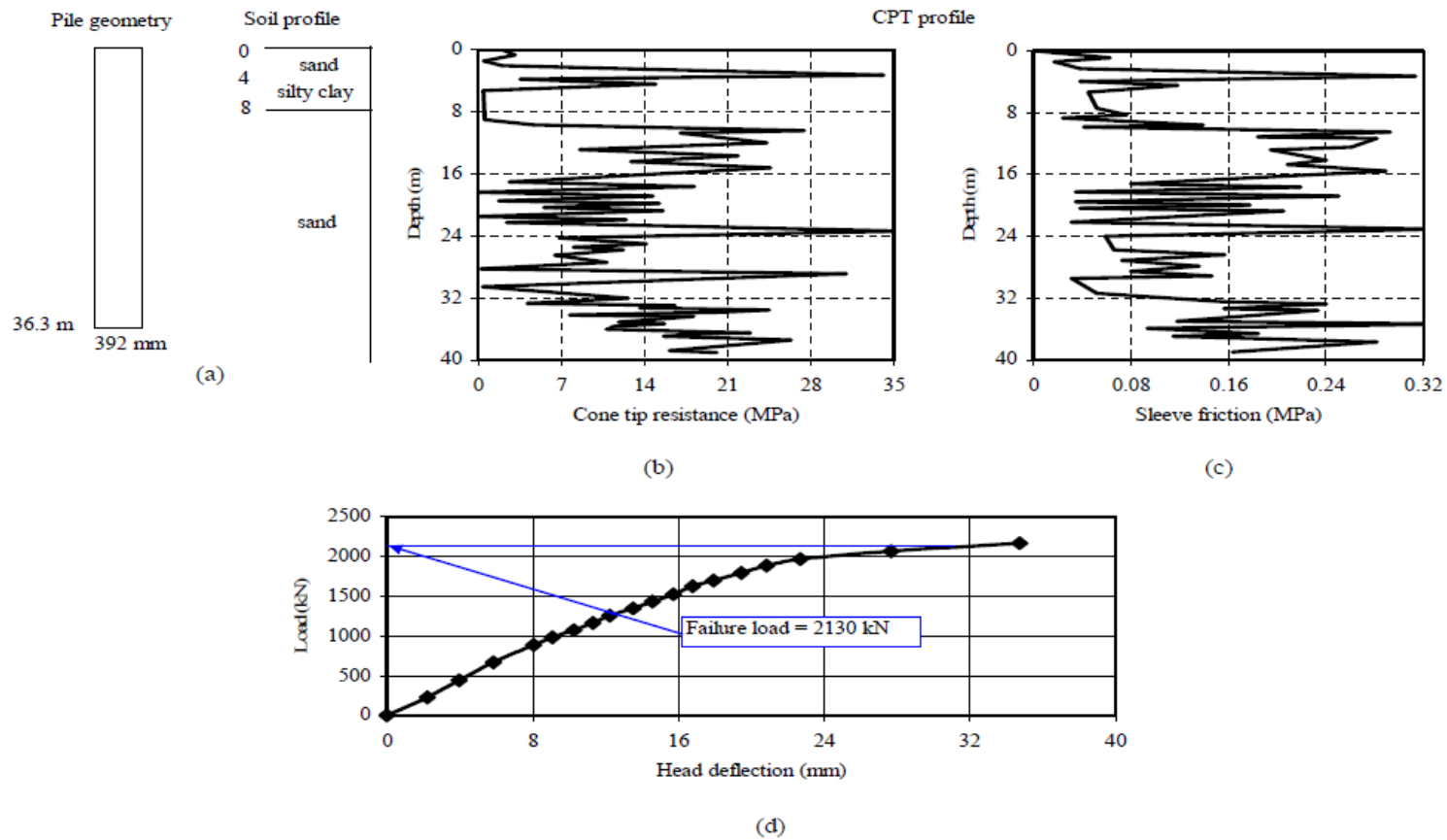


Figure C.20 Summary sheet for case record 20, (a) pile geometry and soil profile, (b) cone tip resistance profile, (c) sleeve friction profile, (d) load deflection plot

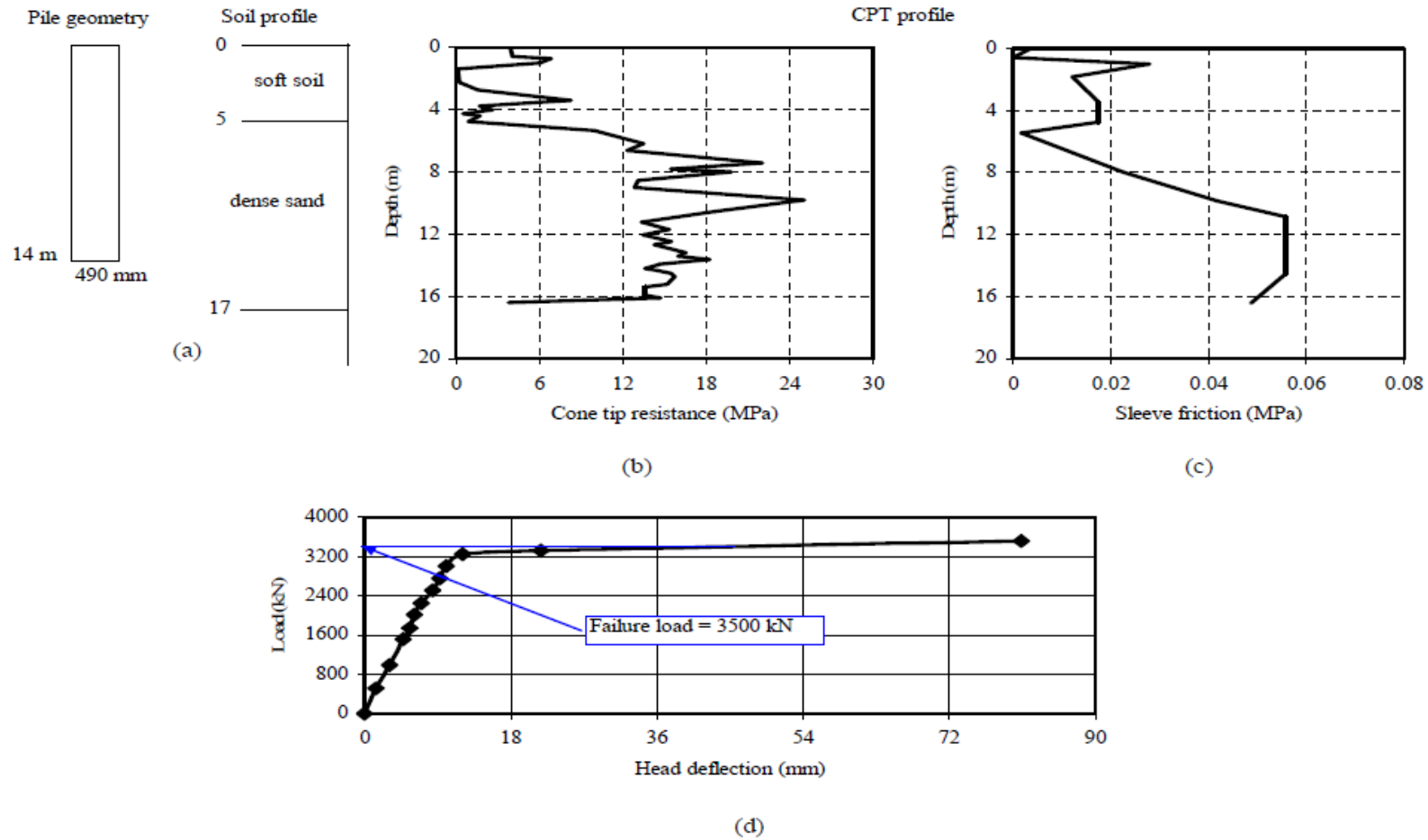


Figure C.21 Summary sheet for case record 21, (a) pile geometry and soil profile, (b) cone tip resistance profile, (c) sleeve friction profile, (d) load deflection plot

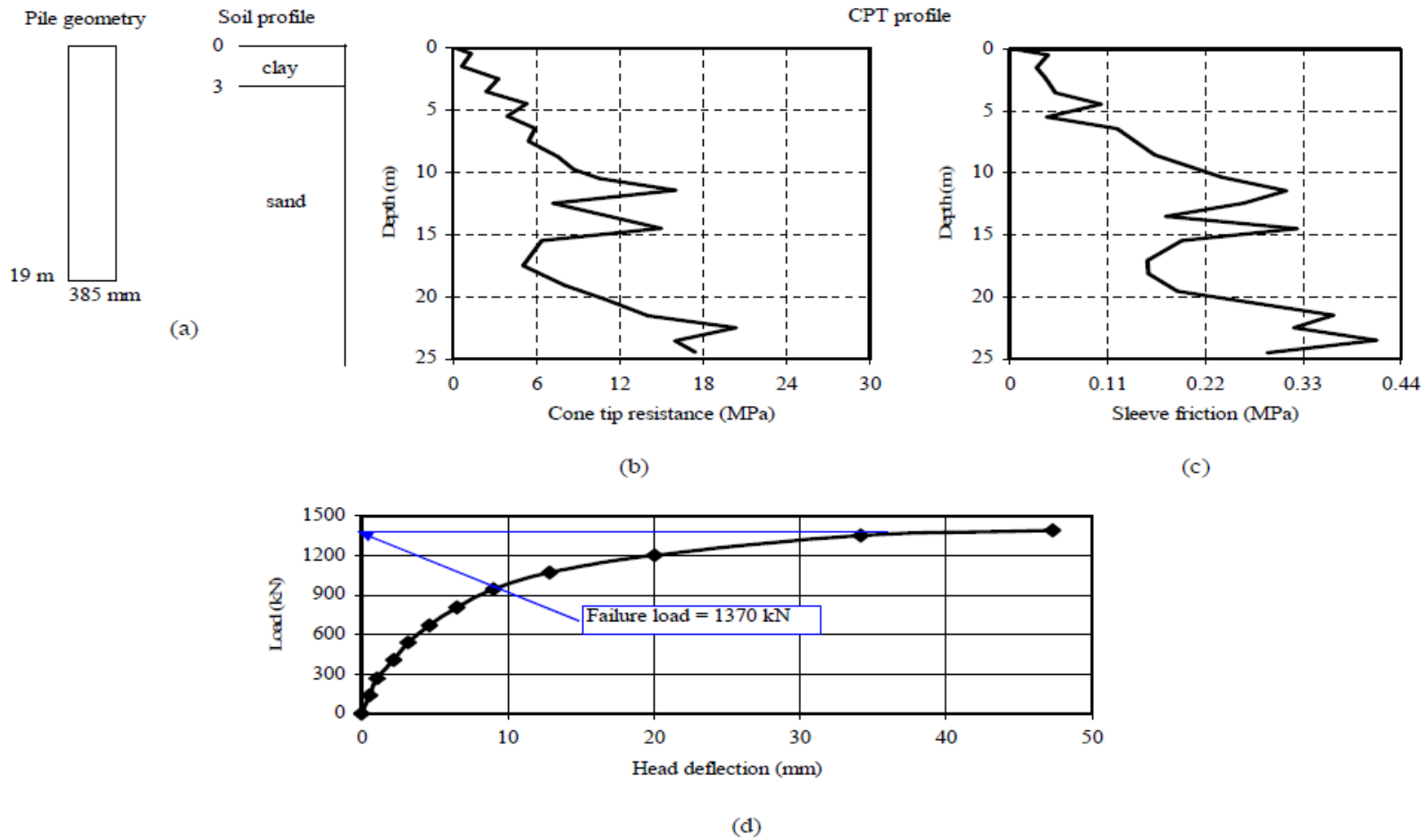


Figure C.22 Summary sheet for case record 22, (a) pile geometry and soil profile, (b) cone tip resistance profile, (c) sleeve friction profile, (d) load deflection plot

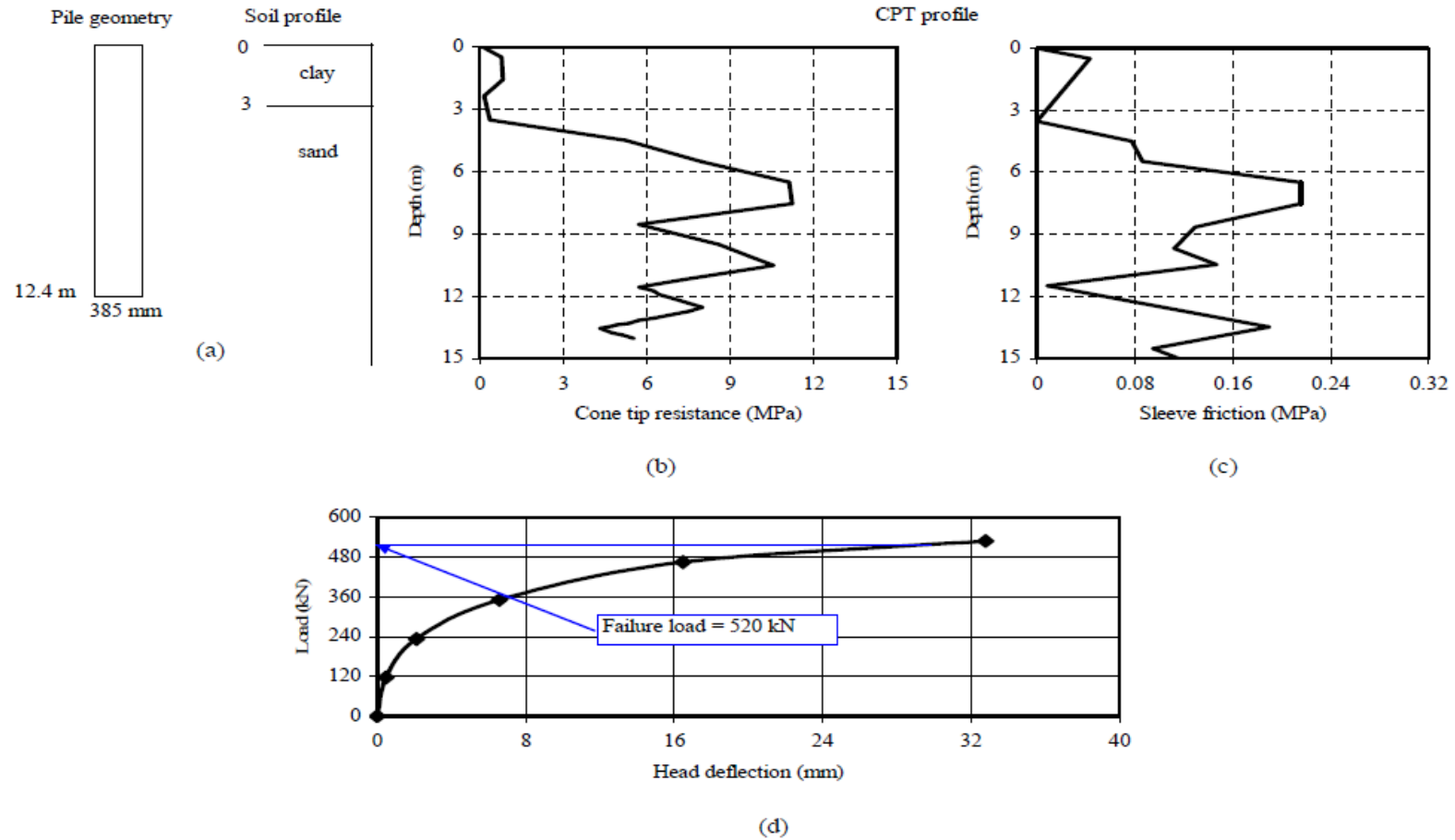


Figure C.23 Summary sheet for case record 23, (a) pile geometry and soil profile, (b) cone tip resistance profile, (c) sleeve friction profile, (d) load deflection plot

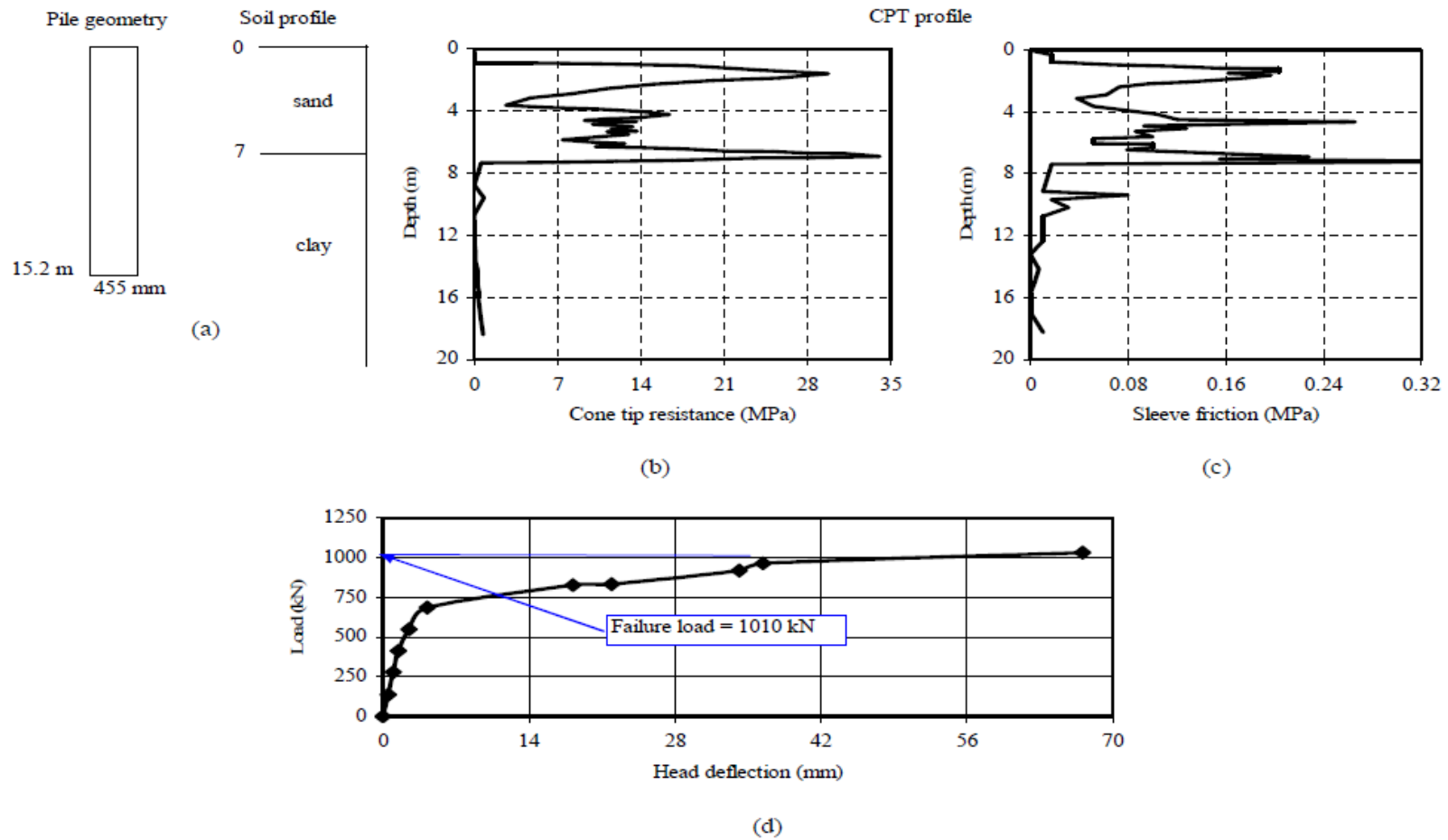


Figure C.24 Summary sheet for case record 24, (a) pile geometry and soil profile, (b) cone tip resistance profile, (c) sleeve friction profile, (d) load deflection plot

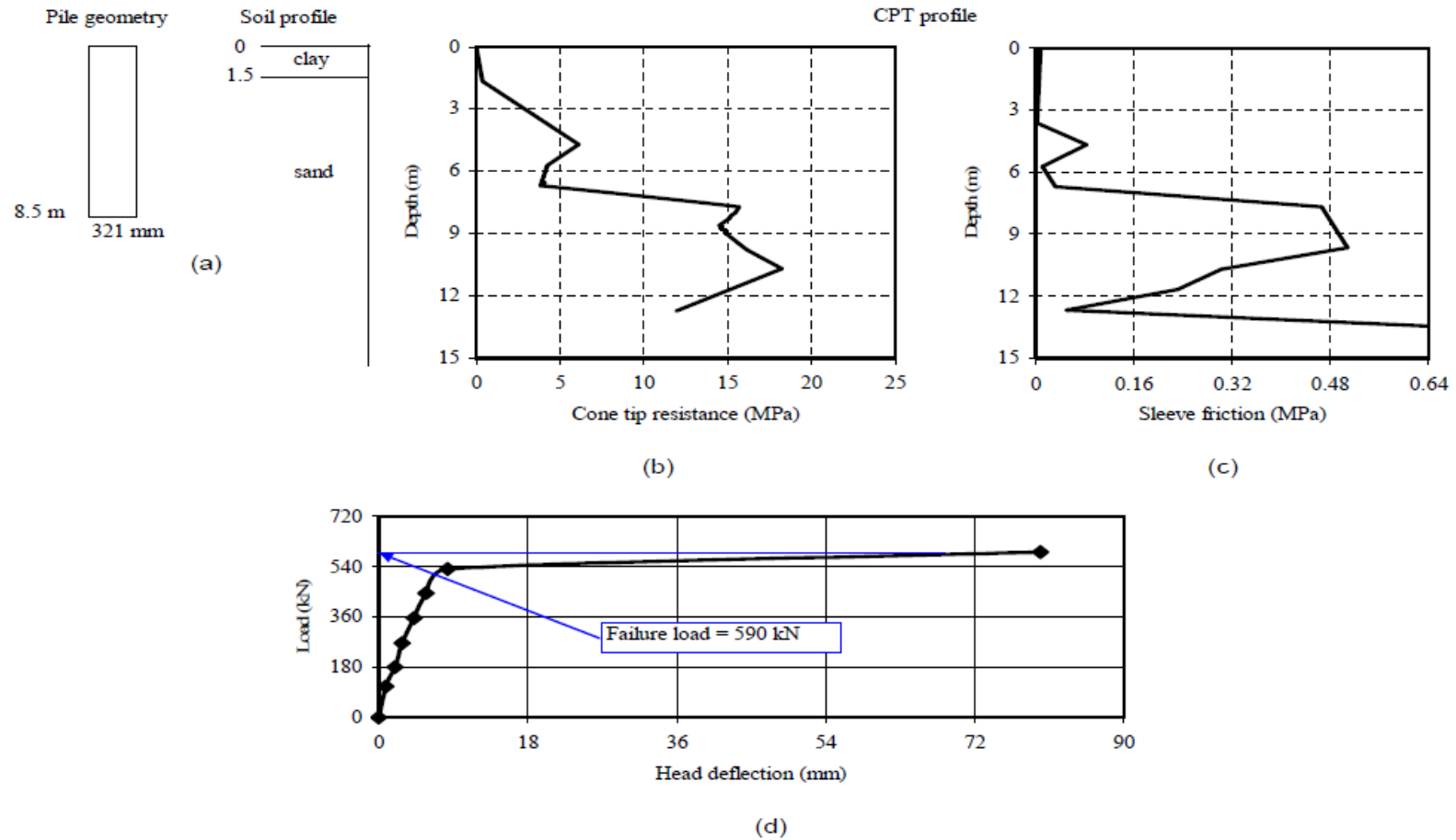


Figure C.25 Summary sheet for case record 25, (a) pile geometry and soil profile, (b) cone tip resistance profile, (c) sleeve friction profile, (d) load deflection plot

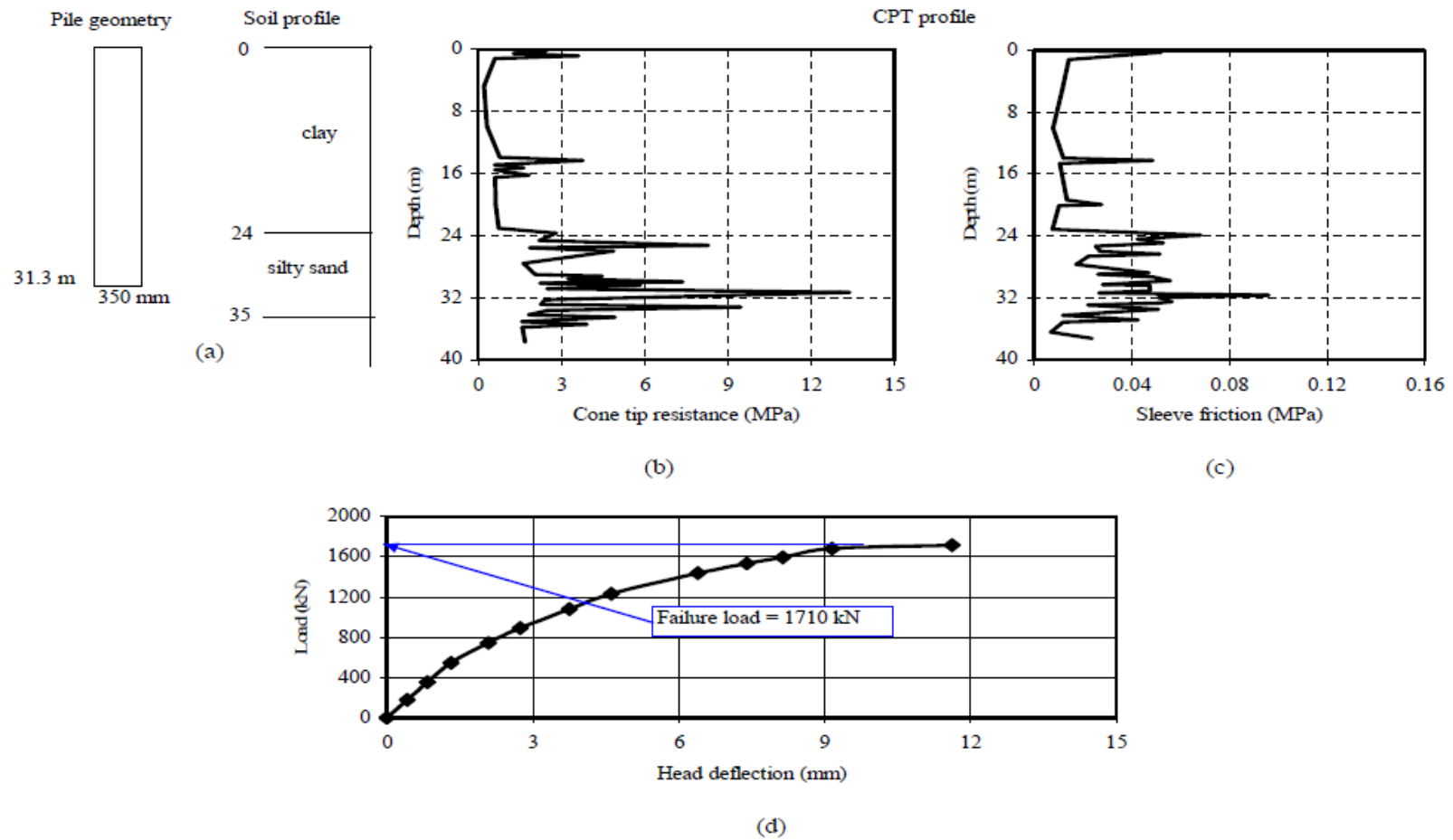


Figure C.26 Summary sheet for case record 26, (a) pile geometry and soil profile, (b) cone tip resistance profile, (c) sleeve friction profile, (d) load deflection plot

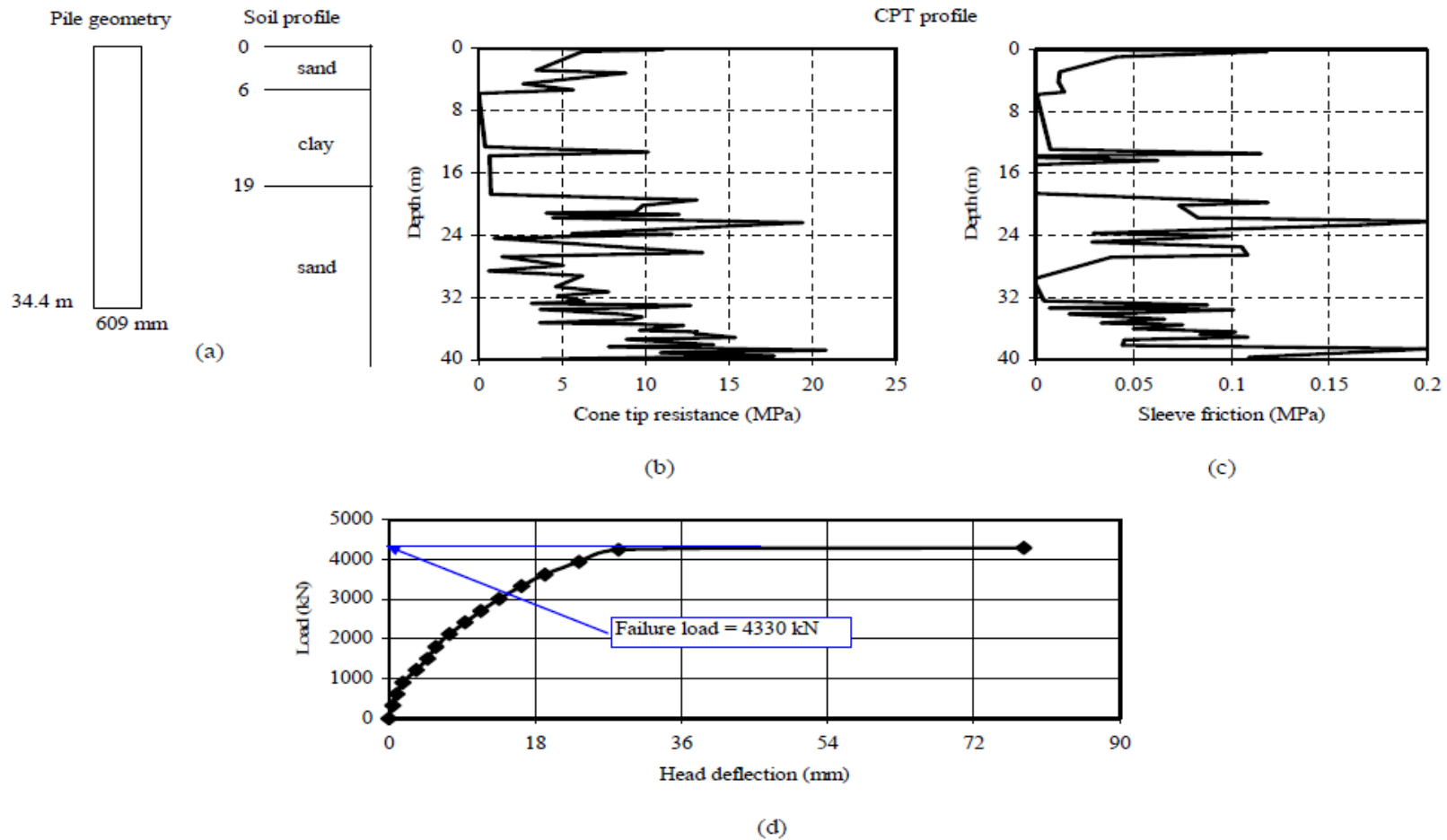


Figure C.27 Summary sheet for case record 27, (a) pile geometry and soil profile, (b) cone tip resistance profile, (c) sleeve friction profile, (d) load deflection plot

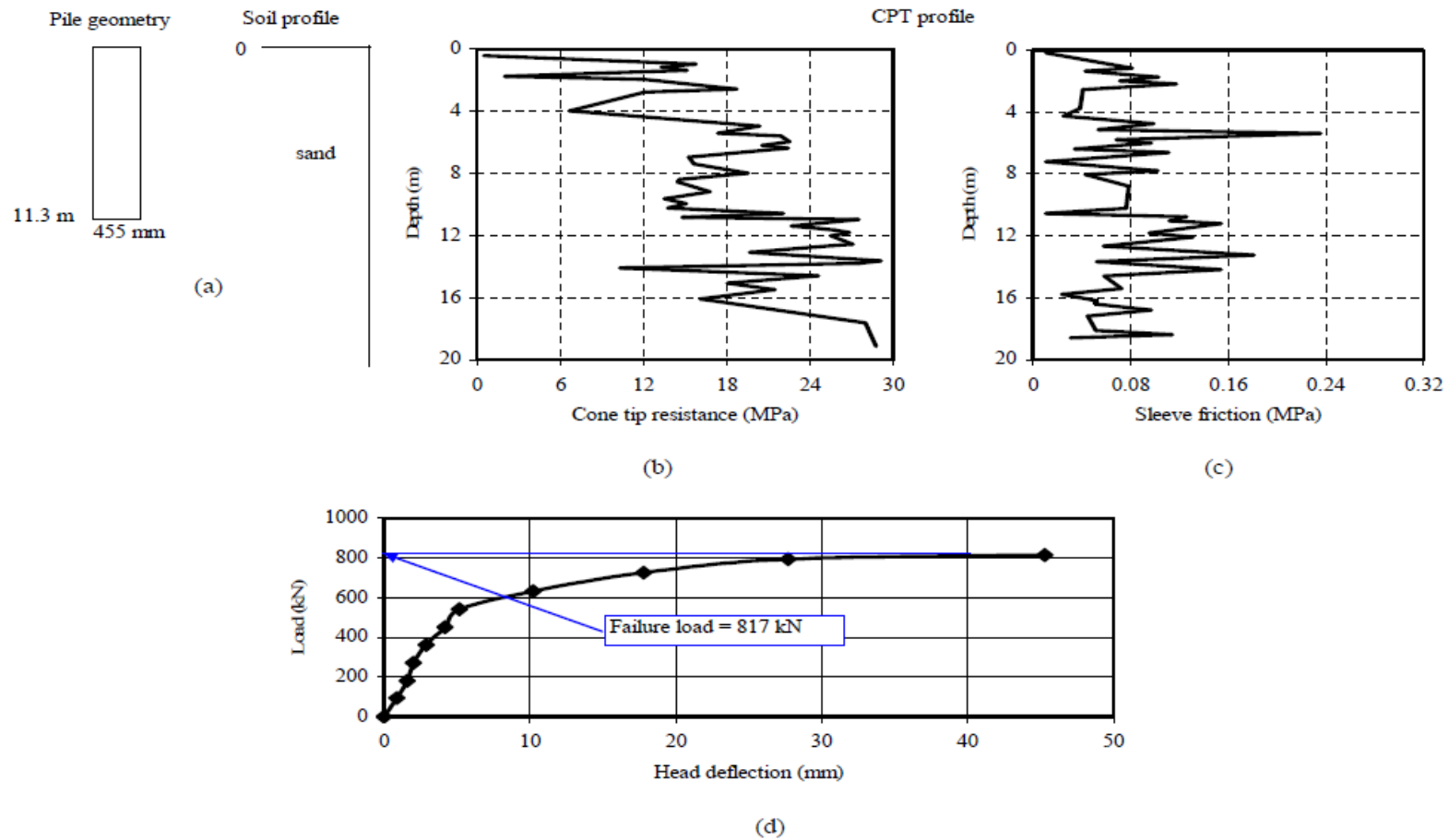


Figure C.28 Summary sheet for case record 28, (a) pile geometry and soil profile, (b) cone tip resistance profile, (c) sleeve friction profile, (d) load deflection plot

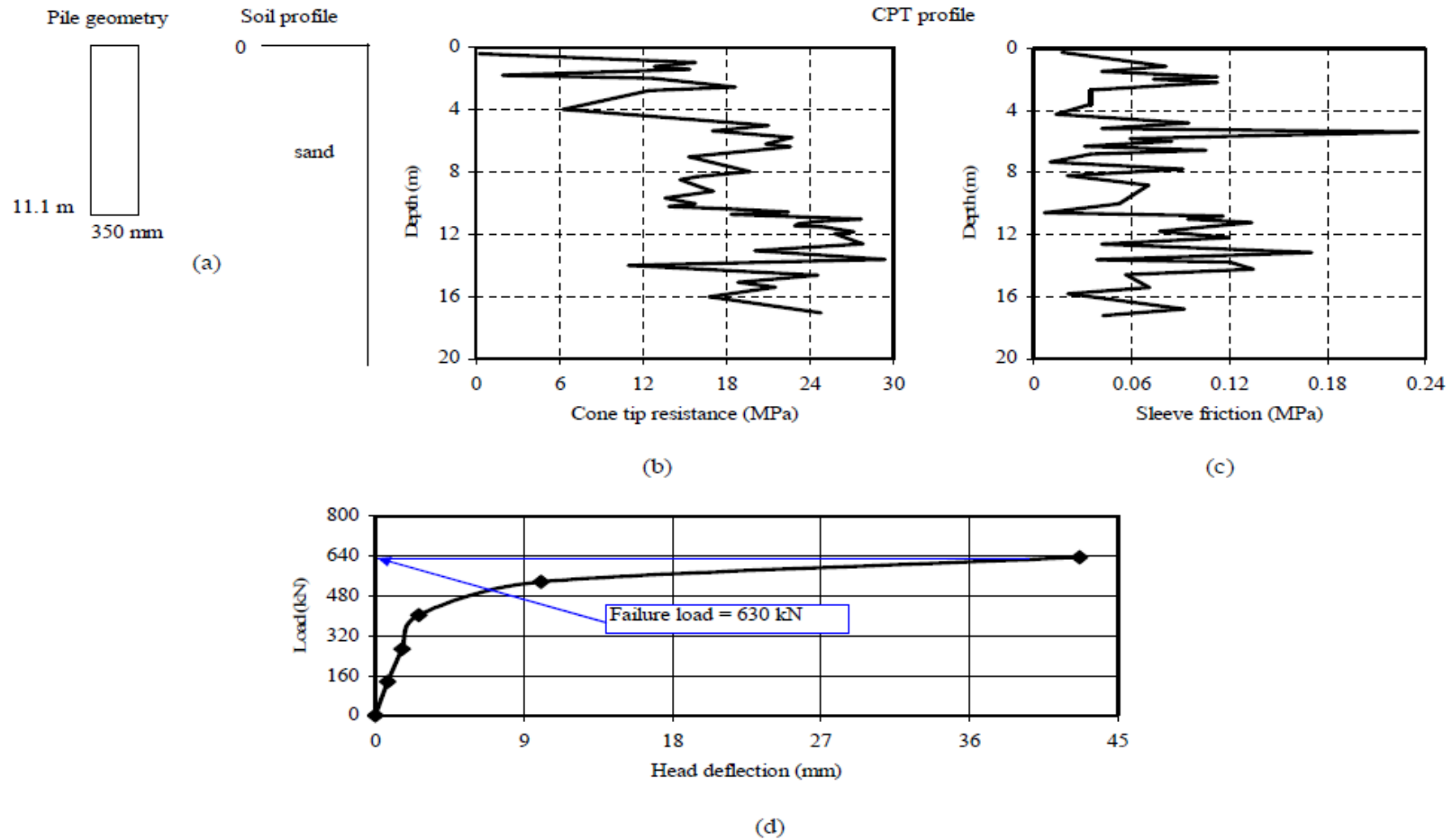


Figure C.29 Summary sheet for case record 29, (a) pile geometry and soil profile, (b) cone tip resistance profile, (c) sleeve friction profile, (d) load deflection plot

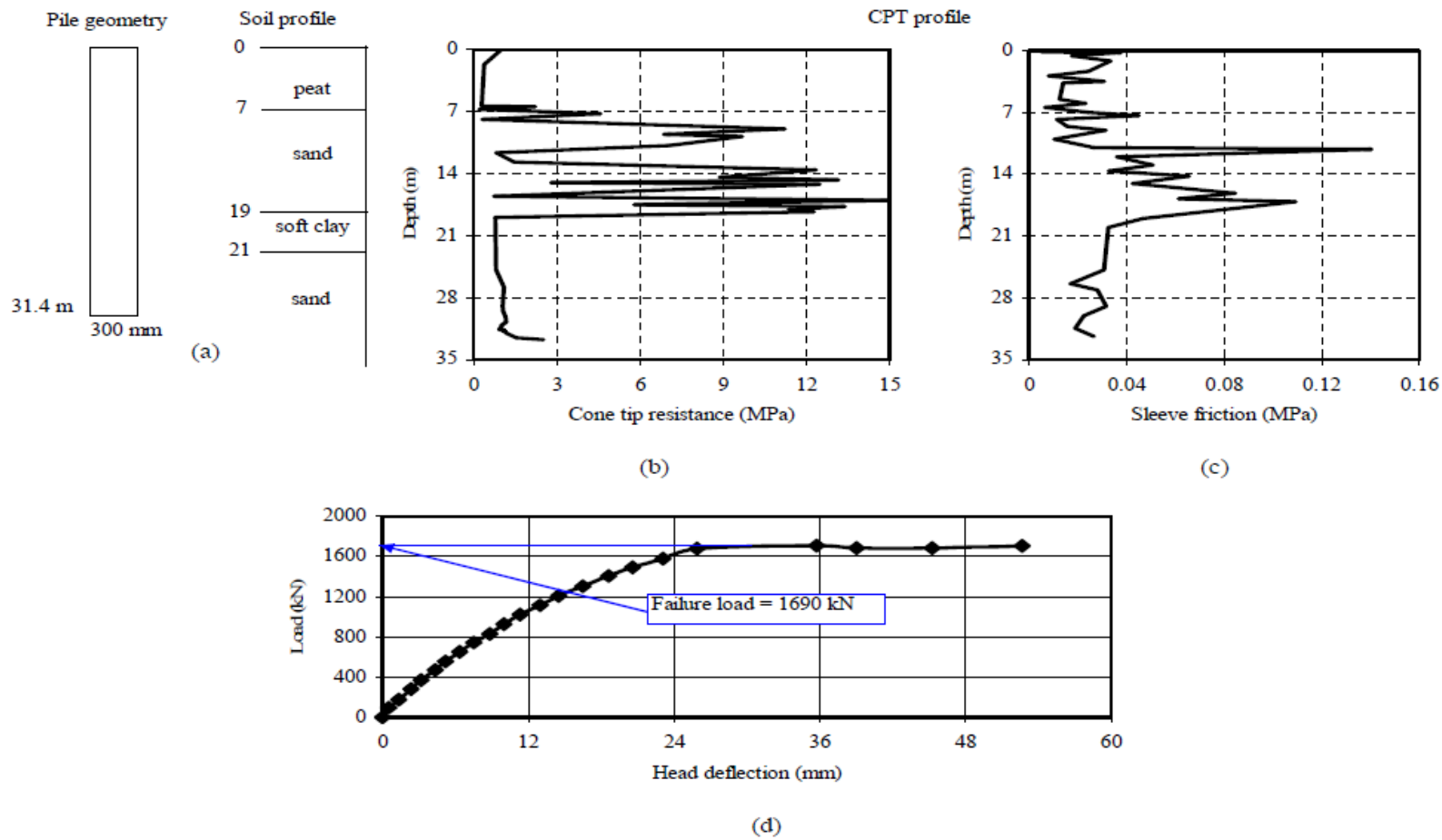


Figure C.30 Summary sheet for case record 30, (a) pile geometry and soil profile, (b) cone tip resistance profile, (c) sleeve friction profile, (d) load deflection plot

Appendix D - Permissions from Copyright Owners

Re: Getting Permission to Use References

iyad.alkroosh@qu.edu.iq

Thu 14/11/2019 12:53 PM

To: Reza Yadak <reza.yadak@postgrad.curtin.edu.au>

On 2019-11-12 19:06, Reza Yadak wrote:

> Dear Dr Iyad,
>
> I wish my email finds you well.
>
> I'm writing to get permission to use some parts of the following
> articles and thesis, submitted by you, as references in my thesis.
> Below are titles:
>
> 1- Alkroosh I, Shahin M, Nikraz H, editors. Modelling load-settlement
> curves of behaviour bored piles using artificial neural networks.
> Proceedings of the 14th Danube-European Conference on Geotechnical
> Engineering; 2010: Slovak University of Technology.
>
> 2- Alkroosh I, Nikraz H. Evaluation of pile lateral capacity in clay
> applying evolutionary approach. International Journal of GEOMATE.
> 2013;4(1):462-5.
>
> 3- Alkroosh ISJ. Modelling pile capacity and load-settlement
> behaviour of piles embedded in sand & mixed soils using artificial
> intelligence: Curtin University; 2011.
>
> 4- Alkroosh I, Bahadori M, Nikraz H, Bahadori A. Regressive approach
> for predicting bearing capacity of bored piles from cone penetration
> test data. Journal of rock mechanics and geotechnical engineering.
> 2015; 7(5):584-92.
>
> My thesis title is: "Comparing CPT Results and Numerical Method
> Investigations to Assess the Behavior of Pile and Sand and Mixed Soil
> Using ABAQUS"
> under the supervision of Dr Amin Chegenizadeh and Co-supervisory of
> Professor Hamid Nikraz at Curtin University.
>
> Thank you in advance for your authorisation and I look forward to
> hearing from you.
>
> Best Regards
>
> Reza Yadak
Dear Reza,

Thanks for your email. Yes you can.

Regards

Iyad

**Canadian Science Publishing LICENSE
TERMS AND CONDITIONS**

Oct 02, 2019

This is a License Agreement between Reza Yadak ("You") and Canadian Science Publishing ("Canadian Science Publishing") provided by Copyright Clearance Center ("CCC"). The license consists of your order details, the terms and conditions provided by Canadian Science Publishing, and the payment terms and conditions.

All payments must be made in full to CCC. For payment instructions, please see information listed at the bottom of this form.

License Number	4681100031562
License date	Oct 01, 2019
Licensed content publisher	Canadian Science Publishing
Licensed content title	Canadian geotechnical journal : Revue canadienne de géotechnique
Licensed content date	Jan 1, 1963
Type of Use	Thesis/Dissertation
Requestor type	Author of requested content
Format	Print, Electronic
Portion	chapter/article
The requesting person/organization is:	Reza Yadak
Title or numeric reference of the portion(s)	Chapter 2, Literature Review, PhD Thesis, Paraphrased
Title of the article or chapter the portion is from	Intelligent computing for modeling axial capacity of pile foundations
Editor of portion(s)	N/A
Author of portion(s)	Shahin, Mohamed A.
Volume of serial or monograph.	47
Issue, if republishing an article from a serial	2
Page range of the portion	
Publication date of portion	Feb 10, 2010
Rights for	Main product
Duration of use	Current edition and up to 10 years
Creation of copies for the disabled	no
With minor editing privileges	yes
For distribution to	Worldwide
In the following language(s)	Original language of publication
With incidental promotional use	no
The lifetime unit quantity of new product	Up to 999
Title	Comparing CPT Results and Numerical Method Investigations to Assess the Interaction between Pile and Sand & Mixed Soils Using ABAQUS, with a Brief Review of ANNs and GEP Methods

Institution name	Curtinuniversity
Expected presentation date	Dec 2019
Billing Type	Invoice
Billing Address	Reza Yadak 633a 80 Stirling Street CampusPerth
	Perth, Australia 6000 Attn: Reza Yadak
Total (may include CCC user fee)	0.00 USD

Terms and Conditions

TERMS AND CONDITIONS

The following terms are individual to this publisher:

None

Other Terms and Conditions:

STANDARD TERMS AND CONDITIONS

1. Description of Service; Defined Terms. This Republication License enables the User to obtain licenses for republication of one or more copyrighted works as described in detail on the relevant Order Confirmation (the "Work(s)"). Copyright Clearance Center, Inc. ("CCC") grants licenses through the Service on behalf of the rightsholder identified on the Order Confirmation (the "Rightsholder"). "Republication", as used herein, generally means the inclusion of a Work, in whole or in part, in a new work or works, also as described on the Order Confirmation. "User", as used herein, means the person or entity making such republication.

2. The terms set forth in the relevant Order Confirmation, and any terms set by the Rightsholder with respect to a particular Work, govern the terms of use of Works in connection with the Service. By using the Service, the person transacting for a republication license on behalf of the User represents and warrants that he/she/it (a) has been duly authorized by the User to accept, and hereby does accept, all such terms and conditions on behalf of User, and (b) shall inform User of all such terms and conditions. In the event such person is a "freelancer" or other third party independent of User and CCC, such party shall be deemed jointly a "User" for purposes of these terms and conditions. In any event, User shall be deemed to have accepted and agreed to all such terms and conditions if User republishes the Work in any fashion.

3. Scope of License; Limitations and Obligations.

3.1 All Works and all rights therein, including copyright rights, remain the sole and exclusive property of the Rightsholder. The license created by the exchange of an Order Confirmation (and/or any invoice) and payment by User of the full amount set forth on that document includes only those rights expressly set forth in the Order Confirmation and in these terms and conditions, and conveys no other rights in the Work(s) to User. All rights not expressly granted are hereby reserved.

3.2 General Payment Terms: You may pay by credit card or through an account with us payable at the end of the month. If you and we agree that you may establish a standing account with CCC, then the following terms apply: Remit Payment to: Copyright Clearance Center, 29118 Network Place, Chicago, IL 60673-1291. Payments Due: Invoices are payable upon their delivery to you (or upon our notice to you that they are available to you for downloading). After 30 days, outstanding amounts will be subject to a service charge of 1-1/2% per month or, if less, the maximum rate allowed by applicable law. Unless otherwise specifically set forth in the Order Confirmation or in a separate written agreement signed by CCC, invoices are due and payable on "net 30" terms. While User may exercise the rights licensed immediately upon issuance of the Order Confirmation, the license is automatically revoked and is null and void, as if it had never been issued, if complete payment for the license is not received on a timely basis either from User directly or through a payment agent, such as a credit card company.

3.3 Unless otherwise provided in the Order Confirmation, any grant of rights to User (i) is "one-time" (including the editions and product family specified in the license), (ii) is non-

exclusive and non-transferable and (iii) is subject to any and all limitations and restrictions (such as, but not limited to, limitations on duration of use or circulation) included in the Order Confirmation or invoice and/or in these terms and conditions. Upon completion of the licensed use, User shall either secure a new permission for further use of the Work(s) or immediately cease any new use of the Work(s) and shall render inaccessible (such as by deleting or by removing or severing links or other locators) any further copies of the Work (except for copies printed on paper in accordance with this license and still in User's stock at the end of such period).

3.4 In the event that the material for which a republication license is sought includes third party materials (such as photographs, illustrations, graphs, inserts and similar materials) which are identified in such material as having been used by permission, User is responsible for identifying, and seeking separate licenses (under this Service or otherwise) for, any of such third party materials; without a separate license, such third party materials may not be used.

3.5 Use of proper copyright notice for a Work is required as a condition of any license granted under the Service. Unless otherwise provided in the Order Confirmation, a proper copyright notice will read substantially as follows: "Republished with permission of [Rightsholder's name], from [Work's title, author, volume, edition number and year of copyright]; permission conveyed through Copyright Clearance Center, Inc." Such notice must be provided in a reasonably legible font size and must be placed either immediately adjacent to the Work as used (for example, as part of a by-line or footnote but not as a separate electronic link) or in the place where substantially all other credits or notices for the new work containing the republished Work are located. Failure to include the required notice results in loss to the Rightsholder and CCC, and the User shall be liable to pay liquidated damages for each such failure equal to twice the use fee specified in the Order Confirmation, in addition to the use fee itself and any other fees and charges specified.

3.6 User may only make alterations to the Work if and as expressly set forth in the Order Confirmation. No Work may be used in any way that is defamatory, violates the rights of third parties (including such third parties' rights of copyright, privacy, publicity, or other tangible or intangible property), or is otherwise illegal, sexually explicit or obscene. In addition, User may not conjoin a Work with any other material that may result in damage to the reputation of the Rightsholder. User agrees to inform CCC if it becomes aware of any infringement of any rights in a Work and to cooperate with any reasonable request of CCC or the Rightsholder in connection therewith.

4. Indemnity. User hereby indemnifies and agrees to defend the Rightsholder and CCC, and their respective employees and directors, against all claims, liability, damages, costs and expenses, including legal fees and expenses, arising out of any use of a Work beyond the scope of the rights granted herein, or any use of a Work which has been altered in any unauthorized way by User, including claims of defamation or infringement of rights of copyright, publicity, privacy or other tangible or intangible property.

5. Limitation of Liability. UNDER NO CIRCUMSTANCES WILL CCC OR THE RIGHTSHOLDER BE LIABLE FOR ANY DIRECT, INDIRECT, CONSEQUENTIAL OR INCIDENTAL DAMAGES (INCLUDING WITHOUT LIMITATION DAMAGES FOR LOSS OF BUSINESS PROFITS OR INFORMATION, OR FOR BUSINESS INTERRUPTION) ARISING OUT OF THE USE OR INABILITY TO USE A WORK, EVEN IF ONE OF THEM HAS BEEN ADVISED OF THE POSSIBILITY OF SUCH DAMAGES. In any event, the total liability of the Rightsholder and CCC (including their respective employees and directors) shall not exceed the total amount actually paid by User for this license. User assumes full liability for the actions and omissions of its principals, employees, agents, affiliates, successors and assigns.

6. Limited Warranties. THE WORK(S) AND RIGHT(S) ARE PROVIDED "AS IS". CCC HAS THE RIGHT TO GRANT TO USER THE RIGHTS GRANTED IN THE ORDER CONFIRMATION DOCUMENT. CCC AND THE RIGHTSHOLDER DISCLAIM ALL OTHER WARRANTIES RELATING TO THE WORK(S) AND RIGHT(S), EITHER EXPRESS OR IMPLIED, INCLUDING WITHOUT LIMITATION IMPLIED WARRANTIES OF MERCHANTABILITY OR FITNESS FOR A PARTICULAR PURPOSE. ADDITIONAL RIGHTS MAY BE REQUIRED TO USE ILLUSTRATIONS, GRAPHS, PHOTOGRAPHS, ABSTRACTS, INSERTS OR OTHER PORTIONS OF THE

WORK (AS OPPOSED TO THE ENTIRE WORK) IN A MANNER CONTEMPLATED BY USER; USER UNDERSTANDS AND AGREES THAT NEITHER CCC NOR THE RIGHTSHOLDER MAY HAVE SUCH ADDITIONAL RIGHTS TO GRANT.

7. Effect of Breach. Any failure by User to pay any amount when due, or any use by User of a Work beyond the scope of the license set forth in the Order Confirmation and/or these terms and conditions, shall be a material breach of the license created by the Order Confirmation and these terms and conditions. Any breach not cured within 30 days of written notice thereof shall result in immediate termination of such license without further notice. Any unauthorized (but licensable) use of a Work that is terminated immediately upon notice thereof may be liquidated by payment of the Rightsholder's ordinary license price therefor; any unauthorized (and unlicensable) use that is not terminated immediately for any reason (including, for example, because materials containing the Work cannot reasonably be recalled) will be subject to all remedies available at law or in equity, but in no event to a payment of less than three times the Rightsholder's ordinary license price for the most closely analogous licensable use plus Rightsholder's and/or CCC's costs and expenses incurred in collecting such payment.

8. Miscellaneous.

8.1 User acknowledges that CCC may, from time to time, make changes or additions to the Service or to these terms and conditions, and CCC reserves the right to send notice to the User by electronic mail or otherwise for the purposes of notifying User of such changes or additions; provided that any such changes or additions shall not apply to permissions already secured and paid for.

8.2 Use of User-related information collected through the Service is governed by CCC's privacy policy, available online here:

<http://www.copyright.com/content/cc3/en/tools/footer/privacypolicy.html>.

8.3 The licensing transaction described in the Order Confirmation is personal to User. Therefore, User may not assign or transfer to any other person (whether a natural person or an organization of any kind) the license created by the Order Confirmation and these terms and conditions or any rights granted hereunder; provided, however, that User may assign such license in its entirety on written notice to CCC in the event of a transfer of all or substantially all of User's rights in the new material which includes the Work(s) licensed under this Service.

8.4 No amendment or waiver of any terms is binding unless set forth in writing and signed by the parties. The Rightsholder and CCC hereby object to any terms contained in any writing prepared by the User or its principals, employees, agents or affiliates and purporting to govern or otherwise relate to the licensing transaction described in the Order Confirmation, which terms are in any way inconsistent with any terms set forth in the Order Confirmation and/or in these terms and conditions or CCC's standard operating procedures, whether such writing is prepared prior to, simultaneously with or subsequent to the Order Confirmation, and whether such writing appears on a copy of the Order Confirmation or in a separate instrument.

8.5 The licensing transaction described in the Order Confirmation document shall be governed by and construed under the law of the State of New York, USA, without regard to the principles thereof of conflicts of law. Any case, controversy, suit, action, or proceeding arising out of, in connection with, or related to such licensing transaction shall be brought, at CCC's sole discretion, in any federal or state court located in the County of New York, State of New York, USA, or in any federal or state court whose geographical jurisdiction covers the location of the Rightsholder set forth in the Order Confirmation. The parties expressly submit to the personal jurisdiction and venue of each such federal or state court. If you have any comments or questions about the Service or Copyright Clearance Center, please contact us at 978-750-8400 or send an e-mail to info@copyright.com.

v 1.1

Questions? customercare@copyright.com or +1-855-239-3415 (toll free in the US) or +1-978-646-2777.

**JOHN WILEY AND SONS LICENSE
TERMS AND CONDITIONS**

Oct 14, 2019

This Agreement between Reza Yadak ("You") and John Wiley and Sons ("John Wiley and Sons") consists of your license details and the terms and conditions provided by John Wiley and Sons and Copyright Clearance Center.

License Number	4687910312440
License date	Oct 14, 2019
Licensed Content Publisher	John Wiley and Sons
Licensed Content Publication	Earthquake Engineering and Structural Dynamics
Licensed Content Title	Dynamic analysis of piles and pile groups embedded in homogeneous soils
Licensed Content Author	P. K. Banerjee, T. G. Davies, R. Sen
Licensed Content Date	Dec 28, 2006
Licensed Content Volume	13
Licensed Content Issue	1
Licensed Content Pages	13
Type of use	Dissertation/Thesis
Requestor type	University/Academic
Format	Print and electronic
Portion	Text extract
Number of Pages	2
Will you be translating?	No
Title of your thesis / dissertation	Comparing CPT Results and Numerical Method Investigations to Assess the Interaction between Pile and Sand & Mixed Soils Using ABAQUS, with a Brief Review of ANNs and GEP Methods
The standard identifier	0098-8847
Expected completion date	Dec 2019
Expected size (number of pages)	1
Requestor Location	Reza Yadak 633a 80 Stirling Street CampusPerth Perth, WA 6000 Australia Attn:
Publisher Tax ID	EU826007151
Billing Type	Invoice
Billing Address	Reza Yadak 633a 80 Stirling Street CampusPerth Perth, Australia 6000 Attn: Reza Yadak
Total	0.00 AUD
Terms and Conditions	

TERMS AND CONDITIONS

This copyrighted material is owned by or exclusively licensed to John Wiley & Sons, Inc. or one of its group companies (each a "Wiley Company") or handled on behalf of a society with which a Wiley Company has exclusive publishing rights in relation to a particular work (collectively "WILEY"). By clicking "accept" in connection with completing this licensing transaction, you agree that the following terms and conditions apply to this transaction (along with the billing and payment terms and conditions established by the Copyright Clearance Center Inc., ("CCC's Billing and Payment terms and conditions"), at the time that you opened your RightsLink account (these are available at any time at <http://myaccount.copyright.com>).

Terms and Conditions

- The materials you have requested permission to reproduce or reuse (the "Wiley Materials") are protected by copyright.
- You are hereby granted a personal, non-exclusive, non-sub licensable (on a stand-alone basis), non-transferable, worldwide, limited license to reproduce the Wiley Materials for the purpose specified in the licensing process. This license, and any **CONTENT (PDF or image file) purchased as part of your order**, is for a one-time use only and limited to any maximum distribution number specified in the license. The first instance of republication or reuse granted by this license must be completed within two years of the date of the grant of this license (although copies prepared before the end date may be distributed thereafter). The Wiley Materials shall not be used in any other manner or for any other purpose, beyond what is granted in the license. Permission is granted subject to an appropriate acknowledgement given to the author, title of the material/book/journal and the publisher. You shall also duplicate the copyright notice that appears in the Wiley publication in your use of the Wiley Material. Permission is also granted on the understanding that nowhere in the text is a previously published source acknowledged for all or part of this Wiley Material. Any third party content is expressly excluded from this permission.
- With respect to the Wiley Materials, all rights are reserved. Except as expressly granted by the terms of the license, no part of the Wiley Materials may be copied, modified, adapted (except for minor reformatting required by the new Publication), translated, reproduced, transferred or distributed, in any form or by any means, and no derivative works may be made based on the Wiley Materials without the prior permission of the respective copyright owner. **For STM Signatory Publishers clearing permission under the terms of the [STM Permissions Guidelines](#) only, the terms of the license are extended to include subsequent editions and for editions in other languages, provided such editions are for the work as a whole in situ and does not involve the separate exploitation of the permitted figures or extracts**, You may not alter, remove or suppress in any manner any copyright, trademark or other notices displayed by the Wiley Materials. You may not license, rent, sell, loan, lease, pledge, offer as security, transfer or assign the Wiley Materials on a stand-alone basis, or any of the rights granted to you hereunder to any other person.
- The Wiley Materials and all of the intellectual property rights therein shall at all times remain the exclusive property of John Wiley & Sons Inc, the Wiley Companies, or their respective licensors, and your interest therein is only that of having possession of and the right to reproduce the Wiley Materials pursuant to Section 2 herein during the continuance of this Agreement. You agree that you own no right, title or interest in or to the Wiley Materials or any of the intellectual property rights therein. You shall have no rights hereunder other than the license as provided for above in Section 2. No right, license or interest to any trademark, trade name, service mark or other branding ("Marks") of WILEY or its licensors is granted hereunder, and you agree that you shall not assert any such right, license or interest with respect thereto

- NEITHER WILEY NOR ITS LICENSORS MAKES ANY WARRANTY OR REPRESENTATION OF ANY KIND TO YOU OR ANY THIRD PARTY, EXPRESS, IMPLIED OR STATUTORY, WITH RESPECT TO THE MATERIALS OR THE ACCURACY OF ANY INFORMATION CONTAINED IN THE MATERIALS, INCLUDING, WITHOUT LIMITATION, ANY IMPLIED WARRANTY OF MERCHANTABILITY, ACCURACY, SATISFACTORY QUALITY, FITNESS FOR A PARTICULAR PURPOSE, USABILITY, INTEGRATION OR NON-INFRINGEMENT AND ALL SUCH WARRANTIES ARE HEREBY EXCLUDED BY WILEY AND ITS LICENSORS AND WAIVED BY YOU.
- WILEY shall have the right to terminate this Agreement immediately upon breach of this Agreement by you.
- You shall indemnify, defend and hold harmless WILEY, its Licensors and their respective directors, officers, agents and employees, from and against any actual or threatened claims, demands, causes of action or proceedings arising from any breach of this Agreement by you.
- IN NO EVENT SHALL WILEY OR ITS LICENSORS BE LIABLE TO YOU OR ANY OTHER PARTY OR ANY OTHER PERSON OR ENTITY FOR ANY SPECIAL, CONSEQUENTIAL, INCIDENTAL, INDIRECT, EXEMPLARY OR PUNITIVE DAMAGES, HOWEVER CAUSED, ARISING OUT OF OR IN CONNECTION WITH THE DOWNLOADING, PROVISIONING, VIEWING OR USE OF THE MATERIALS REGARDLESS OF THE FORM OF ACTION, WHETHER FOR BREACH OF CONTRACT, BREACH OF WARRANTY, TORT, NEGLIGENCE, INFRINGEMENT OR OTHERWISE (INCLUDING, WITHOUT LIMITATION, DAMAGES BASED ON LOSS OF PROFITS, DATA, FILES, USE, BUSINESS OPPORTUNITY OR CLAIMS OF THIRD PARTIES), AND WHETHER OR NOT THE PARTY HAS BEEN ADVISED OF THE POSSIBILITY OF SUCH DAMAGES. THIS LIMITATION SHALL APPLY NOTWITHSTANDING ANY FAILURE OF ESSENTIAL PURPOSE OF ANY LIMITED REMEDY PROVIDED HEREIN.
- Should any provision of this Agreement be held by a court of competent jurisdiction to be illegal, invalid, or unenforceable, that provision shall be deemed amended to achieve as nearly as possible the same economic effect as the original provision, and the legality, validity and enforceability of the remaining provisions of this Agreement shall not be affected or impaired thereby.
- The failure of either party to enforce any term or condition of this Agreement shall not constitute a waiver of either party's right to enforce each and every term and condition of this Agreement. No breach under this agreement shall be deemed waived or excused by either party unless such waiver or consent is in writing signed by the party granting such waiver or consent. The waiver by or consent of a party to a breach of any provision of this Agreement shall not operate or be construed as a waiver of or consent to any other or subsequent breach by such other party.
- This Agreement may not be assigned (including by operation of law or otherwise) by you without WILEY's prior written consent.
- Any fee required for this permission shall be non-refundable after thirty (30) days from receipt by the CCC.
- These terms and conditions together with CCC's Billing and Payment terms and conditions (which are incorporated herein) form the entire agreement between you and WILEY concerning this licensing transaction and (in the absence of fraud) supersedes all prior agreements and representations of the parties, oral or written. This Agreement

may not be amended except in writing signed by both parties. This Agreement shall be binding upon and inure to the benefit of the parties' successors, legal representatives, and authorized assigns.

- In the event of any conflict between your obligations established by these terms and conditions and those established by CCC's Billing and Payment terms and conditions, these terms and conditions shall prevail.
- WILEY expressly reserves all rights not specifically granted in the combination of (i) the license details provided by you and accepted in the course of this licensing transaction, (ii) these terms and conditions and (iii) CCC's Billing and Payment terms and conditions.
- This Agreement will be void if the Type of Use, Format, Circulation, or Requestor Type was misrepresented during the licensing process.
- This Agreement shall be governed by and construed in accordance with the laws of the State of New York, USA, without regards to such state's conflict of law rules. Any legal action, suit or proceeding arising out of or relating to these Terms and Conditions or the breach thereof shall be instituted in a court of competent jurisdiction in New York County in the State of New York in the United States of America and each party hereby consents and submits to the personal jurisdiction of such court, waives any objection to venue in such court and consents to service of process by registered or certified mail, return receipt requested, at the last known address of such party.

WILEY OPEN ACCESS TERMS AND CONDITIONS

Wiley Publishes Open Access Articles in fully Open Access Journals and in Subscription journals offering Online Open. Although most of the fully Open Access journals publish open access articles under the terms of the Creative Commons Attribution (CC BY) License only, the subscription journals and a few of the Open Access Journals offer a choice of Creative Commons Licenses. The license type is clearly identified on the article.

The Creative Commons Attribution License

The [Creative Commons Attribution License \(CC-BY\)](#) allows users to copy, distribute and transmit an article, adapt the article and make commercial use of the article. The CC-BY license permits commercial and non-

Creative Commons Attribution Non-Commercial License

The [Creative Commons Attribution Non-Commercial \(CC-BY-NC\) License](#) permits use, distribution and reproduction in any medium, provided the original work is properly cited and is not used for commercial purposes.(see below)

Creative Commons Attribution-Non-Commercial-NoDerivs License

The [Creative Commons Attribution Non-Commercial-NoDerivs License \(CC-BY-NC-ND\)](#) permits use, distribution and reproduction in any medium, provided the original work is properly cited, is not used for commercial purposes and no modifications or adaptations are made. (see below)

Use by commercial "for-profit" organizations

Use of Wiley Open Access articles for commercial, promotional, or marketing purposes requires further explicit permission from Wiley and will be subject to a fee.

Further details can be found on Wiley Online Library

<http://olabout.wiley.com/WileyCDA/Section/id-410895.html>

Other Terms and Conditions:

v1.10 Last updated September 2015

**ELSEVIER LICENSE
TERMS AND CONDITIONS**

Nov 12, 2019

This Agreement between Reza Yadak ("You") and Elsevier ("Elsevier") consists of your license details and the terms and conditions provided by Elsevier and Copyright Clearance Center.

License Number 4706750091768

License date Nov 12, 2019

Licensed Content Publisher Elsevier

Licensed Content Publication Soil Dynamics and Earthquake Engineering

Licensed Content Title Nonlinear analysis for dynamic lateral pile response

Licensed Content Author M.H. El Naggar, M. Novak

Licensed Content Date Jun 1, 1996

Licensed Content Volume 15

Licensed Content Issue 4

Licensed Content Pages 12

Start Page	233
End Page	244
Type of Use	reuse in a thesis/dissertation
Portion	full article
Circulation	100
Format	both print and electronic
Are you the author of this Elsevier article?	No
Will you be translating?	No
Title	Comparing CPT Results and Numerical Method Investigations to Assess the Interaction between Pile and Sand & Mixed Soils Using ABAQUS, with a Brief Review of ANNs and GEP Methods
Institution name	Curtinuniversity
Expected presentation date	Dec 2019
Order reference number	33
Requestor Location	Reza Yadak 633a 80 Stirling Street CampusPerth Perth, WA 6000 Australia Attn:
Publisher Tax ID	GB 494 6272 12

Total 0.00 AUD

Terms and Conditions

INTRODUCTION

1. The publisher for this copyrighted material is Elsevier. By clicking "accept" in connection with completing this licensing transaction, you agree that the following terms and conditions apply to this transaction (along with the Billing and Payment terms and conditions established by Copyright Clearance Center, Inc. ("CCC"), at the time that you opened your Rightslink account and that are available at any time at <http://myaccount.copyright.com>).

GENERAL TERMS

2. Elsevier hereby grants you permission to reproduce the aforementioned material subject to the terms and conditions indicated.

3. Acknowledgement: If any part of the material to be used (for example, figures) has appeared in our publication with credit or acknowledgement to another source, permission must also be sought from that source. If such permission is not obtained then that material may not be included in your publication/copies. Suitable acknowledgement to the source must be made, either as a footnote or in a reference list at the end of your publication, as follows:

"Reprinted from Publication title, Vol /edition number, Author(s), Title of article / title of chapter, Pages No., Copyright (Year), with permission from Elsevier [OR APPLICABLE SOCIETY COPYRIGHT OWNER]." Also Lancet special credit - "Reprinted from The Lancet, Vol. number, Author(s), Title of article, Pages No., Copyright (Year), with permission from Elsevier."

4. Reproduction of this material is confined to the purpose and/or media for which permission is hereby given.

5. Altering/Modifying Material: Not Permitted. However figures and illustrations may be altered/adapted minimally to serve your work. Any other abbreviations, additions, deletions and/or any other alterations shall be made only with prior written authorization of Elsevier Ltd. (Please contact Elsevier at permissions@elsevier.com). No modifications can be made to any Lancet figures/tables and they must be reproduced in full.

6. If the permission fee for the requested use of our material is waived in this instance, please be advised that your future requests for Elsevier materials may attract a fee.

7. Reservation of Rights: Publisher reserves all rights not specifically granted in the combination of (i) the license details provided by you and accepted in the course of this licensing transaction, (ii) these terms and conditions and (iii) CCC's Billing and Payment terms and conditions.

8. License Contingent Upon Payment: While you may exercise the rights licensed immediately upon issuance of the license at the end of the licensing process for the transaction, provided that you have disclosed complete and accurate details of your proposed use, no license is finally effective unless and until full payment is received from you (either by publisher or by CCC) as provided in CCC's Billing and Payment terms and conditions. If full payment is not received on a timely basis, then any license preliminarily granted shall be deemed automatically revoked and shall be void as if never granted. Further, in the event that you breach any of these terms and conditions or any of CCC's Billing and Payment terms and conditions, the license is automatically revoked and shall be void as if never granted. Use of materials as described in a revoked license, as well as any use of the

materials beyond the scope of an unrevoked license, may constitute copyright infringement and publisher reserves the right to take any and all action to protect its copyright in the materials.

9. **Warranties:** Publisher makes no representations or warranties with respect to the licensed material.

10. **Indemnity:** You hereby indemnify and agree to hold harmless publisher and CCC, and their respective officers, directors, employees and agents, from and against any and all claims arising out of your use of the licensed material other than as specifically authorized pursuant to this license.

11. **No Transfer of License:** This license is personal to you and may not be sublicensed, assigned, or transferred by you to any other person without publisher's written permission.

12. **No Amendment Except in Writing:** This license may not be amended except in a writing signed by both parties (or, in the case of publisher, by CCC on publisher's behalf).

13. **Objection to Contrary Terms:** Publisher hereby objects to any terms contained in any purchase order, acknowledgment, check endorsement or other writing prepared by you, which terms are inconsistent with these terms and conditions or CCC's Billing and Payment terms and conditions. These terms and conditions, together with CCC's Billing and Payment terms and conditions (which are incorporated herein), comprise the entire agreement between you and publisher (and CCC) concerning this licensing transaction. In the event of any conflict between your obligations established by these terms and conditions and those established by CCC's Billing and Payment terms and conditions, these terms and conditions shall control.

14. **Revocation:** Elsevier or Copyright Clearance Center may deny the permissions described in this License at their sole discretion, for any reason or no reason, with a full refund payable to you. Notice of such denial will be made using the contact information provided by you. Failure to receive such notice will not alter or invalidate the denial. In no event will Elsevier or Copyright Clearance Center be responsible or liable for any costs, expenses or damage incurred by you as a result of a denial of your permission request, other than a refund of the amount(s) paid by you to Elsevier and/or Copyright Clearance Center for denied permissions.

LIMITED LICENSE

The following terms and conditions apply only to specific license types:

15. **Translation:** This permission is granted for non-exclusive world **English** rights only unless your license was granted for translation rights. If you licensed translation rights you may only translate this content into the languages you requested. A professional translator must perform all translations and reproduce the content word for word preserving the integrity of the article.

16. **Posting licensed content on any Website:** The following terms and conditions apply as follows: Licensing material from an Elsevier journal: All content posted to the web site must maintain the copyright information line on the bottom of each image; A hyper-text must be included to the Homepage of the journal from which you are licensing at <http://www.sciencedirect.com/science/journal/xxxxx> or the Elsevier homepage for books at <http://www.elsevier.com>; Central Storage: This license does not include permission for a scanned version of the material to be stored in a central repository such as that provided by Heron/XanEdu.

Licensing material from an Elsevier book: A hyper-text link must be included to the Elsevier homepage at <http://www.elsevier.com>. All content posted to the web site must maintain the copyright information line on the bottom of each image.

Posting licensed content on Electronic reserve: In addition to the above the following clauses are applicable: The web site must be password-protected and made available only to bona fide students registered on a relevant course. This permission is granted for 1 year only. You may obtain a new license for future website posting.

17. For journal authors: the following clauses are applicable in addition to the above:

Preprints:

A preprint is an author's own write-up of research results and analysis, it has not been peer-reviewed, nor has it had any other value added to it by a publisher (such as formatting, copyright, technical enhancement etc.).

Authors can share their preprints anywhere at any time. Preprints should not be added to or enhanced in any way in order to appear more like, or to substitute for, the final versions of articles however authors can update their preprints on arXiv or RePEc with their Accepted Author Manuscript (see below).

If accepted for publication, we encourage authors to link from the preprint to their formal publication via its DOI. Millions of researchers have access to the formal publications on ScienceDirect, and so links will help users to find, access, cite and use the best available version. Please note that Cell Press, The Lancet and some society-owned have different preprint policies. Information on these policies is available on the journal homepage.

Accepted Author Manuscripts: An accepted author manuscript is the manuscript of an article that has been accepted for publication and which typically includes author-incorporated changes suggested during submission, peer review and editor-author communications.

Authors can share their accepted author manuscript:

- immediately
 - via their non-commercial person homepage or blog
 - by updating a preprint in arXiv or RePEc with the accepted manuscript
 - via their research institute or institutional repository for internal institutional uses or as part of an invitation-only research collaboration work-group
 - directly by providing copies to their students or to research collaborators for their personal use
 - for private scholarly sharing as part of an invitation-only work group on commercial sites with which Elsevier has an agreement
- After the embargo period
 - via non-commercial hosting platforms such as their institutional repository
 - via commercial sites with which Elsevier has an agreement

In all cases accepted manuscripts should:

- link to the formal publication via its DOI
- bear a CC-BY-NC-ND license - this is easy to do
- if aggregated with other manuscripts, for example in a repository or other site, be shared in alignment with our hosting policy not be added to or enhanced in any way to appear more like, or to substitute for, the published journal article.

Published journal article (JPA): A published journal article (PJA) is the definitive final record of published research that appears or will appear in the journal and embodies all value-adding publishing activities including peer review co-ordination, copy-editing, formatting, (if relevant) pagination and online enrichment.

Policies for sharing publishing journal articles differ for subscription and gold open access articles:

Subscription Articles: If you are an author, please share a link to your article rather than the full-text. Millions of researchers have access to the formal publications on ScienceDirect, and so links will help your users to find, access, cite, and use the best available version.

Theses and dissertations which contain embedded PJAs as part of the formal submission can be posted publicly by the awarding institution with DOI links back to the formal publications on ScienceDirect.

If you are affiliated with a library that subscribes to ScienceDirect you have additional private sharing rights for others' research accessed under that agreement. This includes use for classroom teaching and internal training at the institution (including use in course packs and courseware programs), and inclusion of the article for grant funding purposes.

Gold Open Access Articles: May be shared according to the author-selected end-user license and should contain a [CrossMark logo](#), the end user license, and a DOI link to the formal publication on ScienceDirect.

Please refer to Elsevier's [posting policy](#) for further information.

18. **For book authors** the following clauses are applicable in addition to the above: Authors are permitted to place a brief summary of their work online only. You are not allowed to download and post the published electronic version of your chapter, nor may you scan the printed edition to create an electronic version. **Posting to a repository:** Authors are permitted to post a summary of their chapter only in their institution's repository.

19. **Thesis/Dissertation:** If your license is for use in a thesis/dissertation your thesis may be submitted to your institution in either print or electronic form. Should your thesis be published commercially, please reapply for permission. These requirements include permission for the Library and Archives of Canada to supply single copies, on demand, of the complete thesis and include permission for Proquest/UMI to supply single copies, on demand, of the complete thesis. Should your thesis be published commercially, please reapply for permission. Theses and dissertations which contain embedded PJAs as part of the formal submission can be posted publicly by the awarding institution with DOI links back to the formal publications on ScienceDirect.

Elsevier Open Access Terms and Conditions

You can publish open access with Elsevier in hundreds of open access journals or in nearly 2000 established subscription journals that support open access publishing. Permitted third party re-use of these open access articles is defined by the author's choice of Creative Commons user license. See our [open access license policy](#) for more information.

Terms & Conditions applicable to all Open Access articles published with Elsevier:

Any reuse of the article must not represent the author as endorsing the adaptation of the article nor should the article be modified in such a way as to damage the author's honour or reputation. If any changes have been made, such changes must be clearly indicated.

The author(s) must be appropriately credited and we ask that you include the end user license and a DOI link to the formal publication on ScienceDirect.

If any part of the material to be used (for example, figures) has appeared in our publication with credit or acknowledgement to another source it is the responsibility of the user to ensure their reuse complies with the terms and conditions determined by the rights holder.

Additional Terms & Conditions applicable to each Creative Commons user license:

CC BY: The CC-BY license allows users to copy, to create extracts, abstracts and new works from the Article, to alter and revise the Article and to make commercial use of the Article (including reuse and/or resale of the Article by commercial entities), provided the user gives appropriate credit (with a link to the formal publication through the relevant DOI), provides a link to the license, indicates if changes were made and the licensor is not represented as endorsing the use made of the work. The full details of the license are available at <http://creativecommons.org/licenses/by/4.0>.

CC BY NC SA: The CC BY-NC-SA license allows users to copy, to create extracts, abstracts and new works from the Article, to alter and revise the Article, provided this is not done for commercial purposes, and that the user gives appropriate credit (with a link to the formal publication through the relevant DOI), provides a link to the license, indicates if changes were made and the licensor is not represented as endorsing the use made of the work. Further, any new works must be made available on the same conditions. The full details of the license are available at <http://creativecommons.org/licenses/by-nc-sa/4.0>.

CC BY NC ND: The CC BY-NC-ND license allows users to copy and distribute the Article, provided this is not done for commercial purposes and further does not permit distribution of the Article if it is changed or edited in any way, and provided the user gives appropriate credit (with a link to the formal publication through the relevant DOI), provides a link to the license, and that the licensor is not represented as endorsing the use made of the work. The full details of the license are available at <http://creativecommons.org/licenses/by-nc-nd/4.0>. Any commercial reuse of Open Access articles published with a CC BY NC SA or CC BY NC ND license requires permission from Elsevier and will be subject to a fee.

Commercial reuse includes:

- Associating advertising with the full text of the Article
- Charging fees for document delivery or access
- Article aggregation
- Systematic distribution via e-mail lists or share buttons

Posting or linking by commercial companies for use by customers of those companies.

20. Other Conditions:

v1.9

Questions? customercare@copyright.com or +1-855-239-3415 (toll free in the US) or +1-978-646-2777.

**JOHN WILEY AND SONS LICENSE
TERMS AND CONDITIONS**

Oct 14, 2019

This Agreement between Reza Yadak ("You") and John Wiley and Sons ("John Wiley and Sons") consists of your license details and the terms and conditions provided by John Wiley and Sons and Copyright Clearance Center.

License Number	4687910252007
License date	Oct 14, 2019
Licensed Content Publisher	John Wiley and Sons
Licensed Content Publication	Earthquake Engineering and Structural Dynamics
Licensed Content Title	A model for the 3D kinematic interaction analysis of pile groups in layered soils
Licensed Content Author	Graziano Leoni, Sandro Carbonari, Francesca Dezi
Licensed Content Date	Feb 3, 2009
Licensed Content Volume	38
Licensed Content Issue	11
Licensed Content Pages	25
Type of use	Dissertation/Thesis
Requestor type	University/Academic
Format	Print and electronic
Portion	Text extract
Number of Pages	3
Will you be translating?	No
Title of your thesis / dissertation	Comparing CPT Results and Numerical Method Investigations to Assess the Interaction between Pile and Sand & Mixed Soils Using ABAQUS, with a Brief Review of ANNs and GEP Methods
The standard identifier	0098-8847
Expected completion date	Dec 2019
Expected size (number of pages)	1
Requestor Location	Reza Yadak 633a 80 Stirling Street CampusPerth Perth, WA 6000 Australia Attn:
Publisher Tax ID	EU826007151
Billing Type	Invoice
Billing Address	Reza Yadak 633a 80 Stirling Street CampusPerth Perth, Australia 6000 Attn: Reza Yadak
Total	0.00 AUD
Terms and Conditions	

TERMS AND CONDITIONS

This copyrighted material is owned by or exclusively licensed to John Wiley & Sons, Inc. or one of its group companies (each a "Wiley Company") or handled on behalf of a society with which a Wiley Company has exclusive publishing rights in relation to a particular work (collectively "WILEY"). By clicking "accept" in connection with completing this licensing transaction, you agree that the following terms and conditions apply to this transaction (along with the billing and payment terms and conditions established by the Copyright Clearance Center Inc., ("CCC's Billing and Payment terms and conditions"), at the time that you opened your RightsLink account (these are available at any time at <http://myaccount.copyright.com>).

Terms and Conditions

- The materials you have requested permission to reproduce or reuse (the "Wiley Materials") are protected by copyright.
- You are hereby granted a personal, non-exclusive, non-sub licensable (on a stand-alone basis), non-transferable, worldwide, limited license to reproduce the Wiley Materials for the purpose specified in the licensing process. This license, and any **CONTENT (PDF or image file)** purchased as part of your order, is for a one-time use only and limited to any maximum distribution number specified in the license. The first instance of republication or reuse granted by this license must be completed within two years of the date of the grant of this license (although copies prepared before the end date may be distributed thereafter). The Wiley Materials shall not be used in any other manner or for any other purpose, beyond what is granted in the license. Permission is granted subject to an appropriate acknowledgement given to the author, title of the material/book/journal and the publisher. You shall also duplicate the copyright notice that appears in the Wiley publication in your use of the Wiley Material. Permission is also granted on the understanding that nowhere in the text is a previously published source acknowledged for all or part of this Wiley Material. Any third party content is expressly excluded from this permission.
- With respect to the Wiley Materials, all rights are reserved. Except as expressly granted by the terms of the license, no part of the Wiley Materials may be copied, modified, adapted (except for minor reformatting required by the new Publication), translated, reproduced, transferred or distributed, in any form or by any means, and no derivative works may be made based on the Wiley Materials without the prior permission of the respective copyright owner. **For STM Signatory Publishers clearing permission under the terms of the [STM Permissions Guidelines](#) only, the terms of the license are extended to include subsequent editions and for editions in other languages, provided such editions are for the work as a whole in situ and does not involve the separate exploitation of the permitted figures or extracts, You may not alter, remove or suppress in any manner any copyright, trademark or other notices displayed by the Wiley Materials. You may not license, rent, sell, loan, lease, pledge, offer as security, transfer or assign the Wiley Materials on a stand-alone basis, or any of the rights granted to you hereunder to any other person.**
- The Wiley Materials and all of the intellectual property rights therein shall at all times remain the exclusive property of John Wiley & Sons Inc, the Wiley Companies, or their respective licensors, and your interest therein is only that of having possession of and the right to reproduce the Wiley Materials pursuant to Section 2 herein during the continuance of this Agreement. You agree that you own no right, title or interest in or to the Wiley Materials or any of the intellectual property rights therein. You shall have no rights hereunder other than the license as provided for above in Section 2. No right, license or interest to any trademark, trade name, service mark or other branding ("Marks") of WILEY or its licensors is granted hereunder, and you agree that you shall not assert any such right, license or interest with respect thereto

- NEITHER WILEY NOR ITS LICENSORS MAKES ANY WARRANTY OR REPRESENTATION OF ANY KIND TO YOU OR ANY THIRD PARTY, EXPRESS, IMPLIED OR STATUTORY, WITH RESPECT TO THE MATERIALS OR THE ACCURACY OF ANY INFORMATION CONTAINED IN THE MATERIALS, INCLUDING, WITHOUT LIMITATION, ANY IMPLIED WARRANTY OF MERCHANTABILITY, ACCURACY, SATISFACTORY QUALITY, FITNESS FOR A PARTICULAR PURPOSE, USABILITY, INTEGRATION OR NON-INFRINGEMENT AND ALL SUCH WARRANTIES ARE HEREBY EXCLUDED BY WILEY AND ITS LICENSORS AND WAIVED BY YOU.
- WILEY shall have the right to terminate this Agreement immediately upon breach of this Agreement by you.
- You shall indemnify, defend and hold harmless WILEY, its Licensors and their respective directors, officers, agents and employees, from and against any actual or threatened claims, demands, causes of action or proceedings arising from any breach of this Agreement by you.
- IN NO EVENT SHALL WILEY OR ITS LICENSORS BE LIABLE TO YOU OR ANY OTHER PARTY OR ANY OTHER PERSON OR ENTITY FOR ANY SPECIAL, CONSEQUENTIAL, INCIDENTAL, INDIRECT, EXEMPLARY OR PUNITIVE DAMAGES, HOWEVER CAUSED, ARISING OUT OF OR IN CONNECTION WITH THE DOWNLOADING, PROVISIONING, VIEWING OR USE OF THE MATERIALS REGARDLESS OF THE FORM OF ACTION, WHETHER FOR BREACH OF CONTRACT, BREACH OF WARRANTY, TORT, NEGLIGENCE, INFRINGEMENT OR OTHERWISE (INCLUDING, WITHOUT LIMITATION, DAMAGES BASED ON LOSS OF PROFITS, DATA, FILES, USE, BUSINESS OPPORTUNITY OR CLAIMS OF THIRD PARTIES), AND WHETHER OR NOT THE PARTY HAS BEEN ADVISED OF THE POSSIBILITY OF SUCH DAMAGES. THIS LIMITATION SHALL APPLY NOTWITHSTANDING ANY FAILURE OF ESSENTIAL PURPOSE OF ANY LIMITED REMEDY PROVIDED HEREIN.
- Should any provision of this Agreement be held by a court of competent jurisdiction to be illegal, invalid, or unenforceable, that provision shall be deemed amended to achieve as nearly as possible the same economic effect as the original provision, and the legality, validity and enforceability of the remaining provisions of this Agreement shall not be affected or impaired thereby.
- The failure of either party to enforce any term or condition of this Agreement shall not constitute a waiver of either party's right to enforce each and every term and condition of this Agreement. No breach under this agreement shall be deemed waived or excused by either party unless such waiver or consent is in writing signed by the party granting such waiver or consent. The waiver by or consent of a party to a breach of any provision of this Agreement shall not operate or be construed as a waiver of or consent to any other or subsequent breach by such other party.
- This Agreement may not be assigned (including by operation of law or otherwise) by you without WILEY's prior written consent.
- Any fee required for this permission shall be non-refundable after thirty (30) days from receipt by the CCC.
- These terms and conditions together with CCC's Billing and Payment terms and conditions (which are incorporated herein) form the entire agreement between you and WILEY concerning this licensing transaction and (in the absence of fraud) supersedes all prior agreements and representations of the parties, oral or written. This Agreement

may not be amended except in writing signed by both parties. This Agreement shall be binding upon and inure to the benefit of the parties' successors, legal representatives, and authorized assigns.

- In the event of any conflict between your obligations established by these terms and conditions and those established by CCC's Billing and Payment terms and conditions, these terms and conditions shall prevail.
- WILEY expressly reserves all rights not specifically granted in the combination of (i) the license details provided by you and accepted in the course of this licensing transaction, (ii) these terms and conditions and (iii) CCC's Billing and Payment terms and conditions.
- This Agreement will be void if the Type of Use, Format, Circulation, or Requestor Type was misrepresented during the licensing process.
- This Agreement shall be governed by and construed in accordance with the laws of the State of New York, USA, without regards to such state's conflict of law rules. Any legal action, suit or proceeding arising out of or relating to these Terms and Conditions or the breach thereof shall be instituted in a court of competent jurisdiction in New York County in the State of New York in the United States of America and each party hereby consents and submits to the personal jurisdiction of such court, waives any objection to venue in such court and consents to service of process by registered or certified mail, return receipt requested, at the last known address of such party.

WILEY OPEN ACCESS TERMS AND CONDITIONS

Wiley Publishes Open Access Articles in fully Open Access Journals and in Subscription journals offering Online Open. Although most of the fully Open Access journals publish open access articles under the terms of the Creative Commons Attribution (CC BY) License only, the subscription journals and a few of the Open Access Journals offer a choice of Creative Commons Licenses. The license type is clearly identified on the article.

The Creative Commons Attribution License

The [Creative Commons Attribution License \(CC-BY\)](#) allows users to copy, distribute and transmit an article, adapt the article and make commercial use of the article. The CC-BY license permits commercial and non-

Creative Commons Attribution Non-Commercial License

The [Creative Commons Attribution Non-Commercial \(CC-BY-NC\) License](#) permits use, distribution and reproduction in any medium, provided the original work is properly cited and is not used for commercial purposes.(see below)

Creative Commons Attribution-Non-Commercial-NoDerivs License

The [Creative Commons Attribution Non-Commercial-NoDerivs License \(CC-BY-NC-ND\)](#) permits use, distribution and reproduction in any medium, provided the original work is properly cited, is not used for commercial purposes and no modifications or adaptations are made. (see below)

Use by commercial "for-profit" organizations

Use of Wiley Open Access articles for commercial, promotional, or marketing purposes requires further explicit permission from Wiley and will be subject to a fee.

Further details can be found on Wiley Online Library

<http://olabout.wiley.com/WileyCDA/Section/id-410895.html>

Other Terms and Conditions:

v1.10 Last updated September 2015



Use of evolutionary computing for modelling some complex problems in geotechnical engineering

Author: Mohamed A. Shahin



Publication: Geomechanics & Geoengineering: An International Journal

Publisher: Taylor & Francis

Date: Apr 3, 2015

Rights managed by Taylor & Francis

Thesis/Dissertation Reuse Request

Taylor & Francis is pleased to offer reuses of its content for a thesis or dissertation free of charge contingent on resubmission of permission request if work is published.

BACK

CLOSE